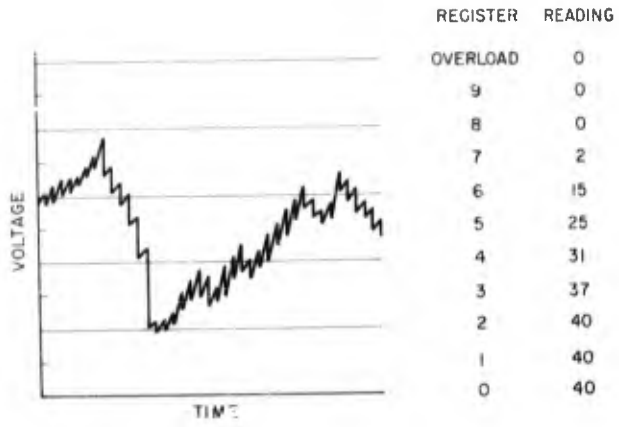

Fig. 4 - Operation of the discriminators in the M. S. mode

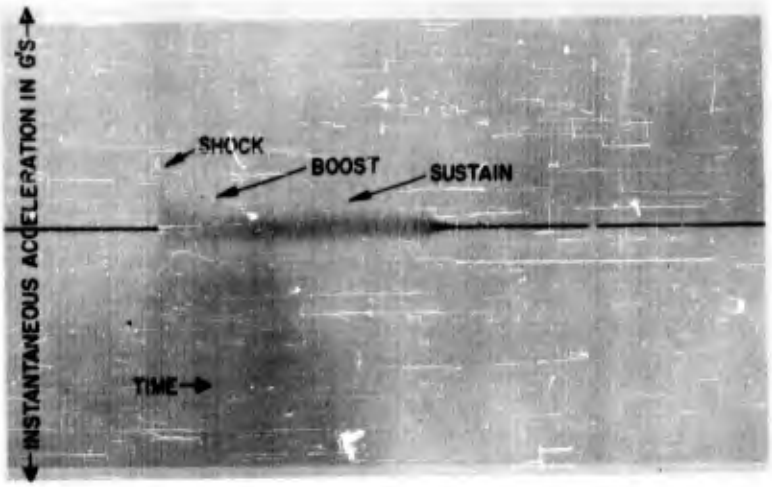

Fig. 5 - Typical acceleration versus time record

APPLICATION TO AN ACTUAL ANALYSIS

To illustrate the operation of this system, its application to the analysis of an actual set of data will be described.

The data presented herein came from a measurement program to determine the vibration occurring at various points on a missile due to the burning of its motor. The missile was held in an especially designed restraining mechanism at the restrained firing facility at NAMTC, Point Mugu.

The duration of the motor burning was approximately 4 seconds. The burning had two distinct phases: (1) a high-rate burning, boost phase, and (2) a lower-rate burning sustain phase. The boost phase lasted approximately 1 second and the sustain phase lasted approximately 3 seconds. Figure 5 shows a typical vibration channel with three characteristics: (1) ignition

shock, (2) high-level vibration during the boost phase, and (3) low-level vibration. There was no shock at burnout. While the ignition shock is no particular problem to analyze, analysis of the vibration is a different story. The record is quite short to be cut into two separate lengths for separate analyses of the boost and sustain phases, although this would be preferable to a single ordinary spectral analysis over the entire vibration duration.

In order to analyze these motor-burning-induced vibrations, the M. S. mode of analysis, described in the preceding section, was used. Figure 6 shows a representative example of one of the oscillograph records obtained as results of this analysis. It represents the variation of the spectral density within one frequency band over the duration of the vibration. Notice that the ignition shock, boost, and sustain phases are clearly defined. Figure 7 shows another oscillograph record, however, this record is for mean-square variation with time of the broadband (unfiltered) signal. The separate phases are also clearly visible. One-fifth-of-a second integration time was used

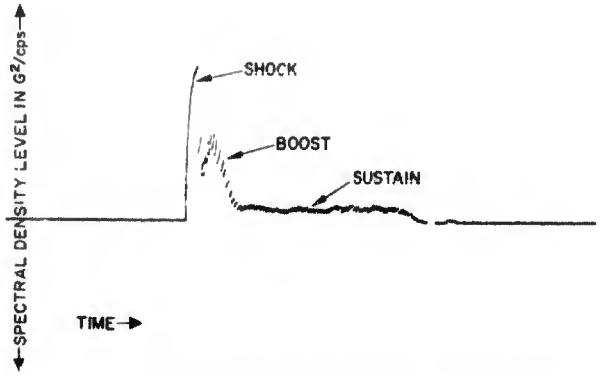

Fig. 6 - Typical spectral density versus time analysis (in a frequency band)

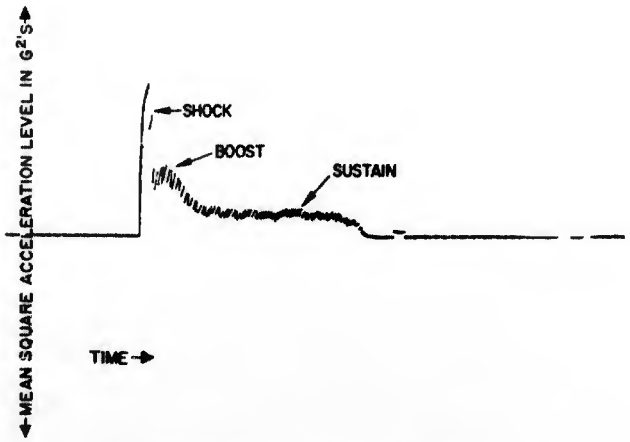

Fig. 7 - Typical mean-square level versus time analysis (of broadband signal)

for this analysis, so that 80 points (1/5-sec integration time by 4-readouts per integration time by 4 seconds) were obtained; this gives fairly accurate resolution of the variation in spectral density, or mean square, with time even over this rather short interval of only 4 seconds.

The final results, obtained from the computer, were in the form of 45 oscillograph records similar to Fig. 6. Each record represents the variation in spectral density, with time, within a frequency band. The optimum form in which to present these data would be a three-dimensional surface whose coordinates are spectral density, frequency, and time; see Fig. 8. Since presenting this three-dimensional plot in a usable form is somewhat of a problem, the results must be presented in some other manner. Several choices are available. As the results come out of the computer, they represent spectral density-time planes in this surface at various points along the frequency axis and they are directly usable as such. One can also take spectral density-frequency planes along the time axis; two such planes are shown in Fig. 9. 9A was taken during the boost and 9B was taken during the sustain phase. These power spectra were obtained by measuring the spectral density at the same two points in time on each oscillograph record. Still another method of presenting the data is to take planes in the frequency-time plane at various spectral density levels, although this is rather difficult and perhaps of not too much value in that form. A comparable and more

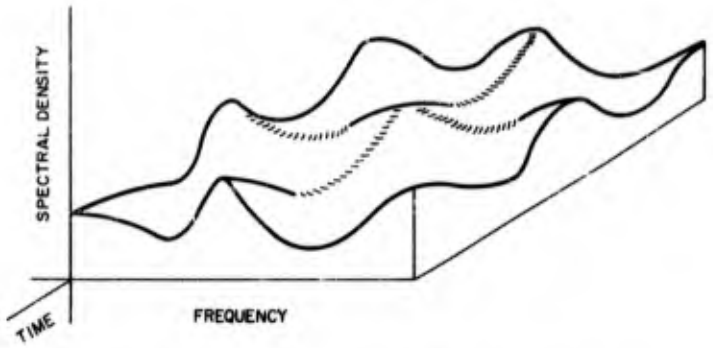

Fig. 8 - Optimum plot of analysis results

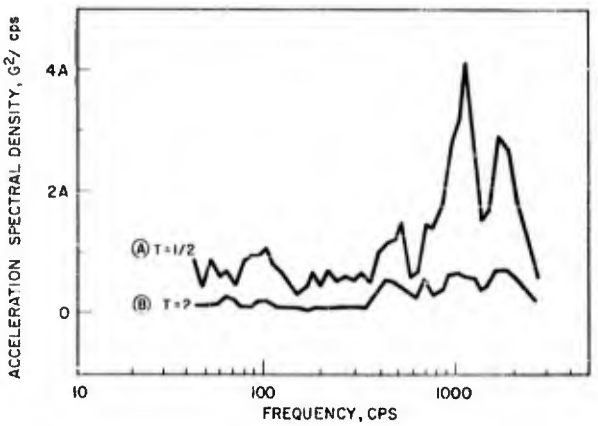

Fig. 9 - Spectra at T seconds from beginning

useful form is to measure the percent of time that the spectral density exceeds various levels for each of the frequency bands; this gives a spectral density distribution curve (Fig. 10). One could calculate this from the oscillograph records, but it can be directly obtained by using the discriminators and counters.

In addition to these types of analyses which are essentially standard, for this particular data it was desired to know the range of variation in the spectrum during both the boost and the sustain phase; to obtain this, the maximum and minimum values of each oscillograph record were measured for both the boost and sustain phases. A separate spectrum showing the band between the maximum and minimum was plotted for each phase (Fig. 11). It can be seen that a great deal of useful information can be obtained by use of this computer.

OTHER ANALYSIS CAPABILITIES OF THE SYSTEM

In addition to analyzing short-duration nonstationary random vibration, the system is capable of analyzing (1) long-duration

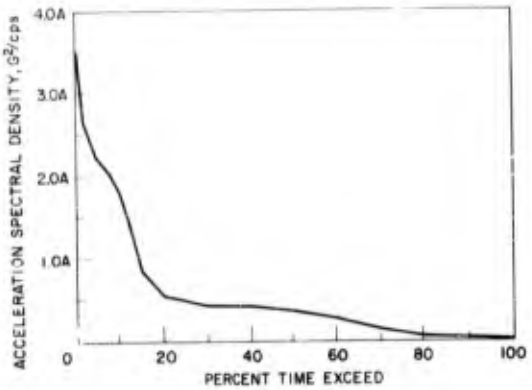

Fig. 10 - Typical spectral density distribution curve (one frequency band)

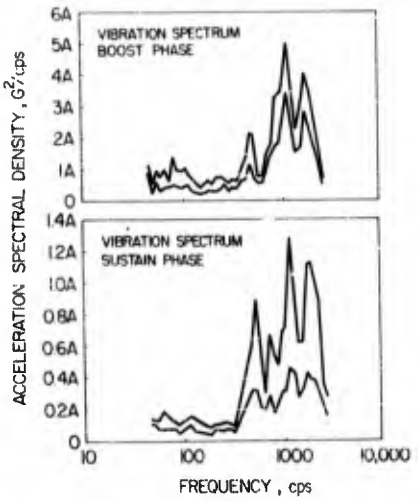

Fig. 11 - Maximum and minimum spectra density occurring during each phase (typical channel)

nonstationary random vibration, (2) stationary random vibration, and (3) periodic vibration. The extension to long-duration nonstationary data is direct; one simply does the same thing over longer times. The computer can analyze stationary data by the same method; however, it is capable of analyzing stationary data by a simpler method, designated as the Spectral Density (S. D.) analysis.

Since the data is stationary, only a short portion is recorded on a continuous loop of magnetic tape. Then the tape is played back and the output of each filter is analyzed one at a time. The output of the filter is squared and integrated as in the M. S. analysis, except that only one integrator is used instead of the commutated bank of five integrators. The output of this integrator is displayed on an oscillograph. To compute the spectral density one merely divides the deflection on the oscillograph by the integration time. Essentially, the computer operates exactly as most conventional vibration analyzers. There is one major difference though. In addition to the data, command signals are recorded on the tape loop. These command signals are recorded on separate tape tracks and their function is to start the integration and stop the integration. After the stop command and before the start command, the integrator's input and output are held to zero. In this manner, one of the annoying problems of loop analysis–what to do about the splice in the tape–is completely eliminated, unless one were to deliberately put the start command before the splice and the stop command after the splice. These command signals also assure that all the filters analyze the same portion of the data and therefore they are used for all methods of analysis in this system. A block diagram of the S. D. analysis mode is presented as Fig. 12. The S. D. analysis mode is identical to the M. S. analysis mode up to the integrators. For the S. D. mode, only one integrator is used. Its integration time is controlled by the duration between the start and stop commands. Also this integrator's output goes to the oscillograph only.

The other type of analysis possible with this computer is designated as the Amplitude Distribution (A. D.) mode. With it the amplitude distribution, actually the probability density function, is computed. This analysis is also for stationary data and permits one to determine if the data is random or periodic. The results of analyzing a sine wave is presented in Part A of Fig. 13; noise is presented in Part B of Fig. 13, and a combination of sine and noise is presented in Part C of Fig. 13. A block diagram of the computer for this mode of analysis is presented in Fig. 14. The circuitry for this mode is identical to that for both the M. S. and S. D. modes up to the output of variable-gain amplifier.

At this point in the A. D. mode, the output of this amplifier is connected to a bank of 11 discriminators biased in equal steps from 0 to full scale. Each discriminator opens a gate whenever its bias level is

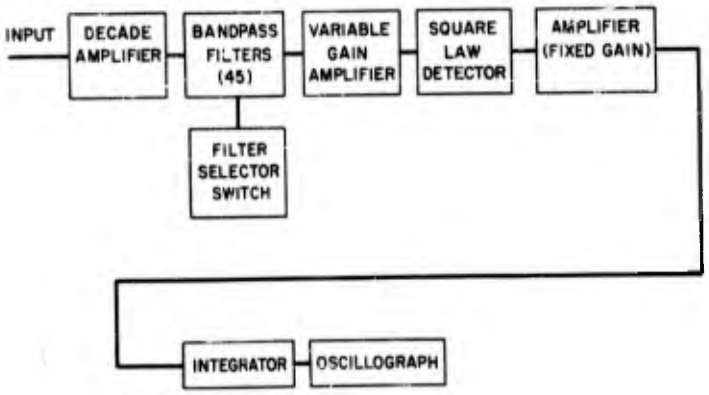

Fig. 12 - The analysis system for the S. D. analysis mode

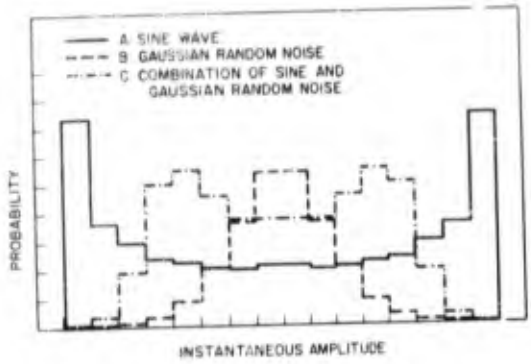

Fig. 13 - Typica. amplitude distribution analyses

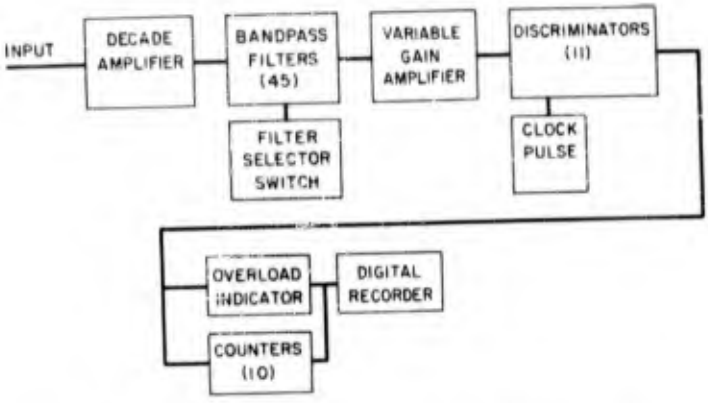

Fig. 14 - Analysis system for the A. D. analysis mode

exceeded. Each gate (except number 11) when opened, then adds a 1-Mc clock to the register (electronic counter), associated with it. The first counter measures the time 0 is exceeded (in one direction) and the eleventh discriminator signals an overload condition, if full scale has been exceeded. To calculate the probability that the signal lies between any two discriminator levels, one merely divides the difference between the two corresponding counter readings by twice the zero counter reading.

CONCLUSION

A special purpose computer that will permit the detailed analysis of nonstationary as well as stationary data has been designed and built. No claim is made that this computer is the answer to all vibration analysis problems. This computer's applications range from the analysis of field measurements to laboratory measurements, from records of a few seconds duration to an hour's duration, and from nonstationary data through stationary data even to periodic data. So it can be seen that in addition to this computer's unique ability to analyze nonstationary data, it also is a very useful tool for the analysis of a large percentage of the total range of vibration analysis.

Dr. Morrow (Chairman, Aerospace Corp.): I had one question in connection with Fig. 13. There were probability density functions plotted versus instantaneous amplitudes. I wonder if you don't mean instantaneous value?

Mr. Kelly: It's not a peak amplitude. I tried to convey what you're saying—instantaneous value. I don't wand to be misleading and say it's versus peak amplitude. It's not. This is the density function.

Mr. Galef (National Engineering Science Co.): I'm very curious to know what you would do with that three-dimensional spectral density, if you had it. To go a little further, why do we want the data in the first place? It would appear that we want the data in order to tell what is going to happen to the equipment. If the process is stationary, the spectral density is extremely useful in telling us what will happen to the equipment. If it is not stationary, I assume somebody, some time, will be able to tell us what will happen, but I haven't seen any results yet of anyone who has analyzed the response to nonstationary random data. I wonder if it might be worthwhile to suggest that, instead of using power spectral analyses when we have very definitely nonstationary data, it might be wise to consider getting something very closely equivalent to a shock spectrum—simply the response of a single-degree-of-freedom system of many different frequencies. In this case it would have to be a damped single-degree-of-freedom system. I think we would like to see a shock spectrum for perhaps 1, 5, or 10 percent damping. This might tell us, in a very concise manner, what the data of your entire 4 seconds is doing, whereas I don't really believe the three dimensional, power spectral density can tell us that.

Mr. Kelly: Well, I have two comments on that: One, somebody has to set up a test level; and the question is how are you going to set up a test level, if you don't know what is happening? The second comment—your reference to using a shock-spectrum type of equivalent—is that I have done a little bit of work on this; in fact, I modified a shock-spectrum computer to have damping. But essentially all you're doing is saying, "Ah hah, now I have a filter whose response curves I know." The only difference I can see is that you have one filter characteristic as compared to another filter characteristic.

Dr. Morrow: May I add a comment to this. I think there has been a little bit too much worry over whether vibration is stationary or not. There is really nothing in the definition of power spectral density which says or implies anything about stationarity. It does turn out that the concept is more useful when the vibration has a certain degree of stationarity, but the idea of stationarity is very closely related to the concept of steady-state conditions when one has periodic or quasiperiodic excitation. It's generally accepted to be reasonable that a peak value and a frequency constitute a good description of a sinusoid at a particular moment, if one can compute the response fairly closely on the basis of this information. Now, whether you can do this or not depends on whether the sinusoid is changing rapidly or slowly by comparison with the response time of the various resonators which may be excited by it. If things happen too fast, the steady-state computation gives you very little insight at all; whereas if things are happening very slowly, then this traditional method of computation works very well. With stationarity, it's much the same story. In those cases where the variations are slow enough so that in the sinusoidal case you could use the steady-state analysis, then for essentially the same degree of slowness in the random case you can get useful results from power spectral density.

Mr. Nute (Convair Astronautics): I would like to suggest an alternate answer to the last question, regarding the usefulness of a three-dimensional power spectrum plot. This relates to some work we have been doing quite recently. So far, we've had no success, but it seems as if it should be promising. Namely, to use this three-dimensional plot to discover cases where you have modulated sinusoids. When developed adequately, this could turn out to be a very powerful diagnostic tool for describing, let us say, the origin of certain types of vibration—particularly where you get two coupled modes of vibration whose frequencies are slightly separated, you will get a

certain frequency modulation of the spectrum. I might say in this connection that I have heard of work done by a different firm (and I do not feel free to divulge too many details), where they took a stochastic process and they analyzed it. They took a power spectral density at one moment; took another density from a different interval of time which overlapped the first interval by about 98 percent; and took a third spectrum which overlapped the last one by 98 percent. Thus they got a sequence of about 50 points–50 spectra. Each of these spectra had about four peaks. The four peaks occurred at the same frequencies but had different amplitudes. So they selected one of these peaks, let us say at 300 cycles, and then they took a height of the 300-cycle peak in each of these 50 spectra which gave them 50 points; they subjected this to another spectral analysis and they found that this was amplitude modulating at a very clear cut frequency. A physical significance was attached to this frequency which brings me to the question that I'm very anxious to see answered: When you are preparing a three-dimensional plot, you have a certain trade-off between the bandwidth and the frequency resolution of a single filter, or the resolution, or the amount of time that you allow to elapse from one sample interval to the other. As I say, in the case I just described, the amount of time elapsing between one sample interval and the other was, you might say, less than zero–they had them overlap. But if you choose a spectral density with a very-high-frequency resolution you have to take a long sample interval and, then, the next sample interval has to start a lot later. Have you seen any work done in answer to this question of how to get the most out of the three-dimensional spectrum?

Mr. Kelly: Offhand, I can't say I've seen any work on that. I'd like to comment on this process a little bit. If you recall Fig. 3 on the commutated integrators, you will remember that during any integration time we read out four values of spectral density. So, we obviously have these values overlapping during that time and this continues for the entire record. I don't know if this is any help or not.

Mr. Galef: I'd like to go back to your answer that you would use the three-dimensional spectral plot to get a specification and to Dr. Morrow's comment that if the spectral density is changing slowly, it is extremely useful. I agree completely with Dr. Morrow; however, for the situation which you have showed which includes the shock of ignition and the very rapidly changing spectral density during first blast, I would hate to have to design something for a spectral density which was derived from the ignition shock. This would be an extremely difficult thing–nor would it be an appropriate thing. This is definitely a shock and should be treated as a shock.

Mr. Kelly: I agree with you wholeheartedly. As a matter of fact, we don't use that bit of data. I mean, you have to use some judgment when you're analyzing this data; and, certainly, if it is a shock, I don't think we should call it vibration.

Mr. Bendat (Ramo-Wooldridge): I want to compliment the speaker for the material presented in his paper. I feel it represents a most significant contribution; and the fact that there has been this discussion, I think, bears that out. As was pointed out in an earlier paper, when a process is ergodic, a single representative record analyzed timewise can give you a great deal of information about the entire ensemble of which it is a part. When the process is stationary, this is no longer necessarily true; and when the process is nonstationary, it's definitely not true. So that, for nonstationary phenomena; one record is never representative of anything, except that one record. Therefore, it is essential in analyzing nonstationary phenomena to always obtain as many samples as possible and do conventional statistical averaging over the results. This was not brought out in the paper, but I'm sure that the speaker is aware of this point. Secondly, the last part of the paper presented some work with amplitude probability distribution analysis. This is another aspect of the problem that has to go hand-in-hand with power spectral analysis. He mentioned the fact that they compute the amount of time that the record will stay above various levels. I would like to ask whether or not they may have considered ways of extending this to also consider the expected number of times per unit of time that you cross various levels–the so-called threshold-crossing problem which has application to fatigue studies?

Mr. Kelly: Yes, frankly, we did consider it but unfortunately the circuitry doesn't lend itself to modification very readily.

Dr. Curtis (Hughes Aircraft Co.): I would like to point out to Mr. Galef that one of the whole purposes of this computer was to be able to separate the shock from the following vibration, so that we didn't commit the sin of which he is accusing us. Secondly, I would like to comment that this business of confidence interval and the probability distribution analysis are very intimately tied together, since it makes no sense to base your confidence interval on having a gaussian, or normal distribution, etc., until after you've found out that you do have such a distribution. Therefore, this is another reason why you have to find out whether these peaks in the spectra really represent narrow band random vibration, or quasisinusoids, or some mixture of the two. Otherwise, you don't know what variation to expect. In case somebody is wondering why didn't we show confidence intervals about this data in this present paper–first, I don't know how to do it for a nonstationary process; and second, we're trying to say what went on during this one burning of a rocket engine for which we had a record of the complete duration. Usually, we're in the position of taking a small sample of a long duration, then confidence intervals come into play.

* * *

A SPECTRAL ANALYZER FOR SHOCK ENVIRONMENT

Ward P. Barnes
Boeing Airplane Company
Seattle, Washington

Recent military specifications require that a shock environment be described in terms of a shock-response spectrum rather than the traditional terms of intensity, duration, and waveform. This paper describes a new method of determining the response to a shock pulse, the analysis equipment, and the results of analyses of both test shocks and actual shock environments.

INTRODUCTION

Recent Research and Development Programs in the Aero-Space industry have emphasized the design and development of electronic packages. The reliability requirements of these packages have in turn attached greater importance to dynamic testing in general, and to shock testing in particular. The definition of shock environment through the use of shock-response spectra is an example of one method developed to refine shock-testing techniques.

The use of shock spectra, however, has necessitated the development of valid methods for determining the response of dynamic systems to shock.

The purpose of this paper is to describe a response analysis method employed at Boeing, to describe the analyzer in detail, and to present the results of some of the analyses.

BACKGROUND

Shock-test specifications have assumed a variety of forms. In general, however, they can be grouped into three categories:

1. Test Conditions Specified. A particular test setup, or shock-test machine, is specified. The test environment, though not defined, can be repeated for each test with a fair degree of accuracy. Shock-test machines of the Naval Ordnance Laboratories are typical of this type of specification.

2. Shock Pulse Specified. The actual shock pulse is described in terms of maximum acceleration, duration, rise time, fall time, and/or wave shape. This type of specification is represented by any one of a number of current MIL specs.

3. Shock Spectrum Specified. Here the response to the shock pulse is specified in terms of the maximum acceleration experienced by simple spring-mass systems. Recent specifications from STL have included test requirements of this type.

The test conditions (drop height, impact medium, pneumatic pressure, etc.) can be readily determined for tests in the first category. The second type of specification required only that the shock pulse be monitored with an accelerometer and displayed. The shock-spectra method, however, requires that an analysis be performed to determine the response to the shock pulse. This requirement prompted the development of the shock-response analyzer described in this paper.

SHOCK SPECTRUM DEFINED

Undoubtedly there are engineers in environmental testing, and even in the particular field of shock testing, that have not yet encountered shock-response spectra. For this reason, it would be advantageous to spend a few moments on a brief description of this type of specification.

A shock spectrum has been defined as follows: "A shock spectrum is the envelope formed by the maximum acceleration response of an infinite number of simple, undamped, single degree of freedom, spring-mass systems when simultaneously subjected to a given shock environment." In simple language, just what does this mean?

Figure 1 shows the steps involved in developing a shock spectrum. Figure 1(a) shows a plate upon which are mounted three simple, undamped spring-mass systems with varying natural frequencies. Assuming the acceleration of the masses may be determined with an accelerometer, their response to the applied half-sine pulse would be as shown in Fig. 1(b), (c), and (d). The maximum positive-acceleration response of each of the systems (a_1, a_2, and a_3) is shown in Fig. 1(e), plotted against natural frequency. If this procedure were to be repeated with an infinite number of spring-mass systems, the maximum positive response would form the envelope indicated by the upper dotted line. This is generally referred to as the primary shock-response spectrum. It should be noted that the maximum negative acceleration response of each of the systems would also form an envelope, referred to as the residual shock-response spectrum. Either the primary or, in some cases, both spectra are used to define a shock-test specification.

SHOCK-TEST INSTRUMENTATION

The system employed at Boeing for instrumenting shock environment is shown in the block diagram in Fig. 2.

Normally, the shock is either produced with a machine in the laboratory or it is an actual, measured-field environment. Measurement of the acceleration level is accomplished with an accelerometer mounted on or adjacent to the test specimen. For part of the work done with shock spectra, however, the signal has been synthesized electrically with a shock pulse simulator.

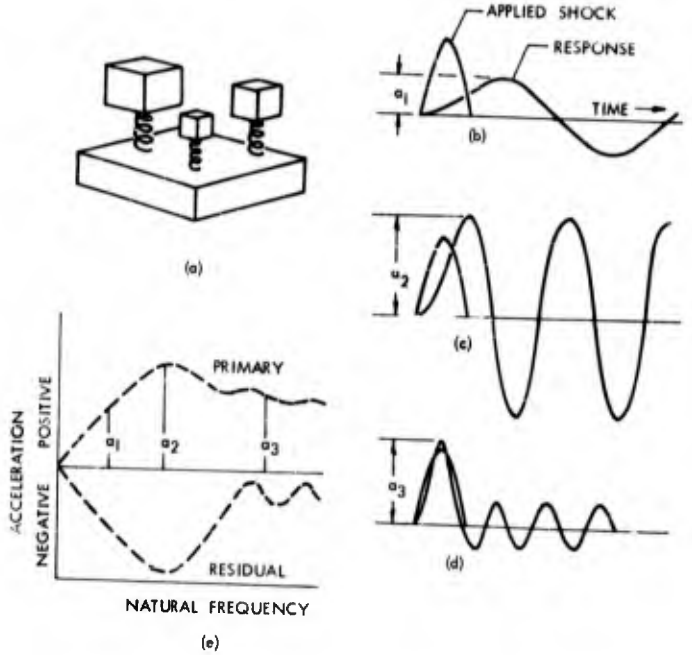

Fig. 1 - Steps involved in developing a shock spectrum: (a), plate with three vibratory systems; (b), (c), and (d), acceleration response of the systems to half-sine shock pulse; (e), resulting shock-response spectrum

The shock pulse is measured by introducing the electronic shock signal to the y axis of an oscilloscope and photographing the resulting trace with a polaroid camera. The response spectra is measured by performing an analysis on the shock pulse with the shock-response analyzer.

SHOCK RESPONSE ANALYZER

The basic analyzer (Figs. 3 and 4) is comprised of a series of simple electronic circuits, each analogous to one simple spring-mass system. The theory behind the operation of the analyzer can be illustrated by analytically comparing an individual electrical circuit to the equivalent mechanical system

x_1 = the displacement of M_1, inches,

x_2 = the displacement of M_2, inches.

The system of differential equations which describe the relationship between M_1 and M_2 is as follows, if friction is neglected:

$$M_1 \frac{d^2x_1}{dt^2} + k(x_1 - x_2) = 0. \qquad (1)$$

$$M_2 \frac{d^2x_2}{dt^2} - k(x_1 - x_2) = F(t). \qquad (2)$$

Eqs. (1) and (2) may be put into a dimensionless form by using the following substitutions.

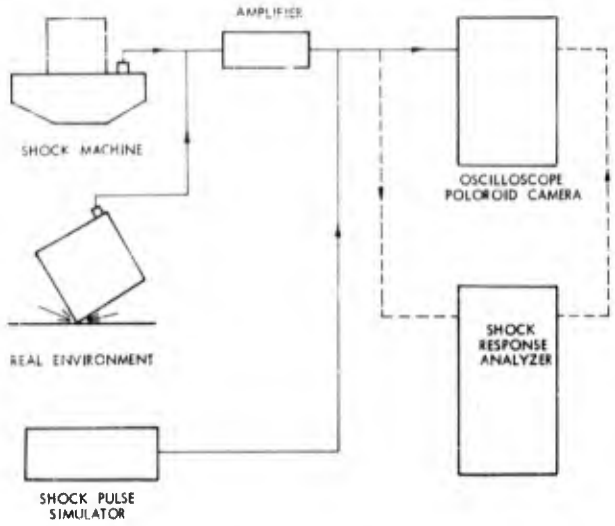

Fig. 2 - Shock-test instrumentation

The Mechanical System

Figure 5(a) shows the symbolic mechanical system where,

M_1 = mass of the equipment being tested,

M_2 = mass of the test equipment table,

k = spring constant of the linkage between M_1 and M_2, pounds per inch,

$F(t)$ = the input shock pulse, inches per second per second,

Let $x_1 = aX_1$

then

$$\frac{dx_1}{dt} = a\frac{dX_1}{dt} = a\frac{dX_1}{dt}\frac{dT}{dT} = a\omega_n \, dX_1$$

$$\frac{d^2x_1}{dt^2} = \frac{d\left(a\omega_n \frac{dX_1}{dT}\right)}{dT}\frac{dT}{dt} = a\omega_n^2 \frac{d^2X_1}{dT^2}$$

let

$$x_2 = aX_2$$

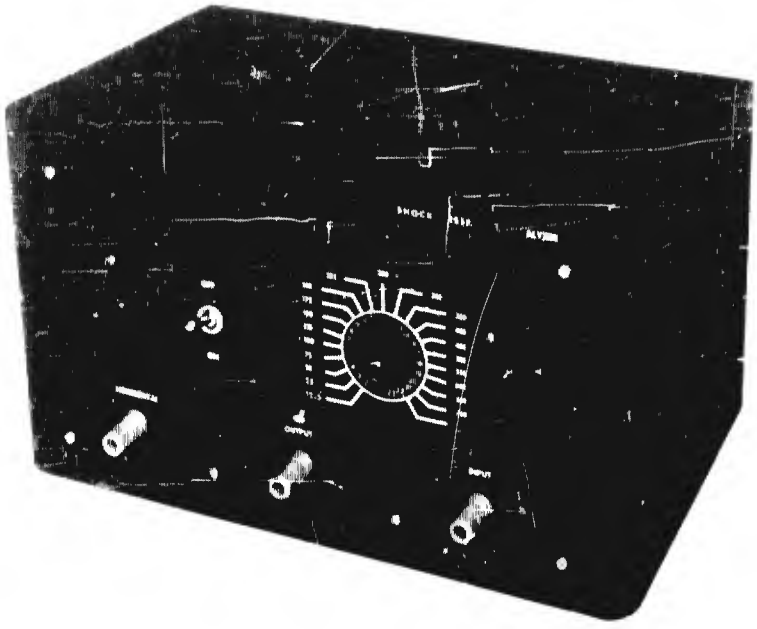

Fig. 3 - The shock-response analyzer

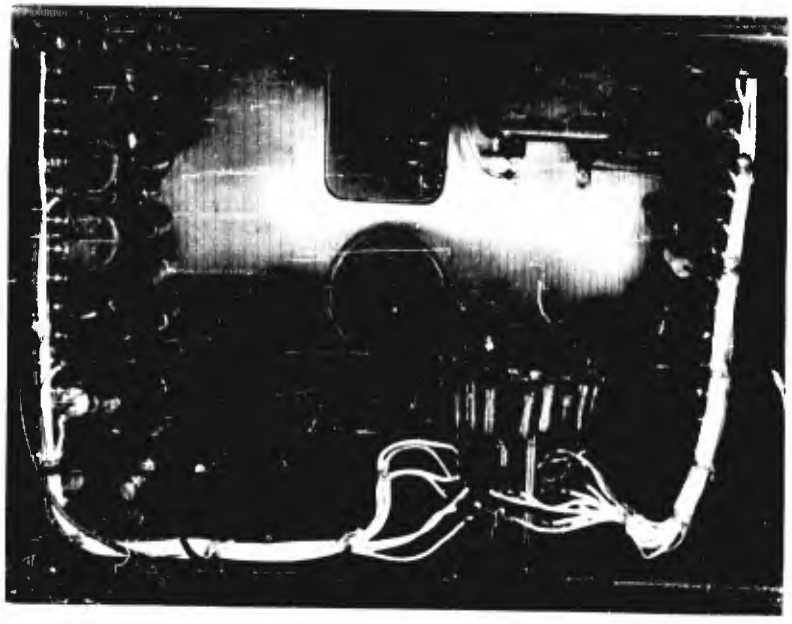

Fig. 4 - Electrical components of the shock-response analyzer

then

$$\frac{dx_2}{dt} = a\frac{dX_2}{dt} = a\frac{dX_2}{dt}\frac{dT}{dt} = a\omega_n\frac{dX_2}{dT}$$

$$\frac{d^2x_2}{dt^2} = \frac{d\left(a\omega_n\frac{dX_2}{dT}\right)}{dT}\left(\frac{dT}{dt}\right) = a\omega_n^2\frac{d^2X_2}{dT^2}.$$

Let

$$T = \omega_n t$$

then

$$\frac{dT}{dt} = \omega_n.$$

Define

$$\omega_n = \sqrt{\frac{k}{M_1}}$$

a = Constant.

From Eq. (1) and the above substitutions, we have

$$M_1 a\omega_n^2\frac{d^2X_1}{dT^2} + ka(X_1 - X_2) = 0. \qquad (3)$$

From Eq. (2),

$$M_2 a\omega_n^2\frac{d^2X_2}{dT^2} - ka(X_1 - X_2) = F\frac{T}{\omega_n} \qquad (4)$$

Eqs. (3) and (4) become,

$$\frac{d^2X_1}{dT^2} + (X_1 - X_2) = 0 \qquad (5)$$

$$\frac{d^2X_2}{dT^2} - \frac{M_1}{M_2}(X_1 - X_2) = \frac{M_1 F\left(\frac{T}{\omega_n}\right)}{M_2 ak}. \qquad (6)$$

The Analogous Electrical System

The electrical circuit which is equivalent to the mechanical system shown in Fig. 5(a) is given in Fig. 5(b) where,

L_1 = inductance, henries

C = capacitance, farads

L_2 = inductance, henries

e(t) = input pulse in volts.

If we neglect the resistance, then the system of differential equations which describe the electrical system are as follows:

$$L_1\frac{d^2q_1}{dt^2} + \frac{(q_1 - q_2)}{C} = 0. \qquad (7)$$

$$L_2\frac{d^2q_2}{dt^2} - \frac{(q_1 - q_2)}{C} = e(t) \qquad (8)$$

Eqs. (7) and (8) can be put into dimensionless form by making the substitutions below:

Let

$$q_1 = \alpha Q_1,$$

then

$$\frac{dq_1}{dt} = \frac{d(\alpha Q_1)}{d\phi}\frac{d\phi}{dt} = \alpha\omega_e\frac{dQ_1}{d\phi}$$

and

$$\frac{d^2q_1}{dt^2} = \frac{d\left(\alpha\omega_e\frac{dQ_1}{d\phi}\right)}{d\phi}\frac{d\phi}{dt} = \alpha\omega_e^2\frac{d^2Q_1}{d\phi^2}.$$

Let

$$q_2 = \alpha Q_2,$$

then

$$\frac{dq_2}{dt} = \frac{d(\alpha Q_2)}{d\phi}\frac{d\phi}{dt} = \alpha\omega_e\frac{dQ_2}{d\phi}$$

and

$$\frac{d^2q_2}{dt^2} = \frac{d\left(\alpha\omega_e\frac{dQ_2}{d\phi}\right)}{d\phi}\frac{d\phi}{dt} = \alpha\omega_e^2\frac{d^2Q_2}{dt^2}.$$

Let

$$\omega_e t = \phi,$$

then

$$\frac{d\phi}{dt} = \omega_e.$$

Define

$$\omega_e = \frac{1}{\sqrt{L_1 C}}$$

α = Constant.

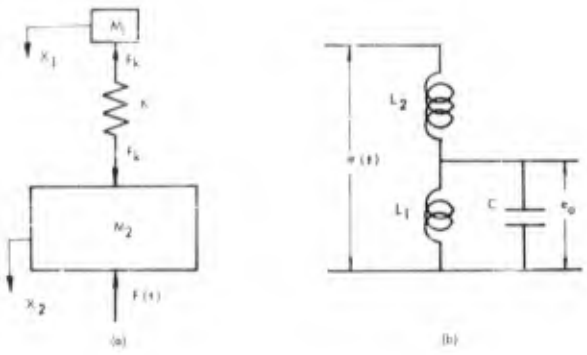

Fig. 5 - Analogous vibratory systems: (a), mechanical and (b), electrical

Eqs. (7) and (8) become,

$$L_1 \alpha \omega_e^2 \frac{d^2 Q_1}{d\phi^2} + \frac{\alpha}{C}(Q_1 - Q_2) = 0. \qquad (9)$$

$$L_2 \alpha \omega_e^2 \frac{d^2 Q_2}{d\phi^2} - \frac{\alpha}{C}(Q_1 - Q_2) = e\left(\frac{\phi}{\omega_e}\right). \qquad (10)$$

Also,

$$\frac{d^2 Q_1}{d\phi^2} + (Q_1 - Q_2) = 0 . \qquad (11)$$

$$\frac{d^2 Q_2}{d\phi^2} - \frac{L_1}{L_2}(Q_1 - Q_2) = \frac{e\left(\frac{\phi}{\omega_e}\right)}{L_2 \alpha \omega_e^2} . \qquad (12)$$

By comparing the mechanical and electrical systems of differential equations, we find the following relations:

$$\frac{L_1}{L_2} = \frac{m_1}{m_2} \qquad (13)$$

$$X_1 = Q_1 \qquad (14)$$

$$X_2 = Q_2 \qquad (15)$$

$$\frac{T}{\omega_n} = \frac{\phi}{\omega_e} \text{ or } \frac{T}{\phi} = \frac{\omega_n}{\omega_e} \qquad (16)$$

$$\frac{T^2}{\omega_n^2} = L_1 C \phi^2 \text{ or } C = \frac{1}{\omega_n^2 L_1} \frac{T^2}{\phi} \qquad (16a)$$

The Analyzer Circuit

Figure 6 shows the circuit diagram of the shock-response analyzer. The complete circuit is essentially an extension of the electrical analogy (Fig. 5), and it comprises 20 tuned L-C circuits, each using the same inductances. It should be noted that L_1 has 20 times the inductance of L_2. The resistance circuit, with its switch coupled to the L-C circuit switch, functions as a voltage divider for locating the position of the response signal on the horizontal axis of an oscilloscope.

Tape Speed Up

The response of circuits with natural frequencies as low as 10 cps was desired. It is extremely difficult, to devise a practical electrical circuit with a resonant frequency much less than 100 cps. This problem was solved by recording the shock on a tape loop and playing the loop back at eight times the recording speed. In this manner, it was possible to use circuits with resonant frequencies from 12.5 to 100 cps.

Damping

In the electrical circuit, as in any real mechanical spring-mass system, there is a certain amount of resistance or damping. The mechanical system called out in the test specification is theoretical, however, with

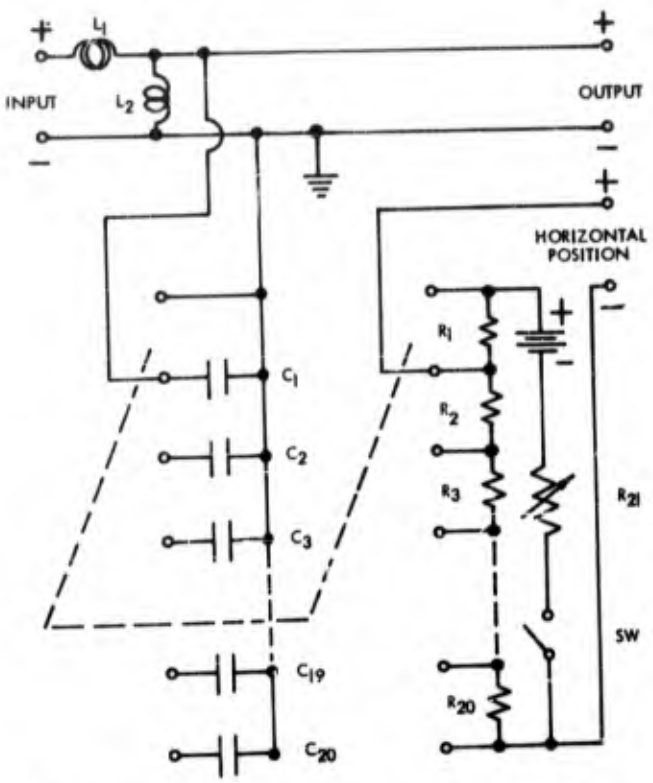

Fig. 6 - Circuit diagram for the shock-response analyzer

no damping. For accurate test results, it is therefore desirable to keep the resistance in the electrical circuit as low as possible. A problem faced in the use of an L-C circuit, is that the coils necessary to produce inductance also create resistance. This resistance is not of sufficient magnitude; however, to have a significant effect on the response of the system to transient signals of short duration. Maximum magnification at resonance of the 20 circuits is shown in the envelope (Fig. 7). Response curves for the 100-, 300-, and 500-cps analyzer circuits (actually 800, 2400, and 400 cps) are shown in detail. The result of the circuit resistance is shown later in the actual test results.

It should be noted that the maximum response envelope is not flat throughout the frequency range. The drop in magnification at lower frequencies is due to the larger parallel capacitances required. The proportionally greater effect of series capacitance in the inductive circuit is responsible for the slight drop at natural frequencies above 3000 cps.

Operation

An analysis of a typical shock pulse would be the best way to demonstrate the operation of the analyzer. The response to a half-sine shock will be used as an example. This shock pulse is selected as it has been the basis for a large percentage of shock-test specifications, and because it is by far the easiest shape to produce, requiring only an elastic impact between two masses. Figure 8 shows the shock pulse, its spectrum, and the response of each of the 20 tuned circuits to the shock. The response spectrum is the result of placing each of the response signals in its respective position according to frequency, with the time base extending into the Z axis, or perpendicular to the plane of the picture.

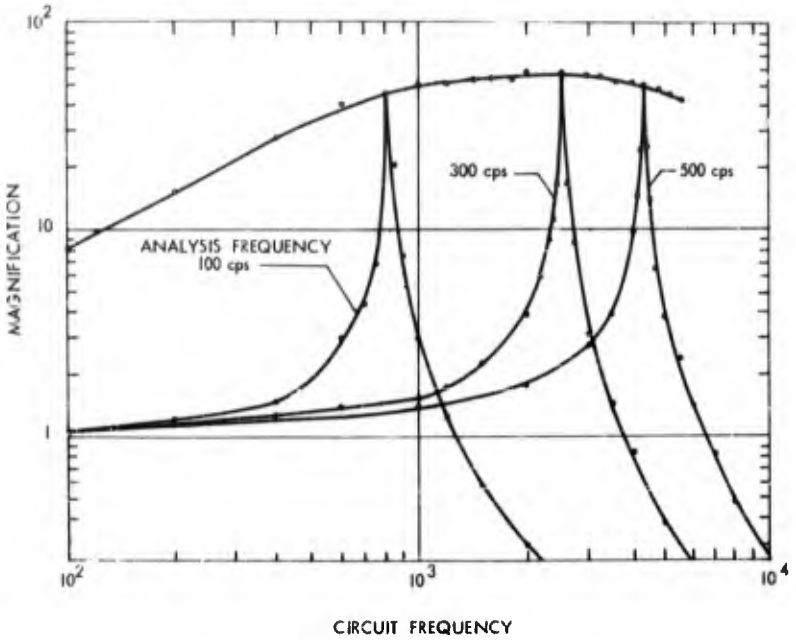

Fig. 7 - Magnification curves for the individual circuits.

$\left(\text{Note: Magnification} = \frac{e_{out}}{e_{in}} \times \frac{L_1}{L_2}.\right)$

Looking now at the response of the individual circuits, the lower frequencies – because of a large mass and/or low spring rate – have only started to accelerate before the transient forcing function is passed. As a result, systems with natural frequencies in this range will not experience an acceleration as high as the level of the shock. Even low acceleration, however, can result in high relative amplitude at low frequencies.

Systems with natural frequencies in the middle range experience what might be called "psuedo-resonance." Response accelerations are considerably higher than the maximum acceleration of the shock pulse and continue at this level until diminished by the damping in the system. This effect can be seen with varying degree in frequencies through 200 cps.

The response of each of the higher natural frequencies can be generally described as a modulated shock pulse. Variation from the shock input acceleration becomes less as the natural frequency of the system increases. The response would be undistinguishable from the input signal if the frequency were sufficiently high.

TEST RESULTS

Spectral analyses have been performed on both laboratory-produced shocks and on actual field data. Several examples of this work follow.

Sawtooth Pulse

Figure 9(a) shows the response of the system to a sawtooth pulse. This type of pulse has formed the basis for the great majority of recent "shock-spectrum" test specifications. The reason is apparent when it is noted that the response accelerations in both positive and negative directions are of high magnitude, even at higher frequencies. It has been proven mathematically that the

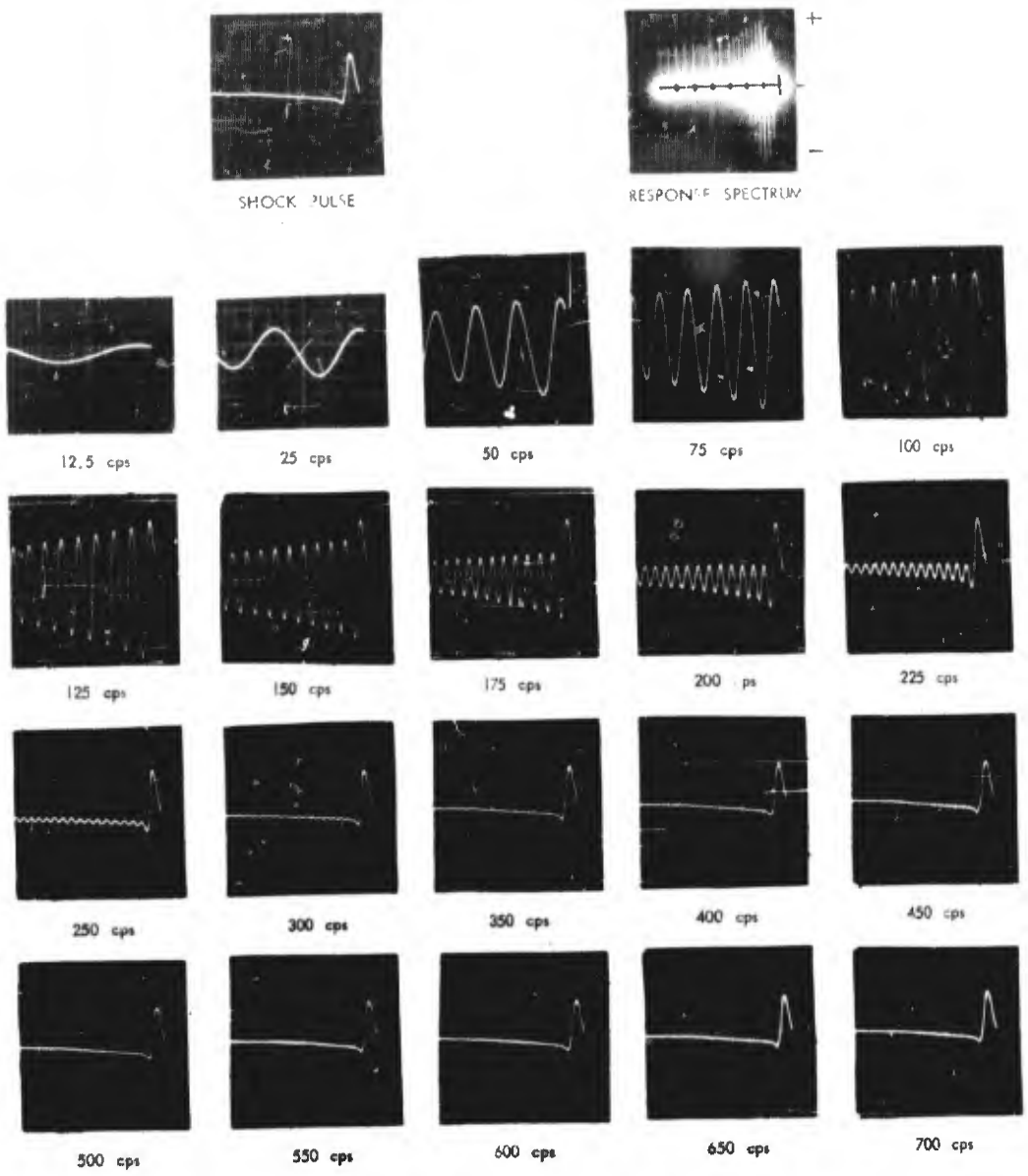

SCALE:	Shock Pulse and Circuit Response	Response Spectrum
Vertical	0.5 Volts / Div.	0.5 Volts / Div.
Horizontal	8 Millisec. / Div.	100 cps / Div.

Fig. 8 - Response of the 20 resonant circuits in the analyzer to a half-sine pulse

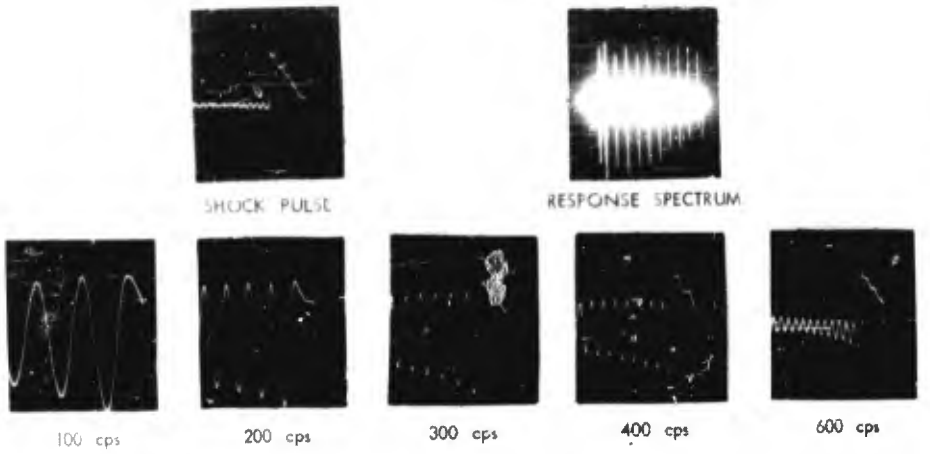

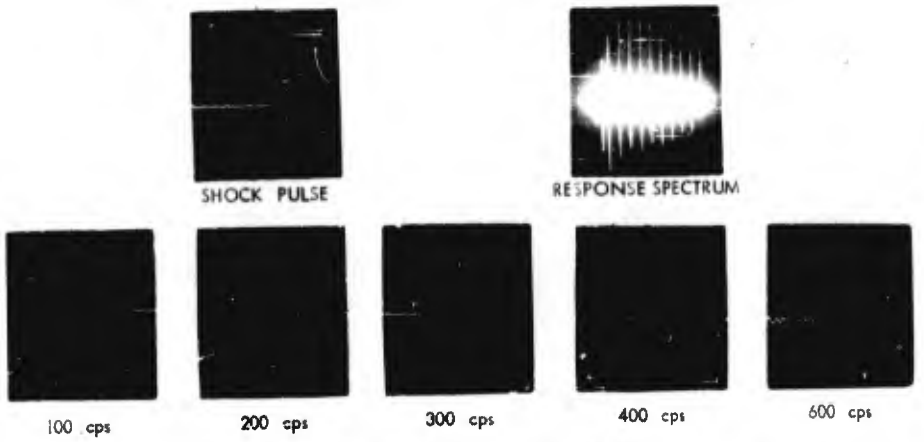

		Vertical	Horizontal
SCALE :	•Response spectrum	0.4 Volts / Div.	100 cps / Div.
	Shock pulse and response	0.4 Volts / Div.	4 Millisec. / Div.

Fig. 9 - Response of the analyzer to sudden acceleration: (a), the response to a sawtooth shock and (b), the response to a reverse sawtooth

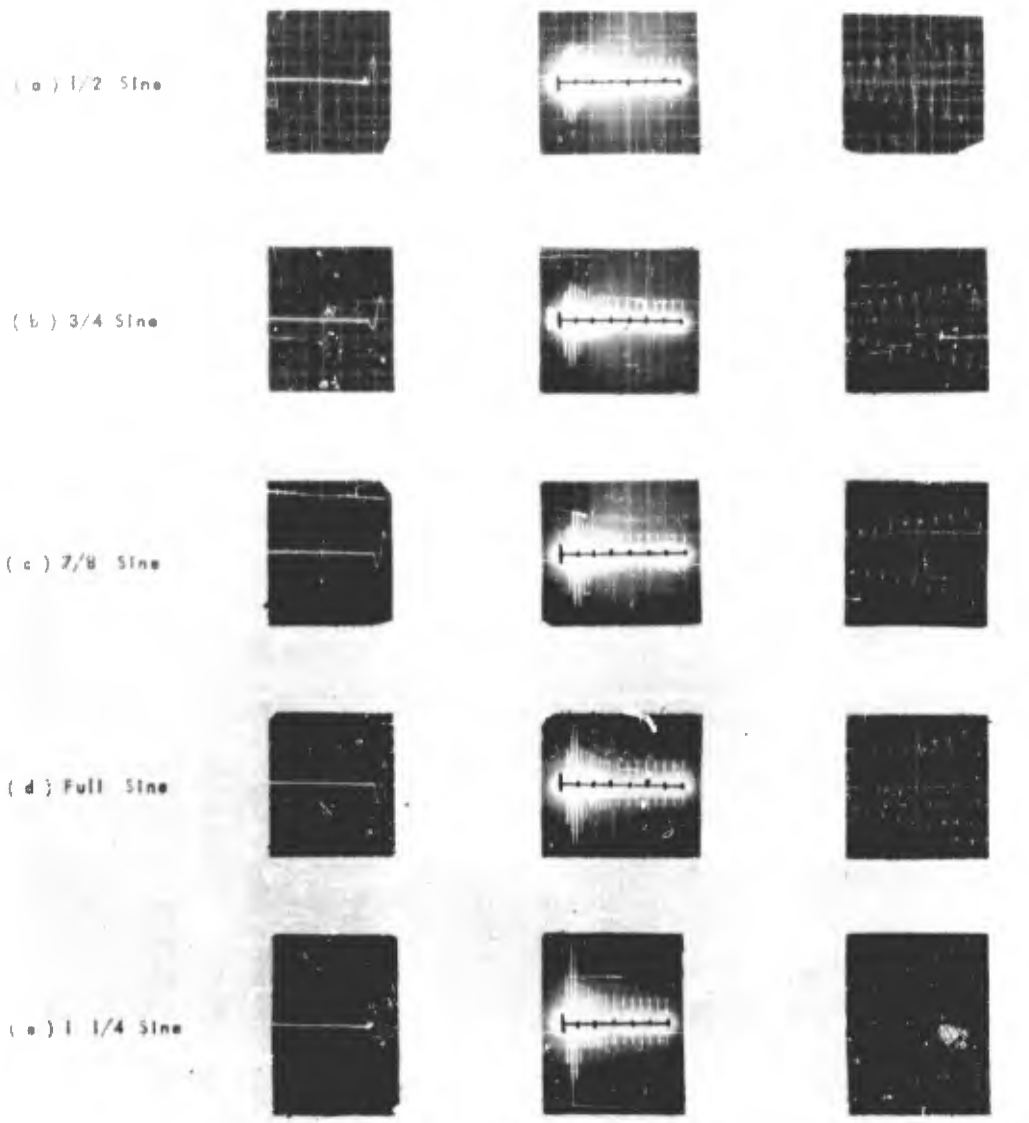

Fig. 10 - The response of the analyzer to various portions of a sine wave

negative response is equal to at least the maximum input acceleration to infinitely high frequencies, provided the input pulse drops from maximum to zero acceleration in zero time. This fact is shown to some extent in the responses to the sawtooth pulse at various frequencies (Fig. 9). Unfortunately, it was impossible to produce a "fall-time" of short enough duration with available equipment.

Reverse Sawtooth

An interesting comparison can be made between the response to the "sawtooth" shock pulse previously shown and the response to the "reverse-sawtooth" pulse shown in Fig. 9(b). It might be assumed that simply reversing the shock pattern would have little effect on the spectrum. This, however, is not the case, as can be seen. The primary difference occurs at the higher frequencies where the short "rise-time" induces a response approximately twice the maximum acceleration of the shock pulse. Again, as before, an infinitely short rise-time result in a flat response spectrum to infinite frequency.

Sine-Wave Response

The response to a half-sine pulse has previously been demonstrated. This shock pulse, its spectrum, and the response at 75 cps are repeated in Fig. 10(a). The results of continuing the shock pulse beyond this half-sine are shown in Fig. 10(b) through 10 (e). As expected, the "pseudo-resonance" at 75 cps to the half-sine pulse approaches a true resonant condition as the sine wave is continued. The maximum response acceleration of the resonant system can be several times the maximum acceleration of the shock pulse under these conditions.

The significance of this effect is demonstrated in Fig. 11. The shock traces in Fig. 11(a) and (b) represent the shocks experienced by large and small electronic packages, respectively, in pivot drop tests. Both shocks, while essentially half-sine in concept, are modulated by several continuous sine-wave pulses. The result of these small sine-waves can be seen in the response spectrums, where theoretical response accelerations at certain frequencies are shown to be at least 5 to 10 times the maximum acceleration of the shock pulse.

A similar response is obtained in the laboratory with shock machines having table resonances less than the maximum frequency of the required shock spectrum.

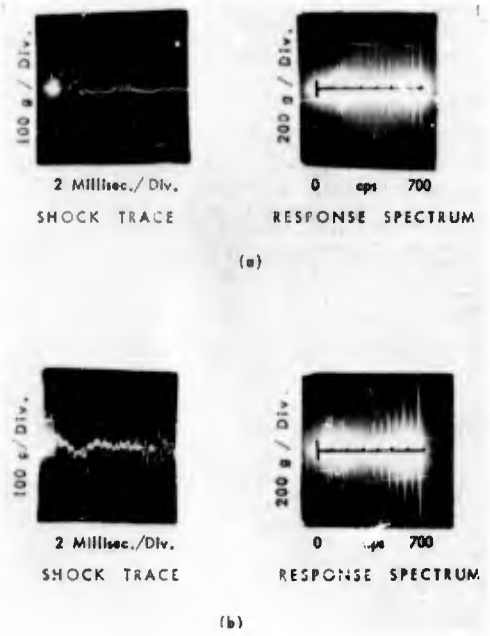

Fig. 11 - The response of the analyzer to shocks resulting from field environment: (a), a pivot drop of a solid, simple structure and (b), the pivot drop of a complex structure

DISCUSSION

It is not intended in this paper to present arguments on the merits or disadvantages of the spectral method of shock measurement. A brief discussion of one important consideration is in order, however.

Figure 12 (a) shows a spectrum from a typical shock-test specification, requiring a level acceleration response from 100 to 700 cps both in the positive (primary) and negative (residual) spectrum. This response must be obtained in three mutually perpendicular axes. From the high-frequency response to the sawtooth shock (Fig. 12 (b)), it is apparent that this type of pulse produces positive and negative response spectra within the required tolerances. As a result, testing is required only in one direction of each axis of the test specimen.

There is a second approved method, however, for meeting the shock-test specifications. The specimen may be tested in each direction of each of three mutually-perpendicular axes. In this case only the primary spectrum must fall within the specified tolerances. Any one of a variety of pulse shapes are than able to produce the desired response.

A comparison of these alternate methods, however, discloses a great difference in damaging potential. The two opposite half-sine shocks (Fig. 12 (c)) are typical of the type of shock pulse used when only one-half of the spectrum requirement need be met at one time. Comparing the response to these "half-sine" shocks with the response to the "sawtooth" pulse reveals a considerable difference in damaging potential at this frequency. The sawtooth shock produces a continuous high-level vibratory response, diminished only by the damping in the resonant system. The use of opposed half-sine shock pulses produces only a single transient half-sine response of this magnitude in each direction.

There is, then, an apparent limitation to the spectral type of shock specification. Even though the peak acceleration each resonant system experiences is specified,

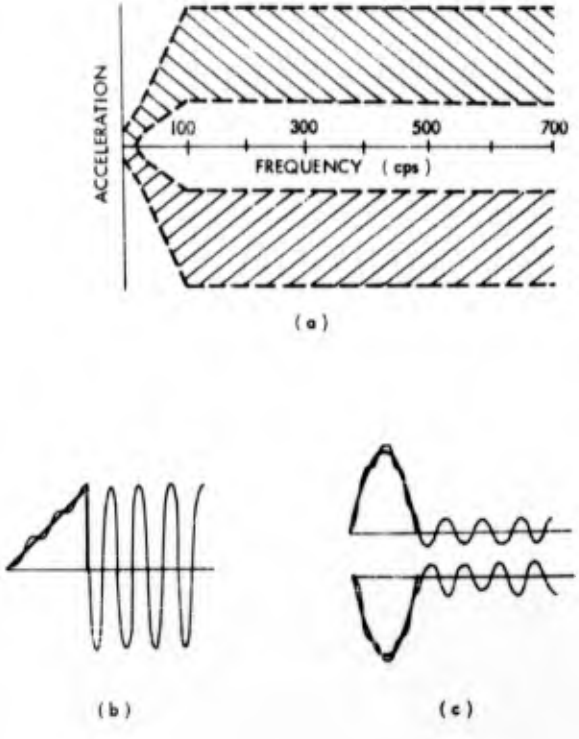

Fig. 12 - Two methods of meeting a spectral shock-test specification ((a), the specification envelope; (b), a single sawtooth shock response; and (c), opposed half-sine shock responses)

no consideration is given to the number of times this acceleration is reached. This becomes of even greater significance when multidegree-of-freedom systems are subjected to the shock, where the vibrating mass of the response system becomes a forcing function for a smaller component.

CONCLUSION

It is apparent that the problems associated with testing to shock-spectrum specifications are not derived from a failure in basic theory, but due to unfamiliarity with the concept. The discrepancy listed previously is a result of this. Engineers, particularly at the test level, still think in terms of the shock rather than the response.

This unfamiliarity results from there being no simple means to demonstrate the acceleration response to a shock pulse. Many shock-testing laboratories have no equipment for spectral analysis. The analyzer, described in this paper and presently in use at Boeing, is a simple low-cost solution to the problem. It represents no new engineering concepts, but only a new application of well-proven principles. This analyzer has made it possible for Boeing engineers to study the response spectrums resulting from a multitude of shock environments. It is likely that equipment developed on the same principles can be as useful elsewhere.

DISCUSSION

Mr. Forkois (U. S. Naval Research Laboratory): I was particularly pleased to see that you showed a positive sawtooth and a negative sawtooth and indicated that the spectra results were different. Last night when we discussed this problem, there was a general feeling on the part of some people that (for a given spectrum) there would be possibly very many shock motions which give you this spectrum. I'm of the opinion that any shock spectrum is a discrete function of a particular shock motion. Would you care to comment on this?

Mr. Barnes: Yes, I'd like to mention one thing. I think a lot of people feel that this particular sawtooth pulse is an answer, and I think it is if we could produce it. It is getting a very rapid fall time that gives you this residual spectrum of high magnitude and high frequency. I agree with the fact that each of a variety of shocks would probably have a different spectrum. This is particularly true if your spectrum is modulated by a sine wave as you would have with a resonant shock table, etc. But there is, I would say, a correlation. These all can meet certain specifications. I can show you a very large number of shock pulses that would all be close enough so that they would probably fall in the same envelope as that required by the test specifications. I think this is one of the advantages of the shock-spectra method. It allows you to use a number of different shocks and still meet your specifications.

Dr. Belsheim (U. S. Naval Research Laboratory): I would like to clarify the positive, negative, and residual shock spectrum. There are really three kinds of shock spectra: the positive, which represents the maximum positive peak; the nagative, the maximum negative peak; and the residual, which is of course the peak after the transient has passed. The residual may be equal to the negative shock spectrum, if the duration of the shock is short compared to the frequency of the responding system. I think this is something worth pointing out. I think also it is worth noting that one can code for shock-spectrum production from a digital computer by sending in the input, coding the computer for the response of a system, and obtaining from the computer all of the positive, negative, and residual shock spectrum – also the Fourier shock spectrum. This is a very general method, perhaps a little more sophisticated, but I also would want to remark that your analyzer is a very useful tool for the laboratory. This is a nondamped system, I believe. Could you add damping to your system?

Mr. Barnes: Yes, I'd like to comment on these one at a time. Your point is extremely well taken. For continuous shocks, of course, we can't consider a residual until the shock pulse has passed. For a simple one-directional shock, such as I've shown, of course the residual is that part that goes below the line – just because it happens to be that way.

I think I might have been confusing on that point. I'd also like to reiterate what we have said. There are several methods of determining shock spectra. We've tried analyzers. We've tried actually mounting accelerometers directly on some reeds and trying to plot these. The problem, of course, in all of these are time and cost. Now your third point regarding damping. We have damping in our system. It's an uncontrolled amount and it's fairly low. It would be very easy, and we have considered this, to add damping to the system so that we can get a more controlled amount. We would also, of course, like to get a system with no damping. I'm afraid it would be impossible with the type of system that we have.

Dr. Belsheim: I think this is possibly one advantage of the computer coding – that there you can set your degree of damping very readily. We have a coding at our computer for obtaining the response of 100 different frequency systems. We can choose the frequency and the damping and obtain various spectra. So, this perhaps is an advantage of a more sophisticated system.

Mr. Barnes: This is definitely an advantage. Of course, you can actually code these things to get a negative damping if you so desire. You can fool around with this sort of thing, if you want and this definitely affords a great deal more flexibility than we have here.

(NOTE: At this point some of the discussion was missed while changing tapes.)

Mr. Hawkins (Sperry Gyroscope Co): Pursuing the same question area, practically to use any spectra to exactly define the original time function, it must be carried to an infinite number of frequencies; and, practically, we're always limited to a rather finite range of frequencies, so that we cannot say that we're rigorously defining the original function in the way in which we use spectra.

Mr. Barnes: Yes, I think that reiterates what we've mentioned.

Dr. Curtis (Hughes Aircraft Co.): I wonder if the author would care to describe briefly how he managed to get all the readout of all the frequencies on the one photograph, which seems to me a very convenient method.

Mr. Barnes: I think you're referring to Fig. 8 showing the spectrum – the shock and the 20 responses. Actually, what we can do as you may have gathered from this, we can analyze each individual frequency by simply displaying the shock pulse across the x-axis of the oscilliscope. When we make a spectrum, of course, we run the time function into the z-axis and all you see then is the vertical response. This is how we make an actual analysis. But if we do care to look at the response and see what is happening, we can change the oscilloscope onto sweep, and then simply run this same frequency back. I mentioned we could put these things on a tape. loop; of course that is necessary to store a transient function such as this. This tape loop is around 10 feet long and we play it back at 30 in. per sec, so that every 4 seconds, approximately, we get another picture of the shock pulse. You can continue to display this shock or any response of any circuit at your leisure.

* * *

METHODS OF VIBRATION ANALYSIS FOR COMBINED RANDOM AND SINUSOIDAL INPUTS

J. P. Stoll
Autonetics
A Division of North American Aviation, Inc.
Downey, California

Generally, the designer needs to be aware of the probability that a specified level of vibration intensity is not exceeded during a given test. This report discusses two methods of determining this probability. In addition to the theoretical studies, an analog computer simulation of the mechanical system was made.

INTRODUCTION

In present vibration tests on many missile components, a program of combined random- and sinusoidal-vibration testing is required. Heretofore, only sinusoidal vibration has been specified in such tests and the inclusion of random vibration has complicated the problem of predicting the effect of vibration on these components. Nevertheless, analysis methods are required in order to predict such things as whether a given component would fail in a combined vibration environment.

The type of failure investigated, and which is the topic of this paper, was a deflection of some physical part due to vibration exceeding some maximum permissible value. For instance, a gas spin bearing (Fig. 1) has a certain clearance C between the fixed and moving parts. If the the deflection $\delta = C$, the bearing "bottoms," and there is metal-to-metal contact. Such a contact can cause damage to the bearing and may be considered a "failure." It was possible to define a ratio $\beta = \delta/C$ where β is the ratio of rotor deflection to the total clearance C. According to this definition, the bearing has "bottomed" when $\beta = 1$. For $\beta < 1$ transfer functions $\beta/\ddot{x}_1$ have been defined for β per g acceleration input, where $\beta/\ddot{x}_1$ is a function of frequency.

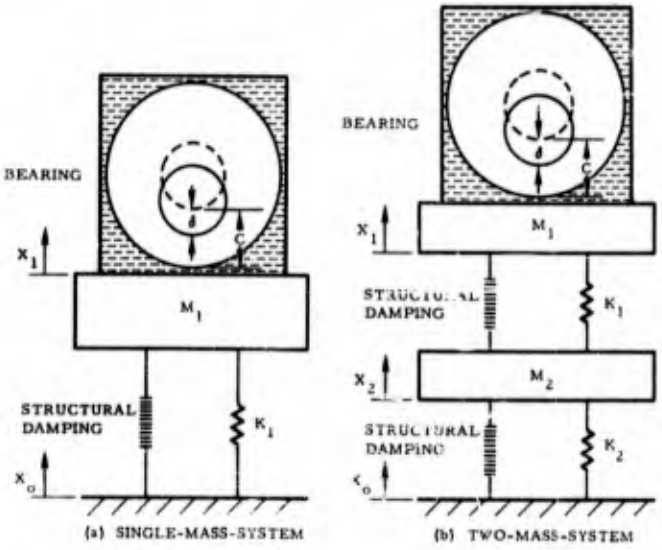

Fig. 1 - Single-mass and two-mass representations of mounting structure and bearing

The investigation was pursued along three lines, each of which will be discussed separately. These methods are: (a) computation of expected peak bearing deflection levels; (b) analog computer simulation of the structure and bearing; (c) theoretical computation of mean number of bottomings per second.

LIST OF SYMBOLS

σ	Standard deviation and rms value of a Gaussian random signal
δ	Deflection of the rotating part of a gas bearing from the equilibrium point with respect to the housing
C	Clearance between the housing and rotating part of a gas bearing
β	Ratio of bearing deflection δ to clearance C
g	Acceleration intensity in multiples of earth's gravity
$\ddot{x}_o$	Input vibrational acceleration, usually measured in g's
$\ddot{x}_1$	Output vibrational acceleration at the bearing
$\ddot{x}^s$	Sinusoidal component of vibrational acceleration
$\ddot{x}^r$	Random component of vibrational acceleration
f	Frequency in cycles per second (cps)
ζ	Damping ratio
$f_1, f_2 \cdots f_n$	Natural or resonant frequencies of supporting structure
τ	Duration of test with random vibration combined with a single sinusoidal frequency
f_A	Lower frequency limit of random-vibration input spectrum
f_B	Frequency above which the sinusoidal- and random-vibration inputs increase to their upper levels
f_C	Cutoff frequency for the sinusoidal and random inputs
f_o	Frequency of the applied sinusoidal vibration component
β_o	A given level of β at which crossings are counted
$\overline{N_{\beta_o}}$	Average number of crossings of β_o per second
σ_β	Total rms value of β
$\sigma_{\dot{\beta}}$	Total rms value of time derivative of β
σ_n	rms component of β due to random vibration input alone
$\sigma_{\dot{n}}$	rms component of $d\beta/dt$ due to random input alone
$p(n,\tau)$	The probability that n bottomings occur in τ seconds
e	Naperian base = 2.718
N_o	$1/\pi(\sigma_{\dot{n}}/\sigma_n)$
Q	Magnitude of sinusoidal component of β measured at the bearing location
$\sqrt{Q^2/2}$	rms value of a sinusoidal process
a	Ratio of Q to the rms of the random component σ_n
y	β_o/σ_n
b	$2\pi f_o Q/\sigma_{\dot{n}}$

$\psi(y)$ The Normal distribution curve for y, given as

$$\psi(y) = \frac{1}{\sqrt{2\pi}} \exp\left\{\frac{y^2}{2}\right\}$$

${}_1F_1\left(-\frac{1}{2}; n+1; -b^2/2\right)$ Confluent hypergeometric function, involving the variables 1/2, n + 1, and $b^2/2$

$\Phi_{nn}(f)$ Power spectral density function of random-vibration input

$k_{s(t)}$ The kth member of an ensemble of sine waves, comprising a sinusoidal process

$|G(f)|$ Magnitude of G(f), the transfer function between the vibration input and β

T Time to take the output to cross a width $d\beta$

m Ratio of the rms of the sine process $\sqrt{Q^2/2}$ to the rms of the noise σ_n

ϵ A measure of the ratio of sine process to that of equivalent fixed sinusoid. $\epsilon\sqrt{1 + m^2}/\sqrt{1 + a^2/2}$

S La place operator

A rms sinusoidal input multiplied by the constant gains of the bearing-support combination

B^2 Acceleration-squared spectral density multiplied by the square of the constant gains of the bearing-support combination

ϕ Phase angle

θ Angle of integration

n An integer, 0, 1, 2, ...

$\Gamma_{(n)}$ Gamma function of n defined as $\Gamma(n) = \int_0^\infty e^{-x} x^{n-1} dx$ for $n > 0$.

COMPUTATION OF EXPECTED PEAK BEARING DEFLECTION

A method which has been often used to treat combined sinusoidal and random vibration is that of computing the peak deflection β for the sinusoidal- and random-vibration inputs separately and adding them together. Since a random signal actually has no definite peak value, it was assumed that the peaks were no greater than 3 times the rms value (the 3σ value). Actually, the random signal has no peak as such but the probability of exceeding 3σ is only 0.26 percent. A block diagram which shows how the random and sinusoidal components of the bearing deflection combine is presented as Fig. 2.

Two forms of transmissibility of the supporting member were considered. The first, a second-order transfer function for a single mass (Eq. (1) and Fig. 1(a)), is a good approximation of the actual transfer function for structural damping, if ζ is sufficiently small. The second form studied was a transmissibility function for a two-mass system (Eq. (2) and Fig. 1(b)).

$$\frac{\ddot{x}_1}{\ddot{x}_0} = \frac{1}{\left(\frac{S}{2\pi f_n}\right)^2 + 2\zeta\left(\frac{S}{2\pi f_n}\right) + 1} \qquad (1)$$

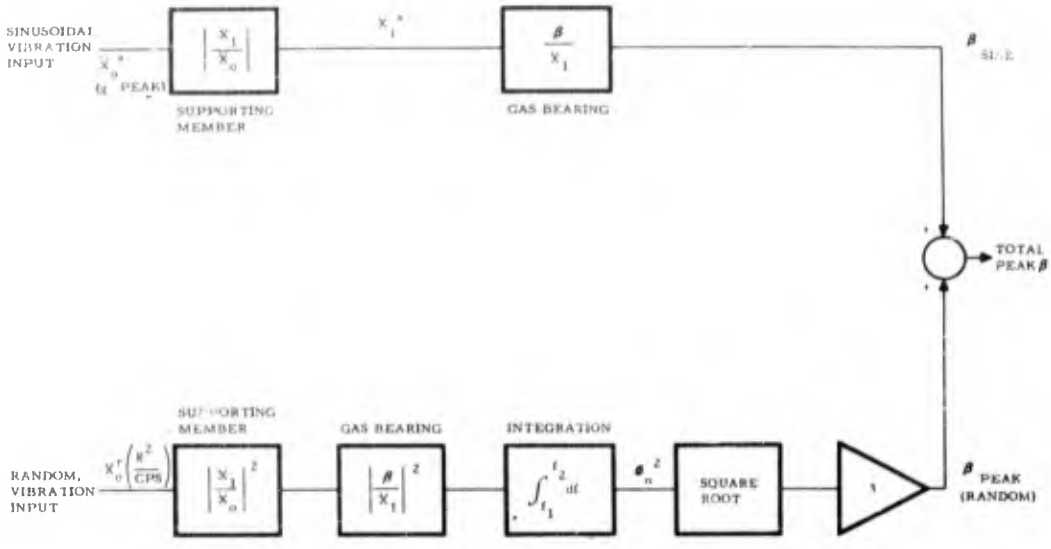

Fig. 2 - Diagram of the manner in which vibration input contribute to bottoming of a bearing

$$\frac{\ddot{x}_1}{\ddot{x}_o} = \frac{\left(\frac{S}{2\pi f_3}\right)^2 + 2\zeta_3\left(\frac{S}{2\pi f_3}\right) + 1}{\left[\left(\frac{S}{2\pi f_1}\right)^2 + 2\zeta_1\left(\frac{S}{2\pi f_1}\right) + 1\right]\left[\left(\frac{S}{2\pi f_2}\right)^2 + 2\zeta_2\left(\frac{S}{2\pi f_2}\right) + 1\right]}. \qquad (2)$$

$$S = j2\pi f$$

The computations indicated in Fig. 2 can be carried out either manually or with the aid of a digital computer for different kinds of transfer functions $\ddot{x}_1/\ddot{x}_o$ and $\beta/\ddot{x}_1$.

Since there is a finite probability that the random signal will at time exceed the 3σ value, it was attempted to find a more realistic method of determining the incidence of bottoming. Next, it seemed feasible to employ analog methods of study.

ANALOG SIMULATION OF BEARING AND SUPPORTING STRUCTURE

As a first attempt in the simulation of a combination of a gas bearing and its support, a crude electrical analog circuit using passive circuit elements, as shown in Fig. 3, was constructed. A random-noise generator and a sine-wave generator were connected in series and, after amplification, the combined output was fed into the network. The output of the network was viewed on an oscilloscope, and the number of crossings of an appropriate output level representing $\beta = 1$ was counted by the operator. Although some useful results were obtained from these tests, it was believed that it would be better to have some more sophisticated investigation carried out with the aid of an analog computer. The computer made it possible to make many experimental runs by using several different sets of parameters for the

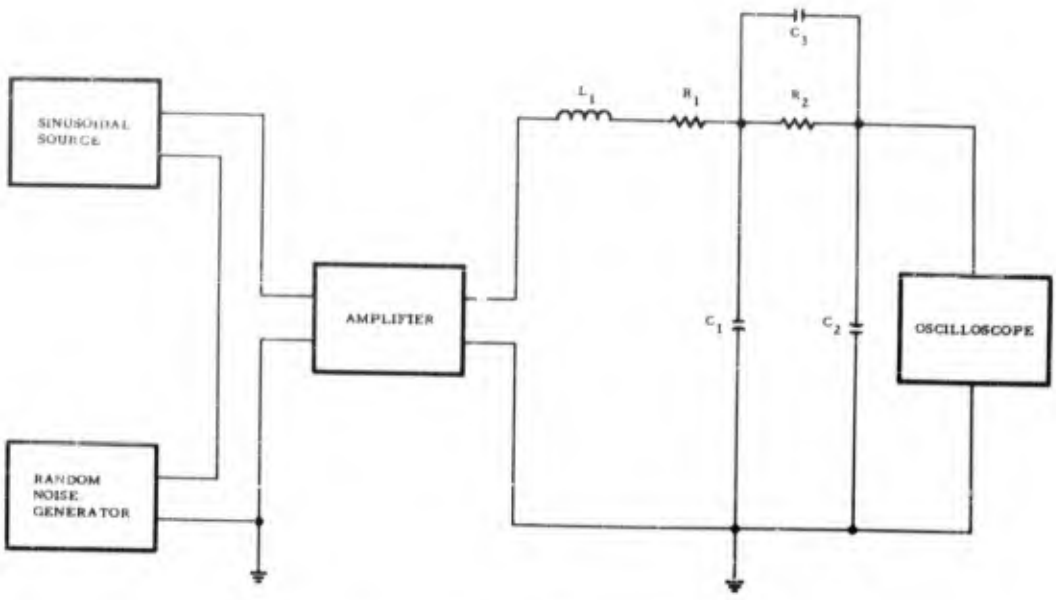

Fig. 3 - Typical circuit diagram for simplified analog study of bearing bottoming

structure and bearing and, therefore, improving the scheme by which bottomings were counted. It was also thought possible to simulate the actual input more exactly. The computer results thus obtained agreed in general with the method using the passive network, thereby demonstrating the validity of that method.

INPUTS

A combination of inputs for a typical vibration test is shown in Fig. 4. The shapes shown allow for the fact that the vibration intensity in the physical system was expected to be larger at higher frequencies. In the proposed shake test these additional restrictions were imposed on the inputs:

1. In addition to the separate low-frequency attenuation of the sinusoidal displacement amplitude, a 3σ-limit was also imposed on the random input.

2. After the inputs were added, hardware limitations caused the peaks of the total acceleration to be clipped at two or three times its total root-mean-square (rms) value and imposed a fixed displacement limit on the total vibration input to the equalized shaker.

These additional criteria had to be mechanized on the analog computer; however, some difficulties were encountered. These are enumerated below:

1. The three times rms acceleration limit was imposed on the random input but not on the combined inputs, because of difficulty in mechanizing the latter. However, on calculation of the rms random input, it was found that it is much greater than the rms of the sinusoidal input in the cases cited here. Hence, this change should not materially affect the over-all results.

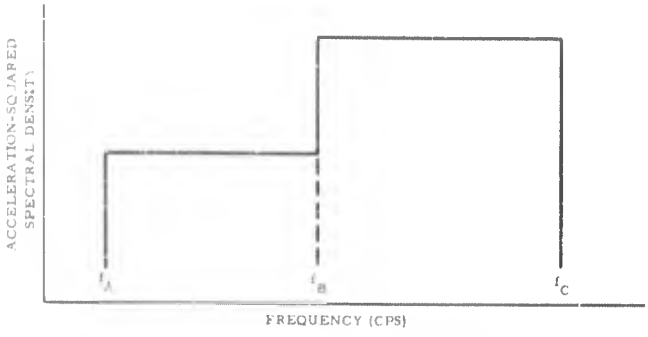

RANDOM INPUT: ACCELERATION - SQUARED SPECTRAL DENSITY

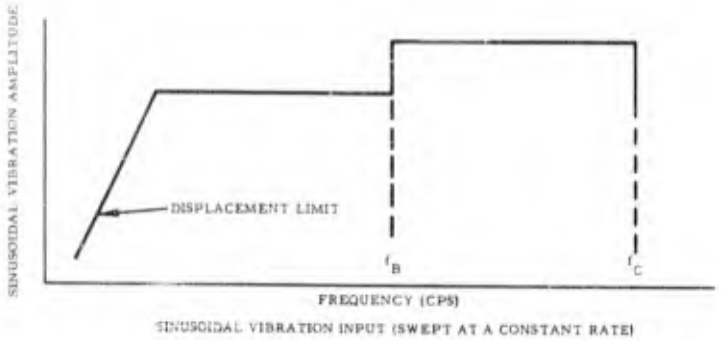

SINUSOIDAL VIBRATION INPUT (SWEPT AT A CONSTANT RATE)

Fig. 4 - Typical acceleration profiles for combined, random- and sinusoidal-vibration input

2. The displacement limit on the total input to the shaker was not mechanized because it would entail a double integration, followed by a double differentiation in the analog computer. The noise and drift introdouced by these operations made it impossible to obtain usable results. However, even without this limit, bottomings were not noticed at the low frequencies where it would apply, because the transmissibility of the mounting structure is small in that frequency range.

3. The sinusoidal sweep was not carried to the upper frequency limit of the original specification in each case, because the highest frequency which the computer would handle was between f_B and f_C. However, this limitation was not expected to affect the final results, because the filters which were used to simulate the transmissibilities transmit relatively little energy above f_B.

4. The computer run was carried out in two separate parts for each case: the first, comprising the lower random input of the entire bandwidth combined with the lower sinusoid, swept from f_A to the upper frequency limit of the computer; the second, comprising the higher intensity random input across the entire bandwidth combined with the higher level sinusoid, swept from f_B to the computer frequency limit. Again, it is the writer's opinion that these changes did not invalidate the results, because little of the random energy above f_B

contributes to the over-all vibration "seen" by the bearing. In the high-frequency run, the number of recorded bottomings would tend to be slightly high because of the high random input in the range from f_A to f_B.

It is expected that these changes in the inputs for the computer simulation would cause the results to err slightly on the conservative side. The grossest single assumption which has been made is that the transfer functions are linear and that there is no "bounce effect," or absorption of energy, when the bearing bottoms. Therefore, it is possible to believe that the computer results do have some factual basis. Some of the computer results have been listed in Table 1.

THEORETICAL CALCULATION OF THE MEAN NUMBER OF BOTTOMINGS PER SECOND

In the course of this investigation, it was learned that the mean number of bottomings per second could be calculated theoretically if a sufficient number of assumtions were made. A theoretical investigation has been followed along two lines: (1) a method by which a sinusoidal process could be substituted for the sinusoidal-vibration input and (2) a more exact but more difficult method involving the use of a fixed sinusoid plus random input. These theoretical results have been compared with the analog computer data and hopefully will be compared with operational test results at a later date.

The chief assumptions which have been made for these theoretical calculations are: (1) the system is linear; (2) the sinusoidal and random inputs are independent and ergodic; (3) there is no "bounce effect" or absorption of energy due to snubbing of the contacting surfaces of the bearing when the bearing bottoms. It is recognized from journal bearing theory that the function $\beta/\dot{x}_1$ is nonlinear in general; however, it appears reasonable to assume linearity in a small region near bottoming. The third assumption causes the calculated results to be pessimistic, because the displacement of an actual bearing is limited and cannot reach as large values as predicted by the linear theory.

SINUSOIDAL PROCESS PLUS RANDOM NOISE

To find the probability of bottoming during a given test, it is first necessary to determine the expression for the average number of bottomings per second of the bearing. This expression is shown as Eq. (3), and its derivation which follows that of Bendat [1] is given in Appendix A.

$$\overline{N_{\beta_o}} = \frac{1}{\pi}\sqrt{\frac{(\sigma_{\dot{\beta}})^2}{(\sigma_\beta)^2}}\, e^{-\frac{\beta_o^2}{2(\sigma_\beta)^2}} \tag{3}$$

where β_o = the level of β at which crossings are counted (in this case, $\beta_o = 1$). $2\pi f_o$ = the angular frequency of the sinusoidal process in radians per second.

$$(\sigma_{\dot{\beta}})^2 = \frac{1}{2}(2\pi f_o)^2\left(\beta_{\substack{\text{rms}\\ \text{sine}}}\right)^2\Bigg|_{f=f_o} + \int_{f_1}^{f_2}(2\pi f)^2\left|\frac{\beta^2}{\text{cps}}\right|_{\text{random}} df \tag{4}$$

Table 1
Summary of Calculated Results and Computer Findings for Bearing Bottoming Study

	Pertinent normalised parameters involved in computation of bottoming probability								Solution using fixed sinusoid				Solution using sine wave process				
										Probability during test				Probability during test			
Type of gas bearing and supporting structure	$N_o = \frac{\sigma_h}{2\sigma_n}$	$a = \frac{Q}{\sigma_n}$	$b = \frac{2\pi f_o C}{\sigma_h}$	$\gamma = \frac{\beta_o}{\sigma_n}$	$(\gamma - a)$	$F(\gamma - a)$	$\frac{P_1(\gamma)}{F(\gamma - a)\sqrt{a}}$	$(P_2(-\frac{1}{2}, b, \frac{b^2}{2}))$	$\frac{\bar{N}\beta_o}{2}$	of no bottomings	of one bottoming	of more than one bottoming	$\frac{\bar{N}\beta_o}{2}$	of no bottomings	of one bottoming	of more than one bottoming	Computed results number of bottomings and number of runs
Bearing which did not bottom; single-mass support	$\frac{356}{\sigma}$	3.79	3.99	9.85	6.06	7×10^{-10}	5×10^{-10}	0.65	2.31×10^{-8}	> 0.999	< 0.001	~ 0	2.06×10^{-3}	0.90	0.095	0.004	2* 20 runs
Bearing which did not bottom; two-mass support — lower peak (f_1)	$\frac{590}{\sigma}$	2.49	2.18	7.05	4.83	5.4×10^{-7}	3.3×10^{-7}	1.33	5.22×10^{-5}	0.98	~ 0.002	~ 0	4.02×10^{-3}	0.844	0.141	0.015	0
upper peak (f_2)	$\frac{590}{\sigma}$	2.93	5.30	17.2	13.9	1.3×10^{-28}	7.8×10^{-29}	0.80	7.55×10^{-27}				7.9×10^{-20}				4 runs
Bearing which bottomed; single-mass support	$\frac{351}{\sigma}$	4.00	4.25	5.67	1.67	0.03	0.015	0.40	0.47	$\sim 1.4 \times 10^{-11}$	$\sim 10^{-10}$	> 0.999	2.4	10^{-55}	~0.001	> 0.999	> 100 2 runs
Bearing which bottomed; two-mass support	$\frac{591}{\sigma}$	2.15	2.38	3.42	1.29	0.054	0.038	0.77	3.5	$\sim 3 \times 10^{-95}$	$\sim 10^{-90}$	> 0.999	4.5	10^{-180}	< 0.001	> 0.999	> 100 3 runs

*Both bottomings occurred in one run

$$(\sigma_\beta)^2 = \frac{1}{2}\left(\frac{\beta}{\text{sine}}_{\text{rms}}\right)^2\Bigg|_{f=f_o} + \int_{f_1}^{f_2}\left|\frac{\beta^2}{\text{cps}}\right|_{\text{random}} df. \tag{5}$$

In the cases considered here, the frequency of the applied sinusoid is swept at a constant rate across the total frequency range, and it is necessary to break up the frequency range into several increments. The sinusoid is then assumed to dwell at a constant frequency within each increment. However, in most problems involving mechanical resonances it is necessary to consider only those frequency increments lying between the half-power points of each resonant peak. Therefore, for the problems discussed here, the time τ spent in the range between half-power points was computed, and the sinusoid was assumed to dwell at the resonant frequency for that period. Thus, in the transmissibility function of Eq. (1), one peak is involved. For the function of Eq. (2), two peaks and two determinations of τ are required, one for each resonant peak.

The values of

$$\sigma_{\dot{n}}^2 = \int_{f_1}^{f_2}(2\pi f)^2\left|\frac{\beta^2}{\text{cps}}\right| df \text{ and } \sigma_n^2 = \int_{f_1}^{f_2}\left|\frac{\beta^2}{\text{cps}}\right| df$$

can be obtained by manual integration. The integration is made much easier, if it can be assumed that $f_2 = \infty$ and $f_1 = 0$. In mose cases the integral over a finite band of filtered random output is nearly equal to the integral from 0 to ∞. If the over-all transfer function $\beta^2/$cps is supplied in graphical form rather than an analytical function, the integrals can be obtained graphically. Thus, experimental data can be used directly without the necessity of a curve-fitting process as required for the analog computer solution. In the problems worked here the integrations were performed graphically, and a typical curve representing $\beta^2/$cps and $(2\pi f)^2|\beta^2/\text{cps}|$ per input $g^2/$cps are shown in Fig. 5. Values for $\sigma_{\dot{n}}$, σ_n and other parameters involved in the bottoming study are presented in Table 1.

When the value of $\overline{N_{\beta_o}}$ is determined it is divided by 2, because there are 2 crossings of $\beta_o = 1$ per bottoming. The probability $p(n,\tau)$ can then be determined, where $p(n,\tau)$ is the probability that there are n bottomings in τ sec. Because it has been assumed that the inputs are normally distributed random functions and because the system is assumed to be linear, the total output should be a normally distributed random function. Therefore, $p(n,\tau)$ follows a Poisson distribution and is given by

$$p(n,\tau) = \frac{\left(\frac{1}{2}\overline{N_{\beta_o}}\tau\right)^n}{n!}\, e^{\frac{-\overline{N_{\beta_o}}\tau}{2}} \tag{6}$$

and $p(0,\tau)$, the probability that there are zero bottomings in τ seconds is given by

$$p(0,\tau) = e^{\frac{-\overline{N_{\beta_o}}\tau}{2}}. \tag{7}$$

The results compare favorably with the analog computer results–that is, the cases yielding a very low probability $p(0,\tau)$ of no bottomings in a given interval corresponded with the cases

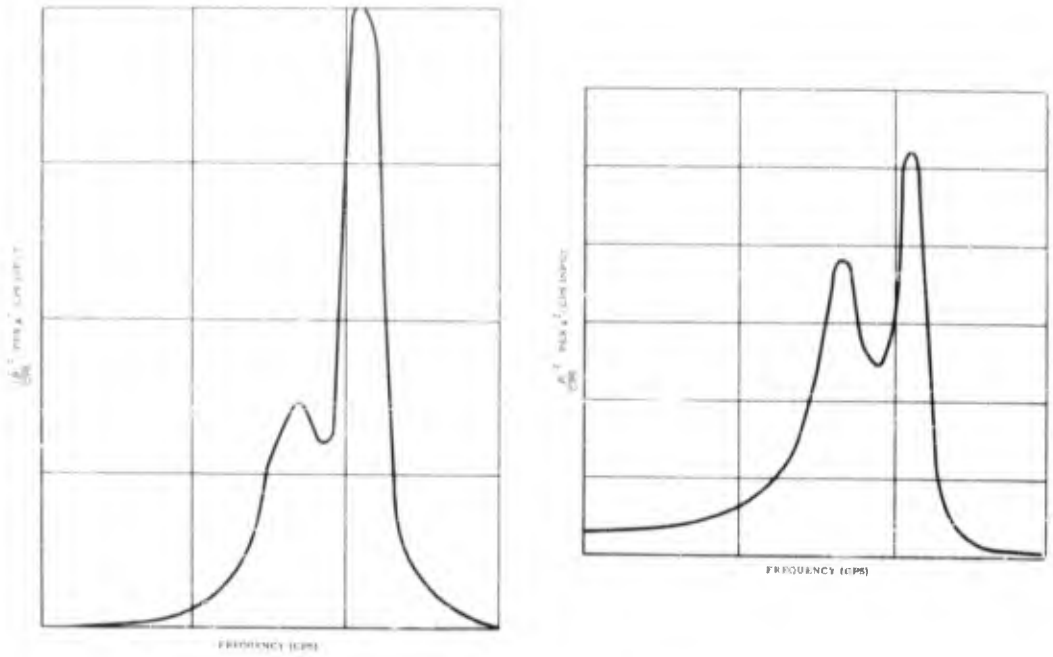

Fig. 5 - Typical curves for β^2/cps and $(\dot{\beta})^2$/cps spectral densities per g^2/cps random input, including transmissibilities of bearing and support

yielding a high number of bottomings in the computer simulation. Conversely, those cases which showed a high probability of no bottomings $p(0,\tau) \geq 0.9$ corresponded with the computer runs giving very few or no bottomings. These results are also presented in Table 1.

The results giving the average number $\overline{N_{\beta_o}}$ of crossings per second of $\beta_o = 1$ are accurate only if the magnitude of the sinusoidal component of β is not much larger than the rms of the random component. From a comparison of the total probability densities of β with random + sine-wave process input and random + fixed sinusoidal input (Appendix A and Fig. 6), it is possible to draw the following conclusions:

1. For a (the ratio of Q, the fixed sine amplitude to σ_n, the rms of the random noise), equal to 1 or less, a sine-wave process of the same rms can be substituted for the fixed sinusoid.

2. For a about 3, a sine-wave process with rms of $1/\sqrt{2}$ that of the fixed sinusoid must be substituted for the applied fixed sinusoid. As shown in Fig. 6, the probability densities are not very similar, yet it was possible to get good agreement with computer results by using this method. If a is much greater than 3, the probability density curves are so different in shape that the substitution of a sine-wave process for purposes of analysis does not appear practical. This situation is discussed in the next paragraph and also in Appendix B.

FIXED SINUSOID PLUS RANDOM VIBRATION

The substitution of a sinusoidal process for the input sine wave in a combined vibration input gives useful results, if the sinusoidal component is not large compared to the random component. However, as in some of the cases studied here, the sinusoidal component is

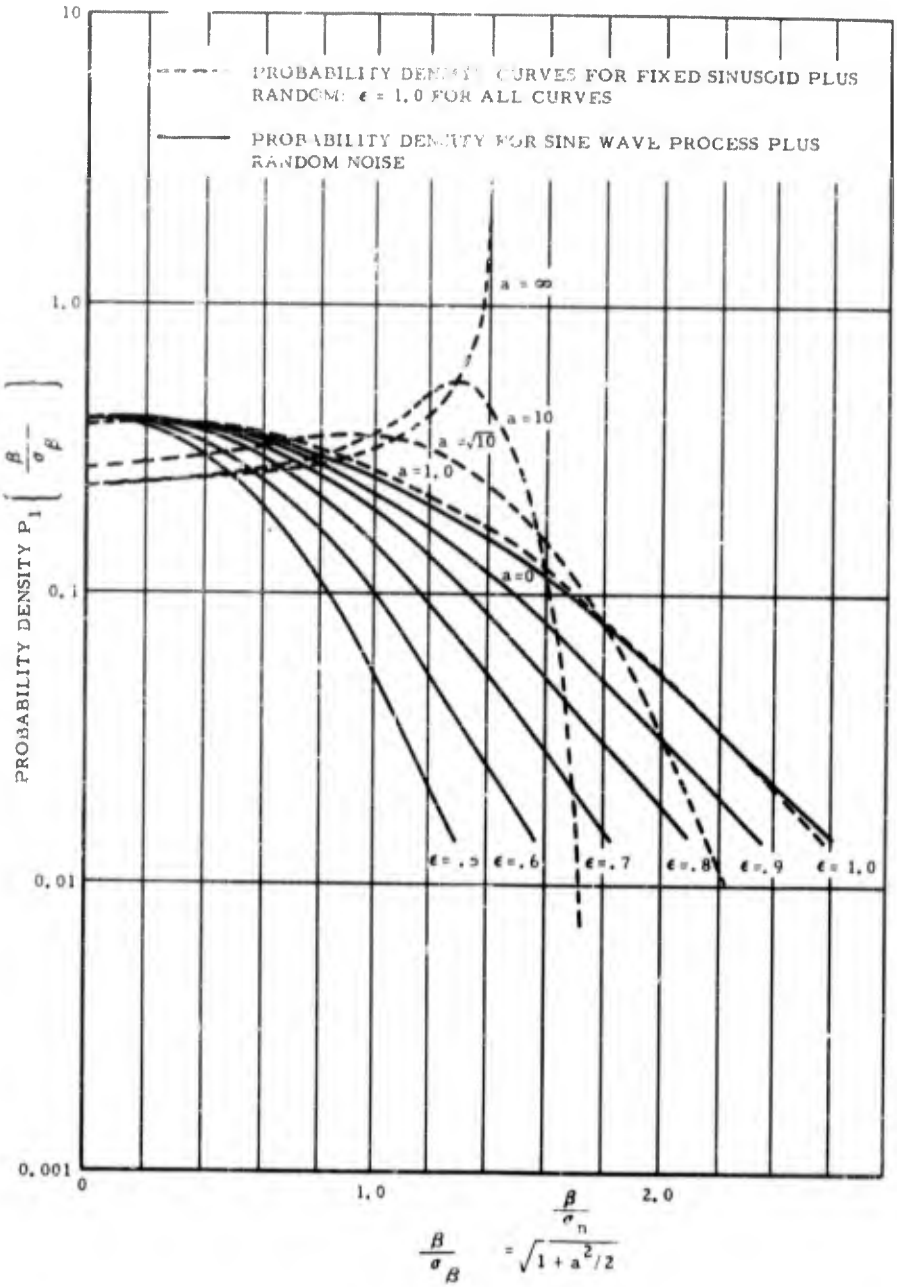

Fig. 6 - Probability density curves of β/σ_β for fixed sinusoid plus random noise and sine-wave process plus random noise

relatively large. Therefore, it appears to be worthwhile to investigate the solution proposed by Rice [4], which is applicable to this situation. The results indicated for this method are approximate and accurate only when the peak of the sinusoid and the level at which bottoming is measured are both fairly large compared to the rms of the random noise. That is, the solution is accurate when a and y are large compared to 1; the method for a and y being less than 1 discussed in the previous section is satisfactory. The average number of crossings per second is given by Eq. (8) in terms of a double summation. The portion designated as

$$ {}_1F_1\left(-\frac{1}{2}; n+1; -\frac{b^2}{2}\right) $$

is called a confluent hypergeometric function, which is the series solution of a special form of Bessel's equation.

$$ \overline{N_{\beta_o}} = N_o \sqrt{\frac{\pi}{2}}\, p_1(y)\, {}_1F_1\left(-\frac{1}{2}; n+1; -\frac{b^2}{2}\right) = $$

$$ = N_o \sqrt{\frac{\pi}{2}} \sum_{o}^{\infty} \frac{\psi^{(2n)}(y)}{n!\,n!} \left(\frac{a}{2}\right)^{2n} {}_1F_1\left(-\frac{1}{2}; n+1; -\frac{b^2}{2}\right) \qquad (8) $$

where

$$ N_o = \frac{1}{\pi}\frac{\sigma_{\dot{n}}}{\sigma_n} $$

$$ a = \frac{Q}{\sigma_n} $$

$$ y = \frac{\beta_o}{\sigma_n} $$

$$ b = \frac{2\pi f_o Q}{\sigma_n} $$

$$ n = 0, 1, 2, 3 $$

$$ \psi^{(2n)}(y) = \frac{d^{2n}}{dy^{2n}}\{\psi(y)\} = \frac{d^{2n}}{dy^{2n}}\left(\frac{1}{\sqrt{2\pi}}\, e^{-\frac{y^2}{2}}\right). $$

It can be shown [4] that $p_1(y)$ can be approximated by

$$ p_1(y) = a^{-\frac{1}{2}} F(y - a) $$

$$\sigma_n^2 = \int_{f_1}^{f_2} B^2 \left| \frac{\beta}{K_o} \right|^2 df = \int_{f_1}^{f_2} \frac{B^2 df}{\left[1 - \left(\frac{f}{f_n}\right)^2\right]^2 + 4\zeta^2\left(\frac{f}{f_n}\right)^2} = \frac{2\pi f_n B^2}{8\zeta}$$

if B^2 is in g^2/cps and we assume that $f_1 \to 0$ and $f_2 \to \infty$.

$$(\sigma_\beta)^2 = \frac{A^2}{4\zeta^2} + \frac{B^2 2\pi f_n}{8\zeta} = \frac{1}{8\zeta^2}\left[2A^2 + B^2\zeta(2\pi f_n)\right].$$

Similarly for $\dot{\beta}$,

$$\frac{(2\pi f_o)^2 Q^2}{2}\bigg|_{f_o = f_n} = \frac{(2\pi f_n)^2 A^2}{4\zeta^2}$$

$$\sigma_{\dot{n}}^2 = \frac{(2\pi f_n)^3 B^2}{8\zeta}$$

$$(\sigma_{\dot{\beta}})^2 = \frac{(2\pi f_n)^2 A^2}{4\zeta^2} + \frac{(2\pi f_n)^3 B^2}{8\zeta} = \frac{(2\pi f_n)^2}{8\zeta^2}\left[2A^2 + B^2\zeta(2\pi f_n)\right]$$

$$\overline{N_{\beta_o}} = \frac{1}{\pi}\sqrt{\frac{\frac{(2\pi f_n)^2}{8\zeta^2}\left[2A^2 + B^2\zeta(2\pi f_n)\right]}{\frac{1}{8\zeta^2}\left[2A^2 + B^2\zeta(2\pi f_n)\right]}}\exp\left\{-\frac{\beta_o^2}{\frac{2}{8\zeta^2}\left[2A^2 + B^2\zeta(2\pi f_n)\right]}\right\}$$

$$\overline{\dot{N}_{\beta_o}} = 2f_n \exp\left\{-\frac{2\beta_o^2\zeta^2}{A^2 + \pi f_n B^2 \zeta}\right\}. \qquad \text{(A-7)}$$

In the cases discussed in this paper, $\beta_o = 1$, and for each gyro bottoming there are 2 crossings of $\beta_o = 1$. For these purposes the average number of bottomings per second is

$$\frac{\overline{N_{\beta_o}}}{2} = f_n \exp\left\{-\frac{2\zeta^2}{A^2 + \pi f_n B^2 \zeta}\right\}. \qquad \text{(A-8)}$$

Then $p(0,\tau)$ is determined by applying Eq. (7):

$$p(0,\tau) = e^{-\frac{1}{2}\overline{N_{\beta_o}}\tau}. \tag{7}$$

For some of the cases given in Table 1, the order of the transfer functions is greater than 2. In these cases, the integrals involved in obtaining σ_n^2 and $\sigma_{\dot{n}}^2$ can be evaluated using Table E, 2-1, of Newton, Gould, and Kaiser [2], or by graphical methods.

APPENDIX B

As indicated in Fig. 6, the shape of the probability density of the combined fixed sinusoidal and random vibration becomes greatly different from that of the sinusoidal process plus random noise if a, the ratio of the peak of the fixed sinusoid to the rms of the random input is greater than about 3. Therefore, for these large values of a, the more exact solution of Rice [1,4] must be resorted to.

Without going into the details of the derivation of the expressions it can be said that the same general considerations apply as in Appendix A. That is, it is necessary to find the value of

$$\overline{N_{\beta_o}} = \int_{-\infty}^{\infty} |\dot{\beta}| \left[\int_0^{\pi} p_1(\beta_o,\theta) p_2(\dot{\beta},\theta) d\theta \right] d\dot{\beta}. \tag{B-1}$$

The probability densities $p_1(\beta_o,\theta)$ and $p_2(\dot{\beta},\theta)$ are quite different from those for a sinusoidal process + random noise. Bendat [1] supplies the derivation of $p_1(\beta_o,\theta)$ and $p_2(\dot{\beta},\theta)$, giving

$$p_1(\beta_o,\theta) = \frac{1}{\pi\sigma_n}\psi\left(\frac{\beta_o - Q\cos\theta}{\sigma_n}\right)$$

$$p_2(\dot{\beta},\theta) = \frac{1}{\pi\sigma_{\dot{n}}}\psi\left(\frac{\dot{\beta} + 2\pi f_o Q \sin\theta}{\sigma_{\dot{n}}}\right) \tag{B-2}$$

where

$$\psi(x) = \frac{1}{\sqrt{2\pi}} e^{-\frac{x^2}{2}}.$$

Substituting Eq. (B-2) into (B-1) we have the result for the number of crossings of any level β_o:

$$\overline{N_{\beta_o}} = \frac{2}{\pi^2\sigma_n\sigma_{\dot{n}}}\int_{-\infty}^{\infty}\dot{\beta}\int_0^{\pi}\psi\left(\frac{\beta_o - Q\cos\theta}{\sigma n}\right)\psi\left(\frac{\dot{\beta} + 2\pi f_o Q\sin\theta}{\sigma\dot{n}}\right)d\theta d\dot{\beta}. \tag{B-3}$$

Rice has solved this double integral directly, in terms of a double summation, giving

$$\overline{N_{\beta_o}} = N_o \sqrt{\frac{\pi}{2}}\, p_1(y)\, {}_1F_1\left(-\frac{1}{2}; n+1; -\frac{b^2}{2}\right)$$

$$= N_o \sqrt{\frac{\pi}{2}} \sum_{o}^{\infty} \frac{\psi^{(2n)}(y)}{n!n!} \left(\frac{a}{2}\right)^{2n} {}_1F_1\left(-\frac{1}{2}; n+1; -\frac{b^2}{2}\right) \tag{8}$$

where

$$N_o = \frac{1}{\pi}\frac{\sigma_{\dot{n}}}{\sigma_n}$$

$$a = \frac{Q}{\sigma_n}$$

$$y = \frac{\beta_o}{\sigma_n} = \frac{1}{\sigma_n}$$

$$b = \frac{2\pi f_o Q}{\sigma_{\dot{n}}}$$

$$n = 0, 1, 2, 3\ldots$$

$$\psi^{(2n)}(y) = \frac{d^{2n}}{dy^{2n}}\{\psi(y)\} = \frac{d^{2n}}{dy^{2n}}\left\{\frac{1}{\sqrt{2\pi}} e^{-\frac{y^2}{2}}\right\}$$

$${}_1F_1\left(-\frac{1}{2}; n+1; -\frac{b^2}{2}\right)$$

is a confluent hypergeometric function given by

$${}_1F_1\left(-\frac{1}{2}; n+1; -\frac{b^2}{2}\right) = \frac{\left(\frac{b^2}{2}\right)^{-1/2}\left(n+\frac{1}{2}\right)}{n!}\left[1 + \frac{\frac{1}{2}\left(n+\frac{1}{2}\right)}{1!\left(\frac{b^2}{2}\right)} - \right.$$

$$\left. - \frac{\frac{1}{2}\left(n+\frac{1}{2}\right)\left(n-\frac{1}{2}\right)}{2!\left(\frac{b^2}{2}\right)^2} + \frac{\frac{1}{2}\left(n+\frac{1}{2}\right)\left(n-\frac{1}{2}\right)\left(n-\frac{3}{2}\right)}{3!\left(\frac{b^2}{2}\right)^3} - \ldots\right]. \tag{B-4}$$

for $b >> 1$.

In the case discussed in this appendix, the sinusoidal component of the combined vibration input is predominant, therefore a is large. It turns out that y is also large, since the bottoming level is considerably greater than the rms for the random noise alone. Fortunately for this case, as Rice points out, the value for

$$p_1(y) = \sum_{n=0}^{\infty} \frac{1}{n!n!} \left(\frac{a}{2}\right)^{2n} \psi^{(2n)}(y)$$

can be approximated by

$$p_1(y) \simeq a^{-\frac{1}{2}} F(y - a)$$

$$\simeq a^{-\frac{1}{2}} \pi \frac{1}{\sqrt{2}} \int_0^{\infty} \psi(z + y - a) z^{-\frac{1}{2}} dz$$

$$\simeq \frac{1}{2\pi} \sqrt{\frac{y - a}{a}}\, \psi\left(\frac{y - a}{\sqrt{2}}\right) K_{\frac{1}{4}}\left(\frac{y - a}{2}\right)^2 \qquad \text{(B-5)}$$

where

$$K_{\frac{1}{4}}\left(\frac{y - a}{2}\right)^2$$

is a modified Bessel function of order 1/4 and is plotted in Fig. 9.

A curve of $F(y - a)$ vs $(y - a)$ has been plotted by Rice [4] and is replotted for a wider range of $(y - a)$ as shown in Fig. 7. The confluent hypergeometric function in this case is simply

$${}_1F_1\left(-\frac{1}{2}; 1; -\frac{b^2}{2}\right)$$

since only the first term (for $n = 0$) of

$$\sum_{n=0}^{\infty} \frac{1}{n!n!} \left(\frac{a}{2}\right)^{2n} \psi^{(2n)}(y)$$

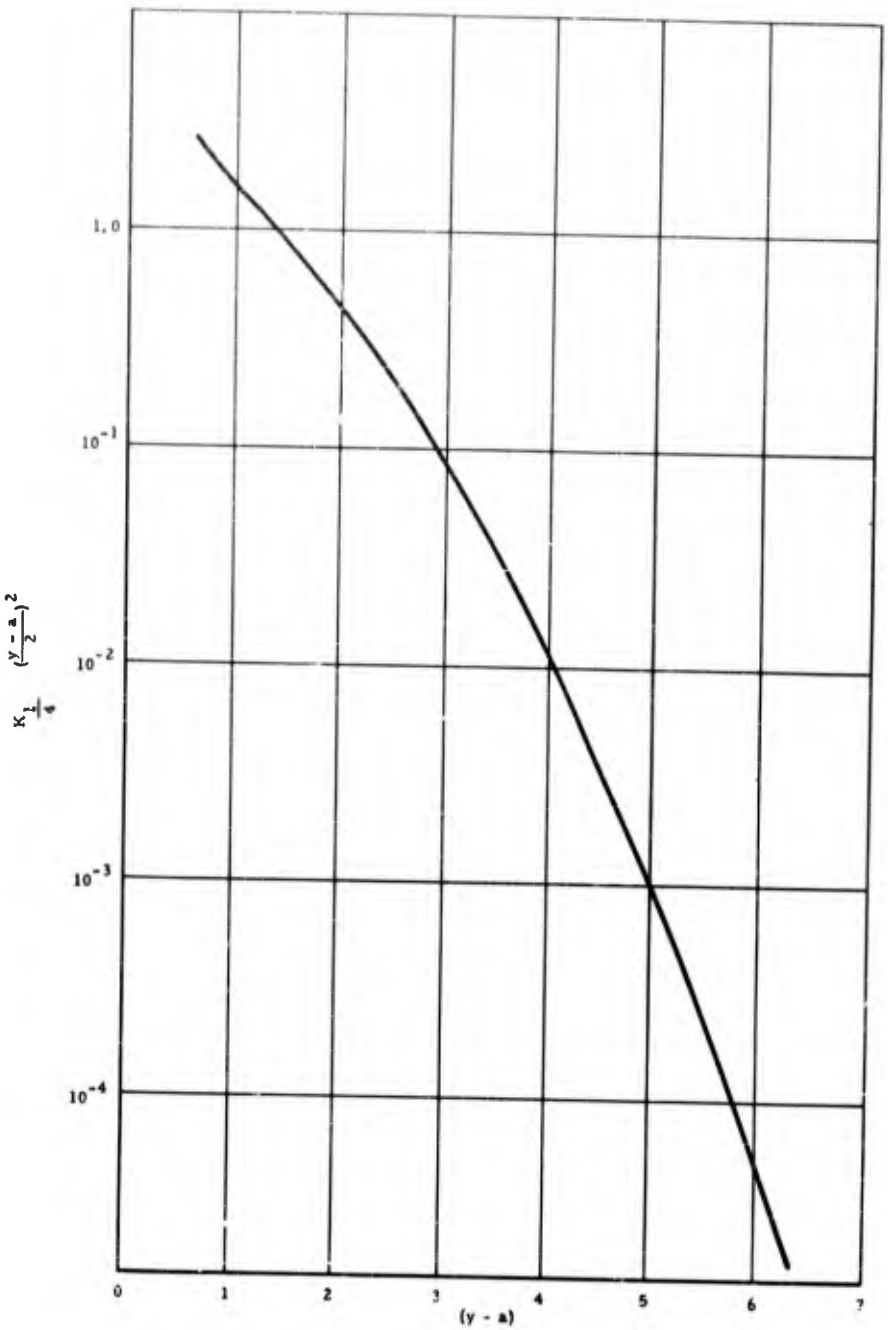

Fig. 9 - Plot of $K_{1/4}(y - a/2)^2$ versus $(y - a)$

is used in Eq. (B-6). A plot of

$$ {}_1F_1\left(-\frac{1}{2}; 1; -\frac{b^2}{2}\right) \text{ vs } \frac{b^2}{2} $$

is shown in Fig. 8, and from these curves it is possible to obtain values of

$$ \frac{\overline{N_{\beta_o}}}{N_o\sqrt{\pi/2}} $$

for values of $(y - a)$ from -4 to +6 and values of $b^2/2$ from 2 to 10.

In almost all of the cases for this study the parameters were in these ranges. Table 1 lists these parameters and gives a comparison of the average number of bottomings per second computed by this method and by the method of Appendix A.

* * *

A "QUICK-LOOK" TECHNIQUE FOR SERVICE VIBRATION DATA

Donald W. Nelson
Boeing Airplane Company
Seattle, Washington

The purpose of this paper is to present a means by which service vibration data can be processed so as to present an accurate picture of the vibration environment with a minimum of engineering and wave-analyzer time.

INTRODUCTION

The basic problem of any missile manufacturer is to produce a missile which will perform in a satisfactory manner. Operating conditions, vibration environment, and weight restrictions combine to pose a formidable engineering problem in the design of satisfactorily operating electronics packages and mechanical hardware.

Unfortunately, the design requirements which meet vibration and weight conditions tend to go in opposite directions. In order to satisfy the demands imposed by these requirements, it is – among other things – necessary to have an accurate picture of the vibration environment to which the equipment is to be subjected. This includes not only vibration amplitude but also the distribution of energy in frequency described by what we call the "power spectral density." An accurate knowledge of power spectral density, which tells us the "color" of the vibration, is extremely important and is found to have more influence on malfunctioning of equipment than does the over-all vibration level.

The purpose of this paper is to present a means by which service vibration data can be processed so as to present an accurate picture of the vibration environment with a minimum of engineering and wave-analyzer time. In order to carry out this objective, a device called a "comb filter" is utilized in the process of selecting data samples which are to be further examined in more detail with the wave analyzer. The following description and figures are presented to show how the comb filter is integrated in the over-all vibration data-handling system.

METHOD

First, the missile location at which the vibration environment is to be analyzed is instrumented with piezoceramic accelerometers and connected to a conventional FM/FM Telemeter channel of suitable bandwidth. The output of the telemeter receiver is recorded on magnetic tape at the ground station.

This step immediately brings up the problem of the selection of a satisfactory gain figure for the entire telemeter channel. The gain must be such that the accelerometer signal is well above the instrumentation noise level but below that which will cause overloading and accelerometer signal clipping. Since random-vibration data and instrumentation noise look alike, the only practical way to differentiate between the two is to have the instrumentation noise absent or, in a real-life situation, present in an insignificant amount.

After obtaining a properly recorded vibration signal, the signal is then played off the tape and recorded on a multichannel oscillograph, with a paper speed of approximately 1/4 inch per second. One oscillograph

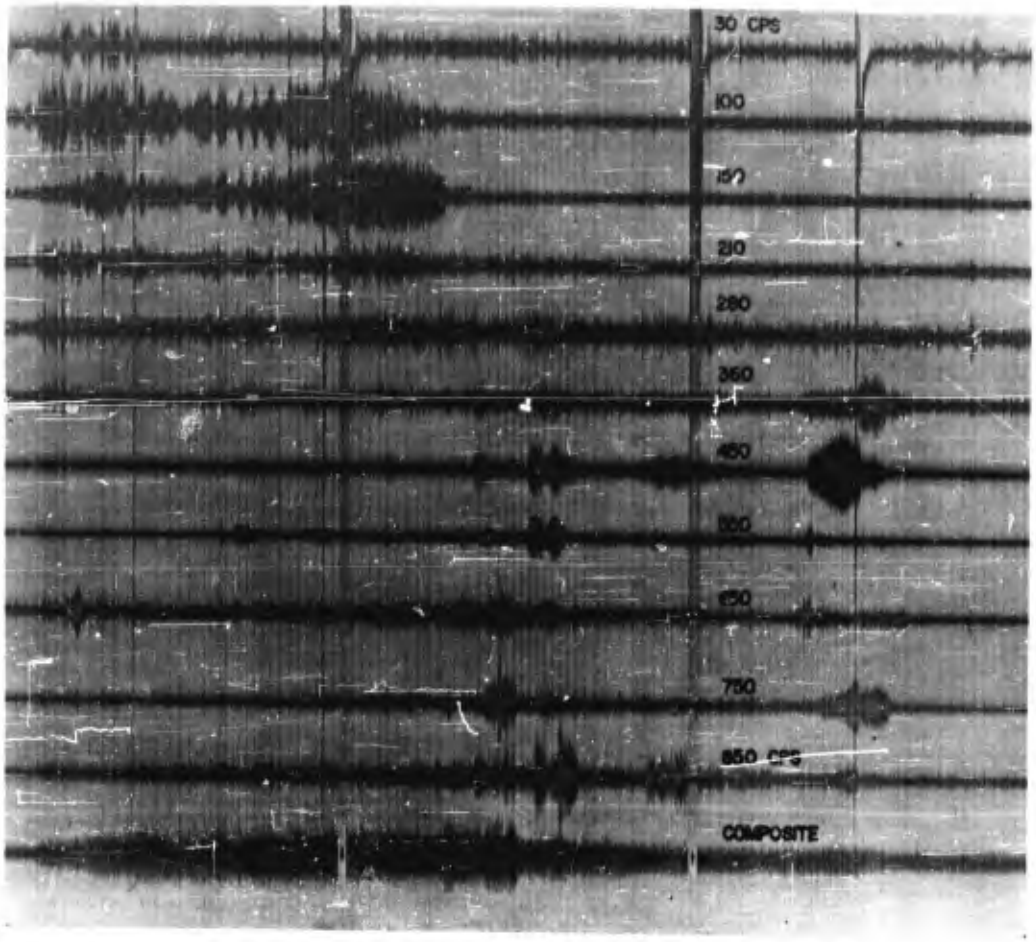

Fig. 1 - A typical comb filter recording

trace represents a direct recording of the accelerometer signal, while the remaining traces show the individual outputs of the "comb filter unit" whose input is connected to the accelerometer output signal. Figure 1 shows a typical "comb filter recording."

The "comb" in this case consists of a group of 24 narrow bandpass filters which are spread out side by side in the frequency domain of interest. The vibration signal is connected to the paralleled inputs of all the filters, and the output of each filter goes to a separate trace on the recording oscillograph. Figure 2 is a block diagram of the comb filter unit.

Several useful purposes are served by making an oscillograph recording of this tape which shows both the raw and the combed data. First of all, it gives – on a comparatively short oscillograph record – an over-all picture of the vibration level and how it varies during the entire missile flight. By examining the remaining traces, which represent the outputs of the individual filters in the comb filter, it is possible qualitatively to measure the frequency distribution of the vibration energy and how this distribution changes with respect to missile flight conditions.

The data presented by the comb filter outputs are very important to structural

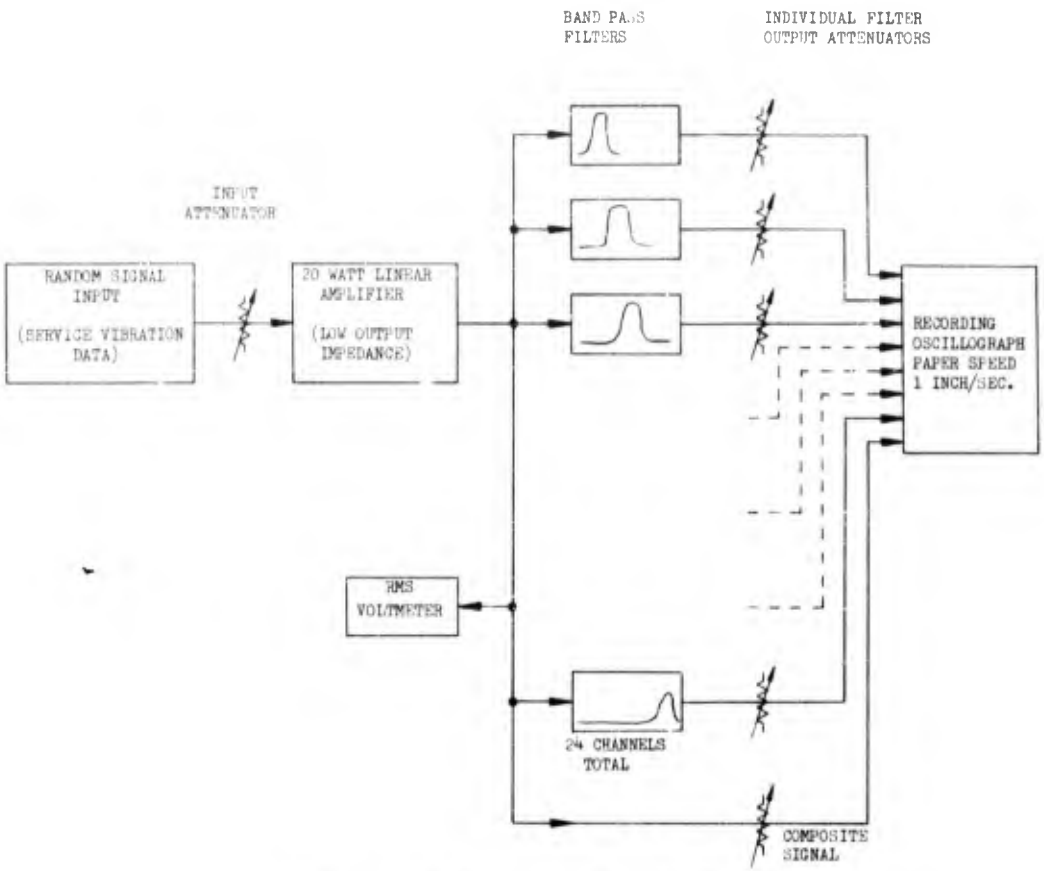

Fig. 2 - Diagram of the comb filter unit

dynamics engineers because these data make it possible for them to select a minimum number of data samples which must be further analyzed on the wave analyzer. Data samples which have been found to be very important are those in which a large amount of energy is distributed over a comparatively narrow band. This characteristic does not show on the unfiltered data trace; and in many instances, the over-all energy level will show an appreciable drop – when, in fact, a critical situation exists. It is also possible, in many instances, to differentiate between true transient-type data and transients which may be caused by instrumentation overloading or other malfunctioning.

The comb filter unit consists of a group of conventional, commercially available L. C. Filters, with approximately constant percentage-bandwidth. The inputs of all the filters are driven by a single 20-watt linear amplifier. Each filter has its own output attenuator which can be adjusted in several ways.

One method is to measure the effective bandwidth of each filter and then to adjust the corresponding attenuators so that the output is indicative of the power spectral density of the input signal. This permits the engineer, by examination of the oscillograph record, to get a rough approximation

of the energy level distribution throughout the frequency spectrum.

The other method, which is used almost exclusively, is to adjust each attenuator so as to get an oscillograph trace of optimum magnitude and dynamic range from each filter. When adjusted in this manner, the oscillograph record is primarily used to observe how the distribution of energy changes with respect to time, so as to select data samples which will give the most vital information.

It is these selected data samples which are run through the spectrum analyzer and yield the final power spectral density curves.

* * *

THE PRINCIPLES INVOLVED IN CHOOSING ANALYZER BANDWIDTH, AVERAGING TIME, SCANNING RATE, AND THE LENGTH OF THE SAMPLE TO BE ANALYZED*

R. C. Moody
Technical Products Company
Los Angeles, California

This paper presents a discussion (from a physical standpoint) of the function performed by the random-wave analyzer in random-wave testing. Other papers [1,2] have discussed the general techniques of random-wave testing, including the preparation of a specification vibration, calibration of accelerometers, and shaker tables.

STATEMENT OF THE PROBLEM

The basic problem in the analysis of random waves resides in the fact that power spectral density is described by an infinite integral. It is necessary to solve this integral by analyzing a sample vibration.† This should be done in a manner which will give a sufficient confidence in the results of the analysis to permit us to make predictions. These predictions must be based on the behavior of the specimen under the conditions described by the infinite integral, and not be our approximate solution.

Solving the infinite integral, by means of the approximate methods we must take, leaves three areas of uncertainty. These are:

1. Having a sample of finite, and often very short length, we can only approximate the total ensemble.

2. Since the filter is of finite bandwidth, it is difficult, in some cases, to produce a power spectral density plot having sufficient resolution to reveal all of the resonances of the specimen under test.

3. We cannot average over an infinite time, and therefore, the power spectral density estimate will fluctuate; that is, it will consist of a fluctuating signal superimposed on the true average.

VARIABLES UNDER OUR CONTROL

There are several variables in the analyzer system over which we have more or less control. It is by the optimum choice of these variables that we will be able to control the accuracy of the results. These variables are length of the sample, bandwidth of filter, and averaging time.

Length of Sample

When the sample is a portion of a real environment, such as telemetered data, the sample length is often not in our control. In some cases we will find that a sample of 1/2 minute or more is necessary to establish a reasonable accuracy. In other cases a sample as short as 1 second may be used. The accuracy of the power spectral density estimate is proportional to the sample length. We are sometimes able to control the sample length when a shake-table type and random analyzing system is used. We can shake the

*This paper was not presented at the Symposium.

†Since we have only a sample to work with, our "solution" is in reality an "estimate," even if all the analyzer operations are mathematically accurate.

specimen as long as we deem desirable to obtain a suitable sample. Later in the memorandum we will discuss methods by which we can predict the probable accuracy of the power spectral density estimate in terms of the sample length.

Bandwidth of Filter

The wider the filter, the more confidence we may have in our power spectral density estimate, but the less detail we will obtain in the power spectral density plot.* This is the area in which the greatest compromise will have to be made. The accuracy of the estimate is proportional to the bandwidth; however, we cannot increase the bandwidth without limit. Figure 1 shows the difference in detail obtained with filters of three different bandwidths.† Note that the 2-cps filter reveals a complex resonance characteristic, whereas the 10-cps filter indicates a single resonance. Figure 1 also illustrates the reason for dividing the infinite integral by the bandwidth of the filter used. The area under the 2-cps filter curve is one-fifth of the area under the 10-cps filter curve. If the area under each curve is divided by the bandwidth used, they will all have the same area.

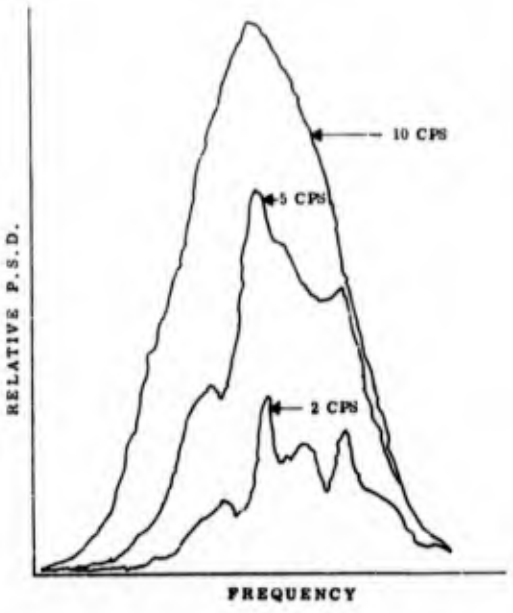

Fig. 1 - Complex resonances which are not shown by a 10-cps filter are revealed by a 2-cps filter. The 10-cps filter has five times as much energy in its passband as does the 2-cps filter, therefore, the area under the 10-cps filter plot is five times greater than the 2-cps plot. Generally, the plots are normalized by dividing the filter output by its bandwidth, and so obtaining the energy per cycle. In such cases, the area under all plots will be the same.

In determining the filter bandwidth we must keep two things in mind. As a practical compromise, the filter should be no more than one-fourth as wide as the narrowest resonance expected to be encountered in the specimen. Under these circumstances the accuracy of the power spectral density plot will be approximately proportional to the filter bandwidth. If, however, the resonances are narrower in width than the filter, the accuracy of the power spectral density estimate will be proportional to the width of the resonance in the specimen and not of the filter. Two solutions have been suggested for this dilemma. One method [3], that of Morrow, is to make two analyses. As an adaption to this technique we shall use the narrowest filter we have to establish the resonances present. We will then make a second analysis, in which a wide filter will be used, and by this analysis we will improve the accuracy of the power spectral density estimate.

This is readily done with the Technical Products Company TP-625 Wave Analyzer System. In the first case a 2-cps filter is recommended for use. The power spectral density plot will reveal a rapid energy versus frequency change if sharp resonances are present. The frequency of the resonances will be noted. These regions of interest can then be scanned with a wider filter, say, of 10 to 50 cps. Scanning can start at any arbitrary point below the resonances in the spectrum and end at any other point above the resonances. When the "integrate" mode

*We might think of a wider filter giving us more data per second, and thus shortening the time of analysis.

†For Figs. 1 and 2, the author owes gratitude to Dr. Wilbur Marks of the David Taylor Model Basin, Navy Department, Washington, D. C.

of the TP-633 Power Integrator is used, a better approximation of the energy within these scanned frequency limits can be obtained. This will establish the Y-axis scale of the first plot, within the frequency band chosen. An example of this technique is shown in Fig. 2.

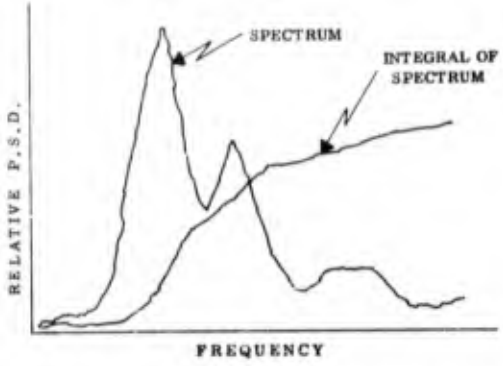

Fig. 2 - Power spectral density is defined by an infinite integral. If the integral is averaged over an infinite time, the result will be approximately as shown in the figure. If the integral is averaged over a short time, the resonances of the specimen under test will be revealed. The ordinate of the integral plot is proportional to the mean square, as is the area under the spectrum plot. The energy between frequencies can thus be estimated.

The second method [4,5], by Press and Tukey, depends on "prewhitening." In this scheme white and random noise is applied to a variable filter, which may become quite complicated in some cases. The output of the variable filter is applied to the specimen under test. The filter is adjusted to remove as many of the hills and dales in the power spectral density plot as possible. If this is done well, we will obtain a "pastel" output from the specimen, which will have no rapid energy changes. The power spectral density plot will reflect the energy distribution when adjusted with the frequency characteristic of the variable filter.

Averaging Time

The infinite integral which defines power spectral density requires an infinite averaging time. The error in not being able to average over an infinite time can be predicted, as will be discussed later. However, the error, or uncertainty, can never be less than that imposed by the sample length.

In the TP-625 Wave Analyzer System there are two modes of averaging. The first, called the "averaging" mode, is variable continuously from 0.1 second time constant to 100 seconds. The second, called the "integrating" mode, has a time constant of about 250,000 seconds and therefore approaches the true infinite average.

When a function is summed over a period of time it must be divided by the time to obtain the time average. When the averaging mode of the TP-625 Wave Analyzer is used, the R-C averaging circuit will discharge as well as charge, this being tantamount to continuous time division. Thus the average is taken over the time constant of the R-C filter. The integrating mode of the TP-625 Wave Analyzer, however, makes use of an operational integrator; and with the consequent high storage capacity the rate of discharge is very slow, or absent, for all practical purposes. Thus, when the integrate mode is used, the average is taken over the entire time of the analysis, and there is no division by time. The area under a power spectral density curve is equal to σ^2 and is, of course, the integral of the power spectral functions over the frequency range $f_b - f_a$. The integrate mode gives this integral directly. Since the integral has the value σ^2, it is a direct check on the measured value of the input, i.e., σ itself, obtained before the analysis is made.

The averaging time, if very long, will tend to obscure the detail in the power spectral density plot. Figure 2 illustrates this. The curve with the detail employs the averaging mode of the TP-625 Wave Analyzer; and, as can be seen, the average value of the function from moment to moment is well established. The smooth curve was made with the integrating mode, and it is in fact the integral of the detail curve. For each value of the abscissa, the ordinate of the

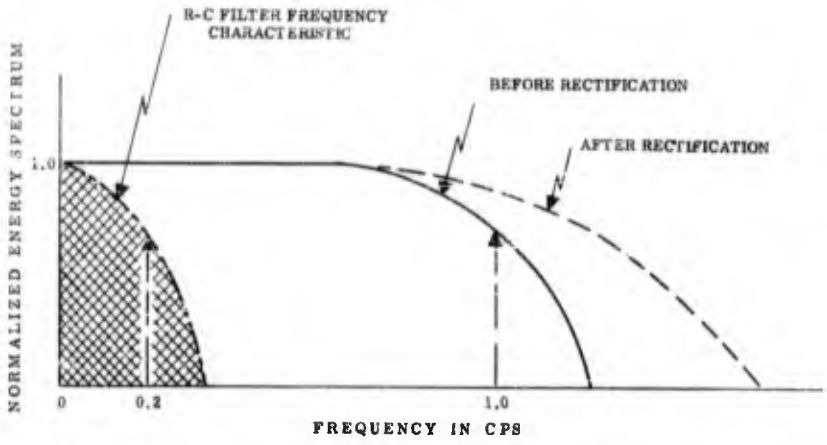

Fig. 3 - The solid curve illustrates the energy distribution in a 1-cps bandpass filter. The dashed curve indicates that the distribution is restored by making the smoothing filter, which follows the rectifier, have a cutoff frequency four or five times lower than that of the bandpass filter. Note that frequencies below about 0.2 cps, shown by the cross-hatched area, are rectified but not smoothed. This has the effect of a very-low-frequency signal superimposed on the smoothed dc output. Therefore, there is an uncertainty as to what the true mean is at any instant of time. The uncertainty can be reduced by making the time constant of the R-C filter large – the condition also required to restore the normal distribution.

Coefficient of Variation =

$$= \frac{\text{Standard Deviation of Estimate}}{\text{Mean of Estimate}}$$

$$\Delta q(\omega) = \frac{\sigma_1}{\langle a^2 \rangle} . \qquad (1)$$

Physically, this coefficient can be interpreted as a fluctuation superimposed on the true estimate. It is the probable error inherent in our estimate due to the finite length of the sample and rate of analysis. The coefficient of variation should not be used as a measure of uncertainty when its numerical value exceeds 0.2 (20 percent). $\sigma_1/\langle a^2 \rangle$ can be calculated [3], or it can be arbitrarily assumed to have some nominal value, say, 0.1. When it is used, we make two assumptions: (1) the power spectral density does not vary in any appreciable degree over the passband of the filter and (2) it does not appreciably change over the averaging time of the analyzer.

According to Morrow [3] we can write

$$\frac{\sigma_1}{\langle a^2 \rangle} = \frac{1}{\sqrt{BW \times SL}} \qquad (2)$$

where

σ_1 = rms deviation

$\langle a^2 \rangle$ = average of the instantaneous squares

BW = effective bandwidth* of bandpass filters in cps

SL = sample length in seconds.

*A method of determining the effective bandwidth is given in the TP-633 Power Integrator handbook. It is also described in a Technical Products Co. memorandum "Effective Squared Bandwidth of TP-218 Filters," Dec. 1, 1959.

smooth curve is directly proportional to the area under the detail curve. With a plot of this sort one can establish the energy between any two frequencies in the detail curve.

Another illustration of how the averaging time can obscure the detail of the plot is shown in Fig. 1. If the averaging time is made long, the curve for the 2 cps filter will tend toward a single resonance shape having the same area as before, but a smooth shape such as the 10-cps filter has.

RELATIONSHIP BETWEEN THE VARIABLES

It is often helpful to the engineer to obtain a physical picture of a mathematical relationship. In this section we will attempt to express the problem in physical terms.

Let us apply a white, and normally distributed, random wave to the analyzer input. We will choose a 1-cps-wide bandpass filter. We will connect a cathode-ray oscilloscope across the output of this filter. The cathode-ray oscilloscope will show a single wavelength of the frequency to which the analyzer is tuned. This single cycle will have a blurred appearance due to its random phase. It will wax and wane in amplitude at a random rate of up to approximately 1 cps and will reach a maximum about each 0.8 second [6]. As we observe this wave, we will be inclined to wait a considerable time before we attempt to state its probable average value. In other words, we require a fairly long sample to make a good estimate.

Now, if the 1-cps filter is switched out of the circuit and replaced by a 10-cps filter, we will find that ten times as many maximums occur in a second than in the previous case. We are now able to make a good estimate in about one-tenth of the time. In other words, for the same degree of accuracy, we need only one-tenth of the sample length. In fact, the product of bandwidth and sample length is a measure of the accuracy of the estimate. In this example we have looked at the instantaneous fluctuations of the filtered signal before they are averaged. The next step is to rectify and smooth these instantaneous fluctuations and obtain their average.

Figure 3 shows the spectrum of the output of a 1-cps bandpass filter before and after rectification. Before rectification, the spectrum is nonlinear and the randomness of the wave thereby is destroyed. The altered spectrum is indicated by the dash line. The passband of the R-C smoothing filter, which follows the rectifier, is shown by the dot-dash line. It has a much lower frequency cutoff than the bandpass filter for two reasons. The first reason is to restore the randomness of the wave. It can be shown [7] that a narrow frequency band of a nongaussian spectrum tends toward normalcy. Now, if the wave does not have a normal distribution, the usefulness of the power spectrum is impaired. Therefore, to avoid this we should make the cutoff frequency of the R-C filter about one-fourth to one-fifth of the bandwidth of the bandpass filter.* This restores the normal distribution.

The second reason is to reduce the fluctuations in the rectifier output. As shown by the continuous spectrum of Fig. 3, there are an infinite number of frequencies in the band, extending from 0 cps to something more than 1 cps, of the rectifier output. The R-C filter will smooth out all of these (average them) above 0.2 cps. Frequencies below 0.2 cps are not effectively smoothed. If the energy below 0.2 cps is a significant part of the whole, we can visualize the effect as that of a very-low-frequency random signal superimposed on the dc output of the rectifier. There will then be an uncertainty as to the exact value of the average at any time. A measure of the uncertainty in the power spectral estimate is the ratio of the cutoff frequency of the R-C filter to the bandpass filter; it is more usual to express this relationship as the product of the bandpass filter width, with the time constant of the averaging filter.

THE MEASURES OF ACCURACY

There are two measures commonly used by which we can establish the accuracy of our estimate. These are approximately equivalent. The first of these is the statistical coefficient of variation.

*The time constant of the chart recorder must be taken into consideration, as it adds to the total time constant.

Example 1

Assume a permissible error of 10 percent.* This makes the coefficient of variation equal to 0.1

$$\frac{\sigma_1}{\langle a^2 \rangle} = 0.1 = \frac{1}{\sqrt{BW \times SL}}. \qquad (3)$$

The required product of BW and SL must then be 100. This can be obtained by either BW = 1 cps and SL = 100 seconds, or by BW = 100 cps and SL = 1 second, or by intermediate values.

How much confidence† can we have in the error being within 10 percent? It has been pointed out [4] that the error has an approximate normal distribution when it is less than 20 percent. Consequently, we can establish confidence bands for the estimated error. Such confidence bands can be established by referring to cumulative distribution tables [8], or from a probability density curve with a cumulative distribution abscissa [9].

Example 2

We ask ourselves, what is the probability that σ_1 will be within the limits necessary for $\sigma_1/\langle a^2 \rangle = 0.1 = 10$ percent? That is, what is the probability of σ_1 remaining in the region of ±1 times its assumed value. Referring to Table A-4 of Ref. 8, or to the probability curve on page 988 of Ref. 9, we see that there is a 34.13-percent probability that σ_1 will be greater than -1 times its assumed value. Thus the probability that σ_1 will be between ±1 is 68.26 percent; or we have a 68-percent confidence that the error will be within 10 percent. There is, therefore, also a 32-percent probability that the error will be greater than 10 percent. We can establish additional confidence bands. Thus, what is the probability that the error will be within 20 percent, in other words, within twice its assumed value? From $\sigma_1 = -2$ to $\sigma_1 = +2$ in the table referenced above is 0.9722 - 0.0228 = 0.9494 ≅ 95 percent. Thus the confidence that the error will be within 20 percent is 95 percent.

The same coefficient, $\sigma_1/\langle a^2 \rangle$, may be used to estimate the uncertainty due to a finite averaging time as well as the error due to sample length. Again, according to Morrow [3],

$$\frac{\sigma_1}{\langle a^2 \rangle} = \frac{1}{\sqrt{2 \times BW \times T}} \qquad (4)$$

where T = averaging time in seconds.

It is the usual case where the sample length is the dominating uncertainty, since T is readily adjustable over wide limits. Also, the uncertainty can never be less than the amount imposed by the sample length. In effect, the above formula says that, for the same confidence level, the averaging time should be half the length of the sample in seconds.

A second measure of the accuracy of our estimate makes use of the chi-square distribution [8,10,11]. Figure 4 is an example which was constructed from Table A6-b in Ref. 8. The ordinate of Fig. 4 is the ratio of the observed to the true power spectral density; the abscissa is "degrees of freedom," and the parameters are confidence bands. Degrees of freedom is a term used by statisticians to indicate the ratio of the mean-square fluctuation of a variable to the true squared average. It is given by [11]

$$n = 2 \times BW \times SL \qquad (5)$$

where

n = degrees of freedom

BW = effective bandwidth

SL = sample length.

Example

If the effective bandwidth is 3.5 cps (typical of a TP-218H Filter) and the sample length is 10 seconds, the number of degrees

*This is not to be confused with instrumentation error in data acquisition, processing, and/or analysis.

†Estimates of error vary in precision. It is important that the estimate be accompanied by a statement of the confidence we have in the estimate.

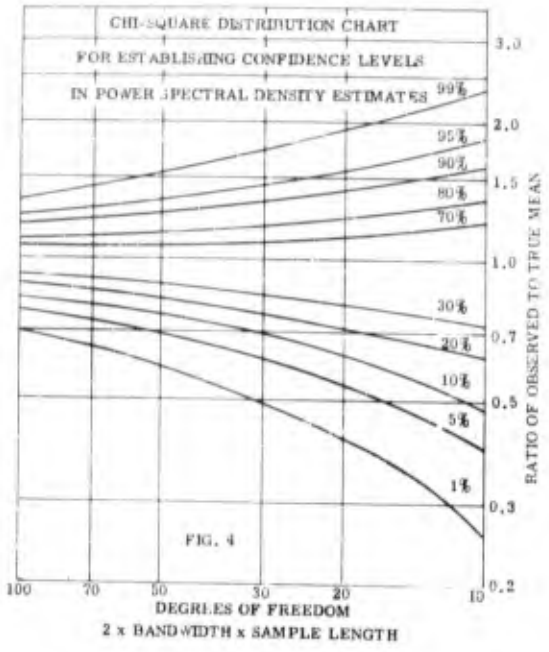

Fig. 4 - The ordinate of the figure gives the ratio of the true mean to the observed mean. As an example of its use with a bandwidth of 10 cps and a sample length of 2 seconds, the degrees of freedom is 40. Entering the abscissa at this point indicates a 1-percent confidence level that the observed mean will be less than 0.55 of the true mean, and 99-percent confidence that it will be less than 1.6. It is also evident that, for the same 40 degrees of freedom, we have a 70-percent confidence that our estimate will be below 1.1, and 30 percent that it will be below 0.88. Our observed mean thus has a dual parameter nature – the interval of the estimate must be accompanied by an expression of the confidence level.

of freedom is 70. The abscissa of Fig. 4 is entered at this point, and we have the following confidence bands:

Table 1

Confidence (%)	That Value Will Be Above	That Value Will Be Below
99	0.649	1.43
95	0.739	1.29
90	0.790	1.22
80	0.856	1.14
70	0.905	1.08

This data could be prepared another way.

Table 2

Confidence (%)	That the Value Will Be Between
98	0.649 and 1.43
90	0.739 and 1.29
80	0.790 and 1.22
60	0.856 and 1.14
40	0.905 and 1.08

It is evident that we need a large number of degrees of freedom to obtain a high confidence in an estimate. The problem is most acute at the low-frequency end of the spectrum due to the narrowness of the filter required to resolve the resonances. At higher frequencies the accuracy increases because we are able to use much wider filters.

A NOTE ON THE SCANNING RATE OF FILTERS

If filters are scanned too rapidly, two phenomena will occur: a growth and a decay transient. The energy will not have time to rise in the filter, and hence we will record an output which is less than the steady-state output. This results in a "blurring" of the output amplitude. Technical Products Company recommends that the maximum scanning rate be chosen from Eq. (6) below

$$CPS/S_{(max)} = \left(\frac{BW}{2}\right)^2 \qquad (6)$$

where BW = filter bandwidth and CPS/S = cycles per second per second. This rate will allow the energy to rise to very nearly the

steady-state value before the filter has been moved in the spectrum by more than 25 percent of its bandwidth. However, it is possible to scan the filter at a faster rate when the power spectrum is comparatively smooth – "pastel," for example. In this case we can use the equation $(BW)^2 = CPS/S$.

All energy contained in the filter must decay as the filter is moved in the spectrum. Decay is not instantaneous; and thus energy present in one bandwidth of the filter will still be present, but at a lesser degree, in the next adjacent bandwidth. This produces a blurring effect; stated in another way, the filter appears somewhat wider than its effective stationary width.

When the filter is scanned at a rate according to Eq. (6), the transient effects of the filter may be regarded as negligible. If scanning is made at higher rates, the apparent increased filter width should be taken into account. Hence, we have an amplitude blurring and a width blurring, which are functions, in a complex way, of the smoothness of the power spectral density plot.

In conclusion, it has been the author's intention to present a brief introduction to the principles involved in choosing analyzer constants. Only the physical aspect has been presented, and it is recommended that the cited references be studied.

REFERENCES

1. Wilbur DuBois, Boeing Airplane Co., "Random Vibration Testing," 27th Shock and Vibration Symposium Bulletin 27.

2. Raymond E. Bell, Lockheed Aircraft Co., Missiles and Space Division, "The Practical Approach to Random Vibration Testing," 27th Shock and Vibration Symposium Bulletin 27.

3. Charles T. Morrow, "Averging Time and Data Reduction Time for Random Vibration Spectra," J. Acous. Soc. Am., Vol. 30, Nos. 5 and 6, June, 1958.

4. Harry Press, NASA, and J. W. Tukey, Bell Telephone Laboratories, "Power Spectral Methods of Analysis and Their Application to Problems in Airplane Dynamics," Agard Flight Test Manual, Vol. VI, Part IVC.

5. R. B. Blackman and J. W. Tukey, Bell Telephone Laboratories, "The Measurement of Power Spectra," Dover Publications, 1958. Also in Bell System Tech. J., Vol. XXXVII, Jan. and March 1958.

6. S. O. Rice, "Mathematical Analysis of Random Noise," Bell System Tech. J., Vols. XXIII and XXIV, July 1944 and Jan. 1945. Also published in Selected Papers on Noise and Stochastic Processes, Wax, Nelson, Dover Publications.

7. D. Middleton, "Noise and Nonlinear Communication Problems," Symp. on Application of Autocorrelation Analysis to Physical Problems, Office of Naval Research, June 1949.

8. W. J. Dixon and J. J. Massey, Introduction to Statistical Analysis, McGraw-Hill Book Co., 1957.

9. Reference Data for Radio Engineers, 4th ed., p. 988, International Tel. and Tel. Co., 1957.

10. J. W. Tukey, "The Sampling Theory of Power Estimates," Symp. on Application of Autocorrelation Analysis to Physical Problems, ONR, June 1959.

11. T. P. Rona, Random Vibration, Chapter 7, Technology Press, MIT, 1958.

* * *

AUTOMATIC TRANSMISSIBILITY PLOTTER*

M. Matrullo and D. R. Thomas
The Martin Company
Baltimore, Maryland

Describes a technique developed to obtain, quickly, vibration transmissibility data. Only equipment which could be considered standard in most aero-space company facilities is used.

INTRODUCTION

Present-day techniques used to obtain vibration transmissibility data on aircraft and missile subassemblies and ground support equipment require an excessive expenditure of engineering manpower solely for data reduction. A typical technique consists of (1) recording the forcing function and the various responses of the article under test on an oscillograph, (2) visually measuring the trace amplitudes, and (3) ratioing these values to obtain the desired transmissibility as a function of frequency. When a large number of data points are to be evaluated, such as in preliminary engineering study tests, one can readily see that the cost and time factors will be quite large. Aside from these important factors, this technique is cumbersome and at times produces inaccurate results because of wave form distortion.

A technique has been developed at the Baltimore Division of The Martin Company to minimize the conditions outlined above, and it is done through the use of equipment which could be considered "standard" in most aero-space company test facilities. The system consists basically of a Technical Products Company Spectrum Analyzer, log converters, difference networks, and X-Y plotters. Figure 1 shows a block diagram of the system.

*This paper was not presented at the Symposium.

EQUIPMENT

The analyzer is the Technical Products Company TP625 wave analyzer system which includes a TP627 wave analyzer and a TP626 oscillator. This analyzer uses the heterodyne principle whereby a local oscillator combines with the incoming signal to produce a new frequency. This frequency is passed by a narrow bandpass filter and recombines with the local oscillator, thus allowing the recovery of the original signal. The process is a continuous one, with the entire frequency spectrum of interest being scanned by automatically changing the oscillator with a constant-speed motor. The center frequency of the filters is in the vicinity of 97 kc, thus allowing the use of crystal filters with their inherent high Q characteristics and making it possible to have highly selective filters in the audio range of frequencies.

The oscillator-modulator, TP643, which is also made by Technical Products Company, is used to provide a method of maintaining synchronization between the shaker driving frequency and the frequency that the analyzer is scanning at any instant of time. If the shaker is driven sinusoidally, it will be necessary that the frequency being scanned by the analyzer is identical to the frequency driving the shaker. This becomes important when extremely narrow bandpass filters are used. For wider filter widths, however, it is only necessary that the driven frequency be within the passband of the filter. The TP643 oscillator-modulator makes it possible to obtain exact synchronization. This is done in the following manner. The oscillator-modulator has a crystal controlled oscillator having a frequency of 97 kc. The local

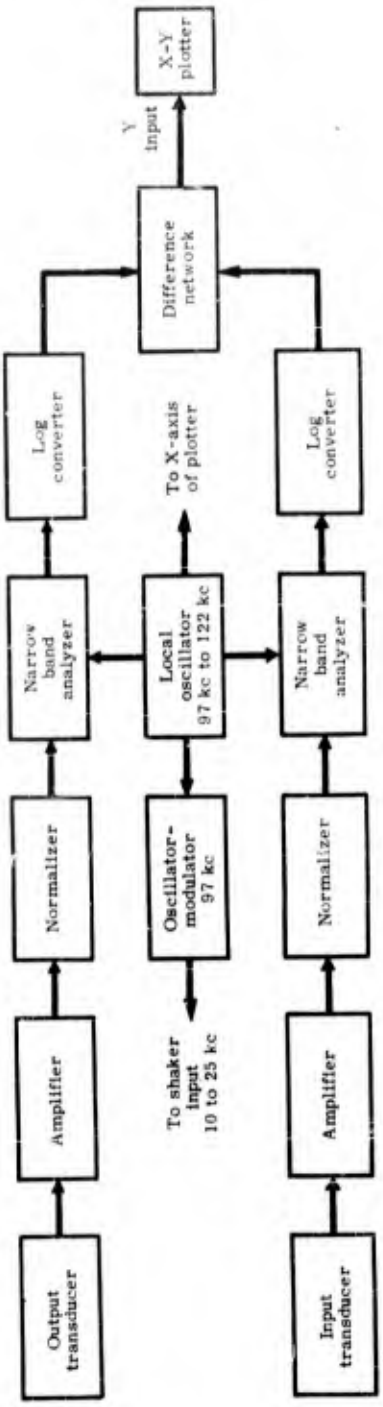

Fig. 1 - Diagram of the automatic transmissibility plotter

oscillator frequency combines with this frequency and the difference frequency is used to drive the shaker. Since the local oscillator is common to both the oscillator-modulator and the wave analyzer, the frequency driving the shaker (input frequency) will be the same frequency that the analyzer will be scanning (output frequency).

The system has a frequency response of from 10 to 20,000 cps. The oscillator scanning can be driven either internally at fixed sweep rates or externally using any scanning rate desired.

The logarithmic converters used are Moseley Model 60B. These units have a dynamic range of 60 db and an adjusted frequency response of 10 to 20,000 cycles. They are used in pairs as computing elements in performing the necessary division to obtain transmissibility, and their outputs are terminated in a resistance-type difference network. The readout device used to detect this difference is a Moseley Model 5 Autograf recorder which has been converted to potentiometer operation (Fig. 2).

The normalizing circuits are calibrated 10-turn potentiometers used in conjunction with step attenuators. Their purpose is to adjust the gain of each transducer and its respective signal conditioner, so that the electrical signals being applied to the analyzers are of equal magnitude when identical physical phenomena are present on each. This unit also serves to attenuate all channels equally in the event that the signal amplitude out of the signal conditioners exceeds the dynamic range of the analyzers. Simultaneously changing the signal level of both transducers into the analyzers will not affect the ratio of the two signals. However, with proper adjustment of the equipment operating range for the physical phenomena expected, dynamic ranges well in excess of 40 db can be obtained with a single setting. The limitations will most likely be determined by the transducer amplifiers used as signal conditioners, since a 60-db dynamic range can be obtained easily in both the analyzers (when used with narrow band filters) and the log converters.

OPERATION

The system functions in the following manner: A transducer is located at an area of interest on the specimen being vibrated, which we will consider the "response" or "output," and a transducer is located at a point on the shaker table fixture where the force is being applied. The signal from this

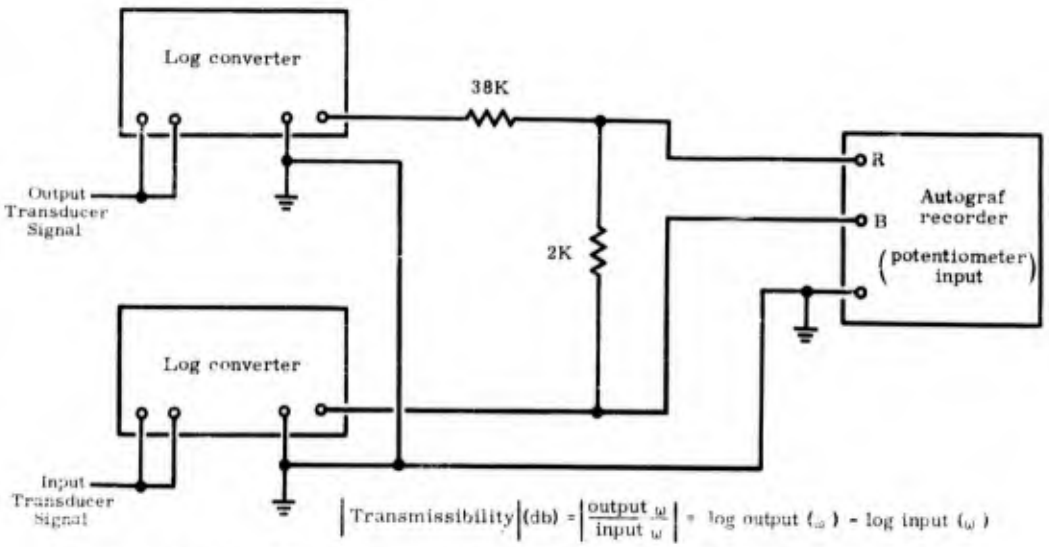

Fig. 2 - Logarithmic converters used as computing elements for performing division

transducer is called the "input" or "reference" signal. These transducers terminate into identical amplifiers which condition the signals for acceptance to the normalizing circuits. The type of signal conditioning needed depends on the transducers being used.

The normalizing circuits adjust the sensitivity of the transducers and their respective amplifiers, so that the ratio of the "output" to "input" will be unity when both transducers experience identical physical units of force.

The normalized signals are then applied to identical analyzers having narrow band-pass filters. The analyzers are made identical, by adjusting the input gain controls so that equal inputs give equal outputs. For sinusoidal testing, we have selected a 10-cycle filter, since it will adequately define resolution for most transmission testing. It is narrow enough to suppress electrical and mechanical distortions ordinarily present in the transducer outputs from approximately 15 cycles up. For resonances lower than this, it is advisable to use narrower filters. The 10-cycle filter also satisfies conditions encountered when synchronizing tape-recorded data which will be explained in greater detail later in this paper.

The frequency sweep rate of the vibration table and the analyzer sweep rate are adjusted so that specimen resonances encountered during the testing will not be blurred. This rate is determined by the Q of the structures at resonance. The sweep rates available with the Technical Products equipment used at the Martin Baltimore Division are 0.185 cps/sec^2 to 0.375 cps/sec^2 for 0 to 250 cps. These rates go up by a factor of 10 when sweeping from 0 to 2500 cps. Thus, if testing is to be performed from 10 to 500 cps, the slowest sweep rate available would be approximately 2 cps/sec^2. This rate is too fast for some resonance conditions, in which case it would be necessary to use an external drive.

The filtered signals from the analyzers are then applied to two identical logarithmic converters which produce an output proportional to the logarithm of the applied signals. Here, again, the gains of the log converters can be made identical by inserting a potentiometer at the inputs of these units or, if preferred, by considering an analyzer with its respective log converter as a unit and adjusting the over-all gain by the gain control of the analyzer. The latter method has been adopted, since it minimizes the number of adjustments to be made when operating the system.

The log converter outputs are combined into a difference network, and the resultant signal is applied to the Y-axis of the Autograf recorder. Since the two signals have been converted into logarithmic form, the difference plotted on the recorder is also in log form. The system thus plots transmissibility in decibels with an accuracy of ±1/2 db. This method offers the advantage of a greater dynamic range than can be obtained using a linear plot.

The frequency is plotted along the X-axis which is driven by a voltage obtained from a potentiometer, mounted on the frequency dial of the local oscillator.

MAGNETIC-TAPE OPERATION

It is often desirable to perform transmission testing on several points of a structure without subjecting the structure to repeated testing. With a limited number of automatic plotters, this can be accomplished by recording the raw data on magnetic tape and then reproducing this tape into the plotter. However, with sinusoidal testing, it becomes necessary that the frequency on tape be synchronized with the frequency being viewed by the analyzer at any instant of time. This synchronization is obtained by using the "speed lock" features of the tape recorder. A block diagram of the system is shown in Fig. 3.

During the recording process, the forcing frequency into the shaker is also recorded on a separate track of the tape recorder. The capstan drive is taken from the tape system's built-in precision standard 60-cycle oscillator. In the playback mode, the recorded forcing frequency is used to control the tape speed. This is accomplished by comparing the recorded forcing frequency with the reference frequency taken from the oscillator-modulator. Any difference between these frequencies will produce a voltage which changes the frequency of the capstan motor source, thus correcting the

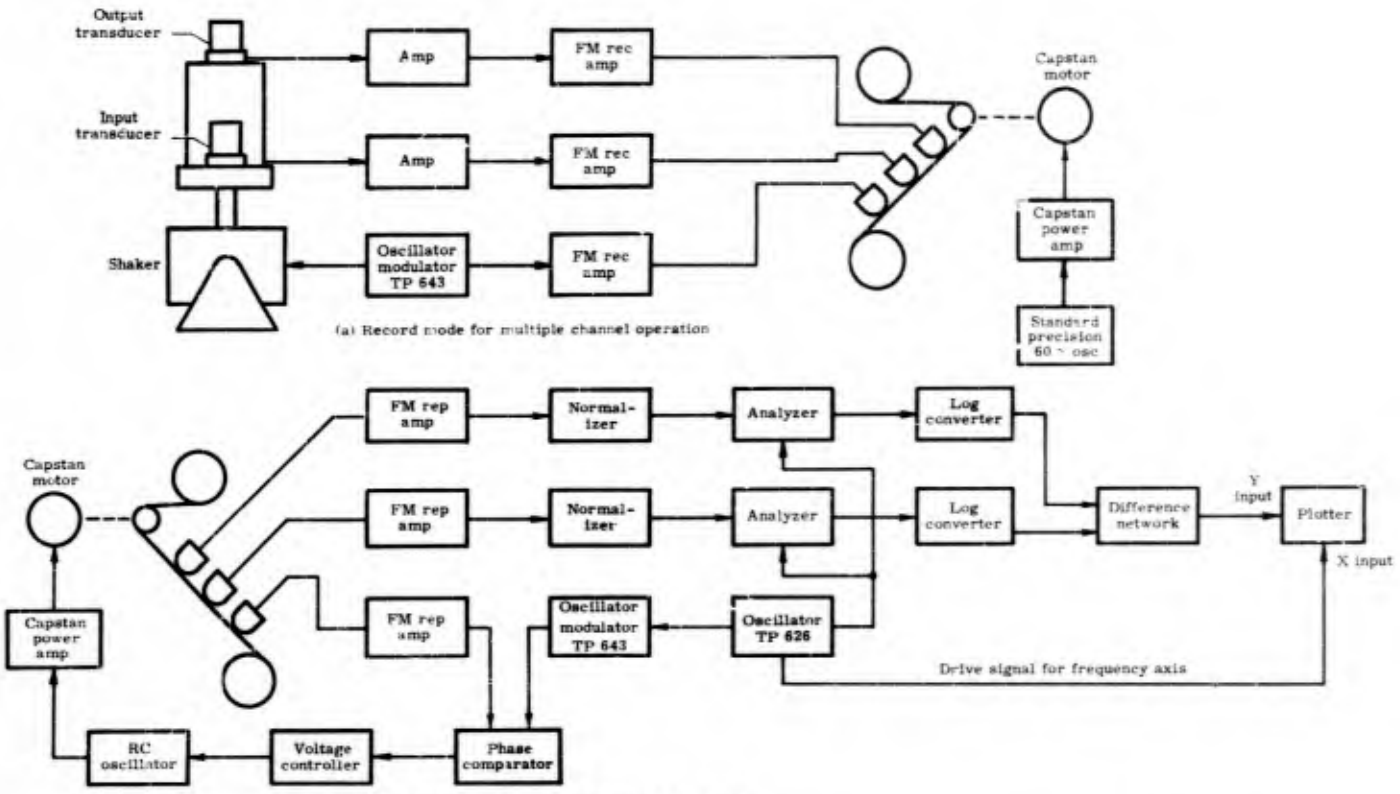

(a) Record mode for multiple channel operation

(b) Reproduce mode for multiple channel operation

Fig. 3 - Diagram of record-and-reproduce modes, using magnetic tapes for a multiple-channel system

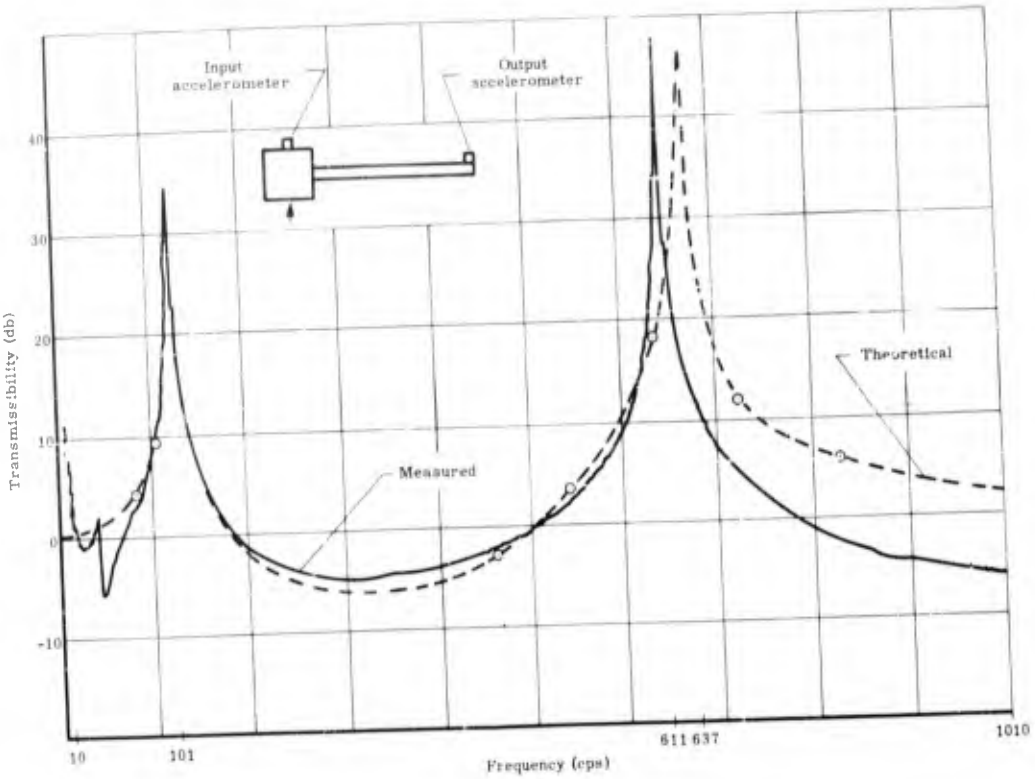

Fig. 4 - Transmissibility of a simple cantilever-beam acceleration output to acceleration input

tape speed until both frequencies are identical. The use of a 10-cycle filter in the analyzer permits analysis at the start of the playback operation until the system is synchronized. Synchronization has been maintained to greater than 500 cps.

To evaluate the performance of the transmissibility plotter, a clamped cantilever beam system was designed and fabricated as a test model. Beam dimensions were 1/2 by 1 inch wide by 12 inches long, with a 3-inch square base (Fig. 4). The beam and base were one piece of aluminum so that proper beam edge conditions could be obtained. The beam base was cemented to the shaker, and a transmissibility plot was obtained as shown in Fig. 4. The dashed curve (Fig. 4) is the theoretical transmissibility which agrees very closely with the measured results. The deviation from the measured curve in the second mode response is due to the assumptions made in the theoretical calculations. The tests do show the accuracy of the system, based on first mode calculations, and the wide dynamic range of the system.

SUMMARY

The system provides a plot of transmissibility versus frequency upon the completion of testing. This represents a considerable saving of engineering manpower. The plots are continuous, and errors due to point-to-point methods of evaluation are eliminated. As a result of the filtering, extraneous signals are rejected, and a true transmission plot is obtained for the frequencies of interest. The filtering action also makes it possible to plot transmissibility using a random input forcing function.

The use of the oscillator-modulator eliminates costly servo systems. This unit also eliminates any tracking errors, since the frequency to which the analyzer is tuned is identical to the forcing frequency applied to the shaker.

* *

Section 3

ANALYSIS AND DESIGN

RESPONSE OF A VIBRATING SYSTEM TO SEVERAL TYPES OF TIME-VARYING FREQUENCY VARIATIONS

A. V. Parker
Collins Radio Company, Cedar Rapids, Iowa

This paper presents an analysis and discussion of two types of sweep methods: the logarithmic sweep function which is used in many testing laboratories and the so-called "log-log" sweep function.

INTRODUCTION

In laboratory testing programs, it is common to use sweep testing in which the test frequency is varied continuously over the frequency range of interest. Many military vibration specifications require this method of testing. Little has been done, however, to determine the best type of frequency variation to use or the effect of using a particular type of sweep.

F. M. Lewis has analyzed the response of a system to a linear sweep, which is characterized by a constant time rate of change of frequency [1]. However, more commonly used in vibration testing laboratories today is the logarithmic sweep, which is produced by turning a logarithmically calibrated frequency control dial at a constant angular velocity.

Both the linear and logarithmic sweeps have a failing which is undesirable for sweep testing purposes. Under each of these sweeps, a piece of equipment being tested receives more significant stress reversals at resonant points of high frequency than at those of low frequency, assuming there is equal damping in each case [1]. Also, sweeping lowers the peak amplitude of the response curve, and under these two sweeps this diminuation in response is more pronounced at low-resonant frequencies than at higher resonant frequencies, again assuming equal damping on the resonant systems being compared [1]. Both of these facts result in less potential damage being administered to the equipment at low-resonant frequencies than at higher resonant frequencies; this results in the completion of the required number of test cycles on resonant frequencies at the upper range of interest before those resonant frequencies in the lower frequency range have completed sufficient testing. By the time sufficient potential damage has been administered to the resonant points at low frequency under the accelerated life testing process, failures may have occurred at the resonant points of higher frequency due to the excessive potential damage administered at those frequencies. A suggested solution to this problem is the use of the so-called "log-log" sweep [2].*

The log-log sweep provides an equal number of stress reversals between the half-power points of all resonant systems with equal damping. It will also be shown that under the log-log

*The log-log sweep is so named because it is generated by turning a frequency control dial calibrated on a log-log scale at a constant angular velocity.

sweep, the diminution in amplitude of vibration due to sweeping is independent of the frequency at which resonance occurs. This paper analyzes and discusses the properties of the logarithmic and log-log sweeps and presents mathematical solutions for the equations of motion; these solutions are presented in the form of transmissibility envelopes. The mathematical model used in the analysis is the simple linear oscillator. Response curves, generated from these solutions, should be useful to engineers in applying the methods of accelerated life testing to sweep tests using these sweep functions.

THE LOG-LOG SWEEP

Consider the differential equation for the forced vibration of a simple linear harmonic oscillator

$$m\ddot{x} + c\dot{x} + Kx = P_o \cos F(t) \tag{1}$$

where m is the mass, with damping coefficient c, which is attached to a spring with constant K. P_o is the amplitude factor on the driving function $\cos F(t)$, and x is the displacement of the mass measured from the relaxed position of the spring.

The present problem, as outlined in the introduction, consists in finding and studying the sweep function $F(t)$ which provides an equal number of cycles between frequencies corresponding to equiamplitude points on the response curve independent of the natural frequency.

For example, if an equipment has resonances at 50 and 250 cps, the function $F(t)$ should generate the same number of cycles between the response curve's half-amplitude frequencies (about 50 cps) as it does between the half-amplitude frequencies (about 250 cps), provided damping is the same in each case (Fig 1).

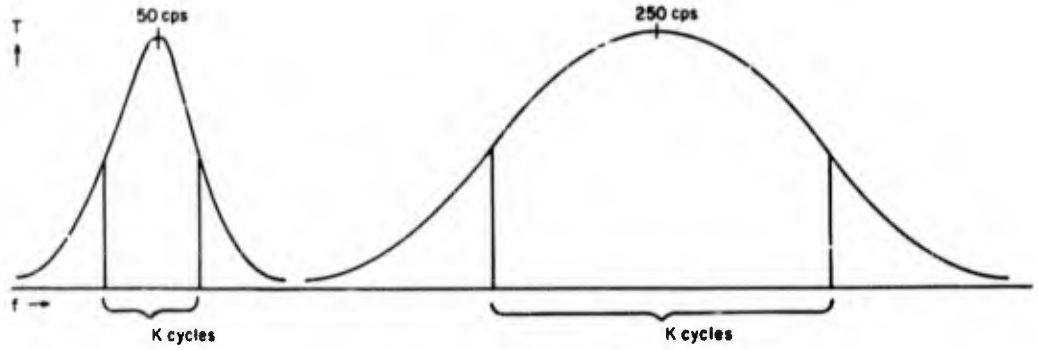

Fig. 1 - Response curves of an equipment having resonances at 50 and 250 cps

It should be kept in mind from the beginning that when the response curve is referred to, what is actually involved is the envelope of the response curve. Maximum response acceleration during a cycle is the desired quantity which permits analysis of the damage due to the cycle, so it is only the acceleration (or displacement) peaks which are of interest. The common method of presenting the response curve is as a plot of transmissibility versus the ratio of driver frequency to natural frequency. Transmissibility is defined as the ratio of transmitted force to applied force. Hence, in the present problem involving the simple linear oscillator, transmissibility is written as

$$T = \sqrt{\frac{(Kx_e)^2 + (c\dot{x}_e)^2}{P_o}}$$

where x_e is the envelope value of x and $\dot{x}_e$ is the envelope value of $\dot{x}$.

Now consider two simple linear oscillators, the first having a natural frequency ω_n and the second having a natural frequency $a\omega_n$ where $a > 1$. Both systems have equal damping. Under frequency dwelling the response curve can be written as

$$T = \sqrt{\frac{1 + \left(2\xi \frac{\omega}{\omega_n}\right)^2}{\left(1 - \left(\frac{\omega}{\omega_n}\right)^2\right)^2 + \left(2\xi \frac{\omega}{\omega_n}\right)^2}}$$

where $\xi = c/c_c$. The quantity $a\omega_n$ replaces ω_n in the expression for the second oscillator. Let H represent the fraction of maximum T where the equiamplitude points are chosen on the response curves. From the expression (just presented) for the response curve, the expression

$$\omega^2 = \frac{\omega_n^2 \left\{2\xi^2(1 - [HT_{max}]^2) + [HT_{max}]^2\right\}}{[HT_{max}]^2} \pm \frac{\omega_n^2 \sqrt{4\xi^4(1 - [HT_{max}]^2)^2 + 4\xi^2[HT_{max}]^2(1 - [HT_{max}]^2) + [HT_{max}]^2}}{[HT_{max}]^2} \qquad (2)$$

is obtained which gives the frequencies about ω_n which correspond to the equiamplitude points which have been chosen on the response curve. The smaller of the two values will be referred to as $\omega_n - \Delta\omega_1$, and the larger will be called $\omega_n + \Delta\omega_2$. By substitution of $a\omega_n$ into Eq. (2) in place of ω_n, the corresponding pair of frequencies associated with $a\omega_n$ are obtained. In this case, the smaller will be called $a\omega_n - \Delta\omega_1'$, and the larger will be called $a\omega_n + \Delta\omega_2'$ (Fig. 2).

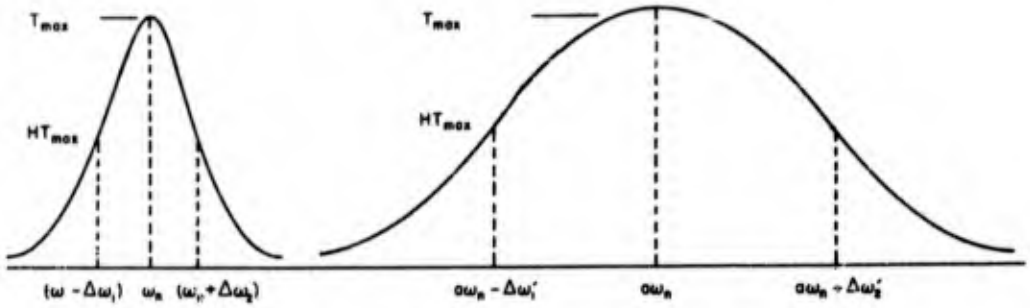

Fig. 2 - Response curves of two simple linear oscillators

From Eq. (2) it follows that

$$(a\omega_n + \Delta\omega_2')^2 = a^2(\omega_n + \Delta\omega_2)^2$$

and

$$(a\omega_n - \Delta\omega_1')^2 = a^2(\omega_n - \Delta\omega_1)^2 .$$

This leads to

$$\Delta\omega_2' = a\Delta\omega_2$$

and

$$\Delta\omega_1' = a\Delta\omega_1 .$$

Thus the condition on the sweep function $F(t)$ can be written as

$$F\left(G\left(a[\omega_n + \Delta\omega_2]\right)\right) - F\left(G\left(a[\omega_n - \Delta\omega_1]\right)\right) = F\left(G\left([\omega_n + \Delta\omega_2]\right)\right) - F\left(G\left([\omega_n - \Delta\omega_1]\right)\right), \tag{3}$$

where $t = G(\omega)$. This is true because $F(t)$ is the angle which the argument of the driving function has passed through from time zero to time t. $F(t)/2\pi$ is then the number of cycles which have occurred between time zero and time t, provided $F(t)$ is expressed in radians. If ω_i represents initial frequency at time zero, $F(G(\omega_i)) = 0$.

Crede and Lunny [2] state without proof that the condition of Eq. (3) is satisfied if

$$h = c\omega^2, \tag{4}$$

where h is the rate of change of driver frequency with respect to time, and c is a constant. The letter h will be referred to as the sweep rate, $F(t)$ will be called the sweep function, and c is the sweep constant. For increasing frequency $c > 0$, and for decreasing frequency $c < 0$.

Now what kind of sweep function is obtained as a result of the hypothesized sweep rate? Since $\partial F(t)/\partial t = \omega$, Eq. (4) is integrated twice to give

$$-\frac{1}{c\omega} = t + a_o \tag{5}$$

and then

$$F(t) = -\frac{1}{c} \ln (-ca_o - ct) + a_1 \tag{6}$$

where a_o and a_1 are constants to be evaluated. Substituting zero into Eq. (5) for t, it is seen that

$$a_o = -\frac{1}{c\omega_i}.$$

Then

$$F(t) = -\frac{1}{c} \ln (1 - c\omega_i t) + \frac{1}{c} \ln \omega_i + a_1.$$

The expression $(1/c) \ln \omega_i + a_1$ is merely the phase angle of the driver which will be called σ. The resulting sweep function is then

$$F(t) = -\frac{1}{c} \ln (1 - c\omega_i t) + \sigma. \tag{7}$$

It will now be shown that this sweep function does indeed possess the property described by Eq. (3), even though the analysis used in its development was based on the response curve associated with frequency dwelling. Differentiating Eq. (6) with respect to time,

$$\frac{\partial F(t)}{\partial t} = \omega = \frac{\omega_i}{1 - c\omega_i t}. \tag{8}$$

Solving Eq. (8) for t results in

$$t = G(\omega) = \frac{1}{c}\left[\frac{1}{\omega_i} - \frac{1}{\omega}\right]. \tag{9}$$

Let t_1 and t_2 be the times at which the driving function attains the instantaneous frequencies $\omega_n - \Delta\omega_1$, and $\omega_n + \Delta\omega_2$, respectively. Likewise let t_1' and t_2' be the times at which the driving function attains the instantaneous frequencies $a[\omega_n - \Delta\omega_1]$ and $a[\omega_n + \Delta\omega_2]$, respectively. Then a necessary and sufficient condition that $F(t)$ satisfies Eq. (3) is that

$$F(t_2) - F(t_1) = F(t_2') - F(t_1') . \tag{10}$$

Substituting into Eq. (10) results in

$$F(t_2) - F(t_1) = -\frac{1}{c} \ln \frac{\omega_i}{\omega_n + \Delta\omega_2} + \frac{1}{c} \ln \frac{\omega_i}{\omega_n - \Delta\omega_1} = \frac{1}{c} \ln \frac{\omega_n - \Delta\omega_1}{\omega_n + \Delta\omega_2}$$

$$= -\frac{1}{c} \ln \frac{\omega_i}{a[\omega_n + \Delta\omega_2]} + \frac{1}{c} \ln \frac{\omega_i}{a[\omega_n - \Delta\omega_1]} = F(t_2') - F(t_1') .$$

Thus the conjecture is established.

This sweep function $F(t)$ has come to be called the log-log function [2]. It is desirable to know if the log-log sweep function shares the property expressed in Eq. (3) with any other possible sweep function. It is conceivable that if another sweep function possesses this property, it may be easier to handle analytically. Assume $\tilde{F}(t)$ is such a function. Then

$$\tilde{F}(t_2) - \tilde{F}(t_1) = \tilde{F}(t_2') - \tilde{F}(t_1') \tag{11}$$

where the subscripted t's have the same significance as before. Also $\tilde{F}(0) = 0$ and $dF(t)/dt = \omega$, since $\tilde{F}(t)$ is a sweep function. Substituting $t_1 = 0$, and expressing time in terms of frequency in Eq. (11), results in

$$\tilde{F}\left(\frac{1}{c}\left[\frac{1}{\omega_i} - \frac{1}{\omega_n + \Delta\omega_2}\right]\right) = \tilde{F}\left(\frac{1}{c}\left[\frac{1}{\omega_i} - \frac{1}{a(\omega_n + \Delta\omega_2)}\right]\right) - \tilde{F}\left(\frac{1}{c}\left[\frac{1}{\omega_i} - \frac{1}{a\omega_i}\right]\right) . \tag{12}$$

Differentiating Eq. (12) with respect to $\omega_n + \Delta\omega_2$, and then with respect to a, results in

$$a\tilde{F}'\left(\frac{1}{c}\left[\frac{1}{\omega_i} - \frac{1}{a(\omega_n + \Delta\omega_2)}\right]\right) - \tilde{F}'\left(\frac{1}{c}\left[\frac{1}{\omega_i} - \frac{1}{a(\omega_n + \Delta\omega_2)}\right]\right) = 0 \tag{13}$$

and

$$\omega_i\tilde{F}'\left(\frac{1}{c}\left[\frac{1}{\omega_i} - \frac{1}{a(\omega_n + \Delta\omega_2)}\right]\right) - (\omega_n + \Delta\omega_2)\tilde{F}'\left(\frac{1}{c}\left[\frac{1}{\omega_i} - \frac{1}{a\omega_i}\right]\right) = 0 . \tag{14}$$

It follows from Eqs. (13) and (14) that

$$\frac{1}{\omega_n + \Delta\omega_2}\tilde{F}'\left(\frac{1}{c}\left[\frac{1}{\omega_i} - \frac{1}{\omega_n + \Delta\omega_2}\right]\right) = \frac{1}{a\omega_i}\tilde{F}'\left(\frac{1}{c}\left[\frac{1}{\omega_i} - \frac{1}{a\omega_i}\right]\right) . \tag{15}$$

Since the right-hand member of Eq. (15) is independent of $\omega_n + \Delta\omega_2$ and the left-hand member is independent of a, it is true that

$$\tilde{F}'\left(\frac{1}{c}\left[\frac{1}{\omega_i} - \frac{1}{\omega_n + \Delta\omega_2}\right]\right) = (\text{constant } c)\,(\omega_n + \Delta\omega_2) . \tag{16}$$

Since $\omega_n + \Delta\omega_2$ can have any positive value, it may as well be replaced by ω. Integrating the resulting equation with respect to $1/\omega$,

$$\tilde{F}\left(\frac{1}{c}\left[\frac{1}{\omega_i} - \frac{1}{\omega}\right]\right) = -(\text{constant } c) \ln \frac{1}{\omega} + (\text{constant } K) . \tag{17}$$

Letting $\omega = \omega_i$ in Eq. (17), it is seen that

$$\tilde{F}(0) = 0 = -(\text{constant } c) \ln \frac{1}{\omega_i} + (\text{constant } K) .$$

Thus

$$\tilde{F}\left(\frac{1}{c}\left[\frac{1}{\omega_i} - \frac{1}{\omega}\right]\right) = \tilde{F}(t) = (\text{constant } c) \ln \frac{\omega}{\omega_i} . \tag{18}$$

Differentiating Eq. (18) results in

$$\frac{d\tilde{F}}{dt} = \omega = (\text{constant } c)\,\frac{\omega_i}{\omega}\,\frac{d\omega}{dt}.$$

Calling the constant in the previous equation $1/c$ results in $h = c\omega^2$, which is known to generate the log-log sweep function. Thus $\tilde{F}(t) = F(t)$ and the uniqueness of $F(t)$ is established.

It is interesting to note that since $\omega = \omega_i/(1-c\omega_i t)$ becomes unbounded as $c\omega_i t \to 1$, the product $c\omega$ sets not only a practical but an absolute limit to the time consumed by a single sweep.

Now, the response curve will be found for a simple linear oscillator excited by a log-log sweeping function. In order to find the transmissibility envelope, the envelopes of the displacement and velocity of the oscillator must be found. This is done by solving the differential equation resulting from the substitution of Eq. (7) into Eq. (1). This results in

$$m\ddot{x} + c\dot{x} + Kx = P_o \cos\left[-\frac{1}{c}\ln(1 - c\omega_i t) + \sigma\right]. \tag{19}$$

The auxiliary solution to this equation is neglected since it represents only transient response which will soon die out under damping. Before finding the particular solution, Eq. (19) is put in a more convenient form by dividing through by m. This results in

$$\ddot{x} + 2n\dot{x} + \omega_n^2 x = \frac{P_o}{m}\cos\left[-\frac{1}{c}\ln(1 - c\omega_i t) + \sigma\right], \tag{20}$$

where

$$2n = 2\xi\,\omega_n = \frac{c}{m} \quad \text{and} \quad \omega_n^2 = \frac{K}{m}.$$

By the usual method of operators a particular solution

$$x = \frac{P_o}{m(\alpha - \beta)}\left\{\epsilon^{\alpha t}\int_0^t \cos F(t)\,\epsilon^{-\alpha t}\,dt - \epsilon^{\beta t}\int_0^t \cos F(t)\,\epsilon^{-\beta t}\,dt\right\} \tag{21}$$

is obtained where $\alpha = -n + i\tilde{\omega}$ and $\beta = -n - i\tilde{\omega}$. ω_n is the usual damped natural frequency $\omega_n\sqrt{1-\xi^2}$.

Rewriting Eq. (21) results in

$$\begin{aligned} x = \frac{\epsilon^{-nt} P_o}{\tilde{\omega} m}\Bigg\{ & \sin\tilde{\omega}t\cos\sigma\int_0^t \cos\left[\ln Z^{\frac{1}{c}}\right]\epsilon^{nt}\cos\tilde{\omega}t\,dt \\ & + \sin\tilde{\omega}t\sin\sigma\int_0^t \sin\left[\ln Z^{\frac{1}{c}}\right]\epsilon^{nt}\cos\tilde{\omega}t\,dt \\ & - \cos\tilde{\omega}t\cos\sigma\int_0^t \cos\left[\ln Z^{\frac{1}{c}}\right]\epsilon^{nt}\sin\tilde{\omega}t\,dt \\ & - \cos\tilde{\omega}t\sin\sigma\int_0^t \sin\left[\ln Z^{\frac{1}{c}}\right]\epsilon^{nt}\sin\tilde{\omega}t\,dt\Bigg\} \end{aligned}$$

where

$$Z = (1 - c\omega_i t) = \frac{\omega_i}{\omega}. \tag{22}$$

In order to obtain the envelope of x it is necessary to find the phase angle σ which extremalizes x and substitute it into Eq. (22) to give x_e. That phase angle is obtained by solving the equation, $\partial x/\partial \sigma = 0$, for σ.

This results in

$$\sigma = \tan^{-1}\left\{\frac{\theta_4 \cos \tilde{\omega}t - \theta_2 \sin \tilde{\omega}t}{\theta_3 \cos \tilde{\omega}t - \theta_1 \sin \tilde{\omega}t}\right\} \tag{23}$$

where

$$\theta_1 = \int_0^t \cos\left[\ln Z^{\frac{1}{c}}\right] \epsilon^{nt} \cos \tilde{\omega}t \, dt$$

$$\theta_2 = \int_0^t \sin\left[\ln Z^{\frac{1}{c}}\right] \epsilon^{nt} \cos \tilde{\omega}t \, dt$$

$$\theta_3 = \int_0^t \cos\left[\ln Z^{\frac{1}{c}}\right] \epsilon^{nt} \sin \tilde{\omega}t \, dt$$

and

$$\theta_4 = \int_0^t \sin\left[\ln Z^{\frac{1}{c}}\right] \epsilon^{nt} \sin \tilde{\omega}t \, dt .$$

Rewriting Eq. (22) in terms of θ's gives

$$x = \frac{\epsilon^{-nt} P_o}{\tilde{\omega}m}\left\{\theta_1 \sin \tilde{\omega}t - \theta_3 \cos \tilde{\omega}t\right\} \cos \sigma + \frac{\epsilon^{-nt} P_o}{\tilde{\omega}m}\left\{\theta_2 \sin \tilde{\omega}t - \theta_4 \cos \tilde{\omega}t\right\} \sin \sigma . \tag{24}$$

Substituting σ from Eq. (23) into Eq. (24) gives

$$x_e = \frac{\epsilon^{-nt} P_o}{\tilde{\omega}m} \sqrt{\phi_1^2 + \phi_2^2} \tag{25}$$

where $\phi_1 = \theta_4 \cos \tilde{\omega}t - \theta_2 \sin \tilde{\omega}t$ and $\phi_2 = \theta_3 \cos \tilde{\omega}t - \theta_1 \sin \tilde{\omega}t$.

Next, the velocity envelope of the oscillator must be found. First, Eq. (22) is differentiated with respect to time to obtain

$$\begin{aligned}\frac{dx}{dt} = \dot{x} = -nx + \frac{P_o \epsilon^{-nt}}{m}\Bigg\{&\cos \tilde{\omega}t \cos \sigma \int_0^t \cos\left(\ln Z^{\frac{1}{c}}\right) \epsilon^{nt} \cos \tilde{\omega}t \, dt \\ &+ \cos \tilde{\omega}t \sin \sigma \int_0^t \sin\left(\ln Z^{\frac{1}{c}}\right) \epsilon^{nt} \cos \tilde{\omega}t \, dt \\ &+ \sin \tilde{\omega}t \cos \sigma \int_0^t \cos\left(\ln Z^{\frac{1}{c}}\right) \epsilon^{nt} \sin \tilde{\omega}t \, dt \\ &+ \sin \tilde{\omega}t \sin \sigma \int_0^t \sin\left(\ln Z^{\frac{1}{c}}\right) \epsilon^{nt} \sin \tilde{\omega}t \, dt\Bigg\} .\end{aligned} \tag{26}$$

It is then necessary to find the phase angle σ which extremalizes $\dot{x}$ and substitute it into Eq. (26) to solve for $\dot{x}_e$. That phase angle is obtained by solving the equation, $\partial\dot{x}/\partial\sigma = 0$, for σ. Substituting the result in Eq. (26) results in

$$\dot{x}_e = \frac{P_o \epsilon^{-nt}}{m} \sqrt{\psi_1^2 + \psi_2^2} \tag{27}$$

where

$$\psi_1 = \left(\frac{n \sin \tilde{\omega}t}{\tilde{\omega}} - \cos \tilde{\omega}t\right) \theta_2 - \left(\frac{n \cos \tilde{\omega}t}{\tilde{\omega}} + \sin \tilde{\omega}t\right) \theta_4$$

and

$$\psi_2 = \left(\frac{n \sin \tilde{\omega}t}{\tilde{\omega}} - \cos \tilde{\omega}t\right) \theta_1 - \left(\frac{n \cos \tilde{\omega}t}{\tilde{\omega}} + \sin \tilde{\omega}t\right) \theta_3 .$$

Recalling that

$$T = \sqrt{\frac{(Kx_e)^2 + (c\dot{x}_e)^2}{P_o}}$$

it is now seen that the response curve may be written as

$$T = \sqrt{\frac{1}{(1 - \xi^2)} (\phi_1^2 + \phi_2^2) + 4\xi^2(\psi_1^2 + \psi_2^2)}\ \omega_n \epsilon^{-nt} . \tag{28}$$

The only remaining problem in the computation of the response curve is the evaluation of the θ integrals. These integrals are oscillatory integrals and extremely impractical to solve by numerical integration techniques. For example, consider θ_1. In most cases of practical interest $\tilde{\omega}$ will be 30 radians per second or larger; and in a great many cases, it will be one to three orders of magnitude larger than that. Thus the factor, $\cos \tilde{\omega}t$, oscillates rapidly about the t axis as t increases. In many vibration testing programs, t runs over 400 seconds. Furthermore, the sweep constant c would necessarily be smaller than 10^{-4}(1/radians) to fulfill many of the government specifications for vibration testing. Thus the integrand factor, $\cos [(1/c) \ln (1 - c\omega_i t)]$, would also oscillate rapidly as t increased. Therefore, a plot of the integrand function would include thousands of peaks and troughs of nearly equal size. Summation of the area under the plot of the integrand function by numerical integration techniques would consequently involve taking extremely small incremental steps to insure that all accuracy wasn't lost. Another complication arises due to the fact that even the larger high-speed digital computers now in use have a floating-point word size of only 9-decimal digit capacity or less. It would be necessary to resort to multiple precision programming, in order to compute the integrand factor ϵ^{nt} with sufficient precision to maintain any accuracy in the final answer. This, too, would slow down the computing process greatly. Considering the fact that θ_1 is only one of four such θ integrals, it becomes apparent that this approach to the solution for the many variations of damping and sweep constant which will be desired is inconceivably time consuming and expensive.

In this light, a series solution approach was taken. First, the θ integrals were written entirely in terms of the variable Z. This resulted in

$$\theta_1 = \int_0^t \cos \left[\ln Z^{\frac{1}{c}}\right] \epsilon^{nt} \cos \tilde{\omega}t\ dt$$

$$= \frac{\epsilon^{\frac{n}{c\omega_i}} \cos \frac{\tilde{\omega}}{c\omega_i}}{(-c\omega_i)} \int_1^e \cos \left(\ln Z^{\frac{1}{c}}\right) \epsilon^{\frac{-nz}{c\omega_i}} \cos \frac{\tilde{\omega}z}{c\omega_i}\ dZ + \frac{\epsilon^{\frac{n}{c\omega_i}} \sin \frac{\tilde{\omega}}{c\omega_i}}{(-c\omega_i)} \int_1^e \cos \left(\ln Z^{\frac{1}{c}}\right) \epsilon^{\frac{-nz}{c\omega_i}} \sin \frac{\tilde{\omega}z}{c\omega_i}\ dZ , \tag{29}$$

$$\theta_2 = \int_0^t \sin\left[\ln Z^{\frac{1}{c}}\right] \epsilon^{nt} \cos \tilde{\omega} t \, dt$$

$$= \frac{\epsilon^{\frac{n}{c\omega_i}} \cos \frac{\tilde{\omega}}{c\omega_i}}{(-c\omega_i)} \int_1^z \sin\left(\ln Z^{\frac{1}{c}}\right) \epsilon^{\frac{-nz}{c\omega_i}} \cos \frac{\tilde{\omega} z}{c\omega_i} \, dZ$$

$$+ \frac{\epsilon^{\frac{n}{c\omega_i}} \sin \frac{\tilde{\omega}}{c\omega_i}}{(-c\omega_i)} \int_1^z \sin\left(\ln Z^{\frac{1}{c}}\right) \epsilon^{\frac{-nz}{c\omega_i}} \sin \frac{\tilde{\omega} z}{c\omega_i} \, dZ. \qquad (30)$$

$$\theta_3 = \int_0^t \cos\left[\ln Z^{\frac{1}{c}}\right] \epsilon^{nt} \sin \tilde{\omega} t \, dt$$

$$= \frac{\epsilon^{\frac{n}{c\omega_i}} \sin \frac{\tilde{\omega}}{c\omega_i}}{(-c\omega_i)} \int_1^z \cos\left(\ln Z^{\frac{1}{c}}\right) \epsilon^{\frac{-nz}{c\omega_i}} \cos \frac{\tilde{\omega} z}{c\omega_i} \, dZ$$

$$- \frac{\epsilon^{\frac{n}{c\omega_i}} \cos \frac{\tilde{\omega}}{c\omega_i}}{(-c\omega_i)} \int_1^z \cos\left(\ln Z^{\frac{1}{c}}\right) \epsilon^{\frac{-nz}{c\omega_i}} \sin \frac{\tilde{\omega} z}{c\omega_i} \, dZ. \qquad (31)$$

and

$$\theta_4 = \int_0^t \sin\left[\ln Z^{\frac{1}{c}}\right] \epsilon^{nt} \sin \tilde{\omega} t \, dt$$

$$= \frac{\epsilon^{\frac{n}{c\omega_i}} \sin \frac{\tilde{\omega}}{c\omega_i}}{(-c\omega_i)} \int_1^z \sin\left(\ln Z^{\frac{1}{c}}\right) \epsilon^{\frac{-nz}{c\omega_i}} \cos \frac{\tilde{\omega} z}{c\omega_i} \, dZ$$

$$- \frac{\epsilon^{\frac{n}{c\omega_i}} \cos \frac{\tilde{\omega}}{c\omega_i}}{(-c\omega_i)} \int_1^z \sin\left(\ln Z^{\frac{1}{c}}\right) \epsilon^{\frac{-nz}{c\omega_i}} \sin \frac{\tilde{\omega} z}{c\omega_i} \, dZ. \qquad (32)$$

For purposes of handling, it was convenient to code $-n/c\omega_i$ as b_1 and $\tilde{\omega}/c\omega_i$ as b_2. Each of the integrands in the integrals in Z was then put in the form of a power series which was integrated to give an infinite series solution to the integral. Thus,

$$\int \cos\left[\ln Z^{\frac{1}{c}}\right] \epsilon^{b_1 z} \sin b_2 Z \, dZ = \frac{1}{2i} \int \cos\left[\ln Z^{\frac{1}{c}}\right] \left\{\epsilon^{(b_1+ib_2)z} - \epsilon^{(b_1+ib_2)z}\right\} dZ$$

$$= \frac{1}{2i} \int \cos\left[\ln Z^{\frac{1}{c}}\right] \sum_{K=0}^{\infty} \frac{Z^K}{K!} \left[(b_1 + ib_2)^K - (b_1 - ib_2)^K\right] dZ$$

$$= \frac{1}{2i} \int \cos\left[\ln Z^{\frac{1}{c}}\right] \sum_{K=0}^{\infty} \frac{Z^K r^K}{K!} \left[\frac{\epsilon^{iK\theta} - \epsilon^{-iK\theta}}{2i}\right] dZ$$

$$= \int \cos\left[\ln Z^{\frac{1}{c}}\right] \sum_{K=0}^{\infty} \frac{Z^K r^K \sin K\theta}{K!} \, dZ$$

$$= \frac{1}{2} \int \left(Z^{\frac{i}{c}} + Z^{-\frac{1}{c}}\right) \sum_{K=0}^{\infty} \frac{Z^K r^K \sin K\theta}{K!} \, dZ \qquad (33)$$

(Continued)

$$= \frac{1}{2}\sum_{K=0}^{\infty} \frac{r^K \sin K}{K!} \int \left(Z^{K+\frac{i}{c}} + Z^{K-\frac{i}{c}} \right) dZ$$

$$= \frac{1}{2}\sum_{K=0}^{\infty} \frac{r^K Z^{K+1} \sin K\theta}{K!} \left[\frac{Z^{\frac{i}{c}}}{K+1+\frac{i}{c}} + \frac{Z^{-\frac{i}{c}}}{K+1-\frac{i}{c}} \right]$$

$$= \frac{1}{2}\sum_{K=0}^{\infty} \frac{r^K Z^{K+1} \sin K\theta}{K!} \left[\frac{(K+1)\left(Z^{\frac{i}{c}} + Z^{-\frac{i}{c}}\right) - \frac{i}{c}\left(Z^{\frac{i}{c}} - Z^{-\frac{i}{c}}\right)}{(K+1)^2 + \left(\frac{1}{c}\right)^2} \right]$$

$$= \sum_{K=0}^{\infty} \frac{r^K Z^{K+1} \sin K\theta}{K!} \left[\frac{(K+1)\cos\left(\ln Z^{\frac{1}{c}}\right) + \frac{1}{c}\sin\left(\ln Z^{\frac{1}{c}}\right)}{(K+1)^2 + \left(\frac{1}{c}\right)^2} \right] \quad (33)$$

where $r = \sqrt{b_1^2 + b_2^2}$ and $\theta = \tan^{-1}(b_2/b_1)$.

In the same manner,

$$\int \cos\left(\ln Z^{\frac{1}{c}}\right) \epsilon^{b_1 Z} \cos b_2 Z \, dZ = \sum_{K=0}^{\infty} \frac{r^K Z^{K+1} \cos K\theta}{K!} \left[\frac{(K+1)\cos\left(\ln Z^{\frac{1}{c}}\right) + \frac{1}{c}\sin\left(\ln Z^{\frac{1}{c}}\right)}{(K+1)^2 + \left(\frac{1}{c}\right)^2} \right], \quad (34)$$

$$\int \sin\left(\ln Z^{\frac{1}{c}}\right) \epsilon^{b_1 Z} \sin b_2 Z \, dZ = \sum_{K=0}^{\infty} \frac{r^K Z^{K+1} \sin K\theta}{K!} \left[\frac{(K+1)\sin\left(\ln Z^{\frac{1}{c}}\right) - \frac{1}{c}\cos\left(\ln Z^{\frac{1}{c}}\right)}{(K+1)^2 + \left(\frac{1}{c}\right)^2} \right] \quad (35)$$

and

$$\int \sin\left(\ln Z^{\frac{1}{c}}\right) \epsilon^{b_1 Z} \cos b_2 Z \, dZ = \sum_{K=0}^{\infty} \frac{r^K Z^{K+1} \cos K\theta}{K!} \left[\frac{(K+1)\sin\left(\ln Z^{\frac{1}{c}}\right) - \frac{1}{c}\cos\left(\ln Z^{\frac{1}{c}}\right)}{(K+1)^2 + \left(\frac{1}{c}\right)^2} \right]. \quad (36)$$

The summation of the resulting series is also a formidable computational job. The factorial term in each denominator insures absolute convergence, but in most cases rZ will be of the order of magnitude of 10^4 or larger, and it would be necessary to sum tens of thousands of terms in each series before suitable accuracy of the final result was insured. And, as in the case of the θ integrals, it would be necessary to use multiple precision programming techniques in order to maintain accuracy when differencing two very large numbers of nearly equal size.

The solution to this enigma is obtained by rearranging the series in a form more tractable for computational purposes. Consider the integral

$$\int \cos\left[\ln Z^{\frac{1}{c}}\right] \epsilon^{b_1 Z} \sin b_2 Z \, dZ .$$

It was shown earlier that

$$\int \cos\left[\ln Z^{\frac{1}{c}}\right] \epsilon^{b_1 Z} \sin b_2 Z \, dZ = \frac{1}{2}\sum_{K=0}^{\infty} \frac{r^K Z^{K+1} \sin K\theta}{K!} \left[\frac{Z^{\frac{i}{c}}}{K+1+\frac{i}{c}} + \frac{Z^{-\frac{i}{c}}}{K+1-\frac{i}{c}} \right].$$

The recursion relation

$$\left(1 + n \pm \frac{i}{c}\right)\sum_{K=0}^{\infty} \frac{(rZ)^K \sin (K+n)\theta}{K!}\left(\frac{1}{K+n+1 \pm \frac{i}{c}}\right) = \epsilon^{rZ\cos\theta} \sin (rZ \sin\theta + n\theta)$$

$$- rZ \sum_{K=0}^{\infty} \frac{(rZ)^K \sin (K+n+1)\theta}{K!}\left(\frac{1}{K+n+2 \pm \frac{i}{c}}\right)$$

is used to rewrite the integral as

$$\int \cos\left[\ln Z^{\frac{1}{c}}\right] \epsilon^{b_1 Z} \sin b_2 Z \, dZ$$

$$= Zc\epsilon^{rZ\cos\theta}\left\{\sin (rZ\sin\theta)\cos\left(\ln Z^{\frac{1}{c}}\right)\sum_{K=0}^{\infty}\frac{\cos K\theta\left(-\frac{\omega_n}{\omega}\right)^K \cos\left(\sum_{j=1}^{K+1}\tan^{-1}\frac{1}{cj}\right)}{\prod_{j=1}^{K+1}\sqrt{j^2c^2+1}}\right.$$

$$+ \sin (rZ\sin\theta)\sin\left(\ln Z^{\frac{1}{c}}\right)\sum_{K=0}^{\infty}\frac{\cos K\theta\left(-\frac{\omega_n}{\omega}\right)^K \sin\left(\sum_{j=1}^{K+1}\tan^{-1}\frac{1}{cj}\right)}{\prod_{j=1}^{K+1}\sqrt{j^2c^2+1}}$$

$$+ \cos (rZ\sin\theta)\cos\left(\ln Z^{\frac{1}{c}}\right)\sum_{K=0}^{\infty}\frac{\sin K\theta\left(-\frac{\omega_n}{\omega}\right)^K \cos\left(\sum_{j=1}^{K+1}\tan^{-1}\frac{1}{cj}\right)}{\prod_{j=1}^{K+1}\sqrt{j^2c^2+1}}$$

$$\left. + \cos (rZ\sin\theta)\sin\left(\ln Z^{\frac{1}{c}}\right)\sum_{K=0}^{\infty}\frac{\sin K\theta\left(-\frac{\omega_n}{\omega}\right)^K \sin\left(\sum_{j=1}^{K+1}\tan^{-1}\frac{1}{cj}\right)}{\prod_{j=1}^{K+1}\sqrt{j^2c^2+1}}\right\}.$$

Note that $crZ = \omega_n/\omega$.

The details of this computation and the results for the other integrals have been completed by the author, along with curves generated from these results. For values of $\omega_n/\omega \leq 1$, the new series converge relatively rapidly. For $\omega_n/\omega < 1$, asymptotic expansions were obtained. It will be noted that

$$\sum_{K=0}^{\infty} \frac{r^K Z^{K+1} \sin K\theta}{K!}\,\frac{Z^{\frac{i}{c}}}{K+1+\frac{i}{c}} = \int \sum_{K=0}^{\infty}\frac{r^K Z^K \sin K\theta}{K!} Z^{\frac{i}{c}}\, dZ$$

$$= \int Z^{\frac{i}{c}} \sum_{K=0}^{\infty}\frac{(rZ)^K \sin K\theta}{K!}\, dZ = \int Z^{\frac{i}{c}}\left[\frac{\epsilon^{rZc\,i\theta} - \epsilon^{rZ\cdot i\theta}}{2i}\right] dZ . \qquad (37)$$

The final expression was integrated by parts using the relation

$$\int x^b \epsilon^{ax} dx = \frac{x^b \epsilon^{ax}}{a} - \frac{b}{a}\int x^{b-1}\epsilon^{ax} dx$$

to obtain a power series in $(rZ)^{-1}$. While the resulting series are divergent, the error in the K^{th} partial sum is quite small if K is chosen properly. This may be seen by examining the remainder integral after K integration by parts. It has the form

$$\frac{(-1)^K \prod_{j=1}^{K} (b+1-j)}{a^{K+1}} \int x^{b-K} e^{ax} dx$$

or in the case at hand

$$\frac{(-1) \prod_{j=1}^{K} \left(\frac{i}{c} + 1 - j\right)}{(re^{i\theta})^{K+1}\, 2i} \int \frac{(rZ)^{\frac{i}{c}}\, e^{rZe^{i\theta}}}{(rZ)^K} dZ \tag{38}$$

is the type of expression encountered. It can be shown that the numerator of the integrand in expression (38) is bounded and the magnitude of the error in the asymptotic expansion is a function of

$$\left(\frac{\omega}{\omega_n}\right)^K \prod_{j=0}^{K-1} (1 + c^2 j^2),$$

since $c << 1$, ω/ω_n need not be much less than one to obtain good accuracy. A detailed error analysis of the asymptotic expansions has been developed by the author, along with the development of the expression for response and the response curves generated therefrom.

A significant point which emerges from the final expressions for response is that they are dependent only on the parameters ω/ω_n, ζ, and c.

THE LOG SWEEP

The development of the analysis of the log sweep is analogous to that for the log-log sweep. The approach to the problem and the techniques used in the solution for the response are the same.

The log-log sweep was characterized as providing an equal number of cycles between frequencies, corresponding to equiamplitude points on the response curve, independent of the natural frequency. It will now be shown that the log sweep spends an equal amount of time between frequencies, corresponding to equiamplitude points on the response curve, independent of the natural frequency. For example, if an equipment has resonances at 50 and 250 cps under the log sweep, the frequency requires the same amount of time to sweep between the half-amplitude frequencies (about 50 cps) as it does to sweep between the half-amplitude frequencies (about 250 cps), provided damping is the same in each case (Fig. 3).

In order to prove this, the functional form of the log sweep must first be found. This function, F(t), is generated by turning a logarithmically calibrated frequency control dial at a constant angular velocity. Let Ⓗ represent the angle through which the dial has turned. Then

$$\frac{\partial (Ⓗ)}{\partial t} = K_1 \qquad (K_1 = \text{constant}) \tag{39}$$

and

$$K_2 \ln \omega = Ⓗ \qquad (K_2 = \text{constant}) \tag{40}$$

by the above conditions. So,

$$K_1 = K_2 \frac{d\omega}{dt}. \tag{41}$$

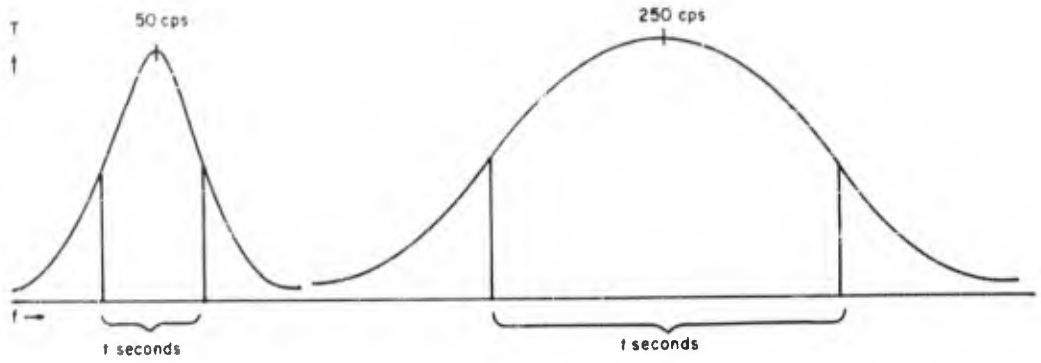

Fig. 3 - Log sweep for an equipment with resonances at 50 and 250 cps

By integrating Eq. (41), there results

$$\ln \omega = \frac{K_2}{K_1} t + K_3 \qquad (K_3 = \text{constant}) \tag{42}$$

or

$$\omega = \epsilon^{\frac{K_2}{K_1} t} \epsilon^{K_3} . \tag{43}$$

Time is measured from $t = 0$, so from Eq. (43) the initial frequency ω_i is

$$\omega_i = \epsilon^{K_3} . \tag{44}$$

Since $\partial F(t)/\partial t = \omega$, integrating Eq. (43) yields

$$F(t) = \frac{\omega_i K_1}{K_2} \epsilon^{\frac{K_2}{K_1} t} + K_3 . \tag{45}$$

K_3 is simply the phase angle σ which will be ignored at present. The constant $\omega_i K_1/K_2$ will be called $\bar{c}$ so that

$$F(t) = \bar{c} \epsilon^{\frac{\omega_i t}{\bar{c}}} . \tag{46}$$

Hence, Eq. (46) gives the logarithmic sweep function. Equation (46) is then differentiated, with respect, to time to give

$$\omega = \omega_i \epsilon^{\frac{\omega_i t}{\bar{c}}}$$

which is solved for t, yielding

$$t = \frac{\bar{c}}{\omega_i} \ln \frac{\omega}{\omega_i} . \tag{47}$$

As in the log-log case, consider two simple linear oscillators with equal damping. The first has a natural frequency of ω_n, while the second has a natural frequency of $a\omega_n$ with $a > 1$. Again the equiamplitude points about ω_n are called $\omega_n - \Delta\omega_1$, and $\omega_n + \Delta\omega_2$. It follows, as before, that

the equiamplitude points about $a\omega_n$ are $a(\omega_n - \Delta\omega_1)$ and $a(\omega_n + \Delta\omega_2)$. The times at which $\omega_n - \Delta\omega_1$, and $\omega_n + \Delta\omega_2$ occur are called t_1 and t_2, respectively, and the times at which $a(\omega_n - \Delta\omega_1)$ and $a(\omega_n + \Delta\omega_2)$ occur are called t_1' and t_2', respectively. Hence, the condition that the frequency under the log sweep spends the same time between $\omega_n - \Delta\omega_1$, and $\omega_n + \Delta\omega_2$ as between $a(\omega_n - \Delta\omega_1)$ and $a(\omega_n + \Delta\omega_2)$ is true, provided

$$t_2 - t_1 = t_2' - t_1' . \tag{48}$$

From Eq. (47), it follows that

$$\begin{aligned} t_2 - t_1 &= \frac{\bar{c}}{\omega_i} \ln \frac{\omega_n + \Delta\omega_2}{\omega_i} - \frac{\bar{c}}{\omega_i} \ln \frac{\omega_n + \Delta\omega_1}{\omega_i} \\ &= \frac{\bar{c}}{\omega_i} \ln \frac{\omega_n + \Delta\omega_2}{\omega_n - \Delta\omega_1} - \frac{\bar{c}}{\omega_i} \ln \frac{a(\omega_n + \Delta\omega_2)}{a(\omega_n - \Delta\omega_1)} \\ &= \frac{\bar{c}}{\omega_i} \ln \frac{a(\omega_n + \Delta\omega_2)}{\omega_i} - \frac{\bar{c}}{\omega_i} \ln \frac{a(\omega_n - \Delta\omega_2)}{\omega_i} \\ &= t_2' - t_1' . \end{aligned}$$

Thus the criterion of Eq. (48) is satisfied, and the conjecture is established.

From Eqs. (46) and (47), it follows that

$$F(t) = \frac{\bar{c}\omega}{\omega_i} . \tag{49}$$

Thus,

$$F(t_2) - F(t_1) = \frac{\bar{c}(\omega_n + \Delta\omega_2)}{\omega_i} - \frac{\bar{c}(\omega_n - \Delta\omega_1)}{\omega_i}$$

and

$$F(t_2') - F(t_1') = \frac{\bar{c}[a(\omega_n + \Delta\omega_2)]}{\omega_i} - \frac{\bar{c}[a(\omega_n - \Delta\omega_1)]}{\omega_i} .$$

So $F(t_2') - F(t_1') = a[F(t_2) - F(t_1)]$, and in contrast with the log-log sweep, the logarithmic sweep provides a greater number of cycles between the equiamplitude points about $a\omega_n$ than it does between the equiamplitude points about the lower frequency ω_n.

The log sweep function is substituted into the differential equation for the linear oscillator resulting in

$$\ddot{x} + 2n\dot{x} + \omega_n^2 x = \frac{P_o}{m} \cos\left[\bar{c}\epsilon^{\frac{\omega_i t}{\bar{c}}} + \sigma\right] \tag{50}$$

which must be solved to obtain the log sweep response curve. Solving the differential equation by the method of operators again results in Eq. (21). The result is rewritten in a form free of the imaginary unit. This gives

$$\begin{aligned} x = \frac{\epsilon^{-nt} p_o}{\tilde{\omega} m} \Bigg\{ &\sin \tilde{\omega}t \cos\sigma \int_0^t \cos\left(\bar{c}\epsilon^{\frac{\omega_i t}{\bar{c}}}\right) \epsilon^{nt} \cos \tilde{\omega}t \, dt - \sin \tilde{\omega}t \sin\sigma \int_0^t \sin\left(\bar{c}\epsilon^{\frac{\omega_i t}{\bar{c}}}\right) \epsilon^{nt} \cos \tilde{\omega}t \, dt \\ &- \cos \tilde{\omega}t \cos\sigma \int_0^t \cos\left(\bar{c}\epsilon^{\frac{\omega_i t}{\bar{c}}}\right) \epsilon^{nt} \sin \tilde{\omega}t \, dt + \cos \tilde{\omega}t \sin\sigma \int_0^t \sin\left(\bar{c}\epsilon^{\frac{\omega_i t}{\bar{c}}}\right) \epsilon^{nt} \sin \tilde{\omega}t \, dt \Bigg\} . \end{aligned} \tag{51}$$

The phase angle σ which extremalizes x is found by solving the equation $\partial x/\partial\sigma = 0$ for σ. Substituting this into Eq. (51) yields the envelope of the amplitude which is

$$x_e = \frac{\epsilon^{-ntP_o}}{\tilde{\omega}m} \sqrt{\phi_1^2 + \phi_2^2}\,, \tag{52}$$

where

$$\phi_1 = \cos \tilde{\omega}t\ \theta_4 - \sin \tilde{\omega}t\ \theta_2$$

$$\phi_2 = \cos \tilde{\omega}t\ \theta_3 - \sin \tilde{\omega}t\ \theta_1$$

and

$$\theta_1 = \int_0^t \cos\left(\bar{c}\epsilon \frac{\omega_i t}{\bar{c}}\right) \epsilon^{nt} \cos \tilde{\omega}t\ dt$$

$$\theta_2 = \int_0^t \sin\left(\bar{c}\epsilon \frac{\omega_i t}{\bar{c}}\right) \epsilon^{nt} \cos \tilde{\omega}t\ dt$$

$$\theta_3 = \int_0^t \cos\left(\bar{c}\epsilon \frac{\omega_i t}{\bar{c}}\right) \epsilon^{nt} \sin \tilde{\omega}t\ dt$$

$$\theta_4 = \int_0^t \sin\left(\bar{c}\epsilon \frac{\omega_i t}{\bar{c}}\right) \epsilon^{nt} \sin \tilde{\omega}t\ dt\,.$$

Equation (51) is differentiated to obtain the velocity of the oscillator mass. This results in

$$\dot{x} = -nx + \frac{\epsilon^{-ntP_o}}{\tilde{\omega}m} \left\{-\tilde{\omega} \sin \tilde{\omega}t\ \theta_4 - \tilde{\omega} \cos \tilde{\omega}t\ \theta_2\right\} \sin \sigma$$

$$+ \frac{\epsilon^{-ntP_o}}{\tilde{\omega}m} \left\{\tilde{\omega} \sin \tilde{\omega}t\ \theta_3 + \tilde{\omega} \cos \tilde{\omega}t\ \theta_1\right\} \cos \sigma\,. \tag{53}$$

The phase angle σ which extremalizes $\dot{x}$ is found by solving the equation $\partial\dot{x}/\partial\sigma = 0$ for σ. Substituting this solution into Eq. (53) gives the envelope of the velocity which is

$$\dot{x}_e = \frac{\epsilon^{-ntP_o}}{m} \sqrt{\psi_1^2 + \psi_2^2}\,, \tag{54}$$

where

$$\psi_1 = \left(\frac{n}{\tilde{\omega}} \sin \tilde{\omega}t - \cos \tilde{\omega}t\right) \theta_2 - \left(\frac{n}{\tilde{\omega}} \cos \tilde{\omega}t + \sin \tilde{\omega}t\right) \theta_4$$

and

$$\psi_2 = \left(\frac{n}{\tilde{\omega}} \sin \tilde{\omega}t - \cos \tilde{\omega}t\right) \theta_1 - \left(\frac{n}{\tilde{\omega}} \cos \tilde{\omega}t + \sin \tilde{\omega}t\right) \theta_3\,.$$

Thus the expression for the response curve has the same form as in the log-log case, that is,

$$T = \sqrt{\frac{1}{(1 - \xi^2)} (\phi_1^2 + \phi_2^2) + 4\xi^2 (\psi_1^2 + \psi_2^2)}\ \omega_n \epsilon^{-nt}\,. \tag{55}$$

The only difference is the form of the θ integrals.

Numerical integration of these θ integrals is out of the question for the reasons set forth in the log-log analysis. A series-solution approach is again used. First, a change of variable is made to facilitate handling. This results in

$$\theta_1 = \frac{\bar{c}}{\omega_i} \int_1^Z \cos(\bar{c}Z)\, Z^{\left(\frac{n\bar{c}}{\omega_i} - 1\right)} \cos\left(\frac{\tilde{\omega}\bar{c}}{\omega_i} \ln Z\right) dZ ,$$

$$\theta_2 = \frac{\bar{c}}{\omega_i} \int_1^Z \sin(\bar{c}Z)\, Z^{\left(\frac{n\bar{c}}{\omega_i} - 1\right)} \cos\left(\frac{\tilde{\omega}\bar{c}}{\omega_i} \ln Z\right) dZ ,$$

$$\theta_3 = \frac{\bar{c}}{\omega_i} \int_1^Z \cos(\bar{c}Z)\, Z^{\left(\frac{n\bar{c}}{\omega_i} - 1\right)} \sin\left(\frac{\tilde{\omega}\bar{c}}{\omega_i} \ln Z\right) dZ ,$$

and

$$\theta_4 = \frac{\bar{c}}{\omega_i} \int_1^Z \sin(\bar{c}Z)\, Z^{\left(\frac{n\bar{c}}{\omega_i} - 1\right)} \sin\left(\frac{\tilde{\omega}\bar{c}}{\omega_i} \ln Z\right) dZ .$$

These integrals are then written in the form of series. For example,

$$\theta_1 = \frac{\bar{c}}{\omega_i} \int_1^Z \left(\frac{\epsilon^{i\bar{c}Z} + \epsilon^{-i\bar{c}Z}}{2}\right) Z^{\left(\frac{n\bar{c}}{\omega_i} - 1\right)} \left(\frac{Z^{\frac{i\tilde{\omega}\bar{c}}{\omega_i}} + Z^{\frac{-i\tilde{\omega}\bar{c}}{\omega_i}}}{2}\right) dZ$$

$$= \frac{\bar{c}}{\omega_i} \int_1^Z \frac{Z^{\left(\frac{n\bar{c}}{\omega_i} - 1\right) + i\frac{\tilde{\omega}\bar{c}}{\omega_i}}}{4} \sum_{K=0}^{\infty} \frac{(i\bar{c}Z)^K}{K!}\, dZ + \frac{\bar{c}}{\omega_i} \int_1^Z \frac{Z^{\left(\frac{n\bar{c}}{\omega_i} - 1\right) - i\frac{\tilde{\omega}\bar{c}}{\omega_i}}}{4} \sum_{K=0}^{\infty} \frac{(i\bar{c}Z)^K}{K!}\, dZ$$

$$+ \frac{\bar{c}}{\omega_i} \int_1^Z \frac{Z^{\left(\frac{n\bar{c}}{\omega_i} - 1\right) + i\frac{\tilde{\omega}\bar{c}}{\omega_i}}}{4} \sum_{K=0}^{\infty} \frac{(-i\bar{c}Z)^K}{K!}\, dZ + \frac{\bar{c}}{\omega_i} \int_1^Z \frac{Z^{\left(\frac{n\bar{c}}{\omega_i} - 1\right) + i\frac{\tilde{\omega}\bar{c}}{\omega_i}}}{4} \sum_{K=0}^{\infty} \frac{(-i\bar{c}Z)^K}{K!}\, dZ$$

$$= \frac{\bar{c}}{\omega_i} \frac{Z^{\left(\frac{n\bar{c}}{\omega_i} + i\frac{\tilde{\omega}\bar{c}}{\omega_i}\right)}}{4} \sum_{K=0}^{\infty} \frac{(1 + \cos \pi K)\, (i\bar{c}Z)^K}{K!} \frac{1}{K + \frac{n\bar{c}}{\omega_i} + i\frac{\tilde{\omega}\bar{c}}{\omega_i}}$$

$$+ \frac{\bar{c}}{\omega_i} \frac{Z^{\left(\frac{n\bar{c}}{\omega_i} - i\frac{\tilde{\omega}\bar{c}}{\omega_i}\right)}}{4} \sum_{K=0}^{\infty} \frac{(1 + \cos \pi K)\, (i\bar{c}Z)^K}{K!} \frac{1}{K + \frac{n\bar{c}}{\omega_i} + i\frac{\tilde{\omega}\bar{c}}{\omega_i}}$$

$$= \frac{\bar{c}Z^{\frac{n\bar{c}}{\omega_i}}}{4\omega_i} \left(Z^{i\frac{\tilde{\omega}\bar{c}}{\omega_i}} + Z^{-i\frac{\tilde{\omega}\bar{c}}{\omega_i}}\right) \sum_{K=0}^{\infty} \frac{(1 + \cos \pi K)\, (i\bar{c}Z)^K \left[K + \frac{n\bar{c}}{\omega_i}\right]}{K! \left[\left(K + \frac{n\bar{c}}{\omega_i}\right)^2 - \left(\frac{\tilde{\omega}\bar{c}}{\omega_i}\right)^2\right]}$$

$$- \frac{\bar{c}Z^{\frac{n\bar{c}}{\omega_i}}}{4\omega_i} \left(Z^{i\frac{\tilde{\omega}\bar{c}}{\omega_i}} - Z^{-i\frac{\tilde{\omega}\bar{c}}{\omega_i}}\right) \sum_{K=0}^{\infty} \frac{(1 + \cos \pi K)\, (i\bar{c}Z)^K \left(\frac{\tilde{\omega}\bar{c}}{\omega_i}\right)}{K! \left[\left(K + \frac{n\bar{c}}{\omega_i}\right)^2 - \left(\frac{\tilde{\omega}\bar{c}}{\omega_i}\right)^2\right]}$$

(56)
(Continued)

$$\frac{\bar{c}\epsilon^{nt}}{2\omega_i}\left\{\left[\frac{n\bar{c}}{\omega_i}\cos\ \ +\ \frac{\tilde{\omega}\bar{c}}{\omega_i}\sin\ \ t\right]\cdot\sum_{K=0}^{\infty}\frac{(1+\cos\pi K)(i\bar{c}Z)^K}{K!\left[\left(K+\frac{n\bar{c}}{\omega_i}\right)^2-\left(\frac{\tilde{\omega}\bar{c}}{\omega_i}\right)^2\right]}\right.$$

$$\left.+\cos\tilde{\omega}t\sum_{K=0}^{\infty}\frac{(1+\cos\pi K)(i\bar{c}Z)^K K}{K!\left[\left(K+\frac{n\bar{c}}{\omega_i}\right)^2-\left(\frac{\tilde{\omega}\bar{c}}{\omega_i}\right)^2\right]}\right\}, \tag{56}$$

Similarly,

$$2\quad\frac{\bar{c}\epsilon^{nt}}{2_i\omega_i}\left\{\left[\frac{n\bar{c}}{\omega_i}\cos\tilde{\omega}t+\frac{\tilde{\omega}\bar{c}}{\omega_i}\sin\tilde{\omega}t\right]\cdot\sum_{K=0}^{\infty}\frac{(1-\cos\pi K)(i\bar{c}Z)^K}{K!\left[\left(K+\frac{n\bar{c}}{\omega_i}\right)^2-\left(\frac{\tilde{\omega}\bar{c}}{\omega_i}\right)^2\right]}\right.$$

$$\left.+\cos\tilde{\omega}t\sum_{K=0}^{\infty}\frac{(1-\cos\pi K)(i\bar{c}Z)^K K}{K!\left[\left(K+\frac{n\bar{c}}{\omega_i}\right)^2-\left(\frac{\tilde{\omega}\bar{c}}{\omega_i}\right)^2\right]}\right\}, \tag{57}$$

$$\vartheta_3=\frac{\bar{c}\epsilon^{nt}}{2\omega_i}\left\{\left[\frac{n\bar{c}}{\omega_i}\sin\tilde{\omega}t-\frac{\tilde{\omega}\bar{c}}{\omega_i}\cos\tilde{\omega}t\right]\cdot\sum_{K=0}^{\infty}\frac{(1+\cos\pi K)(i\bar{c}Z)^K}{K!\left[\left(K+\frac{n\bar{c}}{\omega_i}\right)^2-\left(\frac{\tilde{\omega}\bar{c}}{\omega_i}\right)^2\right]}\right.$$

$$\left.+\sin\tilde{\omega}t\sum_{K=0}^{\infty}\frac{(1+\cos\pi K)(i\bar{c}Z)^K}{K!\left[\left(K+\frac{n\bar{c}}{\omega_i}\right)^2-\left(\frac{\tilde{\omega}\bar{c}}{\omega_i}\right)^2\right]}\right\}, \tag{58}$$

and

$$\vartheta_4=\frac{\bar{c}\epsilon^{nt}}{2\omega_i}\left\{\left[\frac{n\bar{c}}{\omega_i}\sin\tilde{\omega}t-\frac{\tilde{\omega}\bar{c}}{\omega_i}\cos\tilde{\omega}t\right]\cdot\sum_{K=0}^{\infty}\frac{(1-\cos\pi K)(i\bar{c}Z)^K}{K!\left[\left(K+\frac{n\bar{c}}{\omega_i}\right)^2-\left(\frac{\tilde{\omega}\bar{c}}{\omega_i}\right)^2\right]}\right\}, \tag{59}$$

Substitution results in

$$\varphi_1=-\left(\frac{c}{\omega_i}\right)^2\epsilon^{nt}\tilde{\omega}\sum_{K=0}^{\infty}\frac{\sin\frac{\pi K}{2}(\bar{c}Z)^K}{K!\left[\left(K+\frac{n\bar{c}}{\omega_i}\right)^2-\left(\frac{\tilde{\omega}\bar{c}}{\omega_i}\right)^2\right]},$$

$$\phi_2=-\left(\frac{\bar{c}}{\omega_i}\right)^2\epsilon^{nt}\tilde{\omega}\sum_{K=0}^{\infty}\frac{\cos\frac{\pi K}{2}(\bar{c}Z)^K}{K!\left[\left(K+\frac{n\bar{c}}{\omega_i}\right)^2-\left(\frac{\tilde{\omega}\bar{c}}{\omega_i}\right)^2\right]},$$

$$\psi_1=-\left(\frac{\bar{c}}{\omega_i}\right)\epsilon^{nt}\sum_{K=0}^{\infty}\frac{\sin\frac{\pi K}{2}(\bar{c}Z)^K K}{K!\left[\left(K+\frac{n\bar{c}}{\omega_i}\right)^2-\left(\frac{\tilde{\omega}\bar{c}}{\omega_i}\right)^2\right]}$$

$$=-\left(\frac{\bar{c}}{\omega_i}\right)^2\epsilon^{nt}\omega\sum_{K=0}^{\infty}\frac{\cos\frac{\pi K}{2}(\bar{c}Z)^K}{K!\left[\left(K+1+\frac{n\bar{c}}{\omega_i}\right)^2-\left(\frac{\tilde{\omega}\bar{c}}{\omega_i}\right)^2\right]},$$

and

$$+2 \quad -\frac{\bar{c}}{\omega_1} e^{nt} \sum_{K=0}^{\infty} \frac{\cos \frac{\pi K}{2} (\bar{c}Z)^K K}{K! \left[\left(K + \frac{n\bar{c}}{\omega_1}\right)^2 - \left(\frac{\omega\bar{c}}{\omega_1}\right)^2\right]}$$

$$\left(\frac{\bar{c}}{\omega_1}\right)^2 e^{nt} \sum_{K=0}^{\infty} \frac{\sin \frac{\pi K}{2} (\bar{c}Z)^K}{K! \left[\left(K + 1 + \frac{n\bar{c}}{\omega_1}\right)^2 - \left(\frac{\omega\bar{c}}{\omega_1}\right)^2\right]} .$$

For convenience in writing, the quantity $\omega_1 \bar{c} / n$ is called A. The expression for response in terms of transmissibility then becomes

$$T \quad \sqrt{\left(\sum_{K=0}^{\infty} \frac{\sin \frac{\pi K}{2} (cZ)^K}{K! [A^2K^2 + 2A\xi K + 1]}\right)^2 + \left(\sum_{K=0}^{\infty} \frac{\cos \frac{\pi K}{2} (\bar{c}Z)^K}{K! [A^2K^2 + 2A\xi K + 1]}\right)^2}$$

$$\sqrt{+ 4\xi^2 \left(\frac{\omega}{\omega_n}\right)^2 \left\{\left(\sum_{K=0}^{\infty} \frac{\sin \frac{\pi K}{2} (\bar{c}Z)^K}{K! [A^2(K+1)^2 + 2A\xi(K+1) + 1]}\right)^2 + \left(\sum_{K=0}^{\infty} \frac{\cos \frac{\pi K}{2} (\bar{c}Z)^K}{K! [A^2(K+1)^2 + 2A\xi(K+1) + 1]}\right)^2\right\}} . \quad (60)$$

These final series are certainly absolutely convergent and yet, as was the case with the log-log series, the computational problems involved in their summation are formidable. In most cases of interest, the sweep constant $\bar{c}$ will be of the order of 10^3 or larger, $A \leq 10^{-3}$, $\xi \leq 2$, and $Z \geq 1$. Hence, tens of thousands of terms must be summed to attain reasonable accuracy. As in the log-log case, precision is also a problem. Since many of the partial sums in these series would be far more than nine orders of magnitude greater than the sums of the series, multiple precision programming would be necessary throughout the computation. Therefore, as in the log-log case, the series were manipulated into a more tractable form.

As an example of this process, consider that

$$\sum_{K=0}^{\infty} \frac{\cos \frac{\pi K}{2} (\bar{c}Z)^K}{K! [A^2K^2 + 2\xi AK + 1]} = \frac{1}{2\sqrt{1-\xi^2}\, i} \left\{\sum_{K=0}^{\infty} \frac{\cos \frac{\pi K}{2} (\bar{c}Z)^K}{K! [AK + \xi - i\sqrt{1-\xi^2}]} - \sum_{K=0}^{\infty} \frac{\cos \frac{\pi K}{2} (\bar{c}Z)^K}{K! [AK + \xi + i\sqrt{1-\xi^2}]}\right\} . \quad (61)$$

The recursion relations

$$\left\{\sum_{K=0}^{\infty} \frac{\cos \frac{\pi K}{2} (\bar{c}Z)^K}{K! [A(K+N) + \xi \pm i\sqrt{1-\xi^2}]}\right\} \left\{AN + \xi \pm i\sqrt{1-\xi^2}\right\} = \cos \bar{c}Z + A(\bar{c}Z) \sum_{K=0}^{\infty} \frac{\sin \frac{\pi K}{2} (\bar{c}Z)^K}{K! [A(K+N+1) + \xi \pm i\sqrt{1-\xi^2}]}$$

and

$$\left\{\sum_{K=0}^{\infty} \frac{\sin \frac{\pi K}{2} (\bar{c}Z)^K}{K! [A(K+N) + \xi \pm i\sqrt{1-\xi^2}]}\right\} \left\{AN + \xi \pm i\sqrt{1-\xi^2}\right\} = \sin \bar{c}Z - A(\bar{c}Z) \sum_{K=0}^{\infty} \frac{\cos \frac{\pi K}{2} (\bar{c}Z)^K}{K! [A(K+N+1) + \xi \pm i\sqrt{1-\xi^2}]}$$

were then applied to Eq. (61) to obtain

$$\sum_{K=0}^{\infty} \frac{\cos \frac{\pi K}{2} (cZ)^K}{K![A^2K^2 + 2AK + 1]} = \frac{1}{\sqrt{1-\zeta^2}} \left\{ \cos cZ \sum_{K=0}^{\infty} \frac{\cos \frac{\pi K}{2} \left(\frac{\omega}{\omega_n}\right)^K \sin \left[\sum_{j=0}^{K} \tan^{-1} \frac{\sqrt{1-\zeta^2}}{Aj + \zeta} \right]}{\prod_{j=0}^{K} \sqrt{A^2j^2 + 2A\zeta j + 1}} \right.$$

$$\left. + \sin cZ \sum_{K=0}^{\infty} \frac{\sin \frac{\pi K}{2} \left(\frac{\omega}{\omega_n}\right)^K \sin \left[\sum_{j=0}^{K} \tan^{-1} \frac{\sqrt{1-\zeta^2}}{Aj + \zeta} \right]}{\prod_{j=0}^{K} \sqrt{A^2j^2 + 2A\zeta j + 1}} \right\} . \tag{62}$$

The resulting series will obviously converge relatively rapidly for $\omega/\omega_n \leq 1$. The details of this work, including the ultimate expression for response in terms of these series and curves generated therefrom, have been developed by the author elsewhere.

As was done before in the log-log case, asymptotic expansions were developed for the region in which $\omega/\omega_n > 1$. In the case of I_1, note that

$$I_1 = \frac{\bar{c}}{\omega_i} \int_1^Z \cos (cZ)\, Z^{\left(\frac{n\bar{c}}{\omega_i} - 1\right)} \cos\left(\frac{\tilde{\omega}\bar{c}}{\omega_i} \ln Z\right) dZ$$

$$= \frac{\bar{c}}{\omega_i} \int_1^Z \frac{\epsilon^{i\bar{c}Z} + \epsilon^{-i\bar{c}Z}}{2} Z^{\left(\frac{n\bar{c}}{\omega_i} - 1\right)} \left(\frac{Z^{\frac{i\tilde{\omega}\bar{c}}{\omega_i}} + Z^{-\frac{i\tilde{\omega}\bar{c}}{\omega_i}}}{2} \right) dZ . \tag{63}$$

The last integral in Eq. (64) can be integrated by parts repeatedly by the relation,

$$\int x^b \epsilon^{ax} dx = \frac{x^b \epsilon^{ax}}{a} - \frac{b}{a} \int x^{b-1} \epsilon^{ax} dx ,$$

to yield power series in $(rZ)^{-1}$.

An interesting feature regarding the final results for transmissibility in both regions is that they are functions of only ω/ω_n, ζ, and A. The parameter A takes on new significance when it is noted that its value is equal to the log-log sweep parameter c if both sweep functions have the same rate of change of frequency at the natural frequency ω_n. In the log case,

$$\frac{\partial \omega}{\partial t} = \frac{\omega_i^2}{\bar{c}} \epsilon^{\omega_i t/\bar{c}} = \frac{\omega_i \omega}{\bar{c}} ; \tag{64}$$

and in the log-log case,

$$\frac{\partial \omega}{\partial t} = \frac{c\omega_i^2}{(1 - c\omega_i t)^2} = c\omega^2 . \tag{65}$$

If the respective time rates of change of frequency are evaluated at ω_n and equated, the result is

$$c\omega_n^2 = \frac{\omega_i \omega_n}{\bar{c}} .$$

or

$$c = \frac{1}{c'_n} A$$

This provides a convenient method of comparison between the two sweeps.

REFERENCES

1. F. M. Lewis, "Vibration During Acceleration Through a Critical Speed," Journal of Applied Mechanics, p. 253, 1932.

2. Charles E. Crede and Edward J. Lunney, "The Establishment of Vibration and Shock Tests for Airborne Electronics," WADC Technical Report 57-75, ASTIA Document No. AD 142349, Jan. 1958.

DISCUSSION

Mr. Galef (National Engineering Science Co.): I didn't understand why we considered the number of cycles proportional to the frequency to be a disadvantage. Actually, one would think that the 250-cps device would have to remain on the missile for as long as the 50-cps device. It would, therefore, in the life of the missile be subjected to five times as many cycles. If your sweep test is being used as a fatigue test (I rather assumed that it was because of the fact that you are concerned about number of cycles), then you must have the same time within each frequency band and not the same number of cycles.

Mr. Parker: In terms of damage, though—we're not looking at the thing on the missile now. No doubt the missile will not provide a log-log sweep rate. We're in the laboratory; and in carrying out a sweep program, we want to provide the same amount of potential damage for each resonant structure in there. If we provide so many more significant stress reversals at the resonant system of high frequency, we may overtest that before we get done at the low-frequency range.

Mr. Galef: If it fails, it deserves to fail.

Mr. Parker: You're going against the whole philosophy of testing then.

Mr. Galef: No, I disagree. You're trying to design something which will last a certain number of hours or seconds—whatever you call it—in the missile. During this number of seconds, it gets as many stress reversals as it deserves because of its natural frequency. You should give it that many, not some number related to some other natural frequency.

Mr. Parker: I'm thinking we want to give it as much damage as it deserves.

Mr. Galef: Yes!!!

Mr. Stern (General Electric Co.): Just a comment on the previous statement. I think the point that was trying to be made was that in this log-log sweep you're trying to do something that's desirable from a theoretical or a laboratory standpoint, but when you actually test you're trying to simulate. Simulation doesn't mean you do what you'd like to do. You more or less do what usually occurs in the natural environment. My question is this: Can you give a brief description of the hardware? That is, just what would this device look like that would do this log-log sweeping? Just a simple description of how an operator might actually do this.

Mr. Parker: You'd generate it in an analogous manner to the log sweep, the only difference being that your frequency control dial would be calibrated on a log-log scale rather than a log scale.

Mr. Galef: You would drive this at a linear rate then?

Mr. Parker: Constant angular velocity, yes.

Mr. Galef: Oh, then this would be something that would be built into the oscillator when you build it then.

Mr. Parker: Yes. As far as I know no one is doing this at present, however.

Mr. Gertel (Allied Research Associates): I'd like to make a comment on the looseness of terminology we become trapped in—this log-log sweeping. It isn't very explicit because if we're presumably talking about a log-log sweep, which means the sweep rate or df/dt as a function of frequency, it's a straight line. Depending on the exponent of the equation, defining this sweep rate, you can get any number of straight lines and, presumably, could describe these as being log-log sweeps. I think we have to be careful with this terminology because you get completely different results depending on what the slope or exponent of our log-log sweep is. If the exponent of our sweep equation is the first power, this is essentially the same as a linear sweep rate—or one that would be plotted as a straight line on linear coordinates. We wind up with a situation where we have a constant time in the response which, as Arnold Galef tried to point out, gives essentially the same type of condition one might find in a missile. A missile flies for a finite period of time. All the equipments in it, with a first power logarithmic sweep, would experience constant time during the testing process. If, on the other hand, we use a second power, we find a slightly different situation. We find that the responding system experiences a constant number of cycles in the response. This type of testing philosophy is found to be desirable for aircraft use or systems that must be subjected or must withstand say years of life where we really don't care about subjecting them to a constant time test. We really want to get them out to some number of cycles which is well beyond the endurance limit cycles.

Mr. Parker: The accelerated life idea.

Mr. Gertel: Yes. Well in conclusion here I think we want to be extremely careful about the terminology of log-log sweep or log sweep. I think we have to perhaps refer to the equation which defines the sweep rather than this type of terminology.

Mr. Parker: Well, I defined them in terms of how they were generated on a frequency control dial. You have this equation $d\omega/dt$ equals some constant to some power of ω, and I realize that all these will plot linearly on log-log paper. But I was defining these in terms of how they were generated on a frequency control dial, and the log-log case would be the case in which $d\omega/dt$ was proportional to ω^2. In the log case, it's proportional to ω.

* * *

CORRELATION OF SINUSOIDAL AND RANDOM VIBRATIONS

B. M. Hall and L. T. Waterman
Missiles and Space Systems Engineering Department
Douglas Aircraft Co., Inc.
Santa Monica, California

Equations are derived in this paper to show the relationship between a sinusoid at resonance, a sinusoidal sweep, and random Gaussian vibrations. The sinusoids are defined in terms of zero to peak accelerations, whereas the magnitude of the random vibration is given in power spectral density. The work done by internal dampling forces is used as a basis for establishing equal fatigue damage.

INTRODUCTION

There is probably no subject in the field of shock and vibration which is as controversial or as prominent as the subject of random- versus sine-wave vibration testing. The purpose of this paper is to present detailed equations showing a method of finding the equivalence between random- and sine-wave testing. On this basis one may then proceed rationally to the use of either the sine-wave or the random-vibration technique.

Before diving into the mathematics of the problem, it would be advisable to review some of the circumstances which make this investigation such an urgent one. In the field of aircraft and missiles, the rapid transition from propeller driven vehicles to jet and rocket powered vehicles has resulted in a vibration environment which is essentially random. For the thousands of items of structure and equipment which were designed to specifications (such as MIL E 5272), there immediately arises the question of their suitability for operation in random-vibration fields. This question could of course be answered by a gigantic requalification program along with a complete switch from sine-wave facilities to random facilities. The cost of such a program is staggering; and upon closer examination, the complete switch is not particularly desirable, since sine-wave qualification tests are still a valuable tool for locating and examining the nature of resonances in equipment. The common sense approach to the problem is therefore, a program which maintains the sine-wave test technique and adds in addition random tests on large assemblies and structural specimens. These test units would usually be assembled at one of the large companies or at a large government test center where random facilities are rapidly becoming available. The common sense approach also needs a suitable theory to correlate the levels to be used in each type of testing.

PRINCIPLE OF CORRELATION

The principle of correlation developed in this paper is that each type of test produces the same damage on a second-order system model. The equations are derived to show the relationship between a sinusoid at resonance, a sinusoidal sweep, and random vibrations. The sinusoids are defined in terms of zero to peak accelerations, whereas the magnitude of the random vibration is given in power spectral density. The work done by internal damping forces is used as a basis for establishing equal fatigue damage.

A dynamic system subjected to a random fatigue environment will deteriorate with time. This is usually explained in terms of the S-N curve for the material being stressed However, if the environment is stopped short of failure, it is necessary to use Miner's

hypothesis, or the equivalent, to determine the amount of the accumulated damage. Miner's hypothesis establishes a linear relationship between the number of cycles and the percent of fatigue damage; this suggests that the work done on the system can be related to the fatigue damage, and the only sources of dissipative energy in a linear system are the damping forces. Hence, using the work done by the damping forces as a basis for the damage criterion is equivalent to using Miner's hypothesis for accumulated damage.

SINUSOIDAL WORK PERFORMED BY A SINGLE MODE

Although the formulae for the work performed by a simple spring-mass-damper combination are well known, a short derivation will be given in order to introduce the symbols and nomenclature necessary for the ensuing discussion. Consider for instance a single normal mode of a lightly dampled dynamic system.

The equation of motion is

$$M\ddot{y} + \frac{M\omega_N}{Q}\dot{y} + M\omega_N^2 y = \text{Force}.$$

The increment of work done by this system is

$$dW = F_d\, dy = F_d \frac{dy}{dt}\, dt, \tag{1}$$

and

$$F_d = \frac{M\omega_N}{Q}\dot{y}. \tag{2}$$

Substituting Eq. (2) into Eq. (1) and integrating over N cycles gives

$$W = \frac{NM\omega_N}{Q}\int_0^{2\pi/\omega} \dot{y}^2\, dt \tag{3}$$

where

F_d = force due to damping

y = amplitude coefficients of the mode

f_i = amplitude at any station along the mode shape

$y_i = y f_i$

$M = \Sigma M_i f_i^2$ = generalized mass

ω = natural frequency of the mode in radians per second

Q is the reciprocal of twice ζ, where

ζ is the percent of critical damping of the system.

If the system is excited by a force at a sinusoidal constant frequency and constant amplitude, the response is

$$y = R\left(\frac{\frac{\text{Force}}{M\omega_N^2}\, e^{i\omega t}}{\left(1 - \frac{\omega^2}{\omega_N^2}\right) + \left(\frac{i\omega}{Q\omega_N}\right)}\right) \tag{4}$$

$$\dot{y} = R\left(i\omega\, e^{i(\omega t + \theta)}\, |H|\, \frac{\text{Force}}{M\omega_N^2}\right) \tag{5}$$

where R indicates the real part

$$|H| = \frac{1}{\sqrt{\left(1 - \frac{\omega^2}{\omega_N^2}\right)^2 + \left(\frac{\omega}{Q\omega_N}\right)^2}}$$

$$\theta = \tan^{-1} \frac{\frac{\omega}{Q\omega_N}}{1 - \frac{\omega^2}{\omega_N^2}}.$$

Equation (5) may be integrated in Eq. (3) to find the work done for N cycles. It will be noticed that the phase angle drops out by virtue of the integration.

$$W = \frac{\pi NM\omega_N^2}{Q}\left(\frac{\omega}{\omega_N}\right)|H|^2\left(\frac{\text{Force}}{M\omega_N^2}\right)^2. \tag{6}$$

Assume that the structure is being vibrated by a uniform rigid body acceleration. This situation occurs when equipment or structure is fixed to the head of a shake table. Consider for example Fig. 1.

The force on the specimen is given by

$$\text{Force} = \Sigma M_i f_i C_g. \tag{7}$$

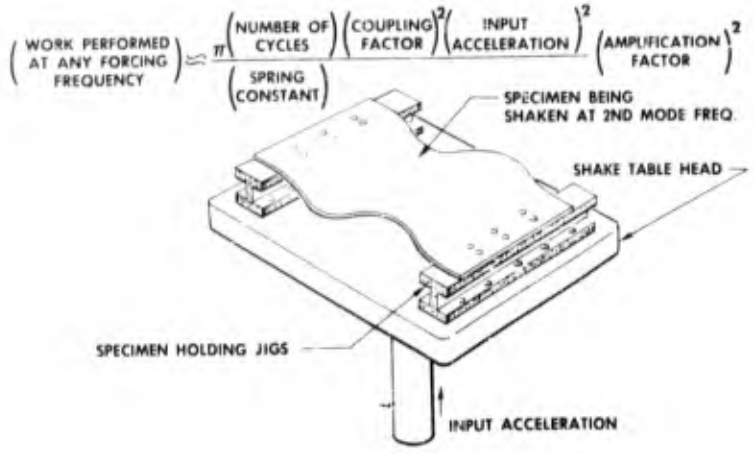

Fig. 1 - Dynamic model

Substituting Eq. (7) into (6) gives

$$W = \frac{\pi N m^2 G^2 |H|^2}{Q M \omega_N^2} \left(\frac{\omega}{\omega_N}\right) g^2 \qquad (8)$$

where

$m = \Sigma M_i f_i$

G = Zero to peak acceleration of the table in g units.

A useful form of Eq. (8) occurs when the forcing frequency is at resonance. This is

$$W_{(resonance)} = \frac{\pi N m^2 G^2 Q g^2}{M \omega_N^2} . \qquad (9)$$

RANDOM WORK PERFORMED BY A SINGLE MODE

For the case of random excitation where S denotes the power spectral density in g^2/cycle/second, the mean-square acceleration response of a general damped second order system is

$$\bar{a}^2 = \frac{1}{2\pi} \int_0^\infty S |H|^2 \, d\omega \qquad (10)$$

where $\bar{a}^2$ is the mean-square acceleration response in g's.

If the power spectral density is constant, the result is response to "white noise." Hence, it may be shown that

$$\bar{a}^2 = \frac{Q \omega_N S}{4} . \qquad (11)$$

This is the total mean-square (ms) acceleration response of a general second-order system. Although there are refined mathematical techniques available by which one may compute the work performed by white noise, a more intuitive approach will be used here. To determine the work done by random vibration, it is convenient to represent the excitations by a sufficiently large number of discrete forces to approximate the continuous state. This is accomplished in the following manner.

It has been established that 90 to 95 percent of the response of a normal mode is obtained from excitation within a bandwidth, say 15 percent for the Q-range of interest, bracketing the resonant frequency. This bandwidth is divided into a number of equal width frequency slots where discrete excitations will be applied at the center frequency of each slot. If these slots are sufficiently small, each random component will have essentially a constant frequency but with randomly varying phase and amplitude.

The problem is to devise an equivalent sinusoid for each slot which will produce the same rms response as the random environment. Starting with the basic

definition of power spectral density, the mean-square excitation is given by:

$$\bar{G}_k^2 = \frac{S\Delta\omega_k}{2\pi} \tag{12}$$

where

$\Delta\omega_k$ = width of slot.

Now, since $\Delta\omega_k$ is constant, $\bar{G}_k^2$ is also constant, the work performed by a sinusoid in the k^{th} slot is from Eq. (8).

$$\Delta W_k = \frac{m^2\ g^2\ G_k^2}{2QM\omega_N^2} N_k \frac{\omega_k}{\omega_N} |H_k|^2 \tag{13}$$

where G_k is the zero-to-peak value of the sinusoidal excitation. The mean-square value of G_k is $1/2\ G_k^2$ which is equal to $\bar{G}_k^2$ in Eq. (12). Since the equivalent sinusoidal excitation will be applied at each slot for the same length of time and ω_k varies between slots, clearly the number of stress reversals N_k must also vary between slots. In order to take care of this problem, the following technique will be employed. Let N be the number of cycles in the slot containing the resonant frequency, then

$$N_k = \frac{\omega_k}{\omega_N} N. \tag{14}$$

Equation (13) may now be rewritten with the aid of Eqs. (12) and (14), and summed over all the frequency slots.

$$W = \frac{Nm^2\ S2g^2}{2QM\omega_N^2} \sum_{k=1}^{\infty} |H_k|^2 \left(\frac{\omega_k^2}{\omega_N}\right) \Delta\omega_k. \tag{15}$$

If the limiting value of the above summation is taken, it may be shown that

$$\lim \Delta\omega \to 0 \sum_{k=1}^{\infty} |H_k|^2 \left(\frac{\omega_k}{\omega_N}\right)^2 \Delta\omega_k = \frac{\pi Q\omega_N}{2}. \tag{16}$$

Notice that this is the same value as given by $\int_0^\infty S|H|^2 d\omega$ in Eq.(11). The total work now becomes

$$W = \frac{\pi Ng^2\ m^2\ S}{2\omega_N M}. \tag{17}$$

Consider a single normal mode of the dynamic system of frequency, ω_N. If random excitation is continued for a time T_1 the number of accumulated fatigue cycles is approximated by

$$N = \frac{\omega_N\ T_1}{2\pi}. \tag{18}$$

Hence the total work done can be written from Eq. (17)

$$W = \frac{T_1\ g^2\ m^2\ S}{4M}. \tag{19}$$

It is to be emphasized that work is independent of the damping in the system. On the basis that the fatigue damage is proportional to the work done by the internal damping forces, the work done by a sinusoid at resonance, Eq. (9) is set equal to the work done by "white noise," Eq. (17), this gives

$$G = \sqrt{\frac{S\omega_N}{2Q}} \tag{20}$$

where

G = zero-to-peak acceleration of sinusoidal excitation at resonance g's

S = power spectral density g^2/cps

ω_N = resonant frequency rad/sec

Q = damping magnification factor.

Hence the equivalent power spectral density is

$$S = \frac{2Q\ G^2}{\omega_N}. \tag{21}$$

It is to be noted that this relationship is identical with that derived by equating the rms response of a sinusoidal resonance to that of the rms response due to a white noise random excitation. This equivalence is not surprising since the work equations are essentially mean-square response equations.

WORK PERFORMED BY A SINUSOIDAL SWEEP

For the sinusoidal sweep, it is necessary to devise a scheme for adding work done at different levels of magnification as the frequency is swept through the frequency spectrum. Assume that the frequency spectrum may be divided into a number of bands each Δf cycles/second wide. Assume also that the number of cycles of work performed by the sweeping sinusoid may be approximated by $\Delta f(f/f')$ where f is the center frequency of the band and f' is the sweep rate in cycles/second/second. From Eq. (8), the work performed in the k^{th} band may be written as

$$W = \frac{m^2 G^2 g^2}{QM\omega_N} \frac{}{4\pi f'} \left(\frac{\omega_k^2}{\omega_N^2}\right) |H_k|^2 \Delta\omega_k . \qquad (22)$$

Summing and passing to the limit as $\Delta\omega_k \to 0$ and the number of segments increases without limit, the integral

$$\int_0^\infty \left(\frac{\omega}{\omega_N}\right)^2 |H|^2 \, d\omega$$

again results and its value is $\pi Q\omega_N/2$. Substituting this result into Eq. (22) gives

$$\text{Work due to sweep} = \frac{m^2 G^2 g^2}{8f'M} . \qquad (23)$$

Now equating this to Eq. (19) to get the random and sinusoidal equivalence, we get

$$\frac{1}{T_1 f'} = \frac{2S}{G^2} . \qquad (24)$$

Notice that the equivalence equations are independent of the system damping and resonant frequency.

APPLICATION OF THE EQUIVALENCE EQUATIONS

A sweeping sine-wave test is very cumbersome to apply if one is required to sweep at a constant rate throughout the entire spectrum as is implied by Eq. (24). It is noted however, that all the work performed by a sweeping sinusoid is done at or near resonance. In view of the foregoing and in the discussion that follows, Eq. (24) may be rewritten by replacing f' with the time necessary to sweep an octave and the octave bandwidth.

$$\frac{T_o}{T_1} = \frac{2S\Delta f_o}{G^2} \qquad (25)$$

where

Δf_o = octave bandwidth

T_o = time to sweep an octave.

This approximation to the equivalence formula is easier to apply and is backed by physical reasoning as seen in the following discussion. This form of the equivalence equation is a good approximation to the logarithmic sweep which is available on most shake tables.

In applying Eq. (25) to an actual system, some careful considerations must be applied. First of all, the equations must be general for a system containing many modes, and, second, due consideration must be given to the nonlinearities of an S-N curve (Fig. 2). The latter consideration may be satisfied by setting T_o/T_1 equal to unity. That is to say that the time taken to sweep through one octave must be equal to the total time the random noise is applied. As experimental data become available it may well indicate that some number other than unity be chosen for T_o/T_1. For the purpose of this discussion it will be assumed that this number is absorbed in the constant 2. This follows from the fact that the sweep can do work only at the frequencies it is sweeping while the random is doing work on all frequencies of the system. The effect is to boost the random levels until they are causing rms stress responses in the same order of magnitude as the sweeping sinusoid. If one were to reduce the interval of consideration to say 1/3 octaves, he would have an even closer equivalence of stress levels.

To demonstrate the applicability of Eq. (25) to a system with many resonances, consider Fig. 3. Assume there is one mode in a given octave.

The random noise is applied to all octaves for T_1 but it is doing work only in the octave containing the resonance. The

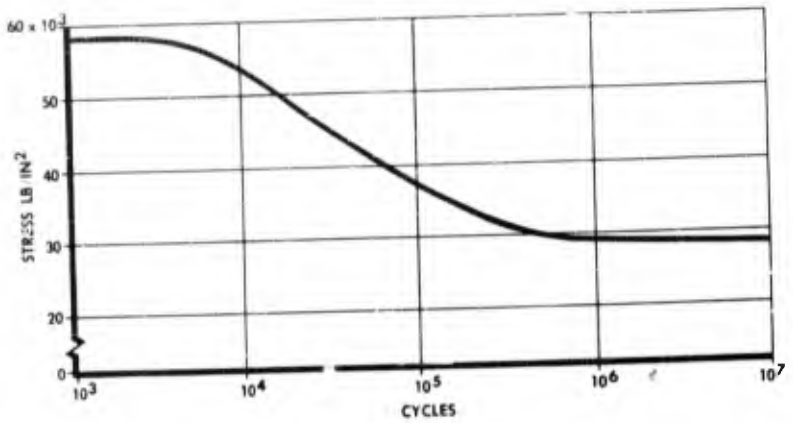

Fig. 2 - S-N diagram, 1020 steel

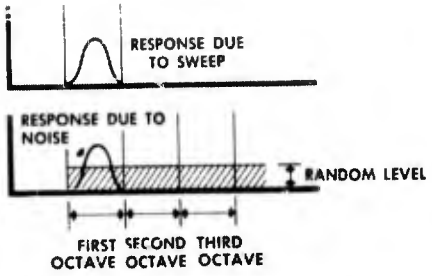

Fig. 3 - Consideration of response due to sinusoidal sweep plus random noise for one mode in a given octave

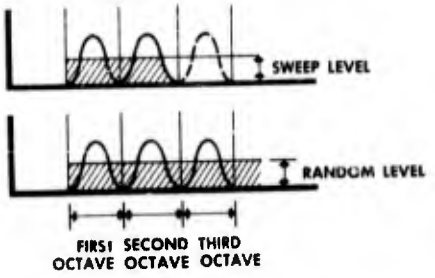

Fig. 4 - Consideration of response due to sinusoidal sweep and random noise for modes in other octaves

sweep is of course only doing work in the octave containing the resonance. The levels are adjusted so that each does the same amount of work in time T_1

Now consider modes in the other octaves, Fig. 4. The random noise is applied at the same level for the same time as previously, but now it is doing work in all octaves since there are resonances there. It is necessary that equivalence be established for each mode independently (or octave as in this example). This equivalence is an approximation for high-Q systems, since in the derivation the integrals were evaluated for a constant level from zero to infinity. Therefore, the sweep time T_1 for the first octave must remain the same as before since the random is doing the same work as in the previous case. By the same reasoning, then the sweep time must be adjusted in octaves two and three so that they are each swept in time T_1. This equivalence is plotted in Fig. 5 as S/G^2 versus frequency. This chart also contains resonance equivalents for reference.

In using the graph, it is assumed that the slope of 6 db/octave is pretty well established from theoretical considerations. The vertical position of the curve is determined by the constant 2 in Eq. (25) and the equivalence time factor. It is assumed that experimental data will become available to better determine the actual value of these constants.

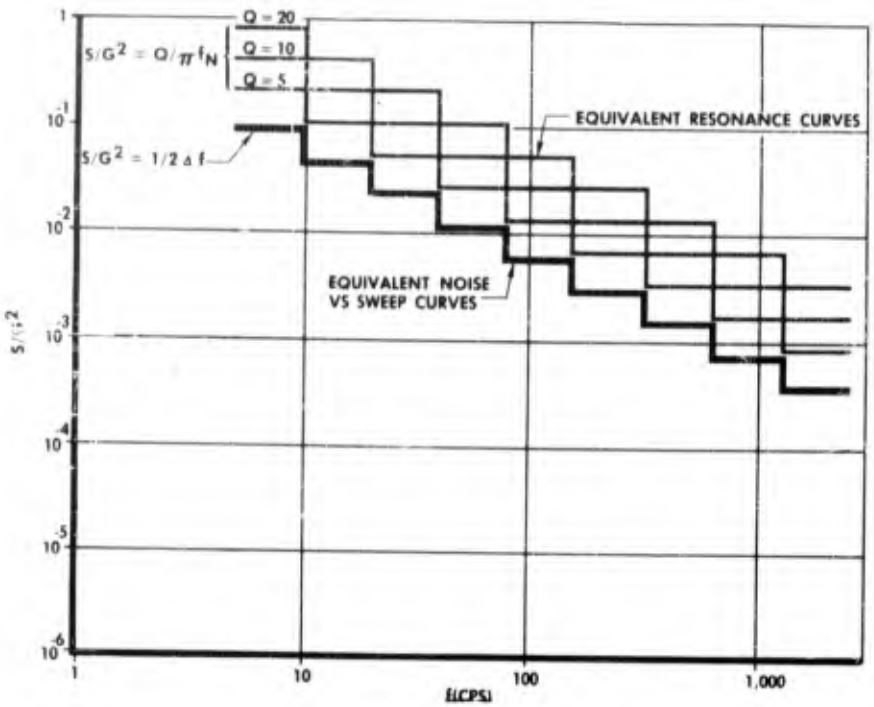

Fig. 5 - Equivalence curves for the ratio of s/G^2

Figure 5 is replotted as S versus G curves (Fig. 6) for easier reference. To use the curves one would first determine the time duration of test and then enter the curves to find the octave levels for the sweeping sinusoid and the white noise inputs.

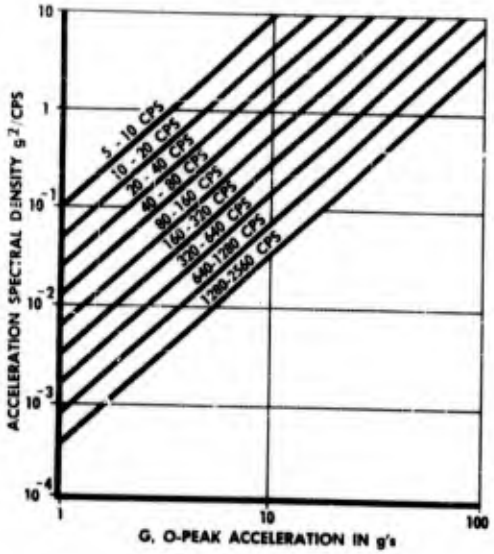

Fig. 6 - Equivalence curves for random noise versus sweep

CONCLUSION

The theoretical analysis given in this paper is intended as a basis for a rational approach to the equivalence of sine-wave and random testing. A test program is currently underway at Douglas to determine experimentally some of the theoretical constants derived in the paper. Due to the difficulties of fatigue testing, these constants will be determined as statistical quantities only.

BIBLIOGRAPHY

1. Stephan H. Crandall, "Notes for the M.I.T. Special Summer Program on Random Vibration," The Technology Press of M.I.T., Cambridge 39, Mass., 1958.
2. J. G. Truxal, Automatic Feedback Control System Synthesis, McGraw-Hill Book Co., N. Y., 1955.
3. W. B. Davenport and W. L. Root, An Introduction to the Theory of Random Signals and Noise, McGraw-Hill, N. Y., 1958.

DISCUSSION

Mr. Parker (Collins Radio Co.): I think I tend to agree with you that the log sweep is better in the case when designing something for a very limited lifetime like a missile. I was thinking more in terms of designing something for an indefinite lifetime.

Mr. Hall: Well, I'm glad you're thinking in those terms. Frankly, we haven't found that kind of a beast yet at Douglas.

Mr. Bieber (Lockheed Missiles and Space Div.): I wonder if you'd clear this up for me. Are you saying that as long as you dissipate the same amount of damping energy in these various tests that you produce the same amount of damage?

Mr. Hall: Providing we work the proper stress levels. Remember we had this discussion on the fact that we can't use a very low-level random vibration because we'd do an infinite amount of work, but we'd never produce any damage. If you can get the stress level high enough, then the criteria that the time taken to sweep one octave must be equivalent to the total time your random is applied. That is correct and that is what our experiments show.

Mr. Galef (National Engineering Science Co.): The argument about the time to sweep one octave being the same as the total time at random would seem to be applicable if the bandwidth of your resonance is one octave. The bandwidths of most resonances that I've seen are much, much less than one octave, sometimes as little as 1, 2, or 3 percent. Would you then say that the time at each 2 percent should be the whole time? Wouldn't you also have to say that now the sweep time is a function of the Q, which it seems you previously said was not a function of the Q?

Mr. Hall: It is definitely not a function of Q. The equivalence is based on the fact that it is completely independent of all the system parameters of the specimen being tested. Now this is on a work basis. Let me point out, if you have a very sharp Q system, there is a possibility, when you consider the nonlinearities of the S-N curve, that we are going to get a statistical scatter in our correlation. But I think that this is minor. I think this is always going to happen. There are nonlinearities in other things that enter into any test system, but these are minor. The point is that we don't have any systems with Q so low that we cannot get all the work done in the particular octave in which the resonance is contained.

Mr. Shoulberg (General Electric Co.): In your future planning do you propose duplicating failures on things other than simple beams? I don't do much testing on simple beams. I am involved in some complex components. I think the criterion here is going to be in duplicating damage or actual failures for a correlation. Am I not right?

Mr. Hall: You have correctly stated a hypothesis. You have also correctly stated that this test was designed for one purpose and one purpose only. That is to check the theory. That beam has absolutely no use to anybody except to check our theory here and it does check that. Now as to the other problem you bring out. What about components? That is a problem which, frankly, we haven't started into yet, but I'm sure that we are going to use the equivalence we derived here as the basic foundation for going into components and deriving the equivalence. I don't know of any other logical way to do it. We've run into relay chatter and things which depend strictly on not very nonlinear-type phenomena. To answer your question, we are going to use this theory in our future testing to start out with. Now what the statistical correlation is going to show the next time I talk to you folks, I don't know.

* * *

EFFECT OF DETUNING IN COUPLED SYSTEMS EXCITED BY SINGLE-FREQUENCY SWEEPS

Charles T. Morrow*
Space Technology Laboratories, Inc.
Los Angeles, California

The response of two resonators, coupled without loading, to excitation by a single-frequency sweep or a periodic vibration has been calculated. The derivative of the response has been taken with respect to the resonant frequency of either resonator. This derivative is expressed in such a way that a value greater than unity shows detuning to be more important than strengthening as a way of improving reliability. Plotted curves serve to emphasize that this is true for a wide variety of conditions.

The measurement of dynamical parameters for quantitative application of the curves is often difficult. A procedure is therefore given for the direct experimental investigation of the effect of detuning in items of practical equipment, by means of temporary additions of mass or stiffness. The procedure leads to design changes that greatly reduce stress.

INTRODUCTION

Most engineers who consider themselves to be shock and vibration specialists are familiar with the phenomena of resonance. Yet, five years ago, little attention appeared to be paid to such phenomena in the practical routine engineering of equipment items when the phenomena were more pertinent to reliability than to nominal performance. Since then, there has been an increasing emphasis on the control of resonance parameters and in particular on the benefits of staggering the resonances of coupled systems. This has received little discussion at symposia, however. Since major changes in the practice of shock and vibration engineering are seldom accomplished without extensive discussion, it appears likely that resonance, on the average, is still not receiving the attention it deserves. The fact that virtually no data are available to equipment engineers on the resonance characteristics of standard parts such as vacuum tubes and relays tends to support this observation.

Vibration test requirements are still chosen with little or no regard for specific characteristics of resonance. It would be too complicated, of course, to try to simulate every peak and valley in the data on which a requirement may be based. In time, it may be possible to arrive at general over-all plans for the resonance characteristics of particular classes of equipment and shape the spectra listed in the various test requirements so as to encourage compliance with the plans. In the meantime, the spectra used are still generally uniform with frequency. The final test for the completed item of equipment may be a complex-wave or random-vibration test, whereas the requirement for testing at lower levels of assembly may be a single-frequency test. Except for this distinction when it is made, there is little variation in spectral shape or over-all severity of excitation according to level of assembly. Since the requirements have so little obvious connection with resonance (except when fixed-frequency excitation of the more prominent structural resonances is a part of a specification), they

*Now at Aerospace Corp., Los Angeles, California.

constitute a distraction from resonance. Even the most sophisticated engineer sometimes becomes so absorbed in the purely formal aspects of compliance with requirements that he forgets to think about resonant frequencies. Yet, the qualification tests for subassemblies, parts, and vendor-supplied items do not ensure satisfactory operation or reliability in a complete assembly unless resonances are subject to some degree of control — either as a recognized but informal supplement to the specifications or as an inadvertent result of the practices of the designer.

The design engineer is not necessarily a shock and vibration specialist. Five years ago, one could say with little fear of contradiction that after a failure of a part in an equipment vibration test, the design engineer would simply "strengthen" the part. This, of course, affected the over-all dynamics and often even resulted in a beneficial detuning, but he did not think in these terms. It is probable that the situation has changed somewhat. It is equally probable that further progress can be made.

There have been powerful practical obstacles to progress in the use of the concepts of resonance even though the applications may seem to many people to be obvious and in little need of further discussion. Simple criteria for routine shock and vibration practices have been essential. Yet habitual use of them tends to dull the imagination. Furthermore, the more enterprising engineer who attempted an investigation of equipment dynamics, even in an emergency situation where drastic measures involving unusual effort were warranted, often found his measurements too complicated and confusing to be useful. He gave up in dispair.

This paper records a brief investigation of detuning of two coupled resonators for the special case of no loading. The presentation of the result is novel, and its quantitative aspects may be useful even to those engineers who are completely conscious of the significance of resonance. Qualitatively, the presentation should serve as a motivation for those who are not. The paper concludes with a discussion of a practical shortcut method of effecting detuning, which though little applied at present, will be found useful in many cases.

THE DYNAMIC MODEL

The model for the analyses is shown in Fig. 1. One resonator is mounted on another

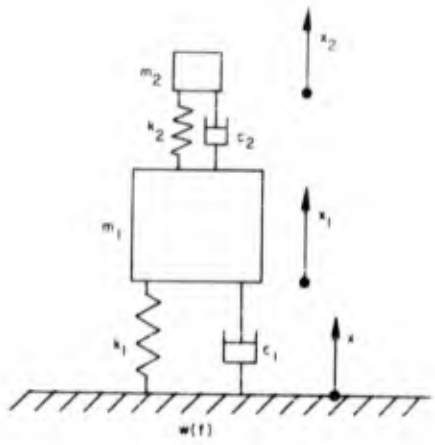

Fig. 1 - Two mechanical resonators, coupled in cascade, and excited by vibration or shock

which in turn is excited by motions of shock or vibration. To relate this model to practice, the lower resonator might represent the frame of an item of equipment, mounted on a damped isolator. The upper resonator might represent a resistor mounted by its leads within the equipment or it might represent the grid of a vacuum tube.* Alternately, the lower resonator might represent a terminal board at its first resonance, supporting the resistor or vacuum tube.

It will be assumed that the upper resonator does not load the lower — that is, the presence of the upper resonator does not significantly affect the motion of m_1; in other words, the upper resonator is of light and flexible construction by comparison with the lower. While this is by no means true in general of coupled resonators in practical equipment, it is a limiting case of importance. Furthermore, the detailed investigation of equipment failures involving coupled resonators is quite likely to disclose not only coincidence of resonance frequencies but light loading. Thus, the coupled resonators under analysis here constitute a better model when equipment must be redesigned than during the early design stage.

Instead of the six quantities, m_1, c_1, k_1, m_2, c_2, k_2, it is more convenient to use the following four parameters in the calculations:

*Leaving the body of the resistor free to vibrate, with no clamping or cementing, is not necessarily the best practice for extreme vibration environments.

$$f_1 = \frac{1}{2\pi}\left(\frac{k_1}{m_1}\right)^{1/2} \quad (1)$$

$$f_2 = \frac{1}{2\pi}\left(\frac{k_2}{m_2}\right)^{1/2} \quad (2)$$

$$Q_1 = 2\pi f_1 m_1 c_1 , \quad (3)$$

and

$$Q_2 = 2\pi f_2 m_2 c_2 . \quad (4)$$

These are sufficient for the calculations to be performed, provided there is no loading.

The aspect of interest is the response of the upper mass, since the response of the lower, under the assumption of no loading, is the same as that of the simple resonator.

STEADY-STATE RESPONSE

The treatment here is limited to considerations of the magnification or transmissibility, without consideration of phase. This is given for a simple resonator by

$$M_o = \left[\frac{1 + f^2/f_o^2 Q^2}{(1 - f^2/f_o^2)^2 + f^2/f_o^2 Q^2}\right]^{1/2} \quad (5)$$

Hence, for the model of Fig. 1, it is given by

$$M = \left[\frac{1 + f^2/f_1^2\, Q_1^2}{(1 - f^2/f_1^2)^2 + f^2/f_1^2\, Q_1^2}\right. \quad (6)$$

$$\left.\frac{1 + f^2/f_2^2\, Q_2^2}{(1 - f^2/f_2^2)^2 + f^2/f_2^2\, Q_2^2}\right]^{1/2} = M_1 M_2 .$$

As Eq. (6) is symmetrical with respect to f_1, f_2, Q_1, Q_2, it does not really matter which subscript is associated with the upper resonator.

For $Q_1 >> 1$, $Q_2 >> 1$ and $f_1 = f_2$, Eq. (6) reduces to

$$M = [Q_1 \cdot Q_2] . \quad (7)$$

Thus, M can have extremely large values for these conditions. For example, if $Q_1 = Q_2 = 10$, $M = 100$. Q's much higher than this are often found in equipment.

EFFECT OF DETUNING

As indicated in the introduction, design engineers often have a tendency to think of redesign, after shock and vibration failures, in terms of strengthening parts. Except when isolators are specifically in mind, it is not entirely common to think in terms of altering the transmission path so as to reduce the stress. Yet Eqs. (6) and (7) suggest that this is often the best basis for redesign. In fact, this is what the designer often actually accomplishes through an inadvertent detuning. The equations also suggest that sometimes manufacturing tolerances have a relation to reliability, not so much through control of strength as through control of the transmission path by means of relative tuning.

These effects can be estimated from Eq. (6). However, for small changes, the derivative of Eq. (6) with respect to f_1 or f_2 is more informative. The question one would like to ask is, "What percentage change in response will result from a given percentage change in mass or stiffness?" When the ratio is greater than unity, one can assume that the detuning effect is more important than any change in strength.

From either Eq. (1) or (2), it follows that

$$\log f = \log \frac{1}{2\pi} + \frac{1}{2}\log k - \frac{1}{2}\log m . \quad (9)$$

Thus

$$\left.\frac{df}{f}\right|_{m=\text{const}} = \frac{1}{2}\left.\frac{dk}{k}\right|_{m=\text{const}} \quad (10)$$

and

$$\left.\frac{df}{f}\right|_{k=\text{const}} = -\frac{1}{2}\left.\frac{dm}{m}\right|_{k\ \text{const}} \quad (11)$$

Consequently, the derivatives of interest should not only be made dimensionless but divided by two.

$$\frac{f_1}{2M}\frac{\partial M}{\partial f_1} = \frac{f_1 M_1}{2M}\frac{\partial M_2}{\partial f_1} + \frac{f_1 M_2}{2M}\frac{\partial M_1}{\partial f_1} \quad (12)$$

$$= \frac{f_1}{2M_2}\frac{\partial M_2}{\partial f_1} + \frac{f_1}{2M_1}\frac{\partial M_1}{\partial f_1}$$

and

$$\frac{f_2}{2M}\frac{\partial M}{\partial f_2} = \frac{f_2}{2M_2}\frac{\partial M_2}{\partial f_2} + \frac{f_2}{2M_1}\frac{\partial M_1}{\partial f_2} . \quad (13)$$

The greatest damage potential occurs when the exciting sinusoid is tuned to one resonant frequency or the other. For a vibration environment of periodic nature, as it occurs during use or transportation of an item of equipment, it would be unnatural to expect the excitation frequency to shift as f_1 or f_2 is changed. However, for a single-frequency sweep as performed during a laboratory test, the maximum responses of the upper mass will occur approximately when $f = f_1$ and when $f = f_2$. It is assumed that these maximum responses are indicative of damage potential, and that the sweep is so slow that the resonators are fully excited. It is further assumed that Q_1 and Q_2 are constant.

Equation (6) is symmetrical with respect to f_1 and f_2; for present purposes, it does not matter whether f_1 is associated with the other. The conditions of greatest interest are therefore summarized adequately by obtaining two expressions for $(f_2/2M)(\partial M/\partial f_2)$ according to whether $f = f_1$ or $f = f_2$. The Q's are assumed to be constant. The expressions for $(f_1/2M)(\partial M/\partial f_1)$, if desired, may then be obtained by symmetry.

Assume first that $f = f_1$.

$$M_1 = \left[\frac{1 + 1/Q_1^2}{1/Q_1}\right]^{1/2} = (1 + Q_1^2)^{1/2} = \text{const} \tag{14}$$

$$M_2 = \left[\frac{1 + f_1^2/f_2^2 Q_2^2}{(1 - f_1^2/f_2^2)^2 + f_1^2/f_2^2 Q_2^2}\right]^{1/2} \approx \left[\frac{1}{(1 - f_1^2/f_2^2)^2 + f_1^2/f_2^2 Q_2^2}\right]^{1/2} \tag{15}$$

provided that Q_2 is large and f_1/f_2 is not too small.

$$\frac{\partial M_2}{\partial f_2} = 0 \tag{16}$$

$$\frac{\partial M_2}{\partial f_2} \approx \frac{2(1 - f_1^2/f_2^2)(2f_1^2/f_2^3) - 2f_1^2/f_2^3 Q_2^2}{2\left[(1 - f_1^2/f_2^2)^2 + f_1^2/f_2^2 Q_2^2\right]^{3/2}} - \frac{2f_1^2/f_2^3 - 2f_1^4/f_2^5 - f_1^2/f_2^3 Q_2^2}{\left[(1 - f_1^2/f_2^2)^2 + f_1^2/f_2^2 Q_2^2\right]^{3/2}}. \tag{17}$$

Hence, from Eq. (13),

$$\frac{f_2}{2M}\frac{\partial M}{\partial f_2} \approx -\frac{f_1^2}{f_2^2}\frac{1 - f_1^2/f_2^2 - 1/2 Q_2^2}{(1 - f_1^2/f_2^2)^2 + f_1^2/f_2^2 Q_2^2} = -\frac{r^2(1 - r^2 - 1/2 Q_2^2)}{(1 - r^2)^2 + r^2/Q_2^2} \tag{18}$$

where $r = f_1/f_2$.

Now assume, alternately, that $f = f_2$.

$$M_1 = \left[\frac{1 + f_2^2/f_1^2 Q_1^2}{(1 - f_2^2/f_1^2)^2 + f_2^2/f_1^2 Q_1^2}\right]^{1/2} \approx \left[\frac{1}{(1 - f_2^2/f_1^2)^2 + f_2^2/f_1^2 Q_1^2}\right]^{1/2} \tag{19}$$

$$M_2 = \left[\frac{1 + 1/Q_2^2}{1/Q_2}\right]^{1/2} = (1 + Q_2^2)^{1/2} = \text{const}, \tag{20}$$

$$\frac{\partial M_1}{\partial f_2} \approx \frac{2(1 - f_2^2/f_1^2)(-2f_2/f_1^2) + 2f_2/f_1^2 Q_1^2}{-2\left[(1 - f_2^2/f_1^2)^2 + f_2^2/f_1^2 Q_1^2\right]^{3/2}} = \frac{2f_2/f_1^2 - 2f_2^3/f_1^4 - 2f_2/f_1^2 Q_1^2}{\left[(1 - f_2^2/f_1^2)^2 + f_2^2/f_1^2 Q_1^2\right]^{3/2}}. \tag{21}$$

Hence, from Eq. (12),

$$\frac{f_2}{2M}\frac{\partial M}{\partial f_2} = \frac{f_2^2}{f_1^2}\frac{1 - f_2^2/f_1^2 - f_2^2/2f_1^2 Q_1^2}{(1 - f_2^2/f_1^2)^2 + f_2^2/f_1^2 Q_1^2} = \frac{(1/r^2)(1 - 1/r^2 - 1/2r^2 Q_1^2)}{(1 - 1/r^2)^2 + 1/r^2 Q_1^2}, \tag{22}$$

which is simply Eq. (18) with r replaced by its reciprocal and Q_2 replaced by Q_1. Thus, a plot of Eq. (18) will enable one to determine values for $(f_2/2M)(\partial M/\partial f_2)$ when either f is constant at f_1 or equals f_2 and changes with it.

By symmetry,

$$\frac{f_1}{2M}\frac{\partial M}{\partial f_1} = \frac{r^2(1 - r^2 - 1/2 Q_2^2)}{(1 - r^2)^2 + r^2/Q_2^2} \tag{23}$$

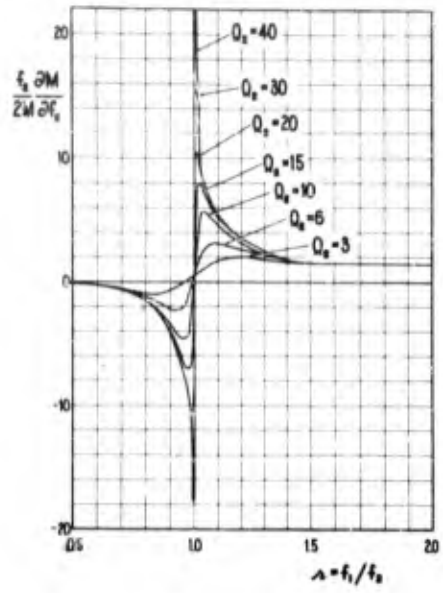

Fig. 2 - Curves of the derivative of the response of the upper mass of Fig. 1

when f equals f_1 and changes with it, and

$$\frac{f_1}{2M}\frac{M}{f_1} = -\frac{1/r^2(1-1/r^2-1/2\,Q_1^2)}{(1-1/r^2)^2+1/r^2\,Q_1^2} \qquad (24)$$

Thus, all necessary information is contained in any one of Eqs. (18), (22), (23), and (24). The first of these is plotted in Fig. 2 for various values of Q_2.* The importance of detuning when $f_1 = f_2$ and a sinusoidal excitation is expected in the neighborhood of either is quite evident. When the ordinate plotted is greater than unity and a failure that occurs in the terminal resonator necessitates a redesign, detuning should be considered as an alternate to strengthening.

Furthermore, when the ordinate is greater than unity, manufacturing variations have more effect on the transmission path by way of detuning than they do by way of effect on local strength. When environment is pertinent to reliability, it is customary to use for conceptual purposes a chart which shows an overlap between the distribution of the environment and the distribution of the strength. The environment and strength are both assumed to be measured at the same point, essentially the location of the failure. It is assumed tacitly that variations in the strength do not affect the environment, and that safety margins may be defined to express the relation of an independent strength to an independent environment. Figure 2 shows that this is not necessarily true for vibration; in fact, the safety margin does not necessarily increase when the strength increases. The chart is conceptually satisfactory only if it is recognized that the variation in the local excitation results in part from the same causes as those of the variation in strength, as well as from variations effectively in the ultimate source of the excitation.

*The fact that each equation involves the Q of only one resonator should be surprising. If the exciting frequency is tuned to either resonator, the Q of that resonator should not affect the derivative so long as that Q is constant, whether or not the frequency of the resonator (and the excitation) is changed.

A PRACTICAL DETUNING TECHNIQUE

It is possible to show that the benefits of detuning are of the same general magnitude when the excitation is random.* A similar result would be expected for shock, although here there is somewhat more uncertainty about what one can say concerning the response of the second resonator than in the case of random or single-frequency excitation. There should certainly be adequate motivation for staggering resonances where possible, regardless of the type of excitation. Applied as a general policy, such staggering provides generous benefits when loading is small, and it does no harm when loading is large. In the latter case, there is some conceptual difficulty from the fact that the resonances of a component are not the same as the resonances of the parts. This is seldom critical, however, and can usually be ignored.

Yet, it can not be said that all designers try to stagger resonances or that there is as yet a systematic approach to the staggering of resonances. Failures during environmental test of an assembled component often occur because of coincidence of resonance frequencies. Yet, little evidence of the cause comes directly to the designer as a result of a qualification test. Usually, he carries out a tentative redesign, and the test is tried again.

*C. T. Morrow, B. A. Troesch, and H. R. Spence, "Random Response of Two Coupled Resonators without Loading," Journal of the Acoustical Society of America, Jan. 1960.

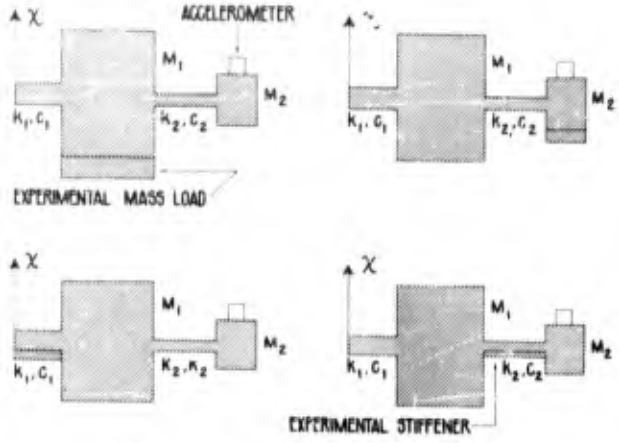

Fig. 3 - Experimental detuning of a two-resonator system

In many cases, valuable indications of the best redesign may be obtained by experiments on the component before it is removed from the shaker — especially if there are any reasons to believe that damping and loading are low.* It is necessary only to have some way of measuring the response in the region of the failure point on a relative basis and to have sufficient access to the interior of the component to make experimental changes that will affect the transmission path. When there is malfunction or performance deterioration without permanent damage, the undesired effect may often be used as a measure of response. Microphonics in vacuum tubes and chattering in relays lend themselves to this. In other cases, it may be possible to apply strain gages, use optical observations or even apply X-ray techniques. Experimental mass loads or stiffeners can usually be applied simply by cementing. A cement or tar that hardens on cooling may be convenient. The possible experiments that can be tried with a two-resonator system are suggested in Fig. 3.

*If there is a heavy schedule of qualification tests, the component may be removed to an auxiliary shaker.

It is not necessary to take time for precise dynamic measurements before using this technique. It is merely necessary to make experimental changes and observe their effect. The final official design change may not always be the same as what is tried experimentally. For example, if mass loading is beneficial, it may be preferable to reduce the stiffness of a spring.

CONCLUSION

It is hoped that this paper will increase the emphasis on detuning techniques where, for one reason or another, they are not consciously used now and that the final suggestions will make their application easier in many cases.

DISCUSSION

Mr. Hawkins (Sperry Gyroscope Co.): This condition that you have here of coupling two masses together which are widely separated in mechanical impedance seems to me a condition that you would necessarily try to avoid in a design that had to meet shock and vibration environments. Wouldn't you say this is true?

Dr. Morrow: I think one should try to avoid it, yes, but it's not necessarily avoided in practice.

Mr. Hawkins: I just want to emphasize, though, that this is a good design principle — to try to avoid this sort of thing. If you do

encounter it this critical tuning that you have here is probably a very good approach.

Dr. Morrow: I'm glad you agree with one of the main points I was trying to make. I would also like to point out that it is relatively easy to get into this type of problem with typical electronic equipment involving vacuum tubes, and also with equipment involving potentiometers with very finely made wipers within. Typically, one designs electronic equipment to a very short time schedule. The main problem the designer encounters is getting all the parts in and when, finally, the man on the board has succeeded in doing this, off the thing goes to the manufacturer. Then it often takes some time to figure out just what we've got and to do something about it if it doesn't work out right. So one can very easily get into this problem because of the practical limitations of the field we're working in.

Mr. Gertel (Allied Research Associates): I just wish to make the simple observation that adding mass changes the frequency by its inverse square root. This has a rather small effect on altering the resonant frequency. Unless the bandwidth of the resonance that you're concerned with is extremely narrow, you would probably have to add considerable mass to effect any significant change.

Dr. Morrow: Well, I think you'll find that the Q's of typical resonances inside a piece of equipment do tend to run fairly high unless special techniques are used to keep them low. For example, if you are trying to design a vibration isolator you find that you have to use quite a bit of care to get the Q a great deal below 10. This is with damping material particularly selected for the purpose. Now, within an item of equipment with the various other problems that are involved in there, often it is necessary to use metal parts with very little damping; it is quite easy to get Q's of 10 or higher. Under these conditions, yes, maybe you do have to add a little bit of mass — maybe you have to add 10 or 20 percent to get very much change — but I think it's interesting that there are times where you gain by weakening a spring, or adding a mass, which you would expect, of course, to increase the stress in the spring.

* * *

NATURAL BENDING FREQUENCIES AND MODE SHAPES OF MISSILES HAVING A MULTIPLE-TANK CONFIGURATION

J. D. O'Rourke and C. L. Conrad
Chrysler Corporation Missile Division
Detroit, Michigan

This paper covers an investigation of the problems of predicting the natural frequencies and mode shapes of a clustered-tank missile. It is shown by illustration that a single-tank representation of multiple-tank configuration is not feasible, and a general method of solution is proposed. A solution is presented for a simplified problem which is proved by a laboratory test. The complexities of the clustered-tank problem are discussed.

INTRODUCTION

The evaluation of the flight dynamics of a particular missile requires a knowledge of the natural frequencies and mode shapes of the structure. If a resonant condition should exist between the natural frequencies of the structure and the control or propellent sloshing frequencies, the mission of the missile could be jeopardized.

As the missions and payloads of the second generation of military missiles and space vehicles have become more demanding, the practice of staging and clustering missiles has become common. The clustered missiles are usually the lower stages of space vehicles and consist almost entirely of propellent tanks with attached engines. The practice of clustering has complicated the problems of accurately predicting the natural frequencies of vibration and forced industry to reevaluate the existing methods of analysis.

The matrix iteration procedure, as applied to a system represented by discrete masses, was chosen as the method of analysis in this paper because it is readily adapted for programming on digital computers of the card punching type, and can accommodate changes in the program as more information becomes available. While this method is not as accurate as many other methods, it has sufficient accuracy for the lower modes of vibration which are of primary importance in structural work.

SINGLE TANK REPRESENTATION

In Reference [1], the fundamental frequency of vibration for a missile, having a multitank booster, was computed by treating the missile as a single beam composed of discrete masses. This assumption is common in vibration problems but could give questionable results in the case of clustered-tank configurations.

Before attempting to establish a general method of solution, an analysis of two parallel tanks was made and compared to a single-tank representation of the two tanks. Both the single-tank and double-tank structures were of constant stiffness EI and had mass distributions simular to that of a missile.

A description of the mathematical models of the two systems is presented in Fig. 1. The springs supporting the attached tank of the two tank structure have stiffness constants which are large enough to produce bending in the supported tank. It was determined that the natural frequency of the system increases as the spring stiffness is increased until a point is reached where the ratio of spring stiffness to tank bending stiffness becomes large, and the frequencies remain nearly constant.

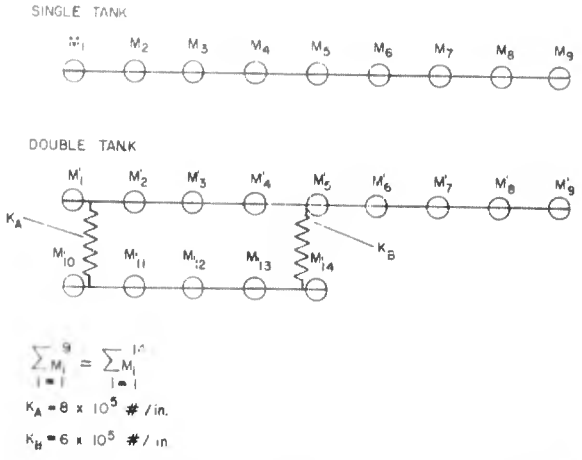

Fig. 1 - Systems represented by discrete masses

A comparison of the unrestrained bending modes is shown in Fig. 2. The single-tank structure has a higher frequency than the two-tank structure, although its stiffness is less than a representative two-tank structure would be. Also, the attached tank mode shape is out of phase with the main tank mode shape. Two conclusions were drawn from this comparison:

1. The two-tank configuration could not be accurately represented by a single equivalent tank.

2. The natural frequency of the system was greatly affected by the phase relationship of the attached tank.

To verify these two conclusions, a laboratory test was conducted on a two-beam system, and the results were compared to the results of an analytical study of the same system.

LABORATORY TEST

The test specimen consisted of a main cantilevered beam from which a second beam was elastically supported at two points. The beams were standard "I" beams with doubler plates and concentrated masses added to present a nonuniform case.

The test specimen was cantilevered from a heavy supporting structure and excited by electrodynamic shakers as shown in Fig. 3. The response of the specimen was determined by placing velocity-type vibration pickups at equal intervals along the beams; these were used to measure both frequency and displacement to obtain a mode shape. The outputs of the pickups were routed through a data-sampling switch, and recorded on an oscillograph recorder. The data-sampling switch was used to select the output from the vibration pickups in an orderly sequence to describe the mode shape.

The test specimen was first subjected to a low-level sinusoidal input from one or more shakers and measurements taken. The frequency was increased from a low level until a resonant condition was reached. Resonance was determined by placing the shaker armature input on the horizontal channel of an oscilloscope and the output from a vibration pickup on the vertical channel. The frequency where the pattern became a straight line at a 45° angle was the resonant condition. The resonant condition was checked by exciting the specimen by single shakers at different points and simultaneously at as many as three points. No significant shift in frequency or mode shapes were noted by these changes.

RESULTS

The first three bending modes of the restrained two beam system are shown in Figs. 4, 5, and 6. Both the test results and analytical results are presented for comparative purposes. Examination of the figures indicates that the mode shapes and frequencies of the analytical results agree reasonably well

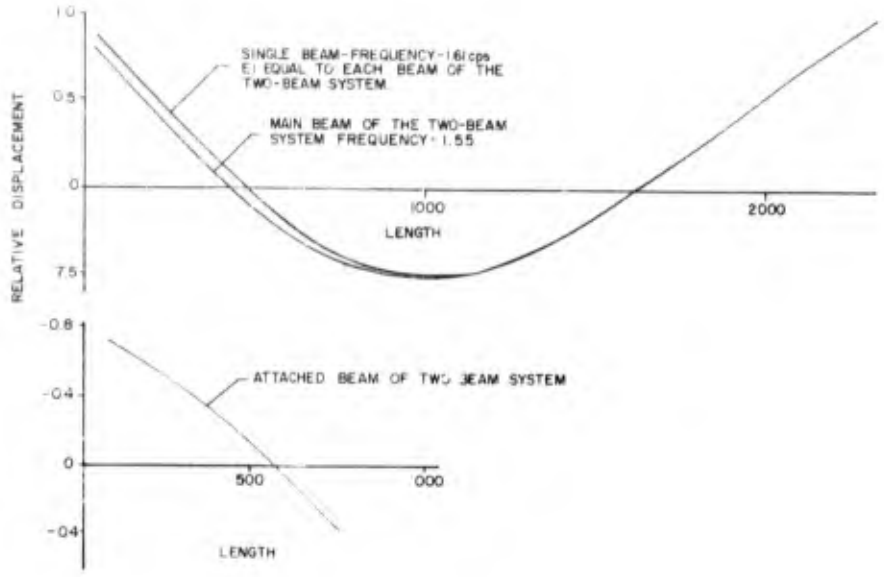

Fig. 2 - Comparison of unrestrained masses

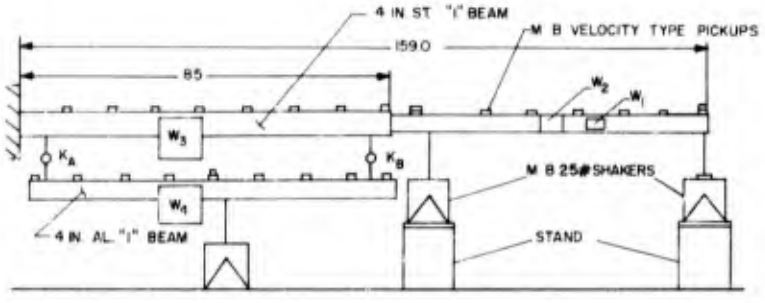

Fig. 3 - Restrained two-beam system (laboratory test)

with the test results for the first two modes. It may be pointed out, that the supported beam showed an out-of-phase relationship with the main beam in the first mode frequency. The main beam in both cases had the normal first-mode deflection curve for a cantilever beam. The third-mode frequency and shape do not correlate, but it was later established that the test frequency was erroneous due to a mounting structure resonance. The curve was left in to show that the third-mode shape for a two-beam system is similar to the normal second-mode shape of a single cantilevered beam.

Small discrepancies between the analytical and the test results can be traced to discrepancies in the mathematical representation of the test specimen. For instance, handbook values of the elasticity modulus, shear modulus, and inertia, etc., were used and the beam assumed perfectly restrained, which could not be duplicated completely in the laboratory. This indicates that while the laboratory test served its purpose of verification of the analytical technique, an estimate of the accuracy of the analysis could not be made.

ANALYTICAL TECHNIQUE

The analytical technique used throughout this paper is the matrix iteration procedure as applied to systems represented by discrete

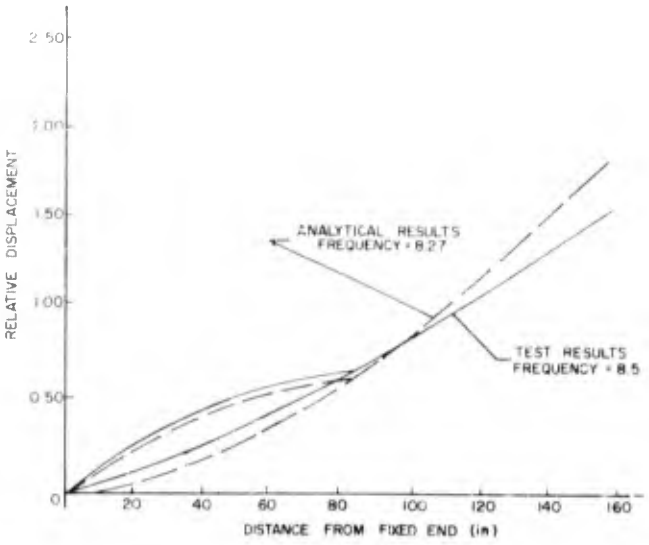

Fig. 4 - Restrained two-beam system (first mode)

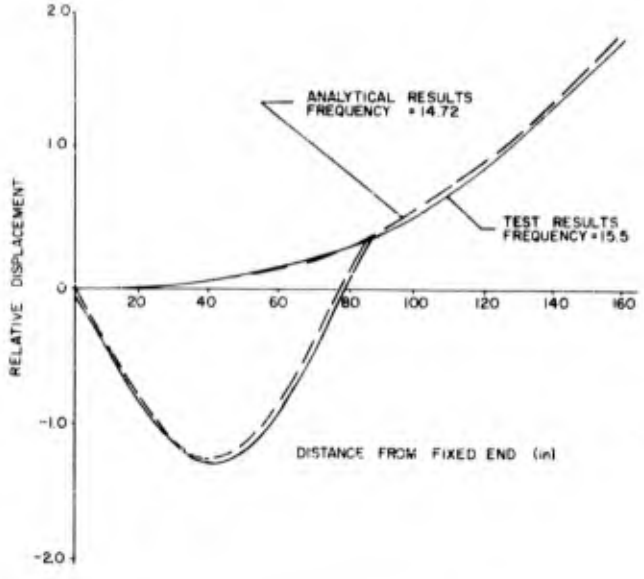

Fig. 5 - Restrained two-beam system (second mode)

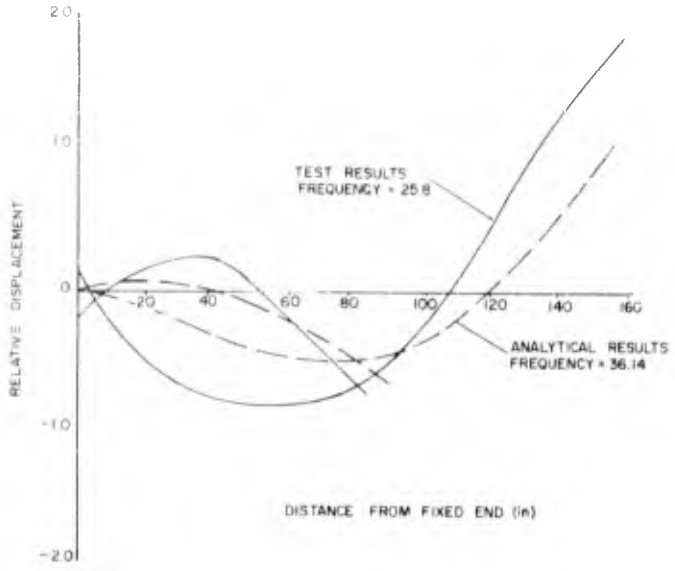

Fig. 6 - Restrained two-beam system (third mode)

masses. This method is widely used and discussed in many text books, and therefore, only the general equations are presented in this paper.

The analysis considers the structure to be divided into rigid segments, with the total mass of each segment concentrated at its center of gravity. The points at which the masses are concentrated are known as control points. The equations of motion for this system were written in terms of flexibility influence coefficients, C_{ij}. These coefficients represent the deflection of control point i due to a load at control point j. The coefficients are obtained by placing a unit load at a control point and calculating the resulting deflections at the remaining control points. The integral form of the influence coefficient equations was used in this analysis to allow solutions of systems having nonuniform properties. The general influence coefficient for a cantilevered beam in bending is as follows.

$$C_{ij} = x_i x_j \int_0^{x_i} \frac{d\lambda}{EI} - (x_j + x_i) \int_0^{x_i} \frac{\lambda\, d\lambda}{EI}$$

$$+ \int_0^{x_i} \frac{\lambda^2}{EI} d\lambda + \int_0^{x_i} \frac{d\lambda}{GK} \quad \text{for } x_i \leq x_j$$

where

x_i = distance from fixed end to i

x_j = distance from fixed end to j

λ = variable along x axis

EI = bending stiffness

GK = shear stiffness.

The influence coefficients obtained from this equation include shear flexibility.

The equations of motion were then transferred to matrix notation, and programmed on a digital computer. The influence coefficient equation was also programmed to expedite the problem solution. The matrix equation is

$$\{y\} = \omega^2 [C] [m] \{y\}$$

where

$\{y\}$ = displacement matrix

ω = frequency

[C] = influence coefficient matrix

[m] = mass matrix.

This equation is solved by an iteration procedure to obtain the fundamental bending frequency and mode shape. This is done by assuming a set of displacements $y_1, y_2, y_3 \cdots$ and performing the indicated operations. The resulting displacements are then made relative to a single displacement which is reduced to unity. Iteration is continued until the displacements stabilize to a definite pattern.

To obtain the higher bending modes of the system the orthogonality relation is introduced. This relation is used to eliminate the lower mode components from the higher modes, allowing convergence to a higher mode. In matrix form this relation appears as a sweeping matrix [s]. The matrix equation for higher modes takes the form of

$$\{y\} = \omega^2 [C][m][s]\{y\}$$

where [s] = sweeping matrix.

For the unrestrained case the beams are first restrained and the [C] matrix computed and then the restraints removed by applying the equations of motion needed for equilibrium of the unrestrained elastic body. The [G] matrix, which is used to compute the unrestrained frequencies, is formed from the following relation

$$G_{ij} = C_{ij} + \frac{S_{x_i} - I_o}{MI_o - S^2} \sum_{k=1}^{n} C_{kj} m_k + \frac{S - M_{x_i}}{MI_o - S^2} \sum_{k=1}^{n} C_{kj} m_k x_k$$

where

I_o = Pitching moment of inertia of both beams about the base

S = Static moment of mass to the right of the base taken about the base

M = Total mass.

DISCUSSION OF THE ANALYTICAL TECHNIQUE

The matrix iteration process for systems represented by discrete masses is a very general method, in that the system can be adapted to cover a variety of structures without changing any of the basic processes. For more complicated structures the complexity of the individual matrices comprising the general equation increases. For instance, the influence coefficient matrix [C] for a single beam in bending comprised of n masses is represented by

$$C_{ij} = \begin{bmatrix} C_{11} & C_{12} & \cdots & C_{1n} \\ C_{21} & C_{22} & \cdots & C_{2n} \\ \cdot & \cdot & & \cdot \\ \cdot & \cdot & & \cdot \\ \cdot & \cdot & & \cdot \\ C_{n1} & C_{n2} & \cdots & C_{nn} \end{bmatrix}.$$

While the influence coefficients matrix for n = 4, combining bending and torsion, is represented by

$$C_{ij} = \left[\begin{array}{cc|cc} C_{11}^{\Delta\Delta} & C_{12}^{\Delta\Delta} & C_{13}^{\Delta\theta} & C_{14}^{\Delta\theta} \\ C_{21}^{\Delta\Delta} & C_{22}^{\Delta\Delta} & C_{23}^{\Delta\theta} & C_{24}^{\Delta\theta} \\ \hline C_{31}^{\theta\Delta} & C_{32}^{\theta\Delta} & C_{33}^{\theta\theta} & C_{34}^{\theta\theta} \\ C_{41}^{\theta\Delta} & C_{42}^{\theta\Delta} & C_{43}^{\theta\theta} & C_{44}^{\theta\theta} \end{array}\right]$$

where

$C_{ij}^{\Delta\Delta}$ = linear deflection at i due to unit force at j

$C_{ij}^{\theta\theta}$ = angular deflection at i due to unit moment at j

$C_{ij}^{\Delta\theta}$ = linear deflection at i due to unit moment at j

$C_{ij}^{\theta\Delta}$ = angular deflection at i due to unit force at j.

It is readily seen from this discussion that the computation of the influence coefficient matrix for a given situation will be the difficult step towards a solution with this method of analysis. However, the influence coefficient matrix for a simple case may be systematically enlarged for more complicated cases. For instance, the influence coefficient matrix for two-beam systems is shown in Fig. 7. The portion of this figure designated as Blocks I and II represents the matrix needed for single-beam problems, while the remaining blocks are needed for solution of the two-beam problem.

It may be noted here that the influence coefficients have the property of symmetry,

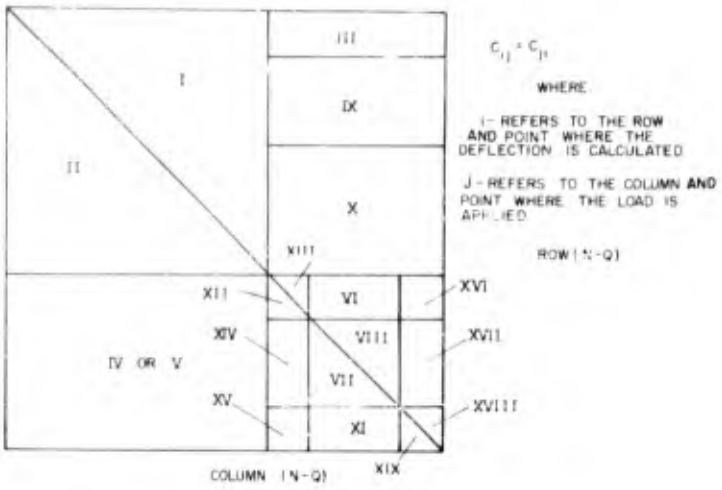

Fig. 7 - Influence coefficient matrix for two-beam system

i.e., $C_{ij}^{\Delta\Delta} = C_{ji}^{\Delta\Delta}$ and $C_{ij}^{\Delta\theta} = C_{ji}^{\theta\Delta}$; thus, only half of the influence coefficients need to be calculated for a given matrix. The [G] matrix does not have the property of symmetry.

At this time the matrix iteration method has been successfully programmed to provide the natural bending and torsional frequencies and mode shapes of such items as shafts, rotors, control surfaces, and complete missiles. In one instance, it was modified to provide for a cantilevered mass off the main structure to predict the bending frequency of the Jupiter missile, where the cantilevered mass represented the rocket engine. This was done in conjunction with a full-scale test to verify that the cause of an additional frequency was the cantilevered engine. Previous methods of analysis could not account for this frequency which was caused by the phasing of the engine and main structure.

The programs, just mentioned, indicate the versatility of the matrix iteration procedure, but they do not provide a clear indication of the advantages and disadvantages of the method. These may be summed as follows:

Advantages:

The matrix iteration procedure can be readily programmed on a digital computer.

The input data for an established program may be obtained through routine calculations.

The inputs may be easily modified to provide a different mass distribution and stiffness, etc.; this allows the program to be used as a preliminary design tool.

Disadvantages:

More sophisticated systems offer greater accuracy, especially in the higher modes which are of interest in elastic body flight dynamics and transient stress analysis.

Only relative deflections of the tanks are known in terms of the simplified configuration, i.e., where the masses are located.

CONCLUSIONS

The ultimate goal is to provide a solution, using the matrix iteration method, which will accurately predict the natural frequencies and mode shapes of a missile having several tanks attached at any angle for combined bending and torsion. The solution for this program would require a complex influence coefficient matrix similar to the case described in the Discussion of the Analytical Technique.

A solution of a multitank missile has been obtained using only the bending portion of the matrix and restricted to one plane. However, no conclusions can be drawn at this time and no attempt has been made to include the

torsion effects. It is felt that the groundwork for the final solution has been prepared and the solution can be obtained in the near future.

REFERENCES

1. "Vibration Analysis of Juno V (3 and 4)," Army Ballistic Missile Agency, Redstone Arsenal, DA Tech. Memo. No. 8-59, Jan. 1959.
2. Michael Dublin and Hans R. Friedrich, "Forced Responses of Two Elastic Beams Interconnected by a Spring Damper System," J. of Aero. Sci., Vol. 23, pp. 824-829, Sept. 1956.
3. G. A. Socks, "Jupiter Missile Bending Frequencies and Modal Shapes," Chrysler Corp. Missile Div. Tech. Memo. AME-M4J, Feb. 1957.
4. Bisplinghoff, Ashley, and Halfman, Aeroelasticity, Addison-Wesley, 1955.
5. C. L. Meikle, "Fundamental Bending Frequency and Mode Shape Analysis for a Clustered Tank Missile," Chrysler Corp. Missile Div. Tech. Note AME-TN-3-59, June 1959, (CONFIDENTIAL).
6. A. L. Ikola, "Experimental Determination of the Vibration Modes of a Two-Beam System," Chrysler Corp. Missile Div. Tech. Memo. No. 755-60-197.
7. J. D. O'Rourke, "The Natural Bending Frequencies and Mode Shapes of a Two Beam System," Chrysler Corp. Missile Div. Tech. Note AME-TN-12-60.

DISCUSSION

Mr. Stern (General Electric Co.): I wondered if any place in your paper you considered the shear and rotary inertia of these discrete masses.

Mr. O'Rourke: We did figure out the shear flexibility, the rotary inertia we didn't take into account.

Mr. Stern: The only reason I mentioned it is that you said that there was somewhat of a disagreement between the two systems when you had the equivalent beam. I would expect it to be somewhat different, but some of the difference might be the result of the fact that the shear and rotary inertia corrections would be somewhat different for these two different systems. You wouldn't have the same error in both and this might be the reason for the difference.

Mr. O'Rourke: This is a good point. I don't know too much about the effects of the rotary inertia, since we don't include it; but we feel that it is probably more effective in the higher modes.

Mr. Stern: Well, what I was thinking of is that if you had, say, an aircraft wing with a pontoon quite a ways below it, if you just broke the wing up into discrete masses and you just stuck the pontoon up on the wing, you would have quite an error. This might be introducing some errors in your solution.

* * *

CONCEPTUAL APPROACH TO VIBRATION CONTROL FOR SYSTEM RELIABILITY

L. I. Mirowitz
McDonnell Aircraft Corporation
St. Louis, Missouri

This paper presents a unified approach of vibration control during system design and subsequent development. Considerable emphasis is placed on a scheme of systematically predicting the vibration environment for new design configurations in which the structural impedance of the airframe is used in the extrapolation process from old to new configurations. The use of data defining the failure susceptibility of equipment in a vibration environment—the Component Functional Profile—is recommended in order to define an Index of Reliability which assesses quantitatively the relative merits of equipment to operate reliably in the predicted environment. Frequency sweep testing is used for the qualification and development tests of equipment, with random-vibration testing preferred in those instances where actual flight failure has been encountered and ground testing must be undertaken to establish corrections.

INTRODUCTION

Many approaches are in use today for controlling the vibration environment existing in airframes. This effort is intended to lead to a reliable weapon system. Advances in the state of the art to date have been concerned primarily with test techniques for simulating the vibration environment in ground reliability testing. Comparatively little work has been done in the field of environment prediction. Because of the many test techniques available, there exists controversy in their utilization. For example, should one use sinusoidal sweep testing versus random-vibration testing, combined environment testing versus separate environment tests, and a number of other combinations. In most cases the test techniques are based on various assumptions of the vibration environment to which the system will be exposed in actual use. Quite often these assumed environments are based on military specifications modified to account for past operational experience on similar vehicles.

It is generally agreed that the state of affairs existing in the area of environmental predictions is less than satisfactory. Also, though a number of sophisticated test procedures and test systems have been developed for more thorough ground testing of equipment, much still has to be done in establishing a quantitative measure of the equipment reliability when exposed to the test and operational environment of the flight vehicle. Furthermore, it is the writer's experience that much of the science of vibration control is based on intuitive thinking and abstract manipulations of data which are difficult for engineering personnel not specializing in this field to comprehend.

The need exists for a more systematic approach to the problem of vibration control for system operational reliability, encompassing the total phase of engineering development of an operational system. In many ways, this approach can be patterned after the methods used in the stress analysis of structures. In this case, one goes through the following basic steps: prediction of the loads, analysis of the structure, predicted margin of safety, proof testing, and operational test experience. In a similar vein, a total program for vibration control should include the equivalent steps followed in stress analysis. These are: predicting the environment—the

vibratory loads, analysis of the structure for resonance response—structural impedance, predicted index of reliability—margin of safety, ground development and proof testing, and operational experience and correction of deficiencies.

The purpose of this paper is to present a unified approach to vibration control during system design and subsequent development based on the systematic procedure used in structural stress analysis and encompassing the five major steps indicated above. Considerable emphasis is given to the proposal of a more systematic method of environmental predictions. The use of data defining the failure susceptibility of equipment to define an index of equipment operational reliability will be stressed. In conjunction with this, the importance of sinusoidal sweep testing is pointed out, with random-vibration testing preferred in those instances where actual flight failure has been encountered and ground testing must be undertaken to establish corrections.

SYSTEM DEVELOPMENT

The development of a system, be it a complete weapon system or a subsystem of the weapon system, involves three distinct phases. These phases are design, prototype development, and production development. These phases, including some important considerations within each phase of engineering development, are shown in Fig. 1. In essence, the design phase is concerned with the initial requirements, the establishment of design criteria, the use of past experience, and—from the standpoint of the environment—the establishment of an environmental control program, including definite design criteria and analysis approaches. In addition, during the basic design, considerable development testing on components is conducted, the results of which are incorporated in the philosophy of the design. The development of the prototype is basically a test phase of the complete system in which the deficiencies in the system are uncovered and in which corrections for these deficiencies are determined and developed. Production development involves operational experience, additional design effort for the production system, flight development and proof testing, and further corrections of deficiencies. A complete plan for vibration control must incorporate a program for each of these engineering development phases.

THE DESIGN PROBLEM

Figure 2 describes the various steps required for the vibration control effort during design. The first problem during this phase is the prediction of the internal structural environment which serves as the input to the various pieces of equipment fastened to the structure. At the present time, the scheme of predicting this internal environment involves military specifications—for example, Ref. [1]—supplemented by past experience on similar airframes intuitively extrapolated to the new configuration.

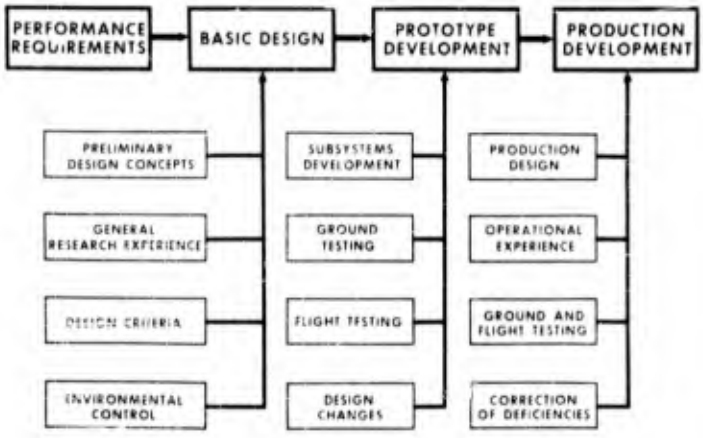

Fig. 1 - Phases of engineering development

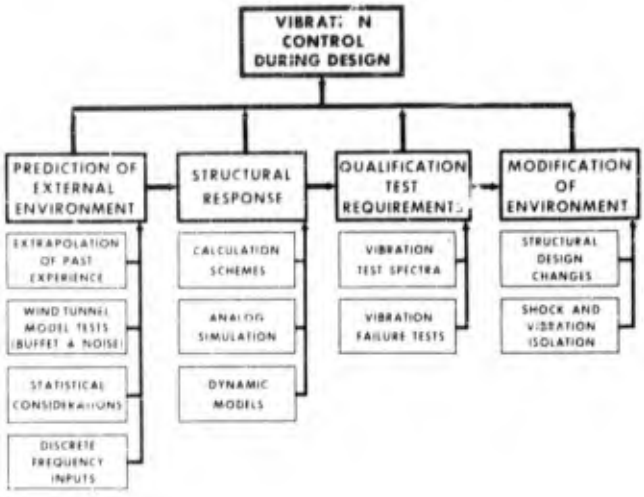

Fig. 2 - The design problem

Predicting the Environment

The vibration environment which is exhibited by an airframe is characterized as random since it is not possible to predict at any instant of time what the level of vibration will be during a mission. The cause of this environment may be such sources as propulsion excitation, rotating machinery, gusts or air turbulence, or the turbulent aerodynamics within the boundary layer surrounding the airframe. Though many of the basic sources of structural vibration (the external stimuli) probably are truly random, the vibration environment internal to the structure, which acts on various items of equipment supported by the airframe, cannot be characterized completely in this form. This is because the structure, through which the external excitation must pass, acts as a filter which shapes the original random (white noise) time-varying environment into one which has more or less distinctly defined frequency characteristics whose amplitudes are not predictable with certainty. Thus the environment concerned with the analysis of equipment reliability should be considered as a frequency selective vibration environment with random amplitudes. The frequency selection is that associated with the resonance characteristics of the structure. This is shown in Figs. 3 and 4 which present in-flight measured vibration data at two points on the F-101 aircraft correlated with the resonant behavior of the structure measured during ground-vibration testing for both the low- and high-frequency range. The data is presented in spectral form as response versus frequency, the in-flight measurements being represented by a harmonic analysis of the time-varying random-vibration environment. As noted, there exists strong correlation between the peaks of the vibration environment and the resonant points of the structure, including reasonable correlative trends with the relative amplitudes of the structural impedance at each resonance.

Assuming that the random internal vibration environment is frequency selective and is shaped by the structural impedance of the airframe and assuming a more or less random white noise external stimulus, the possibility is presented of defining an equivalent random external environment which, when modified by the structural impedance of any airframe, will predict on the average the internal environment for new configurations. In essence this scheme is as follows:

In-flight measurements are taken on existing airframes.

The impedance or frequency response behavior of the structure is measured at the points at which in-flight measurements are obtained on the airframe and the Generalized Impedance at resonance is established.

These data are cascaded in accordance with the output over input response of linear dynamic systems. A solution for a pseudo white noise input or external environment, designated as the Equivalent Random Environment (E.R.E.), can be obtained. This pseudo

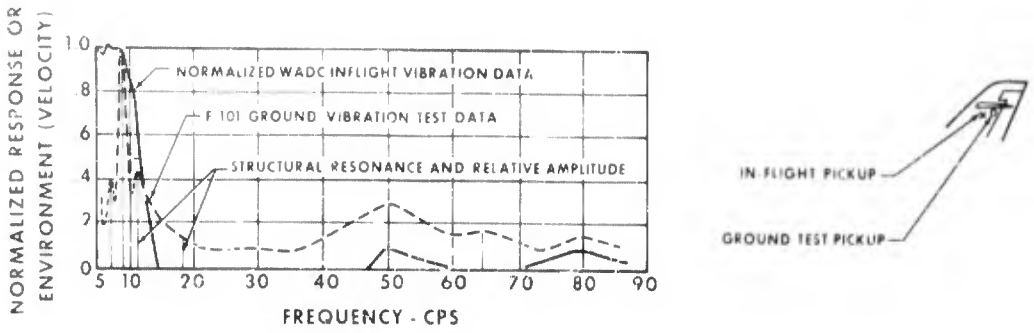

Fig. 3 - Low-frequency correlation of flight-environment and ground-vibration test data

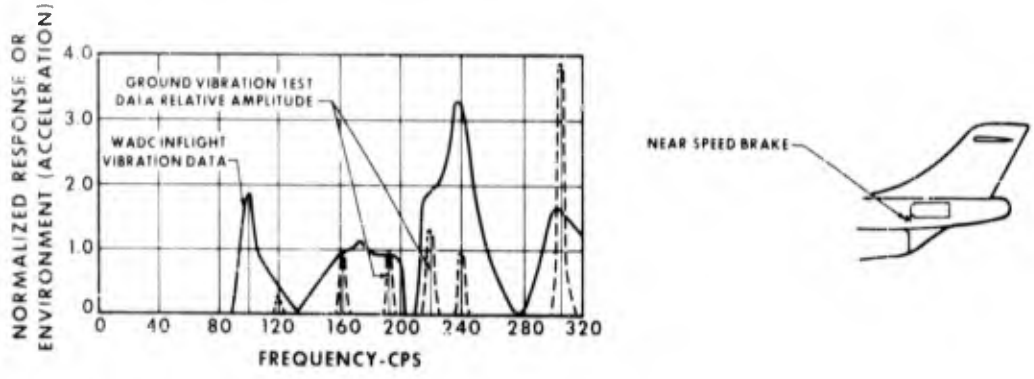

Fig. 4 - High-frequency correlation of flight-environment and ground-vibration test data

environment has the characteristic that, when multiplied by the Generalized Impedance, it will on the average define the structural response environment which is the internal environment acting on equipment. From measurements on existing vehicles, the Equivalent Random Environment, (E.R.E.), can be correlated with aircraft or missile flight parameters to establish trends.

The E.R.E. then serves as the estimate of the external input for a new configuration which is in the design phase. It is then cascaded with the calculated or estimated Generalized Impedance of the new configuration to arrive at a first prediction of the internal environment.

Generalized Impedance of the Structure

The prediction of the environment, using the E.R.E. approach, requires a definition of the so-called Generalized Impedance or Admittance of the structure. The necessity of using a Generalized Impedance becomes obvious when consideration is given to the fact that the external environment acts over a surface rather than at a point on the airframe. Generally, the impedance of a structure is obtained by exciting the airframe with one or at most a small number of mechanical shakers and measuring the response at a finite number of points on the structure. The ratio of the oscillating force applied to the structure to the response of the structure at the point of force application is defined as the point impedance. The reciprocal of this quantity is the point admittance. This is shown in Fig. 5. Since the only structural response of significance is that which occurs at resonance, the point impedance at resonance is a measure of the inherent structural damping. Point impedance data is readily available through ground-vibration testing and model testing and is usually obtained for other reasons during the development program of the airframe. In

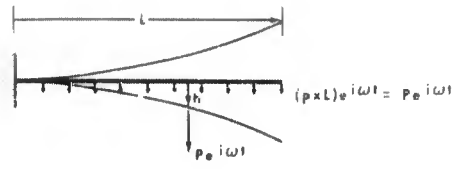

		DEFLECTION	VELOCITY	ACCELERATION
POINT IMPEDANCE - I	:	$\lvert P/h \rvert$	$\lvert P/\dot{h} \rvert$	$\lvert P/\ddot{h} \rvert$
GENERALIZED IMPEDANCE-$\bar{I}$	:	a $I/\int_o^1 \lvert\varphi_\eta\rvert d\eta$ ——→		
		b $I/\int_o^1 \varphi^2_\eta \, d\eta$ ——→		
POINT ADMITTANCE-A	:	$\lvert h/P \rvert$	$\lvert \dot{h}/P \rvert$	$\lvert \ddot{h}/P \rvert$
GENERALIZEDADMITTANCE-$\bar{A}$	:	a $A\int_o^1 \lvert\varphi_\eta\rvert d\eta$ ——→		
		b $A\int_o^1 \varphi^2_\eta \, d\eta$ ——→		

NOTE: η - NONDIMENSIONAL SPAN
$\lvert\varphi_\eta\rvert$ - RESONANCE MODESHAPE

Fig. 5 - Generalized impedance at resonance

particular, ground-vibration tests conducted for flutter and control system coupling are a source of this information. The problem with the point impedance is that all the force enters at a point on the structure. On the other hand, the random environment is distributed over a major part of the surface of the structure. The question then arises what is the impedance of a random pressure acting on a surface in terms of a force acting at a point. Figure 5 shows various methods of modifying the point impedance or admittance to define a surface admittance parameter which is denoted as the Generalized Impedance (or Admittance). These correction factors are based on considerations of generalized work concepts and make use of the mode shape of the structure at its various resonances.

Equivalent Random Environment (E.R.E.)

The following analytical steps define the E.R.E.

$$S_o^2 = s_o(\omega)\, d\omega , \qquad (1)$$

$$s_o(\omega) = \bar{A}^2(\omega)\, s_i(\omega) . \qquad (2)$$

Substituting Eq. (2) into Eq. (1) and assuming $s_i(\omega) = s_i$ (Equiv. Random Environment) then

$$\text{E.R.E. } S_i = \frac{S_o^2}{\int \bar{A}^2(\omega)\, d\omega} = \frac{S_o^2}{\sum_i \bar{A}_i^2 \Delta\omega_i} \qquad (3)$$

where

S_o^2 = Mean square of response

s_o = Power spectral density of response

$\bar{A}_i$ = Generalized admittance at resonance ω_i

$\Delta\omega_i$ = Bandwidth at resonance

ω = Frequency

s_i = Equivalent random environment (E.R.E.).

It is to be noted that, at the higher frequency end of the vibration spectrum, the Generalized Impedance approaches a point impedance since the mode of deformation of the structure at resonance encompasses a smaller and smaller part of the surface. In other words, at the higher frequency end, it is assumed that only the external environment acting near the point of interest influences the motion at that point. It is also important to recognize that known discrete inputs should be eliminated from the

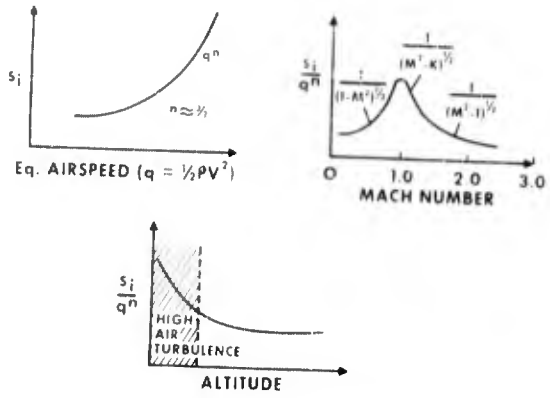

Fig. 6 - Equivalent random-environment E.R.E. trends

data used to calculate the E.R.E. since known frequency inputs would tend to throw the random representation of the external environment out of reasonable tolerance limits. Having obtained numerous E.R.E. values, under a variety of flight conditions for a variety of flight vehicles, it should be possible to obtain trends of the E.R.E. with various flight parameters. Such trends are indicated by the sketches in Fig. 6. In particular, trends with airspeed, Mach number, altitude, load factor, and possibly location on the airframe would be of extreme importance.

With the use of the E.R.E. trend data, the analyst is in a position to choose values of the E.R.E. compatible with the trajectory or design performance boundary of the new configuration. The only remaining step is the calculation of the structural Generalized Impedance of the new configuration or estimates of this impedance at the various resonances. The estimated impedance is then cascaded with the E.R.E. to arrive at the predicted internal structural vibration environment which impinges on equipment. This environment will have the same shape as the structural impedance when plotted on an amplitude versus frequency plot. However, its amplitude will be determined by the appropriate E.R.E. The environment, in spectral form, will exhibit peaks and valleys where the peaks conform to the expected resonance points and the valleys to the antiresonance points of the structure.

Something needs to be said about the calculation or estimation of the Generalized Impedance of the structure prior to having a structure built. There are two requirements: the resonant frequencies and the magnitude at resonance. Frequency analyses are usually conducted as part of the airframe structural analysis by the Dynamics Group at each company. However, the frequency range of interest is usually below 100 cps. For higher frequency resonance, more sophisticated approaches may be required including the dynamics of plates, shells, and local bracketry. Methods are required to do this in an economical manner. For example, analog simulation can be used. McDonnell Aircraft Corporation has a passive network analog which is ideally suited for such studies. In regard to the magnitude of the impedance at resonance, the problem is a much more difficult one. Since the magnitude at resonance is a function of the effective damping provided by the structure, the problem really resolves itself to a definition of structural damping under a variety of complex dynamic deformations. In this regard, models could be built in which some of the details of the actual design are reproduced to a smaller scale. Estimates can be made based on tests conducted on older configurations of comparable design. These tests would define the damping available in built-up structures or plates for dynamic structural deformations at higher resonance modes. More effort needs to go into this area to determine what can be done in a realistic fashion.

Qualification Testing

Once the expected vibration environment has been estimated, the next step is to define qualification test requirements for individual subsystems and components of subsystems.

This is shown on the chart in Fig. 2. As a minimum, qualification tests need to comply with the military specification requirements. These spectra are simplified environmental vibration criteria consisting of straight lines when plotted on a "log-log" vibration spectrum graph. This point is important since it gives consistency and uniformity to equipment fragility levels independent of applications on particular airframes. However, it is necessary to supplement the simplified environmental criteria by the expected internal vibration environment determined by the E.R.E. extrapolation approach for the particular design configuration. This means that the qualification test environment will reflect the expected frequency selectivity of the structure to which the equipment is mounted. For actual qualification testing, sinusoidal sweep testing is preferred since failure during qualification testing can be associated with amplitude and frequency of the failure environment. In fact, it is considered essential that the qualification test process include simplified failure testing of the component, again using a sinusoidal frequency sweep test technique. The fragility or failure level of the equipment can then be determined approximately in terms of the amplitude and frequency of the imposed vibration.

Failure Testing, The Component Functional Profile (C.F.P.)

In essence, the concept of failure under an environment involves two ingredients. One is the characteristic of the environment itself which is defined in terms of amplitude versus time in a time domain, or amplitude versus frequency in a frequency spectrum domain. The other ingredient is the equipment failure susceptibility which can also be expressed in an amplitude-frequency-time domain. It is important to differentiate between an irreversible failure which occurs when performance ceases during the application of the environment and this condition remains after the environmental level has been reduced or removed, and a reversible failure, in which malfunction of the system occurs during the application of the environment with normal operation returning once the environment has been removed. Irreversible failure of a system usually involves considerations of the fatigue of the internal mechanism and therefore the time duration of the environment acting on the equipment is an important parameter. For reversible failures, the duration of the environment is not considered important, but rather the problem is one of the magnitude of the environment.

The boundary defining the susceptibility to failure of the equipment in a vibration environment is defined as the Component Functional Profile (C.F.P.). In the case of irreversible failures, the C.F.P. becomes a surface when plotted in an amplitude-frequency-time domain and is shown in Fig. 7. The Component Functional Profile for the case of reversible failure or malfunction is shown in Fig. 8.

As in the case of the environment, the C.F.P. also exhibits peaks and valleys whose magnitudes are subject to statistical variation. The valleys are representative of environmental regions in which the equipment is most susceptible to failure. The opposite is true for the peaks. It is postulated that the valleys are associated with internal resonance of the equipment itself (in general, structural), which in turn causes system malfunction, failure, or out of tolerance operation. Assuming this to be the case, it can be expected that the frequency location of each valley is more or less fixed and not subject to large variation among various specimens of the same basic unit. This is because the resonant frequency of a dynamic system is sensitive only to the one-half power of variations in the structural parameters.

The critical areas of equipment failure are obviously associated with the valleys of the C.F.P. The frequencies corresponding to these valleys are denoted as the critical frequencies of the equipment. The magnitude of the environment required to cause failure at these critical frequencies is subject to equipment tolerance to a much higher degree than the variation in the critical frequencies themselves. Therefore, one can expect a reasonably large scatter in magnitude of the vibration environment required to cause failure at the critical frequencies of the system. The C.F.P., therefore, must be thought of as the most probable failure surface or boundary within a multitude of similarly shaped failure boundaries. The interesting part of the C.F.P. is that there exists, in all probability, a most critical valley or a region of minimum environment required for failure and that other valleys require a more severe failure environment. This region is denoted as the most critical frequency of the equipment and in all probability is associated with a particular mode of equipment malfunction or failure.

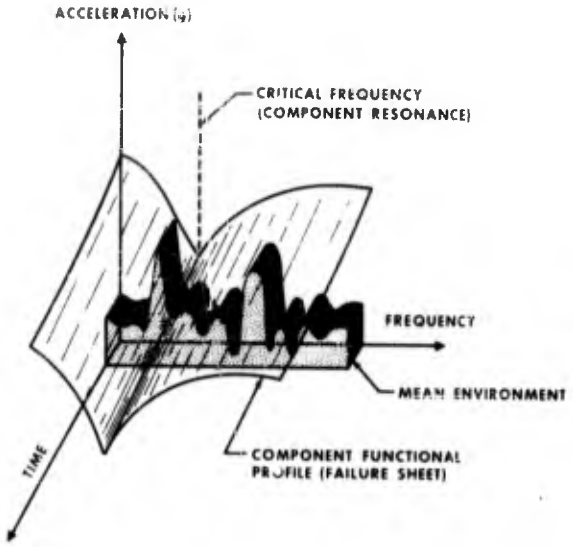

Fig. 7 - The component functional profile concept (irreversible failure)

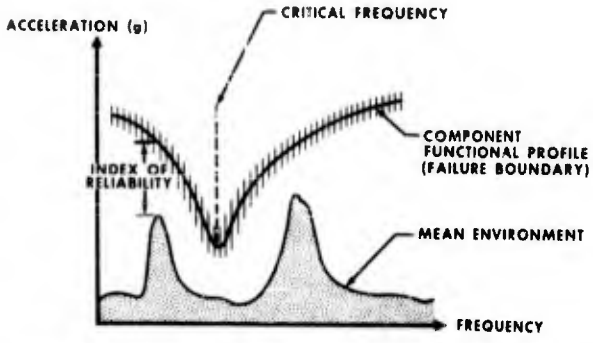

Fig. 8 - The component functional profile concept (reversible failure)

When an item of equipment is exposed to an environment which is characterized by a shaped wide band spectrum (a random amplitude environment with predominant frequencies), damage takes place because of the nearness of the environment to the valleys of the C.F.P. and, in particular, the nearness of only a portion of the environment to the most critical valley of the C.F.P. Thus, in general, failure or malfunction can be associated with a particular mode of failure resulting from a particular internal resonance which is stimulated by a particular portion of the environment. The problem of reliability in a vibration environment, therefore, is associated with mismatching the frequency dependence of the environment with the frequency dependence of the equipment C.F.P. Having estimated, during the design phase, the expected environment based on the E.R.E. approach and having determined the C.F.P. of the equipment as part of the qualification testing of the equipment, it is possible to define an Index of Reliability which reflects the margin of safety available in the installation against failure due to a vibration environment. This is indicated in Fig. 8.

In actual practice, considering the economic consequences of defining with reasonable

statistical accuracy the C.F.P. of a component or equipment, it is not feasible at this time to define the C.F.P. of each system with a confidence level acceptable to the statistician. This is not considered necessary, however. From an examination of Figs. 7 and 8, the really important point is the definition of the critical frequencies of the equipment and, in particular, the most critical frequency of the equipment. It is only of secondary importance to define with a high degree of confidence the mean value and the limits of the failure amplitude at the critical frequencies. Knowing that each piece of equipment must pass a standard qualification test which assures that all valleys are above a minimum level of vibration environment, it is then only necessary to assure that there exists a frequency mismatch between peaks of the expected environment and the most critical valley of the C.F.P. This mismatch should be adequately conservative to account for the fact that a complete statistical analysis of the failure boundary has not been attempted. In the case of reversible failures, it is believed that failure testing of one sample is sufficient to give this type of information. In the case of irreversible failures, possibly three or four samples would be required to define the most critical valley of the C.F.P.

With the Component Functional Profile concept of defining an Index of Reliability of equipment failure in a vibration environment, it becomes immediately apparent that the vibration-test technique to be employed during the design phase of system development should be the frequency sweep technique of testing. Even though this environment is not representative of the actual situation that can be expected to occur in flight, it gives rise to information defining critical parameters of the equipment in a form directly usable with the estimated vibration environment. This estimated vibration environment is given in terms of amplitude versus frequency and takes into account the fact, even in the design stage, that the structure acts as a filter which shapes a random environment into one having predominant frequency components.

Modification of Environment

With the use of the equipment C.F.P. and the frequency dependent vibration environment, the designer is in a position to define the reliability index in a quantitative manner. To improve the index, he can make definite design changes in the structure, provide shock and vibration isolation to modify the environment for better compatibility with the equipment failure boundary, or choose a different equipment component which has a more satisfactory C.F.P. in relation to the expected environment. The complete vibration control program for the design phase is shown in Fig. 9.

DEVELOPMENT PHASE

During and following the design phase, the airframe structure is built and assembled, and preparations are made for ground testing of the prototype airframe; this is the initial stage of the development phase of the system. Figure 9, which presents the total vibration control program proposed during design and development, shows the detailed steps to be followed during the development phase. As a first step, the structural impedance calculations, conducted during the design phase, can be checked through ground-vibration testing using the frequency response technique of testing. Subsequent to the structural ground-vibration tests, the complete system, including the airframe, is to be tested dynamically by driving the airframe with mechanical shakers using the predicted E.R.E. spectrum modified by the other known discrete frequency inputs. All the subsystems of the complete weapon system are operative and their performance is checked during the vibration environment test. Frequency sweep testing again is preferred in order to clearly establish the amplitude and frequency where malfunction may occur. This data can then be used with the C.F.P. of the system to upgrade the Index of Reliability. McDonnell Aircraft Corporation has conducted such complete system environmental tests in which the actual airframe is used to shape the internal environment. This was done on the Alpha Draco Missile and the Mercury Capsule. The environment internal to the airframe, which can be measured during these tests, can also be compared at that point with the qualification test requirements specified during the design phase.

Correction of deficiencies follow the result of the ground proof test and complete system tests. The next phase involves flight testing of the complete system during which measurements of the actual airframe environment can be obtained. These data can then be compared again with the C.F.P. of various equipment to modify and upgrade the Index of Reliability, and to help in the analysis of failures and subsequent correction of deficiencies. As part of this failure analysis effort,

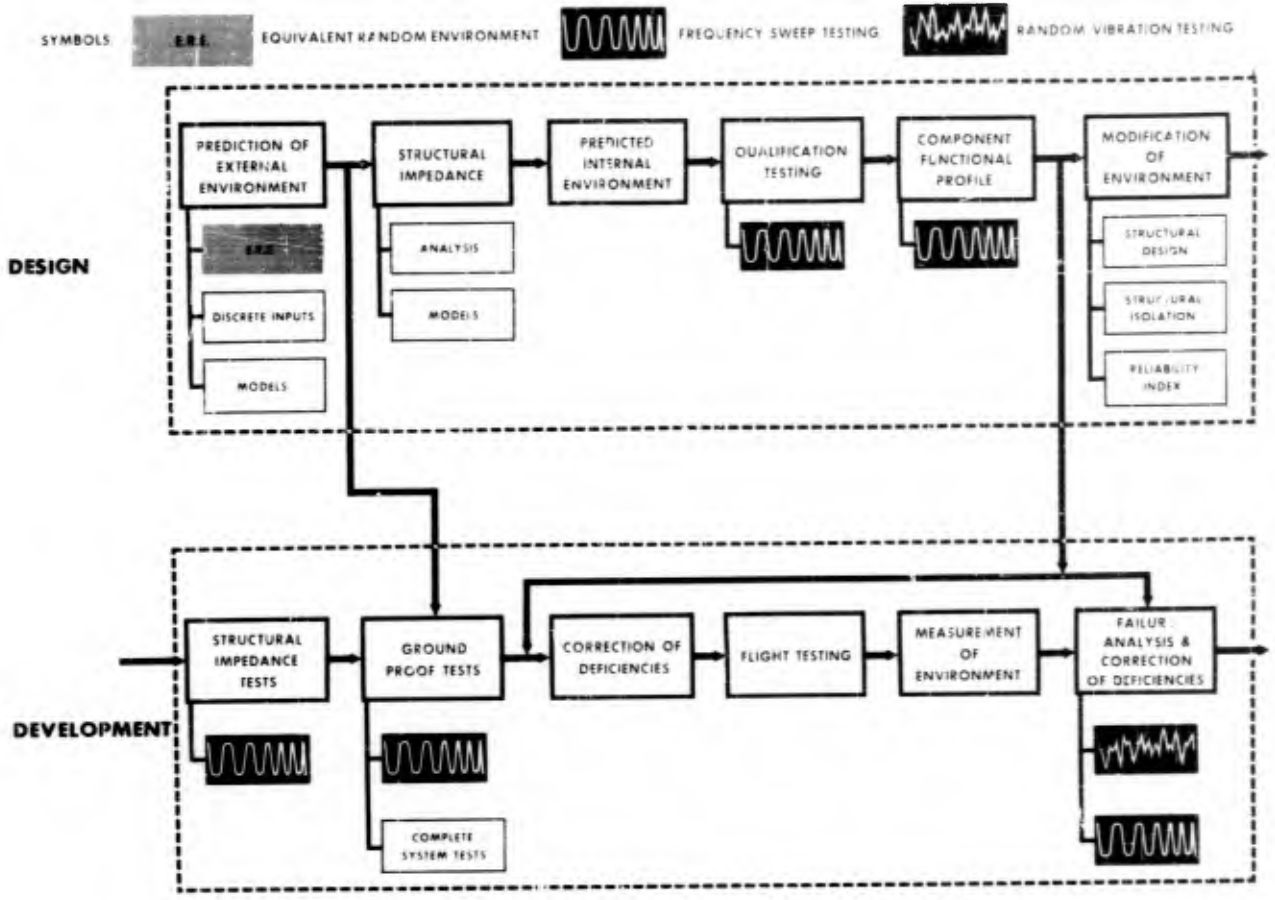

Fig. 9 - Vibration control during design and evaluation

random-vibration testing is employed using the actual in-flight vibration environment as recorded on magnetic tapes. In addition to random-vibration testing, sinusoidal frequency sweep testing also is conducted to pinpoint the frequency amplitude relationship characteristic of the type of failure encountered. This, again, can then be used in conjunction with the C.F.P. to upgrade the reliability of the system. A similar plan is in effect for the production development phase which is the last phase of the development process of a complete weapon system.

CONCLUSIONS

A proposed method of vibration control during the design and development of a weapon system has been presented which should lead to a reliable weapon system. The approach is based predominantly on the sinusoidal-frequency-sweep testing method which permits the determination of failure as a function of frequency and amplitude, thus defining the "Component Functional Profile." A method of systemizing the prediction of the vibration environment for new configurations based on the experience collected on old configurations is proposed. This method, based on the fact that the structure filters a random external environment, is denoted as the Equivalent Random Environment (E.R.E.). Various steps in the vibration control program during design and development are discussed, and importance is attached to the use of ground testing of the airframe structure and the complete system using sinusoidal frequency sweep testing. The use of random vibration testing is preferred in those instances where actual in-flight failure has been encountered and ground testing is undertaken to establish corrections. In this case, the actual environment impinging on the component can be measured in flight and reproduced in the laboratory under controlled conditions.

REFERENCES

1. Military Specification E-5272, "General Specification for Environmental Test, Aeronautical and Associated Equipment"
2. V. C. McIntosh and N. Granick, "Experiments in Random Vibration," WADC T.N. 56-228
3. W. C. Hanson, "The Martin-Denver Component Fingerprinting Program," Shock and Vibration Bulletin No. 27, Part II, June 1959
4. N. Granick, "Status Report on Random Vibration Simulation," Shock and Vibration Bulletin No. 27, Part II, June 1959

DISCUSSION

Mr. Gaiel (National Engineering Science Co.): Can you tell us about any success that you have had in predicting this structural impedance, particularly at the higher frequencies, with models? I don't tend to be too optimistic about it, and I'd like to know about other people's experience.

Mr. Mirowitz: We haven't done this modeling. North American, Columbus, I believe, has built models which duplicate the structural details of the full scale aircraft. They have taken measurements on this for other purposes. I don't have the answers, but I think there is reason to believe something can be done. You could use for example, older structures and determine what your structural damping is by testing those full-scale structures which are similar to the design you are proposing. This structural damping gives you immediately the impedance at resonance. Although I don't know the exact answer, I think it's possible.

Mr. Stern (General Electric Co.): I think the things you are proposing are in the wrong place, judging by that chart you had initially. Many of these things that you can change are the sort of things you can negotiate and discuss while you're still proposing. But once you have signed a contract and you've agreed to do certain tests, this is a contractural obligation. There is no more discussion or negotiation, that is, there shouldn't be if the man who is supplying the item to the customer knows what he is doing and what he has agreed to do. So it would seem that the procedure you have here is the sort of thing that you could

apply while you were still negotiating a contract. Once you have agreed to certain things, particularly "qual tests," you're more or less fulfilling the legal portion of a contract. "Qual tests," for instance, are extremely rigid procedures. It's not a place to experiment. You certainly don't under test or the customer is dissatisfied. You certainly wouldn't over test or the designer will object quite seriously. So, while this proposal and everything you have here does sound quite desirable, what I question is whether this could be put into effect in the manner in which things are negotiated and purchased in day-to-day business.

Mr. Mirowitz: I don't know how much negotiation you have done with the Government. I assume you have done quite a bit. I'm not an expert in negotiation, but I know that in every contract you are continuously negotiating regarding test requirements, design criteria, etc., because new things come up all the time. When you get a contract, years pass by between the original concept of the contract and the final culmination. You get new test data. You get new knowledge which may change the original detailed requirements. That's the reason why we get paid. That's our job, to bring this to the attention of the customer and find out if he will go along with changes. Now, if he doesn't go along, obviously there is no point. Secondly, this is worthwhile just in proposal work. We agree on that. The customer isn't here. Even during preliminary design stages, we can do things which would build more reliability into the system, I believe.

Mr. Stern: Well, let me say this about 2-year development or 2-year delivery. Many times you have to sign a contract and deliver in perhaps 4 months. This happens quite often. Now perhaps there should be a distinction, that you could use this in the development of a large structure where the delivery time is extended. But even then, many times when you're talking to the customer, either you're dealing directly with the Government or subcontracting to, say McDonnell, Boeing, Lockheed—one of the large aircraft companies—they will be quite specific about how these changes can and cannot be made. Even though there may be slight improvements, and there are always breakthroughs day to day, it will really have to make substantial savings, not just in cost but in weight—something really exceptional before they would want to delay the program or do anything to slip the delivery date. That's why I say, I think this procedure is something that would be very difficult to do once you've signed the contract and you have a legal obligation to deliver.

* * *

CUMULATIVE FATIGUE DAMAGE DUE TO VARIABLE-CYCLE LOADING

J. R. Fuller
Transport Division
Boeing Airplane Company
Seattle, Washington

If it is established that structural components or attached equipment items are subjected to random stress cycle amplitudes at essentially a single frequency, then the fatigue life can be estimated by the method proposed herein. If the stress time-history is broadband, there are indications that the life is a function of the stress power spectrum and frequency distribution.

INTRODUCTION

Fatigue failures are difficult to anticipate because so little is known about the basic nature of fatigue. There are questions as to how the cracks originate and how fast they are likely to grow under repeated loadings, when fatigue damage begins, and how it appears to accumulate. Qualitatively, it is known that points of high stress concentration are danger points for fatigue failures. Therefore, actual tests must be conducted on specific parts, which are loaded precisely as they are in service and under similar environmental conditions, before a reasonably accurate estimate of the fatigue life in service can be ascertained.

Since the formation of a fatigue crack is a very localized phenomenon, its place and time of inception depend not only on the geometry and the loads applied to the part, but also on the textural stresses in the metal at critically stressed regions which may arise from forming, heat treating, or machining. The size, shape, and orientation of the individual grains as well as their crystalline structure and the nature of the grain boundaries all influence the formation and growth of the crack from a microscopic or submicroscopic point of weakness until it can be seen with the naked eye. Any influence that affects the mechanical behavior of the metal, such as heat treating or forming can certainly be expected to have an effect on its fatigue properties. However, attempts to predict the fatigue life of a metal from a knowledge of its various measurable properties have not met with complete success for even the simplest type of specimen and a constant stress cycle.

Present theories for estimating fatigue damage due to service stresses can deal only with oscillatory stress time histories with random amplitudes; they cannot deal with the noncyclic character of truly random load time-histories.

In the present state-of-the-art, the distribution of peak stresses is generally assumed to cause the same fatigue damage as an identical distribution of stress cycle amplitudes. The fatigue analysis is then conducted by one of several different methods, some of which will be mentioned or discussed herein. The purpose of the discussion is to review the phenomenological aspects of various pertinent fatigue damage investigations, in order to appraise our present knowledge and to point the way to research needed to attain the objective of being able to estimate the service life of structural and equipment components in the design stages of product development.

The objective of future cumulative-fatigue damage theories should be to estimate service life under truly random loads. It is likely that

rational use of the same statistical parameters that are used in power spectral or generalized harmonic analysis studies can clarify and improve our ability to estimate fatigue life under random loads.

EARLY FATIGUE DAMAGE STUDIES

Studies were started more than 30 years ago to try to correlate the fatigue lives of standard-type specimens which were subjected to cycles of stress of various amplitudes with conventional S-N relationships for the same type of specimen. Most of this research has been done on round-polished specimens stressed in reversed bending; however, some tests have been made using direct axial loads.

The earlier investigations of this type dealt with the effects of cycles of overstress* on the endurance limit of a given material. French [1] defined a so-called "damage line" by this type of testing. This damage line was determined in the following manner: An S-N curve was first obtained, using all new specimens. Then several more identical specimens were run at a low overstress for various fractions of their normal lifetime as determined by the S-N relationship. Each of these "prestressed" specimens was then cycled at the endurance or fatigue limit [2].† If a specimen failed while being run at the fatigue limit, it was assumed to have been damaged by the prestressing operation at the overstress. Specimens that did not fail after prestressing were assumed to have accumulated no damage. Other series of specimens were then tested in a similar manner at other overstresses until it was possible to interpolate between the number of cycles applied to the specimens of each overstress series and determine a point where no damage was inflicted on the fatigue limit. The locus of such points at the various overstresses then determined the damage line.

Similar tests have also been conducted by Moore [3], Kommers [4,5], and others. Kommers determined new fatigue limits for the prestressed specimens. He then expressed the damage as the percent change in the initial fatigue limit caused by the prestressing, where either understresses or overstresses were used as the prestress. His results indicate that there is a rapid increase in damage with an increase in the number of cycles at the higher overstresses. That is, damage increases at an increasing rate with the number of overstress cycles applied. He concluded that a material which has been subjected to an overstress and then to an understress will fail even though the final stress is below the initial fatigue limit, because overstressing causes a decrease in the initial fatigue limit. Other observations showed that there appeared to be an actual increase of the fatigue limit for some materials due to some cycling at low overstresses. Apparently, these materials were not damaged significantly until a very large percentage of the normal fatigue life at these overstresses had been expended.

Lea [6] conducted overstress and understress tests on an annealed 0.32-percent carbon steel having a tensile strength of 72,000 psi and a rotating-beam fatigue limit of 32,000 psi. The estimated fatigue life at 40,000 psi was 12,500 cycles. By cycling a specimen just under the fatigue limit and by repeatedly increasing the stress in small increments up to 40,000 psi, it was possible to apply 40,000,000 cycles at the latter stress level before failure occurred. The normal life at 40,000 psi had been increased 3350 times. Swanger and France [7] also report some interesting results similar to these. This type of testing is reported in many places in the literature and is generally known as coaxing.

Gough [8] and many other investigators believe that understressing tends to work the peak textural stresses in the material into a more uniform distribution and, in effect, increases the fatigue limit. Overstressing, on the other hand, is believed to aggravate the textural stress condition by more severe plastic deformation, particularly in the partially unrestrained material at the surfaces. It is here that fatigue cracks generally form.

Much of the fatigue damage work reported in the literature has been along the lines discussed above. It is not directly applicable to design problems, but it has aided greatly in providing a better general understanding of fatigue damage from a phenomenological viewpoint.

*An overstress or understress is defined as a cyclic stress greater or less than the endurance limit, respectively.

†The American Society for Testing Material, Manual on Fatigue Testing, considers the term "fatigue limit" preferable to endurance limit.

BLOCK-TYPE CUMULATIVE DAMAGE TESTS

Most so-called, cumulative-fatigue damage studies have been concerned with the effects of prestressing at one overstress on the subsequent endurance at another overstress or "test stress." These studies have led to methods for estimating the fatigue lives for variable-stress-cycle loading and can be applied to certain design problems. Important general conclusions can also be drawn from these more recent investigations. For the purpose of discussing these conclusions, the following terminology will be used:

S = Maximum stress of a stress cycle

N = Number of cycles to failure, applied to a specimen at a stress, S

n = The number of cycles endured at any stage of a fatigue test at a stress, S. n always less than N.

R = Cycle ratio, the ratio of the number of stress cycles applied at a given stress level to the expected fatigue life as estimated from the S-N curve for that stress level, $R = n/N$

D = Fatigue damage done to a specimen by previous fatigue stressing, measured as the percent shortening or lengthening of the fatigue life at the final or test stress level.

Palmgren [9,10] is reported to have suggested a method for analyzing data for fatigue tests at several stress levels. The method was then considered by Miner [11], Luthander and Wallgren [12], and others for design purposes. Miner conducted tests on 2024 aluminum-alloy plain sheets and riveted joints, and the method generally carries his name in this country.

In analyzing data by this method, it is assumed that there is a linear relationship between the prestress cycle ratio and damage at any given overstress level, and furthermore, that during the course of any fatigue test, the damage is equal to the summation of all of the prestress cycle ratios. Thus, the damage, D, and the cycle ratio, R, would be equal to n/N for each block of cyclic stresses applied, and would sum to unity at failure.

Müller-Stock, Gerold, and Schulz [13], and Kommers [14], Richart and Newmark [15], Shanley [16], Freudenthal and Heller [17], and other investigators have shown that such a simple relationship between damage and cycle ratio does not actually apply, but that damage more likely varies with some power of the cycle ratio. Freudenthal and Heller [18] are presently conducting a fatigue-damage investigation using a theory based upon a nonlinear relationship between cycle ratio and fatigue damage.

In early investigations, usually only two different stress levels were used. Thus, the effect of a certain block of prestress cycles would show either a healing or damaging effect to the remaining endurance at a different test stress. For example, if after n_1 cycles at a stress S_1, a specimen is cycled to failure at a different stress level, S_2, the cumulative ratio is $n_1/N_1 + n_2/N_2$ and should be equal to 1.0 according to Miner's theory. However, in most cases it was found to be greater or less than unity.

It has been demonstrated that the order in which the stresses are applied makes a difference in the total number of cycles to failure. That is, an initial maximum cyclic stress, S_1, greater than the final stress, S_2, ordinarily gives a cumulative cycle ratio less than 1.0, while an initial stress less than the final stress may give a value of cumulative cycle ratio greater than 1.0.

Richart and Newmark [15] showed that as the number of alternate blocks increased without bound the value of the cumulative cycle ratio appeared to converge to some definite value regardless of which stress block had been applied first. But even then, the cumulative cycle ratio was usually different from unity. It appears that a cumulative cycle ratio most nearly equal to unity will occur when the prestress and test stress are nearly the same. This is to be expected because the constant-cycle fatigue lives at the two stress levels would be very nearly equal.

A point that stands out in nearly all of these tests is that a specimen which is being cycled in fatigue is in a nearly constant state of change, particularly if the maximum stress of the cycle is an overstress. If a given set of specimens were all cycled at a constant maximum stress for an equal number of cycles, and then an S-N diagram determined using these prestressed specimens, and including the cycles of prestress in the new plot, the new diagram would cross the S-N diagram for the original specimens at the value of the prestress. This would occur because continued cycling of a prestressed specimen at the

prestress value would cause failure as predicted by the original S-N diagram. Also, it has been shown by test that prestressed specimens will give a new S-N diagram. However, the fatigue lives are usually more scattered than for tests at a single stress level.

Figure 1 shows test results obtained by Kommers [14] on rotating-beam specimens of SAE 1020 steel. The diagram shows the new S-N relationships that were determined after prestressing the specimens at 36,000 psi for various prestress cycle ratios, R. Figure 2 shows the same test data except that the cycles of prestress are included with the test stress cycles to failure.

It may be noted in Fig. 2 that the "rotation" of the diagrams with respect to the basic S-N curve or a vertical line through the point of rotation is approximately proportional to the cycle ratio of the prestress. Thus, for zero cycles of prestress, R = 0, a test point would lie on the S-N curve, and for R = 1.0, the specimen would fail before any test stress cycles could be applied. In the latter case, the point representing zero cycles of test stress would be plotted on the vertical line through the point of rotation.

From a study by Kommers [14], data and test data obtained by Bennet [19] and others, it appears that S-N diagrams for prestressed

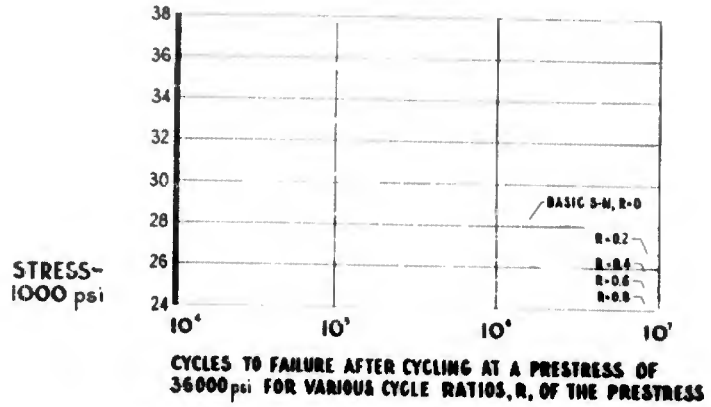

Fig. 1 - Results of rotating-beam tests of SAE 1020 steel, Kommers [14], 1945

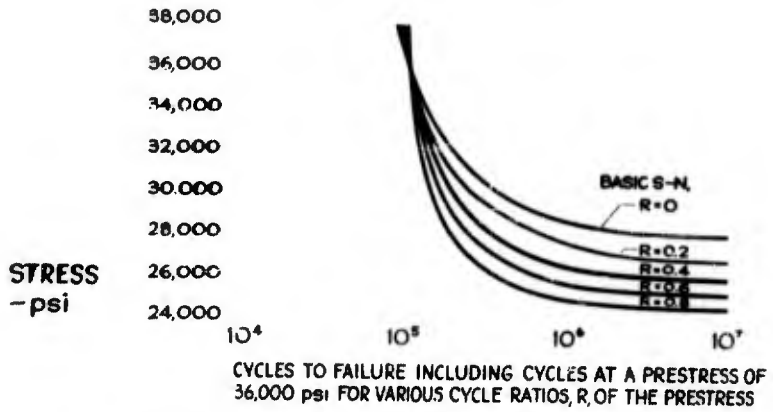

Fig. 2 - Results of rotating-beam tests of SAE 1020 steel, Kommers [14], 1945

specimens will "rotate" in a clockwise fashion about the point on the original S-N diagram corresponding to the value of the prestress. This illustrates some of the principal findings of the earlier fatigue damage studies -- that a high overstress generally has a damaging effect on the subsequent remaining fatigue life at a lower stress, and that a low stress may show a healing effect on the endurance at a subsequent higher stress.

A possible effect of prestressing specimens at one or more values of prestress is further indicated in Fig. 3. In this illustration, it is assumed that an overstress, S_1, is applied to all of the specimens for n_1 cycles. The specimens will be sufficiently changed by this prestressing operation that they will yield an S-N curve different from that of the original specimens. If this new S-N curve is determined and if the cycles of prestress are included in its representation, a curve such as 2-2 in Fig. 3 will result. Two things may be noted concerning curve 2-2: first, it crosses the original S-N diagram at the value of the prestress, and second, it is rotated in a clockwise direction with respect to the original diagram. If, after cycling at S_1 for n_1 cycles, the specimens were subjected to an additional n_2 cycles at S_2 and another S-N relationship were established including the cycles $n_1 + n_2$, a curve such as 3-3 would possibly result.

This implies that if the applied cyclic stresses are always within the finite life range of the basic S-N relationship, the fatigue life can be bracketed on the original diagram between the numbers of cycles required to cause failure at the upper and lower maximum cyclic stresses. Presumably, the location of the point representing the number of cycles to failure would fall within this bracket and would be a function of the general configuration of the blocks of the applied cyclic stresses. Of course, an approximation for an equivalent random variation in stress cycles could be attained only if the pattern of blocks of stresses were repeated a sufficiently large number of times such that the order of the application of the stresses within the pattern or spectrum would make no discernible difference in the total number of cycles to failure.

Damage curves can be used to compare this observation with test data. If the damage is equal to the cycle ratio as Miner and others have surmised, then curves of constant fatigue damage are the same as curves of constant prestress cycle ratio. It is possible, then, to construct curves of constant damage by using Miner's theory and an S-N diagram. For this type of plot, the basic S-N diagram is the curve for a damage of 1.0. The data from Kommers'[14] test data shown in Fig. 1 have been replotted in Fig. 4. The solid curves show the number of cycles to failure after various cycle ratios, R, of the 36,000 psi prestress have been applied. The dashed-line curves are loci of constant fatigue damage determined by Miner's method for prestressing at 36,000 psi. The basic S-N diagram is obtained by test-stress cycles only; therefore, the prestress cycle ratio for this curve is zero. The number of cycles between the dashed-line damage curve, $D = 0.2$, and the basic S-N diagram, $R = 0$, corresponds to 0.8 of the fatigue life at the test stress, because the total or cumulative cycle ratio must be 1.0.

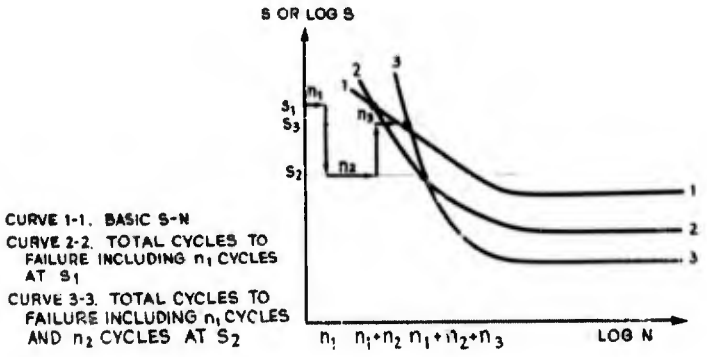

Fig. 3 - Variation of total cycles to failure for various prestressing operations

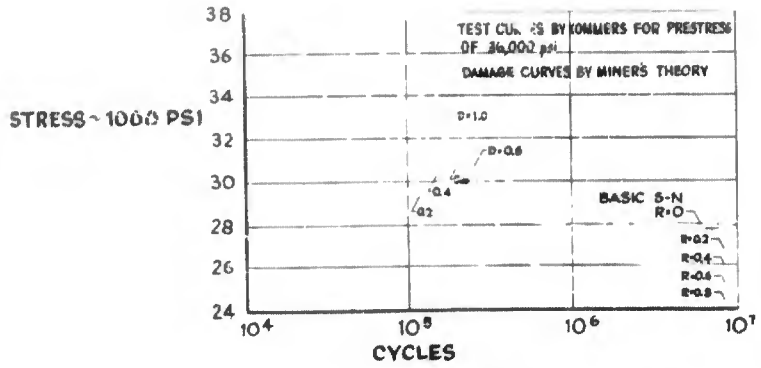

Fig. 4 - Comparison of Miner's theory with test results for SAE 1020 steel, Kommers [14], 1945

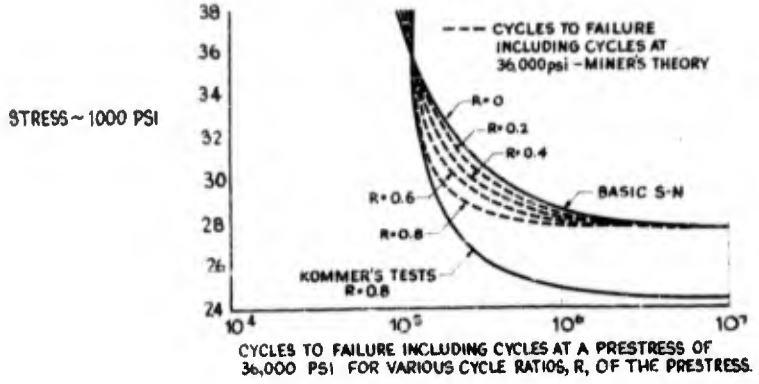

Fig. 5 - Comparison of Miner's theory with test results for SAE 1020 steel, Kommers [14], 1945

Figure 5 shows the total number of cycles to failure for Kommers' tests including the cycles of prestress at 36,000 psi. The dashed-line curves are those predicted by Miner's theory, and the two solid curves, R = 0 and R = 0.8 are those determined by test. These curves clearly illustrate one serious and unconservative defect in Miner's theory — the assumption that no damage is entailed when cycling below the fatigue limit. Figure 5 shows that the failure may occur at 1,000,000 cycles at a stress approximately 3000 psi below the fatigue limit after a cycle ratio of 0.8 had been applied at the prestress. Certainly these stresses below the fatigue limit and their effect on the fatigue life should not be discounted.

DEVELOPMENT OF A CUMULATIVE-DAMAGE CRITERION FOR VARIABLE-CYCLE LOADING

When structural or equipment systems subjected to broadband excitation tend to oscillate at one predominate frequency, then the stress time-histories at given points will have stress cycle amplitudes which are randomly distributed. This type of load cycle environment is often simulated on ordinary fatigue test equipment in so-called, spectrum-type tests. In this type of testing, the load cycles are rearranged and grouped according to increasing or decreasing amplitudes and the resulting spectrum of cyclic loading is repeated many times before the specimen fails.

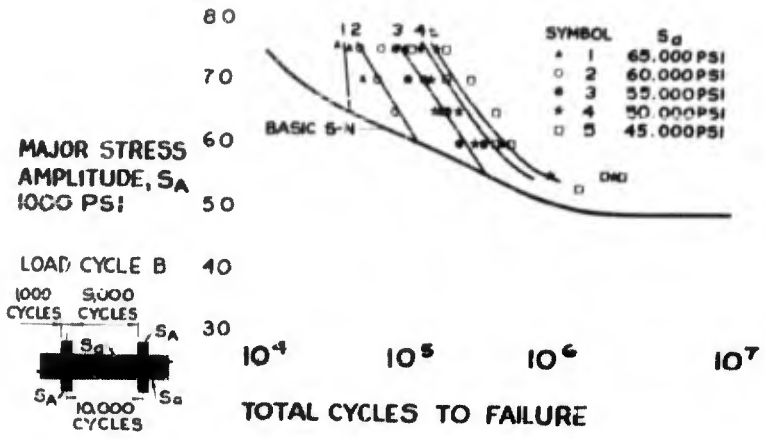

Fig. 6 - Test results for unnotched rotating-beam specimens of SAE 1045 steel, subjected to load cycle B, Dolan, et al [20], 1949

If a specimen is cycled under some variable load pattern between two limiting overstresses, the greater of which is S_A and the smaller S_a, then failure may be expected to occur at some number of cycles greater than that which would cause failure by cycling at S_A alone and less than that which would cause failure by cycling only at S_a. Thus, by cycling under some variable load pattern whose upper and lower bounds are overstresses, it would seem likely that the fatigue life would be a function of the variable load pattern and the stress levels, and that it could be related to the basic S-N diagram.

Dolan, Richart, and Work [20] conducted a rather extensive series of tests on notched and unnotched rotating-beam specimens of several materials using three different variable load patterns, which they refer to as load-cycles B, A, and G. Two of these patterns, B and A, were of the rectangular two-stress-level block type, and the third, pattern G, was a sine wave. All three had a duration of 10,000 cycles. For purposes of discussion, only the results of the tests on the steel specimens from the above paper will be considered. In this work of Dolan, et al, the major (larger) maximum stress, S_A, was always an overstress, and the minor (lesser) maximum cyclic stress, S_a was either an overstress or an understress. Also, the major maximum stress, S_A, was varied from specimen to specimen, while the minor maximum, S_a, was held constant. The results of load-cycle B tests on SAE 1045, where both S_A and S_a were overstresses, are shown in Fig. 6. The variable-cycle test results shown in Fig. 6 are plotted at the major maximum stress value; all test points having the same minor maximum stress are represented by the dashed curves. Thus, Curve 2 represents test results wherein S_a was 60,000 psi and S_A was selected between 60,000 psi and 75,000 psi. Naturally, these dashed curves must intersect the S-N diagram at the value of the minor maximum stress, S_a, because at this point there was no variation in the maximum stress.

It is of particular interest to note that these curves are nearly parallel even though a rather limited amount of data is presented. This suggests that the slopes of the dashed curves may be a function of the loading spectrum used for these specimens and that the ratio of the slope of the S-N curve k_{SN}, to the slope of the variable cycle curves, k_v, may be a constant and may depend only on some function of the variable-cycle pattern.

Other similar tests were conducted on SAE 4340 specimens for which S_a was considerably below the fatigue limit. One group was tested at a value of S_a equal to 78,000 psi and another at 60,000 psi. As in the previous tests, the type-B load cycle was used. The results of these tests are shown in Fig. 7, the authors having approximated the experimental data by the solid curves. However, straight lines would appear to fit the variable-cycle test results equally well.

For the tests of SAE 1045, where both S_A and S_a were overstresses, it was evident that the variable-cycle curves must intersect the S-N diagram at S_a in each case. Also, the

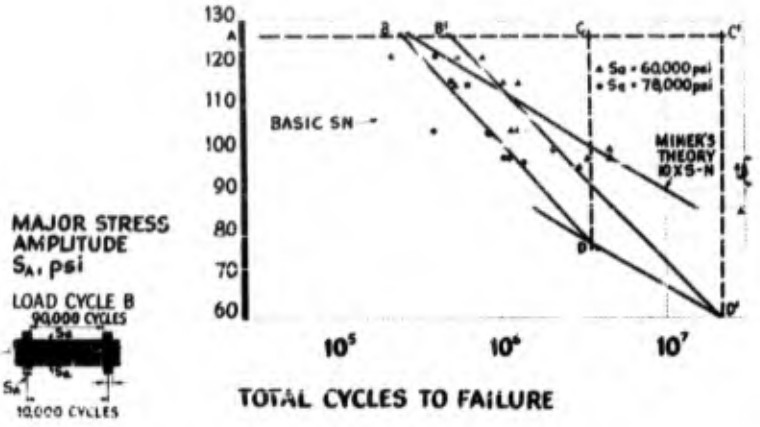

Fig. 7 - Test results of unnotched rotating-beam specimens of SAE 4340 steel, subjected to load cycle B, Dolan, et al [20], 1949

test results for the SAE 4340 specimens show that the variable-cycle straight lines, when extended, intersect the extended "sloped-leg" of the S-N diagram at S_a. This occurs even though a new fatigue limit is different from the fatigue limit of the initial S-N curve.

The type-B load cycle used in the tests of SAE 4340 consisted of 1000 cycles of S_A and 9,000 cycles of S_a, where S_a was below the fatigue limit. Thus, the fatigue lives, as computed by Miner's theory, would be 10 times the number of cycles as indicated for each point on the initial S-N curve. Of course, Miner's curve would terminate at the fatigue limit of the S-N diagram. These curves and those ascertained by the authors may be compared with the test results on the diagrams in Fig. 7. If the slopes of these two variable-cycle curves are a function only of the distribution pattern they should be identical, because the testing apparatus, the specimens, and the load pattern were the same for both series; only the value of S_a was different. An inspection of these curves shows that this may well be the case.

Tests similar to those previously discussed were also conducted using load-cycle A, which consisted of 5000 cycles of S_A and 5000 cycles of S_a. The results of these tests are shown in Fig. 8. From these results it is evident that the variable-cycle curve lies quite close to the S-N diagram even though the test results are somewhat more erratic and even fall to the left of the S-N curve at times. As would be expected, the slope of the variable-cycle curve more nearly approaches the slope of the S-N diagram, because more cycles of S_A were included in the load pattern. Thus, the ratio of k_{SN} to k_v should be nearer unity.

With the data presented from Dolan's tests using the two load patterns B and A as a basis, it is possible to interpolate for the expected relationships for other patterns having different ratios of N_A to $(N_A + N_a)$; where N_A and N_a represent the number of cycles in a load pattern at S_A and S_a, respectively.

If the load pattern were constant at S_A, where S_A is any overstress, then failure would occur on the S-N diagram and the ratio of k_{SN} to k_v would be 1.0. But if only a very small percentage of the load pattern cycles were at S_A and the remainder at S_a, then the slope of a variable-cycle curve so determined would be extremely high and, in theory, would approach a vertical line through the point (N_a, S_a) on the S-N diagram. In the latter case the ratio of k_{SN} to k_v would approach zero as k_v becomes infinite.

If the ratio of k_{SN}/k_v is set equal to β, where

$$0 \leq \beta \leq 1.0$$

then the two limiting points of β (0 and 1.0) together with the two interior points determined from Dolan's tests provide four points on a curve,

$$\beta = f\left(\frac{N_A}{N_A + N_a}\right). \qquad (1)$$

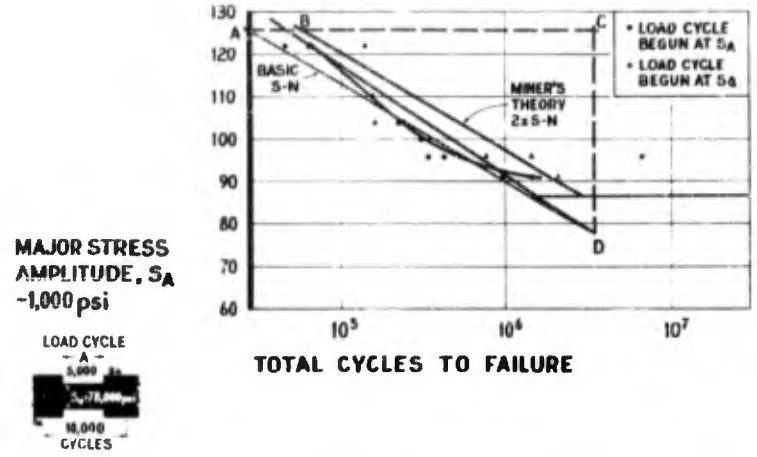

Fig. 8 - Test results for unnotched rotating-beam specimens of SAE 4340 steel, subjected to load cycle A, Dolan, et al [20], 1949

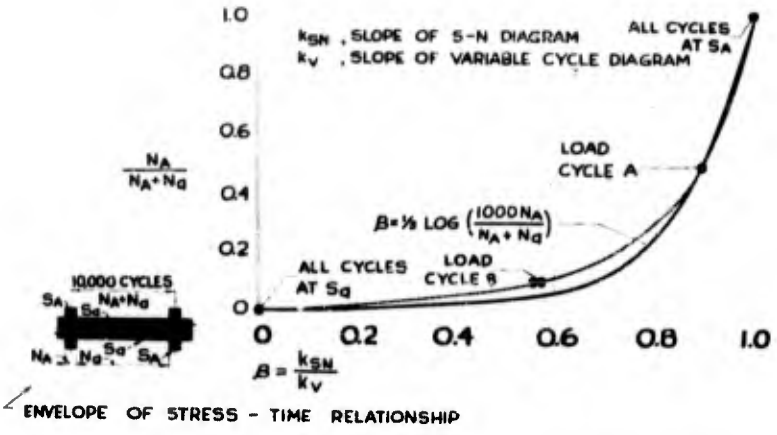

Fig. 9 - Variation of distribution coefficient, β, for loading spectrums of two stress levels of Dolan, et al [20], 1949

This relationship has been plotted in Fig. 9. An approximation to the experimental curve is

$$\beta = \frac{1}{3}\log_{10}\left(\frac{1000\ N_A}{N_A + N_a}\right). \qquad (2)$$

If we consider a decreasing arrangement of load-cycle amplitudes for a 1000-cycle load pattern between S_A and S_a and plot it on a 3-cycle semilog plot, the ratio of the area under this log-distribution pattern (from $\log_{10} 1.0 = 0$ to $\log_{10} 1000 = 3.0$ and from S_A to S_a) to the area of the field on which it is plotted is equal to the distribution coefficient, β, as previously defined. The stress cycles greater than S_a produce a block of area equal to $\log_{10}(1000\,N_A/N_A + N_a)$. Thus, β may be taken equal to the above mentioned block divided by the area of the entire field, which was 1.0 times $\log_{10} 1000$ or 3.0.

On the basis of a 1000-cycle load pattern, load-cycle B of Dolan's tests [20] would have 100 cycles at S_A and 900 cycles at S_a. The minor maximum stress, S_a, is the lower limit of the plot, and cycles at this stress will not contribute to the area being computed, but cycles of greater stress will. Therefore,

$$\beta_B = \frac{\log 100}{\log 1000} = \frac{2}{3} = 0.667 .$$

For load-cycle A there would be 500 cycles at S_A and 500 cycles at S_a, and the distribution coefficient, β_A, could be computed as follows:

$$\beta_A = \frac{\log 500}{\log 1000} = \frac{2.7}{3} = 0.90 .$$

Of course, if all cycles were at S_a, β would be zero; if all were at S_A, β would equal 1.0.

Thus far, patterns having only two stress levels, one at S_A and the other at S_a, have been considered. However, it is necessary to consider continuously varying loading spectra for the method to be of any appreciable value. Dolan's load-cycle G varied as a sine wave between S_A and S_a. The results of these tests are shown in Fig. 10. In this diagram, the dashed-line drawn through the test results has a value of β equal to 0.90. The value of β based on the area procedure, just noted, has been computed for a sine-wave, frequency-distribution spectrum. The diagram on the left side of Fig. 11 shows the frequency-distribution spectrum, and the diagram on the right side shows the resulting 1000-cycle

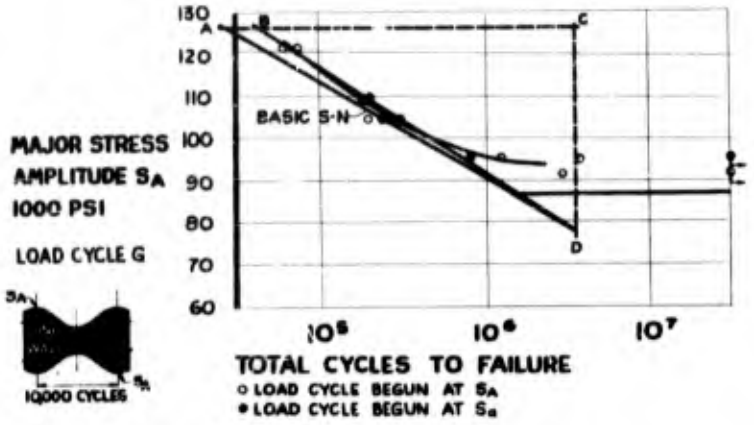

Fig. 10 - Test results for unnotched rotating-beam specimens of SAE 4340 steel, subjected to load cycle G, Dolan, et al [20], 1949

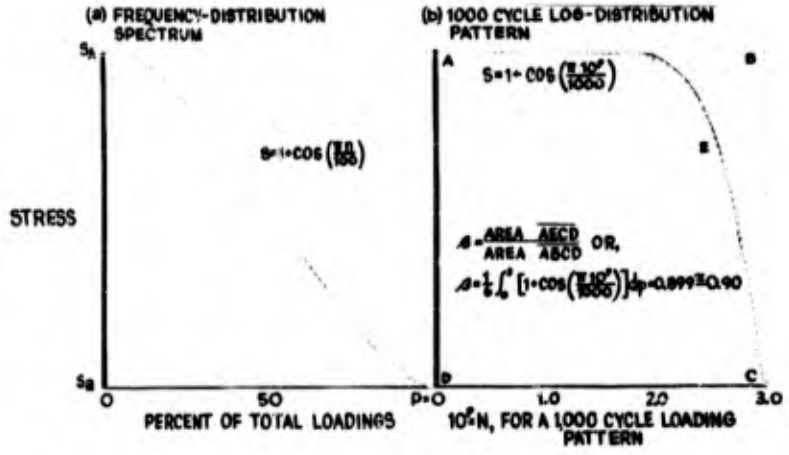

Fig. 11 - Frequency distribution and log-distribution for a sine-wave loading spectrum

log-distribution pattern. It may be noted that the computed value of β is 0.90, which is identical with the above test value.

Another point which is of interest in this discussion is that at any given stress level the value of β may also be represented as the ratio of the actual horizontal distance between the variable-cycle diagram and a vertical line through the S-N diagram (or S-N diagram extended) at S_a, to the distance from the basic S-N diagram to the same vertical line at the same stress level. Thus, for the previous diagrams in Figs. 7, 8, and 10, which show the results of tests by Dolan, et al, the ratio of BC to AC (or in Fig. 7 for S_a = 60,000 psi and load cycle B, the ratio of B'C' to AC') is the same as the ratio of k_{SN} to k_v and is equal to β.

If the distribution coefficient, β, is known, the number of cycles to failure under a spectrum-type loading pattern may be expressed as N_v where

$$\log N_v = \log N_a - \beta(\log N_a - \log N_A)$$

and

$$N_v = N_a\left(\frac{N_A}{N_a}\right)^{\beta} = \frac{N_A{}^{\beta}}{N_a{}^{(\beta-1)}} . \qquad (3)$$

It should be mentioned again, in connection with the previously discussed variable-cycle tests and the foregoing analysis, that all of the variable-cycle results were plotted at S_A, the major maximum cyclic stress. This would seem to be the logical way to identify these test results; however, as will be shown later for random loading, a different stress level may have more significance. If a variable-cycle test value plotted at S_A were projected vertically downward onto the S-N curve, it would indicate a constant stress cycle which would have the same fatigue life and which could be considered as an equivalent constant stress cycle.

Freudenthal [21] has conducted variable-cycle, rotating-beam tests on 2024-T4 and 7075-T6 aluminum alloys. For purposes of comparison, however, only the 7075-T6 tests will be discussed here. In Freudenthal's study, 20 specimens were tested at each of 6 different stress levels for a careful determination of the S-N diagram. Also, 20 specimens were tested at identical stress levels for each of 9 different distribution patterns. The 9 distribution patterns (A, B, C), (A', B', C'), and (A'', B'', C'') are shown in Fig. 12. The 3-cycle log-distributions are plotted adjacent to each frequency distribution pattern. In the log-distribution patterns, the ratio of the shaded area to total block area yields the value of β in each case.

The results of Freudenthal's tests on 7075-T6 are presented in Fig. 13. All points plotted on this diagram were obtained as the anti-log of the mean log N for 20 separate tests. Thus, the 300 tests represented on this figure provide some of the most extensive information yet obtained in a cumulative damage study.

The test results for the 9 variable-cycle load patterns have been plotted at S_A in Fig. 13, and the results based on the computed values of β have been plotted above the actual test results and connected to them by short solid lines for purposes of comparison. The results are also presented in a tabular form in the Table 1. It may be noted that the average net error in β was only 1.52 percent. Those distributions which showed the greatest error are A, C, B', and C'', but no reason for these larger deviations can be determined. If these four patterns are considered alone, the average net error is only 2.91 percent.

Thus, it would appear that the previously described method of estimating the fatigue lives of specimens or parts which are subjected to variable-load patterns need not be complicated to conform exactly with any given set of results. The method appears to yield values that are within the accuracy of the test results themselves.

CORRELATION OF CRITERION WITH RANDOM-LOAD FATIGUE TEST RESULTS

Random-load fatigue tests on 2024-T3 notched and unnotched sheet specimens in reversed bending have been reported by Trotter [22]. The loading was obtained by broadband excitation of an essentially single-degree-of-freedom test system. The test system oscillated at about 40 cps with random amplitudes. A stress-cycle amplitude histogram for 400 cycles was shown to fit the Rayleigh frequency density curve very well with the maximum clearly at the root-mean-square amplitude. The maximum stress-cycle amplitude in the 400 cycles was less than 3.8 times the root-mean-square amplitude.

The Rayleigh probability density function is shown in Fig. 14 and is given by

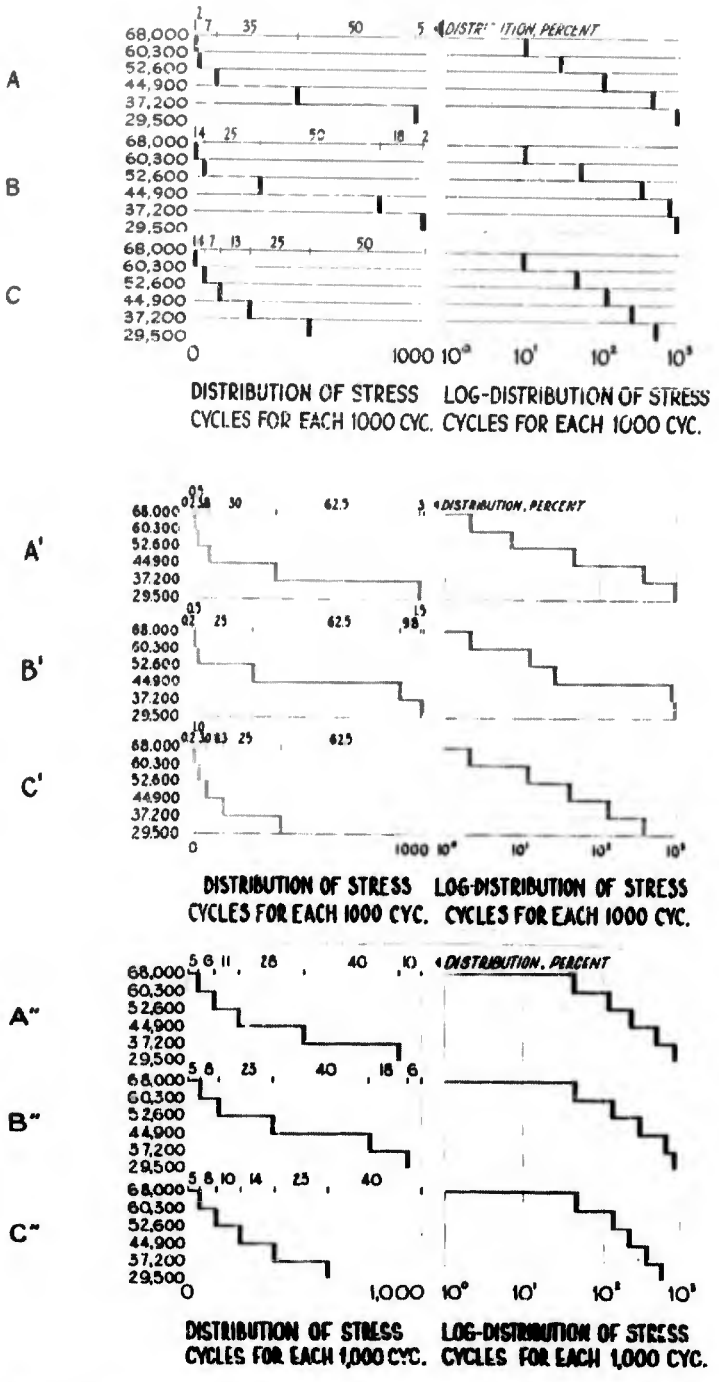

Fig. 12 - Distribution patterns used by Freudenthal [21], 1955 for tests on 7075-T6 aluminum alloy and derived 3-cycle, log-distribution patterns

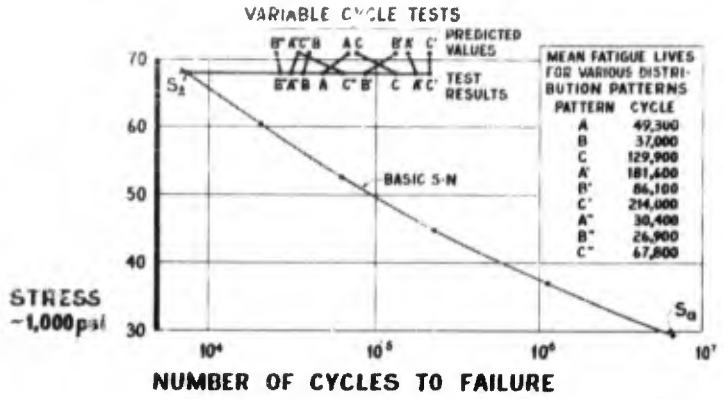

Fig. 13 - Freudenthal's tests of rotating-beam specimens of 7075-T6 aluminum alloy [21], 1955. (Note: These data represent the results of 300 fatigue tests.)

TABLE 1
Comparison of Freudenthal's Test Results on 7075-T6 Aluminum Alloy with Computed Results

Distribution Pattern	Value of β		Difference $\beta_T - \beta_c$	Percent Error
	β_T Test	β_c Computed		
A	0.723	0.673	+0.050	+ 6.91
B	0.766	0.755	+0.011	+ 1.44
C	0.582	0.660	-0.078	- 13.40
A'	0.531	0.554	-0.023	- 4.33
B'	0.642	0.580	+0.062	+ 9.65
C'	0.508	0.509	-0.001	- 0.20
A"	0.794	0.776	+0.018	+ 2.27
B"	0.812	0.822	-0.010	- 1.23
C"	0.677	0.777	-0.100	- 14.79
		Total Net Error, percent		- 13.68
		Average Net Error, percent		- 1.52

$$P(S_P) = \frac{S_P}{S_{P_o}^2} e^{-S_P^2/2S_{P_o}^2} \qquad (4)$$

where

S_p = stress cycle amplitude

S_{P_o} = root-mean-square stress cycle amplitude.

It will be noted that the Rayleigh probability density function would indicate an eventual infinitely large stress-cycle amplitude as a result of the exponential in the probability expression. This fact presents some difficulties in making a fatigue life estimate by any method. However, it must be realized that very large stress-cycle amplitudes are generally limited, because the structural part will not behave linearly under high stresses. Trotter chose to analyze his load-cycle data by Miner's method, and showed a sample computation wherein the maximum stress cycle amplitude was assumed to be 6 times the root-mean-square amplitude.

The random load fatigue life relationships were estimated by the proposed method using

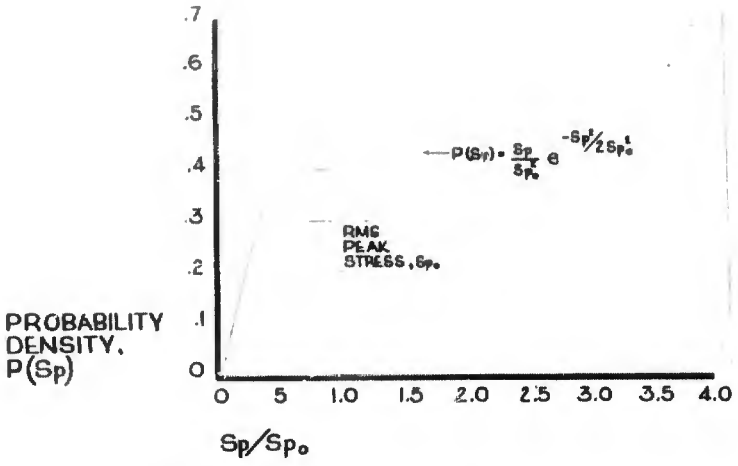

Fig. 14 - Rayleigh probability density function

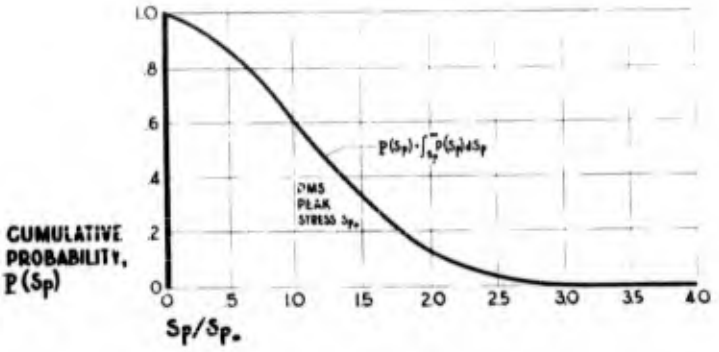

Fig. 15 - Cumulative, Rayleigh probability function

a 1000-cycle load spectrum derived from the Raleigh probability density relationship. For this purpose, it was necessary to compute the cumulative probability function $P(S_p)$, where

$$P(S_p) = \int_0^\infty P(S_p)\, dS_p . \qquad (5)$$

The cumulative probability function is shown in Fig. 15. This function is the envelope of the load-cycle spectrum. The load-cycle spectrum and the corresponding log-distribution function are shown in Fig. 16. It will be noted that only one cycle in 1000 will exceed 3.7 times the root-mean-square, stress-cycle amplitude. Furthermore, the log-distribution plot is parabolic; therefore, the value of β was computed as follows:

$$\beta = \frac{(2/3)(3.7)(3.0)}{(3.7)(3.0)} = 0.667 . \qquad (6)$$

Trotter's S-N relationships and variable cycle test results for the unnotched and notched specimens are shown in Figs. 17 and 18, respectively. The vertical line, CD, representing N_a was established by drawing the steepest tangent, AD, through the S-N data to find the point of intersection, D, at zero stress-cycle amplitude. The point B was then established at 66.7 percent of the distance from A to C, measured from C. The line BC represents the variable-cycle fatigue life for a maximum stress of 3.7 times the root-mean-square stress, if the fatigue data were plotted at the maximum cyclic stress, S_A, divided by the ultimate tensile strength of the material. If the variable-cycle fatigue life is

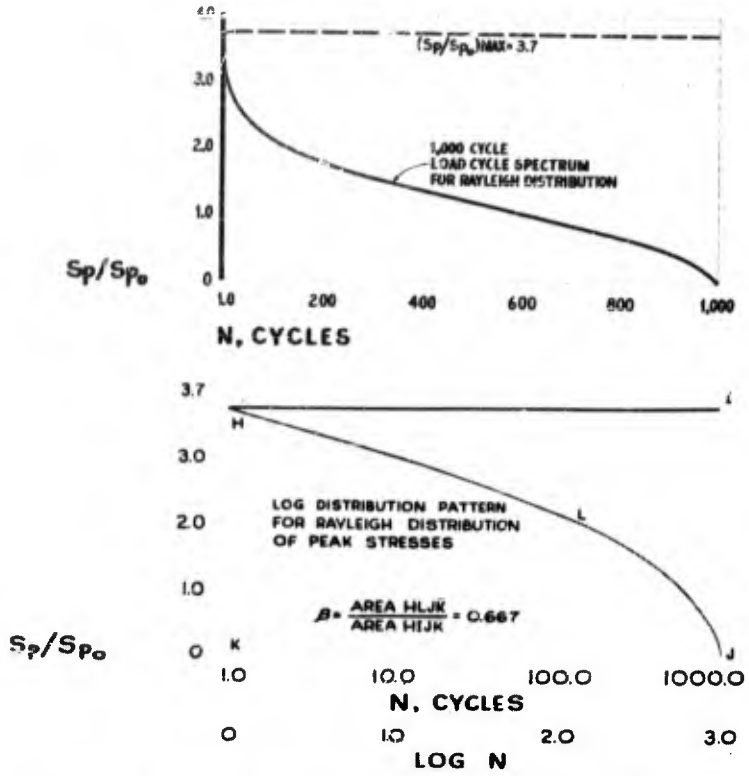

Fig. 16 - The 1000-cycle, load-cycle spectrum and log-distribution pattern for the Rayleigh probability function

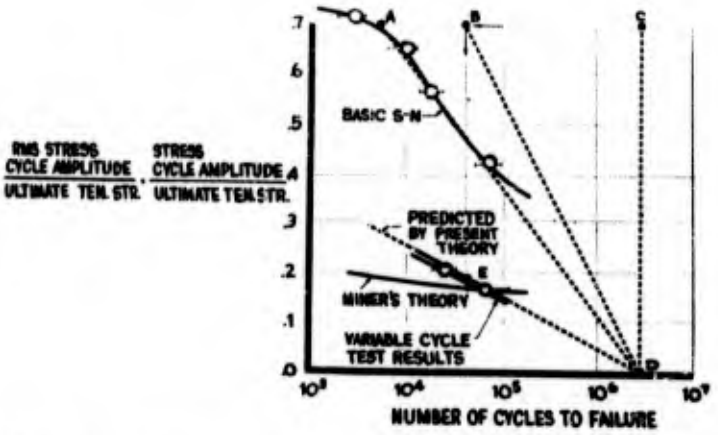

Fig. 17 - Variable-cycle, random-load, fatigue-test results for notched 2024-T3 sheet in reversed bending, Trotter [22], 1958

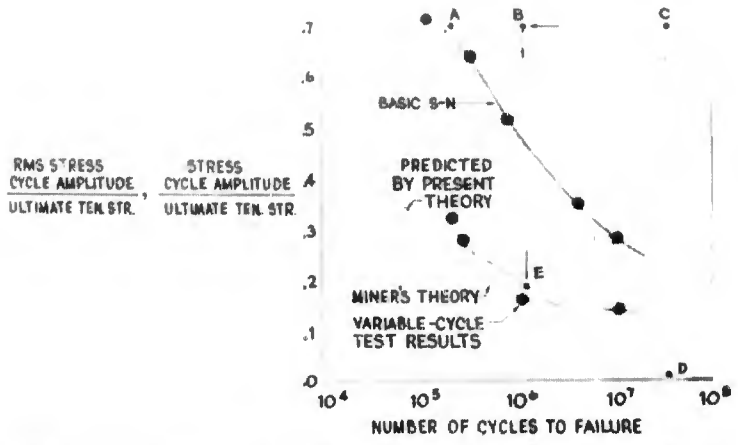

Fig. 18 - Variable-cycle, random-load, fatigue-test results for notched 2024-T3 sheet in reversed bending, Trotter [22], 1956

expressed in terms of the root-mean-square peak stress divided by the ultimate strength. the stresses represented by the line BD are divided by 3.7; that is, the slope of BD is reduced by a factor of 3.7 to obtain ED for both the unnotched and notched data.

It will be noted that the line ED is a fairly good estimate of the variable-cycle fatigue life, particularly for the unnotched specimens. It also appears to be a superior estimate to that predicted by Miner's method.

A PROPOSED FATIGUE LIFE INVESTIGATION FOR BROADBAND RESPONSE

It has been proposed [23] that the two most important parameters for a future cumulative damage theory are those parameters which describe a truly random process, such as the stress at a critical point in a structure. These are the power spectrum and the probability distribution. It is well known that the area under the power spectrum is the variance for a stationary random process. The variance is a measure of the magnitude or severity of the stresses. The power-spectrum shape, on the other hand, shows the relative importance of the various frequency components in the random-stress time-history. For example, a simple relationship involving the second moment of the power spectrum about the zero frequency axis, developed by Rice [24], indicates the number of times that the stress time-history will cross the zero stress level in a given period of time. Thus, it would appear that the second and possibly higher moments might be used in a cumulative damage criterion, since they supply the influence of spectrum shape.

For the simplest possible power spectrum represented as a single, very sharp peak on a "power-frequency" plot, the associated stress time-history is a simple sinusoid of a given frequency. If the power spectrum shows a somewhat broader peak or several peaks of very nearly the same frequency, the associated stress time-history will be roughly sinusoidal at an average frequency and will display random variations in amplitude. These two cases are, in effect, the only cases for which the previously discussed cumulative-damage criteria will apply.

If the stress power spectrum is "broadband," that is, if the power spectral density is significantly different from zero over a wide frequency range, then the associated stress time-history is not cyclic in any way, and existing fatigue damage criteria cannot be applied without making arbitrary simplifying assumptions.

A promising approach for establishing a rational, cumulative-fatigue-damage criterion would be to study the separate effects on fatigue life of stress power spectrum shape and root-mean-square stress for the same stress frequency distribution. Test series of simple, small specimens — subjected to (1) stress time-histories, having different stress power-spectrum shapes but the same root-mean-square stress, and (2) other series, having the same power-spectrum shape but different root-mean-square

Fig. 19 - Typical stress-power spectrum

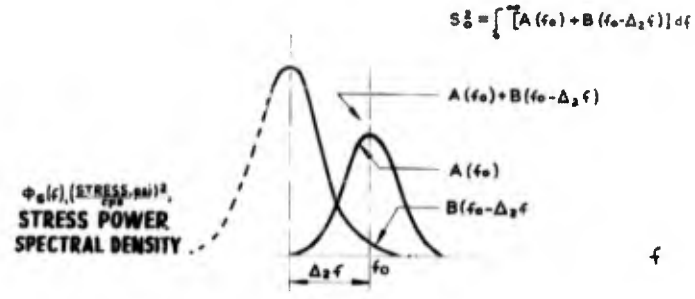

Fig. 20 - Power-spectrum building blocks for a random-load, cumulative-damage test program

stresses — would be required in order to isolate and study the effects of these variables. The stress-power spectral shapes of primary interest are those having characteristics which are more or less typical of actual stress power spectra for structures and equipment components subjected to random service loads. These are often composed of one, two, three, or more very definite peaks such as that shown in Fig. 19. This would suggest that a basic triangular or spike-shaped spectrum building block could be used to approach the more complex shapes. For example, the power-spectrum shape (Fig. 20) could be derived as the sum of the two building blocks A and B. Of course, the first and higher order moments of the power spectra about the zero frequency axis would vary, as block A and block B were shifted on the frequency axis, and would provide a description of the spectral shape. The moments of a power spectrum are defined as follows:

$$M_n = \int_0^\infty f^n \phi(f)\, df . \qquad (7)$$

It was mentioned previously that the number of times that a random stress time-history crosses the zero stress axis with positive (or negative) slope per second is a function of the second moment. This means that the second moment of the power spectrum provides significant information on the shape of the power spectrum and is probably a very meaningful parameter for a fatigue damage theory. The number of zero crossings per second with positive (or negative) slope was related by Rice to the second moment of the power spectrum about the zero frequency axis, and is given by

$$N_0 = \left[\frac{\int_0^\infty f^2 \gamma(f)\, df}{\int_0^\infty \gamma(f)\, df} \right]^{1/2} \qquad (8)$$

The second moment of the power spectrum is somewhat analogous to the moment of inertia in elementary mechanics, where the moment of inertia of the area of a structural section provides information on the shape and bending properties of the section.

DISCUSSION OF RESULTS

In general, previous fatigue damage studies can be separated into the following categories.

1. Studies in which the changes that occur in the fatigue limit due to prestressing at overstresses and understresses were investigated.

2. Those wherein the effects of prestressing are studied in terms of the change in the number of cycles to failure at a different stress level.

3. Investigations designed to study fatigue service life by subjecting test specimens to load patterns which are repeated a relatively large number of times before failure occurs.

4. Studies for single-degree-of-freedom systems oscillating at a nearly constant frequency but with random amplitudes.

The findings of studies in the first two categories indicate, in general, that cycling at an overstress for a portion of the fatigue life damages the specimen by causing the fatigue limit after prestressing to be lower than the fatigue limit displayed by the basic S-N diagram. However, there are indications that some cycling at very low overstresses can raise the fatigue limit preceptibly for some materials.

Understressing just below the basic fatigue limit can raise subsequently determined fatigue limits for some materials. In some studies successive increases in the stress level from an initial high understress has led to extremely long lives at final stresses considerably above the initial fatigue limit. This type of manipulation is known as coaxing.

Generally, it has been observed (1) that overstressing tends to reduce the ordinary fatigue life at a subsequently lower overstress and (2) that it tends to increase the fatigue life at a subsequently higher overstress.

Cumulative-damage studies have been directed toward the expression of fatigue damage as a function of the prestress cycle ratios. Miner and some other investigators assumed the fatigue damage was equal to the summation of the cycle ratios, but others have shown that fatigue damage varies in a more complex manner with the total or cumulative cycle ratio. Richart and Newmark proposed that damage might vary with a power of the prestress cycle ratio for a given prestress and test stress. They also emphasized that the order of application of a small number of blocks of different cyclic stresses had a very definite effect on the fatigue life, but that as the number of applications of the pattern of blocks increased, the order became less significant.

In the present investigation of fatigue under variable-cycle loading, extensive use has been made of test data from previous fatigue damage studies. In most of these investigations tests were conducted at two or more stress levels on small rotating-beam specimens. Rotating-beam tests are relatively easy to conduct, and the cycling rate is usually high; therefore, many investigators have used this type of test to obtain a large number of results in a reasonable period of time.

The method for estimating fatigue life, under variable-cycle loading proposed in this study, has been derived from the extensive variable-cycle test data obtained by other investigators. Data from two studies, in particular, have proved very useful for this investigation. These data were obtained by Kommers [14] and Dolan, Richart, and Work [20].

Kommers obtained new S-N relationships after separate series of identical specimens had been subjected to various cycle ratios of a single high overstress. Thus, the effects of this overstress were demonstrated for other stress levels. In the present study these data were used to demonstrate the changes that are likely to occur in S-N relationships which show the total cycles to failure including the cycles of the initial overstress. This was accomplished by merely "adding-in" the

cycles of the initial overstress or prestress to show the total cycles to failure.

This "adding-in" of the prestress cycles causes curves for prestressed specimens to "rotate" in a clockwise direction about the value of the prestress on the basic S-N diagram. The limiting rotation appears to be a vertical line through the point of rotation on the basic S-N curve. This vertical line represents the limit as the prestress cycle ratio approaches unity. Furthermore, a study of this type of plot indicated that the rotation between the basic S-N diagram and the vertical line was approximately proportional to the prestress cycle ratio. Other test data are needed, however, to evaluate this rotation effect further.

Qualitatively, the rotation effect illustrates two of the important findings of previous fatigue damage studies. It indicates that an overstress has a damaging effect on the fatigue life at a subsequently lower overstress, and that it appears to have healing effect on the fatigue life at a subsequently higher overstress. Quantitatively, it indicates a range of cycles wherein failures should occur for variable-cycle tests if the maximum cyclic stresses are all overstresses.

If all of the maximum cyclic stresses for a given loading pattern are overstresses, then cycling at the major or greatest maximum stress alone would cause failure at N_A cycles as determined from the basic S-N diagram. By cycling at the least or minor maximum cyclic stress alone, failure would occur at N_B cycles. Thus, the inverval for any pattern of maximum cyclic stresses can be defined by vertical lines through the major and minor stress levels on the basic S-N diagram. The present study proposes that the number of cycles to failure within this interval is a function of the pattern of maximum cyclic stresses.

A review of the variable-cycle test data, obtained by Dolan, et al, provided information for an evaluation of β in the relationship,

$$N_v = \frac{N_A^{\beta}}{N_B^{(\beta-1)}} . \qquad (9)$$

In this equation, N_v is the fatigue life for a variable-cycle pattern of loading. The distribution coefficient, β, relates the cycles to failure for the variable-cycle loading to the endpoints of the interval, N_A and N_B.

It was also observed from some of Dolan's test data, where the minor maximum cyclic stress was below the initial fatigue limit, that the life interval could be established by extending the basic straight-line S-N diagram to the value of the least or minor maximum cyclic stress. Therefore, to predict the variable-cycle fatigue life by the present method, it is only necessary (1) to define the interval of possible failure from an accurately determined S-N relationship and (2) to evaluate the distribution coefficient, β, for the loading pattern at hand.

The distribution coefficient, β, as it is presently evaluated, may be computed as a simple ratio of areas. For simplicity and convenience, a 1000-cycle envelope of maximum cyclic stresses is plotted on a semilog basis from 1 cycle to 1000 cycles. This is done by plotting the difference between the major and minor maximum stresses, S_A, and S_B, in order of decreasing magnitude from 1 cycle to 1000 cycles. Then the ratio of the actual area under this plot to the area of the field on which it is plotted, is the value β. With this information, the variable-cycle fatigue life, N_v, may then be computed.

The results of this study reaffirm the fact that stress cycles below the fatigue limit can be helpful if applied initially and can be damaging if they are preceded by stress cycles considerably above the fatigue limit. Also, the variation in β with $(N_A/N_A + N_B)$, would imply that an occasional high-stress cycle is not "remembered" by the material if it has a probability of occurrence of less than about 0.001, provided it would not damage the part if it were applied statically. Any static preloading, or machining, or forming operation that would change the basic S-N relationship can also be expected to affect the fatigue life under variable-cycle loading.

The method presented herein has been applied to tests reported by A. M. Freudenthal. This extensive program of tests with various loading patterns shows good agreement with the method. An example was also shown as to how fatigue lives computed by the proposed method compared to random amplitude constant frequency test data reported by Trotter. In general, the correlation of computed life with actual life was good, particularly for the unnotched series of specimens. The computed lives, for either case, provided better estimates than given by Miner's method.

CONCLUSIONS

The results of study of the data of previous fatigue damage investigations indicate that it is possible to estimate fatigue life under variable-cycle loading with reasonable accuracy. In order to estimate the variable-cycle fatigue life by the method outlined herein it is necessary to know the basic constant-cycle S-N relationship and the pattern of cyclic stress variation.

The range of stresses in the variable-cycle load pattern establishes an interval of cycles to failure on the constant-cycle S-N diagram. The number of cycles to failure falls within this interval and is established by the use of a distribution coefficient which accounts for the distribution of stresses within the load pattern.

Another manner of interpreting the data of this variable-cycle study is in terms of an equivalent fatigue strength, which is simply the constant-cycle fatigue loading which provides the same fatigue life as the variable-cycle loading.

If it is established that structural components or attached equipment items are subjected to random stress-cycle amplitudes at essentially a single frequency, then the fatigue life can be estimated by the proposed method. If the stress time-histories do not show a single frequency, then it is theorized that the fatigue life is also dependent on the stress power spectrum as well as the probability function for the random process.

ACKNOWLEDGMENT

The initial portion of the study reported herein was conducted at the University of Illinois under N. M. Newmark, Head of the Department of Civil Engineering, and W. H. Munse, Research Professor in Civil Engineering, and was sponsored through a cooperative agreement between the Engineering Experiment Station of the University of Illinois, the Illinois Division of Highways, the Department of Commerce - Bureau of Public Roads, and the Research Council on Riveted and Bolted Structural Joints. Later portions of the study were conducted at the Transport Division, Boeing Airplane Company under the supervision of E. L. Webb, Chief of the Structures Development Unit.

REFERENCES

1. H. J. French, "Fatigue and the Hardening of Steels," Transactions, American Society for Steel Treating, Vol. 21, pp. 899-946, Oct. 1933.

2. Committee E-9 on Fatigue, Manual on Fatigue Testing, Special Technical Publication No. 91, American Society for Testing Materials, Philadelphia, Pa., 1949.

3. H. F. Moore, "How and When Does a Fatigue Crack Start"?, Metals and Alloys, Vol. 7, pp. 297-299, 1936.

4. J. B. Kommers, "The Effect of Understressing on Cast Iron and Open-Hearth Iron," Proceedings, American Society for Testing Materials, Vol. 30, pp. 368-381, 1930.

5. J. B. Kommers, "The Effect of Overstressing and Understressing in Fatigue," Proceedings, American Society for Testing Materials, Vol. 45, pp. 532-543, 1943.

6. F. C. Lea, "Effect of Repetition Stresses on Materials," Engineering, Vol. 115, pp. 217-219, 252-254, 1923.

7. W. H. Swanger, and R. D. France, "Effect of Zinc Coatings on the Endurance Properties of Steel," Proceedings, American Society for Testing Materials, Vol. 32, pp. 430-452, 1932.

8. H. J. Gough, The Fatigue of Metals, Scott, Greenwood and Son, London, pp. 113-136, 1924.

9. Palmgren, "Die Lebensdauer von Kugellagern," Zeitschrift des Vereines Deutscher Ingenieure, Vol. 68, No. 14, pp. 339-341, 1924.

10. H. J. Grover, S. A. Gordon, and L. R. Jackson, Fatigue of Metals and Structures, Battelle Memorial Institute, Prepared for Bureau of Aeronautics, Department of the Navy, Superintendent of Documents, U. S. Government Printing Office, Washington, D. C., p. 45, 1954.

11. M. A. Miner, "Cumulative Damage in Fatigue," Journal of Applied Mechanics, Vol. 12, pp. A-159 - A-164, Sept. 1945.

12. S. Luthander, and G. Wallgren, "Determination of Fatigue Life with Stress Cycles of Varying Amplitude," The Aeronautical Research Institute of Sweden, FFA Report No. 18, Translated and Distributed by the Royal Swedish Air Board, Stockholm, as Translation No. 10, 1949.

13. H. Müller-Stock, E. Gerold, and E. H. Schulz, "Der Einfluss einer Wechselvorbeanspruchung auf Biegezeit und Biegewechselfestigkeit von Stahl St. 37," Archiv für das Eisenhüttenwesen, Vol. 12, pp. 1-148, 1939.

14. J. B. Kommers, "Effect of Overstress in Fatigue on the Endurance Life of Steel," Proceedings, American Society for Testing Materials, Vol. 45, pp. 532-541, 1945.

15. F. E. Richart, Jr., and N. M. Newmark, "A Hypothesis for the Determination of Cumulative Damage in Fatigue," Proceedings, American Society for Testing Materials, Vol. 48, pp. 767-800, 1948.

16. F. R. Shanley, "A Theory of Fatigue Based on Unbonding During Reversed Slip," Report No. P-350, The RAND Corporation, Nov. 1952 (Revised), May 1953.

17. A. M. Freudenthal, and R. A. Heller, "On Stress Interaction in Fatigue and a Cumulative Damage Rule," Journal of the Aero/Space Sciences, Vol. 26, No. 7, July 1959.

18. A. M. Freudenthal, and R. A. Heller, "Eleventh Progress Report on Research on Cumulative Fatigue Damage," Contract No. AF33(616)3982, WADD, ARTC/R&D Report No. 1464, Feb. 1960.

19. J. A. Bennett, "A Study of the Damaging Effect of Fatigue Stressing of X4130 Steel," Proceedings, American Society for Testing Materials. Vol. 46, pp. 693-711, 1946.

20. T. J. Dolan, F. E. Richart, Jr., and C. E. Work, "The Influence of Fluctuations in Stress Amplitude on the Fatigue of Metals," Proceedings, American Society for Testing Materials, Vol. 49, pp. 646-679, 1949.

21. A. M. Freudenthal, "Cumulative Fatigue Damage of Aircraft Structural Materials, Part I, 2024 and 7075, Aluminum Alloy," Wright Air Development Center Tech. Note 55-273, (Columbia University under Contract No. AF33(616)2274).

22. W. D. Trotter, "Fatigue of 2024-T3 Aluminum Sheet Under Random Loading," Test Report T2-1601, Boeing Airplane Company, Nov. 1958.

23. J. R. Fuller, "Development of a Rational Criterion for Estimating Fatigue Life Under Random Loads," An Unsolicited Technical Proposal, Boeing Airplane Company Document, D6 5131, Dec. 1959.

24. S. O. Rice, "Mathematic Analysis of Random Noise," Bell System Technical Journal, Vol. 18, p. 282, 1944, and Vol. 19, p. 46, 1945.

* * *

STATISTICAL INFERENCES ON ENVIRONMENTAL CRITERIA AND SAFETY MARGINS*

R. W. Mustain
Nortronics Division, Northrop Corporation
Hawthorne, California

It is planned to conduct environmental tests to determine safety margins for important components and models of a missile guidance system. For many reasons, the environmental testing has to be limited to small sample sizes. Many analytical questions arise about test levels and applicable statistics. The primary objective of this paper is to present some meaningful statistics on the relationships between failure strength and critical stress.

INTRODUCTION

It is planned to conduct environmental tests in such a manner that actual safety margins can be determined for important components and modules of the GAM-87A guidance system. This proposed environmental test program requires the application of environments greater than the service or critical stress environment to obtain the safety margins that exist between critical stresses and failure strengths. The primary objective of this report is to present some meaningful statistics on the relationships between failure strength and critical stress. Within any program, the amount of strength testing conducted is dependent upon various practical considerations such as the availability of test facilities, the capabilities of these existing facilities to produce the increased environments, the financial limitations, the resultant manpower requirements, and the feasibility of completing the tests in the allotted time.

Certainly, these factors influence the number of items of each module or component that can be tested for the GAM-87A Project. For these reasons, it will be necessary to limit the environmental testing of certain components and modules to small sample sizes. These sampling variations and the empirical test strengths must be amplified, clarified, and supplemented by statistical interpretations. Many analytical questions arise about the test levels and the applicable statistics. What can be reasonably expected from tests wherein different sample sizes are used? What is the effect of small sample size on failure probabilities? What confidence limits can be applied to mean failure stress values? How do variations in safety margins, sample size, range, standard deviation, confidence intervals, etc., reflect on the statistical inferences resulting from the fragility tests?

This report has been prepared to present some usable information on the many questionable areas. In preparation for this report, numerous statistical calculations have been made and supporting pictorial material in the form of graphs have been prepared. These accompanying graphs display data on confidence levels; range/standard deviation ratios; probability of failure for various standard deviations; and probability of failure for range values. The range and standard deviation data have been normalized to the service or critical stress environment. Some fundamental statistics have been prepared and plotted to show information on confidence levels. These data indicate the confidence intervals wherein the mean failure stress, the standard deviation failure stress, and the failure stress range can be expected to occur. In this regard, confidence levels and corresponding intervals

*This paper was not presented at the Symposium.

are presented as a function of n, the sample size. Using these graphical aids, the interval that will be expected to include (1) the mean failure stress or (2) the standard deviation of failure stress or (3) the failure stress range can be found for the desired confidence level and the selected value of n. Range/standard deviation ratios have been used to show range values that are comparable to standard deviations for certain values of n in terms of the critical stress, S_c. Standard deviation data converted to values of the critical stress, S_c, are exhibited graphically for location around the mean failure stress, S_m, and for the resultant probability of failure below critical stress levels. Similarly, data have been prepared to display the expected failure probabilities below the critical stress level for the variables n, S_m, and R, the range of the test data. Thus, failure probabilities can be predicted when the sample size, the sample range, and the mean failure stress have been determined. This provides a convenient tool for statistical inferences on probabilities when limited numbers of specimens are available for environmental testing.

CONFIDENCE LIMITS FOR FAILURE STRESS DATA

Since it is planned to establish fragility levels or strengths of GAM-87A modules and components by empirical tests above the service or critical stress, S_c, consideration must be given to the expected values of S_m, the mean failure stress. What confidence limits can be applied to mean failure stress values that are based on small samples? The answer to this question requires some study and research into the distribution and the variance of means. Research in this direction results in reviewing some fundamental theorems that are applicable to the location of sample means:

1. The mean of the distribution of sample means is the mean of the universe of individual values from which the samples are taken. For example, samples taken from a normal distribution with a population mean, μ, of 50 would have sample means of 50 for $n = 9$, 25, 100, etc.

2. The variance of the distribution of sample means equals the variance of the universe of individual values divided by n, the size of the sample: $\sigma_m^2 = \sigma^2/n$. This is the same as saying that the standard deviation of the distribution of sample means equals $1/\sqrt{n}$ times the standard deviation of the universe of individual values: $\sigma_m = \sigma/\sqrt{n}$. For example, samples taken from a normal distribution with a population standard deviation, σ, of 10 would have means distributed with σ_m equal to 3.33, 2, and 1 for n equal to 9, 25, and 100, respectively.

3. Sample means tend to be normally distributed. This relationship is a function of n. The distribution of the sample means becomes more normal or Gaussian as the size of the sample is increased.

4. When samples are small the distribution of the sample means is described by the t or Students distribution.

5. The sample size, n, affects the confidence interval. The larger the sample size, the narrower the confidence interval and the better the estimate of the universe value. The preciseness of statistical inferences increases with the $\sqrt{n}$.

Having covered the fundamentals that essentially define the location of sample means, it is appropriate that the discussion continue with some typical assumptions and examples to illustrate some of the possible mean statistics or parameters. Let it be assumed that tests on n (begin with $n > 50$) modules or components have been conducted and that the mean failure stress, S_m, has been determined. In addition, assume that the standard deviation of the universe from which the sample was taken is known to be σ. Then, certain confidence statements can be made about the mean failure stress based on large samples (say $n > 50$). The distribution of the means is considered to be normal or approximately normal. Therefore, confidence limits for the mean failure stress can be determined in terms of observed values of sample statistics. The confidence level, β, expressed in percent is called the confidence coefficient. The normal curve areas are used to determine confidence limits for large values of n. For each β value, there is a corresponding multiple, t, that is used to calculate the confidence interval. Confidence limits for the mean failure stress are defined by:

$$\text{Confidence Limits} = S_m \pm t\, s/\sqrt{n}. \qquad (1)$$

Multiples for some β values applicable to the normal distribution are shown in Table 1. Suppose that a confidence level of 95 percent is desired for the test; thus, using the multiple for $\beta = 0.95$, the mean failure stress can be expected to fall within the interval described by the values of $S_m \pm 1.96\, s/\sqrt{n}$. That is, 95 out of 100 times the sample mean of n items will lie between the value

TABLE 1
Multiples for Some t Values Applicable to the Normal Distribution

	t
0.50	0.67449
0.75	1.1503
0.90	1.6449
0.95	1.9600
0.975	2.2414
0.99	2.5758
0.995	2.8070
0.999	3.291

of $S_m - 1.96\ s/\sqrt{n}$ and the value of $S_m + 1.96\ s/\sqrt{n}$. In like manner, for a desired confidence of 99 percent, the confidence interval can be expressed as reaching from $S_m - 2.5758\ s/\sqrt{n}$ to $S_m + 2.5758\ s/\sqrt{n}$.

Now, it must be pointed out that the confidence limits given herein have revolved entirely around samples that are relatively large (say $n > 50$). The next logical step is to define equivalent limits for data based on samples less than 50. What happens to these confidence limits as n becomes less than 50? Actually, the distribution of the sample means (for small values of n) departs from the normal form and tends to assume the "Students" t distribution. The t distribution was originally formulated by W. S. Gosset, a chemist employed by Guinness Breweries, who used the pen name of "Student." Gosset published papers in 1907 and 1908 that discussed statistics from exact sampling tests that led to the "Student" t distribution. Fortunately, because of "Student's" work, the exact distribution for a normal universe has been established for sample values of the statistic

$$t = \frac{\bar{x} - \bar{\mu}}{s/\sqrt{n}},$$

where s represents an estimate of the universe standard deviation and $\bar{x}$ is the sample mean. The t distribution is symmetrical about its mean and departs but slightly from the form of the normal distribution. Whereas the t distribution is founded on empirical data, it seems to be a reasonable guide for statistical inferences on small sample data. The t distribution depends on a parameter, degrees of freedom, which is equal to $n - 1$. There are individual t distributions for the individual degrees of freedom. Thus, for each value of $n - 1$ there is a separate distribution curve of t values versus probabilities. These t values become the multiples for the equation

$$\text{Confidence Limits} = S_m \pm t\ s/\sqrt{n}. \qquad (1)$$

Tables of percentage points of the t distribution can be found in several popular texts on statistics. These tabulations contain values of t corresponding to selected cumulated probabilities for different degrees of freedom. Some typical t values are listed for illustration in Table 2. It can be seen from Table 2 that the confidence interval equals twice the quantity $(t\ s/\sqrt{n})$. Therefore, to state the confidence intervals in terms of standard deviations, t distribution points were multiplied by $(2/\sqrt{n})$ for various sample sizes, n, and for selected confidence levels. These values of $2\ t/\sqrt{n}$ are shown in Fig. 1. They represent the width of the confidence interval in units of sample standard deviation. The confidence intervals in standard deviations for corresponding confidence levels are depicted as a function of n. Sample sizes of 2, 3, 4, 5, 10, 20, 61 and 121 were used for the calculations. These curves indicate the confidence that can

TABLE 2
t Values for Various Cumulated Probabilities, and Sample Sizes (n)

Sample Size n	Probability							
	0.50	0.75	0.90	0.95	0.975	0.99	0.995	0.999
2	1.00000	2.4142	6.3138	12.706	25.452	63.657	127.32	636.619
5	0.74070	1.3444	2.1318	2.7764	3.4954	4.6041	5.5976	8.610
10	0.70272	1.2297	1.8331	2.2622	2.6850	3.2498	3.6897	4.781
20	0.68763	1.1866	1.7291	2.0930	2.4334	2.8609	3.1737	3.883
30	0.68304	1.1739	1.6991	2.0452	2.3638	2.7564	3.0380	3.659

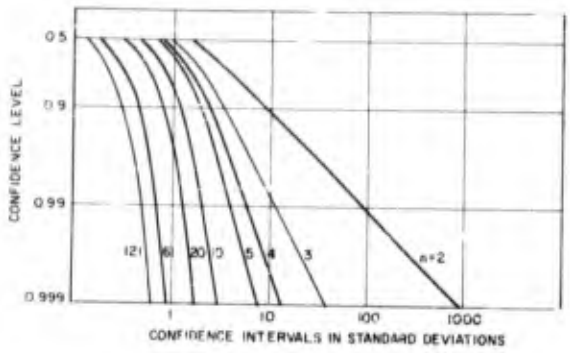

Fig. 1 - Confidence intervals for means $2t/n^{1/2}$

be reasonably expected for mean failure stress values recorded during empirical fragility tests on GAM-87A guidance units.

Perhaps, the most important lesson to be learned from these statistics is that confidence values are meaningless unless both the confidence level and the corresponding confidence limits, or interval, are clearly defined. Figure 1 shows that the larger the sample size, the narrower the confidence interval and the better the estimate of the true environmental failure level. For example, the 95-percent confidence levels for $n = 2, 3, 4, 5, 10, 20, 61$, and 121 exhibit confidence intervals of 17.97, 4.97, 3.18, 2.48, 1.43, 0.936, 0.512, and 0.36, respectively. It is seen also that for a fixed confidence interval, the confidence level increases directly with sample size. For instance, with a constant confidence interval of ±2 standard deviations, the confidence levels for $n = 2, 3, 4$, and 5 are 78.5, 92.5, 97.2, and 98.9, respectively. Tabulated data used to construct Figure 1 are presented in the Appendix (Table A).

To provide similar information on sample standard deviations, calculations have been made to establish confidence intervals for population standard deviations estimated from sample statistics. Confidence data, defining the expected spread of standard deviations, have been prepared by different methodologies. In compiling these confidence data, several approaches have been investigated. Consideration has been given to the relevance of the normal distribution, the t distribution, the χ^2 distribution, and some constants commonly used in quality control statistics.

First, the determination of confidence intervals for the standard deviation of the population based on large samples was accomplished in a manner analogous to that for the mean. Confidence limits for a general parameter are given by

$$\text{Confidence Limits} = g \pm t\,\sigma_g . \qquad (2)$$

σ_g is the standard deviation or the standard error of the statistic. Previously, the confidence limits of the mean failure stress were given as $S_m \pm t\, s/\sqrt{n}$. The ratio of $s/\sqrt{n}$ represents the standard error of the mean and s is an estimate of the population standard deviation taken from sample data. Similarly, the confidence interval (under certain conditions), for the population standard deviation, is defined by

$$\text{Confidence Interval} = s \pm t\, s/\sqrt{2n} . \qquad (3)$$

The term $s/\sqrt{2n}$ is derived from the fact that the standard error or the standard deviation of the distribution of sample standard deviations from a normal population is approximately $\sigma/\sqrt{2n}$. Therefore, the preciseness of the estimate of the population parameter increases with the square root of $2n$. The expression $s \pm t\, s/\sqrt{2n}$ becomes reasonably accurate for large values of n where applicable t values are taken from the normal distribution. For values of n less than 30 the χ^2 distribution is generally used. The β values and the corresponding t values for the normal distribution given in Table 1 can be used with Eq. (3) to determine the confidence intervals for the standard deviation of the population based on standard deviations from large samples. For instance, it can be expressed with 95-percent confidence that the population standard deviation lies in the range $s \pm 1.96\, s/\sqrt{2n}$ when n is large (say $n > 30$, preferably larger). In like manner, 99-percent confidence exists when the population standard deviation lies in the region

between $s + 2.5758\, s/\sqrt{2n}$ and $s - 2.5758\, s/\sqrt{2n}$.

The χ^2 distribution is considered a fairly accurate representation for standard deviation limits when n is less than 30. This distribution is skewed to the right and tends to approach the normal curve as n increases. Thus, there is a trade off point between the χ^2 distribution and the normal distribution that occurs somewhere above the value of $n = 30$. Since the t distribution also approaches the normal distribution for large values of n, it can be used to fill the void between $n = 30$ and the χ^2 - normal trade-off point. The relationship between the t and the normal distribution as n increases is clearly shown in the portion of a t table in Table 3. The normal distribution is equivalent to the case of $n = \infty$.

TABLE 3
Portion of a t Table Showing the Relationship Between the t and the Normal Distribution as n Increases

n	β			
	0.90	0.95	0.99	0.999
30	1.699	2.045	2.756	3.659
31	1.697	2.042	2.750	3.646
41	1.684	2.021	2.704	3.551
61	1.671	2.000	2.660	3.460
121	1.658	1.980	2.617	3.373
∞	1.645	1.960	2.576	3.291

The curves in Fig. 2 show confidence intervals based on the t distribution that are equivalent to the value of $2\, t\, s/\sqrt{2n}$ for n equal to 2, 3, 4, 5, 10, 20, 61, and 121. Again it is seen that the larger the value of n, the smaller the confidence interval. Furthermore, the confidence interval approaches zero as n becomes infinite. Thus, it can be seen that the larger the sample, the better the estimate of the population parameter from the sample statistic. Tabulated data used to construct Fig. 2 are presented in the Appendix (Table B).

Some supplementary confidence data on population standard deviations were prepared by utilizing statistical factors taken from quality control tables. The confidence intervals shown in Fig. 3 were computed by using quality control factors c_2 and c_3 with an applicable equation for t values. The mathematical derivation for this new approach follows. The exact formula for the standard deviation of the distribution of sample standard deviations from a normal population is:

$$s = \frac{\sigma'}{\sqrt{2n}} \sqrt{2\,(n-1) - 2n c_2^2}\,, \qquad (4)$$

where σ' is the standard value of σ and c_2 equals a constant that varies with n, relating the average standard deviation $\bar{\sigma}$ for samples of n observed values each to the standard deviation σ' of the universe sampled, the relation being $\bar{\sigma} = c_2 \sigma'$.

$$c_2 = \sqrt{\frac{2}{n}}\, \frac{\left(\frac{n-2}{2}\right)!}{\left(\frac{n-3}{2}\right)!}\,. \qquad (5)$$

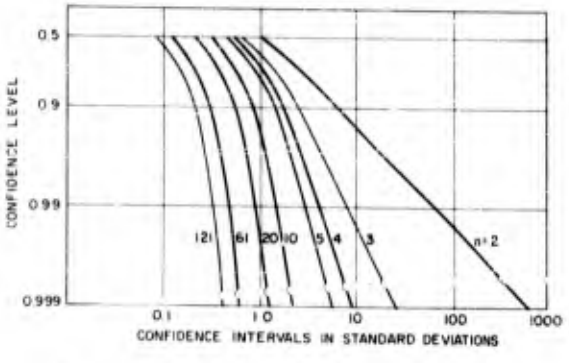

Fig. 2 - Confidence intervals for standard deviations $s \pm t\, s/\sqrt{2n}$

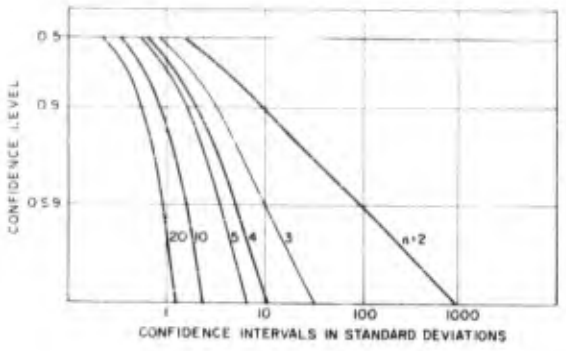

Fig. 3 - Confidence intervals for standard deviations $2\,t\,(c_3/c_2)$

The factor c_3 is a constant also that varies with n and is defined mathematically as:

$$c_3 = \sqrt{\frac{n-1}{n} - c_2^2}\,. \qquad (6)$$

Equations (2) and (4) can be combined to formulate the specific confidence limit equation:

$$\text{Confidence Limit} = s \pm t\frac{\sigma'}{\sqrt{2n}}\sqrt{2(n-1) - 2n c_2^2}\,. \qquad (7)$$

Using the relation $\bar{\sigma} = c_2\sigma'$, Eq. (7) becomes:

$$\text{Confidence Limit} = s \pm t\,\frac{\bar{\sigma}}{c_2\sqrt{2n}}\sqrt{2(n-1) - 2n c_2^2}\,. \qquad (8)$$

This is simplified to:

$$\text{Confidence Limit} = s \pm t\,\frac{\bar{\sigma}}{c_2}\sqrt{\frac{n-1}{n} - c_2^2} \qquad (9)$$

which is condensed to:

$$\left.\begin{aligned}&\text{Confidence Limit} = s \pm t\,\frac{c_3}{c_2}\bar{\sigma}\\ \text{or}\quad&\\ &\text{Confidence Limit} = s \pm t\,\frac{c_3}{c_2}s\end{aligned}\right\}. \qquad (10)$$

This solution is easily verified by using other relationships commonly used to establish 3 sigma limits for quality control charts. In this case the value of 3 is equivalent to the selected t value from a normal distribution. In quality control statistics, the upper limit for a sigma chart is given as $B_4\bar{\sigma}$ and the lower limit is given as $B_3\bar{\sigma}$.

$$B_3 = B_1/c_2 \qquad B_4 = B_2/c_2 \qquad (11)$$

$$B_1 = c_2 - 3c_3; \qquad B_2 = c_2 + 3c_3 \qquad (12)$$

$$B_3 = \frac{c_2 - 3c_3}{c_2} = 1 - \frac{3c_3}{c_2} \qquad (13)$$

$$B_4 = \frac{c_2 + 3c_3}{c_2} = 1 + \frac{3c_3}{c_2}\,. \qquad (14)$$

Then

$$B_4\bar{\sigma} = \bar{\sigma} + \frac{3c_3}{c_2}\bar{\sigma}\,. \qquad (15)$$

Similarly,

$$B_3\bar{\sigma} = \bar{\sigma} - \frac{3c_3}{c_2}\bar{\sigma}\,. \qquad (16)$$

Since the t value is equal to 3 in these two equations

$$\text{Sigma Limits} = \bar{\sigma} \pm t\,\frac{c_3}{c_2}\bar{\sigma} \quad \text{or} \quad s \pm t\,\frac{c_3}{c_2}s. \qquad (17)$$

It can be seen that Eq. (17) is the same as the confidence expression previously derived as Eq. (10). Values of $2\,t(c_3/c_2)$ for $n = 2, 3, 4, 5, 10$, and 20 have been plotted in Fig. 3 from data that are presented in the Appendix (Table C).

The χ^2 distribution has been used to prepare the confidence data on universe standard deviations that are shown in Fig. 4 and tabulated in the Appendix (Table D). For values of n less than 30, the distribution of the sample variances (σ^2) takes the form of

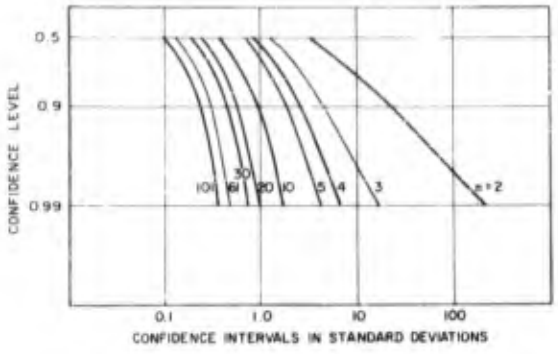

Fig. 4 - Confidence intervals for standard deviations χ^2 distribution

the χ^2 distribution. Percentage points of the χ^2 distribution can be found in most statistical textbooks. The form of the χ^2 distribution varies with the number of degrees of freedom which is $n-1$ in this case. The chi-square distribution exhibits a distinct curve for each value of n and is a skewed distribution that approaches normality for large values of n.

Confidence limits for universe standard deviations were obtained from the χ^2 expression,

$$\frac{n\sigma^2}{\chi^2_{n-1}};$$

The chi-square value is equivalent to a selected percentage point from χ^2 tables for $n-1$. For example, the lower and upper 0.99 confidence limits for the universe variance are

$$\frac{n\sigma^2}{\chi^2_{0.005}} \text{ for } n-1 \quad \text{and} \quad \frac{n\sigma^2}{\chi^2_{0.995}} \text{ for } n-1 . \qquad (18)$$

The square roots of these values yield the upper and lower limits for the universe standard deviation with a confidence of 0.99. Values of $\sqrt{n/\chi^2}$ for different values of n for confidence levels of 0.50, 0.80, 0.90, 0.950, 0.980, and 0.990 have been computed and are presented in the Appendix (Table D). Corresponding confidence intervals have been determined also and are listed in Table D and portrayed graphically in Fig. 4.

The next set of confidence data to be presented applies to the range parameter, R. Again, some quality control factors have been used to obtain confidence intervals for universe ranges. The confidence intervals shown in Figs. 5 and 6 were established by using quality control factors d_2 and d_3 with applicable equations for limits. The distribution of the range is not symmetric for small sample sizes. If samples are drawn from a normal distribution with standard deviation σ', the average of the distribution of the range is $d_2\,\sigma'$ and the standard deviation is $d_3\,\sigma'$. The variance of the range is $(d_3/d_2)^2$. The factor d_2 is a constant that varies with n, relating the average range $\bar{R}$ for samples of n observed values each to the standard deviation σ' of the universe sampled, the relation being $\bar{R} = d_2\,\sigma'$. The factor d_3 is a constant also that varies with n and is often designated as σ_w, the standard deviation of the range for the specific value of n. The ratio R/σ' is equal to w. The standard deviation of the range, σ_R, was given as $d_3\,\sigma'$. Now, since σ' can be estimated by $\bar{R}/d_2$, then σ_R becomes equal to $(d_3/d_2)\,\bar{R}$. This last expression fits neatly into the equation for the confidence limits of a general parameter (Eq. 2) to yield the universe range:

$$\text{Confidence Limits} = \bar{R} \pm t\,\frac{d_3}{d_2}\,\bar{R} . \qquad (19)$$

This equation is indeed similar to the equation derived for the standard deviation limits given in Eq. (17) with the exception that Eq. (19) contains symbols associated with the range parameter. Equation (19) can be easily verified by using other relationships that are used in quality control statistics to determine 3 sigma limits. Once more, the value of 3 is assumed to be the selected t value. In quality control statistics, the upper limit for a range chart is given as $D_4\bar{R}$ and the lower limit is given as $D_3\,\bar{R}$.

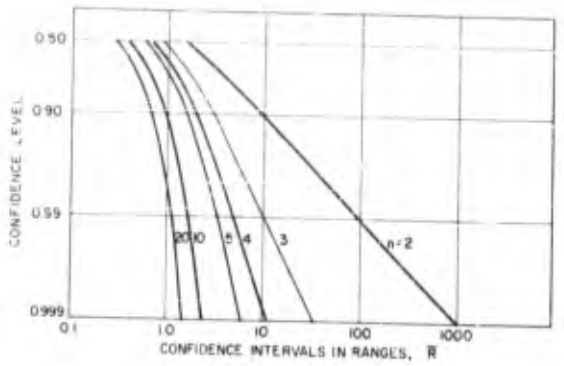

Fig. 5 - Confidence intervals for ranges $2\ t\ (d_3/d_2)$

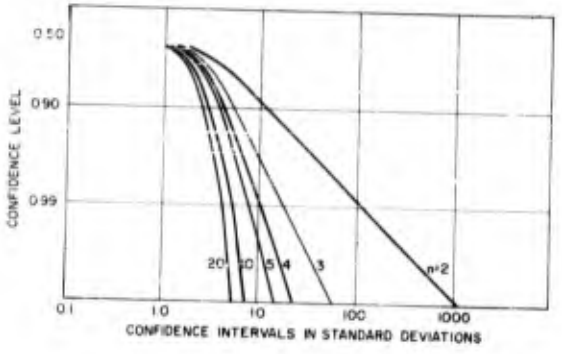

Fig. 6 - Confidence intervals for ranges $2\ t\ d_3$

$$D_3 = D_1/d_2\,; \qquad D_4 = D_2/d_2 \tag{20}$$

$$D_1 = d_2 - 3d_3\,; \qquad D_2 = d_2 + 3d_3 \tag{21}$$

$$D_3 = \frac{d_2 - 3d_3}{d_2} = 1 - 3\frac{d_3}{d_2} \tag{22}$$

$$D_4 = \frac{d_2 + 3d_3}{d_2} = 1 + 3\frac{d_3}{d_2}\,. \tag{23}$$

Then

$$D_4\bar{R} = \bar{R} + 3\frac{d_3}{d_2}\bar{R}\,. \tag{24}$$

Similarly,

$$D_3\bar{R} = \bar{R} - 3\frac{d_3}{d_2}\bar{R}\,. \tag{25}$$

Since the t value is equal to 3 in these last two equations

$$\text{Range Limits} = \bar{R} \pm t\frac{d_3}{d_2}\bar{R}\,. \tag{26}$$

Equation (26) is identical to the confidence limits previously given in Eq. (19). Values of $2\ t\ (d_3/d_2)$ for $n = 2, 3, 4, 5, 10$, and 20 are shown in Fig. 5. Tabulated data for $n = 2$ through $n = 25$ are listed in the Appendix (Table E), for confidence levels of 0.50, 0.75, 0.90, 0.95, 0.975, 0.990, 0.995, and 0.999.

Another confidence expression for the range is easily formulated by combining Eq. (2) with the standard deviation, σ_R, of $d_3\sigma'$. This new confidence equation is

$$\bar{R} \pm t\,d_3\sigma' = \bar{R} \pm t\,d_3 s\,. \tag{27}$$

This confidence limit equation can be easily substantiated by additional quality control relationships used to determine 3 sigma limits. Again, the value of 3 is considered to be the selected t value. In quality control statistics, the upper limit for a range chart is given as $D_2 \sigma'$ and the lower limit is given as $D_1 \sigma'$.

$$D_1 = d_2 - 3d_3; \qquad D_2 = d_2 + 3d_3 \quad (28)$$

$$D_1 = d_2 \sigma' - 3d_3 \sigma' \quad (29)$$

$$D_2 \sigma' = d_2 \sigma' + 3d_3 \sigma'. \quad (30)$$

Now since σ' can be estimated by $\bar{R}/d_2$, then Eqs. (29) and (30) become

$$D_1 \sigma' = \bar{R} - 3d_3 \sigma' \quad (31)$$

$$D_2 \sigma' = \bar{R} + 3d_3 \sigma'. \quad (32)$$

Whereas the t value is equal to 3 in these last two equations, the range limits are:

$$\bar{R} \pm t\, d_3 \sigma' = \bar{R} \pm t\, d_3 s. \quad (33)$$

This equation is the same as the limits that were defined by Eq. (27). Values of $2\,t\,d_3$ for n = 2, 3, 4, 5, 10, and 20 are displayed in Fig. 6. Tabulated values of $2\,t\,d_3$ are given in the Appendix (Table F), for confidence levels of 0.50, 0.75, 0.90, 0.95, 0.975, 0.990, 0.995, and 0.999. Sample sizes from n = 2 through n = 25 are included in the Appendix (Table F).

A third set of confidence data for the range parameter has been prepared based on probability information that is depicted in Fig. 7. Several distributions of the relationship $w = R/\sigma$ from a normal universe are plotted on probability paper for n = 2, 4, 6, 8, and 10. The abscissa represents the probability that the value of w (for the selected value of n) will be less than the corresponding ordinate value of z. It can be seen that this relative range distribution varies with n and tends to become normal with increasing sample size. The deviation from normality appears to be greatest near the lower left corner of the graph for small percentile points.

Confidence limits can be calculated from these probability points, $P(w < z)$, by multiplying the z value for the selected percentile point by σ'. Since σ' is estimated as being equal to $\bar{R}/d_2$, the limits for any chosen confidence level are given by

$$z \sigma' = z \bar{R}/d_2. \quad (34)$$

Values of z/d_2 have been calculated for n = 2 through n = 12 and are listed in the Appendix (Table G). Tabulated values are given for probabilities of 0.001, 0.005, 0.010, 0.025, 0.050, 0.950, 0.975, 0.990, 0.995, and 0.999. The tabulated values can be multiplied by the sample range to obtain the desired upper and lower range limits. For example, the upper range limit for n = 10 with a probability of 0.999 is equal to 1.94 $\bar{R}$. The corresponding lower limit for n = 10 with a probability of 0.001 is 0.351 $\bar{R}$.

FAILURE PROBABILITIES

Any discussion concerned with the problems of environmental criteria and their corresponding safety margin tests requires the consideration of applicable statistics such as

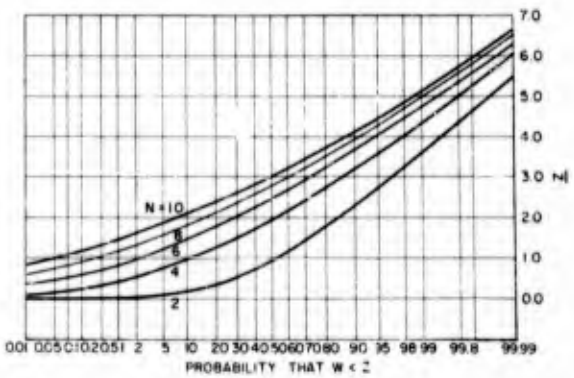

Fig. 7 - Probability of the relative range $\omega = R/\sigma$ for various sample sizes

averages, standard deviations, and ranges. Confidence data for these statistics related to universe parameters were thoroughly expounded in the previous section to lay a solid foundation for statistical inferences on failure probabilities. Primarily, this study is aimed at tests wherein small sample sizes, $n < 50$ or $n < 30$, are used for practical and economical reasons. The discussion will continue for the purpose of establishing failure probabilities for mean failure stress values as a function of range or standard deviation. In turn, the reliability of these failure probabilities can be determined by application of the confidence limits that were presented in the previous section.

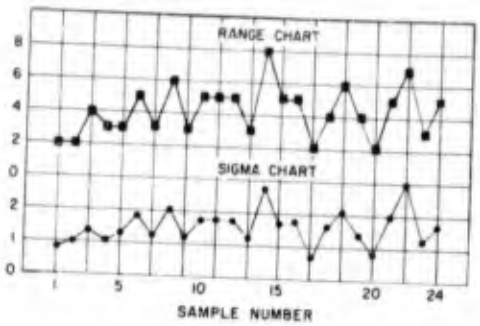

Fig. 8 - Range and standard deviation similarity

In small samples the range and standard deviation are likely to fluctuate together. If the standard deviation is large, the range is also likely to be large. If the standard deviation is small, the range is likely to be small. In large samples, however, the occurrence of one extreme value will cause the range to be large, but it may have less effect on the standard deviation. On the other hand, if the problem is to analyze variability wherein small samples are the rule, then the range may be employed as a substitute for the standard deviation. In addition to being an efficient substitute for the standard deviation in small samples, the range is easy to calculate. For that reason, it is usually preferred to the standard deviation in quality control analysis. Some small-sample data are shown in Fig. 8 that demonstrate the concurrent fluctuations between standard deviations and ranges. Twenty-five random samples of Size 5 were drawn from a normal distribution. Their standard deviations and ranges were computed and plotted. Even with this simple statistical exercise, it is seen that the range and the standard deviation closely follow each other. In fact, the two curves are almost identical in shape; the peaks and valleys are in agreement. This clearly substantiates the fact that the range is an efficient substitute for the standard deviation when small samples are used.

Several useful statistics, i.e., mean, range, standard deviation, etc., can be calculated from data of a sample and from these, estimates can be made of population parameters. Sometimes it is necessary to find approximate values of certain statistics rather than calculate them. For an individual large sample (say $n > 50$), the estimate of population standard deviation is the sample standard deviation (s). If i samples of size n are taken, the average standard deviation, $\bar{s}$, is equal to $\Sigma s/i$, and for this condition the average standard deviation is a better estimate of the population standard deviation than any single sample standard deviation. Another method of estimating the standard deviation of the population is by using the statistical relationship of $w = R/\sigma$ (see previous section and Fig. 7). The standard deviation is estimated from the w relationship by using the value of the mean of w which is represented symbolically by d_2. Thus, the standard deviation is equal to R/d_2. This approximation is good if the universe distribution is nearly normal. Appropriate values of d_2, the average value of w, have been used to show the relationship between range and standard deviation for the environmental statistics which are the primary objective of this report. Range/standard deviation ratios are presented in Fig. 9 to show range values that are comparable to standard deviations for constant values of n in terms of the critical stress, S_c. A family of curves for $n = 2, 3, 4, 5, 10, 20$, and 450 are displayed for the range, R, and the standard deviation, s, both normalized by the critical stress. Thus, values of range, R, over critical stress, S_c, for corresponding values of standard deviation, S, over critical stress, S_c, can be obtained from this graph for various sample sizes. An examination of these data shows that, for small samples, the R/S_c values approach the s/S_c values. For instance, the value of R/S_c is equivalent to $1.128\ s/S_c$ for the case where $n = 2$. This is in contrast to the general approximation of six standard deviations per range that is used often in statistics. Actually, the six standard deviations per range become fairly valid for sample sizes as great as 450. More precisely, the range over critical stress value is 6.009 times the standard deviation over critical stress value for $n = 450$.

Now, that some pertinent points regarding ranges and standard deviations have been

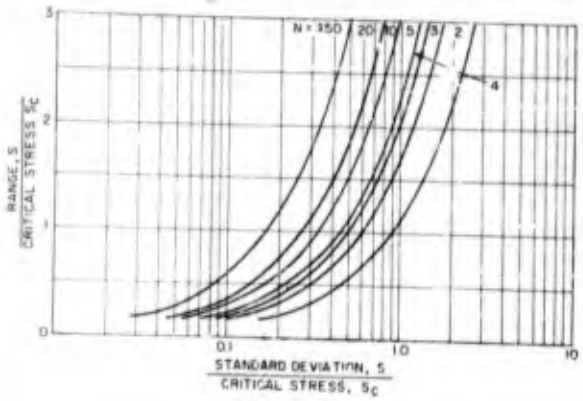

Fig. 9 - Range vs standard deviation as a function of n

covered and explained, this report will present statistical information designed to provide probabilities that components and modules will fail at environments below the service, specified or critical stress environment. That is, statistical data will be given so that failure probabilities (below the critical stress, S_c) can be inferred from statistics obtained during environmental tests of GAM-87A components and modules. First, probabilities based on standard deviations above the critical stress will be presented and then equivalent probabilities determined from normalized range values will be given. To illustrate standard deviation probabilities, assume a normal or near normal distribution for the population or universe. Then, the individual values of the stress failure levels will be normally distributed, the mean failure stress will be fairly representative of the universe mean, and the standard deviations of the sample stress failures will tend to be distributed in a form ranging from the skewed chi square to the normal distribution. Next, calculate the mean failure stress and the standard deviation in units of critical stress. What can be inferred about failure probabilities from these two sample statistics? Based on these statistics, what percentage of components and modules can be reasonably expected to fail at amplitudes below the critical environmental stress? These questions can be answered by proper application of the test statistics to predict the percentage of items (similar to the sample items) that can be expected to fail below the critical stress level.

The methodology of establishing component and module failure probabilities is fairly simple. The environmental amplitude between the mean failure stress, S_m, and the critical stress, S_c, is defined in multiples of standard deviation (normalized by the critical stress). Basically, the problem is to determine what portion of a statistical distribution is either above or below the critical stress amplitude. With an assumption of normality and with the number of safety margins (standard deviations) determined, the areas of the normal curve that are above and below the critical stress level can be found and their corresponding probabilities can be established. The area of the normal curve that falls below the critical stress limit is equivalent to the probability that items similar to those used in the test sample will fail.

The determination of the normal curve tail that lies below this critical line is accomplished by calculating the value of the transformation $S_m - S_c/s$ and, in turn, finding the corresponding probability from tables of the normal distribution. For example, if the standard deviation, s, is equal to 0.5 S_c and if S_m is equal to 3.5 S_c, then $S_m - S_c/s$ becomes $3.5\ S_c - S_c/0.5\ S_c$. Thus, the transformation value is 5 standard deviations which represents a failure probability of 0.0000003. In other words, it can be reasonably expected, with the stated conditions, that only three items out of 10 million will display fragility levels that are less than the critical or specified environmental level.

The fragility levels of the components and modules are assumed to originate from populations that display normal or Gaussian distributions. A normal distribution is defined by this noncumulative formula, where $\bar{x}$ is the mean and σ is the rms or standard deviation:

$$f(x) = \frac{1}{\sigma\sqrt{2\pi}} \exp\left[\frac{-(x-\bar{x})^2}{2\sigma^2}\right] \quad (35)$$

The noncumulative curve of the normal distribution is symmetrical about the mean and is bell-shaped. It is well known that the area within the $\pm 3\sigma$ limits is equivalent to 99.7 percent of the total area and that the turning points occur at $\pm 1\sigma$ values. The cumulative normal distribution function is given by:

$$\text{cum } f(x) = \frac{1}{\sigma\sqrt{2\pi}} \int_{\infty}^{x} \exp\left[\frac{-(x-\bar{x})^2}{2\sigma^2}\right] dx . \quad (36)$$

This equation is frequently altered to show integration over the area from $-x$ to x instead of the area from $-\infty$ to x. There are many tables in statistical literature with values for the ordinate and area of the normal frequency curve. An excellent set prepared by the National Bureau of Standards contains precise values of the normal ordinate and the normal area from $-x$ to x. These latter values, cum f (x; from $-x$ to $+x$) are related to cum f(x), Eq. (36), as follows:

$$\text{cum } f(x) = \text{cum } f\ (x; -x \text{ to } +x) + \frac{1 - \text{cum } f\ (x; -x \text{ to } +x)}{2} . \quad (37)$$

Equation (37) is equivalent to the area of the normal curve that lies above the critical limit. In this case, the critical stress, S_c, is indicated by $-x$ and, since the normal curve is symmetrical about the mean, the probability of success (Eq. 37) consists of the area between $\pm x$ plus the area of an upper tail. This upper tail extends from $+x$ to $+\infty$ and is numerically equal to

$$\frac{1 - \text{cum } f\ (x; -x \text{ to } +x)}{2} .$$

Notice that this is the second expression of the right side of Eq. (37). This upper tail has the same area as the tail that is below the critical stress level. Therefore, the area of interest and the probability of failure is given by

$$P_f = \frac{1 - \text{cum } f\ (x; -x \text{ to } +x)}{2} . \quad (38)$$

Values of Eq. (38) are plotted as a function of safety margins (mean failure stress, S_m over critical stress, S_c) for constant values of standard deviation, s, in Fig. 10. This family of curves shows the probability of an item failing below the critical or specified environment when the standard deviation is equal to S_c, 0.5 S_c, 0.333 S_c, 0.25 S_c, 0.2 S_c, and 0.166 S_c over a range of safety margins from 1 to 4.5. It is shown that the probability of failure, P_f, becomes greater with larger values of the standard deviation and conversely, P_f decreases for increases in the ratio of S_m/S_c. The highest P_f value plotted on the graph is 0.50 for the reason that calculations were made only for cases wherein S_m was equal to or greater than S_c. The probability of failure is 0.50 when the mean failure stress is equal to the critical stress for then half of the symmetrical normal curve lies above the critical stress level.

Usage of the data in Fig. 10 to predict failure probabilities requires that test data be

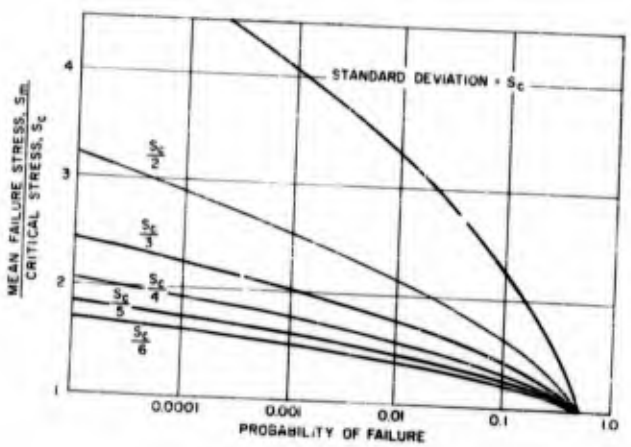

Fig. 10 - Failure probabilities

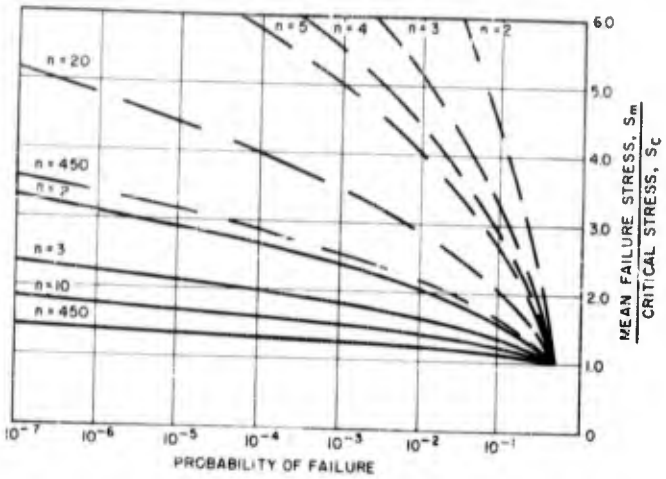

Fig. 11 - Probability of failure vs mean failure stress, as a function of sample size for two ranges: R = 3.00 S_c and R = 0.500 S_c

converted into values of the ordinate (mean failure stress, S_m over critical stress, S_c) and standard deviation. Whereas the statistics shown in Fig. 10 are based on proven statistics, the validity of utilizing this graph requires some meaningful confidence statements regarding the sample data. Some indication of the validity of sample mean failure stress values and sample standard deviation stress values can be obtained from the confidence information presented in the previous section (Figs. 1 through 4).

Failure probabilities have been presented in terms of standard deviations and mean failure stress that can be supplemented by applicable confidence data. In establishing these confidence data, an attempt was made to remove biased values by corrections that reflected the sample size and the statistic or parameter. However, it is desirable to show additional data on failure probabilities that display more vividly the effects of sample size on the possible failure of components and modules at test levels below the critical stress environment. For this reason, numerous computations have been made to provide failure probabilities on the range, R, statistic for different values of n, the sample size. The use of range values yields additional graphs that clearly indicate the relationship between sample size, n, and the probability of failure. Several graphical displays that exhibit the effect of sample size on range failure probabilities are presented in Figs. 12 through 19.

These range data have been prepared by combining the w relationship shown in Figs. 7 and 9 with values of the transformation $S_m - S_c/s$. More specifically, range values in terms of the critical stress have been divided by the appropriate value of d_2 for n to obtain equivalent values of the standard deviation in terms of the critical stress. In turn, these standard deviations have been used in the transformation $S_m - S_c/s$ to find failure probabilities for the range at various sample sizes. Thus, for a given range, a given sample size, and given value of $S_m - S_c$ (or S_m/S_c),

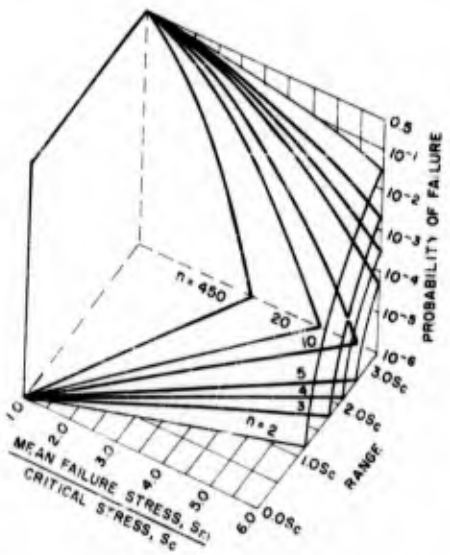

Fig. 12 - Probability of failure

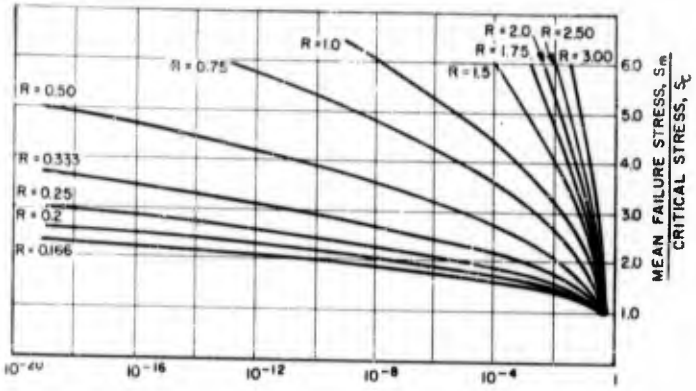

Fig. 13 - Probability of failure vs mean stress for n = 2, as a function of range

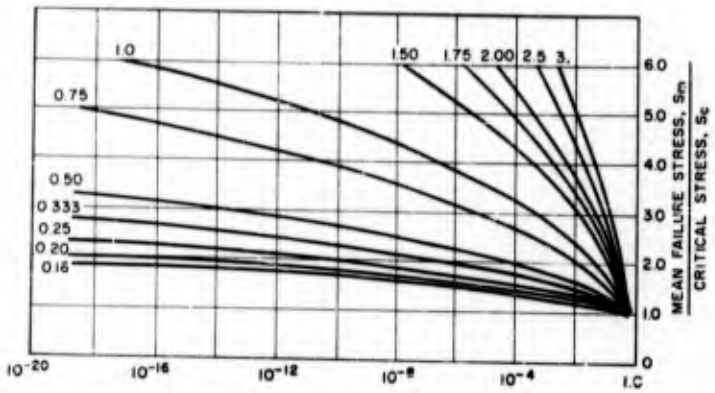

Fig. 14 - Probability of failure vs mean stress for n = 3, as a function of range

the probability of failure below the critical stress can be established.

Figure 11 shows the effect of change in range and sample size on failure probabilities. This figure contains data for n = 2, 3, 4, 5, 20, and 450 and for R = 0.500 S_c and R = 3.00 S_c. An examination of these data shows that increasing values of mean failure stress are associated with decreasing failure probabilities for any constant value of n. It is seen that smaller failure probabilities accompany larger values of n for constant range values. Also, this graph shows clearly that the smaller the range, the smaller is the probability of failure. The three-dimensional spectrogram of Fig. 12 shows failure probabilities as a function of range and mean failure stress for various sample sizes. This field diagram approaches a four-D illustration by virtue of the several failure blankets created by the different n values. An excellent indication of the relationships among the range, the mean failure stress, the sample size, and the failure probabilities is provided by this three-dimensional plot. The data tend to peak near the high range values and the low mean failure stress values. The n blankets clearly display the lower failure probabilities that occur for greater sample sizes with constant range and mean failure stress values. Figures 13 through 19 show detailed failure probabilities as a function of range for seven individual values of n. They also show families of curves for n = 2, 3, 4, 5, 10, 20, and 450, respectively. For example, Fig. 13 shows failure probabilities for n = 2 with range values of 0.166 S_c, 0.20 S_c, 0.25 S_c, 0.333 S_c,

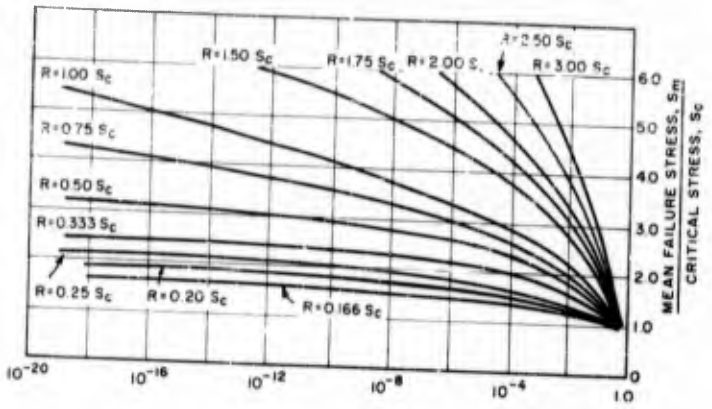

Fig. 15 - Probability of failure vs mean stress for n = 4, as a function of range

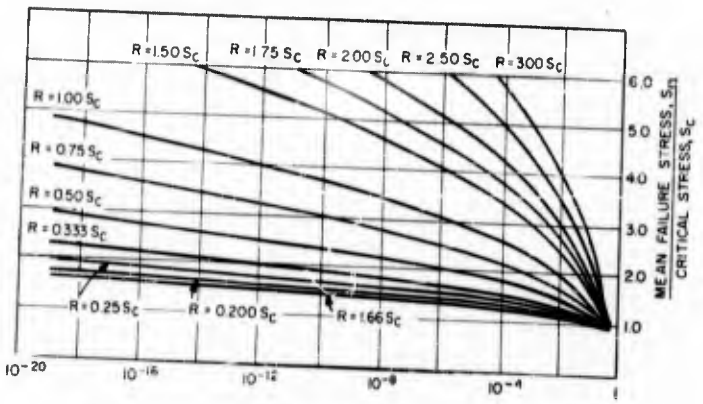

Fig. 16 - Probability of failure vs mean stress for n = 5, as a function of range

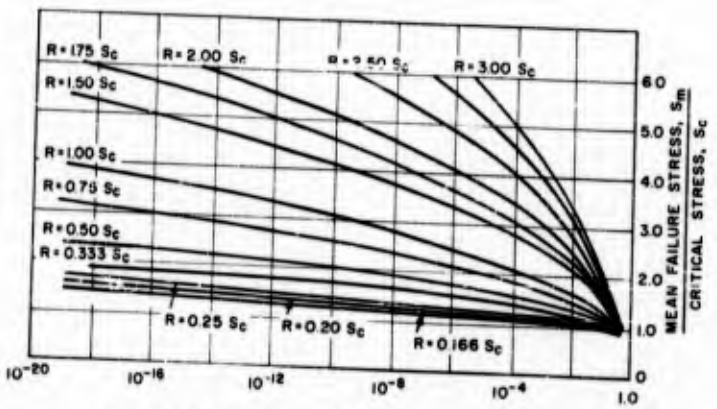

Fig. 17 - Probability of failure vs mean stress for n = 10, as a function of range

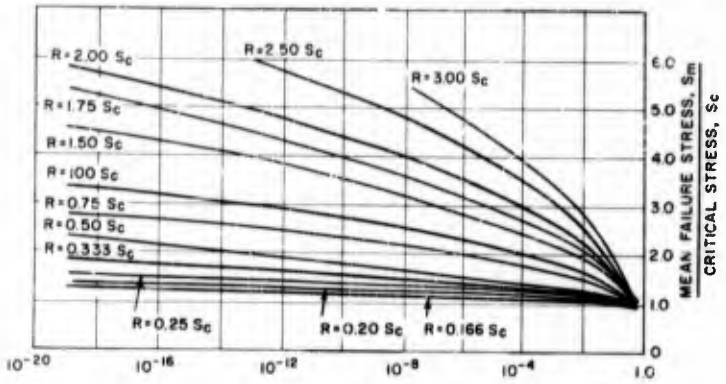

Fig. 18 - Probability of failure vs mean stress for n = 20, as a function of range

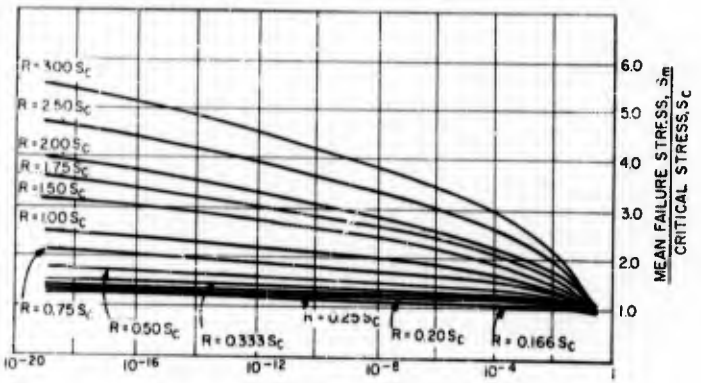

Fig. 19 - Probability of failure vs mean stress for n = 450, as a function of range

0.50 S_c, 0.75 S_c, 1.0 S_c, 1.5 S_c, 1.75 S_c, 2.0 S_c, 2.5 S_c, and 3.00 S_c. These graphical presentations provide an adequate representation of failure probabilities as related to the sample size, the mean failure stress, and the range. An analysis of these data shows (1) lower failure probabilities for the lower range curves, (2) less probability of failure with greater stress levels, and (3) less chance of failure with greater values of n for constant range and constant mean failure stress. This last effect is easily seen when Fig. 13 (n = 2) is compared with Fig. 19 (n = 450).

SUMMATION

This report has encompassed the results of an extensive statistical investigation that was designed to provide supporting data for environmental tests to failure of modules and components from the GAM-87A guidance system. Although, these statistics were studied with this test to failure program in mind, it is felt that the statistics of this report are applicable to many similar statistical sampling problems. Statistics were presented that thoroughly expounded confidence data on means, standard deviations, and ranges. Several methods of establishing confidence limits for each of these universe parameters were given. Failure probabilities below the environmental specification or critical stress level were displayed for modules and components. These failure probabilities were determined with the assumption that fragility levels of the various items were normally distributed. Data were included for failure probabilities based on (1) standard deviations and (2) ranges as functions of the mean failure

stress. Range failure probabilities were presented in considerable detail to illustrate the effect of variations in range and sample size on failure probabilities. The usage of the range statistics is especially recommended for sample sizes less than 12. The mean, the standard deviation, and the range confidence intervals and levels were discussed, displayed, and tabulated for ease of utilization. Sufficient information has been given on these parameters so that meaningful statistical inferences can be made on the parameters and their corresponding failure probabilities.

The confidence data can be used to provide some degree of assurance that a test value obtained will be reasonably indicative of the true universe parameter, i.e., the mean failure stress, the failure stress range, or the standard deviation of the failure stress. These confidence data can be used to set limits which may be expected to include the parameter value that would have been obtained if the test engineers had conducted fragility tests on an exceedingly great number of test specimens. Now then, the establishment of confidence limits on either large or small samples is akin to making a statistical inference. Essentially, this statistical inference consists of using sample statistics from a universe to estimate the parameter of that universe.

Since statistical inferences are usually made in terms of probability percentiles, the test engineer or the analytical engineer must select the degree of assurance required for the tests. Suppose that 99-percent limits have been selected; then it can be reasonably expected with 99-percent confidence that the universe or population parameter will fall within these limits. In a similar manner, an inference could be made that the parameter would be in limits 99 times in 100 and out of limits 1 time in 100.

Use of the confidence inferences provides the test engineer with some practical feeling for the validity of the test data. It becomes a simple matter to proceed from the selected degree of assurance on the estimated parameter to the determination of the failure probability of future specimens. This is easily accomplished with the use of the failure probability charts given in this report.

ACKNOWLEDGMENT

The writer is greatly indebted to D. Butterfield and R. O'Donnell of the Nortronics Division, Northrop Corporation, for preparing the tables and the supporting pictorial data that made this paper possible. The writer is also greatly indebted to Mrs. M. C. Harris for typing this paper.

BIBLIOGRAPHY

1. Walter A. Shewhart, "Economic Control of Quality of Manufactured Product," Van Nostrand, New York, 1931
2. "Control Chart Method for Controlling Quality During Production," American Standards Association, American War Standard, Z1.3, 1942
3. John M. Howell and Ben K. Gold, "Elementary Statistics," Wm. C. Brown Co., 1954
4. R. W. Mustain, "Power Spectral Density Nomogram," Environmental Quarterly, July 1959
5. R. W. Mustain, "Extended Environmental Tests of SM-62 Missile Components," Shock and Vibration Bulletin No. 27, Part II, Office of the Secretary of Defense
6. Tables of Normal Probability Functions, National Bureau of Standards, Applied Mathematics Series 23, 1953
7. Reference Data for Radio Engineers (Fourth Edition), International Telephone and Telegraph Corporation
8. A. J. Duncan, "Quality Control and Industrial Statistics," Irwin Inc., 1955
9. I. W. Burr, "An Advanced Course—Quality Control by Statistical Methods," Purdue University, 1957
10. C. A. Bennett and N. L. Franklin, "Statistical Analysis in Chemistry and the Chemical Industry," John Wiley & Sons, Inc., 1954
11. H. Arkin & R. R. Colton, "Statistical Methods," Barnes and Noble, Inc., 1953
12. M. J. Moroney, "Facts from Figures," W. Clowes and Sons, 1957
13. Mil-Std-414, "Sampling Procedures and Tables for Inspection by Variables for Percent Defective," Department of Defense, 1957

14. Mil-Std-105A, "Sampling Procedures and Tables for Inspection by Attributes," Department of Defense, 1950

15. S. S. Wilks, "Mathematical Statistics," Princeton University Press, Princeton, 1943

16. A.S.T.M. Manual on Quality Control of Materials, American Society for Testing Materials, 1951

17. Hall, P. C., "Introduction to Mathematical Statistics," John Wiley & Sons, Inc., 1947

APPENDIX

TABLE A
Confidence Intervals for Means

Tabulated value = $2\,t/\sqrt{n}$

n \ β	0.50	0.75	0.90	0.95	0.975	0.990	0.995	0.999
2	1.4142	3.4142	8.9291	17.969	35.995	90.025	180.06	900.32
3	0.94281	1.8517	3.3717	4.9683	7.1652	11.460	16.269	36.486
4	0.76489	1.4226	2.3534	3.1825	4.1765	5.8409	7.4530	12.941
5	0.66250	1.2024	1.9067	2.4833	3.1264	4.1180	5.0064	7.7010
6	0.59334	1.0622	1.6452	2.0989	2.5829	3.2892	3.8974	5.6003
7	0.54242	0.96252	1.4689	1.8497	2.2441	2.8025	3.2632	4.5046
8	0.50285	0.88692	1.3397	1.6720	2.0090	2.4745	2.8491	3.8219
9	0.47093	0.82687	1.2397	1.5373	1.8343	2.2369	2.5550	3.3607
10	0.44444	0.77773	1.1593	1.4307	1.6981	2.0554	2.3336	3.0238
11	0.42200	0.73647	1.0930	1.3436	1.5882	1.9112	2.1597	2.7661
12	0.40267	0.70119	1.0369	1.2707	1.4971	1.7931	2.0188	2.5617
13	0.38578	0.67058	0.98664	1.2086	1.4200	1.6943	1.9017	2.3952
14	0.37087	0.64362	0.94659	1.1548	1.3537	1.6101	1.8027	2.2562
15	0.35756	0.61973	0.90953	1.1076	1.2960	1.5372	1.7174	2.1379
16	0.34560	0.59835	0.87650	1.0658	1.2450	1.4734	1.6430	2.0365
17	0.33476	0.57903	0.84689	1.0283	1.1995	1.4168	1.5775	1.9476
18	0.32489	0.56144	0.82005	0.99457	1.1588	1.3662	1.5191	1.8691
19	0.31585	0.54541	0.79566	0.96396	1.1218	1.3207	1.4667	1.7995
20	0.30752	0.53066	0.77328	0.93602	1.0882	1.2794	1.4194	1.7365
21	0.29981	0.51709	0.75272	0.91041	1.0575	1.2418	1.3763	1.6803
22	0.29266	0.50448	0.73371	0.88675	1.0292	1.2073	1.3369	1.6284
23	0.28600	0.49276	0.71608	0.86487	1.0032	1.1755	1.3006	1.5814
24	0.27978	0.48181	0.69970	0.84454	0.97894	1.1461	1.2672	1.5379
25	0.27394	0.47156	0.68436	0.82556	0.95640	1.1188	1.2362	1.4980
26	0.26846	0.46193	0.66997	0.80780	0.93532	1.0933	1.2074	1.4611
27	0.26328	0.45287	0.65649	0.79116	0.91560	1.0695	1.1804	1.4268
28	0.25841	0.44437	0.64380	0.77551	0.89706	1.0472	1.1552	1.3947
29	0.25379	0.43631	0.63177	0.76075	0.87964	1.0263	1.1316	1.3645
30	0.24941	0.42865	0.62042	0.74680	0.86314	1.0065	1.1093	1.3361
31	0.24525	0.42139	0.60969	0.73361	0.84759	0.98783	1.0883	1.3097
41	0.21260	0.36460	0.52596	0.63129	0.72743	0.84475	0.92805	1.1091
61	0.17378	0.29746	0.42782	0.51222	0.58874	0.68123	0.74635	0.88602
121	0.12301	0.21016	0.30140	0.35998	0.41271	0.47589	0.51998	0.61327
	0	0	0	0	0	0	0	0

Note: Tabulated value x standard deviation = confidence intervals.

TABLE B

Confidence Intervals for Standard Deviations

Tabulated value = $2t/\sqrt{2n}$

n	0.50	0.75	0.90	0.95	0.975	0.990	0.995	0.999
2	1.0000	2.4142	6.3138	12.706	25.452	63.657	127.32	636.62
3	0.66667	1.3092	2.3842	3.5132	5.0666	8.1036	11.504	25.800
4	0.54086	1.0059	1.6641	2.2504	2.9532	4.1301	5.2703	9.1507
5	0.46846	0.85027	1.3483	1.7560	2.2107	2.9119	3.5402	5.4454
6	0.41955	0.75107	1.1634	1.4841	1.8264	2.3258	2.7559	3.9600
7	0.38355	0.68061	1.0387	1.3079	1.5868	1.9817	2.3074	3.1852
8	0.35557	0.62715	0.94730	1.1823	1.4206	1.7497	2.0146	2.7025
9	0.33300	0.58468	0.87658	1.0871	1.2971	1.5817	1.8067	2.3763
10	0.31427	0.54994	0.81979	1.0117	1.2008	1.4534	1.6501	2.1381
11	0.29840	0.52076	0.77285	0.95007	1.1231	1.3514	1.5271	1.9559
12	0.28473	0.49581	0.73317	0.89855	1.0586	1.2679	1.4275	1.8114
13	0.27279	0.47417	0.69908	0.85460	1.0041	1.1981	1.3447	1.6937
14	0.26225	0.45511	0.66934	0.81655	0.95723	1.1385	1.2747	1.5954
15	0.25284	0.43821	0.64314	0.78317	0.91637	1.0870	1.2144	1.5117
16	0.24438	0.42310	0.61978	0.75360	0.88031	1.0418	1.1618	1.4400
17	0.23671	0.40944	0.59884	0.72712	0.84820	1.0018	1.1154	1.3771
18	0.22973	0.39700	0.57987	0.70327	0.81937	0.96607	1.0742	1.3217
19	0.22334	0.38566	0.56261	0.68162	0.79326	0.93387	1.0371	1.2725
20	0.21746	0.37524	0.54679	0.66187	0.76951	0.90470	1.0036	1.2279
21	0.21200	0.36564	0.53225	0.64375	0.74778	0.87808	0.97316	1.1881
22	0.20694	0.35672	0.51881	0.62702	0.72779	0.85370	0.94530	1.1515
23	0.20223	0.34843	0.50634	0.61156	0.70934	0.83122	0.91968	1.1182
24	0.19783	0.34070	0.49476	0.59718	0.69221	0.81040	0.89605	1.0874
25	0.19370	0.33344	0.48391	0.58376	0.67628	0.79108	0.87412	1.0592
26	0.18983	0.32664	0.47374	0.57120	0.66137	0.77309	0.85374	1.0331
27	0.18618	0.32023	0.46421	0.55943	0.64743	0.75627	0.83471	1.0089
28	0.18273	0.31422	0.45523	0.54837	0.63432	0.74050	0.81689	0.98619
29	0.17946	0.30852	0.44673	0.53793	0.62200	0.72568	0.80015	0.96483
30	0.17636	0.30310	0.43870	0.52807	0.61033	0.71170	0.78441	0.94475
31	0.17342	0.29797	0.43111	0.51874	0.59934	0.69850	0.76957	0.92608
41	0.15033	0.25781	0.37191	0.44639	0.51436	0.59733	0.65623	0.78428
61	0.12288	0.21033	0.30252	0.36220	0.41630	0.48170	0.52775	0.62651
121	0.08698	0.14861	0.21312	0.25455	0.29183	0.33651	0.36768	0.43365
∞	0	0	0	0	0	0	0	0

Note: Tabulated value × standard deviation = confidence intervals.

TABLE C

Confidence Intervals for Standard Deviations in Standard Deviations

Tabulated value = $2\,((c_3 - c_2)$

n	0.50	0.75	0.90	0.95	0.975	0.90	0.995	0.999
2	1.50	3.62	9.47	19.1	38.2	95.5	191	955
3	0.853	1.68	3.05	4.50	6.48	10.4	14.7	33.0
4	0.646	1.20	1.99	2.69	3.53	4.93	6.30	10.9
5	0.537	0.976	1.55	2.02	2.54	3.34	4.06	6.25
6	0.470	0.842	1.30	1.66	2.05	2.61	3.09	4.44
7	0.422	0.748	1.14	1.44	1.74	2.18	2.54	3.50
8	0.386	0.681	1.03	1.28	1.54	1.90	2.19	2.93
9	0.359	0.630	0.944	1.17	1.40	1.70	1.95	2.56
10	0.335	0.586	0.874	1.08	1.28	1.55	1.75	2.28
11	0.316	0.552	0.818	1.01	1.19	1.43	1.62	2.07
12	0.301	0.524	0.775	0.950	1.12	1.34	1.51	1.92
13	0.287	0.498	0.735	0.898	1.06	1.26	1.41	1.78
14	0.274	0.476	0.701	0.855	1.00	1.19	1.33	1.67
15	0.264	0.458	0.672	0.818	0.957	1.14	1.27	1.58
16	0.254	0.440	0.644	0.784	0.915	1.08	1.21	1.50
17	0.246	0.415	0.622	0.755	0.880	1.04	1.16	1.43
18	0.237	0.410	0.600	0.727	0.847	1.00	1.11	1.37
19	0.231	0.399	0.582	0.705	0.820	0.965	1.07	1.32
20	0.224	0.387	0.564	0.683	0.794	0.934	1.04	1.27
21	0.218	0.376	0.548	0.662	0.770	0.904	1.00	1.22
22	0.213	0.368	0.535	0.646	0.750	0.880	0.974	1.19
23	0.208	0.359	0.522	0.630	0.731	0.857	0.948	1.15
24	0.204	0.351	0.510	0.615	0.713	0.835	0.923	1.12
25	0.199	0.343	0.498	0.600	0.695	0.813	0.899	1.09

Note: Tabulated value × standard deviation = confidence interval.

TABLE D

Confidence Limits and Intervals for Standard Deviations

Tabulated limits = $\sqrt{n\ \chi^2}$

n	0.50 Lower Limit	0.50 Upper Limit	0.50 Interval	0.80 Lower Limit	0.80 Upper Limit	0.90 Interval	0.90 Lower Limit	0.90 Upper Limit	0.90 Interval
2	1.229	4.439	3.210	0.859	11.2	10.3	0.722	22.6	21.9
3	1.040	2.283	1.243	0.807	3.77	2.96	0.708	5.40	4.69
4	0.9867	1.816	0.829	0.800	2.62	1.82	0.715	3.37	2.65
5	0.9636	1.613	0.649	0.802	2.17	1.37	0.726	2.65	1.92
6	0.9516	1.498	0.546	0.806	1.931	1.125	0.735	2.28	1.54
7	0.9446	1.423	0.478	0.813	1.785	0.973	0.745	2.07	1.32
8	0.9409	1.371	0.430	0.817	1.682	0.865	0.753	1.92	1.17
9	0.9384	1.332	0.394	0.819	1.604	0.785	0.762	1.82	1.06
10	0.9370	1.302	0.365	0.825	1.548	0.723	0.769	1.73	0.96
11	0.9362	1.278	0.342	0.829	1.503	0.674	0.775	1.67	0.89
12	0.9359	1.258	0.322	0.833	1.466	0.633	0.780	1.62	0.84
13	0.9356	1.241	0.305	0.838	1.436	0.598	0.787	1.58	0.79
14	0.9360	1.227	0.291	0.841	1.410	0.569	0.791	1.54	0.75
15	0.9360	1.214	0.278	0.843	1.387	0.544	0.796	1.51	0.71
16	0.9363	1.204	0.268	0.847	1.368	0.521	0.800	1.48	0.68
17	0.9368	1.195	0.258	0.850	1.351	0.501	0.804	1.46	0.66
18	0.9373	1.186	0.249	0.852	1.335	0.483	0.808	1.44	0.63
19	0.9379	1.178	0.240	0.855	1.320	0.465	0.811	1.42	0.61
20	0.9386	1.172	0.233	0.857	1.307	0.450	0.815	1.41	0.59
21	0.9387	1.166	0.227	0.860	1.301	0.441	0.818	1.39	0.57
22	0.9394	1.160	0.221	0.862	1.291	0.429	0.820	1.38	0.56
23	0.9398	1.155	0.215	0.864	1.282	0.418	0.824	1.37	0.55
24	0.9404	1.150	0.210	0.866	1.273	0.407	0.826	1.35	0.52
25	0.9409	1.146	0.205	0.868	1.262	0.394	0.829	1.35	0.52
26	0.9413	1.142	0.201	0.869	1.255	0.386	0.830	1.34	0.51
27	0.9419	1.138	0.196	0.871	1.249	0.378	0.833	1.32	0.49
28	0.9423	1.135	0.193	0.874	1.244	0.370	0.836	1.31	0.47
29	0.9429	1.131	0.188	0.875	1.239	0.364	0.838	1.31	0.47
30	0.9433	1.128	0.185	0.876	1.231	0.355	0.839	1.30	0.46
31	0.9438	1.125	0.181	0.877	1.227	0.350	0.841	1.29	0.45
41	0.9479	1.103	0.155	0.8896	1.188	0.298	0.8575	1.244	0.386
51	0.9515	1.089	0.137	0.8985	1.163	0.265	0.8692	1.211	0.341
61	0.9543	1.080	0.126	0.9055	1.146	0.240	0.8783	1.188	0.310
71	0.9567	1.073	0.116	0.9111	1.133	0.222	0.8856	1.171	0.285
81	0.9586	1.067	0.108	0.9158	1.122	0.207	0.8916	1.158	0.266
91	0.9609	1.062	0.101	0.9196	1.114	0.195	0.8970	1.147	0.250
101	0.9622	1.059	0.097	0.9232	1.107	0.184	0.9014	1.138	0.237

Note: Tabulated limit × standard deviation = confidence limit.
Tabulated interval × standard deviation = confidence interval.

TABLE I - Continued

Confidence Limits and Intervals for Standard Deviations

Tabulated limits = $\sqrt{n/\chi^2}$

n	0.950 Lower Limit	0.950 Upper Limit	0.950 Interval	0.980 Lower Limit	0.980 Upper Limit	0.980 Interval	0.990 Lower Limit	0.990 Upper Limit	0.990 Interval
2	0.631	45.1	44.5	0.549	112.9	112.4	0.504	225.6	225
3	0.638	7.70	7.06	0.571	12.2	11.6	0.532	17.3	16.8
4	0.654	4.30	3.65	0.595	5.90	5.30	0.559	7.47	6.91
5	0.671	3.21	2.54	0.613	4.10	3.49	0.579	4.91	4.33
6	0.685	2.69	2.00	0.630	3.30	2.67	0.599	3.82	3.22
7	0.697	2.38	1.68	0.646	2.83	2.19	0.616	3.22	2.60
8	0.707	2.18	1.47	0.658	2.54	1.88	0.628	2.84	2.21
9	0.717	2.03	1.31	0.669	2.34	1.67	0.640	2.59	1.95
10	0.725	1.92	1.19	0.679	2.19	1.51	0.651	2.40	1.75
11	0.733	1.84	1.11	0.689	2.07	1.38	0.661	2.26	1.60
12	0.740	1.77	1.03	0.697	1.98	1.28	0.669	2.15	1.48
13	0.747	1.72	0.97	0.704	1.91	1.21	0.678	2.06	1.38
14	0.753	1.67	0.92	0.711	1.846	1.135	0.686	1.98	1.29
15	0.758	1.63	0.87	0.718	1.794	1.076	0.692	1.92	1.23
16	0.763	1.60	0.84	0.723	1.750	1.027	0.699	1.865	1.166
17	0.768	1.569	0.801	0.729	1.711	0.982	0.704	1.820	1.116
18	0.772	1.543	0.771	0.734	1.676	0.942	0.710	1.777	1.067
19	0.777	1.519	0.742	0.739	1.646	0.907	0.715	1.742	1.027
20	0.780	1.498	0.718	0.744	1.618	0.874	0.720	1.710	0.990
21	0.784	1.480	0.696	0.747	1.594	0.847	0.724	1.681	0.957
22	0.787	1.462	0.675	0.752	1.572	0.820	0.729	1.655	0.926
23	0.791	1.446	0.655	0.756	1.553	0.797	0.733	1.632	0.899
24	0.794	1.432	0.638	0.760	1.535	0.775	0.737	1.610	0.873
25	0.797	1.419	0.622	0.762	1.515	0.753	0.740	1.590	0.850
26	0.800	1.409	0.609	0.766	1.504	0.738	0.746	1.573	0.827
27	0.803	1.398	0.595	0.769	1.488	0.719	0.748	1.552	0.804
28	0.805	1.385	0.580	0.772	1.473	0.701	0.751	1.541	0.790
29	0.807	1.376	0.569	0.775	1.460	0.685	0.754	1.523	0.769
30	0.810	1.369	0.559	0.778	1.448	0.670	0.757	1.513	0.756
31	0.812	1.358	0.546	0.780	1.437	0.657	0.760	1.498	0.738
41	0.8312	1.296	0.465	0.8023	1.360	0.558	0.784	1.407	0.623
51	0.8450	1.255	0.410	0.8184	1.310	0.492	0.801	1.350	0.549
61	0.8557	1.227	0.371	0.8308	1.276	0.445	0.814	1.310	0.496
71	0.8644	1.207	0.343	0.8409	1.250	0.409	0.825	1.281	0.456
81	0.8717	1.190	0.318	0.8493	1.230	0.381	0.835	1.258	0.423
91	0.8778	1.177	0.299	0.8563	1.214	0.358	0.842	1.240	0.398
101	0.8828	1.167	0.284	0.8624	1.201	0.339	0.849	1.225	0.376

Note: Tabulated limit × standard deviation = confidence limit.
Tabulated interval × standard deviation = confidence interval.

TABLE E

Confidence Intervals for Ranges (in $\bar{R}$)

Tabulated values = $2\,t\,(d_3\ d_2)$

n	0.50	0.75	0.90	0.95	0.975	0.990	0.995	0.999
2	1.51	3.65	9.54	19.2	38.4	96.2	193	962
3	0.856	1.58	3.06	4.52	6.50	10.4	14.8	33.2
4	0.654	1.21	2.02	2.72	3.58	5.00	6.38	11.1
5	0.550	0.998	1.58	2.06	2.60	3.42	4.16	6.40
6	0.486	0.870	1.35	1.72	2.12	2.70	3.20	4.60
7	0.442	0.784	1.19	1.51	1.83	2.28	2.66	3.68
8	0.410	0.722	1.09	1.36	1.64	2.02	2.32	3.12
9	0.384	0.674	1.01	1.25	1.50	1.83	2.08	2.74
10	0.364	0.636	0.950	1.17	1.39	1.68	1.91	2.48
11	0.348	0.606	0.900	1.11	1.31	1.57	1.78	2.28
12	0.334	0.580	0.858	1.05	1.24	1.48	1.67	2.12
13	0.322	0.558	0.822	1.01	1.18	1.41	1.58	1.99
14	0.310	0.538	0.792	0.966	1.13	1.35	1.51	1.89
15	0.302	0.522	0.766	0.932	1.09	1.29	1.45	1.80
16	0.294	0.508	0.744	0.904	1.06	1.25	1.39	1.73
17	0.286	0.494	0.724	0.878	1.02	1.21	1.35	1.66
18	0.280	0.482	0.706	0.856	0.996	1.17	1.31	1.61
19	0.274	0.472	0.690	0.834	0.972	1.14	1.27	1.56
20	0.268	0.464	0.672	0.818	0.950	1.12	1.24	1.52
21	0.264	0.454	0.660	0.800	0.928	1.09	1.21	1.48
22	0.258	0.446	0.648	0.784	0.910	1.07	1.18	1.44
23	0.254	0.438	0.638	0.770	0.892	1.05	1.16	1.41
24	0.250	0.432	0.626	0.756	0.876	1.03	1.13	1.38
25	0.248	0.426	0.618	0.744	0.862	1.01	1.11	1.35

Note: Tabulated values × range = confidence intervals.

TABLF F

Confidence Intervals for Ranges in Standard Deviations

Tabulated value = 2 t d_3

n	0.50	0.75	0.90	0.95	0.975	0.990	0.995	0.999
2	1.71	4.12	10.8	21.6	43.4	109	217.2	1090
3	1.45	2.85	5.18	7.64	11.0	17.6	25.0	56.2
4	1.35	2.50	4.14	5.60	7.36	10.3	13.12	22.8
5	1.28	2.32	3.68	4.80	6.04	7.96	9.68	14.88
6	1.23	2.21	3.42	4.36	5.36	6.84	8.10	11.64
7	1.20	2.12	3.24	4.08	4.94	6.18	7.20	9.92
8	1.17	2.06	3.10	3.88	4.66	5.74	6.60	8.86
9	1.14	2.00	3.00	3.72	4.44	5.42	6.20	8.14
10	1.12	1.96	2.92	3.62	4.28	5.18	5.88	7.62
11	1.10	1.92	2.86	3.50	4.14	4.98	5.64	7.22
12	1.09	1.89	2.80	3.42	4.04	4.84	5.44	6.90
13	1.07	1.86	2.74	3.36	3.94	4.70	5.28	6.64
14	1.06	1.84	2.70	3.30	3.86	4.60	5.14	6.44
15	1.05	1.81	2.66	3.24	3.78	4.50	5.02	6.26
16	1.04	1.79	2.62	3.20	3.72	4.42	4.92	6.10
17	1.03	1.77	2.60	3.16	3.68	4.34	4.84	5.96
18	1.02	1.76	2.56	3.12	3.62	4.28	4.76	5.86
19	1.01	1.74	2.54	3.08	3.58	4.22	4.68	5.74
20	1.00	1.73	2.52	3.06	3.54	4.18	4.62	5.66
21	0.994	1.72	2.50	3.02	3.50	4.12	4.56	5.58
22	0.988	1.70	2.48	3.00	3.48	4.08	4.52	5.50
23	0.982	1.69	2.46	2.96	3.44	4.04	4.46	5.44
24	0.976	1.68	2.44	2.94	3.42	4.00	4.42	5.36
25	0.972	1.67	2.42	2.92	3.40	3.96	4.38	5.32

Note: Tabulated value × standard deviation = confidence interval.

TABLE G

Probability Limits for Range

Tabulated values = $w\,d_2$

n	0.001	0.005	0.010	0.025	0.050	0.950	0.975	0.990	0.995	0.999
2	0	0.0089	0.018	0.035	0.080	2.46	2.81	3.23	3.52	4.12
3	0.035	0.077	0.11	0.18	0.25	1.96	2.17	2.43	2.61	2.99
4	0.097	0.17	0.21	0.29	0.37	1.76	1.93	2.14	2.28	2.58
5	0.16	0.24	0.28	0.37	0.443	1.66	1.81	1.98	2.10	2.36
6	0.21	0.30	0.34	0.418	0.493	1.59	1.72	1.88	1.98	2.22
7	0.26	0.24	0.388	0.462	0.532	1.54	1.66	1.80	1.90	2.12
8	0.29	0.379	0.421	0.495	0.562	1.51	1.62	1.75	1.85	2.04
9	0.32	0.407	0.451	0.522	0.586	1.48	1.58	1.71	1.80	1.99
10	0.351	0.432	0.478	0.542	0.604	1.45	1.56	1.68	1.76	1.94
11	0.378	0.457	0.498	0.561	0.621	1.43	1.53	1.65	1.73	1.90
12	0.399	0.476	0.516	0.577	0.635	1.42	1.51	1.62	1.70	1.87

Note: Tabulated values × range = confidence limits.

THE COUPLED-COMPRESSION ISOLATOR FOR SHOCK AND VIBRATION*

R. D. Hawkins
Sperry Gyroscope Company
Great Neck, New York

An experimental design for an isolator, called a coupled-compression isolator, has been developed. This paper describes the design and presents results for two isolators: one intended for wide-range attenuation of aircraft vibration and the other for protection of shipboard equipment from high-impact shock.

INTRODUCTION

Isolators are essential to the reliable performance of military vehicles and weapons systems. Yet isolators are an unwanted necessity. They take space and add weight, require special design considerations and, in some cases, worsen the effect of the environment on the equipment. Some of the disadvantages, common to most isolators, have been largely overcome by an experimental design developed by this Company. This new type of isolator is called the Coupled-Compression Isolator. The design is capable of meeting a wide range of isolator applications. In this paper, description and results are presented for the coupled-compression isolator designed for wide-range attenuation of aircraft vibration and another designed for protection of shipboard equipment from high-impact shock.

DESCRIPTION

In its elemental form, the isolator consists of a pad of resilient material, four metal plates, and straps or cables, connecting the assembly. Figures 1 and 2 provide a good picture of how the assembly is put together. The dimensions of the isolator depend on the environments, the load, and the function to be performed. For performance equivalent to conventional isolators it might be one third or less in height, although possibly covering more area.

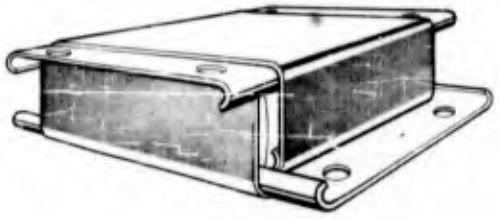

Fig. 1 - The coupled-compression isolator

The characteristics of the resilient pad and the connecting straps are important. These determine completely the performance of the isolator. In all experimental designs tested to date, the resilient pad has been a molded rubber pad of cellular construction, called a buckling pad. The buckling pad possesses unique nonlinear spring properties in compression which make it particularly versatile for use as an isolation medium. The buckling pad, initially stiff in compression, gets softer as the walls begin to buckle. How this characteristic is used to advantage will be shown later. The straps of the isolator are of primary importance because they hold the mount together and thus secure the equipment. They must be very strong in tension and yet be able to buckle freely in compression.

*This paper was not presented at the Symposium.

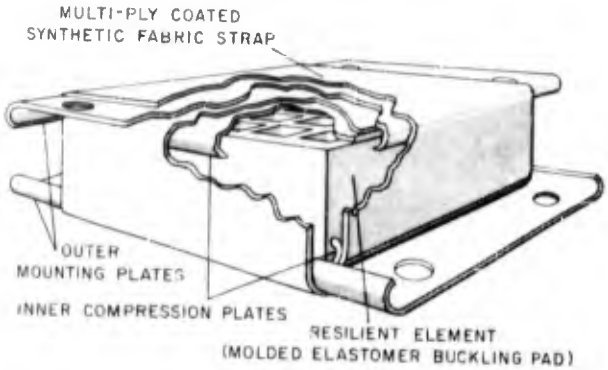

Fig. 2 - Cutaway view showing interior construction of the coupled-compression isolator

Coated synthetic-fiber fabrics are able to meet most, or all, requirements for strap material. The straps also influence the directional properties of the isolator and the orientation of the tension fibers is sometimes important.

OPERATION

The coupled-compression isolator is designed so that, regardless of the direction of the applied load, the resilient pad will be compressed. The action of the isolator is illustrated in Fig. 3. Under compression the straps buckle allowing unrestrained compression of the pad. Under tension the straps go into tension, and with a coupling action cause pad compression. Under shear loads, the straps go into diagonal tension, again causing pad compression. The compressive elastic properties of the pad provide the restoring force for all directions of loading. Thus, a single thickness of pad serves for tension, compression, and shear loads but is itself always compressed. Conventional isolator designs which are self-capturing require separate pads for tension, compression, and shear loads plus clearance space. A comparison of a conventional cup-type vibration mount with an equivalent coupled-compression isolator is shown in Fig. 4.

The action of the straps and pad, at large amplitudes, is inherently nonlinear and is accompanied by considerable energy loss. As a result, maximum vibration transmissibilities at resonance range between 2 and 5, and shock energy is attenuated in an optimum

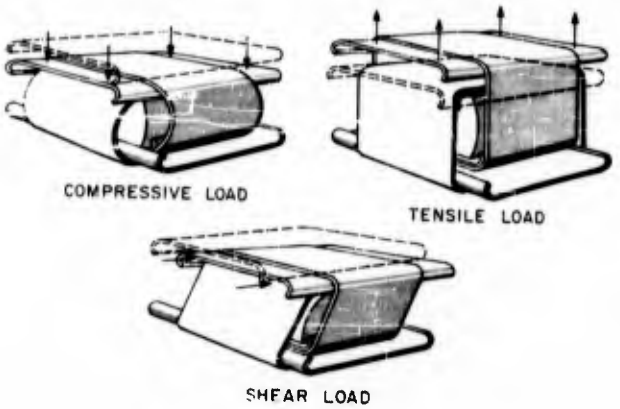

Fig. 3 - Action of the coupled-compression isolator under load

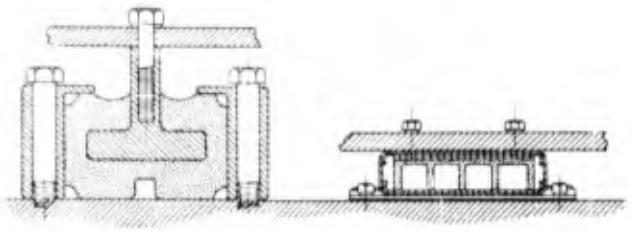

Fig. 4 - Size comparison of coupled-compression isolator with conventional elastomer mount

manner. Attenuation of vibration is equal to that obtained with the best conventional isolators.

The performance under shock and vibration is largely determined by the characteristics of the buckling pad. The buckling pad has been made in a variety of sizes, thicknesses, and cell configurations to meet different requirements. All the pads, however, have the same property of developing a lower spring constant when compressed. The load-deflection curve shown in Fig. 5 is typical. The nonlinearity and hysteresis, shown by the curve, result in low magnification at resonance and excellent absorption of energy. The best wide-range vibration attenuation is achieved when the pad is statically loaded by gravity or precompression, so that its normal position is one of partial buckling. This desired preload is automatically maintained by the coupled-compression isolator, regardless of orientation in the gravity field.

For installations requiring precise returnability, such as inertial systems or shock protection where low-frequency vibration isolation is not important, the buckling pad would not be precompressed to partial buckling but would normally remain in the stiffer, initial position. For shipboard shock protection, this initial stiffness would readily provide mounting frequencies above propeller excited frequencies, but shock loads would cause soft protective-buckling action. Yielding metal braces have been used to obtain similar shock protection, but such designs are not good for repeated shocks; and they are bulkier and more directional.

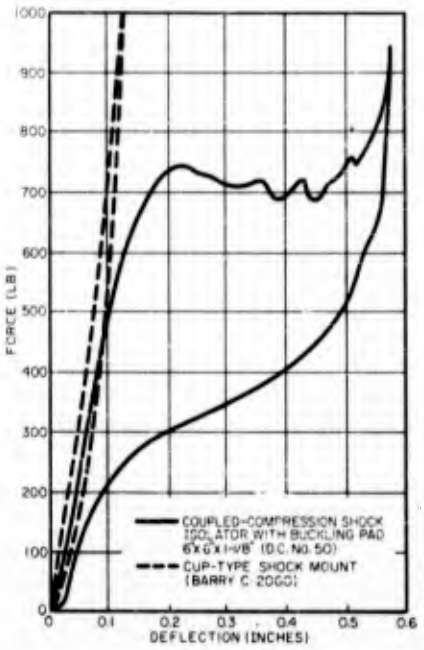

Fig. 5 - Load-deflection characteristics of coupled-compression shock isolator, compared with equivalent cup-type shock mount

ADVANTAGES

In the foregoing discussion, several unique advantages of the coupled-compression isolator have been indicated. It might be useful to review what these advantages are for different applications. For aircraft and missile installations, large savings in space and weight are possible. One ounce of isolator weight per 20 pounds of equipment is practical. The clearance between the isolated equipment and the support structure need be only a fraction of what is usually required for mounts. For MIL-E-5272C vibration environment, a 3/8-inch clearance would be sufficient for all sizes of equipment. Heavy equipment would normally require more mounting area than light equipment, but additional area is likely to be available on heavy equipment. In some applications, this new design will require more

mounting area than conventional mounts. This might seem to be a disadvantage but several benefits are obtained from increased mounting area. First, support loads are distributed over the base of the structure permitting a lighter base design, with less reinforcing. Second, an increase of the support area raises the natural frequency of the isolated structure and provides more damping of modes that do develop.

For shipboard shock protection, space and weight are usually not critical – even so the space normally used by conventional mounts – when used by coupled-compression isolators results in a stable mounting with two to four times more shock protection. This is because the new isolator provides much greater available displacement plus the soft buckling action which allows this displacement to be fully used for maximum shock protection.

A major advantage is the flexibility of application of the coupled-compression isolator. Because it is adaptable in area and stiffness and does not require extra reinforcement at mounting locations, it is much easier to obtain desired elastic centers which minimize rocking and other undesirable isolator modes. For that matter, the buckling pad can be employed by itself as an isolation cushion for equipment that is normally surrounded or contained.

PERFORMANCE TESTS

Development of the coupled-compression isolator has proceeded in the direction of two major areas of need: aircraft vibration isolation and shipboard shock isolation. For aircraft vibration isolation, the effort was towards space saving and wide-range vibration attenuation; for shipboard shock isolation, the objective was better shock attenuation with no greater height than standard shock mounts. Applicable specifications for the aircraft isolator were MIL-C-172B (Vibration Mounts for Electronic Equipment in Aircraft) and MIL-E-5272C (Environmental Testing of Electronic Equipment). Applicable specifications for the shipboard isolator were MIL-M-17185 (Tests for Resilient Mounts in Shipboard Applications) and MIL-T-17113 (Shock and Vibration Specifications for Electronic Equipment). For both types of isolators, experimental models were built and evaluated under laboratory conditions comparable to those required in the above specifications. The results in all cases were highly successful.

AIRCRAFT VIBRATION ISOLATOR

The design of the coupled-compression isolator for aircraft application started with the selection of a buckling pad. Various pads of 1- by 1- by 1/4-inch size were molded of different types of elastomers and with different cell shapes. Practical considerations required that only one pad be selected for complete testing and evaluation. A pad of Dow Corning No. 50 silicone rubber, having 16 cells to the square inch, was chosen. This pad had the best all-around performance when supporting a 7-1/2-pound load. For the initial experimental tests, the strap material used was 1-inch-wide, self-adhering, silicone, rubber-coated, fiberglass tape which was readily available. Plates were 1/32-inch-thick aluminum. Special vibration test fixtures were built to insure precise control of input motion over the entire test spectrum and to permit testing of one isolator at a time (Fig. 6). Vibration transmissibility was measured from 5 to 2000 cps at .036-inch double amplitude (5 to 70 cps) and at 10 g (70 to 2000 cps). Vibration attenuation was uniformly good for all directions of static loading, tension, compression, and shear; and it was comparable to the best conventional isolators. Resonant frequency magnification varied between 3 and 5. One of the transmissibility curves is shown in Fig. 7.

Separate vibration experiments with the silicone elastomer buckling pads showed their operation to be unaffected by high-altitude pressures equivalent to 60,000 feet or by extreme cold temperatures of -65°C. Normal operation at temperatures up to +150°C was not tested but can be safely predicted because of the known properties of the silicone elastomer used. Available strap material of synthetic rubber-coated nylon fabric can also meet all of these environmental requirements and have adequate strength for the 30-g crash safety shock.

SHIPBOARD SHOCK ISOLATOR

The coupled-compression isolator for shipboard shock is a scaled-up version of the aircraft type. A 50-pound capacity was selected for experimental evaluation. The buckling pad, for this capacity, was 6 by 6 by 1-1/8 inches and had 3/4-inch square cells. Plates were 1/8-inch-thick steel and the strap was Permacel 161 Strapping Tape, containing fiberglass tension strands. The complete assembly was 7-1/4 by 7-1/4 by 1-5/8

Fig. 6 - Vibration test fixture for coupled-compression isolator (aircraft type)

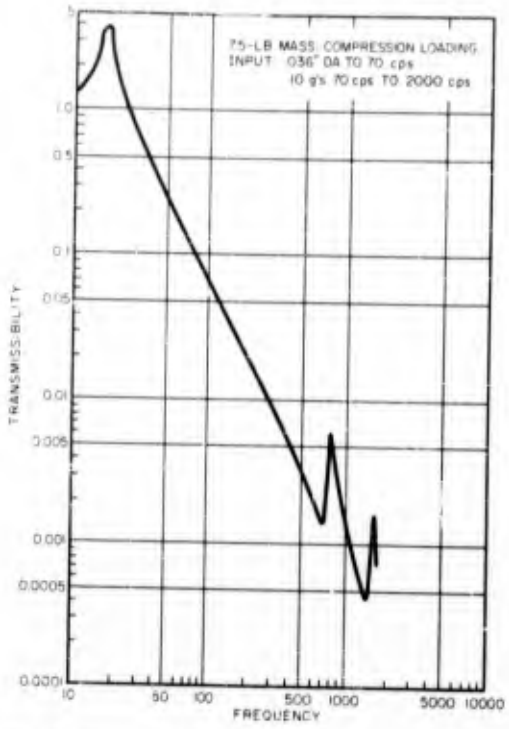

Fig. 7 - Vibration transmissibility for coupled-compression isolator (aircraft type)

inches. Figure 8 shows how this experimental mount was assembled.

Testing consisted of static load versus deflection measurements, vibration up to 55 cps, and high-impact shock testing on the standard Navy High-Impact Shock Machine for Lightweight Equipment. For comparison purposes, identical tests were conducted on two types of cup-type shock mounts: Barry Controls Corp. C-2060 and NC-2060. The latter uses silicone elastomer elements, and it is not specifically recommended for shipboard shock use. These mounts are 1-1/2 inches high; they take less mounting area than the coupled-compression isolator and are rated at 50-pound load for shipboard application.

The results of the load-deflection tests are shown in Fig. 5. The high initial stiffness and the large, soft-displacement capacity of the coupled-compression insulator are clearly shown. The cup-type mount becomes increasingly stiff and has limited capacity.

The results of the vibration tests are summarized in Fig. 9. Resonant frequencies were approximately 35 cps, as planned, except for the coupled-compression isolator, in the shear direction, for which resonance occurred at 15 cps. This was attributed to the vertical orientation of the tension fibers for the strap material used in the experimental mount. The addition of diagonal tension fibers would considerably stiffen the mount in shear. For equipment employing isolators in different mounting planes, unequal axial and shear stiffness is often desirable and may actually simplify the problem of maintaining elastic centers at the center of gravity. Resonant frequency transmissibility was much lower for the coupled-compression isolator than for the standard cup-type shock mount.

The instrumentation used for shock-test measurement is shown in Fig. 10. The load weight for four shock mounts was a 200-pound, one-inch-thick steel plate. Shock waveforms were measured in the center of the load plate and were recorded on a high-speed oscillograph by instruments having flat response to 3000 cps. Comparison of peak accelerations for various shock amplitudes and directions

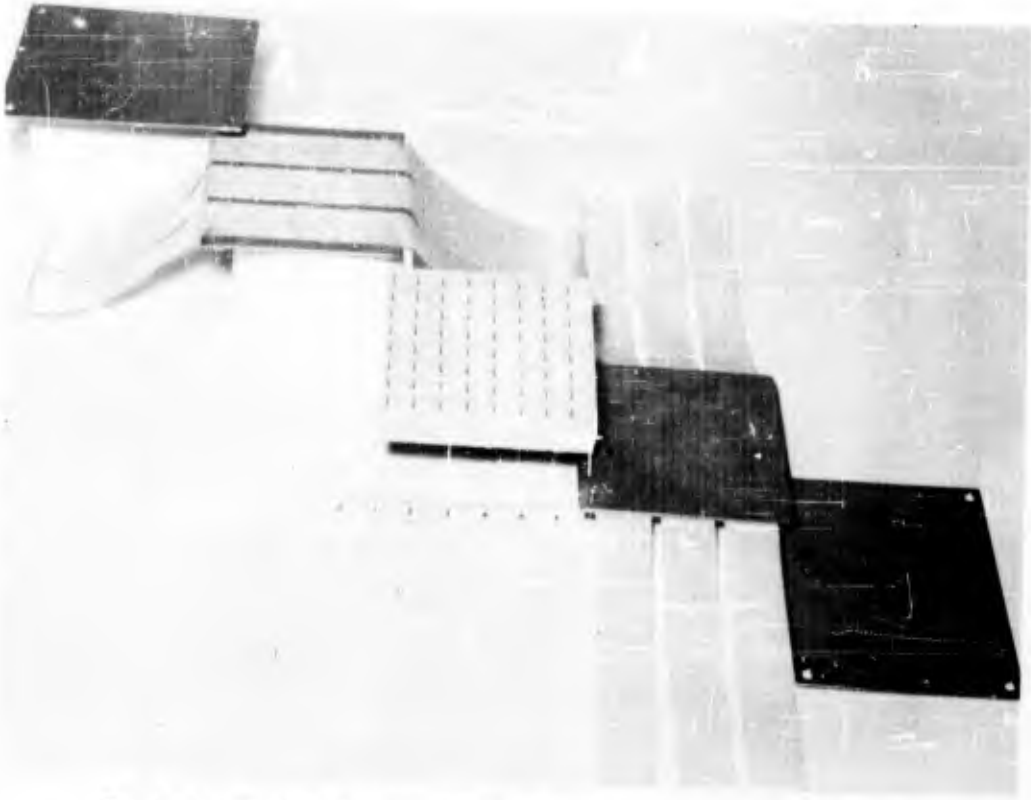

Fig. 8 - Assembly of the experimental coupled-compression shock isolator

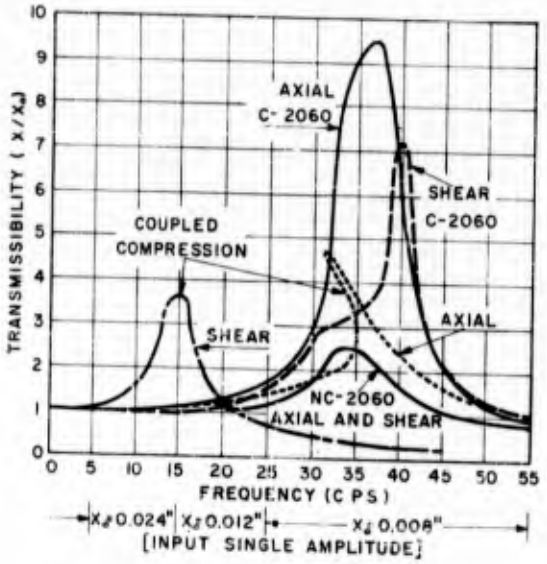

Fig. 9 - Vibration transmissibility for the coupled-compression shock isolator, compared with equivalent cup-type shock mounts

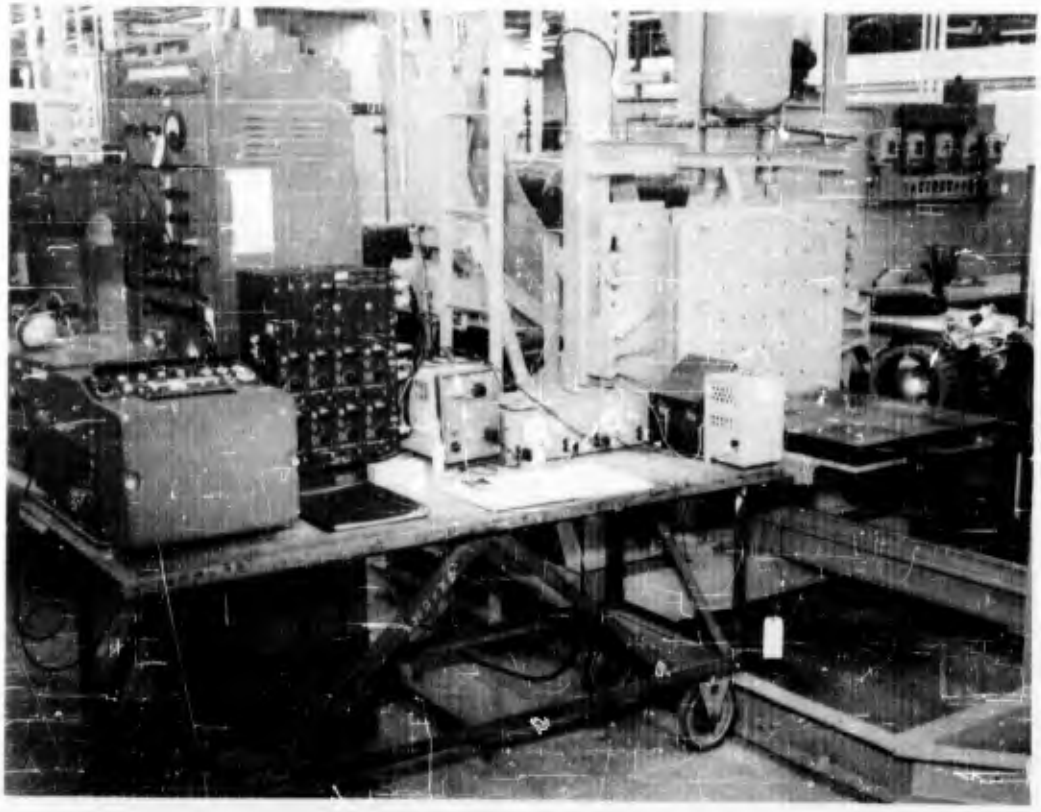

Fig. 10 - The instrumentation used for Navy shock-test measurement

showed the coupled-compression isolator to be lower in all cases by a factor of 1-1/2 to 4; however, a much more meaningful comparison was made by the use of shock spectra. The acceleration-time records were digitized, and undamped shock spectra were computed by electronic digital computer. The results for a 5-foot vertical, hammer-drop shock are presented in Fig. 11. The coupled-compression isolator has better attenuation in the lower frequency range by a factor of 2 or more and by a factor of 1-1/2 at the higher frequencies; the peaking up at 300 cps is due to resonance of the load plate.

Greater improvement in shock attenuation was expected than was actually obtained. Theoretically, because of the softer characteristics and the much greater available displacement, the coupled-compression shock isolator should transmit 4 to 5 times less shock than the equivalent cup-type mount. An investigation as to why this didn't occur revealed several reasons. First, the timing of the basic oscillatory motion of the shock machine table coincided in a critical way with the natural oscillations of the coupled-compression isolator — which caused a compounding of shock input energy across the mount. The cup-type mount, having much higher natural frequency under shock, was not affected in this way. Second, the metal elements of the cup-type mount deformed elastically under tension loading and thus provided additional displacement not initially considered. Another factor concerned the amplitude of the shock which was somewhat less severe than might be expected on a larger test facility, or in actual service. Larger shock amplitude, of course, would favor the coupled-compression isolator because of its greater displacement capacity.

Certain improvements in the pad material and changes in its dimensions are expected to improve its shock-attenuating abilities further. Another change would be the use of heavier strap material. Nonmetallic strap materials are available which have adequate strength for heavy equipment under large shock loads; however, there is no reason why metal cable

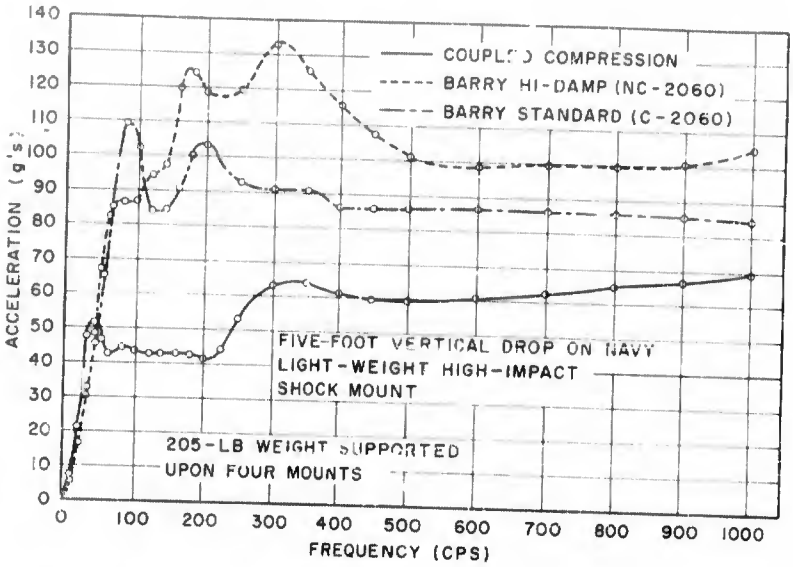

Fig. 11 - Transmitted shock spectra (peak acceleration versus frequency) for Navy high-impact shock test measurement

cannot be incorporated into the strap material if additional strength is desired.

CONCLUSION

It should be emphasized that the results reported in this paper are for an experimental program to evaluate a new-type isolator, and additional work must be done before product use can be planned. Construction and evaluation of additional sizes, inclusion of newer strap and pad materials, and complete qualification testing are yet to be done. The success of these initial tests has been significant. The unique nonlinear properties of the buckling pad and the space and weight saving features of the coupled-compression action promise to advance the art of shock and vibration isolation. It is hoped that reporting the results to date will incur critical appraisal of this new isolation device and will be a step toward better shock and vibration protection in the future.

* * *

VIBRATION INTERACTION OF FOUNDATION EQUIPMENT AND PIPING

V. H. Neubert and J. E. Cadoret
Electric Boat Division
General Dynamics Corporation
Groton, Connecticut

For some types of equipment, the vibration coupling between various components may be neglected and each component studied separately, either analytically or experimentaly, to determine natural frequencies and mode shapes. However, in many cases interaction must be considered to determine adequately vibrational characteristics of the system. As an example, this paper presents the results for a typical small ship component in which interaction between piping, foundation, machine, and mounts was investigated. In the IBM 704 solution, 132 static and 69 dynamic degrees of freedom were considered.

INTRODUCTION

Shock or vibration response of various system subcomponents is often predicted by experimental or theoretical studies of individual components. In many cases this is justified. In other instances, it is necessary to consider the entire system in order to predict vibratory behavior of any part of the system at the drawing board stage. Usually, it is quite obvious whether interaction will be important; however, the complexity of the system may make it impossible to perform a reliable theoretical analysis, or too costly to make an experimental mockup for each item on a ship, for example.

When machines are sound mounted on foundations, vibration coupling between the machine and foundation is usually not important. Piping or conduits connected to the shock- or sound-mounted machines may have undesirable "shorting" effects on their response. A particular example is presented in which foundations, equipment, piping, and mounts were studied simultaneously to determine the importance of mass and flexibility of the various parts of the system.

SYSTEM STUDIED

The system includes a small machine that is fairly typical of several small components

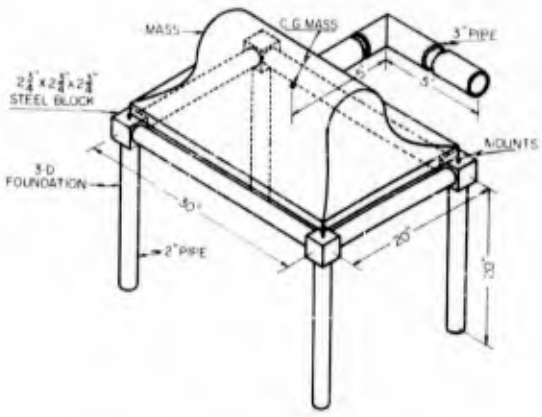

Fig. 1 - Diagram of the system

on submarines (Fig. 1). The foundation is made of 2-inch schedule 40 piping, connected with solid-steel corner blocks. This foundation has been studied quite thoroughly previously for steady-state vibration and shock [1]. A 3-inch pipe has been connected to the machine, for the purpose of this theoretical study only. The piping lies entirely in the xz or horizontal plane. The mount stiffnesses used are those of a Mare Island 6E100 resilient mount. A total of four mounts

were used - one connected to each corner of the foundation.

Four cases were investigated analytically and are presented in this paper. They are the following:

Case A. The entire system

Case B. The system excluding mass of the piping

Case C. The system excluding mass and flexibility of the piping

Case D. The entire system excluding only the rubber mounts. (That is, the machine is bolted directly to the foundation.)

In all cases the machine was considered perfectly rigid, although it was recognized that this assumption is justified only in the low-frequency range. Machine flexibilities can be included and they assume greater importance for equipment without rubber mounts.

ANALYTICAL APPROACH

In this relatively simple system, the qualitative effect of interaction on the lowest natural frequencies could be estimated by slide rule, at least for the cases where the mounts essentially decouple the foundation from the rest of the system. However, in this and more complex problems quantitative results can best be obtained from a high-speed digital computer or by experiment. Faith in calculated results naturally depends on correlation with, or direct use of, experimental measurements as much as possible.

The discrete-mass method was used for which the computer technique has been described previously [2, 3]. Bending, shear, stretching, and torsional deformations of piping and structural elements were included. Damping was not included. Rotary inertia was included for the machine but not for pipe or foundation elements. Fourteen mass points were included for the foundation and seven for the 3-inch pipe.

For this problem, the flexibility or influence coefficient matrix δ was obtained by inverting a 132 by 132 static stiffness matrix. The dynamic matrix equations for free vibrations were then of the form,

$$x = -\delta m\ddot{x} .$$

Since rotary inertia was not included (except for the machine), 69 dynamic degrees of freedom were used for Case A. The mathematical model is shown in Fig. 2. The total mass of the machine is 326#/g which corresponds to 6.6M on the diagram. Other masses are also related to M.

RESULTS

Natural frequencies, mode shapes, and impedances were determined for the four cases. Natural frequencies up to 500 cps are tabulated.

TABLE 1
Natural Frequencies of System (cps)

Case A	Case B	Case C	Case D
6.7	6.9	6.3	
9.7	10.0	7.1	
13.6	14.6	7.7	
20.2	23.5	14.0	
32.3	65.1	20.0	
58.8	82.4	20.9	
97.4			
114.2	114.2	114.2	43.8
120.7	120.7	120.7	50.9
139.6	139.6	139.6	54.5
163.8 (pipe)			98.2
184.4 (pipe)			162.1
217.8	217.8	217.8	164.5
238.8 (pipe)			233.9
286.7 (pipe)			245.3
370.6	370.6	370.6	394.8
414.2	414.2	414.2	447.0
443.1	443.1	443.1	460.4
463.7 (pipe)			490.8
488.5 (pipe)			

For cases A, B, and C inspection of the table as well as impedance curves (Figs. 3-7) reveals that the mounts effectively decouple the foundation from the rest of the system. The natural frequencies, identical in each of these three cases, are those involving motion only of the foundation. The first six values for Case C represent rigid body motion of the machine on the mounts. In Case B, these values are slightly higher because the stiffness of the piping has been included. In Case A, each of the six values is slightly lower than for Case B because the mass of the pipe has also been considered. Inspection of Figs. 3 and 4 reveals this same trend in resonances.

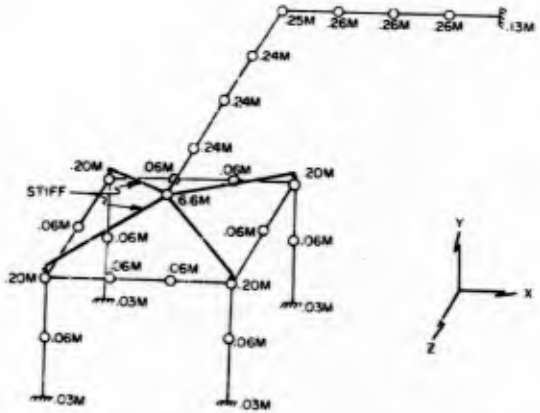

Fig. 2 - Theoretical model of the system

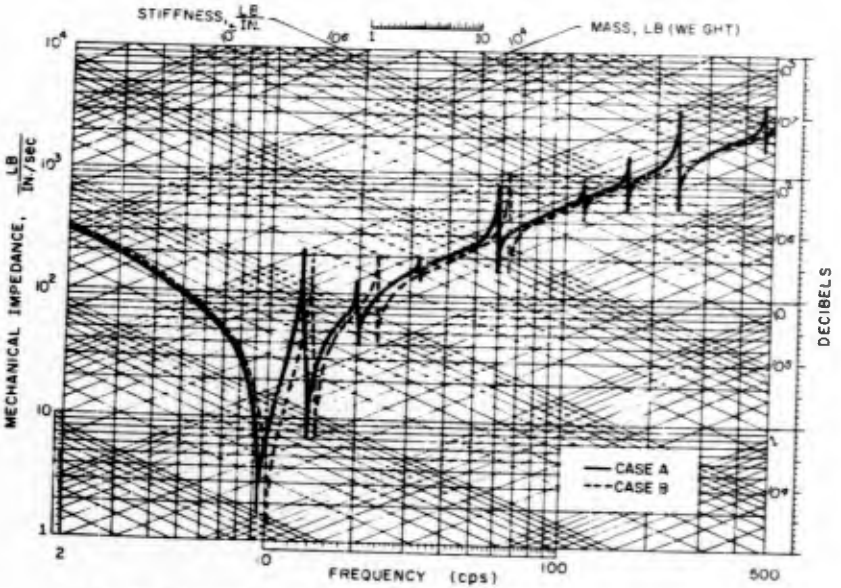

Fig. 3 - Point impedance in x-direction at c.g. of machine

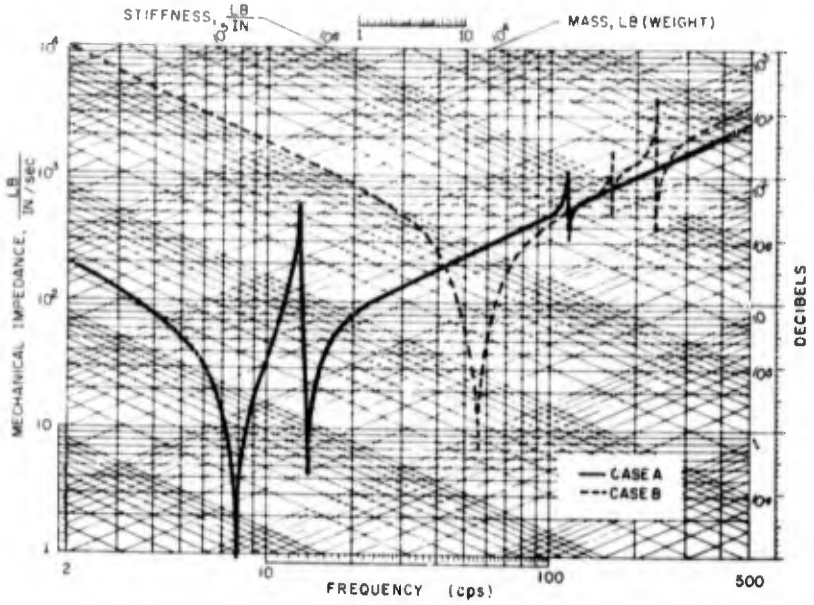

Fig. 4 - Point impedance in x-direction at c.g. of machine

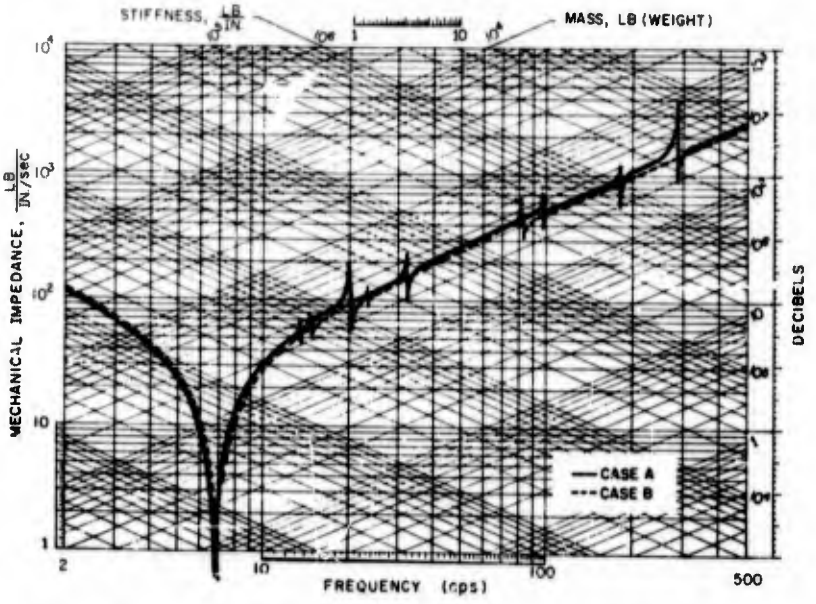

Fig. 5 - Point impedance in y-direction at c.g. of machine

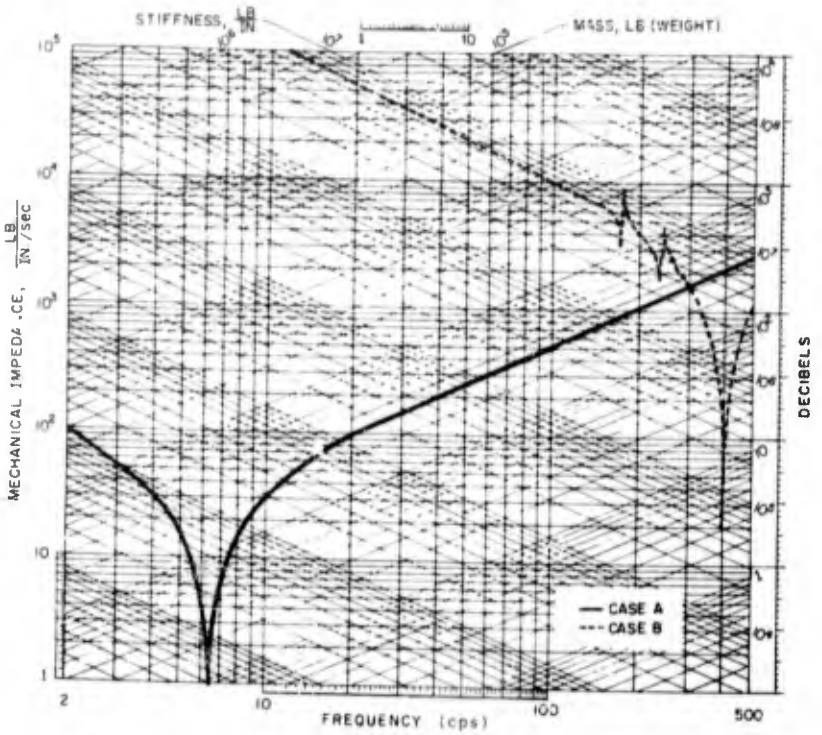

Fig. 6 - Point impedance in y-direction at c.g. of machine

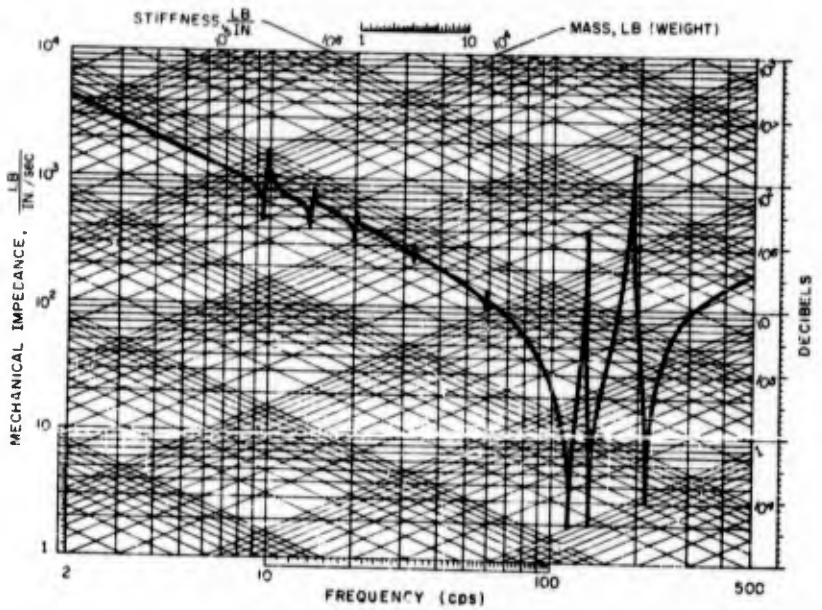

Fig. 7 - Point impedance in x-direction at corner of foundation, Case A

The natural frequencies, labeled "(pipe)" in Table 1, are those which appear because the mass of the piping has been included in the calculation. These, therefore, disappear in Cases B and C.

Some of the calculated mode shapes are shown in Figs. 8 through 13. Long dashed lines indicate the displacement amplitudes for a modal pattern. The short dashed lines, connecting mass points, indicate the components of motion parallel to the coordinate axes. The first mode for Case A (Fig. 8) indicates vertical motion of the machine on the mounts. The pipe must also participate, but the foundation does not. The second mode of Case A (Fig. 9) involves translation of the machine in the horizontal plane and slight twisting about the y-axis. The sixth mode (Case A) shows pure rotation of the machine about the y-axis (Fig. 10). The eighth mode of Case A (Fig. 11) indicates that the machine stands still while the foundation bends in the x-direction.

Only one mode, the ninth, has been plotted for Case C (Fig. 12). Piping is excluded for Case C. Here the foundation twists and the machine on the mounts is motionless.

In the first mode for Case D, only the pipe participates (Fig. 13), each mass moving in the vertical direction. The dotted impedance curve in Fig. 4 indicates that the most significant motion in the x-direction of the machine plus foundation occurs at 54.5 cps. At low frequencies, the impedance curve approaches a stiffness line which is primarily that of the foundation legs as clamped-clamped beams.

Point impedances for the center-of-gravity of the machine in the vertical direction are shown in Figs. 5 and 6. Mount effectiveness is shown for Cases A through D, in that the impedance curve approaches the mass line of the machine. For Case D, the stiffness line (Fig. 6) is that of the stretching or axial distortion of the legs of the foundation. In an actual case, the machine and bedplate mass and elastic properties would greatly reduce this impedance.

Since damping was not included, the impedances at resonances would be zero, and at antiresonances, infinite. For this presentation, these values have been arbitrarily cut off rather than continued as straight vertical lines off the graphs.

EXPERIMENTAL CONFIRMATION

This study was primarily a computer exercise. In a separate study using the same

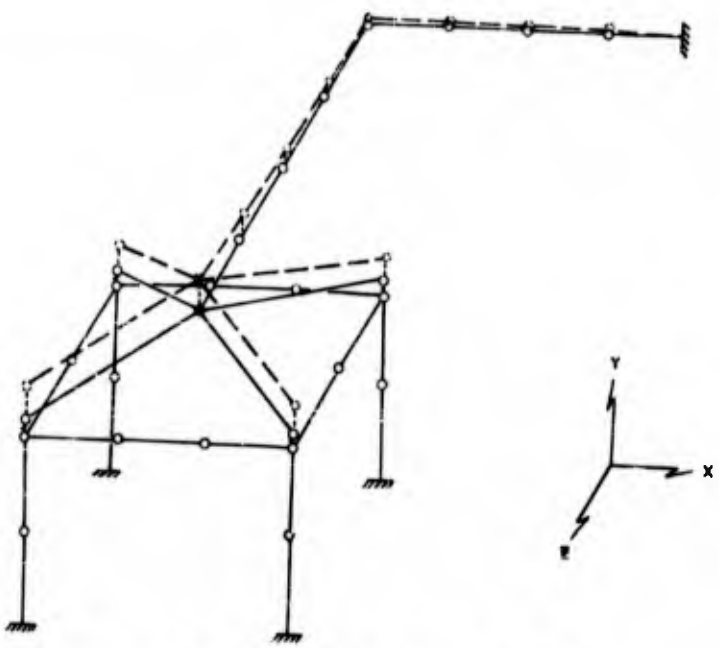

Fig. 8 - First mode (6.7 cps), Case A

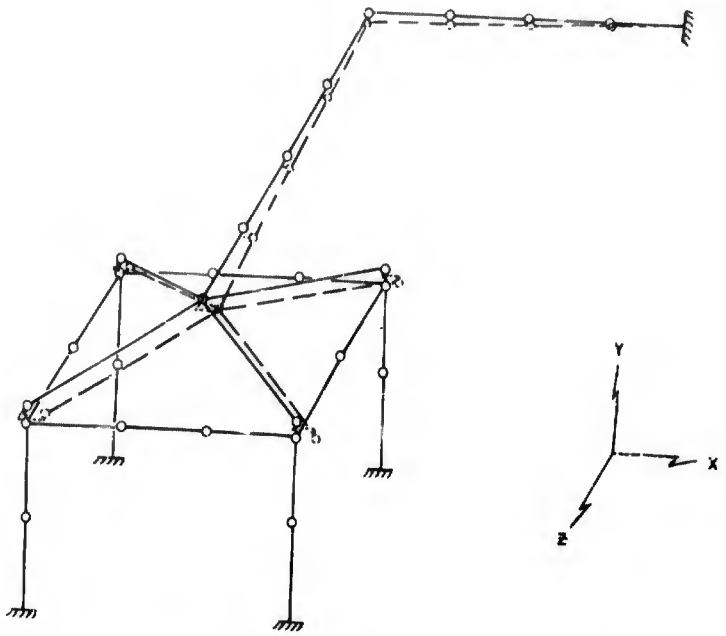

Fig. 9 - Second mode (9.7 cps), Case A

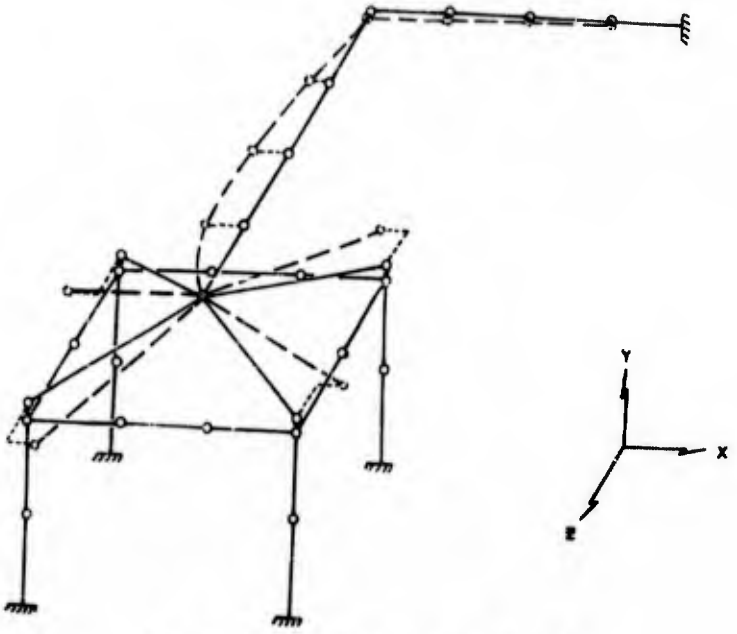

Fig. 10 - Sixth mode (58.8 cps), Case A

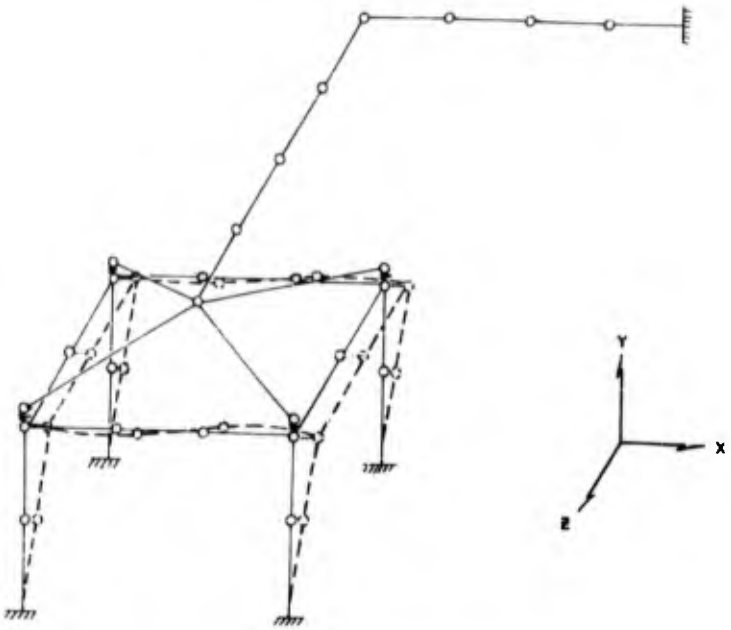

Fig. 11 - Eighth mode (114.2 cps), Case A

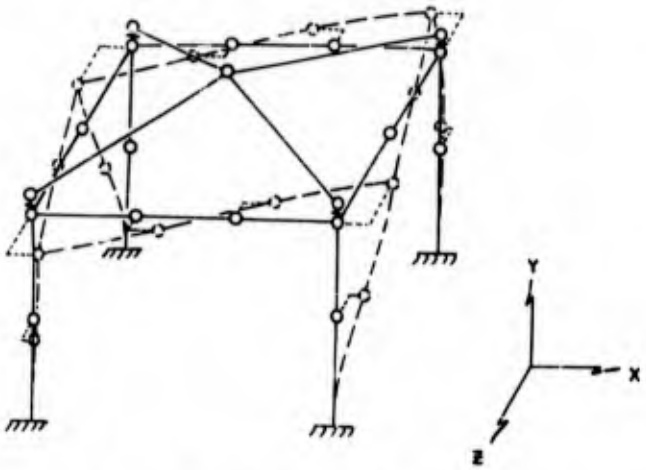

Fig. 12 - Ninth mode (139.6 cps), Case C

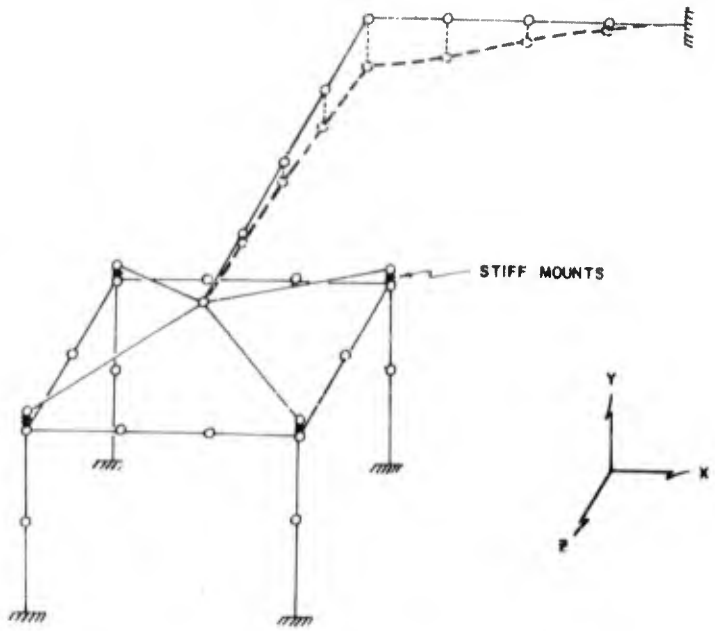

Fig. 13 - First mode (43.8 cps), Case D

foundation, the decoupling due to resilient mounts was demonstrated [4] experimentally for a situation similar to Case C. It was shown that the measured point impedance was almost identical with that of the bare foundation. Experimental and analytical studies of the impedance properties of the foundation, such as given in Fig. 7 for Case A, are also reported elsewhere [2], and the agreement is excellent. The machine and pipe combination used here is a hypothetical one which has not been studied experimentally.

SUMMARY AND CONCLUSIONS

Results demonstrate the importance of piping mass and flexibility, and machine mass on the frequencies, mode shapes, and impedances of a particular system. Machine flexibility should also be considered, depending on the frequency range of interest.

Decoupling of the system by resilient mounts is demonstrated. This as well as the appearance of the mode involving stretching of the foundation legs is felt to be a demonstration of accuracy of computer approach used.

Impedance curves indicate the ratio of force to resulting velocity at the same point. Transfer impedance can also be obtained and used to relate the velocity at a point to a driving force at another point.

Structural damping has not been included. For shock response, the amount of damping neglected would not have a significant effect on maximum stresses. Obviously, for steady-state problems a small amount of damping will be quite significant near resonant frequencies.

ACKNOWLEDGEMENTS

The calculations for the particular numerical example were carried out by the Applied Mechanics and Computer Sections. The assistance of Mr. D. Steinhorn, of the Applied Mechanics Section, in the calculations is gratefully acknowledged.

REFERENCES

1. V. H. Neubert, "Dynamic Shock Analysis of Structural Components and Piping Networks," Shock and Vibration Bulletin No. 27, pp. 92-109, June 1959.

2. V. H. Neubert and W. H. Ezell, "Dynamic Behavior of a Foundation-like Structure," A.S.M.E. Colloquium on Mechanical Impedance Methods, pp. 77-86, Dec. 1958.

3. V. H. Neubert, "Computer Methods for Dynamic Structural Response," Proceedings of the Second National A.S.C.E. Conference on Electronic Computation, Sept. 1960.

4. W. S. Penballow and V. H. Neubert, "Dynamic Behavior of a Foundation under Machine Excitation," E. B. Division, Phase IV, Final Report, NObs 66253, April, 1959.

* * *

Section 4
ACOUSTIC ENVIRONMENTS

ACOUSTIC PROBLEMS ASSOCIATED WITH UNDERGROUND LAUNCHING OF A LARGE MISSILE

H. N. McGregor, et al*
The Martin Company,
Denver, Colorado

Acoustic problems associated with the underground launching of a large missile were investigated by high-intensity, random-noise testing of missile components and structures. A high-intensity, random-noise test facility was constructed for this purpose. Acoustic treatments for the reduction of the acoustic environment were evaluated. Components were functionally tested in a reverberation chamber at over-all random levels from 130 to 168 db. Structural segments were tested under simulated launch loads at random levels from 157 to 166 db.

INTRODUCTION

Two of the important tactical requirements of an ICBM weapon systems are a minimum reaction time and protection against nuclear bombardment. To achieve this twofold tactical requirement, hardened underground silos containing missiles in the ready-to-launch condition will be employed for certain ICBM's. Underground launching causes the missile to be subjected to severe acoustic and and acoustically induced vibration environments because of the confinement of the acoustic energy within the silo launch and exhaust ducts.

Martin-Denver has completed studies and tests with the following objectives: Obtaining information for the prediction of the in-silo launch acoustic and vibration environments; determining the functional and structural responses of missile components and structures to simulated acoustic environments; and of evaluating selected acoustic treatments for use in the silo launch duct to reduce the acoustic environment to levels compatible with missile components and structures.

To achieve these objectives the program was divided into four test phases as follows: Vibration and acoustic measurements obtained during aboveground captive missile firings; localized high random acoustic testing of selected missile structural segments; high-level random acoustic testing of certain missile components; measurement of the acoustic performance of launch duct acoustic treatments.

Since there were four distinct test phases and a facility development phase to the over-all program, this paper has been prepared in five sections and the appropriate credit is given with each section.

*This paper contains several sections. Appropriate credits are given with each section.

Fig. 1 - Acoustic facility

ACOUSTIC SOURCES AND TEST FACILITY*

In order to meet the required objectives of the program, an acoustic facility with high-intensity random and sinusoidal acoustic sources incorporated was built at the Martin-Denver plant. An over-all view of the facility is shown in Fig. 1.

The anticipated silo acoustic environment dictated the performance requirements for the random noise source. Specifically the source was to be capable of producing sound pressure levels up to approximately 170 db† over a 3- by 3-foot section of missile structure and in a 74-cubic foot reverberation chamber.

Various methods of producing high-intensity random acoustic energy were investigated, taking into account cost, reliability, conversion efficiency, frequency response, and the acoustic energy per unit surface area of the transducer. The latter becomes quite significant when the amount of acoustic energy that must be concentrated over a 9-square foot area is considered.

Based on these factors, the method of generating random noise with a multiple disc siren as established at the Wright Air Development Center [1] was selected for the noise source. An acoustic source based on this concept was designed and built.

The siren consists of four concentric counter-rotating discs with randomly positioned ports contained in a cylindrical cast-aluminum housing (Fig. 2). The rotors are driven circumferentially by standard size "V" belts from four electric motors. The first prototype unit built employed variable speed motors to establish optimum rotor speed ratios relative to sound pressure level and spectrum shape. The random siren is coupled to an exponential horn with a theoretical cutoff frequency of 22 cps. The horn is of heavy laminated glass cloth and honeycomb sandwich construction to provide fatigue strength and damping.

A narrow-band analysis (5 cps) shows the presence of irregularities in the spectrum. Although these irregularities present problems in the analysis of test data, the spectrum shape was adequate for proof testing of components and structures. To improve the spectrum shape, two sirens were connected in parallel (Fig. 3). Rotor speeds of the two sirens were adjusted so that the summation of the output of the sirens produced a smooth spectrum. A narrow-band analysis of the single and parallel siren arrangement is shown in Fig. 4. Sound pressure level measured at the mouth of the horn radiating into free space for the single and parallel siren arrangement as a function of inlet air pressure

*Prepared by H. N. McGregor.
†Reference level 0.0002 dynes per square centimeter.

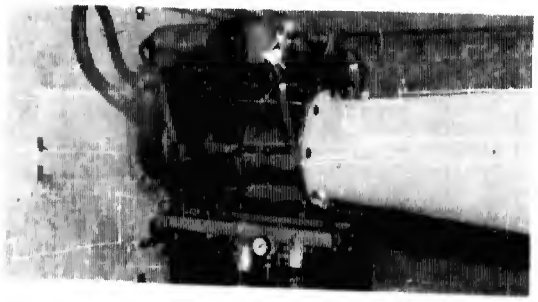

Fig. 2 - Random siren

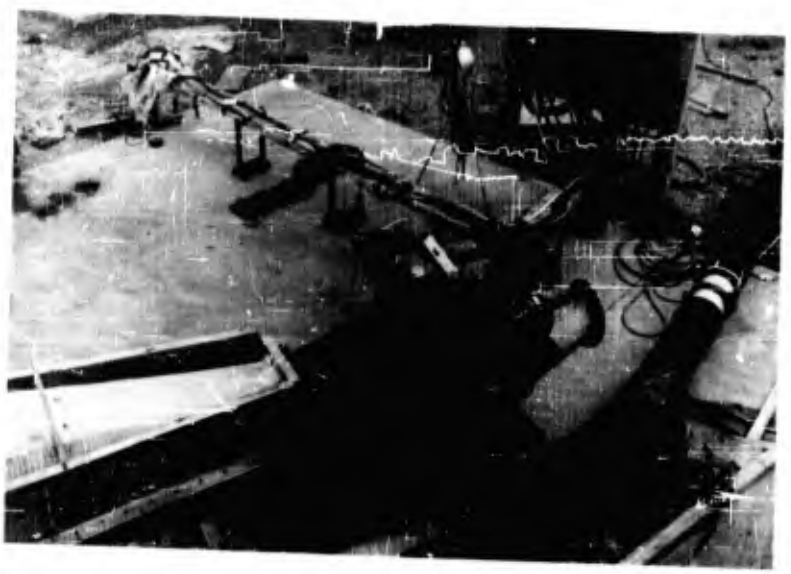

Fig. 3 - Parallel sirens

is shown in Fig. 5. Also shown in Fig. 5 are the sound pressure levels measured in the reverberation chamber and near the surface of a missile structure.

In addition to the random acoustic source, a sinusoidal source was required with the ability to produce sound pressure levels of 160 db from 30 to 1000 cps over a 55-ft^2 area. This was achieved by constructing a high-pressure sinusoidal siren (Fig. 6), employing components from the random siren, where possible.

The 20-port rotor of the siren is belt driven by a variable-speed, 10-hp, dc motor. Pulley ratios are changed to allow operation over the frequency range from 20 to 1000 cps. Frequency response at 40 psig is shown in Fig. 7.

Compressed air to operate the random and the sinusoidal sirens is obtained from an Allison TE-1 compressor unit which consists of two T-56 turboprop engines, geared together and coupled to a modified compressor section from a T-56 engine. Compressor performance curves for various temperatures, at the facility elevation of 6000 feet above sea level, are shown in Fig. 8.

Acquisition and measurement equipment located in the instrumentation and control building provides a centralized integrated instrumentation system for the recording and analysis of acoustic, vibration, strain, and temperature data.

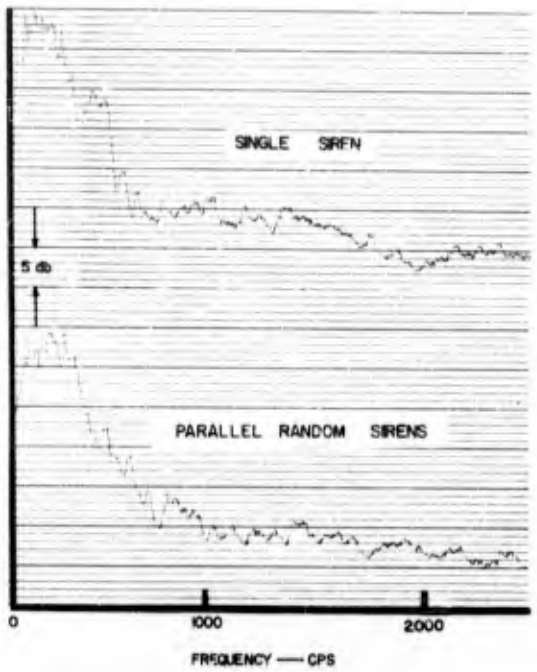

Fig. 4 - Narrow-band analysis

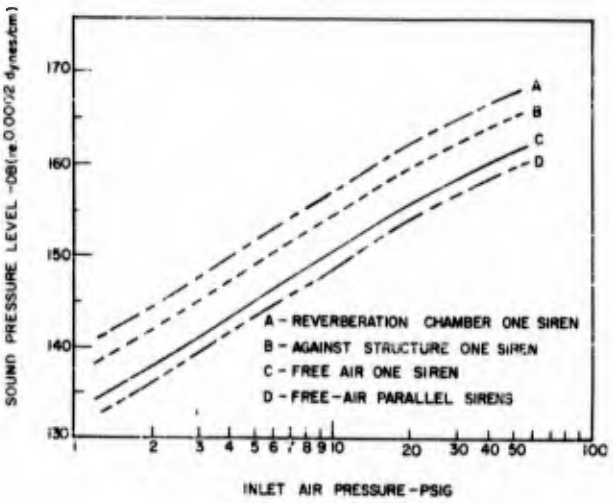

Fig. 5 - Random siren performance
(single and parallel arrangement)

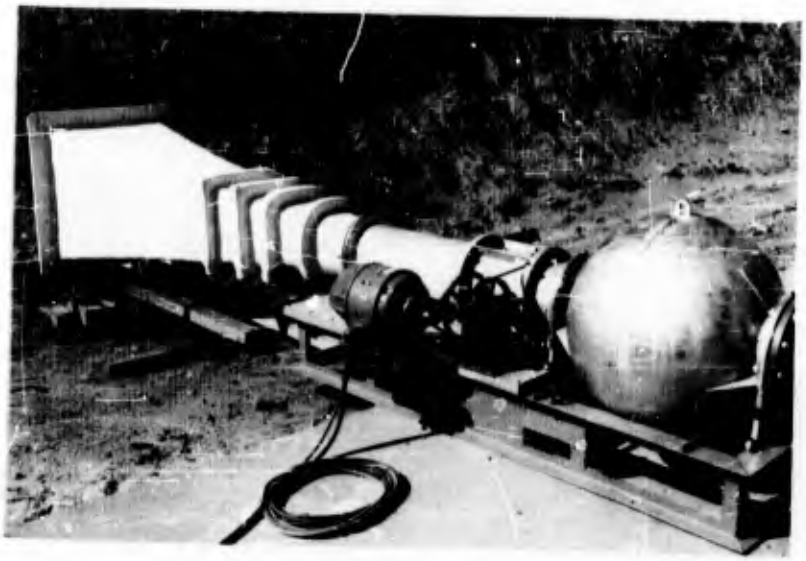

Fig. 6 - Sinusoidal siren

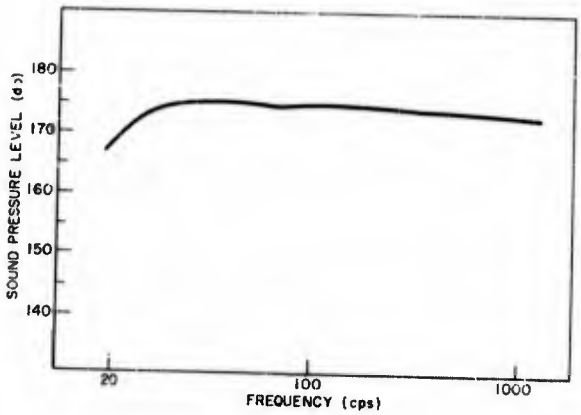

Fig. 7 - Sinusoidal siren performance

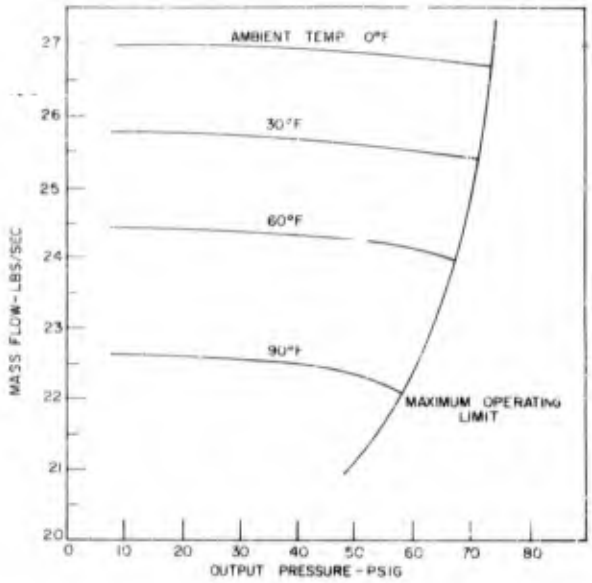

Fig. 8 - Compressor performance curves

ACOUSTIC TEST OF STRUCTURES*

In order to establish the probability of acoustically induced fatigue failure of the missile structure during the in-silo launch, segments of the missile structure were tested with localized high level random acoustic excitation [2]. Simulated launch loads were applied to the segment with a hydraulically operated loading fixture (Fig. 9). Normal incidence was employed for these tests. Preliminary studies and limited testing indicated that the areas on the missile most susceptible to acoustically induced fatigue would be the sections not containing propellants. Such sections, typically, are constructed of ring frames, stringers, and riveted skin; in contrast, the propellant tanks are made from chemically etched continuous structures with a minimum of stress risers.

Seven structural segments were tested at sound pressure levels from 157 to 167 db for a period of 10 minutes per specimen. Of the seven specimens tested, three experienced failure. A typical failure is shown in Fig. 10.

In most cases the failure originated in the form of a "hairline crack" at the junction of the skin panel and stringer. This crack then propagated parallel to the stringer for several inches and either terminated or was deflected towards the central area of the panel. In one instance the ring frames were damaged at the junction of the ring frame and stringer.

Structural modifications were made to the structure to increase its resistance to acoustically induced fatigue and to enable it to withstand a transient overpressure occurring in the silo during engine start-up. To meet the structural requirements imposed by the overpressure pulse, additional ring frames were added to the structure. The original long unsupported skin panel bays were broken up into smaller panels by the installation of a spacer element between the ring frame and skin panel.

The segment which exhibited the shortest time to failure was modified and retested. This segment was the conically shaped transition section located between the first and second stages of the missile. Extensive tests were performed [3] to determine the vibration response of the structure to acoustic excitation and its ability to withstand the anticipated silo acoustic environment. A vibration survey was conducted to determine the major resonant frequencies and mode shapes of the structure under simulated launch loads; this was accomplished by applying a constant (25 pounds) sinusoidal force input at the junction of a ring frame and stringer and measuring the acceleration response at the driven point

*Prepared by D. Dinicola and H. Williamson

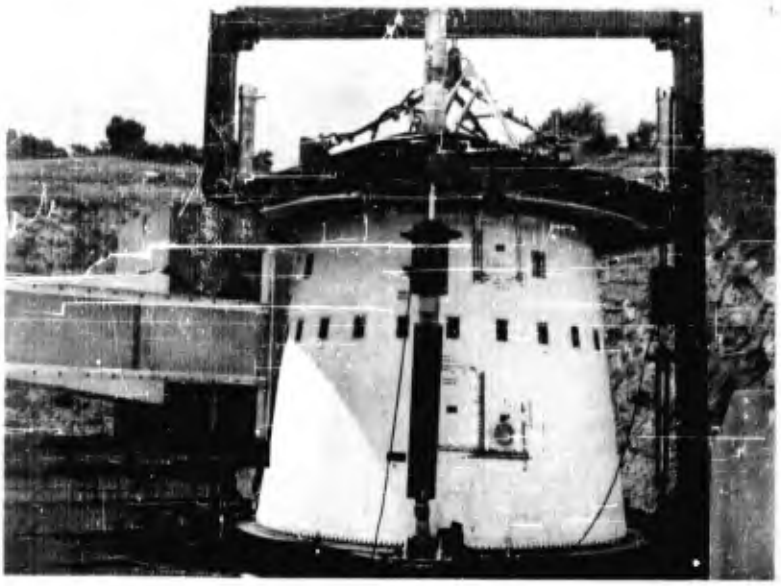

Fig. 9 - Loading fixture

Fig. 10 - Typical failure

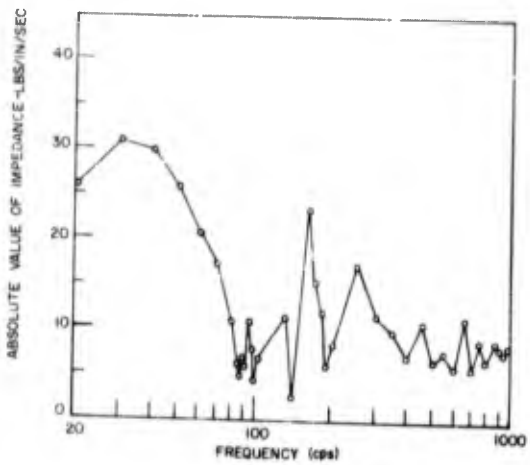

Fig. 11 - Driving point impedance

and at several other points on the structure. Driving point impedance as a function of frequency was computed and is shown in Fig. 11.

The significance of the localized acoustic excitation used for these tests had to be determined in relation to the actual environment in which the total surface of the missile is excited. The interpretation of high-level, localized, acoustic excitation tests depends upon the knowledge of the dynamic properties of the missile structure and the acoustic field within the silo. Although the dynamic properties of the structure can be experimentally measured and (within a limited frequency range) computed, establishment of the spatial time distribution of the acoustic pressures upon the surface of the missile during silo launch presents a difficult problem.

The following analysis was applied in an attempt to correlate the results of localized acoustic tests and to predict the probability of structural failure during silo launch. The response of the structure to localized acoustic excitation, assuming a linear system, can be represented as follows:

$$A_1 = P_1 a_{11}$$

where

A_1 = acceleration response at section of excitation

P_1 = localized acoustic excitation

a_{11} = coefficient relating acoustic excitation and acceleration response.

The coefficient can be determined experimentally and can be used to express the acceleration response of the structure to a random acoustic input over a broadband, or for a series of discrete frequency bands, depending upon the definition of a_{11}. The acceleration response of the structure during complete acoustic excitation as would occur in the silo can be represented as follows:

$$\bar{A}_1 = P_1 a_{11} + P_2 a_{12} + \cdots + P_n a_{1n}$$

where

$\bar{A}_1$ = sum total of all acceleration responses occurring at Section 1

P_n = acoustic excitation over Section n

a_{1n} = coefficient relating acoustic excitation at Section n to response at Section 1.

This technique can be used to predict the response of the structure in the silo environment with reference to the response measurements made during localized excitation tests if the following assumptions are made:

1. The acoustic field is random and uncorrelated.
2. The coefficients, $a_{11}, a_{22}, \ldots, a_{nn}$ are approximately equal due to the symmetry of the structure.
3. The coefficients relating the response at a given section to the acoustic excitation at another section, and conversely, are equal, i.e.; $a_{nm} = a_{mn}$.

4. The root-mean-square acceleration response at a given section is the root-mean-square summation of the individual contributions from all the sections.

Thus,

$$\bar{A}_1 = \sqrt{\sum_{n=1}^{n=K} (A_{n1})^2}$$

where

K = number of equal area sections on the surface of test specimen.

The difference in acceleration response between localized and complete excitation can be used to express the localized acoustic sound pressure level in terms of the equivalent silo sound pressure level.

$$\text{db (localized test)} = \text{db (silo)} + 20 \log_{10} \frac{\sqrt{\sum_{n=1}^{n=K} (A_{n1})^2}}{\bar{A}_1}$$

The structure was excited with random acoustic excitation over a 9-square foot area at a sound pressure level of 136 db. This level was used to minimize the possibility of fatigue of the structure during the test. The acoustically induced acceleration occurring on the remaining 9-square foot areas of the structural segment was recorded on tape. A 1/3-octave analysis of the data was performed and the average acceleration level in 1/3-octave bands for each of the 9-square foot areas was computed. Results of this test indicate approximately a 6-db difference in the acceleration response between localized and complete acoustic excitation for the structure tested.

As the final phase of this test effort, the structure was proof tested at 166 db with the static load on the structure programed to simulate the dynamic loads during silo launch. After 10 minutes of testing at this level, no significant failures were observed which would have affected the flight of the missile.

ACOUSTIC TEST OF MISSILE EQUIPMENT*

A total of 40 missile components were tested [4] in a random acoustic noise field at test levels up to 172 db, in order to establish their acoustic threshold of malfunction or damage. Selection of the components was based upon previous vibration test results and the criticality of the component function during silo launch. During the tests, the components were functionally operated, and all critical operational parameters were monitored or recorded. The components were exposed to a series of acoustic excitation levels in the reverberation chamber starting at 130 db and increasing in 6-db increments until the components malfunctioned, or until the limit of the test facility (168 db) was reached. Higher test levels (172 db) were achieved for small components, such as relays, which could be positioned in the throat of the exponential horn, coupling the random noise source to the reverberation chamber. The components were either mounted rigidly on an interior surface of the reverberation chamber or suspended with shock cord. A typical component installed in the reverberation chamber is shown in Fig. 12.

The ideal method would have been to mount the components on a fixture with the same mounting-point mechanical impedence as encountered in the missile; however, the engineering and hardware fabrication required to simulate mounting-point impedence could not be accomplished within the time span of the program. Of the 40 components tested, which included control system, electrical, cryogenic, hydraulic, and pneumatic components, only four experienced out-of-specification deviation when subjected to the acoustic environments.

In conjunction with the vibration and acoustic tests of the transition section discussed previously, a guidance component was installed on its mounting hardware in the structure and functionally operated while the surface of the structure supporting the component mounting bracketry was excited with random acoustic energy at 158 and 165 db. The electrical signals from the component, together with the accelerations on the component, were recorded on tape. The recording of the electrical signals from the component were played back into a missile-control-system mockup. Engine displacement and accelerations were measured to determine the effect of the acoustically induced error signals upon missile guidance and the structural vibration produced by the engine gimbling. Results of these tests, along with random vibration tests of the component at predicted acceleration power spectral densities, showed that vibration isolation of the component was necessary.

*Prepared by J. M. Otera.

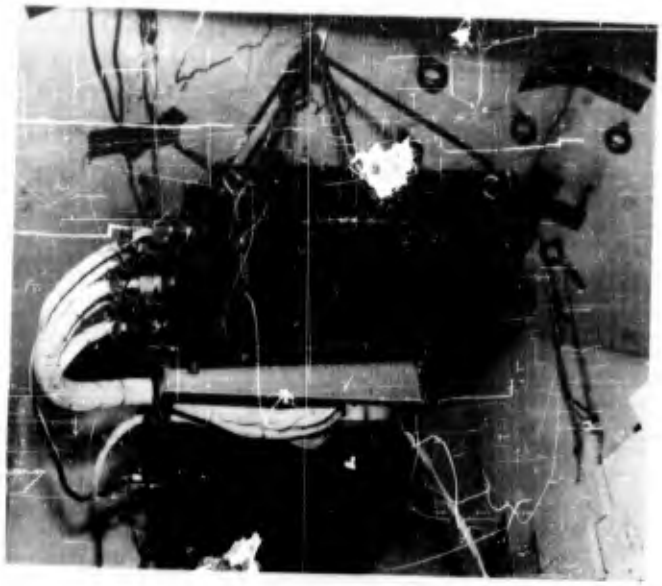

Fig. 12 - Component installation

In general, missile components which have successfully passed airborne vibration requirements will withstand short term direct acoustic excitation up to 160 db without malfunction or failure. Relatively simple methods of protection can be provided for most components which exhibit acoustic sensitivity.

In another respect, however, a high percentage of component malfunctions, or failures, will occur due to the increased acoustically induced vibration environment during silo launch [5]. To overcome this problem, components must be either relocated to areas of the missile having lower vibration environments, isolated, or as a last resort redesigned to withstand the environment.

SILO ACOUSTIC LINER INVESTIGATIONS*

Measurements and computations indicate an expected sound pressure level in the silo of approximately 165 to 170 db at the tailskirt of the missile. If no method is used to attenuate the acoustic energy propagating up the launch duct, these sound pressure levels will occur throughout the launch duct and expose the missile to levels considerably higher than those encountered during above-ground launch.

The object of this phase of the test program was to evaluate various launch duct acoustic treatments and to obtain a practical treatment that provided sufficient attenuation to reduce the sound field about the missile to levels approaching above-ground operation [6].

Silo launch-duct acoustic treatments were evaluated with a 50-foot-long, 1/16-annular segment of a full-scale silo launch facility. The test facility is shown in Fig. 13. The test duct is joined by a conical transition section to an exponential horn fitting, either the sinusoidal or random siren. A removable 22-foot extension of the test duct provides an acoustic termination to prevent the generation of undesirable standing waves in the test section of the duct. Acoustic treatments evaluated were: wedges, multilayer structures, and uniformly continuous structures of (1) metal wool, (2) bonded glass wool, and (3) unbonded glass wool. As a result of these tests, a 3-foot-thick, bulk, unbonded, glass-wool configuration was selected for the acoustic material with which to line the experimental silo-launch facility. Plane wave attenuation performance of this liner is shown in Fig. 14.

In addition to the acoustic attenuation tests, tests were conducted to determine compatibility of selected acoustic materials with missile propellents.

*Prepared by J. R. Pitsker, Jr.

Fig. 13 - Liner test facility

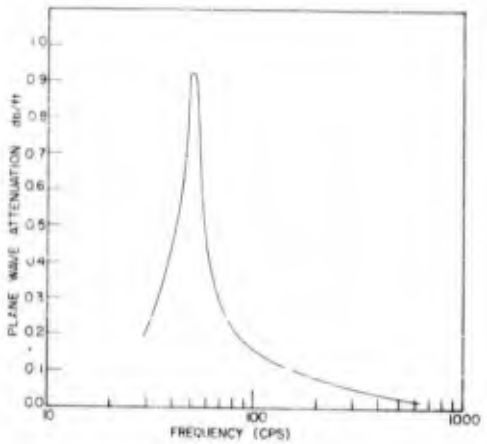

Fig. 14 - Liner attenuation

PREDICATION OF VIBRATION LEVELS*

Introduction

This section describes how the acoustic field surrounding the Titan missile, determines the vibration environment seen by the components within the missile, summarizes the measured above-ground Titan acoustic and vibration environment, and presents a method for predicting the vibration environment when the acoustic field surrounding the missile is altered to that of an underground in-silo launch condition, or to that of a larger but similar missile.

The discussion is limited to the method of predicting the in-silo vibration environment. The actual prediction of vibration levels for an underground launching of the Titan involves a detailed discussion of the in-silo acoustic environment and is beyond the scope of the present paper.

Description of Titan Vibration Environment

From the beginning of the W/S107A-2 Captive and Flight Test Program, vibration measurements were made throughout the various compartments of the missile at the mounting points of equipment, such as the three-axis reference system, guidance equipment, rate gyro, and electrical inverter. Measurements were also made on primary airframe structure, on items such as

*Prepared by F. M. Condos.

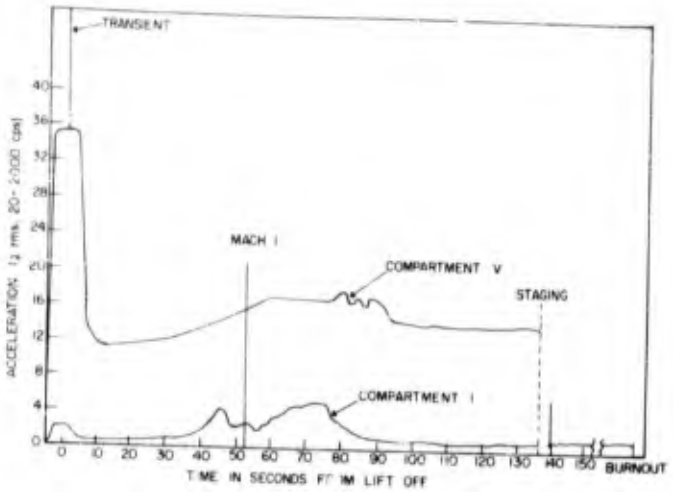

Fig. 15 - Typical vibration time history

stringers and frames which were typical small component mounting locations.

The measurement program covered all phases of the missile test program: Stage I ground firing, Stage II ground firing, Stage I ground firing with Stage II on top of Stage I (the flight configuration), and Stage I and Stage II flights. The data indicated that the ground firing of Stage I and Stage II represented the most severe vibration environment (exceeding or equaling the flight levels), and it was possible therefore to concentrate most of the measurement effort on ground firings, using landline instrumentation which was more readily available than high-frequency telemetering channels.

The typical flight vibration history for the fore and aft compartments is shown in Fig. 15. The initial ground level occurs with engine ignition and thrust build-up. The missile is held down a nominal 4 seconds after engine start and then released. The release results in a rather large launch transient caused by release of strain energy and explosion of the launch bolts. The transient can have a peak value of 250 g at the aft end and 6-10 g at the forward end. This transient decays very rapidly, and the vibration returns to the level noted before lift-off. There is no evidence that the missile vibration environment has been instantaneously changed by the release of the missile.

Following lift-off, the vibration levels gradually decrease in all compartments to a minimum level at about 15 seconds after lift-off. The minimum level is less than 1 grms for the forward compartments. Compartment V, the booster engine compartment, has the highest level of any compartment at this time. From this data, it must be concluded that the before-lift-off vibration is caused primarily by acoustic excitation. As mentioned earlier, the absence of a sudden reduction in missile vibration just after lift-off precludes any effect of the missile being tied down. The gradual reduction from lift-off to lift-off plus 15 seconds must then be the result of loss of ground-reflected acoustic energy and shifting of the sound source farther aft as the missile rises above the rocket flame deflector plate. The Mach number at 20 seconds is on the order of 0.2, which is too low to effect the sound field.

After lift-off, the next period of high vibration occurs during the transonic region and at maximum aerodynamic pressure. These are caused by aerodynamic disturbances on the surface of the missile. The over-all level is approximately equal to the prelift-off level. The vibration spectrum shape during the period of aerodynamic excitation is very nearly the same as that of the ground spectrum, except for a slight increase in low-frequency energy up to 200 cps.

Beyond the aerodynamic disturbance region, the level again drops to a minimum. Stage separation results in some minor shock transients with levels of 40- to 50-g peak in the aft portion of Stage II. Stage II flight has vibration levels of less than 3 grms in any compartment. The vibration is relatively

constant throughout the flight of Stage II and represents the amount of vibration mechanically transmitted through the Stage II structure, since no acoustic field can exist above the atmosphere.

There are several conclusions which may be drawn from these flight characteristics which aid in the prediction of vibration levels expected for an underground launching, and for larger missiles.

1. The major portion of the vibration environment is the result of acoustic excitation of the structure, since the structure is not capable of transmitting vibration any appreciable distance. This is evident from the gradual decrease in vibration after lift-off and the very low-vibration levels during Stage II flight.

2. The aerodynamic disturbances in the transonic region result in nearly the same vibration environment as the ground acoustic field. As expected, the aerodynamic effects are the most pronounced at the conical sections, and less pronounced at the cylindrical sections of the missile airframe.

3. Propellant loads have very little effect on the structure's ability to transmit vibration. This is concluded from the fact that the vibration level near the end of flight for both Stage I and II is the same as the level earlier in the flight.

4. The vibration environment before lift-off appears to be related to the flight environment in frequency content as noted from the similarity of spectrum shapes before lift-off and during flight.

Statistical Method of Data Analysis

It was deemed most practicable to specify Titan design and test vibration levels on a compartment basis, one level for each compartment. In this manner, a component could be located in any position within the compartment and would not be restricted to a specific location by environmental requirements.

Since the vibration environment at every location within a compartment could not be measured, a number of typical locations were selected for measurement. From these measurements, it was necessary to predict a composite compartment environment which would apply to any component. The acceleration spectral density analysis of measured vibration was observed to have variations from location to location and from flight to flight, but measurements from the same compartment were found to exhibit the same general spectrum shape. It was decided to make a statistical approach to the problem.

The acceleration spectral-density data for each compartment was divided into 50-cps bands. The highest g^2/cps value in each band was used as a data point. All data points of the same frequency band taken from the same test condition, such as side-by-side, tandem captive, or flight, constituted the population. No grouping by axis or direction was made. The population was evaluated to determine its distribution. The log normal distribution was chosen as the best fit. With the establishment of a log normal distribution, it became a simple process to predict the probability of certain g^2/cps levels occurring.

The 90-percent probability level was selected as a good design criteria. This level may seem rather low but there is justification for this. First, the data points are always the maximum level in that band width. Secondly, data from all directions or axes and from light and heavy components were combined in the population. This tends to broaden the distribution. Thirdly, overlaying the maximum points which make up the population shows that the majority of these points fall at or below the 90-percent level. Figure 16 is a presentation of the 90-percent probability levels for each compartment. Note that there are levels for both Stage I and Stage II ground firings.

Advantages and Shortcomings of Statistical Analysis

The value of a statistical method is that it allows one to extrapolate vibration data out into a region beyond the measured levels with a degree of confidence greater than that obtained by taking maximum measured values and increasing these by a safety factor. A statistical analysis is less influenced by a single high value, which may be the result of improper calibration, than is a maximum envelope approach. At the same time it does not completely ignore an extreme high or low actual value. Disadvantages are that the statistical method results in a higher overall, root-mean-square vibration level than that indicated by any individual measurement. This is because one assumes that the maximum g^2/cps level is constant over the 50-cps band, when it may actually occur over a

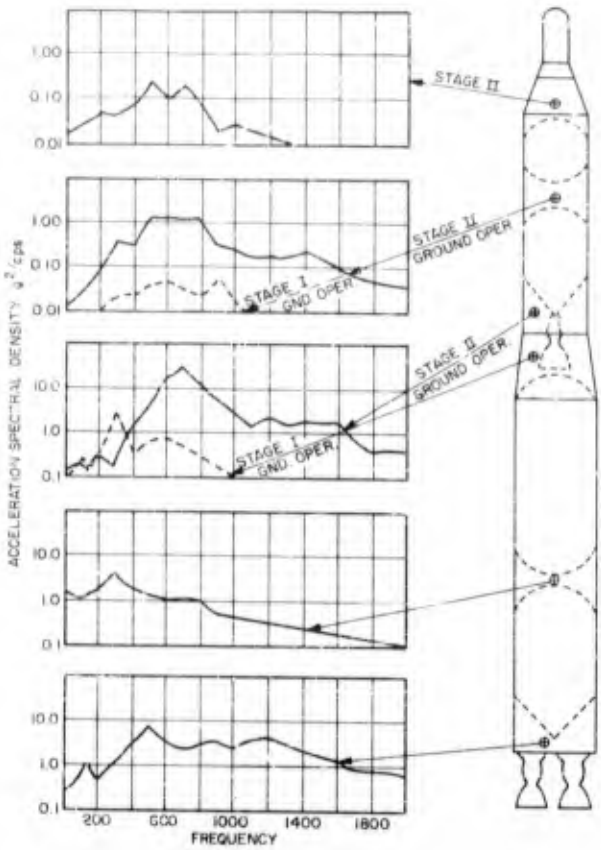

Fig. 16 - Titan vibration levels
(90-percent probability)

narrower band. It is felt that this conservatism is not detrimental since any single resonance responds to the energy admitted by its band width and is a little affected by the overall, root-mean-square level. In addition, a particular structural resonance may shift in frequency slightly from missile to missile, further reducing the need for resolution. Additional previously mentioned disadvantages are those which tend to broaden the distribution and induce conservatism. A final disadvantage is the inability to establish an accurate confidence level relative to the actual environment because of the large number of variables associated with the data samples.

Acoustic Levels

Acoustic levels were measured in and about the missile to establish the acoustic profile applicable to the missile for captive firings [2]. The acoustic profile is shown in Fig. 17. These are average levels. There was evidence of a 1- to 2-db shadow effect on the side opposite the deflected flame. The levels, shown for Stage II when it is placed on top of Stage I, are extrapolated because all data were taken with Stage II beside Stage I. Typical spectrum shapes are shown in Fig. 18.

Prediction of Equipment Vibration Levels from the External Acoustic Field

The preceding paragraphs have dealt with the environment of an existing missile, established after the missile had been developed. Obviously, this information is of little value except to verify the accuracy of the original predictions and design criteria. The principal value of these data lies in their use for predicting vibration environments for an underground launching, or for a larger missile.

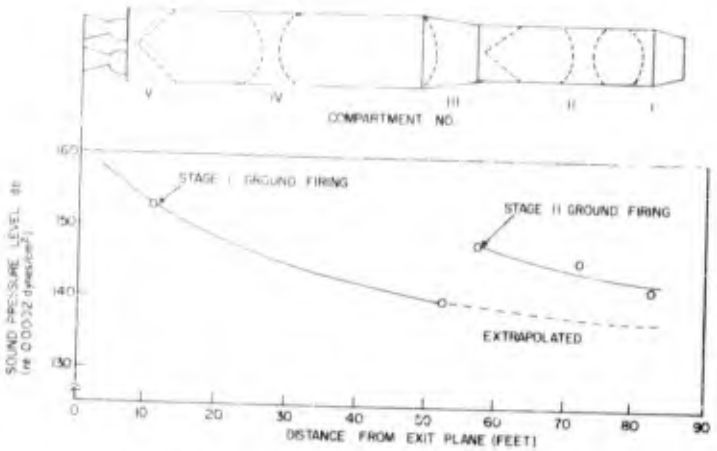

Fig. 17 - Titan acoustic profile (ground firing)

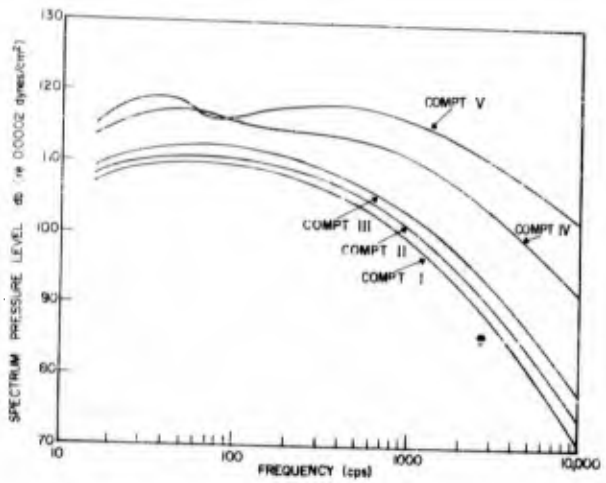

Fig. 18 - Titan sound spectra by compartment

To predict the vibration environment of another missile, or for an underground launching, it is necessary to consider the expected acoustic field and the new structure and to make certain assumptions based on engineering judgement.

A detailed description of the acoustic levels and of the acoustic prediction methods for above-ground or underground launchings is beyond the scope of this paper. It suffices to say that the acoustic field can be determined by analytical and empirical means sufficiently accurately to apply the method outlined here.

Structural differences between the missiles providing the vibration data and the missiles used for an underground launching have to be considered. The Titan structure is of typical aircraft construction with frames and skin riveted and welded together. Equipment is installed on brackets attached to stringers and frames or on trusses attached to the structure. A larger missile will have a similar configuration appropriately sized to increased loads. Major dynamic modes will remain similar to the Titan and will fall below 30 cps. In general, it can be concluded that the structure will respond to the acoustic

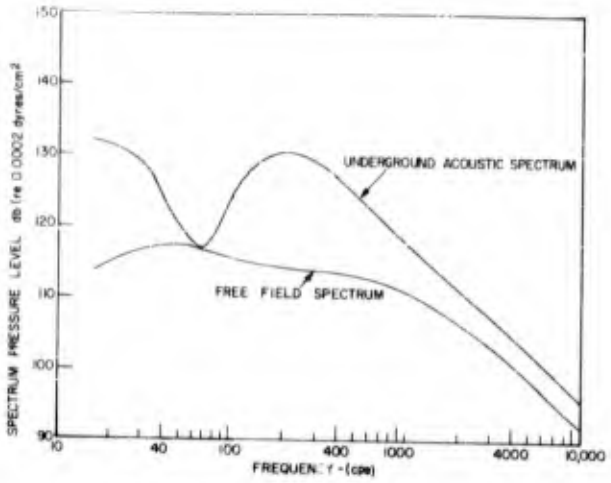

Fig. 19 - Typical acoustic spectral difference

environment in much the same manner as the Titan did because of the similarity. Changes which would most effect the response are increased skin mass and increased local stiffness. Since stiffness control is limited to frequencies below panel resonance, the effect is apparent only up to about 200 cps. Because of this and because analysis of panel stiffness is cumbersome, it was ignored as a significant factor. Only the mass effect was used as a structural consideration. As previously mentioned, the vibration is predominantly a result of acoustic excitation. For the purpose of prediction, it is assumed to be the only source.

The remaining assumption is that the structural response to acoustic excitation is a linear function. This was quickly established by structural acoustic tests which indicated the response of stringers and frames to be linear over an acoustic level of 140 to 165 db.

The prediction of vibration levels becomes a matter of applying a factor (F) to the 90-percent probability level of the acceleration spectral density level for each frequency, based on the following relationship:

$$F = \text{antilog} \frac{\Delta db}{10} \frac{M_1}{M_2}$$

where

M_1 = skin mass per square foot for the Titan

M_2 = skin mass per square foot for new missile

Δdb = difference in acoustic spectrum level for a given location on Titan and new missile

Typical acoustic spectra for Compartment IV of Titan for above-ground and underground firings are shown in Fig. 19. By the use of the above relationship, the vibration environment for Compartment IV during an underground firing of a "new" missile was calculated yielding the random vibration spectrum shown in Fig. 20.

The aerodynamic flight environment of the "new" missile is considered to be similar

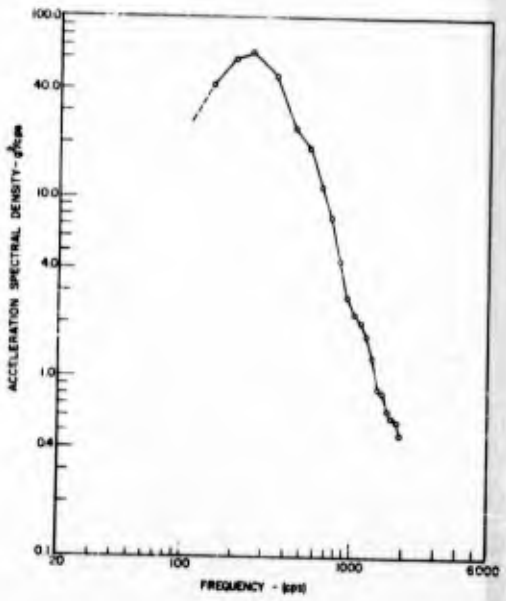

Fig. 20 - Predicted level for underground launching (Compartment IV)

to that of the Titan, which is a function only of the re-entry vehicle shape. Trajectory will effect the duration and time of occurrence of the maximum flight vibration but should not alter the maximum level. Levels for equipment attached directly to the engines can be established on the basis of increased mechanical energy since the low area-to-mass ratio precluded the possibility of high acoustic response.

Conclusion

The foregoing is a simplified method for establishing vibration levels on structurally similar missiles prior to actual measurements or tests. The method avoids the use of mathematical analyses of structural response, which are tedious and tend to give an appearance of accuracy unwarranted by the data, assumptions, or calculations required.

CONCLUSION

Acoustic problems associated with the underground launching of a large missile c be solved by the employment of launch-duct acoustic treatments, minor modification to the missile structure, and vibration isolation of components where required.

In general, most missile components are relatively insensitive to direct acoustic excitation up to sound pressure levels of 160 db. Component vibration levels, due to acoustically induced structural vibration, are higher than levels occurring during above ground launch and in general require vibration protection of the components.

REFERENCES

1. J. N. Cole, H. E. Von Gierke, M. L. Oestreicher, and R. G. Powell, "Simulation of Random Acoustic Environments by a Wide-Band Noise Siren," Bulletin No. 27, Shock, Vibration & Associated Environments, Part II, Dec. 1957
2. H. Williamson, D. Dinicola, and H. McGregor, "Missile Structural Segments Acoustic Test, Silo Launch Technical Investigation, Final Report," Martin Company Technical Report CR-60-22, Vol. 3, Aug. 1960
3. P. Rader, "Acoustic and Vibration Test of Lot VS Stage I Transition Section," Martin Company Report (to be published)
4. J. M. Otera and H. McGregor, "Missile Component Acoustic Testing, Silo Launch Technical Investigation, Final Report," Martin Company Technical Report CR-60-22, Vol. 1, Aug. 1960
5. J. M. Otera and R. A. Vigil, "Silo Launch Test Facilit · Component, Vibration Test," Martin Company Technical Report (to be published)
6. R. Pitsker and H. McGregor, "Silo Liner Acoustic Testing, Silo Launch, Technical Investigation, Final Report," Martin Company Technical Report CR-60-22, Vol. 2, Aug. 1960
7. F. Condos and W. Butler, "Silo Launch Technical Investigation, Final Report," Martin Company Technical Report CR-60-22, Vol. 4, Oct. 1960

DISCUSSION

Mr. Fuller (Boeing Airplane Co.): What was the philosophy of this random test with the horn? How did you interpret this in terms of life? Did you know anything about the correlation of pressures over the panel or did you know anything about the shaping of the power spectrum to the proper value? What did you do with the test data once you got it?

Mr. McGregor: There were several problems involved. First, the acoustic spectrum generated by the siren approximated the spectrum which was anticipated for the silo. The question arose, how shall we test the structure? Shall we use normal incidence, grazing incidence, or some angle between? After many discussions it was agreed to disagree.

We said go ahead and test with normal incidence. The interpretation of failures is, I think, a rather difficult thing to assess from these tests. Actually the tests were merely proof tests. If the structure withstood this excitation for at least 10 minutes, it was considered that it would withstand the silo environment. We're now conducting tests on the panel which I showed you there in which a little more refined techniques are being employed to correlate exposure time and fatigue life.

Mr. Trotter (Boeing Airplane Co.): I wonder if you could tell us what were your spectral shapes and levels that you could achieve with your random sound generator?

Mr. McGregor: The sound pressure levels achievable were 166-167 db when the horn was placed against the structure. In the 70 ft^3 reverberation chamber sound pressure levels were up to 168 db. and to 172 db in the horn.

Mr. Barnes (Boeing Airplane Co.): Is there any technique that you people have developed for providing shaping of your spectrum?

Mr. McGregor: To be honest with you, no. While we were building the acoustic facility we did not have a compressed-air source in which to run an evaluation program on our siren, so every weekend we would pack the siren and all the instrumentation associated with it and take it up to Climax, Colorado, up to the molybdenum mine up there, and use the compressed-air source up there. Every Sunday night we'd come back with all the pieces and work the rest of the week and try it the next weekend. We finally got a siren which was structurally sound and we were very fortunate that the spectrum of the siren output very closely approximated the missile spectrum. You can get some shaping of the spectrum by varying rotor speeds. You run into some problems in which you have a set of speed ratios on the rotors, I guess you could call them forbidden speeds, at which the thing turns into a sinusoidal generator.

(Note: At this point, part of the discussion was lost while changing tape reels.)

Mr. Klein (Space Technology Laboratories): Could you tell me how you determined the duration of the structures test?

Mr. McGregor: The structures tests were performed in increments in which the structure was irradiated, for the first series of tests, for a 2-minute burst and then we went out and inspected the structure. The philosophy was that it lessened the mean time to failure. If it lasted for 10 minutes, we would have a reasonably high degree of confidence that it would withstand the relatively short exposure time during silo launch.

Mr. Brown (Varian Associates): I am wondering about the setup where you used the two sirens in parallel—where they tended to smooth out the field of your wave. What do you attribute the better results to? Is it more or less the two waves impinging there at that y-throat? Do they tend to randomly cancel some of the more spurious points?

Mr. McGregor: I think the reason the spectrum smoothed out is because both of the sirens are not running at exactly the same speed and are not producing exactly the same spectrum. We did not have sufficient time to go into more detailed tests because of our current test program. What we plan to do is to set up the two sirens in parallel and take a look first at one siren and look for the peaks and valleys in the spectrum, and then set up the other siren so that it would fill in the valleys and maybe knock off the peaks.

Mr. Brown: Would there possibly be an application for using two smaller sirens then using again a duplicate y-throat and coupling four together like that? Could that smooth it out even more, do you think?

Mr. McGregor: Well, I think so. I think if you went to many-many sirens you would probably get a very smooth spectrum.

Mr. Brown: Now how about in the exponential horn in there, you placed the blast right up to the test item, more or less a surface contact. What would be the difference if you removed it possibly a meter or so. Is it more advantageous to have it next to the horn?

Mr. McGregor: Yes, it is. As we pull the horn away, the sound levels drop down.

Mr. Brown: What's the shape of the wave? Do you consider that it is extremely plane for a full-zero-degree incidence?

Mr. McGregor: I can say this. We placed the random siren against a concrete block and measured the sound distribution across the face of the block—no phase measurements now, just pressure measurements—and the pressure measurements in 1/3-octave bands seemed to be reasonably uniform across the

face of the horn. Of course when you go against the structure, you have a panel resonating here and one over there, and you will get some change in the sound field.

Mr. Fuller: When you tested these at normal incidence, didn't you see any standing wave phenomena that would change the shape of the spectra that you were trying to reproduce? In other words, when you measure the spectra from the random source did you measure it with something in front of it, like the block, or was this a free-field measurement that was analyzed to give the spectrum?

Mr. McGregor: We found, with the siren radiating into free space and then against the concrete block, that the change in the spectrum shape was very small. This was not true in the reverberation chamber.

Mr. Fuller: You didn't notice any resonances due to the air column even in the random test, then? You had no air column effect?

Mr. McGregor: No appreciable effect. Of course, the horn itself is a little over eleven feet long. The theoretical cut-off frequency was 22 cycles.

Dr. Vigness (Chairman, U.S. Naval Research Laboratory): I think in all of this kind of work, which is really rather new, that we don't have a feel, in terms of db, as to what constitutes a magnitude which really would give damage. If we would speak of it in terms of psi, then around 150-160 db it begins to be appreciable in psi. When you get something less than 1/10th of a psi it probably won't hurt anything if you are worrying about structural damage. But when you begin to get something greater than 1/10th of a psi, then you might begin to worry about structural damage caused by resonant effects and such. So, if you begin to convert mentally until you have a feeling, in terms of the db values, of the pressures involved, I think you'll begin to feel what might cause damage. Of course, the levels would be entirely different when you are worrying about microphonics and noise in your equipment generated by the excitation noise. But if you're worrying about fatigue and structural damage, then try to get an idea as to the forces involved, the pressures and the area.

* * *

EMPIRICAL PREDICTION OF SPACE VEHICLE VIBRATION*

Kenneth McK. Eldred
Western Electro-Acoustic Laboratory, Inc.
Los Angeles, California

The material presented in this paper has been drawn from a much larger study† of Structural Vibrations in Space Vehicles [1]. The paper gives a brief background of the sources of space vehicle vibration, and illustrates the variation of the two major exciting sources, rocket noise and boundary layer pressure fluctuations, during a typical launch. This introduction is followed by a summary of available vibration data for current missiles at both launch and maximum dynamic pressure flight phases. Two empirical correlations between the excitation and resulting vibration are presented and discussed.

INTRODUCTION

Vibration is of major concern in the design and development of a successful missile or space vehicle. This concern stems directly from the flight failures which have been traced to excessive vibration of structure or equipment. Usually, excessive vibration manifests itself either in the fatigue failure of skin and structure, or in the malfunction of electronic and mechanical equipment. Although fatigue failure is normally associated with relatively long exposure periods, it can occur in a short time if the vibration is very severe or the frequency high. On the other hand, equipment malfunctions are usually amplitude sensitive and independent of exposure duration. However, either type of problem can be disastrous to the successful accomplishment of a mission by a complex vehicle, which requires the coordinated and precise functioning of many systems and their diverse components.

Consequently, it is desirable to assess the probable operational vibration environment of a vehicle while it is still on the drawing board. Correct evaluation of the probable environment at this early date can provide a realistic basis for considering vibration requirements, together with all other basic vehicle requirements, in the preliminary design stage. This consideration can, in turn, guide both system and mission concepts toward increased reliability at minimum penalty.

The major sources of excitation for vibration in space vehicles and high performance aircraft are jet or rocket noise, boundary layer and base pressure fluctuations, and other phenomena which are characterized by continuous frequency spectra and random amplitudes. Hence, the task of predicting vibratory responses and stresses for these vehicles is more formidable than formerly when the exciting forces were primarily sinusoidal in nature. Furthermore, although structural fatigue is predominant at frequencies below 500 cps, equipment malfunction and electronic component fatigue extend the frequency range of concern to at least 10,000 cps. Hence, in many cases, when predicting vibration response for advanced aircraft and space vehicles all frequencies below 10,000 cps must be considered.

The vibration response of any portion of the vehicle resulting from a source of mechanical energy depends on the characteristics of the source, the path between the source and the receiver, and the characteristics of the receiver itself (Fig. 1). At low frequencies, the response of the entire vehicle to external sources is a maximum at the basic body modes,

*This paper was not presented at the Symposium.

†The study was conducted by the Norair Division of Northrop Corp., and the Western Electro-Acoustic Laboratory, Inc., as co-contractors, and was sponsored by the United States Air Force, Vibration and Acoustical Section, Dynamics Branch, Structures Laboratory, Wright Air Development Division, under Contract AF33(616)-6486.

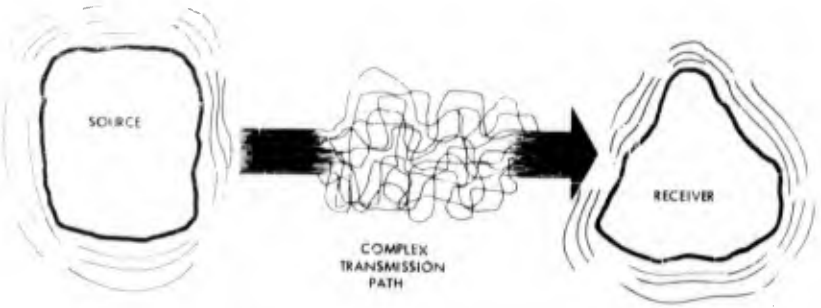

Fig. 1 - Sketch of the complex transmission of mechanical energy from source to receiver

and the magnitude of the response depends primarily upon the location relative to the body mode shape, the magnification factor for the mode, and the magnitude of the forcing function over the entire vehicle. At higher frequencies, the maximum responses occur at the resonances of the various panels and the magnitude of the response depends on the characteristics of the source, the panel, the transmission path between panel and receiver, and upon the receiver. At frequencies above the panel, fundamental resonances, the factors influencing response, become very complex and the possibility of resonances along the path becomes sufficiently high as to suggest that the path be treated as a transmission line with lumped parameters which, in addition to source and receiver characteristics, determine the vibration response.

From this brief discussion, it is clear that a detailed stepwise approach for the prediction of vibration for any general case would be exceedingly complex and cumbersome. Further, it is clear that a practical analytical solution of the vibration characteristics of a mechanical system must lie in judicious simplification of the system to a series of subsystems whose solutions are known. It is also clear that an analytical approach is not feasible for general prediction at the early design stages where the structure is not reasonably fixed in concept; however, many preliminary decisions regarding equipment location, isolation and specification and the definition of potential structural fatigue problem areas must be resolved in the early design stage. Therefore, it is desirable to examine available vibration data to determine its usefulness as a predictive tool for the probable vibration environment of new designs.

The purpose of this paper is the presentation of vibration data, the comparison of data obtained in different classes of vehicles and different flight phases, and an analysis of the broad trends which can be of assistance in the prediction of vibration environments. Before discussing the data, it is necessary to consider some of the circumstances regarding the measurements and analysis.

COMPARABILITY OF VIBRATION DATA

The nature and quality of reported vibration data is profoundly influenced by the techniques employed in selecting, locating and mounting the vibration transducers, and by the recording and analysis of the data, in addition to the procedures used in designing and specifying the test conditions. The many optimum requirements for measurement procedures are not always simultaneously attainable and, consequently, much data must be obtained under less than desirable circumstances.

The various major difficulties which arise in the comparison of vibration data taken by several organizations, assuming all data to have been corrected for the usual response factors, stem directly from three basic problem areas. These are:

1. Alteration of the frequency response of the mounted transducer from its laboratory calibration because of the interaction between the vibratory characteristics of the transducer, mounting device, and local structure.

2. Nonuniformity of the measured quantity, e.g., acceleration as velocity, as an average, as a root-mean-square, a mean peak, or peak, etc., together with the lack of measured statistical distributions to determine the relationship between these quantities.

3. The analysis of data with a variety of filter bandwidths, and often the reduction of

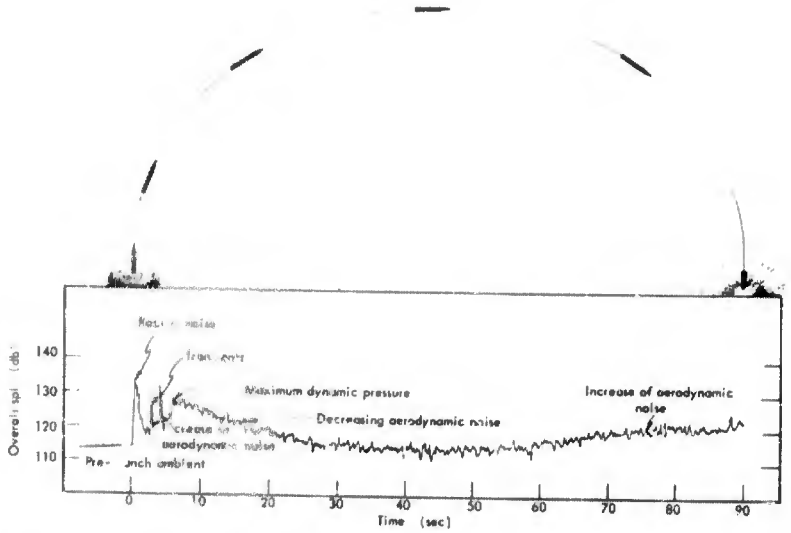

Fig. 2 - Graphic level recording of variation of over-all noise level inside forward compartment of a small missile during its flight

data, measured by a filter whose bandwidth is wider than the bandwidth of a vibration resonance, to a fictitious power spectral density.

Because of the latter two factors, comparison of much of the valuable data presently available is only possible when the data are transferred to an arbitrary standardized form of presentation. For standardization of the data in this paper, certain ground rules were followed which were felt to introduce the least error in determining and comparing the various empirical trends. The data which were available to the author have been reduced by filters of one of the following bandwidths: 1/2 octave, 100 cps, and a series of smaller bandwidths ranging down to 2 cps. The results were reported as displacement or acceleration in terms of mean square per cycle, root-mean-square (rms) for the bandwidth, mean peak, etc. Statistical distributions of either peak amplitude or instantaneous amplitude were also occasionally presented.

To obtain standardization for comparison, all acceleration data were converted to the rms amplitude for the original bandwidth. Where the analysis bandwidth was narrower than the bandwidth of the resonant phenomena, the energy under each resonance was summed and the result reduced to the rms amplitude which is associated with the single resonance. Sinusoids, where identifiable, were considered separately as appropriate to each of the summary figures. Where only the maximum mean square amplitudes per cycle of resonant peaks were reported, the rms value for the total resonant vibration associated with each peak was estimated, assuming that the q of the resonance was 15, which seems typical for many missile structures. Where mean peak data were given for the value of resonant vibration, it was assumed that the resonant peak amplitudes would follow a Raleigh peak distribution and the rms amplitude was computed by dividing the mean peak amplitude by 1.19. Furthermore, although a few of the reported results gave data above 1000 cps, the lack of reported calibration of the installed transducers (except for one organization) made these data suspect and of indeterminate value.

SUMMARY OF AVAILABLE MISSILE VIBRATION DATA

The vibration environment in a missile varies rapidly with time during a typical flight profile. This rapid variation can be illustrated by the continuous recording of the noise in a forward compartment of a small ground-to-ground missile. It might be noted that a recording of noise is illustrated rather than a recording of vibration simply because of the availability of the former.

Figure 2 from [Ref. 2] illustrates the several phases of noise or vibration environment which are usually found in missile flight data. The rocket noise at launch provides a high

level of vehicle response, which decreases rapidly as the vehicle leaves the pad and accelerates. However, as vehicle velocity increases, the pressure fluctuations in the turbulent boundary layer increase in magnitude and the vehicle response begins to increase. The transients shown on the graphic level recording represent a shock as the vehicle passed through the transonic region, and a second shock when the sustainer engine was ignited. As can be seen, the response continued to increase until the maximum dynamic pressure (8) was reached, at which time in the flight profile the boundary layer pressure fluctuations are maximum. As the vehicle continued to accelerate into less dense atmosphere, the q decreased, as did the response. However, when the vehicle descended into more dense atmosphere in the terminal portion of the flight, the vehicle q and response both increased.

It is evident from Fig. 2 that the two most severe vibration environments are a result of rocket noise at launch, and aerodynamic phenomena at maximum q. The relative severity of these two forcing functions and their responses in a specific vehicle depends on many factors, including the flight profile and the launch configurations, as discussed in [Ref 1]. It should be noted that, for some vehicle types, other forcing functions may also be of comparative severity.

The quest for missile vibration data which has general application toward empirical correlation studies is very laborious and difficult. This difficulty results from the problems encountered by vibration engineers in industry when they are forced to compete with other important groups for the assignment of telemetering channels. In most cases, this competition severely limits the number of transducers which can be used and requires commutation of the various transducers. Furthermore, these limitations require that potential problem areas and important equipment receive priority for transducer locations, so that ideal surveys, which trace vibration at various structural locations throughout the vehicle, are seldom realized.

Figure 3 presents data obtained at the launch of rocket powered ballistic missiles from transducers located on structure in the middle and forward portions of the vehicles. The data were obtained from [Refs. 3 - 18], which include five missiles with gross launch weights less than 15,000 pounds, and three missiles which have gross launch weights in the 100,000- to 300,000-pound range. The lightweight vehicles are denoted by open symbols and the heavier missiles by the solid symbols. It is evident from the figure that the vibration amplitudes in the heavy missiles are on the order of 20 to 25 percent of the amplitudes measured in the lightweight vehicles.

Figure 4 gives similar data for vibration at the maximum q flight phase for six missiles, four of which are lightweight and two of which are in the heavyweight class. Again, it is clear that the vibration of the heavy missiles is significantly lower than the vibration of the light missiles. It is noted that the vibrations given in the figure are thought to result only from pressure fluctuations in the boundary layer along the vehicle's skin. Thus, the figure does not include the data from a missile which responded to the high turbulence created by the wakes of its dive brakes or another vehicle which was excited by base pressure fluctuations. These two known special cases of aerodynamic excitation are discussed in [Refs. 16, 17, 19, 20].

Figure 5 presents available data for vibration of missile structure located near the engine. There is a rather large scatter in the data, and no consistent division is seen between light and heavy missiles. Rather, it appears that much of the data represents power level vibration. This is not at all unexpected because of the large variability of the vibratory energy output of different types of rocket engines.

Figure 6 summarizes the data obtained on four pieces of equipment, two of which were located in each of two types of heavy missile. The range of data represents many repeat flights with the transducers located at the same positions. In general, the vibration appeared to be sinusoidal at several harmonically related frequencies which were generated by the particular equipment. Obviously, these data represent specific cases and are included here only because of the large amount of data measured on each of these equipments, and to give some feeling for the range of amplitudes which might be encountered on or near equipment vibratory sources; however, the prediction of vibration near any equipment vibratory source should be predicated on measurements of the specific type of equipment when mounted on a foundation of known impedance.

In each of the figures in the preceding discussion of missile vibration, a median curve was fitted to the data. These curves, taken from Figs. 3, 4, and 5, are summarized

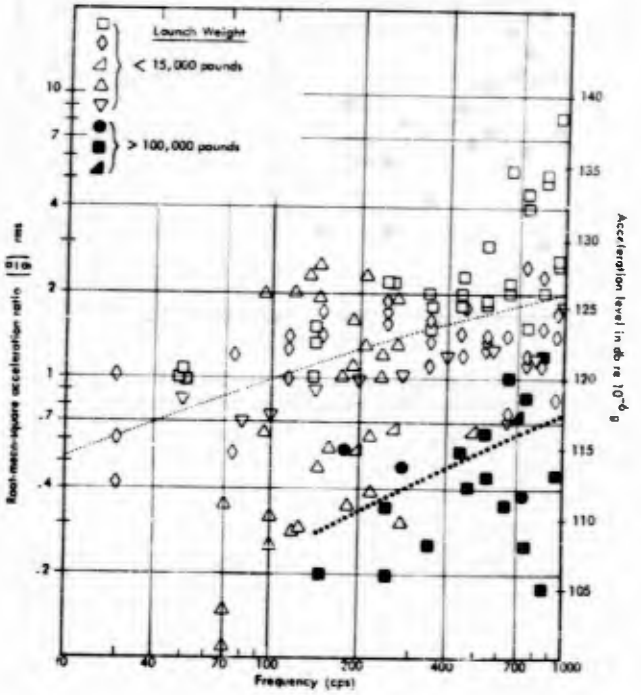

Fig. 3 - Missile launch accelerations obtained on structure in forward half of vehicle

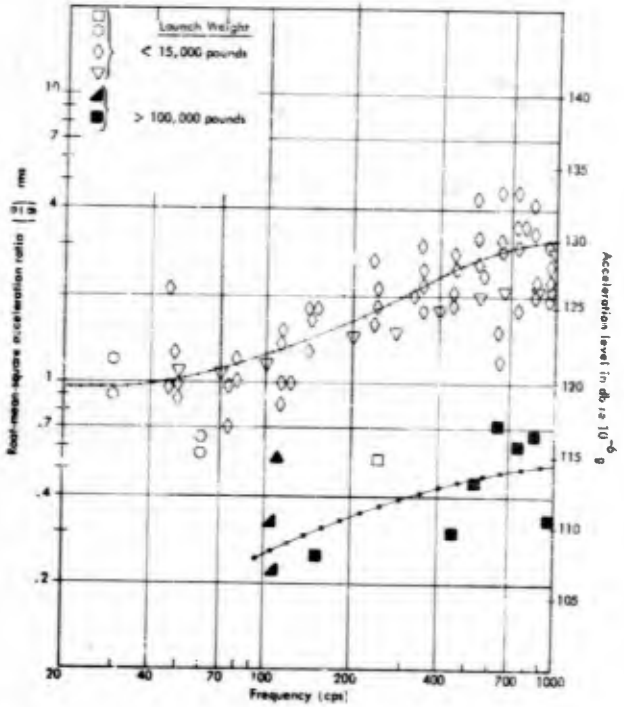

Fig. 4 - Missile flight accelerations on structure in forward half of venicle and obtained near maximum dynamic pressure, flight phase

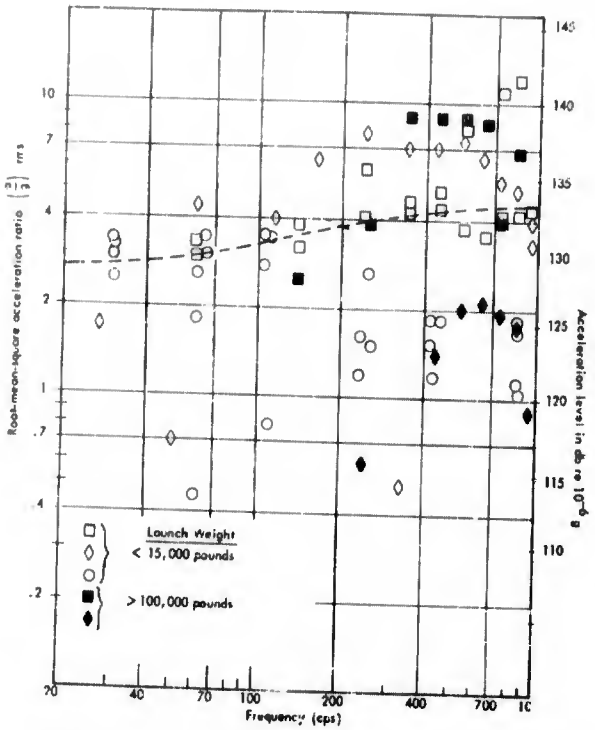

Fig. 5 - Missile flight accelerations on structure adjacent to rocket engine

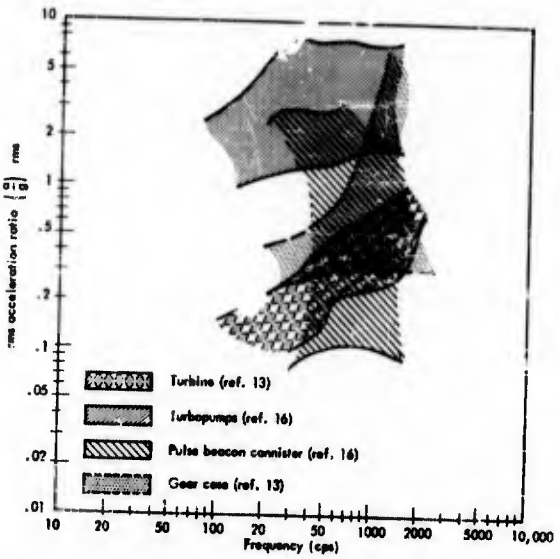

Fig. 6 - Range of accelerations for four types of self-excited missile equipment

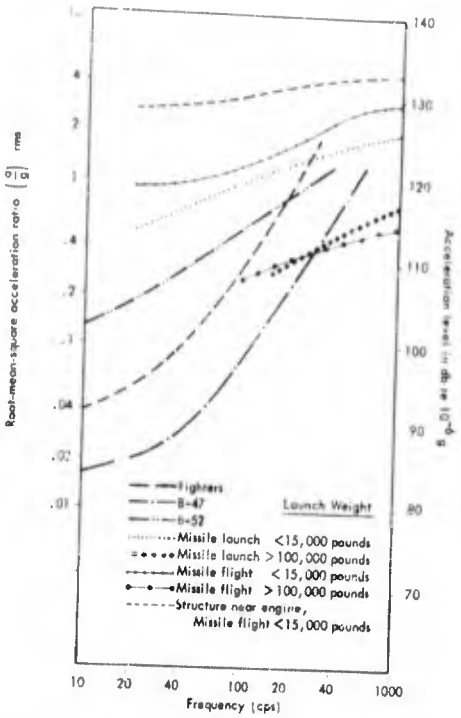

Fig. 7 - Summary of median curves for aircraft and missile accelerations

in Fig. 7. In addition, medians for the rms acceleration amplitudes measured in several types of aircraft [21] are presented for comparison with the missile data. It can be seen that the median of the data for the B-52 exceeds that for the B-47, whereas the median for the jet fighter vibration data lies between the medians of the two bombers. The medians for light missile launch and maximum q flight are generally higher than those for the aircraft, whereas the medians for the heavy missiles are significantly lower and are of the same order as the jet fighter and B-47 vibration. Note that the vibration on structure located near the rocket engine is considerably higher. Thus, this figure clearly demonstrates that the severe portions of the vibration environment in the light missiles generally exceeded those experienced in high performance jet aircraft; however, the vibrations in the heavy missiles of the IRBM and ICBM category have been generally of the same order as those of the aircraft. It should be emphasized that Fig. 7 only shows trends, since a very large scatter around the median exists for all the data.

It should be noted again that the relative severity of launch and maximum q flight phase vibration depends upon both the flight profile and the launch configuration. For example, all the launch data result from surface launches rather than silo launches. A comparison of the surface launch noise environment with the silo launch environment based on the information of [Ref. 1] indicates that the magnitude of vibration might be on the order of 3 to 5 times greater in a silo than on the surface. Thus, the silo launch vibration equipment for heavy missiles might be expected to approach the surface launch vibration environment in the light missiles.

EMPIRICAL PREDICTION OF VEHICLE VIBRATION

The objective of the comparison of vibration data in this paper is to assist the engineer in his understanding of the phenomena which are responsible for, or control, the vibration in a space vehicle, and to assist him in the prediction of the resulting vibration environment. As is the case in many young technologies, when the state of the art is not sufficiently complete to perform direct analytical solutions of specific problems, or when the analytical approach involves excessive complexity, it is desirable to attempt to derive direct empirical correlations which may be used as predictive tests and which define apparent trends.

The success of an empirical correlation generally depends upon the degree to which the correlating parameters represent the actual physical phenomena under study, and their actual scaling laws. In addition, the development of an empirical correlation which will stand the test of time often depends upon the relationship between the presently available range of each of the parameters and the range of the parameters which will eventually be encountered. For example, empirical correlations of jet noise from data which represents only a small range of jet velocities would, in all probability, not result in a proper scaling law for the velocity parameter, and in consequence, be a very inaccurate predictive tool for velocities which differ significantly from those considered. The preceding cautionary factors represent the basic hazards of the empirical approach, and suggest that empirical correlations be re-examined constantly to assure that they remain consistent with advances in the general "state of the art."

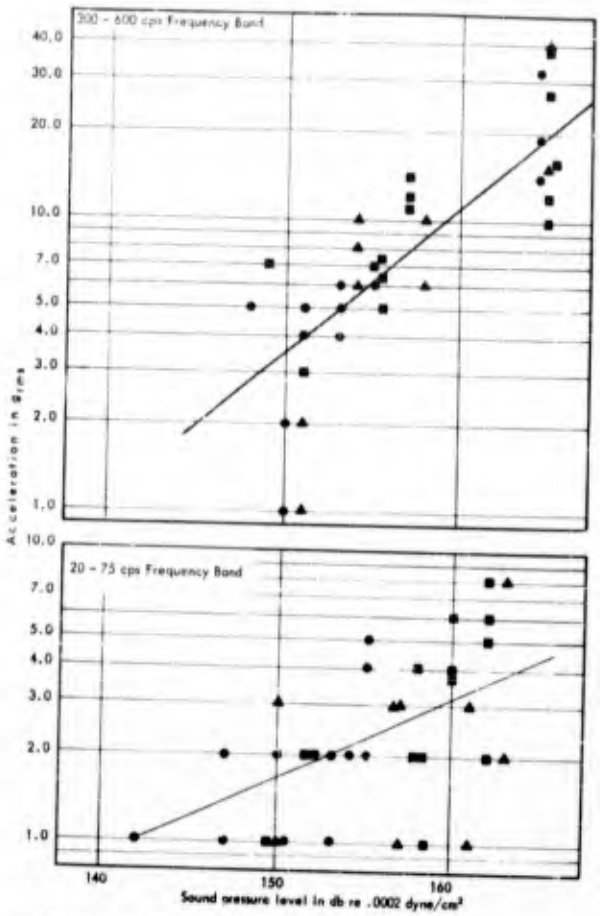

Fig. 8 - Comparison of internal vibration of structure and adjacent external sound pressure level for two frequency ranges from [Ref. 28]

Direct Correlation of Noise and Adjacent Structural Vibration in Aircraft

One approach to the correlation of vibration response of aircraft with external noise has been suggested previously by Convair [22 - 24]. This correlation was obtained by direct comparison of the external sound pressure level on the B-58, resulting from jet engine noise, with the vibratory response of adjacent internal structure. Thus, vibration measurements in the nose of the aircraft were compared directly to sound pressure levels measured on the external skin of the nose section, and vibration measurements in the aft end of the aircraft were compared to sound pressure levels measured on the external skin of the aft section, etc. Since the external noise environment on the B-58, and other types of jet aircraft varies considerably from the relatively low noise levels forward to the very high levels toward the aft end, a comparison of this type includes a range of external noise levels of the order of approximately 30 db.

A similar comparison of external noise and internal vibration from Snark data [25, 26] is given for two frequency bands in Fig. 8. The lower sound pressure levels and their associated vibration data are obtained at forward fuselage stations, and the higher sound pressure levels and the associated vibration data are obtained at afterfuselage stations adjacent to the rocket booster exhaust. It should be noted that the small variations in sound pressure level at one microphone position result from data of repeated firings

and that the acceleration data include some from transducers attached to airplane structure and oriented in various directions.

As might be expected, the data exhibit considerable scatter, so that it is possible only to estimate a trend line through the points; however, more significant than the scatter, is the slope of the trend line. Note that if the acceleration amplitude increases by a factor of 10 for an increase of 20 db spl, a direct linear relationship exists between the internal structural vibration amplitude and the adjacent external sound pressure amplitude. In this event, the trend line through the data gives a constant of proportionality between external sound and internal vibration. However, if the trend line has a slope of less than unity, as is the case of the low-frequency data of Fig. 8, a direct linear relationship between internal vibration and adjacent external sound pressure cannot be proved by the correlation.

Several factors might, individually or collectively, be responsible for slopes less than unity. These factors include:

1. Structure borne transmission of vibration from high external noise level areas to those of lower external noise level;

2. Nonuniform structure throughout the fuselage (which undoubtedly contributes to scatter);

3. Nonlinear response of the structure;

4. Unfortunate selection of transducer location with respect to model response.

Before considering any of these factors in more detail, it is helpful to examine the slopes of the trend curves as a function of frequency. Figure 9 summarizes the results of this type of direct correlation for four aircraft type structures, including the B-66 of [Ref. 27], together with Snark, B-58 and B-52. The upper portion of the figure gives the slopes of the trend curves and the lower portion gives the average rms acceleration for each octave band when the adjacent external octave band spl is 150 db. It is clear from Fig. 9 that some correlation between adjacent external noise may exist above 150 cps for the Snark and at the higher frequencies for the other aircraft where the slopes of the trend curves approach unity. Since a large number of randomly selected transducer locations are included in the various surveys, it is doubtful that the accidental location of transducers with respect to the various vibration modes accounts for the lower slopes at the lower frequencies. Similarly, since several experiments give the same general conclusion with regard to the trend curves, it is not felt that structural nonuniformity is a particular factor in the determination of the slope of the trend curve, although it undoubtedly is a most significant factor in the scatter of the individual data.

The role of nonlinear behavior in the structure cannot be evaluated with respect to the trend curves from the available data; however, it is considered to be less important than the fact that the response at any general position in the structure is given by the sum of the noise energy transmitted directly to adjacent structure, plus the noise energy received at more remote locations and transmitted as vibratory energy through the structure to the position. Thus, at higher frequencies better correlation would be expected between adjacent acoustical excitation and response because the vibrational energy transmitted through the structure from remote locations has been attenuated and makes only a minor contribution. Conversely, at low frequencies the vibrational energy transmitted from the areas which have the highest external noise levels to those with lower external noise levels would be expected to exceed the local excitation. This general result might be anticipated since the attenuation of vibratory energy transmitted by bending waves along the fuselage is essentially constant per wavelength. Thus, the high-frequency energy suffers considerably more attenuation than does low-frequency energy when both are transmitted for the same distance through the fuselage.

Correlation of Ballistic Missile Launch Noise and Response

The vibration data given in Figs. 3 and 4 for structure forward of the engine area of ballistic missiles during both launch and maximum dynamic pressure flight, consistently showed that the vibration environment of the large and heavy missiles was significantly less than the vibration of the smaller and lighter missiles. This suggests that the next generation of space vehicle launch platforms, which are anticipated to be considerably larger than the present ICBMs, might have even less severe vibration. On the other hand, changes in launch configuration, engine parameters, or maximum q could result in increases.

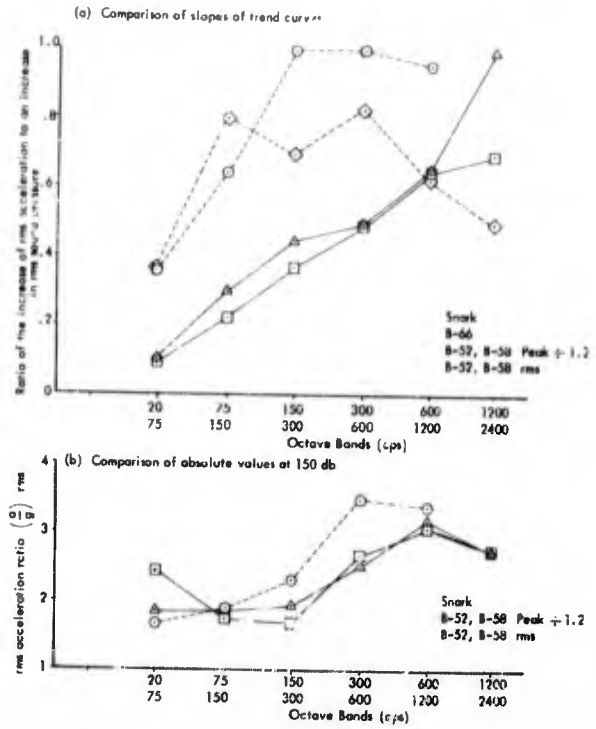

Fig. 9 - Summary of aircraft empirical correlation of external noise with acceleration of adjacent structure

It is, therefore, desirable to determine an empirical relationship between the response and the forcing function, appropriately modified by the vehicle's structural parameters.

It is believed that an empirical correlation can be found by equating the available energy of the forcing function with the mechanical energy of the resulting vibration. It is fundamental that these two quantities are related since all of the incident acoustical energy which is absorbed by the vehicle must result in vibration and be dissipated through damping. Unfortunately, the results of this approach have been inconclusive, probably indicating insufficient sophistication in the definition of one or more of the pertinent parameters.

However, an alternative approach to the correlation of the launch acoustical forcing with vehicle response appears to give encouraging results, and will be discussed in detail. It is well known that complicated (and even simple) structure has many resonances, distributed throughout the frequency range, which occur at frequencies above the fundamental resonant frequency. Consequently, the response of a structure to a random forcing function, which has energy approximately equally distributed over a broad frequency range, exhibits many resonant peaks. Similarly, the majority of the missile launch data in Fig. 3 are representative of the vibration amplitudes associated with one or more of the many resonances which occur in the missile.

It is well known that the natural vibration characteristics of many complex structures can be approximated by individual consideration of each resonance or mode of vibration, assuming it to be essentially unaffected by, or decoupled from, any other mode. The response of the vehicle in any one of these modes can be obtained from expressions similar to those developed for the single degree of freedom if an appropriate definition can be obtained for the amount of the total mass which is involved in actual vibratory motion, and for the effective or "generalized force" on the vehicle. Viewed in this perspective, the total response of the vehicle at any location is simply the sum of the contributions from all of the vehicle's vibratory modes.

The mean square displacement response of a single degree of freedom system to a continuous random forcing function is given by:

$$\overline{x^2} = \frac{Q\,\omega_n\,\overline{F(f)^2}}{k} \qquad (1)$$

where

$\overline{x^2}$ is the mean square displacement,

Q is one divided by twice the damping ratio,

ω_n is the natural frequency in radians/second,

$\overline{F(f)^2}$ is the mean square force per cycle/second

and

k is the stiffness of the system.

The mean square acceleration ratio $\overline{(a/g)^2}$ associated with this response can be readily obtained from Eq. (1) to give:

$$\overline{\left(\frac{a}{g}\right)^2} = \frac{\omega_n\,Q\,\overline{F(f)^2}}{4W^2} \qquad (2)$$

where

W is the weight of the mass.

In order to apply this simple concept of the single degree of freedom system to the empirical correlation of multimode missile vibration, it is necessary to consider the relationship between the generalized force and generalized mass of the vehicle with the single forcing function and single mass in the single degree of freedom solution. For example, the generalized force on a panel in a space vehicle resulting from acoustic excitation depends, in addition to the actual magnitude of the sound pressure, primarily upon the spacial correlation of the sound pressure, or the distances over which the pressure is in phase, in relationship to the distance between modes in the panel's bending response. It is also known that when acoustic phenomena are similar, except for a scale factor, their spacial correlations are similar when compared on a wave number basis. Here, the wave number (kr) is equal to the number of radians per unit distance $(\omega/c = k)$ times a distance characteristic of the size of the object or missile. For the purpose of this correlation, r is defined as the radius of the vehicle, and it is assumed that the spacial correlation is essentially similar at launch for geometrically similar vehicles and similar launch configurations when compared at equal values of kr.

Now, the natural frequency of any mode of two geometrically similar panels varies inversely with the ratio of the panel dimensions (or the scale factor). Consequently, since the distance between nodes on the panel varies directly with the scale factor, the relationship between the scaled spacial correlation of the sound pressure and the scaled shape of the bending panel remains unaltered when compared on a constant kr basis. It can also be shown that the generalized mass of the scaled panel would be the same proportion of the total mass for the same mode of vibration. Hence, it would be expected that any empirical correlation for geometrically similar structures would be a function of kr and that for this purpose Eq. (2) should be written

$$\overline{\left(\frac{a}{g}\right)^2} = \frac{\beta^2\,\omega_n\,Q\,\overline{F(f)^2}}{4W^2} \qquad (3)$$

where

β^2 represents the constant of proportionality for all factors in Eq. (2) and is a function of kr.

It is clear that both the damping in the structure and the type of structure will affect any correlation of response with forcing function, as both additional damping or additional stiffness in a specific vehicle will reduce the response for a fixed forcing function. Therefore, in absence of sufficient data describing these two factors for the various missiles of Fig. 3, a constant q of 15 was assumed for all missiles and all natural frequencies. The missile weight (W) was taken as the gross launch weight, but the stiffness variable remains in the correlation as an additional unknown.

The forcing functions were calculated for surface launch of each of the eight missiles represented in Fig. 3, using Figs. 7 and 10 from [Ref. 1], together with the appropriate engine parameters, to define the external noise environment. The estimated value of mean square force per cps was obtained by integrating the predicted mean square pressure per cps on the vehicle and multiplying this result by the square of the vehicle's surface area. It is obvious that this quantity cannot represent the true generalized force on the vehicle, but it should be proportional to the generalized force for constant values

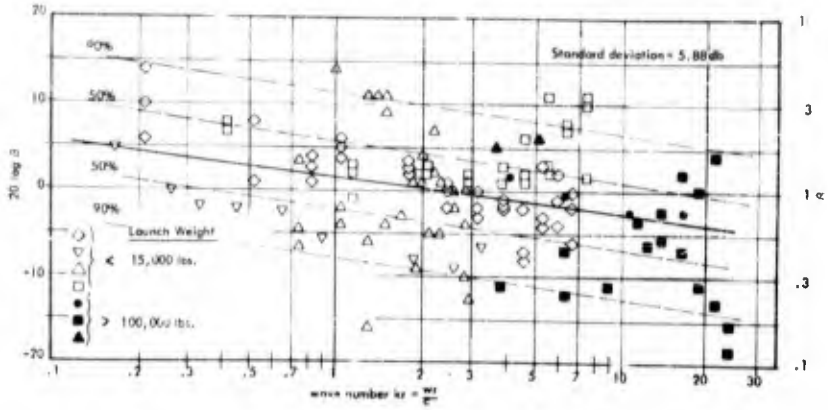

Fig. 10 - Variation of the parameter β with kr for the data of Fig. 3, where

$$\beta^2 = \left[\frac{4 \left(\frac{\eta}{g} \right)^2 W^2}{\omega_n \, Q \, \overline{F(f)^2}} \right]$$

of kr. Equation (3) was then solved for β for each of the (η/g) data points in Fig. 3.

The results are given as a function of kr in Fig. 10. β appears to be almost constant, slowly decreasing with increasing wave number. The standard deviation of 20 log β is approximately 3 db, which indicates that 68 percent of the values of β are between 0.5 and 2.0, as seen in the histogram of Fig. 11. Although it would be desirable to effect a reduction in the scatter of the values for β, it is actually somewhat surprising that the scatter is so small when all the assumptions are considered. Several comments are pertinent, including:

First, it is improbable that all of these missiles are dynamically similar, since a wide variety of structural design concepts are represented.

Second, the forcing functions have been estimated through necessity, as insufficient measured launch noise data has been made available. While it might be thought that the use of an estimator rather than measured data would help to insure consistency, the estimation did not consider minor and largely unknown variations in rocket deflectors and other configuration details.

Third, the assumption of constant Q for all missiles and all frequencies.

Fourth, it is well known that the launch noise environment has a relatively short duration and that the response cannot be considered stationary from the statistical viewpoint. Consequently, variation in response can be expected at the same location for different launches or short duration engine runups.

Fifth, the scatter at various transducer locations and various flights of one missile is seen to be almost as great as the total scatter in the figure.

When these and other factors are considered, the results of this correlation are encouraging. Perhaps the most startling result is the fact that the mean value of β is approximately one, as in the single degree of freedom case. This indicates that the ratio of generalized force to generalized mass remains constant with wave number and that the method of obtaining the forcing function used for the correlation fortuitiously gives the ratio exactly equivalent to the single degree of freedom case.

It would be highly desirable to test this empirical correlation with additional data and, wherever possible, to use measured launch noise data in the comparison. It would be desirable also to test an extension of these concepts to the maximum dynamic pressure portion of flight; however, the necessary flight parameters were not available for such an extension. In lieu of this test, it appears that the value of β in Fig. 11 could be used at a desired confidence level, together with the

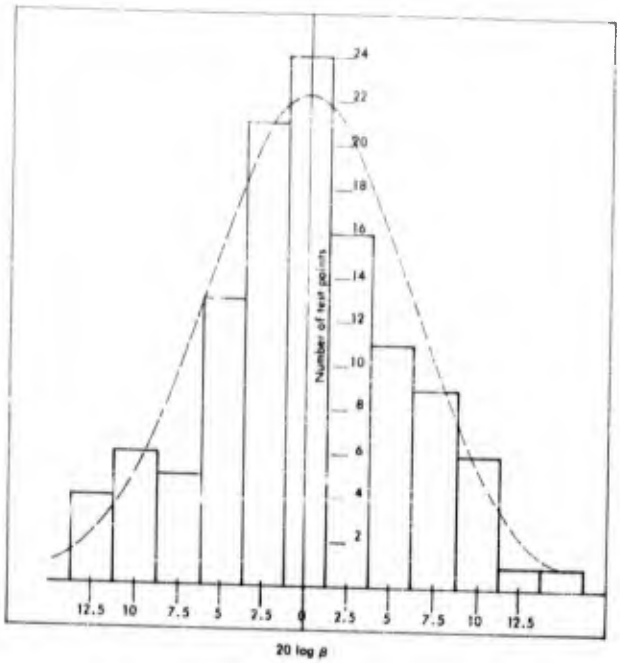

Fig. 11 - Histogram of β from Fig. 10

boundary layer pressure fluctuation forcing function in section 3 of [Ref. 1] to estimate this response.

As a final note on the broad trend exhibited between vibration amplitude and weight of missile, the data obtained in the calculations indicated that the mean square acceleration at a constant value of kr varies roughly inversely with the square of the radius of the missile, or inversely with the two-thirds power of the gross weight. This relationship, illustrated in Fig. 12, is subject to innumerable restrictions and should be interpreted only in this vein. For example, a change in launch configuration to a silo might bring a fivefold increase in the vibration, or less, depending upon the acoustical treatment in the silo. Also, a change in the thrust-weight ratio, mass-stiffness ratio, damping, type of rocket stream, etc., can each affect this generalization, and should be interpreted analytically with Fig. 10 as a possible guide or reference.

CONCLUSIONS

The data and discussions suggest the following conclusions:

1. In general, the maximum vibration in space vehicles occurs either at launch, as a result of rocket noise, or during the maximum, dynamic pressure flight phase, as a result of boundary-layer pressure fluctuations;

2. The rms accelerations on missile structure associated with the resonant amplification of either of the above random noise inputs appears on the order of 2 g for light missiles weighing less than 15,000 pounds, and on the order of 0.5 g for heavy missiles weighing over 100,000 pounds. Note that these amplitudes result from surface launch and present maximum q values and that variation in launch configuration or increase in maximum q will change these values;

3. The rms accelerations of various vehicle resonances increase in level with increasing frequency, at a rate approximately proportional to the square root of frequency;

4. Rms acceleration amplitudes on missile structures near operating rocket engines in both heavy and light missiles are on the order of 3 to 10 g, independent of flight phase.

A correlation between external noise and vibration of adjacent structure showed promise for aircraft at the higher frequencies; however, the results were negative at low frequencies, indicating that the vibration of structure in

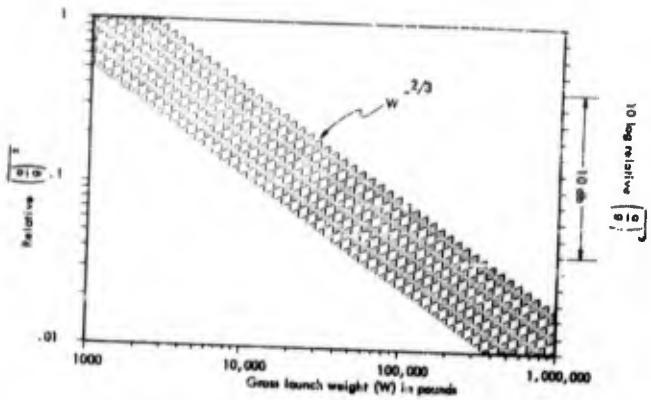

Fig. 12 - Approximate trend for surface launch acceleration as a function of gross launch weight based on present vehicles and engines

regions remote from the location of the maximum noise levels is a summation of direct local excitation and vibration transmitted through the structure from the areas of maximum noise. The results are consistent with the concept of a constant value of attenuation per wavelength of the transmitted vibration bending wave, as demonstrated from a Snark experiment. The data also exhibited differences between types of aircraft which may result from differing structures.

An empirical correlation of missile-launch vibration data showed that prediction of resonant vibration could be made by considering the mean square force per cycle input to the vehicle regardless of spacial correlation, the vehicle's weight, and frequency. The data indicate that the ratio of generalized force on the vehicle to the generalized mass taking part in the motion is constant for constant values of the wave number associated with the noise input.

It is hoped that the discussions of this paper will stimulate the release of additional data regarding missile vibration and the testing of these data against the two methods of empirical comparison discussed herein, as well as stimulate further efforts toward effecting usable empirical correlations.

REFERENCES

1. "Structural Vibrations in Space Vehicles" (to be published as a WADC TR)
2. K. M. Eldred, "Analysis of Noise Data for Convair, Pomona, Tartar LTV-1, SN-3 and SN-6," Paul S. Veneklasen and Associates Report dated 10 Sept. 1958
3. C. Gates, "Environment of Corporal Missile XSSM-A-17," JPL Progress Report 20-185, Apr. 1953
4. R. Blake and M. Oleson, "Vibration Data Obtained During Firings of Vanguard," NRL Report 5102 and Memos 6261-292, -315, and -46 from Oct. 1957 to Feb. 1958
5. H. Beckwith and D. Douglas, "Vibration Data on Thor," Space Technology Laboratories, TR-59-0000-00566, Jan. 1959
6. S. Morrison, H. Beckwith, R. Vargas, and D. Douglas, "Vibration Data for Thor," STL Reports No's. 112, 114, 115, 117, 118, 119, 123, 126, 138, 140, 146, 164, and 176
7. D. Douglas, "Quick Look," Vibration Report of Titan A-5, STL Report, Mar. 1959
8. R. Mains, "Flight Vibration Measurements from Talos," Johns Hopkins Report APL/JHV, CF-2284

K. Kuoppamaki, L. Burns, and R. Lewis, "Program for Determination of Polaris Vibration Environment," Lockheed LMSD 480002, May 1959

10. B. Cameron, "Report of Polaris FTV-1 Series Vibration Environment," Lockheed LMSD 460029, Sept. 1958

11. R. Blake, "Report of Polaris FTV-1 Series Vibration Environment," Part II, Jan. 1959

12. V. Paul, "Predicted Flight Vibration and Acoustic Environment in Polaris," Lockheed LMSD 461291, Oct. 1958

13. B. Cameron, "Preliminary Analysis AX-6 Structure," Lockheed DD 16920, July 1959

14. H. Beckwith, "Vibration Data on Atlas Series A," STL GM-TR-0165-0048, Sept. 1959

15. M. Hines, H. Beckwith, and D. Douglas, "Vibration Data for Atlas #3B, 4B, 5B, 8B, 9B, 11A, 11B, 13A, 15A, 16A." STL Reports Oct. 1958 to Nov. 1959

16. A. Fine and D. Bell, "Captive Firings of Terrier," NOLC Report 215, Sept. 1955

17. G. Tatum and B. Delaney, "Review of Shock and Vibration Test Requirements for Terrier," Vitro TR-34, Feb. 1952

18. H. Beckwith, "Vibration Data on Final Stage Able-1," STL Report, July 1958

19. W. S. Shipley and N. F. Jacobson, Jet Propulsion Laboratory, p. 61, Shock and Vibration Bulletin, No. 26, Part I, Sept. 1958, CONFIDENTIAL

20. K. M. Eldred, "Base Pressure Fluctuations" (to be published in Journal of Acoustical Society)

21. E. J. Lunney and C. E. Crede, "Establishment of Vibration and Shock Tests for Airborne Electronic Equipment," WADC TR57-75, Jan. 1958

22. Convair Report FZS-4-149, "Method for Predicting B-58 Vibration Environment," Oct. 1957

23. Convair Report FZM-4-803, "B-58 Environmental Vibration Qualification Tests," Feb. 1958

24. Convair Report FZS-4-160, "B-58 Predicted Vibration Environment and Vibration Range Curves for Environmental Test," Feb. 1958

25. D. T. Egbert and W. W. Harter, "Vibration and Acoustic Environment Measurements as Applied to Snark Missile Equipment," Shock and Vibration Bulletin, No. 24, Feb. 1957

26. R. Mustain and B. Vermer, "Snark Acoustic and Vibration Data Analysis," Northrop Report NAI-56-686, Vols. I and II, 1956, N69D Missile N3305, Nov. 1956; NAI-57-584, Nov. 1957; NAI-57-582, "Internal Acoustical Treatment," Jan. 1958; NAI-57-584, "Salted Grain Booster Bottles," July 1958; NAI-29-25, "Summary of Acoustic and Pressure Data Booster Blast Off Program," Dec. 1958

27. D. C. Kennard, Jr., "Some Vibration as Exemplified by the RB-66B Airplane," WADC Technical Note 59-156, May 1959

* * *

AN ESTIMATE OF MISSILE ENVIRONMENTAL ACOUSTIC PRESSURES RESULTING FROM A SUBSURFACE LAUNCH, BASED ON MODEL TESTS*

Edwin C. Kamps
Convair
San Diego, California

The tests employed a 1/30-scale model Atlas, normal operating exit temperature and jet velocity and approximately 1/900 of full-scale model thrust and mass flow. Excellent correlation was achieved between the acoustic output of the model and of the full-scale Atlas.

INTRODUCTION

Vulnerability of the Atlas missile to attack while in the surface launch configuration prompted a study to determine the feasibility of a subsurface launch. To preclude the possibility of a missile failure due to equipment malfunction resulting from the expected increase in environmental acoustic pressures in the subsurface installation, a number of tests were run to provide a reasonable estimate of the expected sound pressure levels.

Tests using a 1/30-scale model of the Atlas missile were employed to establish the full scale acoustic environment for several proposed conditions. This model was selected because it was considered that it would provide accurate data for a minimum expenditure of time and materials.

Free-field measurements [1], made previously by Bolt Beranek and Newman, of full scale surface static firings had established near- and far-field sound pressure levels. Operation of the model under similar free-field conditions was required so that correlation between the acoustical outputs of the two sources could be effected. That is, a comparison between sound pressures at particular corresponding locations was required so that amplitude and frequency scale factors could be established. These factors were required so that they might be applied to data derived from subsurface model firings to enable a reasonable estimate of full scale pressures.

MODEL RELATIONSHIPS

The physical dimensions of the model employed were 1/30 those of the full-scale Atlas missile. The operating parameters were identical to those of the Atlas at the time this study was made, although considerable improvement in performance has been obtained since that time. The approximate operating exit temperature was 5000-degree fahrenheit and the exit velocity was approximately Mach 3. Model thrust and mass flow were direct functions of the scale and were approximately 1/900 full scale or 180 pounds per booster and 1 pound per second per booster, respectively.

The establishment of a sound pressure level in a particular volume is dependent upon the acoustic power of the source. If identical directivity indices are assumed, a ratio of acoustic powers between two sources can be established by comparing a sound pressure level resulting from one source with that resulting from a second source, provided the point of measurement remains fixed. Since

*This paper was not presented at the Symposium.

the estimated ratio of acoustic powers between the Atlas missile and the model was 900:1, measurements at equal distances would prove difficult. Therefore, a comparison was made between sound pressure levels at identical angles but at more convenient radial distances.

Lighthill established that the acoustic power (PWL) generated by a source of this type is a function of the exit cross sectional area (A), the exit velocity of the fluid (V), the density of the fluid (ρ) and the atmospheric speed of sound (a).

$$PWL \approx \frac{AV^n\rho}{a^5} .$$

Considering that the model and the Atlas had identical V, ρ and a, the ratio of acoustic powers was merely a function of the area ratio which was 900:1.

The sound pressure level (SPL) at a particular radius R is equal to the acoustic power per unit area.

$$SPL = \frac{PWL}{4R^2} .$$

If the ratio of the acoustic powers were 900:1, the sound pressure level resulting from the operation of the Atlas, measured at a particular radius (R) and angle, would be equal to that resulting from operation of the model when measured at a distance of R/30 at the same angle. Verification of this relationship would establish equivalence of the sound pressure levels resulting from operation of the model with those of the Atlas, provided that a factor of 30 was applied to all linear distances.

The initial assumption of equivalent directivity indices was necessary due to limited full-scale data. Nevertheless, examination of WADC studies of fourteen types of rockets [2] indicated that this assumption was valid. Further verification was provided by the agreement of the model test and full-scale data at two points (Figs. 1 and 2).

Frequency distribution differences between the model and full-scale sources were resolved by utilization of the Strouhal Number

$$\frac{fD}{V} ,$$

where

f = frequency

V = jet velocity

D = exit diameter of the source.

FREE-FIELD MODEL TESTS

Acoustic pressures were measured by means of two Altec Lansing M-14 microphone systems employing two 21 BR 180 microphones. FM recording techniques were employed and the signals were recorded on an Ampex 800 series magnetic-tape recorder. The frequency response of the entire system was 40 to 15,000 cps.

The model was operated in an upright position with the jet exhaust deflected at an angle of 90 degrees (parallel to the ground). There were no reflecting surfaces in the vicinity of the test area.

Two microphone positions were selected to facilitate comparison with full-scale data, as well as to provide free-field data at the particular points. One microphone was located 3.7 feet from the deflector face at an angle of 34 degrees from the thrust axis. The face of the microphone pointed up to minimize ground effects and was located in the horizontal plane of the jet exhaust. The second microphone was positioned 4 inches from the body of the missile with the face located 9 inches above the booster exit.

Acoustic pressures resulting from static firings of an Atlas missile [1] indicate that the sustainer rocket does not significantly contribute to the acoustic levels which result from booster rocket operation. Therefore, to simplify operation of the model, all measurements reflect the result of booster operation only.

The data resulting from several model firings are compared with full scale Atlas data in Figs. 1, 2, and 3. Figures 1 and 2 are plots of octave level sound pressures versus Strouhal Numbers for the two measurement positions. Figure 3 is a replot of the data of Fig. 2 to show the actual octave levels occurring in the area of the missile instrument pod compared to the scaled pressures created by the model.

Examination of the figures indicates that reasonable agreement was obtained by applying the scale factors discussed earlier and the 2- to 3-db differences noted were probably not due to error in scaling theory but rather to measurement errors.

FLY-OUT TUBE MODEL TESTS

Establishment of correlation between full-scale and 1/30-scale model free-field data

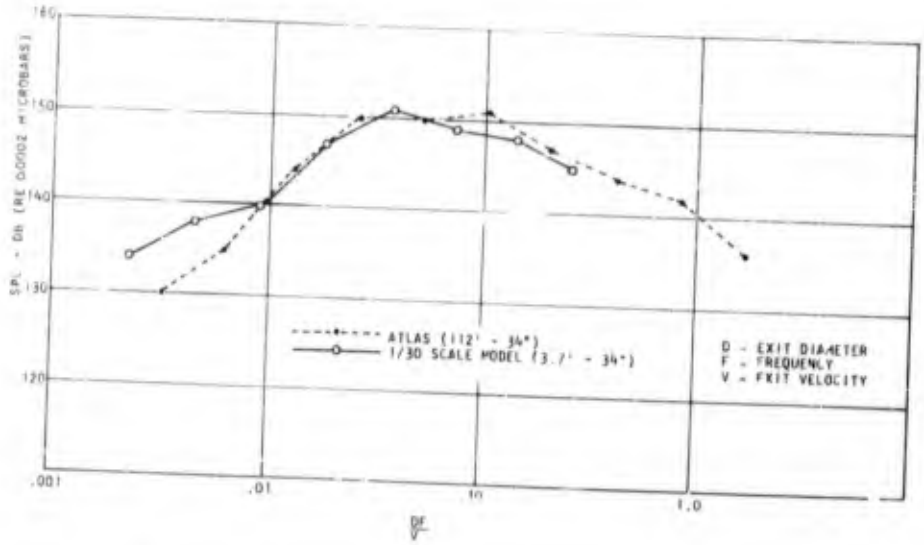

Fig. 1 - Free field. Octave sound pressure levels versus Strouhal number (DF/V)

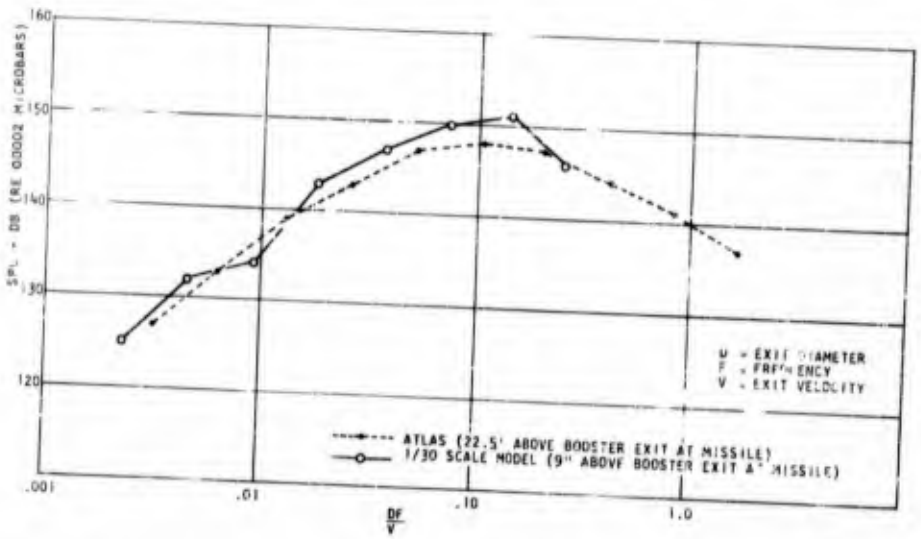

Fig. 2 - Free field. Octave sound pressure levels versus Strouhal number (DF/V)

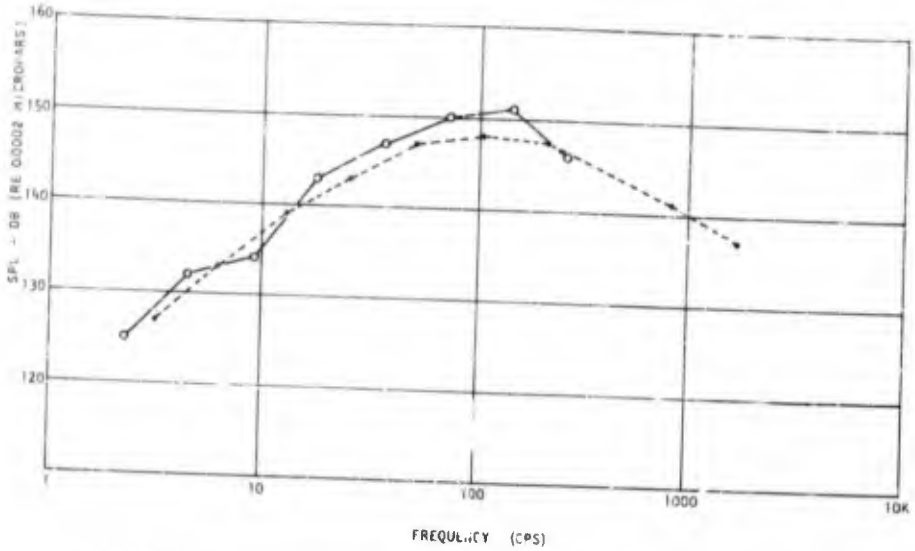

Fig. 3 - Free field. Octave sound pressure levels versus frequency in cps

gave reasonable assurance that scaling could be successfully applied to the model under confined conditions and that full-scale pressures could be accurately described from 1/30-scale model pressures. Therefore a 1/30-scale model of the proposed "fly-out tube" was employed in conjunction with the 1/30-scale missile model to simulate the desired mode of operation.

The "fly-out tube" model consisted of a U-tube configuration. The legs were circular stainless steel tubes approximately 38 inches long with wall thicknesses of 0.050 and 0.125 inch and inside diameters of 8.8 and 7.2 inches, respectively, for the intake and exhaust tubes (Fig. 4). A flame deflector, consisting of a hollow graphite block, joined the two tubes and directed the rocket exhaust at an angle of 180 degrees. The entire assembly was buried in sand so that acoustic radiation from the walls of the tubes would not influence the desired data.

Four Altec-Lansing 21BR200-1 microphones were employed to measure the acoustic pressures in and about the fly-out tube model. Two microphones were flush mounted in the intake tube; one was located 9 inches above the plane of the booster nozzle outlet (a point corresponding to the center of the equipment pod on the full-scale missile) and the other was mounted 32 inches above the same reference level. The microphones were resiliently mounted to minimize spurious signals which could result from excessive microphone vibration. Acoustic pressures at the mouth of the intake tube were measured by a microphone mounted 4 inches above ground, in an upright position, and 4 inches from the intake tube. Another microphone similarly mounted in relation to the exhaust tube, was used to measure pressures at this point. An accelerometer was mounted on the rocket model directly opposite the microphone located 9 inches above the plane of the booster nozzle outlet. The purpose of obtaining the accelerometer data was to assure that vibration of the missile model did not distort the desired acoustic data. Thermocouples were also employed at several locations in the tube to preclude possible errors due to microphones exposed to excessive temperatures during the tests. All data were recorded on magnetic tape using the same equipment as in the free-field tests.

Sound pressure levels were recorded under constant thrust conditions, as a function of the position of the missile in the tube. The selected positions were 0, 6, 8.25 and 18 inches above the initial launch positions, which corresponds to 0, 15, 20.6 and 45 feet for the full-scale tube.

The acoustic pressure data resulting from these tests were analyzed in octave and fixed frequency bands of 5 and 200 cps.

Comparison of the data obtained at the various operating conditions indicates that the position of the missile in the tube affects only

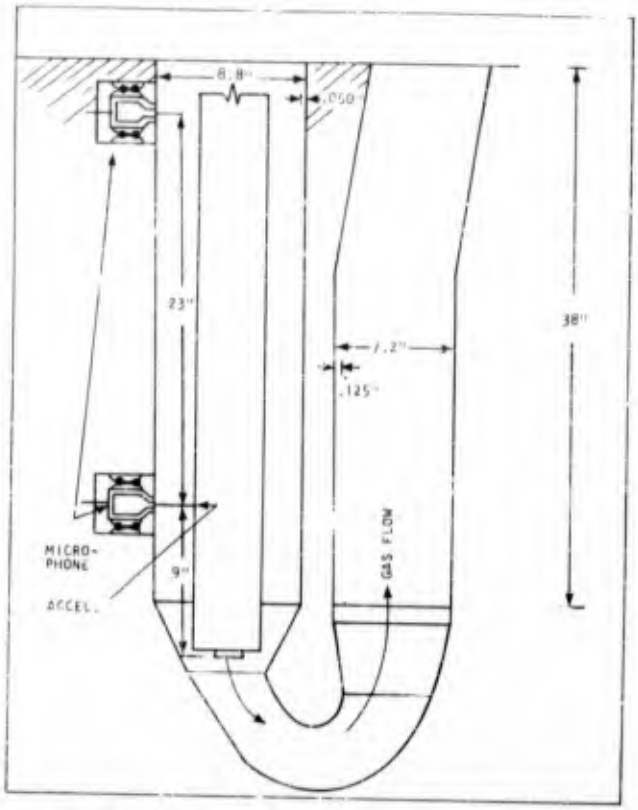

Fig. 4 - 180-degree U-tube subsurface launcher

the acoustic pressures at the frequencies related to the harmonic modes of an open-open pipe whose effective length is equal to the total length of the "fly-out" tube. For the model configuration tested, the fundamental frequency was approximately 75 cps, which is equivalent to 2.5 cps full scale. Extrapolating the measured pressure levels at this frequency with the pressure distribution function in the tube indicates that a maximum rms pressure level of 171 db (re 0.0002 microbar) will occur at the center of the equipment pod as the missile leaves the tube. This corresponds to an rms pressure of 1.0 psi.

Octaves not containing this frequency component did not appear to vary as a function of either missile or microphone position. Therefore, other acoustic pressures were averaged for the four missile positions and the two microphone positions. These data are shown in Fig. 5 as Octave Sound Pressure Levels versus Strouhal Number. A comparison of the octave pressures of the confined model with those of the free-field condition shows that the increase due to confinement ranges from 7 to 20 db per octave. The narrow-band data analyses indicated that no outstanding discrete frequency peaks were present. It appeared that reverberation was the primary factor influencing the increase in acoustic pressure over the free-field condition.

An additional requirement of this investigation was to determine the effect, if any, of variation of the exhaust deflection angle on the internal sound pressure levels. Therefore, another test model U-tube was constructed similar to the 180-degree U-tube just described with the exception that the rocket exhaust was directed at an angle of 150 degrees rather than 180 degrees. Instrumentation and test procedures were the same as for the 180-degree U-tube test.

Analysis of the data resulting from these tests indicated that no significant differences existed between the resultant acoustic pressures generated in the 180-degree or the 150-degree U-tube. The fundamental mode of the open-open pipe was again strongly stimulated and the general level at other frequencies did

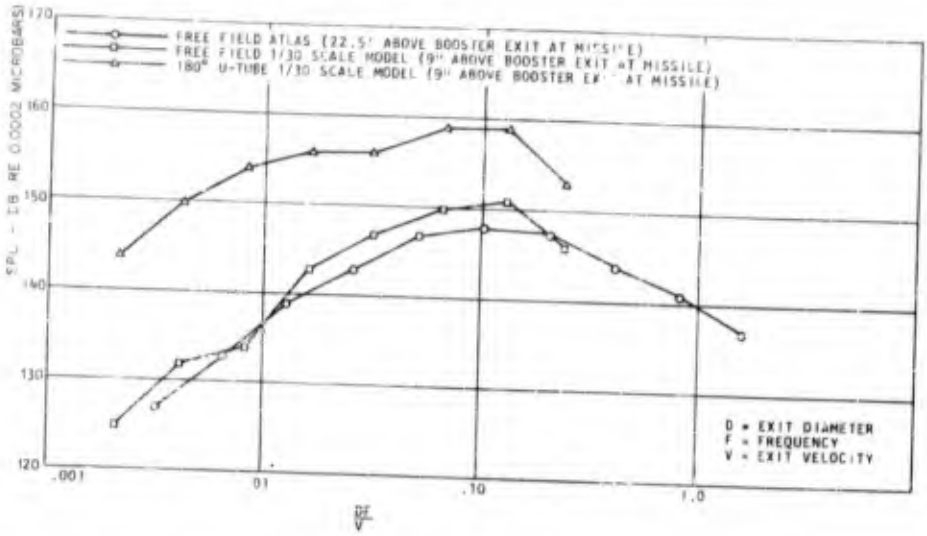

Fig. 5 - Octave sound pressure levels versus Strouhal number (DF/V)

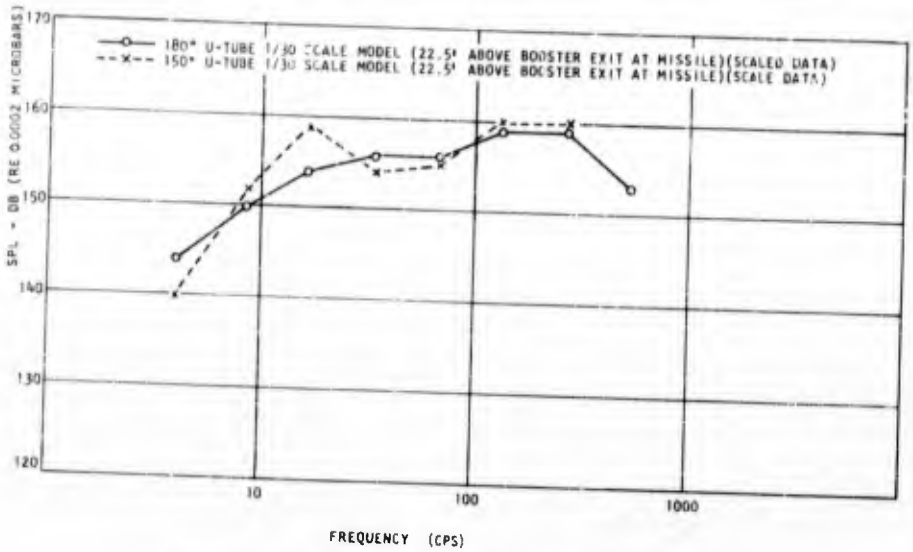

Fig. 6 - Octave sound pressure levels versus frequency in cps full-scale Atlas missile

not vary significantly from the 180-degree levels. Comparative data are presented in Fig. 6 as octave sound pressure levels versus frequency for both the 150-degree and 180-degree U-tubes.

CONCLUSIONS

The conclusions based on the results of this study were:

1. A reasonable estimate of the expected acoustic levels accompanying a proposed subsurface launch of an Atlas missile had been provided.

2. An equipment fragility study would have to be made to preclude possible equipment malfunction, but in the event of a possible problem it appeared a reasonable solution could be effected by improving the noise reduction of the equipment canisters

or by increasing the absorption of the "fly-out" tube.

3. The possibility of structural fatigue damage was considered slight excluding a possible coincidence of the basic missile mode and the open-open tube resonance. If this occurred, determining one or the other could easily resolve this difficulty.

Therefore, it appeared that no unusual acoustical problems would emerge as a result of a full scale effort.

Doubts had been expressed concerning the reliability of test results obtained by employment of a model of such reduced scale. However, considering the excellent correlation achieved between the full-scale and 1/30-scale model data, this method has been shown to produce reliable design information at minimum cost.

REFERENCES

1. Bolt, Beranek, and Newman, Inc., "Acoustical Environment and Structural Vibration of Model 7," Report No. 507, dated 13 Sept. 1957.

2. J. N. Cole, et al, "Noise Radiation from Fourteen Types of Rockets in the 1,000 to 130,000 Pounds Thrust Range," WADC TR 57-354, dated Dec. 1957.

* * *

Section 5
PANEL SESSION

THE ESTABLISHMENT OF TEST LEVELS FROM FIELD DATA

Moderator: Professor Charles E. Crede
California Institute of Technology

Panelists: Mr. Maurice Gertel
Allied Research Associates, Boston
Mr. Neal Granick
NASA, Goddard Space Flight Center
Dr. Thomas Rona
Boeing Airplane Company, Seattle
Dr. Robert Mains
General Electric Company, Schenectady
Dr. Allen Curtis
Hughes Aircraft Company, Culver City

Those concerned with determining the probability that a given equipment will fail in service are faced with the problem of translating environmental data into realistic laboratory tests. Simulation is the art of laboratory testing to create a condition that is representative of the actual environmental condition to which equipment will be subjected. In this context, a simulated environment is not necessarily similar to the actual environment but rather has the same damaging potential. Various criteria of damage have been proposed to evaluate this damaging potential. These, together with analytical and empirical techniques for establishing laboratory test levels were considered by the panelists and form the subjects of the prepared presentations. In presenting the general discussion which followed, a verbatim transcript has not been attempted, but comments have been condensed and consolidated under a number of general headings.

OPENING STATEMENT OF THE MODERATOR

Dr. Crede

This panel has been assembled (1) to present a cross section of the latest thinking on the problem of establishing test levels from field data and (2) to give members of the audience an opportunity to obtain comments on their problems from the experts on the panel. I have deliberately avoided saying that the experts will answer your questions because there are no known answers to many questions that can be asked.

Essentially everyone engaged in the design or manufacture of equipment for military use has a problem in determining test conditions. The very stringent requirements for reliability of such equipment dictates that the equipment should be subjected to shock and vibration tests in the laboratory. The objective of such tests is relatively easy to state: The laboratory tests should cause all failures and malfunctions that would later occur in

field service test should not be so stringent as to require excessive overdesign of equipment. This objective sounds innocent enough, but attempts at its implementation have introduced problems of enormous complexity.

It was common practice before World War II to subject at least some types of equipment to laboratory shock and vibration tests; however, the experiences gained during World War II brought about some drastically different viewpoints on laboratory tests. In the first place, the severity of shock encountered during naval warfare was found to be much greater than formerly assumed, notably in connection with naval ships. In the second place, some of the problems which arose brought about a greatly increased interest in the measurement of field conditions and in treatment of equipment design by theoretical methods. The measurement of shock and vibration during those early days was handicapped by the unavailability of good instruments and by the lack of good techniques in the use of such instruments as did exist. We have had great advances in instrumentation have occurred in recent years, and lack of field data of good quality no longer is an important obstacle to the orderly formulation of laboratory testing procedures. An insufficient quantity of data may be a limitation in some instances; however, the major problem at the moment is in the area of applying measured field data to the specification of laboratory tests. Perhaps some of the discussion during this evening may point the way to a better understanding of this problem.

Laboratory tests, as laid down in specifications for equipment, are in many cases a mixed blessing. On the whole, they represent a better estimate of the requirements to be placed upon equipment than could be expected from every user of the specification, many of whom are unacquainted with the actual field conditions. To this extent specifications are desirable. From a contractual viewpoint, specifications are necessary to define the conditions which the contractor is required to meet. Unfortunately, specifications which set forth required tests create the impression that ultimate field conditions are well known and will be effectively simulated by the laboratory test specified. It has been my experience that users of specifications have much more confidence in the requirements set forth therein than have the persons who formulated these requirements initially.

Before we had many valid measurements of field conditions, we had specifications that required shock and vibration tests. Often the testing requirements were based upon concepts best known only to those responsible for formulating the requirements. At the present time, even with a much greater quantity of measured data, laboratory tests must be specified even though the measured data cannot be applied directly to the specification of tests. Our panelist Mr. Granick has had extensive experience in laboratory testing and is familiar with the concepts used to formulate testing procedures. I will ask him to outline the considerations that are important when specifying laboratory tests when field measurements are available for this purpose.

EMPIRICALLY FORMULATED SHOCK AND VIBRATION TESTS

Neal Granick

I remember a session from another Shock and Vibration Symposium, not long ago, in which a young man rose to ask a very searching question. As I recall, the topic of that session also was the interpretation of field data. The discussion that preceded his question had centered largely on data reduction and analysis with the usual quarrelsome details that bear so importantly on the value of the data that had been presented. Now, what he wanted to know was simply this: After the current controversies were settled, and agreement somehow is reached on the correctness of the information . . . what will be done with it? He asserted that he too had collected data from field measurements, but still was at a loss to see how this could be fitted validly into a specification. Could anyone there in the audience help him answer this question? After a few moments of stunned silence, some of the more courageous souls in the audience tried. It seemed to me that the opinion of each successive speaker only confused him all the more, for each idea was different.

It is almost axiomatic that the more one knows about the possibilities for error in trying to interpret and employ field measurements for developing specifications, the less confident he will become in using this approach, alone. For the core of the problem does not just reside in whether the environment is random, quasi-sinusoidal, or some complex combination. Nor is it simply a question of the extent of errors introduced by instrumentation and telemetry limitations. There are so many other critical factors that bear on the value of a closely derived

specification that have nothing whatever to do with the measurements that underly it. Let me cite a few of these.

To begin with, how many measurements should be taken to state the environment expected at every different component location in a flight vehicle of today's complexity? Would you say ten thousand, a hundred thousand, or a million? I'm sure I don't know the answer, but the number must be astronomical. In the second place, if we had all these measurements, how well do you suppose we could duplicate them in the laboratory? Isn't it almost universal practice to test with rigid fixtures and colinear vibration; conditions that are practically non-existent in the field? Thirdly, when vibration in a laboratory test becomes uncontrollably noncolinear, what relation does this bear to a field measurement that we were trying so vainly to reproduce? If we take time enough to reflect on these matters, then sooner or later we arrive at a single conclusion. There is a restricted use to which measurements can be put, so we must augment our data with certain experience and judgment factors.

In my opinion, field measurements can be applied directly only for specialized problems. For example, measurements can be used to describe the conditions that exist at the interface of a payload with a boost vehicle. This is particularly true if we have some knowledge of the structural impedance conditions that exist at this interface; however, even here one must be cautious not to extend these measurements to include other payloads indiscriminately.

For the problem of testing a multiplicity of separate components which may be used in the same payload, I am equally convinced that we must rely heavily upon other sources of information to write our vibration test levels. The specification which defines component tests always must be written well in advance of the flight vehicle's operational readiness date. Hence, usually there are few measurements from the vehicle itself that would be pertinent to this task. Nevertheless, there are other sources of information from which we can draw. For example, extrapolated data taken from other vehicles can be used if the measurements are numerous enough and have been interpreted with a liberal factor of safety. Secondly, we can perform transmissibility studies on likenesses of the vehicle or payload which can yield rewarding details about the component vibration. Lastly, past testing history can be employed for classifying component vulnerability. This information can be used for deciding which components will need to be protected without even running a test.

I am sure there are people in the audience who have used these empirical techniques with reasonably good success to develop a component evaluation program without benefit of accurate pertinent field data. The point is, that to be successful one must embrace a rather conservative attitude about what one will accept when the tests reveal the component to be marginally acceptable. Since the test that was specified is not truly related to a known field environment, but was employed for the very purpose of screening possible weaknesses, to accept marginal performance from a component is to invite disaster. These are the building blocks of the systems. Reliability cannot be built on a weak foundation.

To summarize, I would advise that we employ field measurements directly for specifying tests only to the extent that they are modified to take into account limitations in their number, dependability, and in our own ability to reproduce these field conditions in a laboratory. Any decision to modify previous specifications after analysis of flight data should be carefully weighed against the confidence level that these few measurements truly reflect all the conditions implied by their usage.

Dr. Crede

When a person attempts to define shock and vibration independently, he encounters some difficulty because he often finds that in some respects one is a special case of the other, or vice versa. Nevertheless, in a non-technical sense, shock and vibration are considered separately. They are discussed in different paragraphs of equipment specifications, and the shock and vibration tests are usually conducted upon different types of testing machines. The distinction is further justified because, even though the two phenomena are generically related, different concepts of data analysis are found convenient at least for purposes of specifying laboratory tests.

The fundamental components of a measurement system are a transducer which creates a signal proportional to the instantaneous value of some parameter of the vibration, for example, acceleration, and a recorder which transcribes a time-history of the signal from the transducer. This signal may be transcribed on paper, film or magnetic tape, as a function of elapsed time. This time-history

is the fundamental form of the measured data, although with some types of instrumentation systems it may be transformed to another form before the analyst has an opportunity to work it over. Although the time-history is the fundamental form of the data, usually it is not useful except in its most elementary form as a basis for the specification of laboratory tests. Some data reduction or data analysis must first be done, often applying one concept of data reduction if the ultimate objective is a vibration test and another if the objective is a shock test. Dr. Curtis has had extensive experience in data reduction, and I will ask him to outline some important considerations in the reduction of data for the purpose of specifying laboratory vibration tests.

REDUCTION OF MEASURED VIBRATION DATA FOR USE IN SPECIFYING LABORATORY TESTS

Allen Curtis

To restrict these comments to the reduction of measured data rather than the evaluation of data, we should perhaps start on the basis of following assumptions:

> The measured data to be reduced must have adequate accuracy and fidelity.
>
> The data must have been obtained at a sufficient number of known operational conditions to define, with some confidence level, the complete environment.
>
> The locations at which measurements were made were chosen to yield data which can be interpreted by designers or those responsible for deriving test levels.

Before analysis can commence, it is necessary to know a few rather obvious facts such as the frequency range over which the data is valid, the sensitivity of the particular instrumentation channel, etc. Let us assume that all these "details" have been taken care of and that we have a record of the time-history over some time-period, during which the physical processes which generate the vibration are not necessarily constant. Now what are the quantities needed by the person who has to evaluate the data? If we leave for the moment, the techniques of correlation in the time domain, and confine ourselves to the more common (though not necessarily superior) techniques of spectral analysis in the frequency domain, there are probably four major quantities of interest:

> The variation, at a particular time (or over a restricted time interval) of the vibration magnitude as a function of frequency, i.e., spectral analysis.
>
> The variation, at a particular frequency (or in a particular frequency band) of the vibration magnitude with time. The variation with time can then be correlated to physical processes. This I like to call magnitude time-history analysis.
>
> The characteristics of the vibration magnitude, e.g., is the vibration sinusoidal, quasi-sinusoidal or a random process.
>
> The accuracy of, or the confidence band which must be placed about, the observed values due to uncertainties caused by the measurement techniques and/or the method of data analysis employed.

Of these four items, I think the first, spectral analysis, has been much discussed, and I would like to pass to the second one, which perhaps has received less attention. We can probably all agree that a significant proportion of vibration failures are caused by fatigue. Thus, if our knowledge of cumulative damage in fatigue is to be exploited, the time periods for which the vibration magnitude equals or exceeds various levels must be provided in describing the field environment. Ideally the variation in each frequency band should be given although experience shows that the variation of the overall magnitude often suffices since the shape of the spectrum is usually maintained.

A paper presented at this Symposium by Mr. Kelly* describes such a time variation analysis carried out to ascertain the variation of vibration during the burning of a rocket motor, and illustrates the fallacy of averaging the vibration over the total burning time.

The last two items, which are somewhat interrelated, have perhaps received the least attention. Consider the question of the

*R. D. Kelly, Hughes Aircraft Company, "A Method for the Analysis of Short-Duration Nonstationary Random Vibration," p.

characteristics of the vibration magnitude. It is just as incorrect to assume that all vibration is random and should be described in terms of spectral density as it is to assume that all is sinusoidal. If meaningful tests are to be specified, then the data reduction process must determine the appropriate quantities by which to describe the vibration magnitude. In general, this means that a statistical analysis of the vibration in each frequency band must be carried out. Only in this way can we know for example, whether a peak which shows up in a spectral analysis is really a sinusoid, or at least a coherent signal, superimposed on a general random process. We have had a very real example of this in the vibration due to resonant burning at the recent finding of a vintage solid-propellant rocket motor. Also, in this way, we may justifiably specify a random, sinusoidal or combination test procedure.

The last item regarding the confidence bands which must be placed about the measured data is probably rather new, and I think I see some members of the audience who I hope will contribute more than I on this subject. Essentially the problem can be reduced to giving up our gay practice of saying, "The vibration level is so much," and adopting a more realistic attitude by saying, "The vibration level observed is so much," and, based on the sample size and data reduction method used, lies within these two levels with a certain probability. Of course, this can only be done if we have made a statistical analysis of the signal so that we know how to go about establishing these confidence bands.

A final comment which seems appropriate concerns the format in which this reduced data is presented. Assuming that the analysis has yielded some sort of plot of vibration level versus frequency, it would appear desirable to add to the curve some ancillary information to aid in the evaluation of the data, either by the immediate user, or at some later time. For example: the bandwidth of any filters used; the filter sweep rate employed, if any; the integration or averaging time employed; the time duration of the data sample; and perhaps something regarding instrumentation employed. Of course, the employment of confidence levels takes most of these factors into account and serves the same purpose. I mention this because many of us have managed to obtain data from one source or another but hesitate to use it for lack of this type of information. Thus, inclusion of this type of information with the reduced data would broaden its usefulness considerably.

Dr. Crede

Now, if the objective is to specify shock tests rather than vibration tests, it is common practice to take a somewhat different viewpoint of data reduction methods. I will ask Mr. Gertel to outline some important considerations in data analysis for the purpose of specifying laboratory shock tests.

REDUCTION OF MEASURED SHOCK DATA FOR USE IN SPECIFYING LABORATORY TESTS

Maurice Gertel

My purpose on this panel is to present a technique for analyzing and reducing transient environmental shock and vibration data into a form which will permit a rational development of future laboratory shock test procedures. The methods of shock data reduction that I will present are known to many of you as Shock Spectra techniques. I will review the concept briefly for the benefit of those who may be new to the problem. Shock Spectra (sometimes called system response spectra) are in effect an analytical extension of a philosophy which has been successfully used in the development of some of the empirical shock tests which are currently in vogue. In particular, I wish to cite the example of the Navy's Hi-Impact shock machine. This test machine was developed on the basis of producing damage in equipment similar to the damage which was experienced under actual combat conditions. Equipment response deflections are associated with damage if high stresses result, hence the association of shock spectra with damage. The shock time-history of the Navy test machine bears little, if any, resemblance to the actual shipboard shock environment, yet it has successfully demonstrated its ability to screen out equipment which in all probability would not withstand the rigors of Naval combat.

The important point in my presentation is that shock procedures should be developed on the basis of producing a desired degree of damage in equipment. The method of data reduction should therefore be capable of discerning the damaging potential in the environment as opposed to defining the environment itself. This approach doesn't rule out shock tests which are an exact reproduction or duplication of an actual shock environment. In some instances where the waveform is simple, this might be desirable. The concept of damage simulation, however, does open the possibility

of shock tests whose time histories have no physical resemblance to actual environments, as in the example of the Navy shock machine. Just to make the case a bit stronger, the method of shock data reduction which is applicable for the damage simulation concept is equally useful for describing both simple and complex shock conditions; whereas other techniques concerned primarily with defining the input (such as Fourier analysis) are extremely difficult to apply to complex shock patterns.

The data reduction parameters involved in the damage simulation or shock spectra concept may be readily determined by examining the idealized equipment shown in Fig. 1. Here each idealized mass spring combination may be considered as a separate, simple component in a large equipment, or as the effective mass and compliance of each normal mode of vibration in a complex structure. In either case, it can be seen from the equation of motion in Fig. 1 that the response acceleration—of mode or component—is proportional to the relative deflection across the elastic element of the system. (Damping in most structures is small and can be ignored here.) Inasmuch as stress in any element is proportional to its deflection (or strain), the stress in each element of the system is proportional to the response acceleration of the mass. In general, the response of a structure to shock is vibratory motion and continues for an appreciable number of oscillations. The damage which can occur in each structural element (or mode) in Fig. 1 is a function of whether the vibratory response accelerations produce deflections and stresses which exceed ultimate stress or safe fatigue allowables. Unless the shock is extraordinarily severe—e.g., resulting from a crash or explosion—failure rarely occurs during a single application of shock. Rather, damage tends to accumulate progressively during several repetitions of the shock and repeated reversals of vibratory response until failure ultimately occurs.

With this brief background, it is perhaps evident to many of you that the concept of data reduction for shock damage simulation has much in common with defining fatigue inputs for structural materials. By analogy with structural fatigue problems, the parameters for shock data reduction are (1) response acceleration (or stress) and (2) the number of cycles or repetitions of response peaks. Natural frequency is of course an important parameter here so that the damaging potential of the shock can be examined in relation to different components.

Figure 2 shows, step by step, the process of reducing shock data into a form which is useful for developing shock tests with damage simulation as the objective. First, the time-history of the shock input is applied to a single-degree-of-freedom analog of a simple equipment and response time histories are obtained for different system natural frequencies. An operational analog computer representation of the simple system is used here for illustrative purposes. Actually, mechanical analogs or numerical computation techniques can be used to determine the response; however, operational analog computers are generally conceded to be most versatile and convenient for the type of fine-tuning control of the system natural frequency and damping which is required here. I might add that there is no standard on the value of damping to use in this analysis, although Q's of 50 to 100 are usually convenient and represent typical values for structures.

The second step in the shock data reduction process is to summarize in digital form

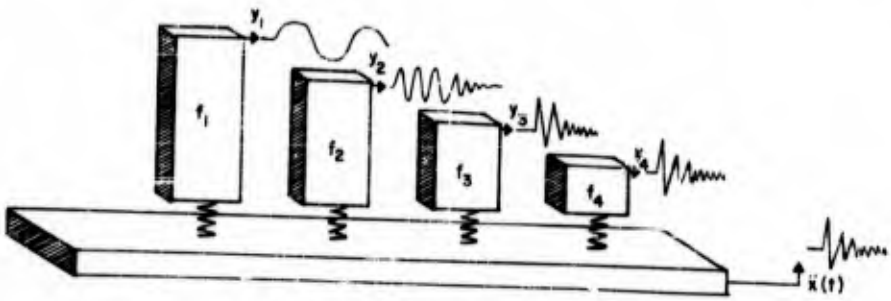

Fig. 1 - Idealized equipment

the important characteristics embodied in the system response time histories. A convenient way of accomplishing this is to obtain histograms or bar charts denoting the number of cycles of response peaks embodied in the response time history. There are perhaps many ways of accomplishing this and one method is illustrated in Fig. 2. Horizontal graph lines of any convenient increment are superimposed on the response. The procedure is to count the number of times the response crosses each incremental level. Dividing the total number of crossings at each increment by 4 gives the cycle count. (It is usually convenient to lump positive and negative amplitudes together for the cycle count.) In Fig. 2 the length of each bar in the chart indicates the number of peak responses which exceed the response amplitude represented by the bar. For example, 5 peaks exceed increment 1 but only 3 peaks exceed increment 2. I would like to inject a word of caution here that there is no standard technique for making cycle counts of peak responses. If the data are intended for developing a shock test, the counting technique is not too critical because only relative comparisons of data severity are involved. If the data are intended for design purposes, then it would be desirable to cull the fatigue literature for more sophisticated counting methods. In any event it can be seen that converting a response time history to digital form results in a loss of detail, e.g., the order of occurrence of high and low peaks is not evident. Therefore, it is desirable to include a copy of the original time history with the reduced data.

The next step is to assemble the data into a form which will show at once the effect of the shock transient on systems with any natural frequency. A three dimensional presentation which accomplishes this is shown in Fig. 3. The reduced data are presented as a surface whose coordinate axes are peak response, natural frequency of the responding system and the number of response cycles which exceed any given value. The surface is faired through the ends of the bars in each histogram since in the limit the width of these bars can be made to approach zero and define a smooth surface.

The surface I have described is known as a Three-Dimensional Shock Spectrum. A simplified and much older version of this is the Two-Dimensional Shock Spectrum. The two-dimensional spectrum is actually the intercept of the three-dimensional spectrum at N = 1 in Fig. 3. The two-dimensional spectrum is of particular value when defining a very severe shock which is expected to cause failure in a single application of the shock. Obviously, in this case there is no need to consider the fatigue effect introduced by lower levels of response.

In summary, I have described an analytical technique for reducing shock transients in a manner which discloses their relative damaging potential. If two shock surfaces are compared the higher surface is considered the more damaging. If they intersect, then it is reasoned that each shock is more critical than the other only in the region where each is higher. The principal limitation of the data reduction method described lies in the analogy which is implied between equipment failure and structural failure. Insofar as equipments, broadly construed, are fabricated of structural elements, the failure analogy is reasonable and vibration endurance data on electronic and other components tends to confirm this.

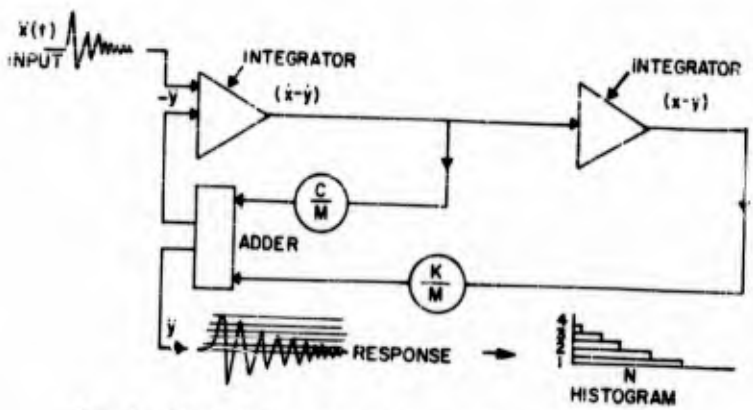

Fig. 2 - Block diagram of shock-data reduction process

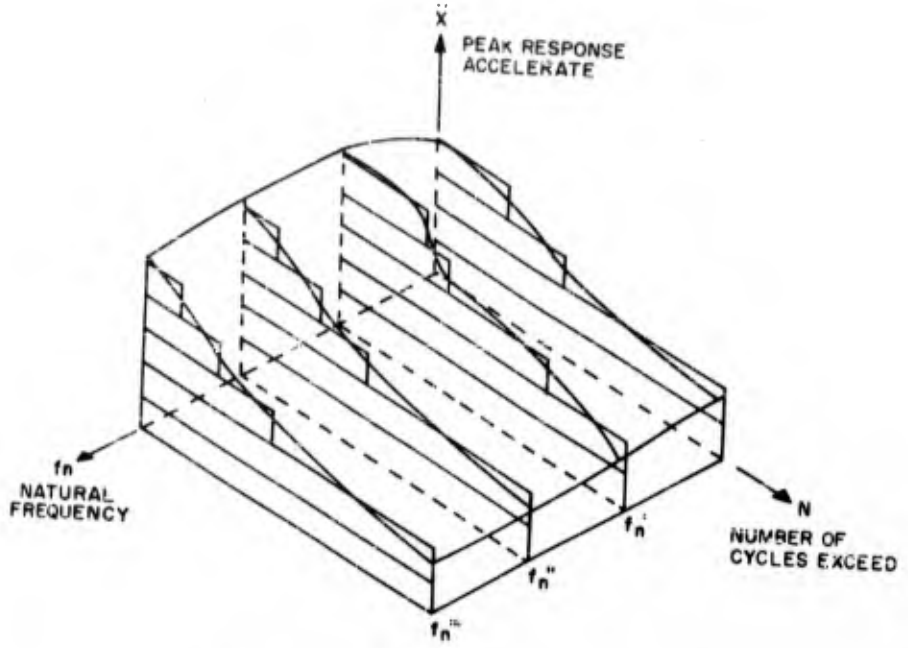

Fig. 3 - Three-dimensional shock spectrum

I must point out, however, that there is a class of equipment failure, described as "temporary malfunction," e.g., electrical noise, loosening of fasteners, etc., for which the presented data reduction technique doesn't fully apply. This isn't a major handicap, however, and until we find a way to design tests for malfunctions the present method based on simulating structural damage will ensure the structural integrity of the equipment we place in future vehicles.

Dr. Crede

Now, if we have followed the advice of Dr. Curtis and Mr. Gertel, we will have separated out from the complexities of a time-history certain numerical parameters which indicate the nature and severity of the field conditions. From our knowledge of these field conditions, we can determine the over-all time during which the equipment will be subjected to these conditions. For example, equipment installed in a manned aircraft may be required to endure hundreds or thousands of hours of vibration, whereas that installed in a ballistic missile must withstand only a very few minutes of vibration. Finally, we may know something of the nature of the equipment to be tested which can be applied in selecting appropriate tests. Dr. Rona, if you were supplied with reduced data as outlined by Dr. Curtis and Mr. Gertel, together with the other information that I mentioned, what concepts would you apply in devising a laboratory test to best simulate the field conditions?

TEST PROGRAM BASED ON MEASURED ENVIRONMENT

Thomas P. Rona

The question, as phrased, may imply that the only thing I can use is the data supplied by my copanelists. Actually, what I shall try to do is to limit the proportion of the test designer's judgment which enters into the definition of the test, and attempt to increase the rational elements. We should not delude ourselves by thinking that by rational we mean absolutely incontrovertible. It is simply a matter of where the elements of judgment do come in the picture.

Specifying a rational shock and vibration test program is, in general, impossible on the basis of measured environment only. While "environment," translated as meaning here input and output phenomena connected with

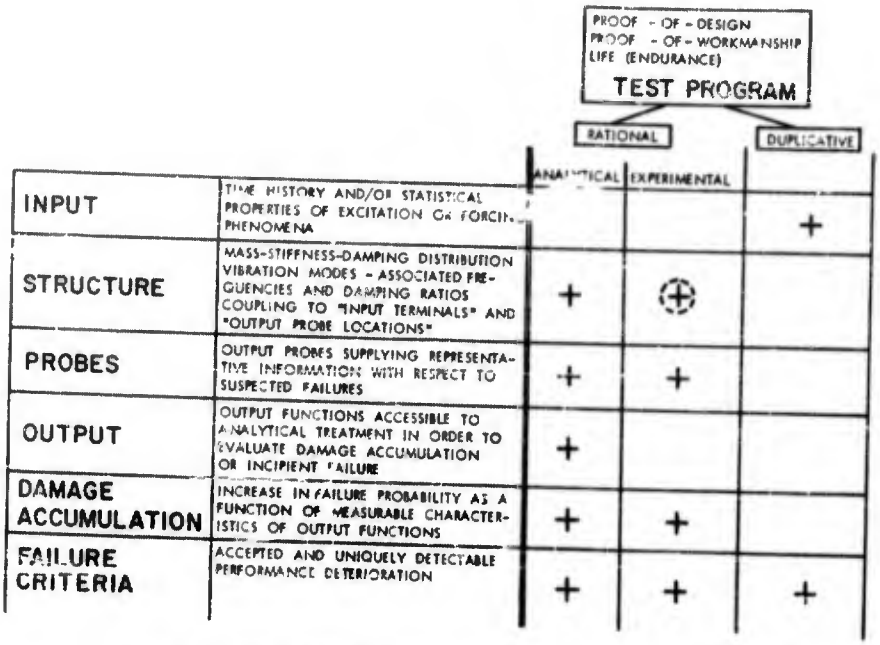

Fig. 4 - Proof of design, workmanship, and life (endurance) of "rational" and "duplicative" test programs

vibration and shock, is one of the essential ingredients of such rational test programs, other information types are just as indispensable. Figure 4 characterizes the components of what may be thought of as being an ideal situation. Two "rational" test program determination processes are compared with a "duplicative" process in order to illustrate the specific requirements of both types.

Before examining the detailed nature of such requirements, the following preliminary statements should be clearly spelled out:

Practical considerations of operational nature often do impose constraints that dominate the technical considerations discussed here. It cannot be our purpose to conceive methods that would modify the respective weights given to operational and technical constraints.

Certain items of information about the type of equipment to be tested (among others, the safety factors, mission success probability and performance penalty paid for overdesign) will often supply valuable indications in order to decide between "rational" or "empirical" test programs.

The objective pursued here is to clarify the differences in input requirements and in quality of test results expected rather than to take a definite stand in favor of one or the other of the approaches discussed.

Figure 4 shows proof of design, proof of workmanship, and life (endurance) test programs in two categories. "Rational" test programs are the ones which, presumably, would start from all the available necessary information in order to obtain results with a minimum of equipment and effort. For want of better description, we call "duplicative" the type of test performed when only the shock and vibration input characteristics to a given piece of equipment are known together with some arbitrary failure criteria. Our efforts are exerted toward duplicating inputs as accurately as possible in order to produce, hopefully, identical failures.

The horizontal lines represent types of information necessary to design test programs. These types are:

Input quantities, in our terminology, are time-history and/or statistical properties of excitation or forcing phenomena. When vibration and shock inputs are not transmitted through specific mounting points, the spatial distribution of input phenomena is also required.

For structure, ideally, the information needed is that which would lead to a complete, detailed dynamic history of the whole structure (including its smallest component) under any arbitrary vibration input. It is clear that such complete information would never be available; however, mass stiffness and damping distribution, possibly the vibration modes (normal or not), associated natural frequencies and damping ratios, as well as the relationship between these vibration modes and excitation input terminals and measuring probe locations are of importance. As a matter of practical limitation, the degree of resolution that is necessary for the knowledge of the structure is determined largely by the shortest "wavelength" that is conceivably present in the structure.

Under the heading "probes," we mean accelerometers, displacement meters, velocity meters, strain gages, strain indicators, and, in general, any device which will give information with respect to the absolute or relative motion of one portion of the structure. As stated above, the information required includes relation of the output probe indications and the structural motions. In addition to this, it is necessary to be in position to relate probe indication with respect to suspected or expected failures.

The output function, in certain cases, must satisfy a certain number of analytical conditions in order to evaluate damage accumulation or incipient failure threat. A typical example would be that a random vibration environment is required to be Gaussian and reasonably narrow band before a meaningful prediction of amplitude distribution probability or peak distribution probability can be made on an analytical basis.

Damage accumulation is the process serving at the base of our prediction that the failure probability of a given structure or subassembly will increase monotonically with the duration of shock and vibration history. The small number of damage accumulation concepts now available should not prevent us from recognizing that they are central to the whole idea of rational test program planning.

Finally, failure criteria are necessary in order to establish a clear-cut end point for failure test programs. Such criteria are quite evident when physical rupture of structural components are involved; they are, however, not so obvious when failure is a function of performance deterioration of electronic equipment, or of a change in temperature, chemical structure, etc.

Figure 4 also illustrates the role of these various input data categories with respect to test program planning. It is readily apparent that if by "environment" we mean shock and vibration input phenomena these are only required for duplicative programs. They are not essential (and possibly not even useful) to the so-called "rational" processes.

If the measured output is of sufficiently simple form to allow analytical application of the available and accepted damage accumulation formula, and if, further, the measured output is uniquely related to the expected failure(s) the test program is decided without difficulty in principle. The practical application of such a process, however, is a matter of some complexity (Fig. 5).

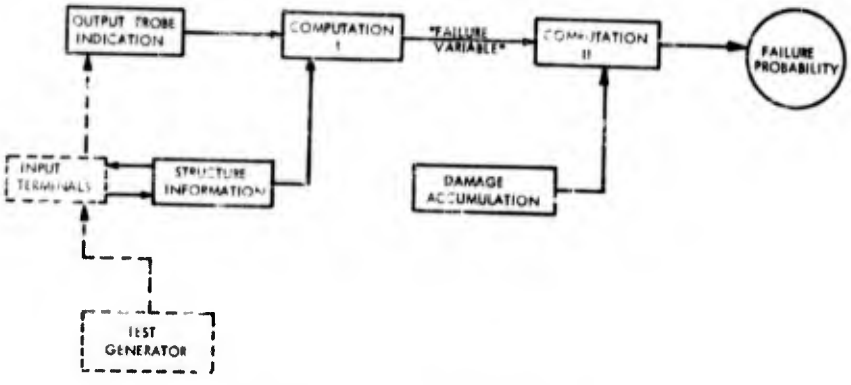

Fig. 5 - Rational test program design

The experimental approach to the "rational" test program design has been described previously. Essentially it uses automatic machine computation for Step II and consequently does not require the analytical simplicity of the output functions. Requirements on structure information are often less stringent than in the analytical approach.

To conclude, the "rational" and empirical approach for test program design are complementary rather than competing. When sufficient data is on hand; when talent, manpower and time are not restricted; when design is critical with respect to performance and reliability, the rational approaches are advocated. When manpower and time are the predominant constraints, the empirical test program has considerable merit and may even be the only possible approach.

Dr. Crede

Some of us have had occasion to explore in detail the problem of specifying laboratory tests on the basis of a detailed analysis of the field data. Personally, I can recommend that as a most stimulating type of mental exercise; however, I have some reservations that the concepts outlined by Dr. Rona lead to more generally useful results than those outlined by Mr. Granick. The fifth member of our panel, Dr. Mains, has over the years run head-on into the problem of making a choice between these alternatives, or possibly compromising between the alternatives and thereby devising an optimum test. I will ask him to compare the relative merits of the two approaches and to indicate how he would use the data from various sources in arriving at the best test.

RELATIVE MERITS OF EMPIRICALLY FORMULATED TESTS VS TESTS FORMULATED FROM MEASURED DATA

Robert M. Mains

In devising a test, it is necessary at the outset to consider the problem carefully and determine which of the following conditions is applicable:

1. The "environmental loads" are known, and the "damage processes" are known, so that it is reasonable to devise a test in which the same damage processes are developed in the test as in field service.

("Environmental loads" = whatever phenomenon causes damage.

"Damage process" = the process leading to eventual malfunction or failure.

"Same" = identical in nature, rate, and extent.)

2. Either the loads or the damage processes (or both) are not known, so that any test is at best only a sorting process of doubtful correlation with field service.

3. A middle-ground between Cases 1 and 2, in which the loads are partly known and the damage processes partly understood.

In addition to the load-damage process categories, let us consider the various types of tests and their purposes:

The prototype acceptance test, in which the effort is to prove the adequacy of a design under as near to service conditions as can be managed.

The design development test, in which the effort is to gain information useful in establishing the characteristics of a design, in developing data for design improvement, or in choosing between various design alternatives.

The quality control test, in which the effort is to sort the "good" ones from the "bad" ones, and to hold the bad ones within some acceptable reject rate.

When we speak of degree of realism or simulation in a test, the key to the degree of realism is the similarity of the damage processes involved. Since this is the case, it is entirely possible to have an empirically developed test which is nearly 100-percent realistic because it causes the same damage processes as the field service. On the other hand, it is equally possible to have a test formulated from measured data which is only 10-percent realistic because the essential damage processes are not developed. To achieve these two extremes, one might say that it would require a very lucky empiricist in the first case, and a very uninformed or unobservant applier of data in the second case.

We could define "relative merit of a test" as the odds in favor of the test being

*Thomas B. Rona, "Equivalent Vibration Program from the Fatigue Viewpoint," Bulletin No. 27, Shock, Vibration and Associated Environments, Part II, p. 129, UNCLASSIFIED.

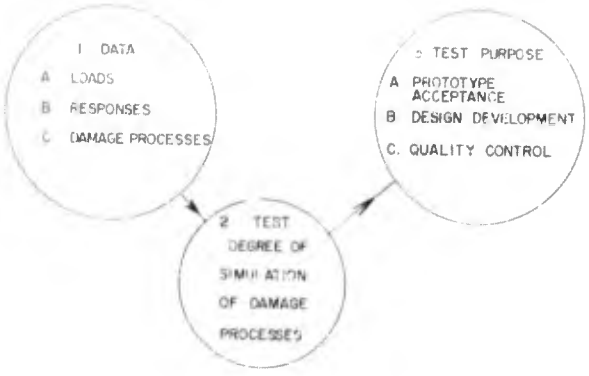

Figure 6

100-percent realistic, or alternatively the maximum percent of realism which could be expected from the test under normal circumstances. This would be a good measure of relative merit for a prototype acceptance test, but a poor measure for a quality control test.

If we define relative merit of a test as the degree of achievement of the test purpose, then this applies equally well to the prototype acceptance, design development, and quality control tests. From this point of view, the prototype acceptance test is the only one which needs to be realistic as to nature, rate, and extent of the damage processes. It should be derived directly from measured data, and the loads should be monitored to produce 100-percent realism, once it has been shown that the resulting damage processes are correct. (Be wary of attempting to accelerate the rate of damage by arbitrarily increasing the load. This often leads to nonlinearities: twice the load rarely produces twice the damage.)

The design development test needs to involve the same damage process as the field service in nature only. The rate or extent of damage may be juggled to suit the particular design aspect being tested. This test need not be based on measured data except indirectly since the cause and effect relationship between the test load and the desired damage process must come from somewhere.

The quality control test needs no measured data for simulation purposes. What it needs are measurements to establish that it is controlling quality: field failure rate versus factory reject rate and the like.

To summarize the situation, consider the illustration (Fig. 6). In Circle No. 1, we see the available data in terms of what we know about the loads, the responses to the loads, and the resulting damage processes. In Circle No. 3, we see the purpose of the test, prototype acceptance, design development, or quality control. Circle No. 2, then, is the simulation or test which translates the data into the accomplished purpose. For a high degree of realism, tests based on measured data are to be preferred. When realism is not so important, then empirically developed tests are adequate. Much of our work at present seems to fall somewhere between these two cases because the loads are not adequately known, or the structural action is too complex, or the damage process is not understood. It does little good to argue the relative merits of one test versus another unless this can be done on the basis of answers to the questions: what is the field service damage process, and how well does the test in question simulate this damage process in nature, rate, and extent?

Dr. Crede

Now that our panel of distinguished experts have stated their views on the several topics put to them, there may be persons in the audience with different opinions on these subjects, or with questions on points touched by the panelists but not answered explicitly. The subject of laboratory testing and failure of equipment is a very broad one, much broader than could be discussed this evening or in any other reasonable period of time. To gain maximum benefit from the discussion this evening, we should limit ourselves to those explicit topics discussed by the panelists. You may address your comments to anyone of the panelists directly or to the panel in general; in the latter case, if no member of the panel then volunteers to comment, I will direct the question to a member of the panel whom I select.

NECESSITY FOR EMPIRICAL TESTS IN THE EARLY STAGES OF A PROJECT

Dr. Stallard (The Martin Company, Denver) commented that Dr. Mains in his illustration (Fig. 6) seemed to have put the cart before the horse for most programs, because he had started out with environmental data. Dr. Stallard cited the case of the Titan II program. It was a new program, an in-silo launch, and no one had done anything like it before on the scale of the Titan II thrust. Confidential drawings were out already and as far as the environment went, it was a question of making as good a guess as possible. By the time real environmental data became available, tests to qualify components would be underway on the basis of the guesses. In favor of this method he could point to the Titan I program where, with the same approach, there had been, so far, something like 18 successful flights out of 25. It would be very nice to have all the environmental data on hand so as to specify a realistic test but there was not the time. A lot of judicious guessing was necessary to get a program on the road.

Dr. Mains agreed entirely with Dr. Stallard and was hurt that any other views should be imputed to him. He said, "If you've got to start and you don't have any data, then you go ahead and start. You do so on the basis of your reasoned, best judgment at the time and if you've overshot, you back up. You jiggle in . . . on the proper test as you gain experience."

INCREASING VIBRATION TEST LEVELS TO ACCOUNT FOR DAMAGING EFFECTS OF OTHER ENVIRONMENTS

Mr. Fine (The Martin Company) noted that in real environments, vibration stresses would be superimposed on other stresses, for instance, those due to temperature of humidity. He asked, "Should we not, in designing our laboratory tests, raise the vibration test levels to try to account for the damage due to these other stresses?"

Dr. Mains said that it would be admirable to do this, if we knew how. If we knew the damage processes and the way in which damage accumulated from the various stresses, then perhaps we should be able to increase the vibration level to account for these other environments. He did not believe we had this knowledge yet.

Mr. Fine agreed, but pointed to cases where items had passed vibration tests and, although temperature could have been added as well, this was not done because the people had been falsely led into a feeling of security since these items has passed the vibration test with a good margin. He asked if some factor of safety should not be added, although he realized it would not be easy to obtain.

Dr. Mains said that he knew of at least one case, quite recently, where only the addition of the temperature as well would have found the trouble. In that case no amount of increase in the vibration level would have done the job.

CONFIDENCE LEVELS FOR DATA

Mr. Barkham (Lockheed) addressed Dr. Curtis with regard to analysis of data. "You mentioned that specification writers should give greater consideration to confidence bands with regard to analyzed data. What do you mean and where does this lack of confidence in the data come from? I presume you are speaking of power spectral density plots and random-type presentations. Could you elaborate a little more on this, Dr. Curtis?"

Dr. Curtis responded, "Assuming we have a stationary process and a normal distribution, the probable error is based on the fact that when we take a certain length of time over which we obtain the mean squared value, we have taken a certain sample size. The bigger the sample size, the better is our estimate of the mean-squared value. Similarly, the wider the bandwidth, the more frequencies we're averaging over. True, resolution is lost in the shape of the spectrum, but confidence is gained because, to put it in the statisticians' terms, we wind up with more degrees-of-freedom. They're not vibration degrees-of-freedom; they're some other kind that I don't understand too well. Anyhow, the wider the bandwidth, the more are the degrees of freedom and the greater is the confidence that the observed value is truly the mean squared value of the random process."

Mr. Barkham, referring to a figure of 20 percent that Dr. Curtis had previously mentioned, said, "Normally when we attempt to establish a mean-squared value, we take a sample about 2 seconds long. Are these values that you express representative of a particular length of sampling time?"

Dr. Curtis replied, "No, the figure I used was just one I happened to have around. I took a loop of tape 4-1/2-seconds long and used it at 10-percent bandwidth filter. The number of degrees-of-freedom is twice the bandwidth times the integration time of the effective bandwidth. Since we have a Gaussian process, the mean-squared value which I compute from a particular observed sample should have a chi squared (χ^2) distribution. With the many degrees-of-freedom and using χ^2 tables, I can find the 80- or 90-percent confidence limits. Without being too rigorous statistically, this means that, for the 80-percent confidence interval, if I observed a value of 1 g^2/cps at 100 cycles, the upper limit was 1.2; the lower limit was 0.8. Thus, if I have a stationary process and sample over and over again, 80 percent of these samples will be between 0.8 and 1.2. The one sample I made came out at 1, so I'm only 80 percent confident that it actually is between 0.8 and 1.2."

Mr. Kuoppamaki of Lockheed, Sunnyvale, remarked that this confidence interval was concerned with details of the analyzer and had little to do with the test levels. He mentioned that there are confidence intervals which are directly connected with test levels. These consider the damage process. There are the go, no-go tests and we speak of test levels with respect to the expected environments. That phase of the problem should be gone into. Mr. Kuoppamaki referred to a paper by Dr. Mains in the 28th Bulletin* in which he discussed simulation, described damage processes and explained that we are concerned with statistical distributions. He asked, "Dr. Mains, would you amplify a little on the same subject from the standpoint of test levels? Should we place our test levels somewhere in the mean of our expected environments, or should we probably be a little above the mean and how much above the mean?"

Dr. Mains replied, "The answer to your question would take much longer than we have, but I will comment briefly. First of all, the margin that you want to put into a test should be predicated upon the degree of disaster that results from the failure. If it doesn't make a great deal of difference whether the failure occurs or not, I'd be willing to hit for the middle of the statistical range for my test level. But if the result of the failure is catastrophic, I would want to double or maybe triple that test level, depending on the situation. I like to temper my mathematics with judgment rather heavily.

*R. M. Mains, "Introduction to Shock and Vibration Simulation," Bulletin No. 28, Shock, Vibration and Associated Environments, Part IV, p. 225, UNCLASSIFIED.

ON SHOCK TESTING

Dr. Morrow (Aerospace Corporation) considered that none of the panelists had really come to grips with the problem of establishing test levels from field data. He thought Mr. Granick had come closer than the others and he had been talking about establishing test levels without field data. There were many things that must be considered, some of which had already been mentioned, but there was one important subject about which little had been said. This subject was feasible tests and their limitations. He asked Mr. Gertel if he would like to say something on feasible methods of shock testing; about how he would use some of the data he had discussed in arriving at test levels for shock test equipment; and in particular how he would make use of the three-dimensional (3-D) shock spectrum (Fig. 3), in view of the fact that in practice we deal with systems having multiple degrees of freedom.

Mr. Gertel began his reply by pointing out that the 3-D spectrum was an extension of the well known two-dimensional (2-D) shock spectrum. As to devising a machine to do the shock tests, he believed that it was a question of the severity of the test. If a test was very severe, then the 2-D spectrum was all that was needed. The test item would be proved in one or two blows. On the other hand, if the shock in question was one that had to be repeated say 100 times, then it would be desirable to incorporate in the shock machine features which would impose the damaging factors over a number of applications. The third axis in the 3-D spectrum then came into the picture; however, whether you had a 2-D or a 3-D spectrum the process of arriving at a test machine could be rather empirical. You would create some sort of a shock device and obtain a shock spectrum of either variety, as need dictated, and compare this spectrum with required service condition. He knew of no technique other than the empirical for making the machine approach the required spectrum. He wanted to emphasize again that the principal value of the spectrum is for comparison of one environment with another.

Dr. Crede took up Dr. Morrow's query about using the shock spectrum when in practice we are dealing with multidegree of freedom systems. He considered the answer lay in a comparison of the shock spectrum as a

design tool and as a means for specifying a shock test. From a design standpoint, the shock spectrum left many questions unanswered. Based as it was on a linear, single-degree-of-freedom system, evidently it would not apply to systems with many degrees of freedom, nor to systems which have nonlinearities or that have feedback loops, nor to many other types of systems. But as a simple yardstick for comparing a field condition with a laboratory test, the shock spectrum had considerable utility.

Mr. Davis (General Electric Company) wondered if some of the shock test specifications were really satisfactory. In particular he had in mind a component shock test which called for 3 shocks in 6 directions for a total of 18 shocks, each at the same g level and for the same duration. "If we are going to do 3 shocks in a given direction, it seems to me it might be more logical to specify that the duration be changed from shock to shock, so that we would tend to excite different resonances in the particular component."

Mr. Gertel replied that if the shock spectra of the machine which was called upon to do the test embodied frequency components representative of the real environment, as it should, then there would be no need to modify the shock durations. He continued, "Actually, you'll find in a particular shock test that there are two aspects which create the damaging condition. One is the velocity change embodied in the shock test. Certain low-frequency systems will respond primarily to the velocity change rather than to the acceleration time history. The stiff components will respond primarily to the peak acceleration of the shock pulse and to the high-frequency components that may be embodied in the pulse."

Dr. Crede mentioned some of his experience concerning the Navy lightweight shock-testing machine that, he thought, bore on the question. The shock is produced in this machine by a hammer striking an anvil to which the equipment is mounted by a suitable test fixture. The horizontal velocity which is produced by the blow is arrested by the bottoming of springs. In writing the test specifications, it was recognized that one rather severe frequency condition was introduced to the exclusion of others, thus the specification was written to call for hammer drops of 1, 3, and 5 feet successively. This would give the table three different velocities. The distance to the stop was deliberately kept constant in order to produce three different periods from the initiation of the motion until the termination of the motion. Dr. Crede asked Mr. Forkois of NRL to comment on this reasoning.

Mr. Forkois verified that the 1, 3, and 5-foot hammer drops were still specified for the lightweight machine test.

Dr. Vigness of NRL felt that Dr. Crede might have been referring to the medium-weight shock machine. An attempt was made to make the shock test fairer to different equipments by reducing the travel distance of the anvil from 3 to 1-1/2 inches. (Blake at NRL at one time reduced it to 3/4 inch.) The travel time is frequency sensitive because if the equipment being tested has a natural frequency corresponding to the period of travel of the anvil, the equipment would be at the wrong position when the anvil is brought abruptly to a stop. The test would be unfair to equipment that might be tuned to cause damage, and easier on other equipment. In addition to natural frequencies of the anvil, the four-way mounting plates and other things would discriminate against equipments having the same natural frequency. These frequencies may not exist on shipboard, yet the frequencies present on the ship may be in the same area. The machine is not perfect and NRL would like to change a lot of things.

Dr. Vigness then asked the panel to comment on the following point. "Although we know all shipboard conditions are different, we have attempted to duplicate shipboard conditions fairly exactly. This is impossible, but we attempt to do it by generating the same frequency components as on the ship. Of course we can't include on our shock machine all the frequency components involved. The present trend in the design of shock machines is not to try to simulate exact field conditions, but to use a simple pulse for a shock output; the latest is the sawtooth pulse. I rather think the simple pulse is a good thing since a simple pulse does not discriminate against a particular frequency which only by accident would exist in the field."

Dr. Curtis referred back to the question by Mr. Davis (of GE) and commented as follows. "We are trying to attain two things by controlling the frequencies of a shock pulse so that it will be a good shock test. First, all resonances in the test object should be excited, thus the pulse must have a certain duration compared to the lowest resonant frequency. Secondly, the pulse should have a rate of change, rise time or decay time, fast enough to excite the higher resonant frequencies. Assuming that the pulse is long enough and

sharp enough we find that, unless the wave shape is sloppy, the positive spectrum seldom has valleys; it may have some peaks. Mr. Davis is doing his test three times in each direction. When he changes direction the positive becomes the negative, thus, altogether, he will have tested all frequencies in each direction. This ties in with Dr. Vigness' comment in that we now try to use pulse shapes for which we can predict the spectra ahead of time, and know what kind of spectra we're going to get out of the machine, rather than building the machine and measuring what we get. This is not a criticism, but perhaps reflects how some machines come about.

Dr. Mains, commenting on Dr. Vigness' remarks, said, "This is almost a put-up deal since I'm reasonably sure Irwin knew I wanted to say something on this subject. I'd like to see our shock specifications in some other form than a machine, such as in the 901 test, or a shock response spectrum; I can't do anything with these things. What I need is either a time pulse or its Fourier Transform. It doesn't matter which, since they're both the same. We can then do something toward being more rational. As long as we're stuck with a test that's required to be done on a given machine in a given way, or as long as the shock test is described only in terms of a single-degree-of-freedom response spectrum, we can't go anywhere."

Mr. Gertel commented that the simple shock pulse is desirable in that it is getting away from attempting to recreate the exact time-history of the field environment. On the other hand, the triangular- or sawtooth-type pulse does subject all components to equal responses. If the actual environment has holes in its spectra, the use of a sawtooth pulse would prevent our taking advantage of these holes and may result in overdesign.

Mr. Bob Hawkins (Sperry Gyroscope) made the following comments: "The panel has chosen to make a dividing line between empirical test methods and rational test methods. When the subject of shock testing and the possibility of going toward an idealized pulse came up, I noticed that the question of whether we are testing in an attempt to simulate, arose. Empirical testing is still an attempt to simulate. The examples that Mr. Granick gave are really simulation, not by measurement but by observation. When we talk about a triangular pulse or white noise, however we're really no longer trying to simulate the environment but are attempting to make it easy to perform the test. We're also trying to make it easy to understand and control the test. This may be a more likely objective when one considers the difficulties of simulating the environment.

The question came up regarding the value of shock spectra and Dr. Mains mentioned the desirability of Fourier Transform information. We have discovered in our laboratory that if you take a shock spectrum and divide it, as many people have, between the maximum response during-the-pulse shock spectrum and the after-pulse shock spectrum, the ringing responce that occurs after the end of the pulse, the after-pulse shock spectrum divided by omega (ω) is equivalent to the Fourier Integral Transform. We have used this very conveniently because we have the same computer program for both sets of information. The Fourier Transform is useful to do a mathematical operation on a multidegree-of-freedom-system and to come up with response information. The shock spectrum is convenient if you want to talk about the severity of a shock, the equivalence of shock data, or design information from a magnitude point of view. Both have merit. One is for a highly analytical purpose and the other for comparative evaluation purposes. Both can be obtained by a similar type of calculation. There is some equivalence there. We observed it by coincidence and then developed a mathematical proof."*

Dr. Mains said that he was glad to know about this residual spectrum being the same as the Fourier Transform and asked, "Did your residual spectrum have an amplitude and phase?"

Mr. Ralph Blake (Lockheed, Sunnyvale) answered as follows: "The computer people at the Naval Research Laboratory got the jump on us in this same way. We asked them for shock spectra while others were asking for Fourier spectra of miscellaneous signals. They used the same program for both of us. They gave the Fourier spectra people the after-shock or ringing, and they gave us the peak value. There is an amplitude and phase. You can express the ringing as a sine and cosine term."

HOW MUCH SHALL WE OVERTEST?

Mr. Ray Yaeger (Chrysler Corporation) commented as follows: "Legislative technology is a great favorite of mine and I greatly favor the simple pulse. The major reason is

*See Information Exchange, this Bulletin.

'hat I know of no one who can tell me that my simple pulse is not duplicated in the field sometime. Neither can I guarantee that a complex pulse is going to replace the measured field pulse at any given time.

You've been running around the question of time, which is one that I get frequently. You discussed orders of magnitude and how far off we are. In the missile business when we're talking about short-term flight problems, I feel that we're always off by at least a factor of 3 because of this 3-directional business. We go to great lengths to set up a test in terms of time, magnitude, etc., then turn around and run it three times as we should because we've got to run along three different axes. I frequantly get into differences of opinion, particularly with designers. They accuse me, or people in the laboratories, of overtesting their equipment by factors of 3, since their equipment may not have failed until it was tested in the third direction. I would appreciate comments on this."

Mr. Gertel was inclined to agree with the designers, particularly if the test excited a coupled type of response that doesn't occur in the direction of the input. When a vibration is applied to a system which is nonisoelastic, it will have a strong tendency to vibrate in some cross axis other than the direction of the input. A very strong likelihood of overtesting exists if the cross-sensitivity persists when the test is repeated in the other input direction. Mr. Gertel felt that, if a resonance of that nature did occur and the test called out a prescribed duration of testing at resonance, a duration test should not be repeated at a cross-sensitive resonant frequency when the same input frequency had been tested on some other axis.

Mr. Granick felt that we must go back and look at the objective of the test. He said, "If we're attempting to qualify components and our objective is to attain a margin of safety in these components, I would be concerned about accepting a component which passes 2 or 3 shocks but won't take the fourth. You can feel more confident about a component that takes all 6 or 18 shocks and still survives. Since a component is a building block of a system, a weak component will get you in trouble on the complete system. A system test is another matter. Here we want to be closer to the real environment."

Dr. Mains asked Mr. Yaeger, "Are you talking about a prototype acceptance test or a quality control test in this case? Is this something you do as a production checkout?"

Mr. Yaeger answered, "All vibration testing is involved, but particularly qualification testing where one is in a very formal part of the program and is demonstrating to the customer that the equipment will work in the specified environment. Someone mentioned fatigue failures, but these are not always fatigue considerations so that we can carefully pin them down as to their directional nature. Sometimes we're talking about noise in a circuit."

Dr. Mains continued, "Yes, sometimes you're talking about gyro precession; sometimes you're talking about just general deterioration of performance; however, most of these things have to do with something that has a damage versus time or damage versus number-of-cycles relationship like a fatigue relationship. I find it difficult to believe that these other processes, about which we know very little at the moment, are any less variable in their distribution than the fatigue of a piece of steel. You do very well if the spread in life for a piece of steel in a fatigue test is no more than a factor of 5. I would be surprised if the deterioration of a vacuum tube had any smaller deviation than a factor of 5. So if your people are complaining about failures in the test, I haven't much sympathy for them unless the test is already a factor of 5 longer than the service life. Do you see my point?"

Mr. Yaeger said, "The only thing is that I've sat in on too many meetings where people have spent hours debating whether to run a test at 5 or 10 g, or sometimes even 5 or 6 g. These debates between customer and contractor have been very bitter and sometimes there's a great deal of money involved. This is why I mentioned this order of magnitude in the answer. We're off 3-1 or 10-1 in some of these, yet I know of cases in which people have seriously debated the requirements within one digit."

Dr. Mains commented, "I'll probably be looking for a new job when I get back to Schenectady if I say this, but as far as I'm concerned, the customer is not always right. I personally have no objection to telling him so."

Dr. Rona commented that, in the light of these enormous spreads in the results and in the use to which we put the results, the confidence limits defined by Dr. Curtis were not as frightening as they looked at first sight. A power spectrum out by only 20 percent is pretty good.

Dr. Curtis said, "I would agree with you, but unfortunately I picked the wrong curve.

Perhaps I should have taken the more usual case of the 1-second integration time and the 2-cps bandwidth which is so popular. I think you would have found they were a little wider. But this is only one of many in-series inaccuracies in the process, all I would like to do is reform and not kid ourselves that it isn't there."

ESTABLISHMENT OF TEST LEVELS FROM FIELD DATA

Mr. Julius Bendat (Ramo-Wooldridge) commented as follows: "The subject is the establishment of test levels from field data. ---By its very nature, it seems to me that the underlying aspect of the whole problem is statistical. This has been stressed to some extent by Dr. Curtis and by a couple of the questions, but has been largely ignored by the others. Field data is, by its very nature, random. You are going to take samples out of a population which is unknown to you and are going to try to use these samples as a basis for simulating the environment in question. It seems to me that one makes certain assumptions, usually about the underlying environment, and, if we're going to make a science out of this work, we have to test these assumptions. Tests need to be established for randomness, for periodicity, and for stationarity or nonstationarity of the data, particularly as a missile undergoes various changes. Tests need to be established for normality, if normality becomes a strong assumption for later conclusions. Tests need to be established for the nature of the probability distribution of peak values, etc. Dr. Mains, I think your diagram emphasized the need for repeated experiments and for statistical analysis of repeated experiments. I wonder if you would comment on that point."

Dr. Mains said, "If people were to go away from this meeting thinking that they would have to get busy and try to devise tests to test tests to test tests to determine whether a time function is truly statistical, I would feel that we had failed miserably. I couldn't care less whether we have a stationary time function. I couldn't care less whether we have white noise. What I want to know is, when I design a family of missiles of which several hundred are going to be made, what is the environment for which I must design that missile? We did not start this business about random vibration for the purpose of making an argumentative device for the mathematicians. We were concerned with trying to find a means of generalizing the design environment so we could draw intelligent conclusions for design choice. Once you realize that you have a random-like function, this then allows you to make an intelligent design choice. It doesn't matter whether it's a stationary time function or not. And so on for some of the other things."

* * *

Section 6
EVENING SESSION

ZERO SHIFT IN PIEZOELECTRIC TRANSDUCERS

An informal session on this problem was held at the U.S. Naval Supply Center, Oakland in conjunction with the 29th Symposium on Shock, Vibration and Associated Environments.

Mr. Smart (Sandia Corporation, Albuquerque) opened the session by presenting and discussing some records of zero shift phenomena obtained during field tests by Sandia Corporation.

Mr. Smart: Figure 1 is a playback of a tape that we obtained from the 300-foot drop tower at Sandia, Albuquerque. You can see in the upper trace from an Endevco 2216 that this one does have zero shift, the result of a cross-axis g load. The 2216 is a compression-type accelerometer. It has a wafer element with a mass and a spring load (preload, it is generally called); and ordinarily in an accelerometer of this type, we don't experience any appreciable zero shift in the sensitive axis, especially at these levels (approximately 1000 g). The cross lines (Fig. 1) are roughly a hundredth of a second. In a compress-type accelerometer, subjected to a ballistic drop, you get a considerable cross-axis component which, acting on the relatively heavy mass causes it to slide across the crystal element. Even if it does not get a displacement because of surface roughness, it can give you either a positive or a negative shift. In this case, it went positive. We have examples, however, that go in either direction and in some types of accelerometers we get a much more pronounced shift than this. In some cases, it will be way off scale, but this one is pronounced enough so that you can tell the signal has been completely masked.

A voice: How much lateral movement do you think you get?

Mr. Smart: It doesn't depend on how much lateral movement you get; say you have two rough surfaces and you shift them slightly with respect to each other, you can then affect the preload of the spring. Three microinches of compression or release of compression in one of these accelerometers will give you about 100 v.

Figure 2 is a record of a drop on which I had a number of accelerometers that we were trying out. We had not been able to make any of them shift in the laboratory on our drop tables, but this was on an actual tower drop in an actual weapon. Notice the one at the top, in particular, has a tremendous shift, roughly equivalent to 600 or 700 g. This particular one was an Endevco 2224 and the load was in the sensitive axis. Now, I might mention that the 2224 is not a compression type, it is an annular-shaped element that is captive on a post in the center, and the mass is on the outside so that there is no preload; and also there can be no shift of the mass and element with respect to each other. Now, this gets into another type of a zero shift not caused by movement but by something else which I won't go into at this time. The time base in Fig. 2 is 1 ms between small pips and 10 ms between the larger pips. That shock signature would be roughly 2 or 3 ms. Notice the second record from the top is a Clevite 2C1 which gave us satisfactory results. There was no observable shift. The third record is a 2216 shocked cross-axis, but it did not shift. The bottom one is a Clevite 2C1. On these two (the second from top and the bottom), we had asked that the weight be reduced to a minimum to get away from what we thought might be an overstressing of the piezoelectric element which would result in a shift; and of the two samples of the test, neither one shifted, which in some measure bears out our contention, but it will

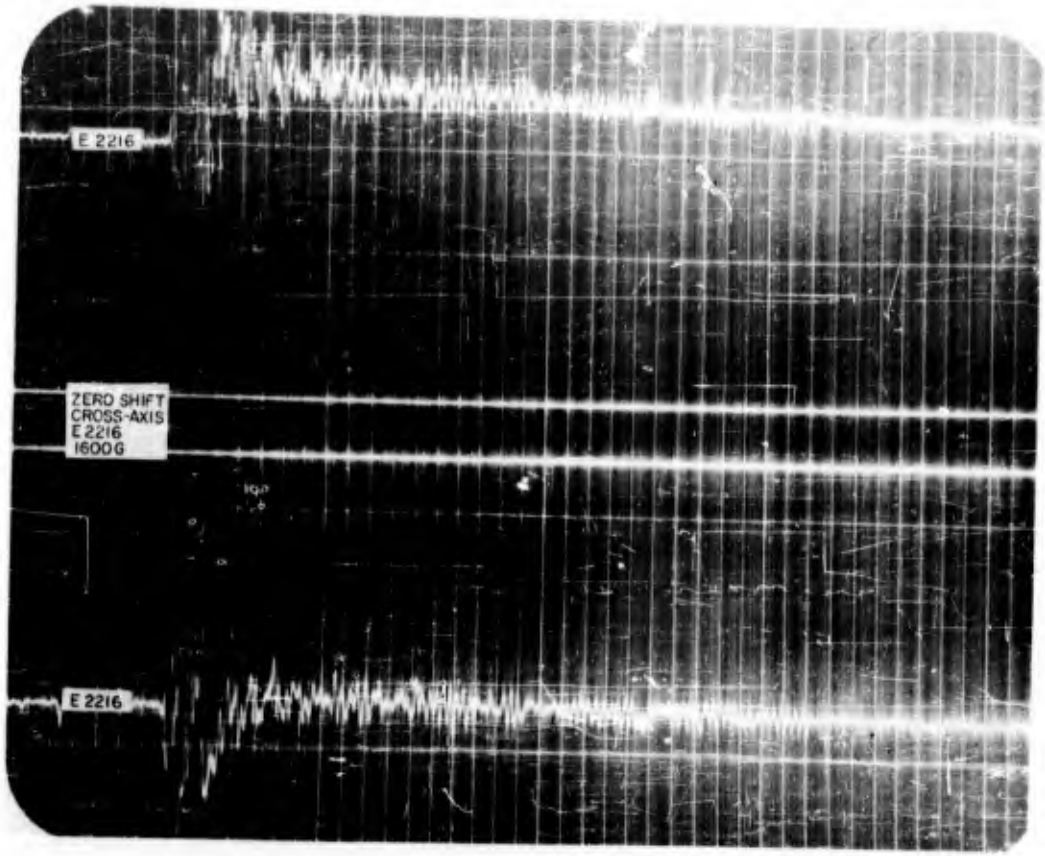

Figure 1

need more than just the one drop of two accelerometers to give us anything definite. Now I might mention, we had two Endevco 2224's on that test. One shifted, one did not.

Figure 3 is from the same test as Fig. 2. The top record is from the Clevite 5C1 which shifts negatively just slightly. That again was in the sensitive axis. Out where you see the second signal is a bounce. This was a ballistic drop; the test item landed on the nose and then bounced on the cable. The second one down is another Endevco 2216 which shifted slightly. The Endevco 2216, we have found, shifts less often than any of the other compression types that we've tried. The next one down is a Glennite A316 mounted cross-axis and you can see we've got some shift there also. So we seem to get it in the bender design too.

Figure 4 is the final record of this particular test. The top trace is from another Endevco 2216 which had a slight positive shift. The second one down is an Endevco 2224 which gave a good signal. The third one down is another Endevco 2216 with a slight shift, and the bottom was another Glennite which kind of rattled after it was all over. You can see it had somewhat of a shift and then it really went. Cross-axis, the bender construction doesn't seem to be very strong. Again, those time marks are 1 ms apart.

Figure 5 is from another drop. The angle there, the attitude, was 45°. This one I put in to show you one shift in particular; see the arrows (Fig. 5). That one started out where it says Clevite 5C1, on left side. The shock was about 200 g. Now that is a real one. We don't always get them that large, but often enough to really mess things up. Notice also the Endevco 2216 there; we get a slight negative shift. Notice the long time constant on these, even on that one which had a shift in base line of maybe 10,000-g equivalent, according to the calibrations (that one was calibrated for 2000 g).

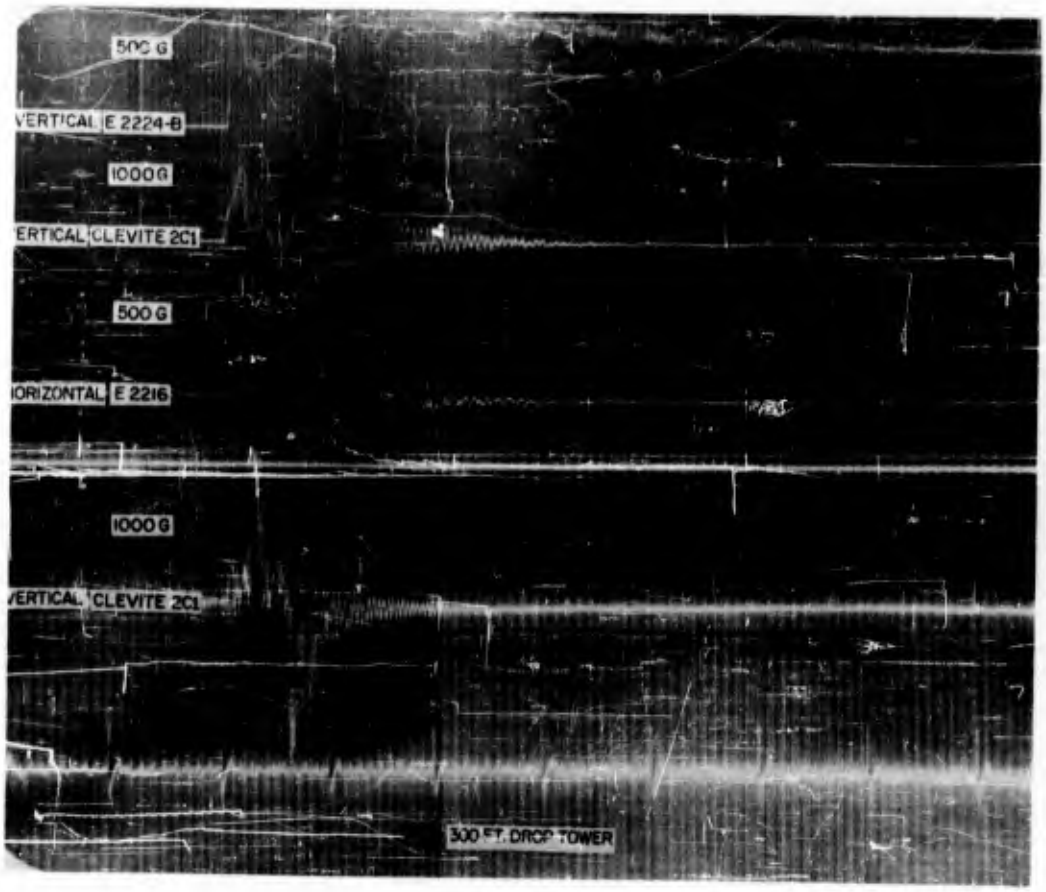
500 G
VERTICAL E 2224-B
1000 G
ERTICAL CLEVITE 2C1
500 G
IORIZONTAL E 2216
1000 G
VERTICAL CLEVITE 2C1
300 FT. DROP TOWER

Figure 2

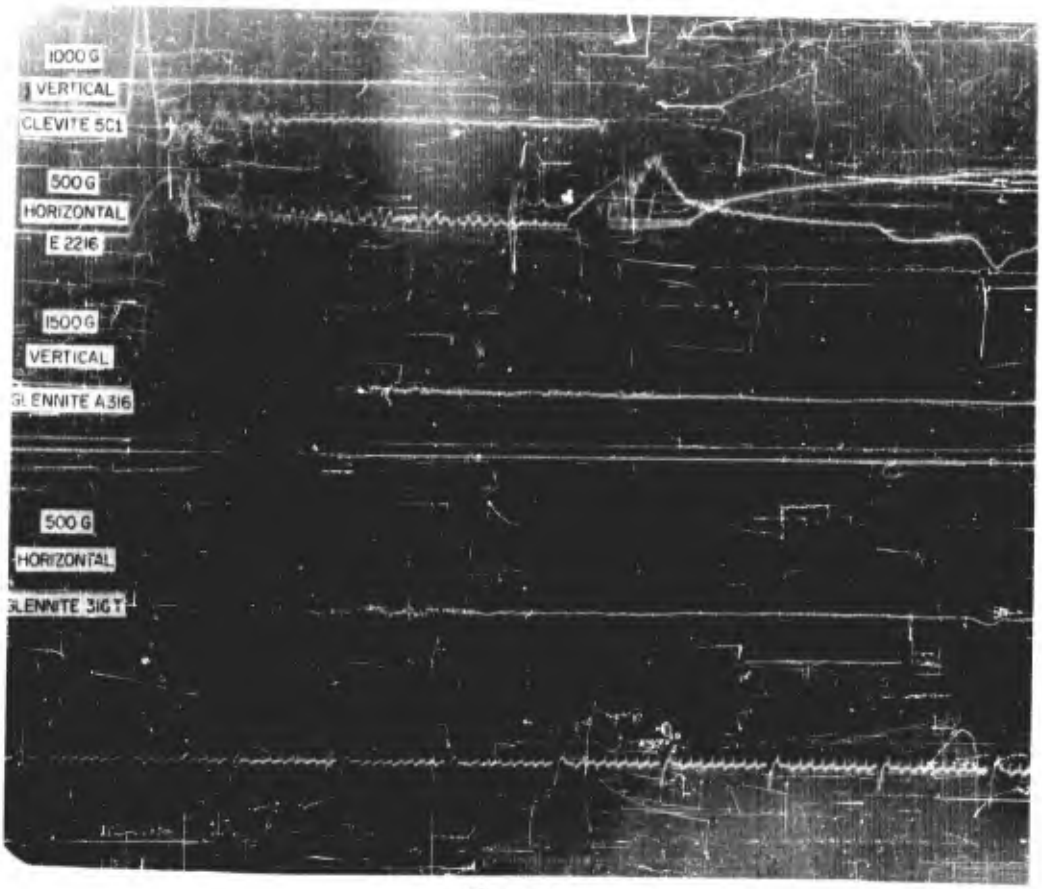
1000 G
VERTICAL
CLEVITE 5C1
500 G
HORIZONTAL
E 2216
1500 G
VERTICAL
GLENNITE A316
500 G
HORIZONTAL
GLENNITE 316T

Figure 3

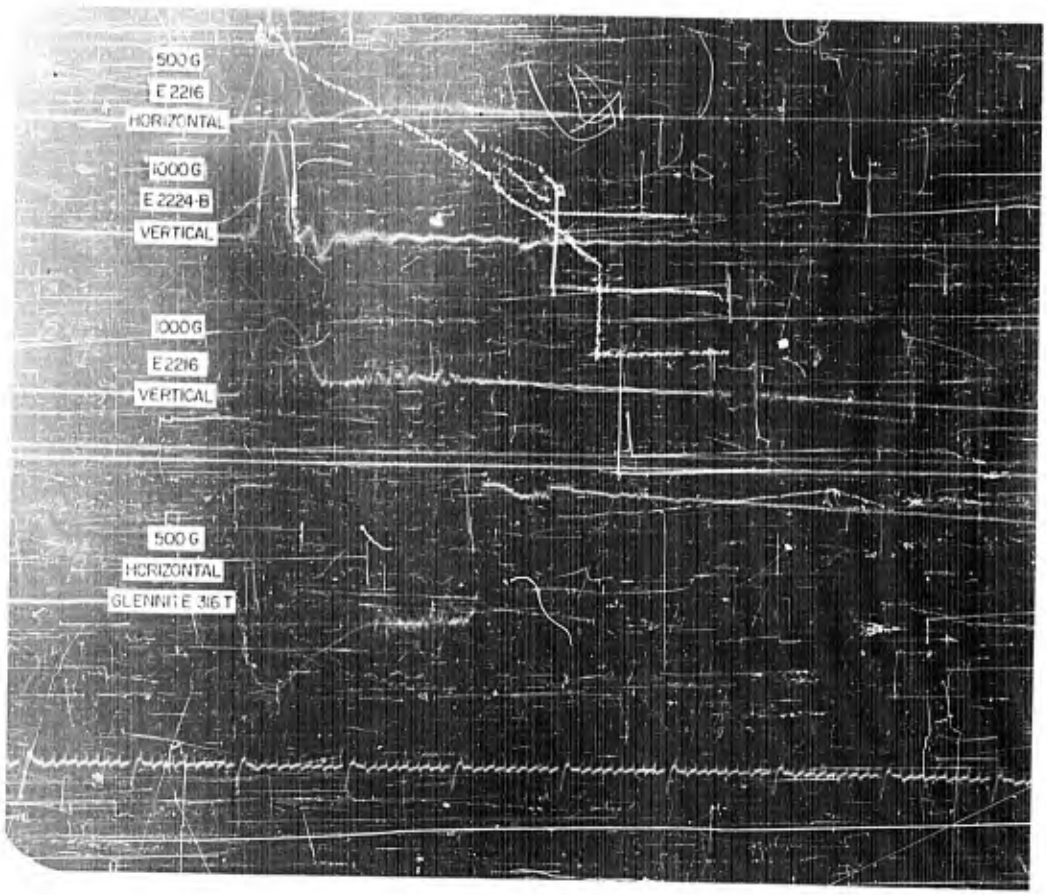
500 G
E 2216
HORIZONTAL
1000 G
E 2224-B
VERTICAL
1000 G
E 2216
VERTICAL
500 G
HORIZONTAL
GLENNITE 316 T

Figure 4

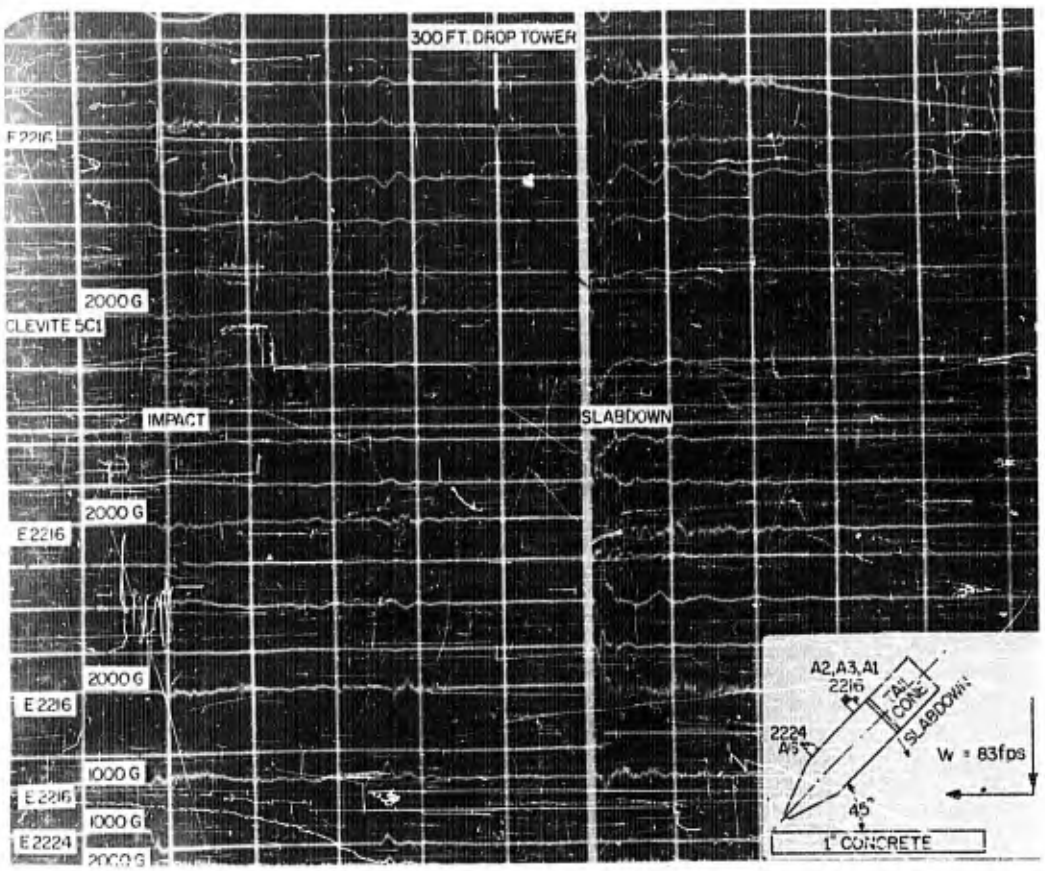
300 FT. DROP TOWER
E 2216
2000 G
CLEVITE 5C1
IMPACT
SLABDOWN
2000 G
E 2216
2000 G
E 2216
1000 G
E 2216
1000 G
E 2224
A2,A3,A1
2216
TAIL CONE
SLABDOWN
2224
A5
W = 83fps
45°
1" CONCRETE

Figure 5

Figure 6 shows traces from another one in the same series of tests, but these were not recorded on tape. They are direct recordings on the Consolidated unit before we had our tape unit working, so we didn't have as much control over how "pretty" they come out as we do when we use the tape. I wanted to show you the fifth from the top (circled), a characteristic type of zero shift. The signal is completely obliterated, you can't get anything out of it. The fourth from the top here is another one, these are about 3000-g shocks. Those two were both cross-axis. The first and second from the top are 1200-g shocks; so you see that out of five crystals, we didn't get a good trace. These were compression-type accelerometers shocked in a cross-axis sense, and these I think, characteristically, will give you more movement than any of the others because of the mechanical shift.

Now on the 155-mm recoilless gun (Fig. 7), using the Endevco 2224 type and employing a doughnut-shaped (annular) element, the third trace from the top is a kind of a nonreturn-to-zero type of thing. Breach pressure is the top curve. The second from the top is the breach strain curve so that we know by these curves when the acceleration should be back to zero. Again, the intervals are one millisecond. The fourth from the top is about a 3000-g shock pulse with a rise time of about 2 ms, so it is not a particularly sharp pulse. Both of these had the shift.

Also from the 155-mm recoilless rifle, Fig. 8 shows that the acceleration curve didn't come back to zero at the same time that the pressure curve did. This is seen again in Fig. 9, the second trace. The shock was about 3500 g and almost 3-ms rise time. Notice the tail off there, and notice that the third trace actually goes negative. The cable on these are cut out there somewhere and when you get into the area marked on Fig. 9, you're getting a cable deformation that can affect the signal.

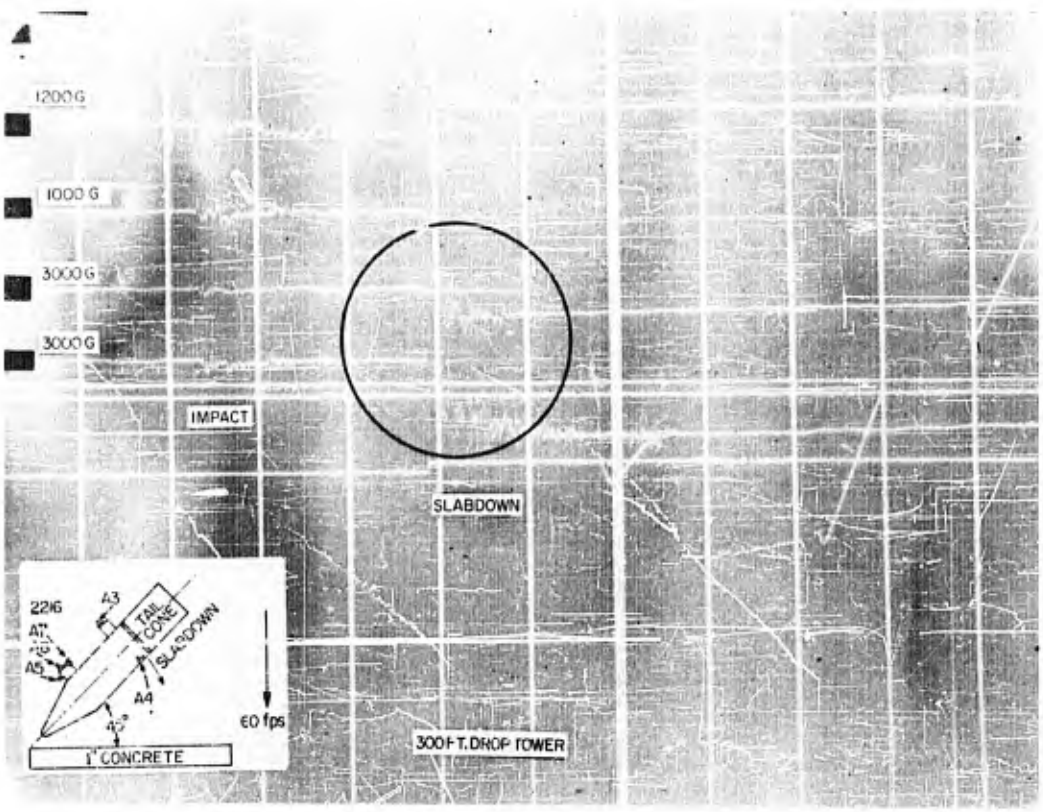

Figure 6

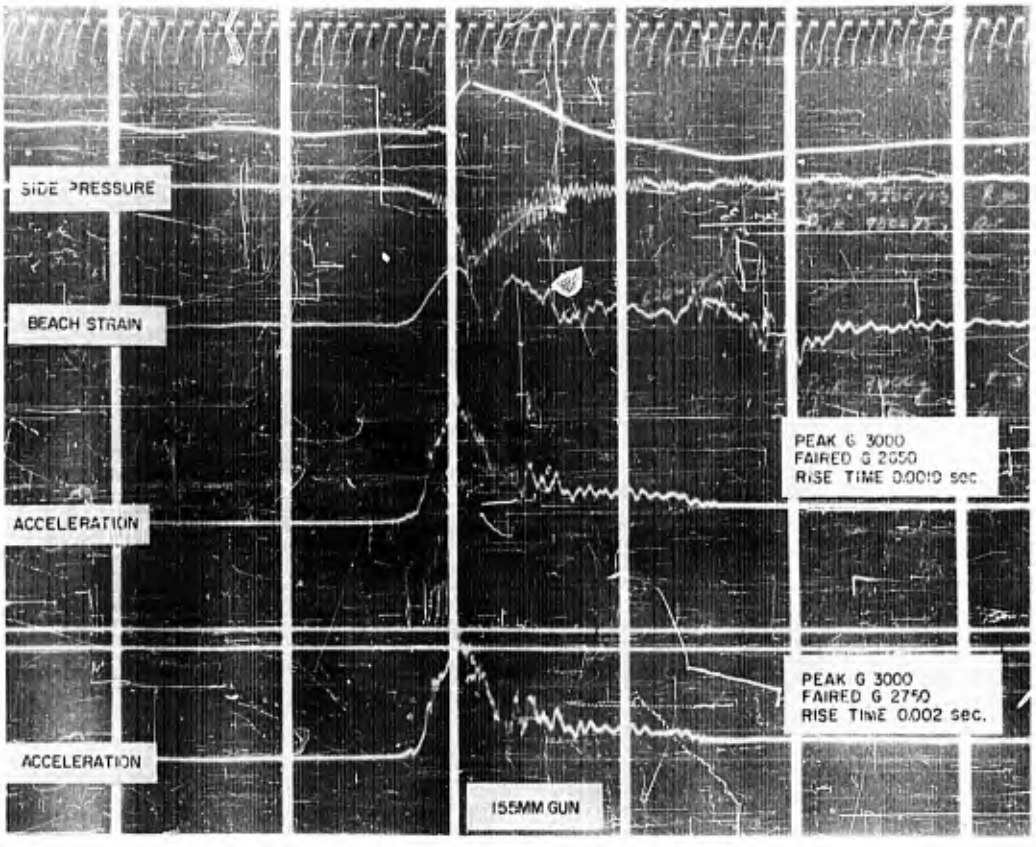
SIDE PRESSURE
BEACH STRAIN
ACCELERATION
ACCELERATION
PEAK G 3000
FAIRED G 2550
RISE TIME 0.0010 sec
PEAK G 3000
FAIRED G 2750
RISE TIME 0.002 sec.
155MM GUN

Figure 7

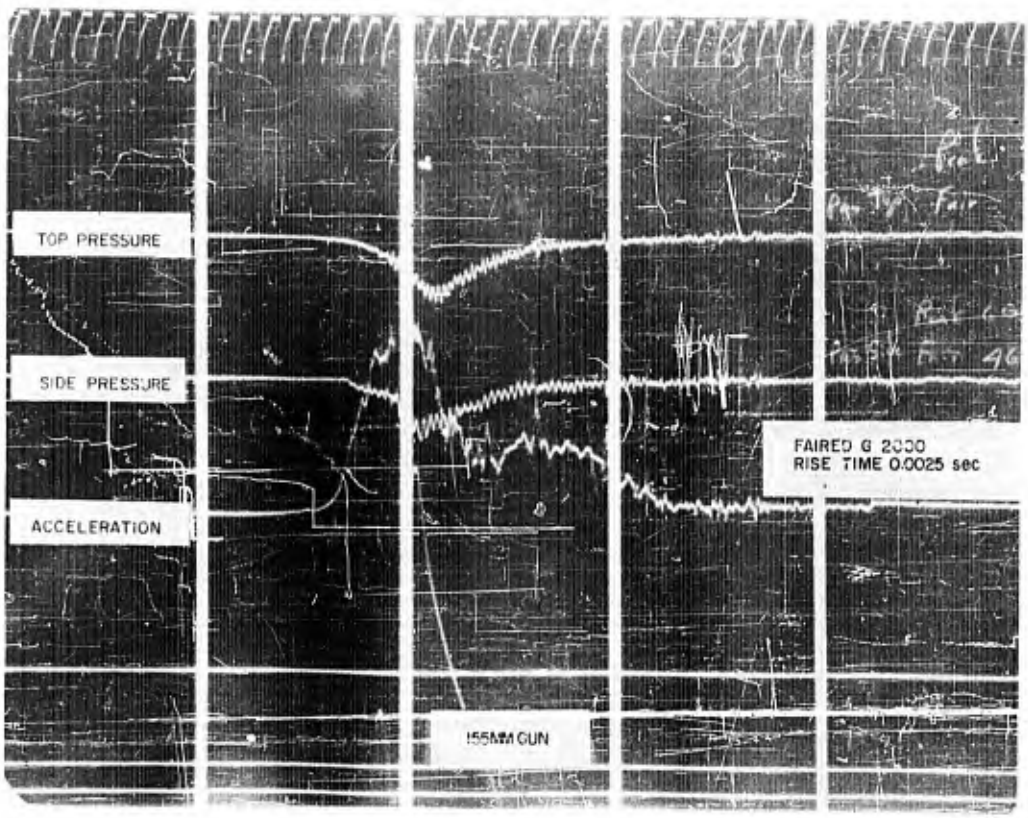
TOP PRESSURE
SIDE PRESSURE
ACCELERATION
FAIRED @ 2000
RISE TIME 0.0025 sec
155MM GUN

Figure 8

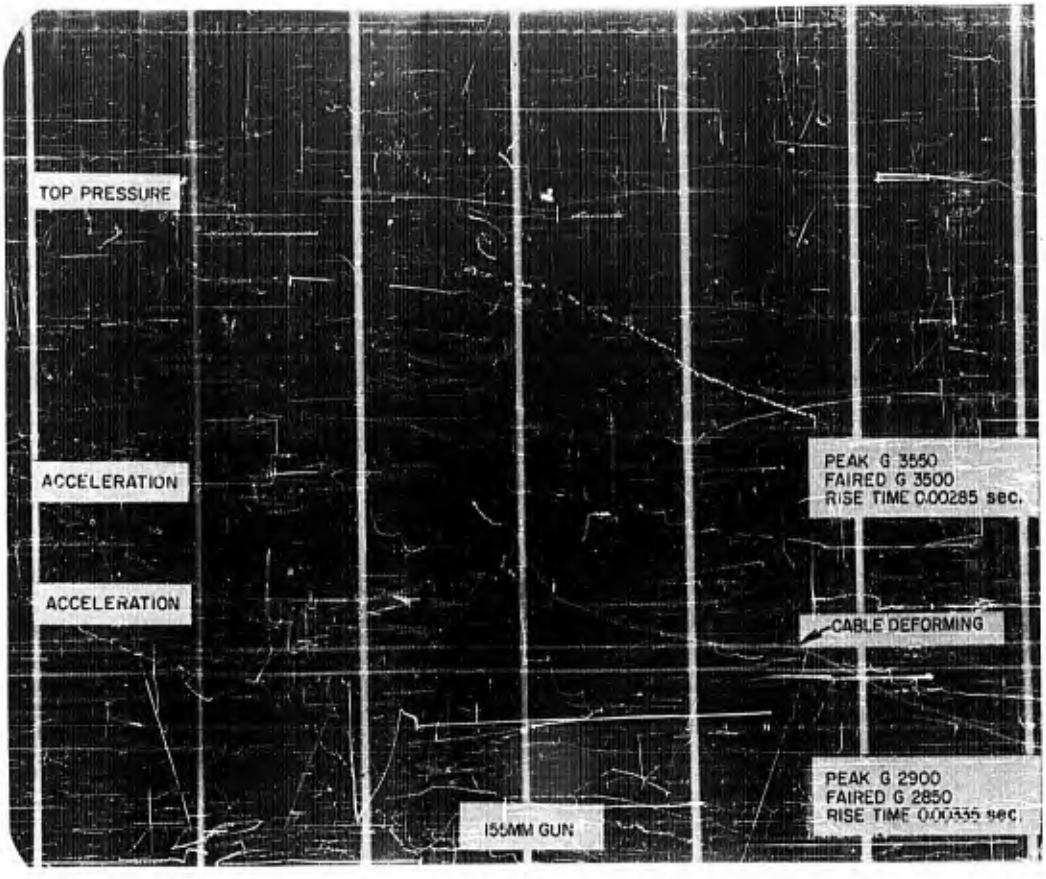
TOP PRESSURE
ACCELERATION
ACCELERATION
PEAK G 3550
FAIRED G 3500
RISE TIME 0.00285 sec.
CABLE DEFORMING
PEAK G 2900
FAIRED G 2850
RISE TIME 0.00335 sec.
155MM GUN

Figure 9

Figure 10 is a 5-1/2-inch, air-gun test which again doesn't give you a real sharp input spike. The gun is built to give a triangular wave so it is not a sharp rise time device. Looking at the second trace, the point where the cable is cut is circled, so disregard that; it is not a zero shift. These are Endevco 2224's.

In Fig. 11, the second is about a 1000-g pulse peak. This one shows one of the effects we get. The trace hasn't come clear back at the time that it is cut. It actually looks as if it may have started up a little right at the circled point. The rise time was about 7 ms on that one.

In Fig. 12, the second trace has very definitely started back up. Rise time is about 7 ms on that one, so these are not sharp rise times. And again, this was an annular element. Figure 13 shows the same thing, a negative baseline shift of some kind. Now I can't convince myself that this is the same phenomenon that we're getting on the drop tower. Maybe some of you can help me figure out what the difference is, but this does not look like the same type of shift. If you remember, the others came to a specific place, broke sharply, and from then on had a normal RC recovery. But you see what I've been calling a zero shift is something that takes off and you can't even tell what the peak is, whereas on the others we get a pretty good signal, except that it tails off. Those are actual records from field test data.

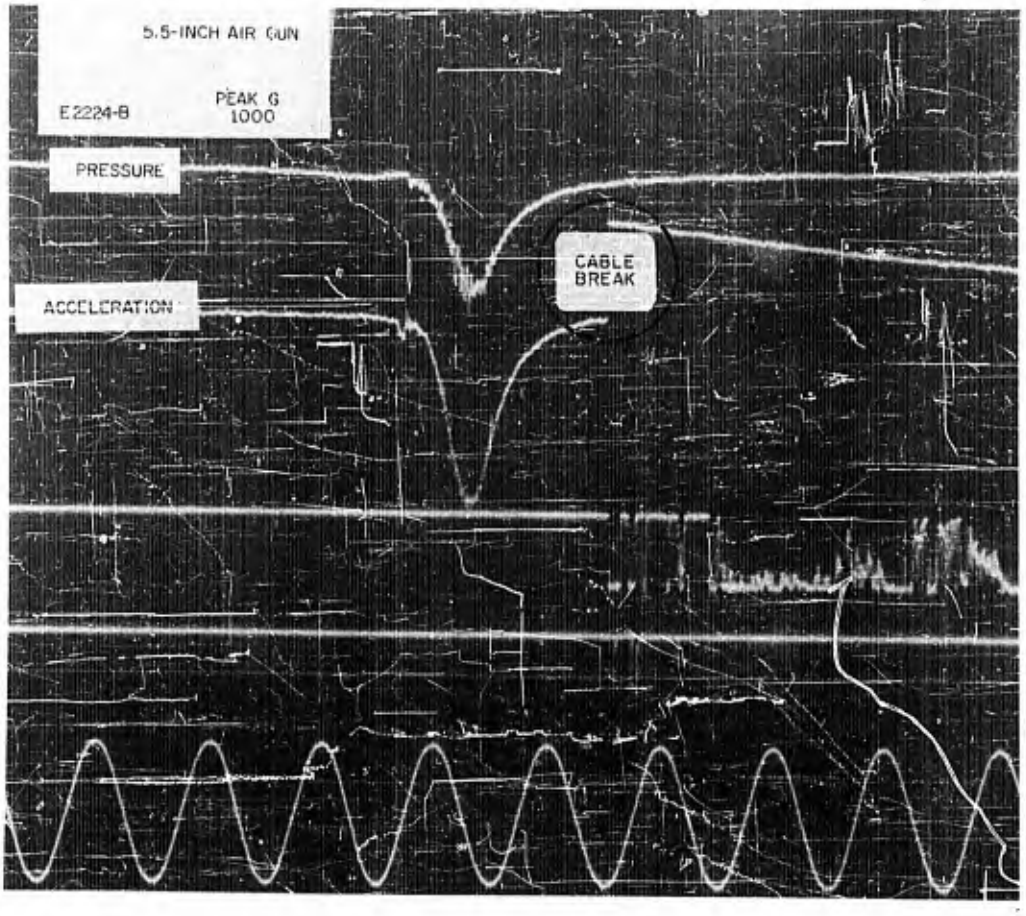

Figure 10

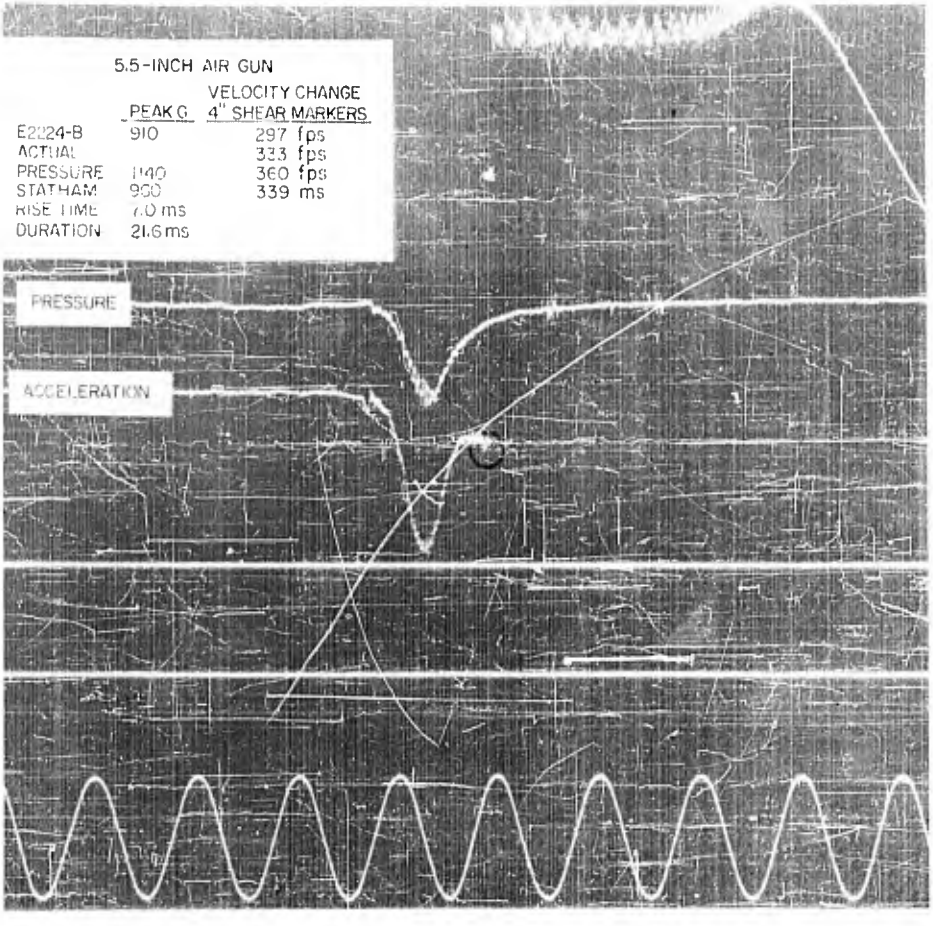
5.5-INCH AIR GUN
PEAK G
VELOCITY CHANGE 4" SHEAR MARKERS
E2224-B 910 297 fps
ACTUAL 333 fps
PRESSURE 1140 360 fps
STATHAM 990 339 ms
RISE TIME 7.0 ms
DURATION 21.6 ms
PRESSURE
ACCELERATION

Figure 11

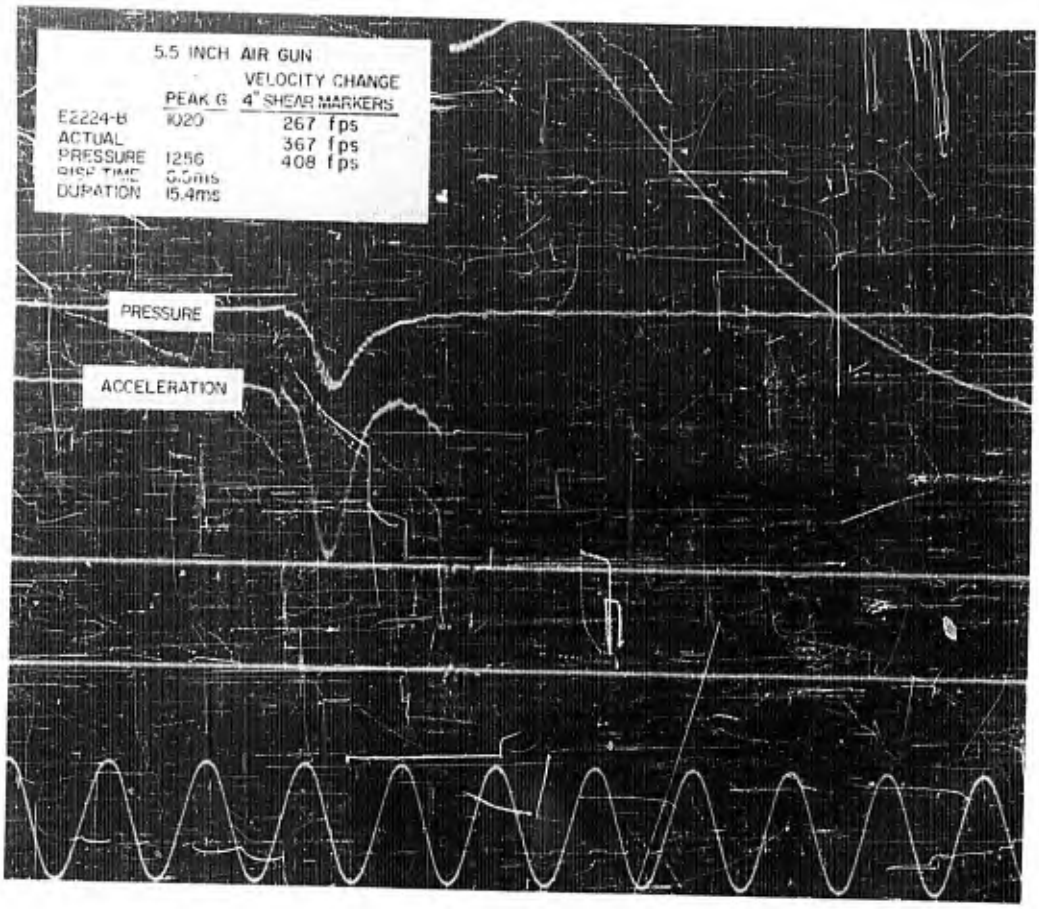
5.5 INCH AIR GUN
VELOCITY CHANGE
PEAK G
4" SHEAR MARKERS
E2224-B
#020
267 fps
ACTUAL
PRESSURE
1256
367 fps
408 fps
DURATION
15.4ms
PRESSURE
ACCELERATION

Figure 12

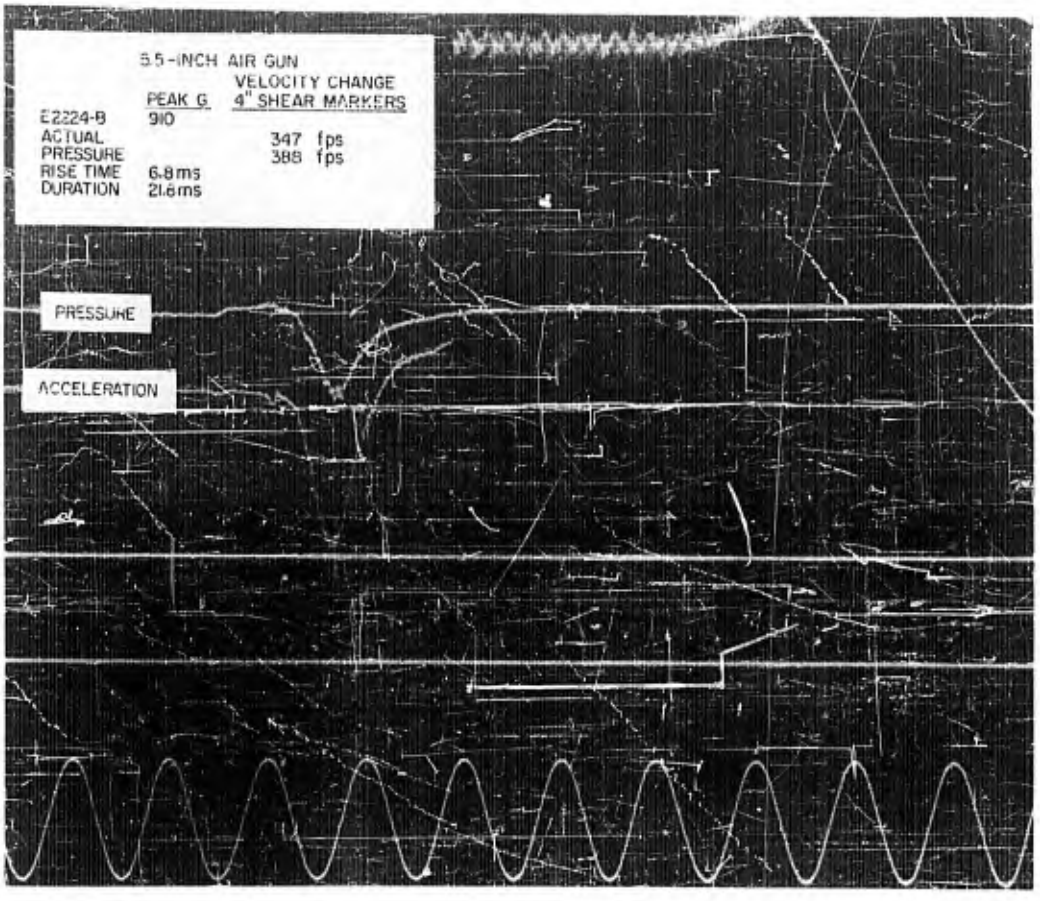
5.5-INCH AIR GUN
VELOCITY CHANGE
PEAK G
4" SHEAR MARKERS
E2224-B
910
ACTUAL
347 fps
PRESSURE
388 fps
RISE TIME
6.8 ms
DURATION
21.6 ms
PRESSURE
ACCELERATION

Figure 13

Dr. Bouche (Endevco Corporation, Pasadena) then discussed the results of a survey* which had been made at Endevco.

Dr. Bouche: I'll tell you about a survey we made, as the result of a number of people mentioning that this "something" was happening. I gathered together some 14 or 15 pickups, and we applied a series of drop tests to them and tried to discover just what the general characteristics of this zero shift were. I'd like to classify the zero shift a little bit more definitely, so that we can focus our attention and distinguish it from so-called negative undershoot, resulting from insufficient RC time constants of the pickup and input resistance to the amplifier, and insufficient frequency response in the following amplifier. To distinguish it from these, I'd like to call it an effect such that an accelerometer continues to have a measurable voltage output that persists for a finite period of time after the shock motion is completed. And, I think, because the voltage output does not immediately return to zero, we've been calling it "zero shift."

To perform this type of survey test, we used a little drop-ball shock machine we developed at Endevco. It consists of nothing more than an anvil about 1 or 2 inches in diameter and 1 or 2 inches long. We attached the accelerometer to the bottom of the anvil and impart the shock motion by dropping a ball on the anvil. One can perform an absolute calibration of the anvil, or the accelerometer attached to the anvil, by measuring the velocity of the anvil after impact. With this, we're able to apply shock motions up to as high as 16,000-g, half-sine pulse, with a duration of 50 ms. If we want lower acceleration, we put rubber pads on the anvil and get correspondingly lower accelerations. With 1-1/2-ms duration, the acceleration applied is about 325 g. In the test we connected the pickup, in most cases, directly to an oscilloscope and put some capacity in parallel across the pickup to reduce the pickup output and also to obtain sufficient time constant. In some cases, we did put a cathode follower or preamplifier between the accelerometer and the oscilloscope, but no filtering circuits were used.

In this series of tests we applied first, a series of increasing accelerations, 1600 g, 2400 g, 4500 g, 8500 g, and 16,000 g, all along the sensitive axis of the pickup. Then we applied 1800 g in a direction inclined 45 degrees from the sensitive axis of the pickup. This motion was preceded and followed by shock motions of 8500 g or higher. After that we applied 2300 g along the sensitive axis of the pickup in one direction, and followed it by a shock in the other direction, of the same magnitude, generally speaking. We applied about five series in both directions for a total of 10 shots; that is, we applied the acceleration into the base of the pickup, out of the base, and so forth. You notice that in Fig. 14, for example, there is a negative shift which is about 5 or 7 percent of the total acceleration. In Fig. 15 there is a positive shift which is on the order of 15 percent of the peak acceleration, and in Fig. 16 it is about 20 percent of the peak acceleration. The frequency with which we obtain these shifts is indicated in Table 1. In the second column of Table 1, the various accelerometers are designated by letters; the basic design of those of letter A is the same, and those of letter B is the same, etc. One thing that we could tell from the results that we obtained is that, generally, the shifts occurred more frequently, the higher the accelerations that were applied in the 8500- to 16,000-g region, with the exception of one of the pickups. Pickup No. 5, exhibited shifts almost everytime we dropped it at accelerations as low as a few hundred g; however, in that particular case, we were subjecting the pickup to accelerations far in excess of rated acceleration, by a factor of 20 or so. One thing that I thought was a little interesting about this, is that the shifts seemed to be somewhat of a unpredictable thing that was not tied down to the compression-type accelerometer, as Mr. Smart has already pointed out. There were shifts in annular-type accelerometers and shifts in other types of accelerometers, so we couldn't predict it on that basis. And, for the results of the tests that we conducted, I couldn't draw any conclusions that would indicate the zero shifts exhibited a definite trend because of the accelerometer's previous

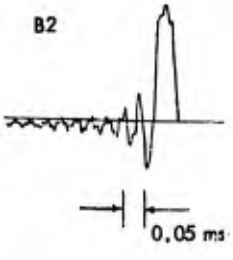

Fig. 14 - Output of acceleration pickup of Design B2 subjected to a 16,000-g, 50-ms shock pulse. (The negative shift is 6 percent of the peak output of the pickup.)

*R. R. Bouche "Survey Report on Quasi-Constant Voltage Outputs from Piezoelectric Acceleration Pickups Subjected to High Shock Motion Accelerations," Endevco Technical Data, Nov. 11, 1960.

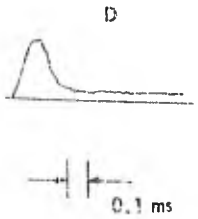

Fig. 15 - Output of acceleration pickup of Design D subjected to a 4500-g, 200-ms shock pulse. (The positive zero shift is 20 percent of the peak output of the pickup.)

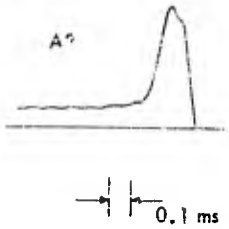

Fig. 16 - Output acceleration of pickup of Design A2 subjected to a 2400-g, 250-ms shock pulse. (The positive shift is 20 percent of the peak output of the pickup.)

TABLE 1
Summary of Quasi-constant Voltage Output Shifts from Piezoelectric Acceleration Pickups Subjected to the Same Applied Accelerations up to 16,000 G, Except Where Otherwise Indicated

Pickup No.	Pickup Basic Design	Pickup Model Number	Number Shock Motions Applied	Number Voltage Shifts Occurred
1*	A1	Endevco 2211	13	1
2	A1	Endevco 2213	22	3
3	A1	Endevco 2215	20	0
4	A1	Endevco 2242	25	0
5†	A2	Endevco 2219	11	9
6‡	B1	Endevco 2225	14	3
7	B1	Endevco 2225	20	0
8	B1	Endevco 2225	21	0
9	B1	Endevco 2225	22	0
10	B2	Endevco 2224	18	1
11	B2	Endevco 2224	17	2
12§	B2	Endevco 2224	11	2
13#	C	Manufacturer X	8	2
14§	D	Manufacturer Y	8	6

*Only increasing accelerations between 1600 g and 16,000 g as well as 1800 g inclined accelerations applied.
†Only increasing accelerations between 325 g and 8500 g were applied.
‡Only increasing accelerations between 1600 g and 16,000 g as well as 2300 g alternating direction accelerations applied.
§Only increasing accelerations between 1600 g and 16,000 g were applied.
#Only increasing accelerations between 8500 g and 16,000 g were applied.

history, or that it was a function of the transverse component of the applied acceleration. I think some of the other people who have made these tests have indicated that they have observed some trend in one or other of these directions, but in our particular tests, limited in that we were using relatively short duration pulses, I could not draw such conclusions. There seems to be a trend, though, that the shifts were a function of the stress applied to the crystal in the accelerometers; that is the stress in the crystal for the same applied acceleration. For example, in Table 1, the stress in Accelerometer A2 was 10 times the stress in Accelerometer A1 for the same applied acceleration. Likewise, the stress in Accelerometer B2 is 10 times the stress in Accelerometer B1 for the same applied acceleration. You will notice in the case of Accelerometer A2, that the frequency of occurrence of the shifts was much greater than in A1. The frequency in B2 was greater than the frequency in B1. In fact, I did try to use some sort of a philosophy in making the test. Once it was determined that a particular design of accelerometer shifted, I lost a little interest in that accelerometer, because if I found one that did not shift, I wanted to do everything to that one to make it shift. I wanted to build up some evidence for the tendency for it not to shift and this is why you'll notice that the Endevco 2225 accelerometer was tested so many times. I tested four of them and subjected them to quite a number of shock motions; and of the four, only one shifted and that one shifted only three times out of 14 shots. Figure 17 is a picture from the same pickup as in Fig. 16 but using a less-sensitive time scale to have a look at what happens to the output after the shock—what happens to the zero shift as it progresses as a function of time. It seems that the decay of the final portion of the zero shift is consistent with the time constant of the measuring circuit, which in this case was 5 ms. That is, the zero shift had returned to zero within 5 ms after the pulse was completed. But on the other hand, there seems to be slightly flat portion for a period of about 4 ms. This might suggest that some crystal deformation is occurring in the crystal of the accelerometer after the shock motion is completed; and this deformation in the accelerometer, if it were to continue to give an output, would be a deformation that would be changing over this short period of time of 4 ms.

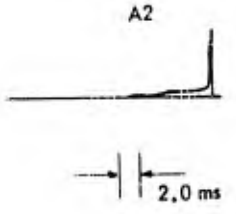

Fig. 17 - Acceleration pickup of Design A2. (The acceleration pulse and zero shift is similar to that shown in Fig. 16. The input time constant of the pickup and electric circuit was 5 ms.)

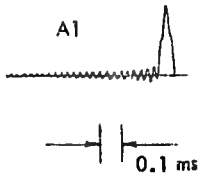

Fig. 18 - Output of acceleration pickup of Design A1 subjected to an 8500-g, 80-ms shock pulse

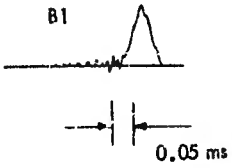

Fig. 19 - Output of acceleration of Design B1 subject to an 8500-g, 80-ms shock pulse

I think the general type of thing that we can tell from these tests is that the zero shift is present, that it seems to be a result of something happening in the accelerometer, and that it appears to happen at the higher accelerations, and that the frequency of occurrence of this shift does seem to vary from one design of accelerometer to another. In something like the Endevco 2225 accelerometer, in which the stresses in the crystal are very low compared to other accelerometers, zero shifts did not occur nearly as frequently as in other cases, so this is maybe a direction we can start in in designing accelerometers to correct for this. The indications are so far that the Endevco 2225 has been used quite successfully in field tests, although I think that Mr. Jensen will probably mention that he did get a shift from one out of the four that I tested.

After Mr. Jensen's account of his investigations, Mr. Kapiloff (Westinghouse, Sunnyvale) inquired about the possibility of using an electrometer on the accelerometer and cathode follower to try for any latent change on the cable on the disconnect. Mr. Smart (Sandia Corporation, Albuquerque) replied that they had used electrometers, they had shorted the grid just before the pulse, and when they had got a shift the only difference had been that it lasted much longer. There was still an RC return, but it was very long because now there was no grid-leak resistor. Mr. Smart was then asked why should a change continue to be

generated long after the source or physical reason for the charge had disappeared. He replied that, when polarized, there was a constant charge on the crystal. Now, if the lattice were overstrained, the configuration might actually be changed slightly as it would if a voltage or force were applied. Then would it not be possible to have a permanent or semipermanent change in the total charge? Such a change would be analogous to the change of magnetism when a magnet was shocked. You could polarize a ferroelectric by shock.

Mr. Bradley (Endevco) agreed but said that would not mean that you would continue to have a latent charge. You could change crystal configuration to such a degree that you would get a different charge pattern or characteristics. Mr. Smart suggested that leak-off would then follow the circuit parameters. He pointed out that in his particular circuit, the time constant was about 2 seconds and all the zero shifts they had observed, except those from the guns, had leaked off at the circuit rate (Figs. 1-6). What he was suggesting as a hypothesis to think about was a change in the remanent polarization caused by the shock overstressing the element, analogous perhaps to exceeding the elastic limit in a metal, or something of the sort. In reply to a query from Mr. Bradley, Mr. Smart said he would expect it to return to zero eventually.

Mr. Fowler (U. S. Sonics) pointed out that to make any appreciable changes in the characteristics of the crystal you would have to put on enough force to get about 1500 v across the normal thickness of the crystal used in accelerometers. The force would be between 10,000 and 15,000 psi to make any appreciable difference. He went on to say, "I believe there are a whole series of different effects in the zero shifts shown. Some of the figures of the waveforms were clearly due to cable motion which upsets the characteristics of some accelerometers very much indeed. So you would have to throw out some of the results for that reason. Some of them may have been frictional decelerations after the shock—that is, they may have been genuine accelerations. Both the cable and the coupling capacitors and some amplifiers have a semipermanent shift, a shift in the electrical characteristics after you put a pulse in and some of the figures clearly show that. Some of the experiments with the cable show that they were doing this. It is a well known effect." As a final possibility, he suggested that a few accelerometers with a number of mechanical connections in them really do have a capacitance shift on experiencing high shocks.

Mr. Smart inquired if Mr. Fowler was saying that there really was no zero shift. If the things Mr. Fowler had mentioned were so clearly evident, would he point them out. Mr. Fowler pointed out one case where the shift had occurred before the pulse and said this was very much like cable motion. Mr. Jensen agreed but said he had pointed this out at the time. Mr. Smart said that they went to great lengths to immobilize cable and to get the electronics out of it. If it could be shown there was an electronic problem, he would be happy to try eliminating it. Mr. Fowler said he did not mean that no accelerometers really showed the effect. However, there were a lot of accelerometers in which there were many mechanical connections and putting stress on the case of accelerometer could affect the sensitivity. He had been associated with Raytheon in developing a line of crystal accelerometers and, broadly speaking, he would say that they had not shown these effects at all. Mr. Smart asked Mr. Arndt (Clevite Corporation) to comment.

Mr. Arndt confirmed the high stresses needed to change the polarization of any of the ceramics. He gave a typical figure of from 15,000 to 20,000 psi. He went on to say, "If you do stress a ceramic to the point where you affect the remanent polarization, the effect of this is a reduction in the piezoelectric effect, but it does not imply any permanent voltage appearing across the electrodes. You just sort of squeeze some of the energy out of it so to speak, so that on further stressing, the output is less than it was originally.

Mr. Jensen went on to describe the results of an investigation* which had been made at Sandia Corporation. Mr. Jensen:

The investigation was carried out with a Gulton AT-2 Ballistic Pendulum. With this machine shocks can be repeated at about 40-second intervals, but maximum accelerations are limited to about 600 g for 9/10 ms. It was necessary, therefore, to use transducers likely to be most sensitive to the phenomenon, and from past experience Gulton A391TM were chosen.

The test set up was as follows: Gulton Pendulum, the cathode followers supplied with it, a Tektronix 536 oscilloscope, and a Hughes memo-scope. The oscilloscope was used as

*H. J. Jensen, "Zero Shift in Piezoelectric Transducers," Sandia Corporation, Report SCDC 2006.

a trigger generator to supply the memo-scope with an initiating pulse at the proper time. The pulse from the reference accelerometer was amplified by the Tektronix 536 and used for self-triggering. The trigger set the horizontal sweep on the 536 into operation. The rise time of the sweep was then used to control delay of the sweep initiation on the Hughes memo-scope, the delay being necessary because a period of time elapses while the shock travels the length of the pendulum slug.

It was then required that assurance be obtained that the cathode followers would not be overloaded. It was found that these would accept a 30-v, peak-to-peak signal through a 1000-micromicrofarad capacitor. The deflection sensitivity of the Hughes memo-scope was set at 1/10 v per centimeter and remained at that level throughout the entire test. The gain of the cathode-follower, low-pass filter combination was 0.48. In addition, accelerometers with higher sensitivities were mounted in the test position and the shocks passed through the system undistorted. These two tests should be satisfactory evidence that zero shift was not being caused external to the transducer.

The next step was to round up all the Gulton A391TM's available. Several of these had been used at one time or another and several were new. All told, about 80 samples were tested. These were installed on the pendulum and the first 3- to 6-shock pulses were recorded on the memo-scope and then photographed.

It has observed that the majority of transducers shifted to some extent at least and several shifted quite radically. It was immediately apparent that the outputs of these accelerometers on the first to third shock pulse bore no resemblance either in amplitude or wave form to the true shock pulse.

The tests were repeated the next day after the transducers had been disconnected and stored inactively overnight. Shifts were again observed on those whose tendency it had been to do so on the previous test. The magnitude of the shift seemed to be about 25 to 50 percent less.

A transducer was then selected from this group which repeatedly showed significant amounts of "zero shift," the intention being to use this for the balance of testing. This was done not with the idea that it would be representative but that the effects could more readily be studied under the limited laboratory conditions. The observations which had been made from the inactive storage effects naturally lead one to wonder if the same phenomena would redevelop if the entire test set up were left active for long periods of time. Toward this end, a test series was conducted with the selected transducer left actively installed with all associated electronics in active operation. The transducer was given three consecutive shocks at 40-second intervals after periods of: 3, 6, 12, 24, and 48 minutes; 1 hour and 36 minutes; and 18 hours. At no time was a "zero shift" observed.

At this point, one might reason that the tendency to "zero shift" could be a result of charges accumulated during storage or induced by a potential on the cable used to connect the transducer to the cathode follower. It was then observed that a small "zero shift" (less than 25 percent of that observed after storage) took place after each momentary disconnection of the cable at either the transducer or the cathode follower. The transducer was installed after an overnight shelf period and given several 550-g shocks. After showing decreasing shifts, the transducer performance again became normal. The cable was then removed momentarily at the transducer, reconnected, and the transducer was shocked three times. There was a small amount of "zero shift," at first—and then the transducer again achieved stability. The connector was then removed momentarily at the cathode follower. It was then noted that the shift took place in the opposite sense when the disconnect was made at the cathode follower rather than at the transducer and a series of tests was conducted to confirm this observation. The observation was found to be true.

An attempt was then made to exaggerate this condition by placing a battery across the transducer. With this arrangement, the battery could be placed across the transducer in either sense without also placing it across the cathode follower. It was noted that the sense of the "zero shift" was a function of the sense in which the battery was placed across the transducer. This test was also conducted with a 10-minute waiting period between the point at which the battery was placed across the transducer, and the point at which it was shocked. No decay in the tendency to shift was observed during this period of time. A number of the above tests were then performed on the Clevite ICI Serial Number 002. This unit was selected because it was on hand and readily adapted to the mount and for no other reason. This unit did not exhibit a tendency to shift under any of the above conditions.

It is recognized that these investigations are not complete. No attempt has been made to make them so, nor can the results be interpreted as being representative of a product or class of products. What is significant is that "zero shift" has been shown to exist in a transducer. Furthermore, this "zero shift" has been induced and controlled by strictly electrical means. This is not to say that mechanical effects do not contribute but rather to say that "zero shift" must be thought of in "inclusive" terms rather than "exclusive." It has been observed that certain transducers within a type are less subject to "zero shift" than others. Further investigation should be directed to finding out what design parameters are involved in eliminating this undesirable phenomenon. Until a solution has been achieved, we are forced to the conclusion that a very serious limitation on the use of piezoelectric transducers for shock measurement has been imposed.

Mr. Bradley asked if Mr. Jensen had any explanation for the change in zero shift with disconnection of the cable at one end or the other. He felt there were adequate theories to account for all the other happenings. Mr. Jensen did not have a theory.

Mr. Bradley then outlined his views.

"It seems to me that there are two major effects, and they can probably be broken down into several subcategories. Certainly in some kinds of designs there are mechanical shifts, particularly, you'd expect to see them in compression accelerometers when impacted at 90 degrees to their sensitive axis. I think this has been pretty well shown by some of the figures. This could also be tied into the case stress effects that have been mentioned by Mr. Fowler. These are all quite easily explainable but then we get into the units with which the bulk of Mr. Smart's field tests and the bulk of our tests at Endevco were conducted; these are either a bender element which exhibits these characteristics repeatedly, or the annular type. If I'm not mistaken, in the bender element the crystal is totally isolated from the case. In fact, it's up on a pedestal where the diameter of the pedestal is something like 30/1000 inch, and it is hard to see where any stresses from the case can be coupled into crystals. I would say that in a bender element, the case effects or physical shifts, must be ruled out. The same is true in the annular concentric crystal where the crystal is supported on a post or around a post and the mass is around the crystal. These are some of the kinds which are shown in the figures, and also I believe some of them are the Clevite units. There could be complete failure I believe, because the only thing that can shift are the bond lines between crystal and mass and this would be a total failure rather than a change in preload or change in the mechanical pressures on the crystal. So, it seems quite evident to me that something is happening in the crystal. I wish it were not true, but I think we have to face it: We have long experience which tends to indicate that it does not take 10,000 pounds per square inch to affect the polarization of a crystal. As long as 5 years ago, we started cycling our accelerometers for a period of some 3 weeks in terms of all kinds of shocks: hot shock, cold shock, and something on the order of 30,000 g. Now this was done, not because we were trying to beat them to death, but because we found that they were not as stable as they should be until we went through this process We have documents on, I would guess, thousands of units showing that as they went through this process, there were shifts in polarization. This shift in polarization is observed as a shift in sensitivity; however, a shift in sensitivity is a shift in polarization. And if you were to observe it during the time it was shifting, you would discover that it would appear just like the dc shift in the figures: because when the polarization changes, the crystal either gives up or takes on charges, and this in essence changes the voltage across the crystal until the charges have a chance to leak off and equalize. So I think the problem is with us and very much in the crystal.

"Let me go one step further to say that it is probably not unusual to expect this to happen, because most metals when dynamically loaded will show hysteresis; and I assume, therefore, it is reasonable to expect dielectric materials will also show hysteresis and particularly a hysteresis that is time sensitive, a hysteresis where the material on the first cycle never returns to zero but on subsequent cycles usually does return to zero. If you wait a few hours or days and do it again, you very often find that you go through the first hysteresis again. I'm not saying that this is what is happening, but I'm saying that it seems to be analogous and that this is the sort of thing that is going on within the crystal. The best solution to it is what I think has been shown here, that is to reduce the stress on the crystal so that hysteresis becomes small. It does seem to be stress sensitive."

The following discussion then occurred.

Mr. Fowler: You are discussing here the shift in sensitivity. I don't deny that over a

period of time, particularly when these crystals are new, they spontaneously will slowly lose a certain amount of their polarization. I would make a very, very strong distinction between the sensitivity of the accelerometer and the sensitivity of the crystal element. You're saying that in the ring accelerometers which are cemented onto a post, that you're not changing the stress in the crystal when you stress the case. If you work out how many tenths of a micro inch deflection it takes in the crystal to upset its sensitivity, I think you might change your mind a little. Have you tried actually measuring the sensitivity of the crystal—that is, for instance, the ratio of its resonant frequencies?

Mr. Bradley: Very definitely.

Mr. Fowler: You're relating the change in actual sensitivity of the crystal to the shock testing and so on that you've done to it. It seems to me that you would have to make some very careful measurements to show whether the shift in sensitivity that you measured on the crystal after you've taken it out of the accelerometer and you've got it mounted between a pair of whiskers, whether this was due to shock or due to temperature cycling, etc.

Mr. Bradley. I don't think we have done anything exactly as you've laid it out. I will say though that we have put stresses into the case on these concentric-ring accelerometers that are so great that they permanently deform the case and this has no effect on the crystal.

Mr. Fowler: Well, that's very interesting.

Mr. Bradley: In other words, we have verified that the stresses from the case into the crystal have no effect on the crystal.

Mr. Fowler: I think you said you didn't understand what happened to the experiment with the battery in the cable.

Mr. Bradley: The battery, I can understand. Just why, when you disconnect the cable at one end, you get a positive shift and when you disconnect the cable at the other end you get a negative shift—this is very hard to understand.

At this point, a 10-minute break was taken. Resuming the discussion, Mr. Fowler said, "The suggestion has been made that all of these experiments should be repeated without an accelerometer but with a good quality mica capacitor; there are some uncased ones for computer use which are of extremely good quality. They should be of the same capacity as the accelerometer, and then subject this apparatus to all these tests including the shock test."

Mr. Smart: We did this on the air gun using regular 5-percent silvered mica capacitors and we got nothing, absolutely nothing. In other words, in place of the accelerometer we had a capacitor with the plates in the same axis that the plates of the accelerometer would be, and as I recall, we got nothing except a little line noise.

A voice: Have you tried putting batteries and switches in series with it to put pulses in it?

Mr. Smart: No, we have not. However, it was charged with the cathode voltage of the cathode follower. So it did have about 30 v across it. Our cathode follower has about 40 v on the input. We have an 0.01-microfarad input capacitor. The accelerometer had about 500-microfarad capacity, so it would have had all the voltage across it, or pretty near all. We fully expected a signal. We did not get one that I can recall.

Mr. Bradley: One of the conclusions that we have reached here is that the whole system ought to be tested under all these conditions, without using the crystal and the accelerometer. The best indication to me that there may be another effect in addition to the crystal effect is this cable disconnect business where disconnecting at one end you get one effect and at the other end you get another effect. It seems more important to put a single pulse generator—not a train of pulses, but a single pulse—into the system and look for shifts. Do you get any shifts?

Mr. Smart: Right across the accelerometers?

Mr. Bradley: Yes.

Mr. Smart: Well, I've done it both ways. I've used a single-pulse, Tektronix pulse generator both with the accelerometer disconnected and with a capacitor where the accelerometer was. When I disconnected the accelerometer, I fed the capacitor in series, simulating a voltage circuit with a series capacitor. In other words, it would be the Thevenin equivalent of the piezocircuit which would be a charge generator with shunt capacitance. So, then, when I put the shock pulses in, I put in a voltage and a series capacitor. And I'm fairly confident of the cable when stationary; now I'm not so confident of it in

the test. Mr. Fowler probably has a point. The ones he said were to him, at least, clearly cases of cable deformation, whereas in the gun tests, we do not have much control over the cable. This is a good point, maybe; but in those also, we have used the capacitor to replace the accelerometer on the 5-1/2-inch air gun and have never had a signal.

I have very exhaustively tested, under single pulse conditions, the entire system that we use. Not only in the laboratory, but at the tower and in places where they are actually used. We actually calibrate with a simulated accelerometer.

Mr. Fowler: There is one thing I'd like to say that may clarify the position I'm taking. I'm not arguing that some accelerometers don't show the zero shift because I believe some accelerometers do; but, I believe it's faulty mechanical design. I'm just saying that, in general, accelerometers don't have this effect.

Mr. Smart: Have a look at Figs. 2 and 3. Take the Clevites for instance. On the more sensitive one, the 5-millivolt-per-g accelerometer, we got a shift similar to the one at the top (Fig. 3). On this same drop, look at the two 2C1 (Fig. 2). With these there is only a decrease in the seismic mass, and the capacitance is the same. The mass was decreased to where the sensitivity dropped from 8 millivolts per g in the 5C1 to 2.5 millivolts per g in the 2C1. Those two (Fig. 2) did not shift on the same drop with roughly the same g load and the same duration.

Mr. Fowler: That would have been halving the mass?

Ted Smart: That would have been changing the sensitivity by a factor of about 3 to 4, by only changing the seismic mass.

Mr. Fowler: Then apparently for just a 3-to-1 change in the stress in the crystal we go from no effect at all to an effect in which the crystal broke.

Mr. Smart: Right. On this 1-g load. Yes, that's correct. This was about 1000 g, roughly.

Mr. Fowler: If you'd really affected the crystal that much, this accelerometer wouldn't have worked afterwards or would have been so drastically different you would have noticed it. It is not reversible you see, if you damage it.

Mr. Smart: Oh, I realize that. But we're not suggesting that it's been damaged, because we can use it again on the next test and get a perfectly satisfactory signal.

Mr. Fowler: To my mind, and I don't know whether the gentleman from Endevco would agree with this, in this particular case it would really rule out the possibility of it being the crystal.

Mr. Smart: No, I've gone along with you so far, but I can't agree with you there. Why would you say that?

Mr. Fowler: Well, it may be a few-percent shift in capacitance; this is feasible.

Mr. Smart: That particular crystal, like any of these others, may shift on one shock and not on the next. Or, I'll tell you something else, that happened—you can take one accelerometer and subject it to continued shocks, the amount of shift will decrease and after awhile you won't get any. But, if you reverse it, go back the other way, it will start all over again. And we can do this time after time. Isn't that right?

Mr. Jensen: That is correct.

Mr. Smart: And we can do it on the same accelerometer and successive calibrations will not show any difference in sensitivity.

Mr. Fowler: Well, I would suggest in that case, on this particular accelerometer, that it sounds as if it must be a mechanical effect—that somehow you are altering the tension in the case and changing the stress in the crystal. As I say, we have accelerometers which are basically very similar to these, and they don't show the effect.

Mr. Arndt: Well, my only real comment is that I don't understand it. I'm inclined to agree that a reduction of 3 to 1 in the mass and therefore stress on the crystal for a given acceleration, should not make such a tremendous difference such as we saw between the very large zero shift and no apparent zero shift. If the trouble were in the crystal material I would think that it would not be quite so violent. Now, we don't understand what it is, if it is in the crystal, so we can't make any very conclusive statements about it. But the feeling is, that it wouldn't be such a radical change.

Mr. Fowler: Would you think there would be any difference in the behavior of the

low-curie point, comparatively low-activity barium titanate, the almost pure barium titanates, as compared with the very high curie point, very large activity crystals that both our companies make—because I would guess that we've got a mixture of materials in the accelerometers we are talking about, and it is possible that maybe perhaps some of the almost pure barium titanates might behave differently as they are easy to polarize for instance.

Mr. Arndt: Well, I wouldn't be surprised to find a difference. Frankly, I know very little about the physics of these crystals. My interest is more on the application side, and my attitude at the moment is that most anything could happen and I don't think I could say one way or the other. Certainly, in certain respects there are very big differences between, say a straight barium titanate and some of the other materials.

Mr. Bradley: All of the data shown concerning our annular designs, is for lead zirconate titanate with curie points well above 700 degrees, and still we see the dc shift. I would suspect it would be worse than pure barium titanate because the coercive force on alloyed barium titanate is very low, but most commercial barium titanates have calcium and lead in them that raise this coercive force and therefore should improve the stability. Lead zirconate is another order of magnitude a better in coercive force, isn't that right?

Mr. Edleman (National Bureau of Standards): I have a comment which is completely negative, and I offer it only because maybe someone can make something of the experience we've had. We've reported driving several different pickups with sustained sinusoidal accelerations over a fairly long period of time, with acceleration levels up to 12,000 g. We have been doing this while we were calibrating the pickups and in this study we found no sign of any shift. Now from the comments that I've heard tonight, apparently there was no reason to expect any, but perhaps the fact that none showed up is significant. If any had been present we would have found them. We were making very careful calibrations repeatedly and the pickups were exposed to these very high levels of acceleration over a wide frequency range and over a period of several weeks. Now the pickups were of several different kinds, one without any inertial mass, another with a very heavy inertial mass and neither of them had any case, so there was no question of the case effects. I just offer this and hope that perhaps this will tell you what the zero shift is not due to.

Mr. Jensen: May I ask you a question Mr. Edleman? Did you observe any nonlinearity? Mr. Bouche suggested to me sometime back that if on a continuous sinusoid test, zero shift did occur at the end of each half cycle that this would show up as a nonlinearity. Maybe you could clarify that a bit Dr. Bouche?

Dr Bouche: I don't remember the exact subject at the moment except that we were in a general discussion about the fact that one of the pickups that did exhibit shift quite a bit, was nonlinear in its amplitude response. I mention this with some hesitance, because of all of the piezoelectric accelerometers with which I've been associated, it is only with one accelerometer that I've noticed any nonlinearity and this particular one did have the most zero shifts. This particular accelerometer exhibited nonlinearity at low accelerations compared to other accelerometers in which we have no indication of amplitude nonlinearity up to thousands of g.

Mr. Ames (Frankford Arsenal): I can only tell you of our experience. We have noticed dc shifts in fairly low-g ranges of several hundred g and up to maybe 20 or 30,000 and we blamed it on the instrumentation rather than on the accelerometer. To eliminate these dc shifts, an electronic engineer redesigned the cathode follower, and along with this had the technicians make what he called a stumpometer. This was a metal rod in a solenoid, and by pushing a button he could repeatedly hit the accelerometer and produce dc shifts. He tested continuously until, by redesign of the cathode follower, he didn't get any dc shifts. I don't know what bearing that has on the case but that was our experience. And, as far as we're concerned, we don't have that problem now; it might be that by a careful examination of some of our records, it might possibly be noticed in the transverse shocks but, we consider the problem solved as far as we're concerned.

Mr. Jensen: I think there wouldn't be a one of us here that wouldn't agree that this is a possibility, and probably one of the first things that anyone would think of, on the other hand, you can't explain the randomness of occurrence nor can you explain how some particular class of accelerometers will exhibit this much less frequently, especially in the case where the sensitivity of a "nonshifting" accelerometer could be a whole order of magnitude more than in the case where it was shifting.

Mr. Bort (David Taylor Model Basin): The small accelerometers are exactly what

you need for model work if you want to measure response of the models to underwater explosions. We've been trying to use them for the past 5 years and we've always been brought up short by this very zero shift. Since we're mainly interested in things such as velocity and displacement, even a small amount of zero shift will shoot us down, because zero shift amounting to as little as 1 percent of the peak acceleration integrated to get a velocity and double integrated to get a displacement means that it immediately drifts off screen one way or the other. We found the random effect. We've also found that at roughly 2000 g, you get roughly 20-g zero drift (sometimes one direction, sometimes the other). These show up in the integrated records. We generally record into an RC circuit without a preamplifier so there is no voltage on the accelerometer. We follow the RC circuit with an electrometer impedance amplifier which will give us a 1000-megohm input impedance and run our recording equipment. The electronics have been checked with small pulse generators and work fine. We made checks with the cable dead ended rather than connecting it to a capacitor, and got no real cable effects. If we could get rid of this zero shift, it would be real handy because the small accelerometers are just what we need in model work.

Mr. Jensen: Well, I'm in complete agreement. Our problems deal with flight test vehicles, where the installation has to be made several weeks before we can actually conduct the test, and during which time the entire installation and all the associated electronics lie dormant. We can't control some of the factors that might be controlled in laboratory. For instance, we can't very well keep the accelerometers shorted and reliably reconnect them sometime during the flight, and we can't keep a running record of the accelerometers' past history. It becomes a problem of eliminating the source of the trouble rather than trying to correct it.

Mr. Hancock (Endevco): None of the data presented has given any definite indication that the accuracy of the peak amplitude is impaired by the zero shift. Have you, or has anyone demonstrated that the indication of amplitude is off by X percentage or is affected by this shift?

Mr. Jensen: In the investigation* we made and which I described to you earlier we had some good examples. We used a ballistic pendulum to get a half-sine pulse. This was very repeatable and we could demonstrate it with other types of pickup. Well, we took a transducer and installed it after an overnight shelf period and gave it several 550 g shocks. With the initial pulse, the accelerometer indicated zero acceleration and shifted negatively. On the second pulse, there was a little acceleration and with successive shocks performance gradually improved. It was not until the fifth and sixth shocks that it began to approach the half-sine pulse we knew was there.

Another example is Fig. 1 in the report* which shows in the bottom trace a positive zero shift. The pulse was actually a square wave. I believe in this particular case we could have intuitively corrected for the zero shift, but if it had been an unknown waveform, I am sure we could not have justified any particular correction.

A voice: How did you produce a square pulse?

Mr. Jensen: Impacting honeycomb.

Mr. Bradley: It is a possibility that the crystal is acting like a transistor? I'd have to say out of ignorance that I assume it is not a possibility. I wouldn't see how it worked.

Mr. Fowler: You can dope some of these materials until they are semiconductors, but the resistivity of one that is piezoelectric would be far too high; there is just no appreciable conduction. They are tens of megohms at the very least and usually hundreds and even thousands.

Mr. Kapiloff: But, we have been talking about the possibility of a change in the structure due to severe acceleration and we have considered, too, the fact that there may be some impurities in some of these crystals that are not present in others. Also we have potentials, that exist, either from the amplifier or from the counter emf of the crystal itself. Now, would that constitute a transistor effect do you think? I'm trying to see if we can't find some other explanation for these dc shifts and that occurs to me as a possibility.

Mr. Fowler: I don't believe that would be a possibility. There is a possibility that might occur in some of these experiments and which would account for zero shifts far greater than which have been mentioned. Most of these higher resistivity crystals are extremely pyroelectric. For instance, if you take a good crystal out of an oven at 250 degrees and put it down on something cold, if you touch it within the next 10 minutes you would get a pretty nasty

*H. J. Jensen, "Zero Shift in Piezoelectric Transducers, Sandia Corporation Report SCDC 2006.

shock off it. For a matter of only a few degrees centigrade change in a matter of a second or two, you would get more voltage shock than from the zero shift that you're talking about.

Mr. Bradley: I'd like to change the subject a little. We've been talking about all the problems here and how what a problem zero shift is, and it certainly does seem to be, but it seems to me that there is a good chance of overcoming it. In our tests, on two separate designs, not one zero shift showed up in over 50 tests. I don't know whether this will be duplicated under all circumstances, but other tests may show up zero shifts under certain conditions which would give us a clue. It does seem to me that it is an effect that is controllable, and one which will, and is, yielding to some solution. I don't think it is as hopeless as all of us discussing the problem here might make it sound.

Mr. Fowler: Could I ask somebody from Sandia, on the air gun experiments, whether the temperature of the accelerometer at the end of the shock was effectively exactly the same as it was at the beginning?

Mr. Smart: The man who designed it says it is strictly isothermal. I use this word hesitantly. In other words, there is no temperature change in the shock and especially up until the time the cable has been cut. The cylinder is accelerated and, at a later time is decelerated by compressing the air in the muzzle. Up until the time that the cable has been cut, which is approximately 6 feet from the breech (and the thing is 120 feet long), the designer maintains it is completely isothermal. There is no pressure, effectively, in front of the cylinder at that time because he has a low-pressure valve at the other end so that he has no deceleration until he wants it later—so he says. This is a question we brought up when we started seeing this; we said, well, you've got pressure there, your working against a difference in pressures, maybe you're heating these things, and we tried an accelerometer that was temperature compensated or that was supposedly flat (or was flat in our tests at least) up to 500 degrees or so.

Mr. Bort (David Taylor Model Basin): Most of these accelerometers, fed into an electrometer circuit with enough impedance, drift you off screen immediately if you warm them up—this is something you simply avoid when you're working with them, but they are indeed very temperature-sensitive

SUMMARY

Mr. Fowler (U. S. Sonics): The position I would take is that I would suggest that a great many of these results are due to some extraneous factor. It may be a genuine acceleration that you don't realize you've got. It might be a pyroelectric effect which is very active in these crystals. It might be electret effects in the cable or just plain cable. It might be electronic, but most people apparently thought of this and eliminated it. I believe that some accelerometers which have much too much mechanical complication about the holding of the crystal will really show a shift. Also preceptible is shifting capacitance and a shifting in sensitivity. Whether, remaining after that, there is any real zero shift in the way it has been described, from the nature of these ferroelectric crystals I would very much doubt, but from what has been said I look for some results.

Mr. Bradley (Endevco): I think our feeling is that we have eliminated a lot of the extraneous possibilities although there is always cause to suspect anything that hasn't been thoroughly tested out in the system. It appears to us that the mechanical design can be a problem but has been eliminated in most designs that have been brought out in the last few years. The remaining cause seems to be in the ferroelectric material. It appears to us that it is stress level sensitive, since our tests definitely show high-stress level in the crystal will create zero shift while a low-stress level, for the majority of cases, does not. Now why does the crystal show these shifts when it is supposed to be so stable? As has been mentioned, the pyroelectric effect is a very strong effect generating hundreds of volts per degrees centigrade shift in temperature. The piezoelectric effect that's seen in ferroelectrics is a combination of what is true piezoelectric and what is true electrostrictive. In a ferroelectric material, you do get domain movement. Now this is a friction movement, and it would seem reasonable to suspect that some heat is generated internally in this process which could be the source of our shift. This does appear to be internal to the crystal. In final summary, I think that the newer design runs which have been produced in the attempt to eliminate zero shift, have definitely reduced the problem. I believe the users will agree that zero shifts have gotten a great deal smaller and a great deal less frequent with some of the newer designs that have been tested. I think this is the direction that will bring success.

Section 7
INFORMATION EXCHANGE

THE MATRIC COMPUTOR

Pierre M. Honnell
Washington University

INTRODUCTION

At present, matric mathematics are not very extensively employed in vibration theory, although this is inevitable. Examples of the application of matric analysis to the description of vibration generators is given in [Ref. 1], to the description of the theory of elastic structures in [Ref. 2], in mechanics in general [3], in electricity [4] and electronics [5], and in servomechanisms [6]. Increasingly, matric methods are permeating all scientific areas.

An electronic computor specifically designed for the solution of matrically formulated mathematical problems will therefore be of extreme importance both for purely mathematic problems, and as an aid in the analysis and synthesis of physical systems. This is being achieved in The Matric Computor which is presently under development.

Classification of the Matric Computor is simplest by pointing out that it employs electronic amplifiers and network components as does the electronic differential analyzer. It at present does not employ numerical techniques; however, just as the electronic machine has displaced the mechanical differential analyzer, so will the Matric Computor displace the electronic differential analyzer.

The Matric Computor, however, is a more general machine and permits matric mathematic operations to be performed; it is not limited to differential equation systems. These matric operations include sums and products of numerical matrices, inversion, coordinate transformations, and the solution of systems of algebraic and differential equations. Certain problems in linear programming and in least squares are also accessible to the computor.

The outstanding attribute of the new computor is its functional simplicity. It requires neither a schematic diagram, nor programming.

THEORY

A rigorous derivation of the mathematic theory of the computor is given in [Ref. 7] and repeated in [Ref. 8]. Briefly, an ensemble of admittance amplifiers, μ_k, and admittance components, y_{sk}, are interconnected as shown in Fig. 1. The j_k are prescribed current sources, and the w_k are the admittance amplifier outputs, recorded on digital voltmeters for steady problems, or oscillographically for time-varying problems.

To as close an approximation as desired, by making the μ_k amplifier admittance amplification large, the equation of physical state of the electronic network in Fig. 1 is described by the matric equation:

$$\begin{bmatrix} (y_{11} + y_{11}) & \cdots & (y_{1k} + y_{1k}) & \cdots & (y_{1s} + y_{1s}) \\ (y_{21} + y_{21}) & \cdots & (y_{2k} + y_{2k}) & \cdots & (y_{2s} + y_{2s}) \\ \cdots & \cdots & \cdots & \cdots & \cdots \\ (y_{k1} + y_{k1}) & \cdots & (y_{kk} + y_{kk}) & \cdots & (y_{ks} + y_{ks}) \\ \cdots & \cdots & \cdots & \cdots & \cdots \\ (y_{r1} + y_{r1}) & \cdots & (y_{rk} + y_{rk}) & \cdots & (y_{rs} + y_{rs}) \\ (y_{s1} + y_{s1}) & \cdots & (y_{sk} + y_{sk}) & \cdots & (y_{ss} + y_{ss}) \end{bmatrix}$$

$$\begin{bmatrix} w_1 \\ w_2 \\ \cdot \\ w_k \\ \cdot \\ w_r \\ w_s \end{bmatrix} = \begin{bmatrix} j_1 \\ j_2 \\ \cdot \\ j_k \\ \cdot \\ j_4 \\ j_5 \end{bmatrix} \qquad (1)$$

In the above equation, there is a 1-to-1 reciprocal correspondence between each matric entry and the correspondingly ordered physical admittance component illustrated schematically in Fig. 1. In other words, an electronic synthesis network has been devised in which each mathematical term is represented by one and only one physical device; and reciprocally.

This extraordinary property of a 1-to-1 reciprocal correspondence, or homeomorphism, between the matric mathematics and the physics of the electronic synthesis network is the crucial essence of the Matric Computor.

APPLICATIONS

As a concrete example, consider the matric differential equation system

$$\begin{bmatrix} 1.00 + \frac{d}{dt} & -0.667 & 1.33 \\ 0.400 & 1.00 + \frac{d}{dt} & -0.600 \\ 3.00 & 1.50 & 1.00 + \frac{d}{dt} \end{bmatrix} \cdot \begin{bmatrix} x_1 \\ x_2 \\ x_3 \end{bmatrix} = \begin{bmatrix} 43.3 \\ -18.00 \\ 35.0 \end{bmatrix} . \qquad (2)$$

which has the eigenroots $\lambda = 2.96$ and $\lambda = 0.0130 \pm i\ 0.238$. The ideograph or logical schema in the pattern of Fig. 1 for this matric differential equation is shown in Fig. 2 after physical scaling by multiplying all entries in Eq. (2) by 10^{-6}. As seen in Fig. 2, all constant mathematic terms are represented by conductances in microohms, differential coefficients by capacitances in microfarads, and the prescribed constant vectors by microamperes from current sources. The unknowns to be determined, the vectors $[x]$, are scaled in volts, and read from the admittance amplifier outputs.

Figure 3 is an oscillographic record of the solution to this matric differential equation system, obtained on a rudimentary machine. As may be noted from the oscillograph, the solution has the typical oscillatory behavior predicted by the complex pair of eigenroots, and the final steady state magnitude of the solution vector col (x_1, x_2, x_3) converges on (10, -10, 20).

It is clear that ideographs such as Fig. 2 are not necessary to enter the problem on the Matric Computor. That is, the new computor is so organized that the matric equations being solved, themselves represent the programming. No patching and no schematic diagrams are required.

As a second example, consider the single differential equation

$$\frac{d^2x}{dt^2} + \frac{dx}{dt} + x = f(t) . \qquad (3)$$

The matric theory of differential equations teaches that this problem can be replaced by an infinite variety of equivalent first-order mathematic systems. This provides great latitude and flexibility in the logical schemas utilized to solve such equations on the new machine.

In Fig. 4, two of the possibilities of entering the given example on the Matric Computor are shown to emphasize its simplicity. The problem is actually being solved on a very elementary form of machine constructed solely for the purpose of exhibiting certain conceptual aspects of the theory. The "d" in the matrix is a shortened version of "d/dt." As can be seen from the photograph, each constant coefficient of the matrix is entered as a conductance, and each differential coefficient "d" as a capacitance, and both plugged into the elementary computor.

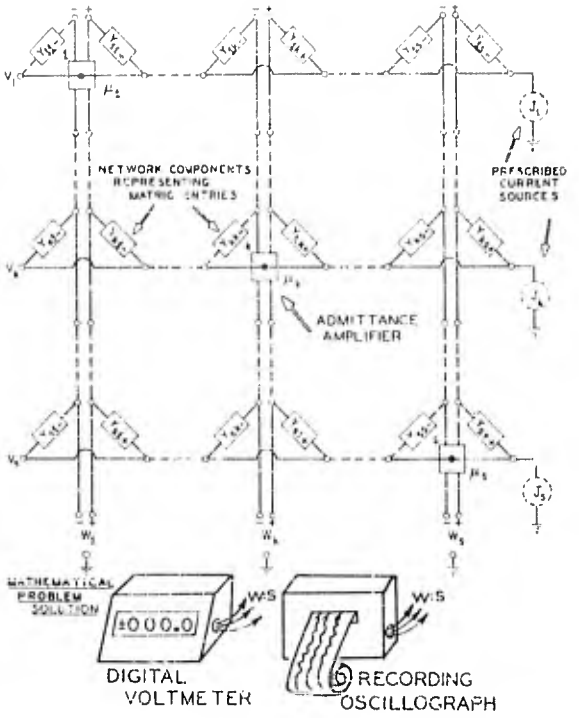

Fig. 1 - Electronic synthesis network which is homeomorphic to mathematical matrix Eq. (1)

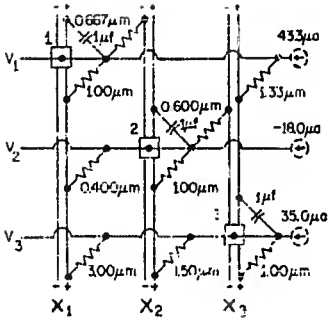

Fig. 2 - Logical schema of matric differential equation system (2)

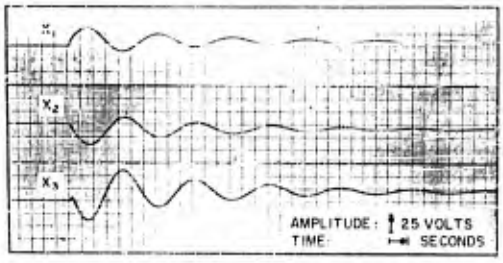

Fig. 3 - Oscillographic recording of solution to matric problem synthesized according to Fig. 2

The 1-to-1 reciprocal correspondence between the entries of the mathematic matrix and the computor entries is clearly evident; each mathematic entry has an admittance component in the corresponding matric array in the machine, and zero mathematic entries are represented by zero admittances (absence of components). In a machine for problem solving, the admittance-magnitudes would be dialed into the appropriate matric array on the machine and not plugged into jacks as shown in the rudimentary machine illustrated in Fig. 4.

EXPERIMENTAL RESEARCHES

A theory is only a theory in the physical domain; it must be verified to discover whether

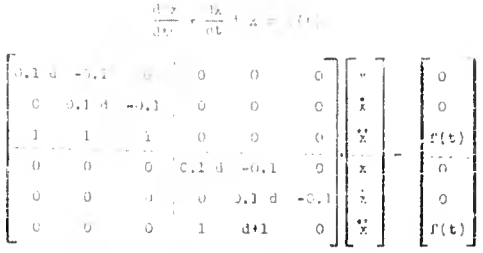

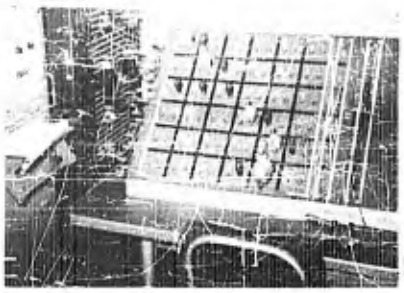

Fig. 4 - Elementary (6 x 6) order matric computor solving differential equation (3) by two methods simultaneously. (Note the homeomorphism between matric entries and computor synthesis components.)

the underlying assumptions and idealizations in the theory are valid. For these well-known reasons, a strong experimental research program has been in evidence alongside the theoretical researches; the two are, in fact, complementary and mutually supporting.

An improved machine is now under development. It will be of (10 x 10) order, and will be truly a Matric Computor. All problems will be entered merely by dialing-in the mathematic coefficients. Obviously, power supplies, means for reading out solutions oscillographically and on digital voltmeters, means for entering initial conditions for differential equation problems, means for obtaining eigenroots, and the like, must all be provided in this final-design, practical machine.

Furthermore, this machine will be adapted to the solution of linear variable-coefficient, and also to nonlinear equations. For the solution of nonlinear problems is well within the purview of the Matric Computor as is easily shown. All the required electronic components for this purpose, however, are not yet available although in principle this can be surmounted.

This is a very ambitious undertaking for a small research group, but the importance of the end result, a new electronic computor based upon a new theory, justifies the efforts.

ACKNOWLEDGMENT

It is a pleasure to acknowledge the support of these researches by a National Science Foundation grant. Without such support, fundamental researches at a university are inevitably curtailed before their final objectives can be reached and their full value realized.

REFERENCES

1. Pierre M. Honnell, "Prescribed-Function Vibration Generator," Journal of the British Institution of Radio Engineers, April 1956, pp. 187-198

2. Borje Langefors, "Analysis of Elastic Structures by Matrix Transformation with Special Regard to Semimonocoque Structures," Journal of the Aeronautical Sciences, July 1952, pp. 451-458

3. Frazer, Duncan, Collar, "Elementary Matrices and Some Applications to Dynamics and Differential Equations," Cambridge University Press, 1938

4. Gabriel Kron, "Tensor Analysis of Networks," John Wiley, New York, 1939

5. Pierre M. Honnell, "The Transmission Matrix Stability Criterion," The Matrix and Tensor Quarterly, Sept. 1951

6. Pierre M. Honnell and Daniel Wolffenstein, "Transfer Matrix Stability Criterion Applied to an Amplidyne Servo Network," Applications and Industry Section, Part II, Transactions of the American Institute of Electrical Engineers, July 1957, pp. 143-149

7. Pierre M. Honnell and Robert E. Horn, "Analogue Computer Synthesis and Error Matrices," Communications and Electronics, Part I, Transactions of the American Institute of Electrical Engineers; Mar. 1956, pp. 26-32

8. Robert E. Horn and Pierre M. Honnell, "Electronic Network Synthesis of Linear Algebraic Matrix Equations," Communications and Electronics, Part I, Transactions of the American Institute of Electrical Engineers, Jan. 1960, pp. 1028-1032

* * *

DERIVATION OF THE RELATIONSHIP BETWEEN THE "RESIDUAL" SHOCK SPECTRA AND THE FOURIER INTEGRAL SPECTRA

H. Southworth, Jr.
Sperry Gyroscope Company
Great Neck, Long Island, New York

During the Panel Session on the Establishment of Test Levels from Field Data at the 29th Symposium on Shock, Vibration and Associated Environments, there was a discussion on the relative value of Shock Spectra compared to Fourier Integral Spectra when used to represent amplitude-time shock pulses in the frequency domain. During this discussion it was mentioned by Mr. R. D. Hawkins, Sperry Gyroscope Company, that there was a mathematical relationship between the Fourier Integral Spectra and the "after pulse" or "residual" shock spectra. This fact evoked considerable interest and therefore the following analytical proof is presented here for the benefit of those interested in this subject.

INTRODUCTION

The following derivation relates the "residual" or "after pulse" shock spectrum to the frequency composition of a time pulse as defined in Fourier Integral Theory. The "residual" shock spectrum is derived in general mathematical notation for continuous functions without damping.

"RESIDUAL" SHOCK SPECTRUM

"Residual" shock spectrum is defined as the maximum absolute value of the acceleration of a one-degree-of-freedom system after the shock pulse, plotted as a function of the frequency of the system.

Consider in Fig. 1 a one-degree-of-freedom mechanical system of natural frequency, fn, mounted on an infinitely rigid base. The base of this system is subjected to an arbitrary input acceleration as a function of time in Fig. 2. This acceleration pulse $\ddot{x}_B(t)$ lasts over the time interval $0 < t < T$ where T represents the completion time of the pulse.

We can write the differential equation of this system as:

$$M\ddot{x}_M + K(x_M - x_B) = 0 . \qquad \text{(i)}$$

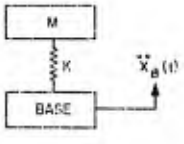

Figure 1

Figure 2

Using the definitions of relative displacements and accelerations between mass and base,

$$x_R = x_M - x_B \tag{2}$$

$$\ddot{x}_R = \ddot{x}_M - \ddot{x}_B \tag{3}$$

we obtain,

$$\ddot{x}_R + \frac{K}{M} x_R = -\ddot{x}_B \tag{4}$$

or

$$\ddot{x}_R + \omega^2 x_R = -\ddot{x}_B . \tag{5}$$

At initial time ($t = 0$) the relative displacement and velocity are zero:

$$x_R(0) = 0 \tag{6}$$

$$\dot{x}_R(0) = 0 . \tag{7}$$

Taking Laplace Transforms of Eq. 5,

$$S^2 x_R(S) + \omega^2 x_R(S) = -\ddot{x}_B(S) . \tag{8}$$

Solving for $x_R(S)$:

$$x_R(S) = -\frac{1}{\omega}\left[\frac{\omega}{S^2 + \omega^2}\,\ddot{x}_B(S)\right] . \tag{9}$$

Since $[\omega/(S^2 + \omega^2)]\,\ddot{x}_B(S)$ is the product of the transforms of $\sin \omega t$ and $\ddot{x}_B(t)$, the inverse transform is then the convolution of these functions.

$$x_R(t) = -\frac{1}{\omega}\int_0^t \sin \omega(t-\tau)\,\ddot{x}_B(\tau)\,d\tau . \tag{10}$$

Taking the time derivative,

$$\dot{x}_R(t) = -\int_0^t \cos \omega(t-\tau)\,\ddot{x}_B(\tau)\,d\tau . \tag{11}$$

At the completion time of the pulse T, the relative displacements and velocities are given by:

$$x_R(T) = -\frac{1}{\omega}\int_0^T \sin \omega(T-\tau)\,\ddot{x}_B(\tau)\,d\tau \tag{12}$$

$$\frac{\dot{x}_R(T)}{\omega} = -\frac{1}{\omega}\int_0^T \cos \omega(T-\tau)\,\ddot{x}_B(\tau)\,d\tau . \tag{13}$$

Since $\ddot{x}_B(\tau) = 0$ for any time domain outside the pulse duration we can extend both limits of integration to plus and minus infinity:

$$x_R(T) = -\frac{1}{\omega}\int_{-\infty}^{\infty} \sin \omega(T-\tau)\,\ddot{x}_B(\tau)\,d\tau \tag{14}$$

$$\frac{\dot{x}_R(T)}{\omega} = -\frac{1}{\omega}\int_{-\infty}^{\infty} \cos \omega(T-\tau)\,\ddot{x}_B(\tau)\,d\tau . \tag{15}$$

After the shock pulse $t > T$, $\ddot{x}_B(t) = 0$ and Eq. (5) can be written:

$$\ddot{x}_R + \omega^2 x_R = 0 \tag{16}$$

with a solution,

$$x_R = A \cos \omega(t - T) + B \sin \omega(t-T) \tag{17}$$

$$x_R = c \sin [\omega(t-T) + \phi] . \tag{18}$$

Differentiating, and dividing by ω,

$$\frac{\dot{x}_R}{\omega} = c \cos [\omega(t-T) + \phi] . \tag{19}$$

Considering the initial conditions $t = T$ for after the pulse, Eqs. (14) and (15) become:

$$-\frac{1}{\omega}\int_{-\infty}^{\infty} \sin \omega(T-\tau)\,\ddot{x}_B(\tau)\,d\tau = c \sin \phi \tag{20}$$

$$-\frac{1}{\omega}\int_{-\infty}^{\infty} \cos \omega(T-\tau)\,\ddot{x}_B(\tau)\,d\tau = c \cos \phi . \tag{21}$$

Squaring Eqs. (20) and (21) and adding:

$$c^2 = \frac{1}{\omega^2}\left\{\left[\int_{-\infty}^{\infty} \sin \omega(T-\tau)\,\ddot{x}_B(\tau)\,d\tau\right]^2 + \left[\int_{-\infty}^{\infty} \cos \omega(T-\tau)\,\ddot{x}_B(\tau)\,d\tau\right]^2\right\} . \tag{22}$$

Expanding,

$$c^2 = \frac{1}{\omega^2}\left\{\left[\int_{-\infty}^{\infty} (\cos \omega T \cos \omega\tau + \sin \omega T \sin \omega\tau)\,\ddot{x}_B(\tau)\,d\tau\right]^2 + \left[\int_{-\infty}^{\infty} (\sin \omega T \cos \omega\tau - \cos \omega T \sin \omega\tau)\,\ddot{x}_B(\tau)\,d\tau\right]^2\right\} . \tag{23}$$

Removing functions independent of the integration outside the integral sign:

$$c^2 = \frac{1}{\omega^2}\left\{\left[\cos\omega T\int_{-\infty}^{\infty}\ddot{x}_B(\tau)\cos\omega\tau\,d\tau + \sin\omega T\int_{-\infty}^{\infty}\ddot{x}_B(\tau)\sin\omega\tau\,d\tau\right]^2 + \left[\sin\omega T\int_{-\infty}^{\infty}\ddot{x}_B(\tau)\cos\omega\tau\,d\tau - \cos\omega T\int_{-\infty}^{\infty}\ddot{x}_B(\tau)\sin\omega\tau\,d\tau\right]^2\right\} \quad (24)$$

Squaring,

$$c^2 = \frac{1}{\omega^2}\left\{\cos^2\omega T\left[\int_{-\infty}^{\infty}\ddot{x}_B(\tau)\cos\omega\tau\,d\tau\right]^2 + \sin^2\omega T\left[\int_{-\infty}^{\infty}\ddot{x}_B(\tau)\sin\omega\tau\,d\tau\right]^2 + 2\sin\omega T\cos\omega T\int_{-\infty}^{\infty}\ddot{x}_B(\tau)\sin\omega\tau\,d\tau\int_{-\infty}^{\infty}\ddot{x}_B(\tau)\cos\omega\tau\,d\tau + \sin^2\omega T\left[\int_{-\infty}^{\infty}\ddot{x}_B(\tau)\cos\omega\tau\,d\tau\right]^2 + \cos^2\omega T\left[\int_{-\infty}^{\infty}\ddot{x}_B(\tau)\sin\omega\tau\,d\tau\right]^2 - 2\sin\omega T\cos\omega T\int_{-\infty}^{\infty}\ddot{x}_B(\tau)\sin\omega\tau\,d\tau\int_{-\infty}^{\infty}\ddot{x}_B(\tau)\cos\omega\tau\,d\tau\right\} \quad (25)$$

Collecting terms and taking a square root of both sides of the equation:

$$c = \frac{1}{\omega}\left\{\left[\int_{-\infty}^{\infty}\ddot{x}_B(\tau)\cos\omega\tau\,d\tau\right]^2 + \left[\int_{-\infty}^{\infty}\ddot{x}_B(\tau)\sin\omega\tau\,d\tau\right]^2\right\}^{1/2} \quad (26)$$

Finding the second time derivative of Eq. (18) and using the fact that $\ddot{x}_B = 0$ after the pulse in Eq. (3) we obtain:

$$\ddot{x}_M = -c\omega^2\sin[\omega(t-T)+\alpha] \quad (27)$$

The positive residual shock spectrum after the pulse $R(\omega)$ is defined as the maximum absolute value of the mass acceleration in this equation. Therefore,

$$R(\omega) = |\ddot{x}_M|_{max} = c\omega^2. \quad (28)$$

Thus,

$$R(\omega) = \omega^2\left\{\left[\int_{-\infty}^{\infty}\ddot{x}_B(\tau)\cos\omega\tau\,d\tau\right]^2 + \left[\int_{-\infty}^{\infty}\ddot{x}_B(\tau)\sin\omega\tau\,d\tau\right]^2\right\}^{1/2} \quad (29)$$

THE FOURIER INTEGRAL

A function $\ddot{x}_B(t)$ can be expanded within a finite time domain by use of the Fourier Series expansion formula.

$$\ddot{x}_B(t) = \frac{a_0}{2} + \sum_{N=1}^{\infty}[a_N\cos N\omega t + b_N\sin N\omega t]. \quad (30)$$

If the frequency spacing between harmonics approaches zero we will approach a continuous distribution of frequency components known as the Fourier Integral Identity over an infinite time domain.

$$\ddot{x}_B(t) = \int_0^{\infty}a(\omega)\cos\omega t\,d\omega + \int_0^{\infty}b(\omega)\sin\omega t\,d\omega \quad (31)$$

where,

$$a(\omega) = \frac{1}{\pi}\int_{-\infty}^{\infty}\ddot{x}_B(\tau)\cos\omega\tau\,d\tau \quad (32)$$

$$b(\omega) = \frac{1}{\pi}\int_{-\infty}^{\infty}\ddot{x}_B(\tau)\sin\omega\tau\,d\tau. \quad (33)$$

Rearranging,

$$\ddot{x}_B(t) = \frac{1}{\pi}\int_0^{\infty}[\pi a(\omega)\cos\omega t + \pi b(\omega)\sin\omega t]\,d\omega \quad (34)$$

$$\ddot{x}_B(t) = \frac{1}{\pi}\int_0^\infty S(\omega)\cos(\omega t + \psi)\,d\omega \qquad (35)$$

where:

$$S(\omega) = \left[\pi^2\left(a(\omega)\right)^2 + \pi^2\left(b(\omega)\right)^2\right]^{1/2} \qquad (36)$$

$$S(\omega) = \left\{\left[\int_{-\infty}^{\infty}\ddot{x}_B(\tau)\cos\omega\tau\,d\tau\right]^2 + \left[\int_{-\infty}^{\infty}\ddot{x}_B(\tau)\sin\omega\tau\,d\tau\right]^2\right\}^{1/2} \qquad (37)$$

$S(\omega)$ in Eq. (37) is defined as the frequency composition of $\ddot{x}_B(t)$.

RELATIONSHIP BETWEEN "RESIDUAL" SHOCK SPECTRA AND FREQUENCY CONTENT OF THE PULSE

By comparing Eqs. (29) and (37),

$$S(\omega) = \frac{R(\omega)}{\omega} = \left\{\left[\int_0^{\infty}\ddot{x}_B(\tau)\cos\omega\tau\,d\tau\right]^2 + \left[\int_0^{\infty}\ddot{x}_B(\tau)\sin\omega\tau\,d\tau\right]^2\right\}^{1/2} \qquad (38)$$

Consequently, the relationship of the "residual" shock spectrum to the frequency composition of a time pulse as defined in Fourier Integral Theory is given by:

$$S(\omega) = \frac{R(\omega)}{\omega} \qquad (39)$$

where $R(\omega)$ and $S(\omega)$ are respectively the "residual" shock spectra and the frequency composition of the Fourier Integral both a function of the angular frequency ω.

* * *

UNCLASSIFIED